

## Chemical Physics of Discharges

Wade L. Fite

University of Pittsburgh

Introduction

The gas discharge as a chemical tool is of interest for the environment which it provides, an environment which in many respects is very close to and in others very far away from thermal and chemical equilibrium. Since achieving this situation in the gas discharge is a result of the physical processes occurring to sustain the electrical characteristics of the discharge it is appropriate to consider some of the basic physical aspects of gas discharges before examining the chemical consequences.

In attempting to understand the physics of discharges one would like first to understand the microscopic processes in discharges and then construct a reasonably complete and accurate synthesis to describe the macroscopic characteristics. This approach of course implies that one has a detailed understanding of the processes involved and know the rates and cross sections for the processes. While one can use this approach successfully up to a point, the extreme complexity of discharge phenomena forces one also to formulate a macroscopic description and work toward a juncture with the microscopic point of view.

In this brief review, the microscopic point of view will be used primarily. Also, in view of the fact that other participants at this symposium will discuss extensively the heavy particle aspects of discharges, i.e., the chemistry, it would appear appropriate to emphasize in this paper the role of the electron in discharges. In the final analysis, the electron is the essential ingredient, the sine qua non of a gas discharge, the agent which transfers energy from an electrical power supply to the gas.

Following some microscopic considerations, some of the macroscopic description of discharges is reviewed briefly and finally the afterglow of a gas discharge is discussed.

## II Electron Motion and Behavior

Be it supposed that a gas is enclosed in a container and that a free electron has been produced--perhaps by a cosmic ray, or by the radiation from the experimenter's watch dial, or from that little piece of uranium glass in a graded seal, or by cold cathode emission by the very strong electric fields around a sharp point on an electrode in the discharge tube.

If a dc electric field is imposed, the electron will respond according to Newton's law,

$$\dot{v} = \frac{q}{m} E \quad (1)$$

and begin to accelerate in free fall. This acceleration will continue until it has a collision with a gas molecule. If the energy of the electron at the time of collision is very low, only elastic scattering will be admitted. At higher energies large amounts of energy can be lost by the electron in exciting the molecule to high-lying states of internal energy and at higher energies yet, ionization can occur. The latter process is, of course, essential to achieve the electron multiplication and convert the gas with a single electron in it into a gaseous medium of high electrical conductivity.

Since each type of collision has separate consequences for the discharge we consider them in turn. The collisions are of course statistical and we must incorporate statistics with particle mechanics in their treatment.

### A. Elastic Collisions: Transfer of Energy

In elastic collisions of electrons with heavy gas molecules, two effects are of importance. First there is a redistribution of directions of travel of the electrons and second there is a very slight loss of energy (and therefore speed) as a very small amount of momentum and energy are transferred to the molecule by the electron.

At low energies, i.e., a few ev and less, electron scattering tends to be isotropic in angle in the center of mass coordinates. This implies that if we examine many electrons immediately after they have had a collision the average vector velocity will be zero, but of course the average scalar speed will not be zero. The probability per unit time that an electron will have a collision (i.e. the collision frequency) is given by

$$Z(c) = n Q(c) c \quad (2)$$

where  $n$  is the number density of molecules,  $c$  is the electron's speed and  $Q(c)$  is the total cross section for elastic collisions. The cross section generally diminishes with increasing speed, although resonances in scattering impart considerable structure in the functional form of the cross section in the case of most gases.

We suppose that an electric field,  $E$ , is imposed in the  $z$  direction, and

inquire about the component of velocity in the z direction, averaged over all electrons,  $\langle v_z \rangle$ , which is identical to  $\langle \vec{v} \rangle$ . Since each electron responds to the field in the same way, the average acceleration due to the field is that of each electron separately. Further, because the average velocity is zero following a collision, the loss of average velocity due to collisions is to good approximation just the product of the average collision frequency  $\langle Z \rangle$  and the average velocity. Thus we can write that for the average velocity in the z direction

$$\frac{d\langle v_z \rangle}{dt} = \frac{q}{m} E - \langle Z \rangle \langle v_z \rangle. \quad (3)$$

When the steady state is achieved the left side vanishes, which implies that the pickup of directed velocity from the field is just balanced by the loss of directed velocity due to the randomization of direction of motion by the collisions. Under steady state collisions, then,

$$\langle v_z \rangle = \frac{q}{m} \cdot \frac{1}{\langle Z \rangle} E = \mu E \quad (4)$$

where  $\mu$  is designated the mobility.

Equation (4) can be re-written in terms of Eq. (2) as

$$\langle v_z \rangle = \frac{q}{m} \cdot \frac{1}{\langle c Q(c) \rangle} \cdot \frac{E}{n}. \quad (5)$$

In this expression the second term gives all the information about the interaction between the electron and the particular gas molecule and the third term contains the parameters available to the experimenter, i.e., the electron field and the gas number density. Since the number density is proportional to the gas pressure, the experimental quantity of major relevance is the ratio  $E/p$ .

Randomization of directions of velocity says nothing whatever about average speeds of the particles. For this we turn to other considerations. Conservation of momentum requires that the energy loss from an electron of mass  $m$  and kinetic energy  $W$  in collision with a heavy particle of Mass  $M$  is given by

$$\Delta W = W \frac{2m}{M} (1 - \cos \theta) \quad (6)$$

where  $\theta$  is the angle of deflection of the electron in the collision. If the scattering is isotropic (as it closely approximates at low energies) then the energy loss in a collision averaged over angle is

$$\overline{\Delta W} = \frac{2m}{M} W = hW \quad (7)$$

where for convenience we let  $2m/M = h$ .

We would expect a steady state ultimately to be achieved between the electron energy picked up from the electric field between collisions and the energy transmitted from the electron to the heavy particles through the collisions. We proceed to evaluate these separately. For simplicity we assume that the collision frequency is independent of speed of the electrons.

Since the electric field acts only in the  $z$  direction, all the increase in kinetic energy of an electron will occur through increasing the  $z$  component of its velocity which is given by

$$v_z = v_{0z} + at \quad (8)$$

where  $v_{0z}$  is the value of  $v_z$  immediately following the collision and  $t$  is the time elapsed since the last collision and  $a = (q/m)E$ . The energy picked up will be

$$\Delta W = qE \int dz = ma \int v_z dt = ma \left\{ v_{0z}t + \frac{1}{2}at^2 \right\} \quad (9)$$

If we now average over all angles of direction of motion immediately following the last collision,  $\overline{v_{0z}} = 0$  so that

$$\overline{\Delta W} = \frac{1}{2} ma^2 t^2. \quad (10)$$

If we now average over all collision times, Eq. (10) becomes

$$\overline{\Delta W}_{av} = \frac{1}{2} m a^2 (t^2)_{av}. \quad (11)$$

To find  $(t^2)_{av}$ , we assume that collisions are random events and the collision frequency is independent of speed. We can then write that the probability of a collision occurring in the interval  $t$  to  $t + dt$  following the preceding collision is

$$p(t)dt = Z e^{-Zt} dt \quad (12)$$

for which the average value of  $t^2$  is  $2\tau^2$  where  $\tau = 1/Z$  is the mean collision time. Eq. (11) then becomes

$$\overline{\Delta W}_{av} = m a^2 \tau^2 \quad (13)$$

If we also average over all speeds of electrons and neglect some of the finer points of statistics, Eq. (13) becomes

$$\langle \overline{\Delta W}_{av} \rangle \approx m a^2 \frac{\lambda^2}{\bar{c}^2} \quad (14)$$

where  $\lambda$  is the mean free path and  $\bar{c}$  is the mean speed of the electrons.

This quantity, in the steady state, will equal the right hand side of Eq. (7) averaged over all electrons. If we let  $W \approx \frac{1}{2} m \bar{c}^2$

$$\frac{1}{2} h m \bar{c}^2 \approx m a^2 \frac{\lambda^2}{\bar{c}^2} \quad (15)$$

Thus we would expect that the mean speed would be given by

$$\bar{c}^4 \approx 2 \frac{a^2 \lambda^2}{h^2} \quad (16)$$

and the mean energy of the electrons in the steady state by

$$\frac{1}{2} m \bar{c}^2 \approx \frac{1}{2} m \bar{c}^2 \approx \frac{1}{2} \sqrt{\frac{M}{m}} g E \lambda. \quad (17)$$

The remarkable aspect of this result comes on the insertion of numbers in Eq. (17). If for example, one has electrons moving through a gas with  $M \sim 30$  AMU, at pressures giving  $\lambda \sim 1$  mm (i.e.  $p \approx 1$  torr) then the mean energy in ev is around 25 times the field strength in volts/cm. With as little as a few tenths of v/cm fields, mean electron energies are several ev. We can thus understand the appearance of high electron "tempreatures" in gas discharges.

It is beyond the scope of this review to go further and question the distribution of electron energies. It is sufficient to indicate that if one takes assumptions similar to those made in this simplified argument and utilizes them in the Boltzmann equation, one can obtain an approximate solution for the distribution of speeds. The result is not the Maxwell-Boltzmann distribution, but rather that known as the Druyvesteyn distribution whose dependence on speed is given by

$$f(c)dc \propto c^2 e^{-\frac{3hc^4}{8\lambda^2 a^2}} \quad (18)$$

This distribution function is similar in shape to the Maxwell-Boltzmann distribution for a given mean speed, except that the most probable speed is slightly higher and the high energy tail is diminished in the Druyvesteyn distribution. Nonetheless, the distributions are sufficiently similar that one can, to good approximation, think of the electrons as having a temperature in the Maxwellian sense which is much higher than the neutral gas temperature; i.e. typically 30,000°K vs 300°K. It is this dichotomy of temperatures which is perhaps the most striking of the non-equilibrium aspects of a gas discharge.

This general effect of collisions randomizing the direction of motion of electrons which have picked up energy from the field between collisions has another important manifestation. It is responsible for the operation of microwave electrodeless discharges. If we consider an electron moving in an ac field which is of the form  $E(t) = E_0 \cos \omega t$ , then Newton's law for the electron becomes, in the absence of collisions,

$$\dot{v} = \frac{q}{m} E_0 \cos \omega t \quad (19)$$

which solves to give

$$\left. \begin{aligned} v &= \frac{qE_0}{m\omega} \sin \omega t \\ x &= -\frac{qE_0}{m\omega^2} \cos \omega t \end{aligned} \right\} \quad (20)$$

The rate of energy pickup from the field i.e. the power, P is given by

$$P = qEv = \frac{q^2 E_0^2}{m\omega} \cos \omega t \sin \omega t = \frac{1}{2} \frac{q^2 E_0^2}{m\omega} \sin 2\omega t, \quad (21)$$

which, it is noted can be negative as well as positive. If we consider the total power pickup over a complete cycle, the sine-cosine product integrates to zero, indicating that there is no net transferral of energy from the electric field to the electron. This is of course a result of the fact that the applied field and the electron velocity are  $90^\circ$  out of phase.

Furthermore, we can note from (20) that the maximum electron velocity will be  $qE_0/m\omega$  and the maximum kinetic energy will be

$$W_{\max} = \frac{1}{2} \frac{q^2 E_0^2}{m\omega^2}. \quad (22)$$

It is noted that if one has a field oscillating at say  $10^9$  cps and a maximum field strength of say 300 volts/cm, equation (22) indicates that the maximum kinetic energy of the freely oscillating electron will be only about 2 ev. This is insufficient energy to ionize gases, and yet breakdown will occur for this type of field.

It is collisions of the type which lead to the Druyvestryn distribution which are responsible for ionization. An electron will be accelerated by the field during a portion of its cycle and then be deflected in a collision. The energy parallel to the electric field is thus converted to energy perpendicular to the field.

The field then proceeds to give the electron additional energy in the direction of the field. Energy is pumped from kinetic energy of motion parallel to the field to kinetic energy in all directions.

If we write Newton's law for an electron, adding a collision term, we are left with Eq. (3), except now,  $E$  is time-dependent. Writing  $E = E_0 \cos \omega t$

$$\frac{d\langle v_x \rangle}{dt} = \frac{qE_0}{m} \cos \omega t - \langle Z \rangle \langle v_x \rangle. \quad (23)$$

The power delivered to an electron by the field, averaged over a cycle, is

$$\bar{P} = \frac{1}{2} \frac{q^2 E_0^2}{m} \frac{\langle Z \rangle}{\langle Z \rangle^2 + \omega^2} \quad (24)$$

This equation shows directly the role of collisions of electrons in conversion of electrical energy to energy of the gas.

Again if this power gain is equated to the loss of energy of electrons in elastic collisions with the gas molecules, as would occur in the steady state, then

$$\frac{1}{2} m \bar{c}^2 h \langle Z \rangle \approx \frac{q^2 E_0^2}{m} \frac{\langle Z \rangle}{\langle Z \rangle^2 + \omega^2} \quad (25)$$

or since  $\langle Z \rangle \approx \frac{\bar{c}}{\lambda}$

$$\frac{1}{2} m \bar{c}^2 \approx \frac{\lambda a}{\sqrt{h}} \left\{ \sqrt{1 + \frac{\lambda^2 \omega^2}{a^2 h}} - \frac{\lambda \omega}{a \sqrt{h}} \right\} \quad (26)$$

where  $a \equiv \frac{qE_0}{m}$ .

From (26) one would expect the electron "temperature" for fixed  $E_0$  to diminish with increasing frequency, but for pressures of the order of one torr and gas masses of around 30 AMU the electron temperature will remain near the dc value for frequencies usually employed for gas discharge work.

#### B. Elastic Collisions, and Diffusion

Since in either dc or ac discharges, the electrons will have high temperatures, one can expect that all the manifestations of a kinetic temperature will be present. Particularly important among these is diffusion through elastic collisions. If only electrons are present in a neutral gas they will tend to diffuse as would any other gaseous component with a current density

$$\vec{S}_e = n \langle \vec{v}_e \rangle = -D_e \nabla n_e \quad (27)$$

where  $n_e$  is the number density of the electrons and  $D_e$  is the diffusion coefficient of the electrons through the gas. If a field is also superposed, the current density will contain a mobility term as well so that

$$\vec{S}_e = -D_e \nabla n_e - n_e \mu_e \vec{E} \quad (28)$$

where the minus sign in the second term indicates that because of the negative charge on the electrons, their motion will try to be in the direction opposite to that of the applied field.  $\mu_e$  is taken to be a positive number. Whether the electron motion is diffusion-dominated or field dominated depends on whether the first term is larger

than or smaller than the second.

In a gas discharge, the electrons will have produced ions and these also will tend to diffuse through the neutral gas as well as respond to any electric fields. The current density of ions will be given therefore by a similar equation

$$\vec{S}_+ = -D_+ \nabla n_+ + n_+ \mu_+ \vec{E}. \quad (29)$$

From Eq. (4) the mobility of either type of particle is  $\mu = |q|V/(m\langle Z \rangle)$  and from kinetic theory, the diffusion coefficient is given by  $D = kT/(m\langle Z \rangle)$ . Since both these parameters have the mass appearing in the denominator the electron will diffuse and respond to an electric field much more rapidly than will the heavy ions.

The case of major interest for discharge physics is that where the number density of ions is very nearly equal to that of the electrons. Clearly because the electron mass is very light these will try to diffuse away from the ions. However, as soon as they do this, an electric field is set up between the electrons and ions so that the electrons are held back by the ions and the ions are dragged along by the electrons. We would thus expect that the current fluxes  $S_e$  and  $S_+$  would be equal.

If we set  $S_e = S_+ \equiv S$ , and  $n_e = n_+ \equiv n$ , to indicate an electrically neutral plasma, Eqs. (28) and (29) can be combined to eliminate the electric field with the result that

$$S = -D_a \nabla n \quad (30)$$

where

$$D_a = \frac{\frac{D_+}{\mu_+} + \frac{D_e}{\mu_e}}{\frac{1}{\mu_+} + \frac{1}{\mu_e}} \quad (31)$$

Since

$$\frac{D_+}{\mu_+} = \frac{\kappa T_+}{|q_+|}$$

$$\text{and } \frac{D_e}{\mu_e} = \frac{\kappa T_e}{|q_e|}$$

and

$$\frac{1}{\mu_+} \gg \frac{1}{\mu_e}, \quad |q_e| = |q_+| = e$$

we can write

$$D_a \approx \frac{\kappa \mu_+}{e} (T_+ + T_e) \quad (32)$$

or

$$D_a \approx \frac{\kappa \mu_+ T_+}{e} \left(1 + \frac{T_e}{T_+}\right) = D_+ \left(1 + \frac{T_e}{T_+}\right). \quad (33)$$

If the electron temperature is equal to the ion temperature, as in the case of late in an afterglow, the ambipolar diffusion coefficient is just twice the value of  $D_+$ . In the active discharge, however, as we have seen  $T_e$  will be large, perhaps of the order of 30,000°K. On the other hand the ion temperature will deviate little from the neutral gas temperature. The reason is that the ion mass is comparable to the mass of the neutral molecules; thus by arguments similar to those leading to Eq. (7) the ion will in a single collision be able very effectively to give to the neutral gas the energy it picks up from the field between collisions. The temperature of the ions will therefore remain very close to the neutral gas temperature. The ratio  $T_e/T_+$  will be of the order of 100 typically in an active discharge and rapid diffusion of the plasma through the neutral gas and to the walls of the container will result.

#### Summary of the Remainder of the Paper

C. Electron production and loss mechanisms are discussed and the plasma balance equation is formulated.

D. Excitation to radiating and metastable states is summarized and some of their consequences for the operation of a discharge are presented.

E. Wall phenomena.

#### III. Macroscopic phenomena.

A. Plasma polarization and the Debye length are discussed.

B. Characteristics of certain types of discharges are reviewed; Glow Discharges, Arc Discharges and rf discharges.

IV. Afterglows. The effects of suddenly reducing the electron temperature are briefly reviewed.

Frederick Kaufman\*

Department of Chemistry, University of Pittsburgh

## I. INTRODUCTION

The size and topical variety of this symposium clearly show that electrical discharges are finding increasing application in many areas of chemistry ranging from the production of simple atomic species such as H, O, or N from their diatomic molecules to the synthesis or specific decomposition of complex organic or inorganic compounds. It is unfortunately true that our understanding of the chemistry of discharge processes is still in a rudimentary state, that the field is more an art than a science, and thus represents one of the last frontiers of chemistry.

There is good reason for this unsatisfactory state of affairs. Glow discharges are complex phenomena in which gases at sub-atmospheric pressure are undergoing excitation and ionization by electron impact and so give rise to highly unequibrated steady-state conditions where the effective temperature of free electrons is typically tens of thousands °K, that of electronically or vibrationally excited states may be thousands of °K, whereas the translational and rotational temperature will only be tens to hundreds of °K above ambient. It should be clear, of course, that apart from the processes occurring at the electrodes, energy from the electric field is coupled to the gas almost entirely through the kinetic energy of free electrons which, due to their small mass, acquire energy more rapidly from the field and lose it more slowly in elastic collisions (the mean fractional energy loss per elastic collision equals  $2 m/M$  in the simplest classical model where  $m$  and  $M$  are the masses of the electron and of the molecule). In this manner, electrons become sufficiently energetic to ionize some of the neutral species and thereby balance their continuous loss by diffusion, attachment, and recombination. As the ionization potentials of most neutral gases are in the 10 to 20 eV range (230 to 460 kcal/mole), an appreciable fraction of the electrons has enough energy to produce electronic excitation (responsible for the emitted glow) and dissociation.

In the following sections, the mechanism of dc and ac glow discharges will be briefly described, with emphasis on high frequency electrodeless discharges ( $f = 10^6$  to  $10^{10}$  sec<sup>-1</sup>) and on the simple geometry often encountered in rapidly pumped steady-state flow systems at pressures near 1 torr. After a brief discussion of the rates and energy dependence of specific collision and diffusion processes, available experimental data will be brought to bear on the problem of H<sub>2</sub>, N<sub>2</sub>, and O<sub>2</sub> dissociation and on the chemistry of some more complicated systems.

Although there are several fine monographs available on electron impact phenomena and discharge physics<sup>1-4</sup>, they contain relatively little information on active high frequency discharges which is pertinent to the problem of dissociation and chemical reaction. The electron physics of microwave discharges is discussed in some review articles.<sup>5,6</sup>

## II. BASIC PHYSICAL PROCESSES

## II. 1. General Mechanism and Frequency Dependence.

Glow discharges are typically observed in the pressure range of about 0.1 to 10 torr. At much lower pressures, the electron mean free path is too long for gas collisions to be important, electrons pick up large amounts of energy from the dc or slow ac field and bombard the anode or the tube wall which may then fluoresce. At

\* This work was supported by the National Science Foundation

much higher pressures, the mean free path is very short, the breakdown field strength is very high, and when it is exceeded, local, highly ionized, but narrow pathways are created for the conduction of current, i.e. spark filaments are formed. The normal dc glow discharge in a long cylindrical tube is characterized by many axially distinct but radially fairly uniform regions of quite different optical and electrical properties such as the Aston Dark Space, Cathode Glow, Cathode Dark Space, Negative Glow, Faraday Dark Space, Positive Column, Anode Glow, and Anode Dark Space, in this order, between cathode and anode. The reason for this complexity is that quite different processes occur in the different regions as is also shown by a very non-uniform voltage rise between cathode and anode. Most of the potential difference is taken up in the 'cathode fall' which comprises the first four regions enumerated above, is dependent on the cathode material as well as on the nature of the gas and on the natural variable  $E/N$  (V cm<sup>2</sup>/molecules) where  $E$  is the field strength (V/cm) and  $N$  the total neutral density (molecules/cm<sup>3</sup>). The latter is a measure of the electron energy under conditions of steady-state drift. Equating energy loss and gain per electron per second,  $\frac{2m}{M} \frac{e\bar{v}}{\lambda} = eEw$ , where  $\epsilon = \frac{1}{2} m\bar{v}^2$  is the electron energy,  $\lambda$  the mean free path for electron-neutral collisions,  $e$  the electronic charge, and  $w$  the electron drift velocity which equals  $\frac{2}{3} \frac{eE\lambda}{m\bar{v}}$  one obtains  $\epsilon = \frac{eE\lambda m^{1/2}}{(6m)^{1/2}} = \frac{E}{N} \frac{em^{1/2}}{2\pi\sigma^2(3m)^{1/2}}$  where  $\lambda$  was replaced by  $1/(\frac{1}{2} \pi \sigma^2 N)$  from simple kinetic theory. The 'cathode fall' and 'anode fall' regions also have large gradients of electron and ion concentrations and a local imbalance of electrical charge. The positive column is simpler in nature (although striated positive columns are still poorly understood), has a small and constant axial voltage drop, and only a small imbalance of charge carriers, because, although electrons initially diffuse to the tube wall faster than ions, the resultant radial field prevents further charge separation and forces electrons and ions to diffuse equally fast. This process is called ambipolar diffusion and is further discussed below. The voltage drop along the positive column is also independent of the total current over a fairly wide range, and since the current,  $i$ , is carried mostly by the electrons whose drift velocity is about 100 times larger than that of the ions,  $i = n_e ew = \frac{2}{3} \frac{e^2 E \lambda}{m\bar{v}} n_e$ , which shows that the electron concentration,  $n_e$ , increases linearly with increasing current because  $E$  and  $\bar{v}$  are constant. In its normal range of electron (and ion) concentrations of  $10^8$  to  $10^{11}$  cm<sup>-3</sup>, the positive column of a dc glow discharge is diffusion-controlled and serves as the electrical connection between the cathode and anode regions.

In high frequency electrodeless discharges the complications of the cathode and anode regions are absent, the entire plasma is approximately neutral and diffusion-controlled, and the discharge often resembles the positive column of an equivalent dc discharge. Yet, there are differences in its fundamental mechanism, especially at microwave frequencies. Free electrons oscillating in an alternating field can not derive power from the field on the average, because their motion is 90° out of phase with the field. They therefore acquire energy only because collisions with neutral molecules change their phase relationship with the field, while at the same time representing a small fractional loss of the energy gained. Under the assumption that the ac frequency,  $f$ , is greater than the elastic collision frequency,  $\nu_e$ , the maximum displacement,  $x$ , of an electron due to the high frequency field is given by  $x = \frac{2eE}{m\omega^2}$  where  $\omega = 2\pi f$ . In an active microwave discharge  $E$  is typically 30 V/cm and  $x$  is therefore less than  $10^{-3}$  cm when  $f = 2.5 \times 10^9$  sec<sup>-1</sup> (as in the widely used Raytheon Microtherm Generator). The corresponding maximum electron energy acquired during the cycle is  $eEx$ , about 0.02 eV, i.e. the electrons slowly accumulate the energy necessary to undergo inelastic, ionizing collisions and to sustain the discharge. When elastic collisions are approximately accounted for, it is convenient to define an effective field strength,  $E_e = E_0 \left( \frac{\nu^2}{\nu^2 + \omega^2} \right)^{1/2}$ , where  $E_0$  is the rms value of the applied field strength. The power gained from the

field per electron is  $\frac{e^2 E^2}{mv}$  and per collision therefore  $\frac{e^2 E^2}{mv^2}$ .

## II. 2. Diffusion of Charged Species.

In the discharges of interest here, the concentration of charged species is greater than  $10^8 \text{ cm}^{-3}$  and a large fractional separation of electrons and positive ions becomes impossible, because it would set up a very large opposing field. The currents of electrons and ions reaching the wall must then be equal,  $i_e = -D_e \nabla n - n \mu_e E'$

$i_+ = -D_+ \nabla n + n \mu_+ E'$  where  $n = n_e = n_+$  is the electron density,  $\nabla n$  the density gradient,  $D$  the diffusion coefficient,  $\mu$  the mobility, and  $E'$  the field due to the (small) space charge. The subscripts  $e$  and  $+$  refer to electron and positive ion. Equating  $i_e$  and  $i_+$  and eliminating  $E'$  one obtains

$$i = - \frac{D_e \mu_+ + D_+ \mu_e}{\mu_+ + \mu_e} \nabla n = D_a \nabla n$$

which serves as the definition of the ambipolar diffusion coefficient,  $D_a$ . Substituting  $\mu_e \frac{kT_e}{e}$  for  $D_e$  and the equivalent expression for  $D_+$  one obtains

$$D_a = \frac{\mu_e \mu_+}{\mu_e + \mu_+} \frac{k}{e} (T_e + T_+)$$

which approximately equals  $\frac{\mu_+ k}{c} (T_e + T_+)$  or  $D_+ (1 + \frac{T_e}{T_+})$  because the electron mobility  $\mu_e$ , is much larger than the ionic mobility  $\mu_+$ . In active glow discharges  $T_e/T_+$  is typically 20 to 100, whereas in the afterglow the electrons thermalize rapidly and  $T_e/T_+ = 1$ . Thus,  $D_a \approx 20$  to  $100 D_+$  in the active discharge, and  $2 D_+$  in the afterglow.

The disappearance of charged species by ambipolar diffusion in the absence of a source term is described by the diffusion equation  $\frac{\delta n}{\delta t} = D_a \nabla^2 n$  where  $n$  is a function of  $r$ ,  $\theta$ ,  $z$ , and  $t$ . The well-known solution of this equation for the case of an infinite cylinder is  $n(r,t) = \sum_{i=1}^{\infty} A_i J_0(\alpha_i \frac{r}{r_0}) e^{-k_i t}$  where  $\alpha_i$  is the  $i$ th root of  $J_0$ , the Bessel

function of zero order and  $k_i = (\frac{\alpha_i}{r_0})^2 D_a = \frac{D_a}{\Lambda^2}$ . The diffusion length,  $\Lambda$ , therefore equals  $\frac{r_0}{\alpha_i}$ . The first few zeroes of  $J_0$  are  $\alpha_1 = 2.405$ ,  $\alpha_2 = 5.520$ ,  $\alpha_3 = 8.654$ ,

$\alpha_4 = 11.792$  which shows that, as diffusion proceeds, the time decay will be increasingly governed by  $k_1 = (\frac{2.405}{r_0})^2 D_a$ , the first (lowest) diffusion mode, because the next three higher modes are damped out more rapidly by factors of 5.3, 12.9, and 24. After a short transient, the diffusion-controlled electron decay or the diffusion controlled loss under steady-state conditions with a spatially well distributed source term can therefore be closely approximated by a first-order rate constant,  $k = 5.78 D_a / r_0^2$ .

This analysis applies when there are only positive ions and electrons present. When negative ions are also present, their principal effect is to accelerate the ambipolar diffusion of the electrons,  $(D_a)_e$ , which now becomes approximately

$$(D_a)_e = (1 + \lambda) D_+ (1 + \frac{T_e}{T_+}) + \lambda (\frac{T_e}{T_+} - 1) \text{ which for active discharges } (T_e/T_+ \gg 1)$$

can be further approximated by  $(1 + 2\lambda) T_e/T_+$ , where  $\lambda = n_-/n_e$ , the concentration ratio of negative ions and electrons. It can be seen that for  $\lambda \gg 1$  electrons

will be lost much more rapidly by diffusion to the wall than in the absence of negative ions.

### II. 3. Electron-Ion and Ion-Ion Recombination.

Although several radiative, two-body, and three-body recombination mechanisms exist, only the fastest ones will be mentioned here. These are the dissociative recombination of electrons and positive molecular ions as exemplified by  $\text{NO}^+ + e \rightarrow \text{N} + \text{O}$  (where the products are likely to be electronically excited), similar ion-ion reactions such as  $\text{I}_2^+ + \text{I}^- \rightarrow \text{I}_2 + \text{I}$  or  $3\text{I}$ ,  $\text{NO}^+ + \text{NO}_2^- \rightarrow$  neutral products, and three-body ion-ion recombinations such as  $\text{NO}^+ + \text{NO}_2^- + \text{M} \rightarrow$  neutral products.

All of these processes have very large rate constants, due to the long range coulombic attraction between reactants, if reasonable paths are available for the dissipation of the large exothermic reaction energy ( $\sim 10$  eV) such as dissociation and electronic excitation. The first of these three processes has been studied in greatest detail, especially by Biondi and coworkers<sup>7,8</sup> who found a value of  $2.9 \pm 0.3 \times 10^{-7} \text{ cm}^3 \text{ molecule}^{-1} \text{ sec}^{-1}$  for the rate constant of  $\text{N}_2^+ + e \rightarrow \text{N} + \text{N}$ , for example. The generally observed range of 1 to  $5 \times 10^{-7}$  ( $6 \times 10^{13}$  to  $3 \times 10^{14}$  lit mole<sup>-1</sup> sec<sup>-1</sup>) means that at an electron and ion concentration  $10^{11} \text{ cm}^{-3}$ , which is near the upper limit of charged particle densities encountered in glow discharges, the effective first order rate constant for electron removal under steady-state conditions will be 1 to  $5 \times 10^4 \text{ sec}^{-1}$ .

Two-body ion-ion recombinations have rate constants in the same general range, although few have been studied in detail, none with precise analysis of reactants and products. Some three-body ion-ion recombinations have recently been studied by Mahan and coworkers<sup>9,10</sup> who found effective termolecular rate constants in the range  $4 \times 10^{-26}$  to  $3 \times 10^{-25} \text{ cm}^6 \text{ molecule}^{-2} \text{ sec}^{-1}$  for  $\text{NO}^+ + \text{NO}_2^- + \text{M}$  near  $300^\circ\text{K}$ . With an approximate  $T^{-5/2}$  dependence, and at a total pressure of 1 torr, such processes would have effective first-order rate constants of ion removal in the 10 to 100 sec<sup>-1</sup> range, too slow to be of importance.

### II. 4. Electron Attachment and Detachment.

Only the fastest of the many possible processes need to be discussed here. Radiative attachment and photodetachment as well as three-body attachment processes are unlikely to be of importance. Dissociative attachment reactions such as  $e + \text{O}_2 \rightarrow \text{O}^- + \text{O}$  have rate constants<sup>11</sup> which rise from zero at an electron energy threshold (4 to 9 eV for the formation of  $\text{O}^-$  from  $\text{O}_2$ ,  $\text{NO}$ , or  $\text{CO}$ ) to a maximum of  $10^{-11}$  to  $10^{-10} \text{ cm}^3 \text{ molecule}^{-1} \text{ sec}^{-1}$  for electrons with 6 to 10 eV. For average electron energies of 2 to 3 eV in an active discharge, the effective rate constant must therefore be lowered about 10 fold to a range of  $10^{-12}$  to  $10^{-11}$ . Moreover, several associative detachment reactions such as  $\text{O}^- + \text{O} \rightarrow \text{O}_2 + e$ ,  $\text{O}^- + \text{N} \rightarrow \text{NO} + e$ ,  $\text{O}^- + \text{H}_2 \rightarrow \text{H}_2\text{O} + e$  have recently been found<sup>12</sup> to be very rapid ( $k = 1$  to  $5 \times 10^{-10} \text{ cm}^3 \text{ molecule}^{-1} \text{ sec}^{-1}$ ) under thermal conditions near  $300^\circ\text{K}$ . This further reduces the likelihood that negative ions are important species in rapidly pumped steady-state glow discharges of diatomic gases. In this regard, active discharges probably differ markedly from their corresponding afterglows in which the electrons are rapidly cooled to ambient temperature and will then readily attach to form  $\text{O}_2^-$ ,  $\text{NO}^-$ ,  $\text{CO}_3^-$ ,  $\text{CO}_4^-$ , and other negative ions even though the electron affinities are quite small.

## II. 5. Charge-Transfer and Ion-Molecule Reactions.

Both positive and negative ion-molecule reactions have recently been studied by a variety of experimental methods, and consistent values for many rate constants have become available. Because of the strong ion-dipole or ion-induced dipole interaction, these reactions usually have little or no activation energy if they are exothermic, and often have rate constants near  $10^{-9}$   $\text{cm}^3 \text{ molecule}^{-1} \text{ sec}^{-1}$ , in accord with the simple theory based on the polarizability of the neutral reactant. Some exceptions such as  $\text{O}_2^+ + \text{N}_2 \rightarrow \text{NO}^+ + \text{NO}$  which is at least  $10^6$  times slower are probably due the large energy requirements for bond rearrangement which in the corresponding neutral four-center reaction gives rise to a very large activation energy. Other unusually slow reactions such as  $\text{O}^+ + \text{N}_2 \rightarrow \text{NO}^+ + \text{N}$  ( $k \sim 2 \times 10^{-12}$ ) are less easily rationalized, particularly since  $k$  rises sharply when the reactant  $\text{N}_2$  is vibrationally excited.

From the magnitude of  $10^{-10}$  to  $10^{-9}$  for many of the exothermic reactions it is clear that the effective first-order rate constant for the transformation of an ionic species by reaction with a major neutral constituent ( $P = 1 \text{ torr} \approx 2 \times 10^{16}$  molecules  $\text{cm}^{-3}$  at the higher temperature of the discharge) is  $2 \times 10^6$  to  $2 \times 10^7 \text{ sec}^{-1}$ , i.e. such reactions will go to completion in a small fraction of the residence time in even the most rapidly pumped flow systems. Minor neutral constituents such as atomic species at 0.1 to 1 mole % will transform ionic species with rate constants of  $10^3$  to  $10^5 \text{ sec}^{-1}$ , still much faster than the rate of traversal through most discharges whose average flow velocities are in the range  $10^2$  to  $10^4 \text{ cm sec}^{-1}$  and whose lengths are 1 to 10 cm.

## II. 6. Electron Impact Ionization.

As shown in section II. 2 above, the electron loss term by ambipolar diffusion can be approximated by a first-order rate constant,  $k = 5.78 D_a/r_0^2$ , which for an active discharge with  $T_e/T_+ \sim 50$ ,  $D_+ \sim 100 \text{ cm}^2/\text{sec}$ , and  $r_0 = 0.5 \text{ cm}$ , makes

$k \sim 1 \times 10^5 \text{ sec}^{-1}$ . Although it is conceivable that chemi-ionization will occur in which two electronically excited molecules with 5 to 10 eV energy react to produce ionization, such processes will normally be of very minor importance. Even with a very large chemi-ionization rate constant of  $10^{-10} \text{ cm}^3 \text{ molecule}^{-1} \text{ sec}^{-1}$ , a concentration of  $5 \times 10^{14} \text{ cm}^{-3}$ , 2 to 3 mole %, of such excited molecules would be required to balance the diffusional loss. It thus seems likely that electron impact ionization is the major source term for charged species in the discharge. Although this requires more than the ionization potential of the atom or molecule, i.e. electron energies in excess of about 15 eV, the large electron velocity and its very high average temperature,  $T_e$ , can easily provide the required magnitude of the rate constant.

The ionization cross section of most atoms and simple molecules rises sharply from zero at the ionization potential and comes to a broad maximum of about 1 to  $5 \times 10^{-16} \text{ cm}^2/\text{molecule}$  at electron energies of 70 to 120 eV. It normally reaches a value of  $1 \times 10^{-17}$  about 2 to 4 eV above its ionization potential, i.e. at electron energies of 12 to 17 eV. For average electron energies of 2 to 3 eV in active glow discharges, this lends to total effective ionization rate constants of  $10^{-11}$  to  $10^{-10} \text{ cm}^3 \text{ molecule}^{-1} \text{ sec}^{-1}$  if a Maxwell distribution is assumed. A somewhat lower range would be obtained for a Druyvesteyn distribution, but since the ratio  $\epsilon/\bar{\epsilon}$  of required to average energy is never very large the error due to the assumption of a Maxwell distribution should be fairly small.

An important, though infrequently applicable ionization mechanism is the direct ionization by collision with sufficiently energetic, metastable neutral species. This process, called Penning ionization, can occur only if the excitation energy of the metastable exceeds the ionization potential of the other reactant. For He, Ne, and Ar the excitation energy of the lowest triplet state is 19.80, 16.62, and 11.55 eV respectively, and since the rate constants for Penning reactions are often gas kinetic,

i.e. near  $10^{-10}$  cm<sup>3</sup> molecule<sup>-1</sup> sec<sup>-1</sup>, this <sup>16</sup> process is likely to be the major ionization source in diatomic gases mixed with excess He or Ne but not with Ar.

## II. 7. Excitation and Dissociation

Molecules can have internal energy in the form of rotation, vibration, or electronic excitation, and they can therefore undergo inelastic collisions with electrons which leave the molecule in one of its many excited states. For the purpose of this review, rotational excitation need not be considered, because rotational energies are small, and the collisional exchange of translational and rotational energy is so rapid that rotational states are unlikely to be substantially out of kinetic temperature equilibrium. Vibration-translation interchange, however, is very inefficient, especially for strongly bound, homonuclear diatomic molecules, so that appreciable vibrational excitation can occur in glow discharges, and effective vibrational temperatures may be established which are intermediate between  $T_i$  and  $T_e$ . Electron impact excitation of vibrational energy is a highly specific process whose cross section can differ by two orders of magnitude from one molecule to another, because it depends on the existence of virtual negative ion states which decay into vibrationally excited ground-state molecules and slow electrons. This mechanism is particularly important in N<sub>2</sub>, CO, and CO<sub>2</sub> which have large cross sections (1 to  $5 \times 10^{-16}$  cm<sup>2</sup>/molecule,  $k = 5 \times 10^{-9}$  to  $2 \times 10^{-8}$  cm<sup>3</sup> molecule<sup>-1</sup> sec<sup>-1</sup> at electron energies of about 2 to 5 ev), but less so in H<sub>2</sub> and O<sub>2</sub> whose cross sections are a factor of 10 to 50 smaller than those in N<sub>2</sub>. The high vibrational temperature,  $T_v$ , of N<sub>2</sub> in glow discharges is likely to be responsible for much of its electronic excitation, because if  $T_v$  approaches  $T_e$ , the internal equilibration of vibrational states will produce appreciable concentrations of molecules with 5 to 8 ev of vibrational energy, consistent with some recent spectroscopic observations in active nitrogen<sup>13</sup> as well as electronically excited molecules by the reverse process of the very fast quenching reactions of the A<sup>3</sup>Σ state of N<sub>2</sub> by N-atoms.

Electronically excited states can be formed directly by electron impact. When the corresponding radiative transition is allowed, the excitation cross section rises to a broad maximum and then slowly decreases, whereas for forbidden radiative transitions, the cross section is sharply peaked at the corresponding energy and falls off rapidly at higher energies. Peak cross sections are often in the  $10^{-17}$  to  $10^{-16}$  cm<sup>2</sup>/molecule range which roughly corresponds to rate constants of  $10^{-11}$  to  $10^{-10}$  cm<sup>3</sup> molecule<sup>-1</sup> sec<sup>-1</sup> for transitions requiring 5 to 10 ev, assuming average electrons energies of 2 to 3 ev.

The principal mechanism for the direct dissociation of a molecule into neutral fragments by electron impact must, of course, be the initial formation of an electronic state with energy greater than D, the dissociation energy. This transition will take place within the limitations set by the Franck-Condon principle. The ensuing dissociation will normally come about in one of three principal ways: (a) the upper state is repulsive and dissociates upon its first pseudovibration, i.e. in about  $10^{-13}$  sec; (b) the upper state is bound, but the molecule is formed on the repulsive part of its potential energy curve at a point above its dissociation energy, and will therefore dissociate on its first vibration, also in about  $10^{-13}$  sec; (c) the upper state is bound, the molecule is formed with less than the dissociation energy of that state, but there is another state of lower dissociation energy with which the first state may interact. Near the crossing point of the two potential energy curves, the states become mixed and there is a probability of crossing and subsequent dissociation. Depending on the degree of mixing, this predissociation process may be very much slower than the first two. The overall cross section and rate constant for dissociation will normally equal that of the primary excitation step, i.e. there will be near unit probability for the subsequent dissociation, because collisional or radiative lifetimes of the excited states can not be shorter than about  $10^{-7}$  to  $10^{-8}$  seconds.

## III. APPLICATION TO THE DISSOCIATION OF SOME DIATOMIC MOLECULES.

### III. 1. Summary of Some Atom Production and Loss Processes

In the following sections much evidence will be cited for catalytic effects in the production of atomic species such as H, N, or O in glow discharges of their diatomic gases. The existence of such effects suggests large changes in the atom production or loss terms upon small variations in gas composition. The principal processes are therefore summarized in this section, and approximate ranges given for their rates. A cylindrical discharge tube of 1 cm diameter, average electron concentration of  $10^{11}$   $\text{cm}^{-3}$ , and electron energy of 2 to 3 eV are assumed corresponding to known conditions in microwave discharges at input power levels of about 10 to 500 watt.

Production terms: (a) Electron impact dissociation via excited states depends on the existence of a dissociating or predissociating state at moderate excitation energy and is therefore quite variable. When the dissociation energy is relatively small, as in H and O, and when states are available at 8 to 10 eV excitation threshold, an atom production rate of 10 to 100 torr/sec can be calculated. For  $\text{N}_2$  whose dissociation energy is larger, the rate will be at least 10 times lower. It should be clear that this process must occur in active discharges, since electron impact ionization, which requires appreciably larger electron energies, is the principal source term for electron production. Therefore, since there are enough electrons present with 15 to 20 eV energy to balance the rapid ambipolar diffusion (and recombination) loss, there must be appreciably more with 8 to 12 eV for excitation-dissociation.

(b) Electron-Ion recombination at the wall (following ambipolar diffusion) or in the gas phase will also produce atomic species in reactions such as  $e + \text{H}_2^+ \rightarrow 2\text{H}$ ,  $e + \text{N}_2^+ \rightarrow \text{N} + \text{N}$ , etc. It is clear that the upper limit to this atom production term is given by the total rate of ionization except for a possible factor of two from the stoichiometry of the dissociation. But as this surface recombination may also lead to the molecular product by the dissipation of energy to the surface, the dissociation rate due to this process is likely to be lower than the corresponding ionization or equivalent ambipolar diffusion term, i.e. < 0.5 to 5 Torr/sec. The gas-phase dissociative recombination will produce atoms at a rate of 0.1 to 0.3 Torr/sec at an electron density of  $10^{11}$   $\text{cm}^{-3}$  and much more slowly at lower densities.

(c) Ion-molecule reactions of primary ions may in exceptional cases be sufficiently exothermic to produce atomic species and ions of lower ionization potential such as in  $\text{H}_2^+ + \text{H}_2 \rightarrow \text{H}_3^+ + \text{H}$ , but the equivalent reactions for  $\text{O}_2$  and  $\text{N}_2$  are endothermic. When such a process is possible, its rate is again limited by the total rate of ionization, but should closely approach it if the neutral molecule is a major species as in the above  $\text{H}_2$  reaction.

(d) Neutral-neutral dissociation reactions may also occur, but little can be said about them in general. As the kinetic temperature of all but the electrons is fairly low (300 to 800°K, mostly near 600°K), two excited, metastable molecules would have to react to transfer their excitation to a predissociating state. Few such reactions are known, and their rate constants are likely to have upper limits in the  $10^{-12}$  to  $10^{-11}$   $\text{cm}^3 \text{ molecule}^{-1} \text{ sec}^{-1}$  range. If that were so, metastable mole fractions as high as 0.1% would only produce atoms at ratios of 0.02 to 0.2 Torr/sec. Such states would also have to be optically metastable, i.e. have radiative lifetimes longer than 0.01 sec, and be resistant to collisional quenching, i.e. have deactivation probability per collision lower than  $10^{-4}$ .

Loss Terms: (a) Homogeneous gas-phase atom recombinations are three-body processes with rate constants near  $10^{-32}$   $\text{cm}^6 \text{ molecule}^{-1} \text{ sec}^{-1}$  so that even for atom mole fractions of 5%, such loss rates are near 0.01 torr/sec, negligibly small.

(b) Surface recombination is a well-known process, usually kinetically first order, and characterized by a rate constant,  $k = \frac{\gamma \bar{c}}{d}$ , for a cylindrical tube of diameter  $d$ .

Here  $\gamma$  is the recombination coefficient, the fraction of surface collisions leading to recombination, and  $\bar{c}$  is the average molecular velocity of the atomic species.  $\gamma$  which is often as low as  $10^{-5}$  outside the discharge for a well-cleaned or suitable poisoned surface, is likely to be  $10^{-3}$  or larger in the active discharge. For  $\gamma = 10^{-3}$ , atom loss rates of 2 to 10 torr/sec can be calculated, and for larger  $\gamma$ , these rates would be larger, but not proportionately so, because large radial concentration gradients would be produced and diffusion would become rate-controlling. Then, an effective first order rate constant,  $k = D/\Lambda^2 = 5.8 D/r^2$ , would be applicable, similar to ambipolar diffusion (Section II.2), but with the smaller molecular diffusion coefficient. For an atom mole fraction of 5%, the upper limit to the diffusional atom recombination rate will be 100 to 300 torr/sec depending on the atomic species.

(c) Ion-molecule reactions can remove atomic species if the ion is polyatomic such as in  $N + N_3^+ \rightarrow N_2 + N_2^+$  or the equivalent oxygen reaction. If the polyatomic ion is a major ionic species, and the reaction is a fast one, its rate at 5% atom mole fraction will be near 5 torr/sec. It will then be limited by the rate of regeneration of the polyatomic ion. Reactions of the type  $O_2^+ + N \rightarrow NO^+ + O$  or  $N_2^+ + O \rightarrow NO^+ + N$  are known to be fast, but as they replace one atomic species by another they need not be considered here.

(d) Neutral, bimolecular atom-molecule reactions such as  $N + O_2 \rightarrow NO + O$  or  $O + H_2 \rightarrow OH + H$  often have appreciable activation energies. Moreover, they, too, only shuffle atomic species and can not be considered loss terms. In the few applicable cases where this does not hold as in  $O + N_2O \rightarrow 2 NO$  or  $N + N_2O \rightarrow N_2 + NO$ , the reactions are known to be negligibly slow.

### III. 2. Hydrogen Discharges

The discussion of the electron collisional aspects of  $H_2$ ,  $N_2$ , and  $O_2$  discharges is greatly aided by the excellent papers by Phelps and coworkers in which elastic and inelastic collision cross sections are obtained by numerical solution of the Boltzmann transport equation and comparison with all available experimental data on electron transport coefficients. For  $H_2$  and  $D_2^{14}$ , the vibrational excitation cross section becomes appreciable ( $10^{-17} \text{ cm}^2$ ) at about 1 eV and peaks near 5 eV at  $8 \times 10^{-17} \text{ cm}^2$ . For dissociation, a threshold at 8.85 eV and peak of  $4.5 \times 10^{-17} \text{ cm}^2$  at 16 to 17 eV was found to be consistent with the data. A recent measurement by Corrigan<sup>15</sup> of the dissociation cross section of  $H_2$  is in good agreement with the above except for a larger peak of about  $9 \times 10^{-17} \text{ cm}^2$  at 16.5 eV. For average electron energies,  $\epsilon_k$ , of 3.0 and 2.0 eV, dissociation rate constants,  $k_d$ , of 11 and  $2 \times 10^{-10} \text{ cm}^3 \text{ molecules}^{-1} \text{ sec}^{-1}$  can be calculated by summation of  $Qv f(\epsilon)$  from  $\epsilon = 0$  to  $\infty$ , using energy increments of 2 or 3 eV, where  $Q$  is the appropriate cross section,  $v$  the electron velocity, and

$$f(\epsilon) = \frac{2}{\pi^{1/2}} \left(\frac{\epsilon}{\epsilon_k}\right)^{1/2} e^{-\frac{\epsilon}{\epsilon_k}} \frac{d\epsilon}{\epsilon_k}$$

is the Maxwell distribution function. Such  $k_d$ 's correspond to H-atom production rates of 200 or 40 torr/sec. An effective ionization rate constant,  $k_i$ , was similarly found to be  $7 \times 10^{-11}$  ( $\epsilon_k = 3 \text{ eV}$ ) and  $6 \times 10^{-12}$  ( $\epsilon_k = 2 \text{ eV}$ ), corresponding to ionization rates of 7 and 0.6 torr/sec, respectively. The latter should be approximately equal to the ambipolar diffusion loss,  $5.8/r_0^2 D_+ T_e n_e / T_g$ , which equals 9 or 6 torr/sec if  $D_+ = 700 \text{ cm}^2/\text{sec}$  at 1 torr pressure. This crude calculation suggests that  $\epsilon_k = 3 \text{ eV}$  is a better choice than 2.0 eV. It neglects the serious deviation from a Maxwell distribution which is to be expected.

More realistic estimates of  $k_d$  and  $k_i$  were obtained by Dr. Phelps by simultaneously adjusting  $E/N$ ,  $\epsilon_k$ , and using the appropriate rate coefficients to balance ionization against diffusion losses. This led to values of  $\epsilon_k = 3.0 \text{ eV}$ ,  $E/N = 1.1 \times 10^{-15} \text{ Vcm}^2/\text{molecule}$  and  $k_i = 7 \times 10^{-11}$ , in surprising agreement with the

above. With that  $E/N$ , an estimate of  $k_d$  can be obtained from ref. 14, Fig. 8 by multiplying the excitation coefficient ( $8 \times 10^{-17}$  cm<sup>2</sup>/molecule) by the drift velocity ( $1.5 \times 10^7$  cm/sec) which gives  $k_d = 1.2 \times 10^{-9}$ , also in fortuitously good agreement with  $1.1 \times 10^{-9}$  above. This excitation coefficient includes other, non-dissociating processes, but since application of Corrigan's<sup>15</sup> larger dissociation cross section would increase total excitation coefficient, its subsequent apportioning would not lead to serious discrepancies.\*

Thus, a very large atom production term of about 200 torr/sec is indicated by all available estimates. In addition, there is the source term due to electron-ion recombination at the wall, and due to the fast reaction  $H_2^+ + H_2 \rightarrow H_3^+ + H$ . Each of these can at most equal the ionization rate, so that their sum will contribute 10 to 20 torr/sec of atomic hydrogen. All other source terms are negligible.

Surface recombination provides the only comparably large loss term in the discharge. For small  $\gamma$ , the first order rate constant,  $k_s = \gamma \bar{c}/d = 2 \times 10^5 \gamma$ , and the steady-state atom concentration,  $[H]_{ss}$  is approximately  $1 \times 10^{-3}/\gamma$ . This shows that  $\gamma$  must always be relatively large, and that the diffusion controlled  $k_s = 5.8 D/r^2 = 2$  to  $4 \times 10^4$  sec<sup>-1</sup> may be applicable which leads to an  $[H]_{ss}$  of 0.5 to  $1 \times 10^{-2}$  torr, less than 1% mole fraction. When  $\gamma$  is lowered to  $10^{-2}$ ,  $[H]_{ss} = 0.1$  torr, and under either condition the half-life for its formation is very short ( $3 \times 10^{-5}$  or  $3 \times 10^{-4}$  sec).

One is thus led to the interesting conclusion that the dissociation yield of such  $H_2$  discharges is mainly controlled by surface recombination and that the surface in the discharge must be moderately to highly efficient for atom recombination. Moreover, the effect of small amounts of added gases such as  $H_2O$  or  $O_2$  in increasing the yield must be through their influence on the surface efficiency, as they can not affect the principal production term and as no homogeneous loss mechanisms of proper magnitude are available. These conclusions are in general agreement with recent work by Goodyear and Von Engel<sup>17</sup> on radio frequency discharges at lower pressure and of different geometry.

The very large body of experimental work on the "catalytic" production of H when small amounts of  $H_2O$  or  $O_2$  are added will not be reviewed here. The effect is unquestionably real, i.e. factors of 10 or so in H-atom yield when switching from "dry"  $H_2$  to  $H_2$  containing 0.1 to 0.3%  $H_2O$  can be demonstrated routinely and reversibly. Rony and Hanson<sup>18</sup> have recently questioned the existence of such an effect at a pressure of 0.075 torr and have reviewed the general subject. Our early experiments do not bear this out, as they show a large catalytic effect for added  $H_2O$ , but they do indicate that the effect is less pronounced at pressures below 0.1 torr. This trend can be expected if the above analysis is correct, because at low pressures, the production terms are decreased and the loss terms increased. Moreover, for a given discharge energy input, the surface should be hotter at low pressure, and this may nullify the deactivation which is probably due to adsorbed water molecules. Several of the relevant experiments are now under way in our laboratory by Dr. D. A. Parkes, using Lyman- $\alpha$  absorption for the down-stream measurement of [H].

### III. 3. Oxygen Discharges

Electron collision cross sections have been calculated by Hake and Phelps<sup>19</sup> from all available experimental data on electron drift velocity and other transport coefficients. The cross sections for vibrational excitation are much smaller than in  $H_2$  and that process can probably be neglected. Electronic excitation is described by

\* It is Dr. Phelps's view that the high  $E/N$  portion of the enelastic collision frequency and the corresponding cross sections will have to be modified in view of recent work by Fletcher and Haydon, Austral. J. Phys. 19, 615 (1966).

three processes with thresholds at 4.5, 8.0, and 9.7 ev. The latter two are larger than the first, and should lead to dissociation, since the upper states have shallow potential energy minima at larger internuclear distances than the ground state. The combined cross section for the 8.0 and 9.7 ev excitation shows a broad first peak of  $1.1 \times 10^{-16} \text{ cm}^2$  at 12 to 15 ev, then drops slightly and rises again to a second peak in the 50 to 100 ev range. With the assumption of an average electron energy,  $\epsilon_k$ , of 3.0 ev the effective dissociation rate constant,  $k_d$ , is about  $2 \times 10^{-9} \text{ cm}^3 \text{ molecule}^{-1} \text{ sec}^{-1}$ .

The corresponding ionization rate constant,  $k_i$ , was calculated to be  $1.3 \times 10^{-10} \text{ cm}^3 \text{ molecule}^{-1} \text{ sec}^{-1}$ . Fitting the  $\text{O}_2$  data in a similar way to  $\text{H}_2$ , Dr. Phelps obtained  $E/N = 9 \times 10^{-16} \text{ V cm}^2/\text{molecule}$ ,  $\epsilon_k = 3.4 \text{ ev}$ ,  $k_d = 1 \times 10^{-9}$ , and  $k_i = 1 \times 10^{-11} \text{ cm}^3 \text{ molecule}^{-1} \text{ sec}^{-1}$ , in fair agreement with the above except for the smaller  $k_i$ , but  $k_i$  is strongly dependent on  $E/N$  near  $10^{-15} \text{ Vcm}^2/\text{molecule}$ , so that a 20% increase of  $E/N$  would lead to a tenfold increase of  $k_i$ .

An O-atom production rate of about 200 torr/sec by dissociative electron impact is thus indicated, and all other production terms are negligible by comparison. Surface recombination of O-atoms is kinetically similar to that of H-atoms except for a lower diffusion coefficient and molecular velocity by a factor of 3. Thus, the effective first order surface recombination rate constant is  $6 \times 10^4 \gamma \text{ sec}^{-1}$  for small  $\gamma$  and  $5 \times 10^3 \text{ sec}^{-1}$  for  $\gamma$  approaching unity.

In pure  $\text{O}_2$ , as in  $\text{N}_2$ , there is another loss term which does not arise in  $\text{H}_2$ . The polyatomic ions  $\text{O}_3^+$  and  $\text{O}_4^+$  can react exothermically and rapidly via  $\text{O}_4^+ + \text{O} \rightarrow \text{O}_3^+ + \text{O}_2$ ,  $\text{O}_3^+ + \text{O} \rightarrow \text{O}_2^+ + \text{O}_2$  to recombine O-atoms. To obtain an upper limit for this loss rate one may assume that  $\text{O}_4^+$  is a major ion, i.e.  $[\text{O}_4^+] = 10^{11} \text{ cm}^{-3}$ , and that it is therefore regenerated by the bimolecular reaction  $\text{O}_2 + \text{O}_2^+ \rightarrow \text{O}_4^+$ . The latter assumption requires that the lifetime of the unstabilized  $\text{O}_4^+$  collision complex be equal to or longer than the collision time,  $3 \times 10^{-7} \text{ sec}$ , which seems excessively long for such a simple species. At its (unreasonable) maximum estimate, such a chain process may recombine O-atoms at twice the rate of  $\text{O}_4^+ + \text{O} \rightarrow \text{O}_3^+ + \text{O}_2$ , i.e. with an effective first order rate constant of  $200 \text{ sec}^{-1}$  if both ion molecule reactions have rate constants of  $10^{-9} \text{ cm}^3 \text{ molecule}^{-1} \text{ sec}^{-1}$ . Even so, it would not seriously limit O-atom production, since the corresponding  $[\text{O}]_{\text{ss}} = 0.5 \text{ torr} = 50\% \text{ mole fraction}$ . Moreover, Knewstubb, Dawson, and Tickner<sup>20</sup> saw no  $\text{O}_4^+$  in their mass-spectrometric study of dc  $\text{O}_2$  discharges at 0.4 torr, though the weakly bound ion could have dissociated in the large electric field at the sampling orifice as Schmidt<sup>21</sup> suggests for  $\text{N}_4^+$  in his mass-spectrometric study of nitrogen ions. The above mechanism does have the desirable property that it is easily quenched by small amounts of added gases such as  $\text{N}_2$  or  $\text{H}_2$  which are capable of transforming the oxygen ions into more stable ions such as  $\text{NO}^+$  or  $\text{H}_3\text{O}^+$ , but it is unlikely to be important here.

The process  $\text{O}^- + \text{O} \rightarrow \text{O}_2 + e$  is known to be fast ( $k = 1.5 \times 10^{-10}$ ) and it should follow the dissociative attachment step  $e + \text{O}_2 \rightarrow \text{O}^- + \text{O}$  which has a threshold of 4.5 ev and a low maximum near 7 ev. Insofar as  $\text{O}^-$  is formed mainly by this reaction and removed by its reverse, and the concentrations of electrons and ions are very much lower than those of neutral species, these steps leave  $[\text{O}]$  unchanged.

If the above large excitation-dissociation rates are approximately correct, the O-atom yield, as the H-atom yield in the preceding section, is principally controlled by surface recombination in the discharge. The smallest calculated  $[\text{O}]_{\text{ss}} (\gamma = 1)$  is about 0.04 torr, 4% mole fraction, considerably larger than experimental values for pure  $\text{O}_2$ . A possible explanation of this discrepancy may lie in the surface properties immediately downstream from the discharge region. Active discharges have a sharp boundary as shown by their light emission, because electron loss processes are very fast. The corresponding transition of the surface from a region where  $\gamma$  is near unity to one where it is less than  $10^{-4}$  is likely to be more gradual, and would provide a

region in which large, highly localized surface loss terms could quickly reduce the atom concentration.

Experimentally, large catalytic effects by  $N_2$ , NO, or  $H_2$  in the production of O-atoms in microwave discharges have been reported.<sup>22</sup> Very pure oxygen gave only 0.6% atoms (still lower yields of 0.3% were later obtained), but small additions (0.01 to 0.05%) of  $N_2$ ,  $N_2O$ , or NO produced O-atoms at the rate of 40 to 45 per added N, and similar additions of  $H_2$  produced 160 to 200 O-atoms per added  $H_2$ . In terms of the present interpretation, the large catalytic effect may be understandable for  $H_2$  additions as due to  $H_2O$  wall effects, but less so for nitrogen compounds which should not be strongly adsorbed at the surface. Conceivably,  $NO^+$  or  $NO_2^+$ , strong Lewis acids, may be involved in poisoning the surface. Thus, our understanding of  $O_2$  discharges is still in an unsatisfactory state. Further experiments are required in which particular attention should be given to the condition and characterization of the surface as well as to the immediate downstream region.

### III. 4. Nitrogen Discharges.

The great complexity of "active nitrogen" is probably due to its larger cross sections for vibrational excitation and to the existence of metastable electronically excited states below the dissociation limit of ground-state  $N_2$ . Consequently, extensive vibrational excitation persists for times much longer than those spent in the discharge zone, and chemionization is observed in regions such as the "pink glow" well downstream of the discharge. The absence of the lowest triplet state,  $A, {}^3\Sigma_u^+$ , in active nitrogen<sup>23</sup> containing N-atoms indicates that these excited molecules are very efficiently quenched by N, and that vibrationally highly excited ground-state molecules are the principal carriers of excitation to the downstream region. Engelhardt, Phelps, and Risk<sup>24</sup> have determined the relevant elastic and inelastic electron collision cross sections. Some of the electronically excited states above the dissociation limit do not lead to predissociation, and therefore only the state with threshold energy of 14V was used in the estimate of dissociation. Assuming an average electron energy,  $\epsilon_k = 3$  ev, and a maxwellian distribution, one obtains an effective dissociation rate constant,  $k_d$ , of  $3 \times 10^{-10}$  (60 torr/sec) and a corresponding ionization rate constant,  $k_i$ , of  $6 \times 10^{-11}$ . The latter is larger (6 torr/sec) than the corresponding ambipolar diffusion loss term (0.5 to 1 torr/sec). The more realistic calculation by Dr. Phelps which simultaneously fits  $\epsilon_k$ ,  $E/N$ , and the known cross sections to make the ambipolar diffusion loss equal the rate of ionization gave  $\epsilon_k = 2.2$  ev,  $E/N = 1.2 \times 10^{-15}$  V cm<sup>2</sup>/molecule,  $k_d = 3 \times 10^{-11}$  (6 torr/sec), and  $k_i = 3 \times 10^{-12}$ . This dissociation rate is very much lower than that of  $H_2$  or  $O_2$  and properly reflects the difficulty of producing extensive dissociation of  $N_2$  in glow discharges. No other source terms of comparable magnitude are available. The principal loss processes include atom recombination at the surface which can be set equal to those of oxygen, because the molecular velocities are similar. The catalytic atom loss mechanism by  $N_4^+ + N \rightarrow N_3^+ + N_2$ ,  $N_3^+ + N \rightarrow N_2^+ + N_2$ , and  $N_2^+ + N_2 \rightarrow N_4^+$  has been suggested by Young et al.<sup>25</sup> The binding energy of  $N_4^+$  is about 0.5 ev<sup>26</sup>, but its direct, bimolecular formation is reported to be very slow<sup>27</sup>. It must be expected that the association of such a simple complex will not be in its second-order (high pressure) limit at 1 torr pressure, and the catalytic loss process then becomes inoperative, as its rate is limited by a relatively slow three-body reaction. The balance of the main production and loss terms here predicts a minimum  $[N]_{SS}$  of 0.1% when  $\gamma$  is near unity and the recombination in the close post-discharge region is neglected. When  $\gamma$  is sufficiently small to make  $[N]_{SS}$  about 20 to 50 times larger, the corresponding surface recombination rate constant,  $k_s$ , is relatively small (100 sec<sup>-1</sup>) and the half life for attaining steady state may become longer than the residence time so that dissociation becomes source-controlled. This has been observed in recent experiments in our laboratory where two microwave discharges in series in rapidly pumped  $N_2$  at 7 torr produced approximately twice the  $[N]$  of each one operating alone.

Experimentally, there is abundant<sup>22</sup> evidence for "catalytic" effects as summarized by Young et al<sup>28</sup> who studied the effectiveness of O<sub>2</sub>, NO, and SF<sub>6</sub> added either before or immediately after a microwave discharge in highly purified, flowing N<sub>2</sub>. All three gases were "catalytic" when added before, but only NO after the discharge, and SF<sub>6</sub> added before "produced" 230 N-atoms per SF<sub>6</sub> molecule. The ESR method employed may give erroneous results, however.<sup>29</sup> At the present writing, these effects, as the similar ones in H<sub>2</sub> or O<sub>2</sub>, can only be understood in terms of surface effects in the discharge. In addition, long-lived vibrational excitation is probably responsible for downstream "pink glow" chemiionization effects. The electron impact cross sections are largest for the production of ground-state N<sub>2</sub> with relatively little vibrational excitation<sup>29</sup> (V = 1 to 4). If these states are extensively populated, the gas will leave the discharge with vibrational energy corresponding to a temperature of 5,000 to 10,000°K, but in a non-equilibrium distribution, lacking its proper complement of highly energetic molecules. These will be formed by vibration-vibration energy transfer which may be relatively slow at the higher levels where the anharmonicity is large.

#### IV. DISCHARGE CHEMISTRY IN MORE COMPLICATED SYSTEMS.

Although this is the area of greatest interest to most chemists, the necessary fundamental information is mostly lacking. Data on some triatomic molecules such as CO<sub>2</sub><sup>19</sup> and H<sub>2</sub>O<sup>31</sup> have been analyzed. Their active discharges will also contain diatomic molecules such as CO, O<sub>2</sub>, OH, or H<sub>2</sub> as well as the free atoms. This means that reactions between the various neutral species must also be considered. These may be much slower than the electron impact processes and may require long residence times in the discharge to reach their steady state. The approach to full steady state may therefore be characterized by several time constants, very short ones for ionization and direct excitation or dissociation, and various superimposed longer ones due to reactions of neutral species requiring an energy of activation (e.g. hydrogen abstraction from hydrocarbons which often has an E of 7 to 10 kcal/mole).

Glow discharges in water vapor are a good example of the chemical complexity of simple polyatomic systems. Their chemistry was long misrepresented on the assumption that dissociation to H and OH was the principal discharge reaction and that their recombination could be measured downstream. Space-resolved line absorption experiments on OH in a fast-flow steady-state system<sup>32</sup> showed however, that negligible amounts of OH were present a few milliseconds downstream of the discharge, but that a little OH was produced further downstream by slow reactions such as  $H + O_2 + M \rightarrow HO_2 + M$  and  $H + HO_2 \rightarrow 2OH$ . Thus the discharge is an excellent source of H-atoms, but the further excitation-dissociation of OH is apparently so rapid that O-atoms are also formed, and the very fast reaction  $O + OH \rightarrow O_2 + H$  accounts for the major discharge products which are H-atoms and O<sub>2</sub>. When the dissociation of OH in the discharge is insufficient to produce the O-atoms needed in the above reaction, OH may leave the discharge, but will react rapidly by  $2 OH \rightarrow H_2O + O$  and  $OH + O \rightarrow O_2 + H$  for an overall stoichiometry of  $3 OH \rightarrow H_2O + O_2 + H$ . Should OH be extensively dissociated in the discharge as appears to be the case at pressures below 0.1 torr, O-atoms will persist, and the overall discharge products will consist of varying amounts of H, O, and O<sub>2</sub>, with H always in great excess. It is clear from this discussion that the primary electron energy and cross section data obtained from transport properties in pure H<sub>2</sub>O are much less applicable in determining principal discharge products and their yields. The ionization threshold and cross sections in H<sub>2</sub>O are very similar to those in O<sub>2</sub>. The excitation-dissociation cross sections have higher thresholds (12.0 and 12.6 ev), but rise more sharply with increasing electron energy, so that one would expect the primary ionization rate to be equal to that in O<sub>2</sub>, and the primary dissociation rate to be a little lower if  $\epsilon_k$  is comparable. All ions will be extensively hydrated which should increase the rate constants of many bimolecular ion-molecule reactions and make it possible for association reactions to take place by simple two-body processes.

In conclusion, the varied aspects of glow discharge chemistry should be summarized once more. In the case of moderately complex reactants, one should have knowledge of many things in order to progress from a cookbook level to one of (partial)

understanding: (a) Electron impact ionization and dissociation rates of reactants and other major species; (b) Surface recombination rates in the discharge; (c) Ion-molecule reaction rates involving major neutral species; (d) neutral-neutral reaction rates and their temperature dependences in and out of the discharge. Much of the necessary information for (a), (c), and (d) is becoming available for many systems. The role of surface, however, is little understood for electrically neutral reactants, even less so for charged species, and seems to be the present bottleneck.

#### Acknowledgement:

The author would like to thank Dr. A. V. Phelps for many interesting discussions and for calculations of important parameters.

#### References

1. H. S. W. Massey and E. H. S. Burhop, *Electronic and Ionic Impact Phenomena*, Oxford University Press, 1952.
2. E. W. McDanel, *Collision Phenomena in Ionized Gases*, John Wiley and Sons, N.Y. 1964.
3. F. Llewellyn-Jones, *The Glow Discharge*, Methuen and Co., London, 1966.
4. S. C. Brown, *Introduction to Electrical Discharges in Gases*, John Wiley and Sons, N.Y. 1966.
5. L. Goldstein, *Advances in Electronics and Electron Physics*, Vol. 7, 399-503 (1955).
6. S. C. Brown, *Handbuch der Physik*, Vol. 22, 531-575 (1956).
7. M. A. Biondi, *Advances in Electronics*, Vol. 18, Academic Press, Inc., N.Y. 1963, p.67.
8. W. H. Kasner and M. A. Biondi, *Phys. Rev.* 137, A317 (1965).
9. B. H. Mahan and J. C. Person, *J. Chem. Phys.* 40, 392 (1964).
10. T. S. Carlton and B. H. Mahan, *J. Chem. Phys.* 40, 3683 (1964).
11. D. Rapp and D. D. Briglia, *J. Chem. Phys.* 43, 1480 (1965).
12. F. C. Fehsenfeld, E. E. Ferguson, and A. L. Schmeltekopf, *J. Chem. Phys.* 44, 1844 (1966).
13. Y. Tanaka, F. R. Innes, A. S. Jursa, and M. Nakamura, *J. Chem. Phys.* 42, 1183 (1965).
14. A. G. Engelhardt and A. V. Phelps, *Phys. Rev.* 131, 2115 (1963).
15. S. J. B. Corrigan, *J. Chem. Phys.* 43, 4381 (1966).
16. D. J. Rose and S. C. Brown, *Phys. Rev.* 98, 310 (1955).
17. C. C. Goodyear and A. Von Engel, *Proc. Phys. Soc.* 79, 732 (1962)
18. P. R. Rony and D. N. Hanson, *J. Chem. Phys.* 44, 2536 (1966);  
P. R. Rony, Lawrence Radiation Laboratory Report UCRL-16050, April 1965.
19. R. D. Hake, Jr. and A. V. Phelps, Westinghouse Research Laboratories, Paper 66-1E2-Gases-Pl, October 1966.
20. P. F. Knewstubb, P. H. Dawson, and A. W. Tickner, *J. Chem. Phys.* 38, 1031 (1963).
21. M. Schmidt, *Beiträge d. Plasmaphysik* 3, 147 (1966).
22. F. Kaufman and J. R. Kelso, *J. Chem. Phys.* 32, 301 (1960); 8th Internatl. Combustion Symposium, Williams and Wilkins, Baltimore, Md., 1960, p. 230.
23. R. A. Young, *Can. J. Chem.* 44, 1171 (1966).
24. A. G. Engelhardt, A. V. Phelps, and C. G. Risk, *Phys. Rev.* 135, A1566 (1964).
25. R. A. Young, C. R. Gatz and R. L. Sharpless, *J. Phys. Chem.* 69, 1763 (1965).
26. R. N. Varney, *J. Chem. Phys.* 31, 1314 (1958); 33, 1709 (1960).
27. C. F. Giese and W. B. Maier, *J. Chem. Phys.* 35, 1913 (1961).
28. R. A. Young, R. L. Sharpless, and R. Stringham, *J. Chem. Phys.* 40, 117 (1964).
29. C. J. Ultee, *J. Chem. Phys.* 41, 281 (1964).
30. G. J. Schulz, *Phys. Rev.* 135, A988 (1964).
31. A. V. Phelps, private communication.
32. F. P. Del Greco and F. Kaufman, *Faraday Discussion*, 33, 128 (1962).

## Ion-Molecule Reactions in Electric Discharges

J. L. Franklin, P. K. Ghosh and Stanley Studniary

Rice University, Houston, Texas

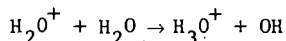
Before the development of good vacuum equipment and techniques, mass spectrometrists observed many ions occurring at masses well above those of the molecules admitted to the instrument. These interfered with the main interests of the experimenters at that time, although in a few instances it was recognized that reactions were occurring between primary ions and molecules. When good vacuum facilities became available in the early 1930s they were adapted to mass spectrometry and for a number of years every effort was made to maintain pressures well below  $10^{-6}$  torr in order to avoid collisions of primary ions with neutrals. However, in 1940, Mann, Hustrulid and Tate (1), in studying water, observed an ion at mass 19, and by vary-

---

(1) Mann, M.M., Hustrulid, A. and Tate, J. T., Phys. Rev., 58, 340 (1940)

---

ing the pressure in their instrument, concluded that it was  $H_3O^+$ , probably formed by the reaction:



During the middle 50s, several groups of mass spectrometrists became curious as to the results that would be observed if source pressures were raised sufficiently to allow a few collisions to occur between ions and molecules. Several ions occurring at masses above those of the parent ion were observed. Because of this, a number of systematic studies were made and increasing interest and emphasis on reactions of ions with neutral molecules has developed, until at present some 50 to 100 papers per year are published on this subject alone.

Perhaps one of the strongest reasons for the interest in ion-molecule reactions is the fact that ions of unusual and unsuspected composition were observed. Most fascinating of these has been  $CH_5^+$ , which was completely unexpected, but which, nevertheless, is now well established as a stable ion. This ion was first announced by Tal'roze and Lyumbimova (2), but it was also reported shortly after the Russians

---

(2) Tal'roze, V. L. and Lyumbimova, A. K., Dokl. Akad. Nauk SSSR, 86, 909 (1952)

---

by several groups in this country (3,4,5,9). Studies of secondary ions from a large number of molecules followed.

---

(3) Field, F. H., Franklin, J. L. and Lampe, F. W., J. Amer. Chem. Soc., 79, 2419 (1957)

(4) Stevenson, D. P. and Schissler, D. O., J. Chem. Phys., 23, 1353 (1955)

(9) Schissler, D. O. and Stevenson, D. P., J. Chem. Phys., 24, 926 (1956)

(5) Meisels, G. G., Hamill, W. H. and Williams, R. R., Jr., J. Chem. Phys., 25, 790 (1956)

---

The earlier studies of secondary ions were largely limited to ions of masses greater than that of the parent ion, but subsequent studies have shown that many secondaries of lower mass also occur. In most instances, the fact that the ion resulted from collision rather than from impurities was demonstrated by varying the pressure in the ion source. If the ion intensity increased as a second power of the pressure, the ion clearly resulted from a collision.

Having established that an ion was indeed the result of a collision, it was obviously of interest to ascertain the primary ion precursor of the secondary ion. Two methods have usually been used for this purpose. The method most often used was to measure the appearance potential of the secondary ion and compare it to appearance potentials of various primary ions occurring in the system in question.

Obviously, the secondary ion must have the same appearance potential as its precursor, and where reasonable agreement of primary and secondary ion appearance potentials was found the identities of reactant and product were established. In some instances, it has been possible to reduce the electron energy to the point where only one or two primary ions were present. Under these conditions, it is often possible by comparing intensities of secondary ions with the disappearance of primaries to identify unequivocally the precursors of the various secondaries. Obviously, both of these techniques suffer from certain difficulties. Where the primary ion spectrum is sufficiently complicated, or where the appearance potentials of several primary ions are sufficiently close together, it is very difficult and often impossible to determine the precursor of a secondary ion satisfactorily. Further, comparison of primary and secondary appearance potentials usually serves to identify only the precursor of lowest appearance potential. Possible precursors of higher appearance potential are obscured and can only be detected by other means. Of course, it is also true that one cannot always simplify the primary spectrum sufficiently by reducing the electron energy to permit satisfactory identification of the precursor. As a result, in recent years a few mass spectrometrists following Lindholm (6) have employed a primary mass sorter to select the primary ion which is then injected into the gas

---

(6) For a survey of Lindholm's work see E. Lindholm, "Ion-Molecule Reactions in the Gas Phase," Advances in Chemistry Series 58, American Chemical Society, Washington, D. C., 1966, pl.

---

with which reaction is desired.

Mass spectrometer ion sources are quite small chemical reactors. It can easily be shown that the reaction time of an ion in the source will normally be in the order of a microsecond, and unless the pressure in the source is well over 100 torr only a small fraction of the ions can undergo collision. It early became apparent that where secondary ions were observed they must, in most instances, have resulted at almost every collision of ion and neutral. Further, in many instances, the heats of formation of ions and neutrals were well established, and in all such instances it was possible to show that the reactions were exothermic. Indeed, it would be impossible under most circumstances to observe a reaction to form secondary ions if the reaction were endothermic. Such endothermicity would appear as activation energy, which would greatly reduce the probability of reaction when the ion and molecule collide. (Later on we mention certain conditions in which this rule is violated, but under most circumstances it holds rigorously.) This rule is so seldom violated that it can be used as a means of helping to eliminate possible precursors of a secondary ion.

It was mentioned above that the secondary ions first observed occurred at masses above those of the parent. However, there was always an expectation that ions of lower mass might also be formed in collision reactions and as the pressure that could be tolerated in the ion source was increased it became apparent that such was indeed the case. For example, it was observed by Munson, Franklin and Field (7)

---

(7) M.S.B. Munson, J. L. Franklin and F. H. Field, J. Phys. Chem. **68**, 3098 (1964)

---

that the  $C_2H_5^+$  ion from ethane and the  $C_3H_7^+$  ion from propane, both present in the primary spectrum, increased with increasing pressure and indeed, in the case of propane the  $C_3H_7^+$  ion increased from a very small proportion of the primary spectrum until it represented some 70% of all the ions present. Many secondary ions of mass less than the parent did not show such spectacular increases and other techniques were sought to establish these. One method of especial interest was that due to Cermak. (8). He employed electrons having energies too small to ionize in the

---

(8) V. Cermak and Z. Herman, Collection Czechoslov. Chem. Commun. **27**, 406 (1962)

---

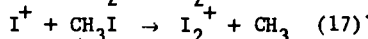
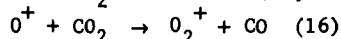
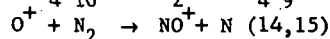
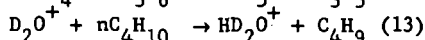
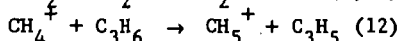
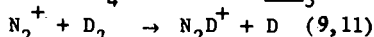
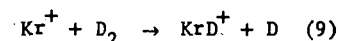
ionization chamber. However, he employed a relatively high variable potential between the ion chamber and the trap anode, so that the electrons were accelerated

in the anode region. Some of these ionized molecules present in that region and the ions were repelled by the potential on the anode and drifted back into the ionization chamber. These primary ions could not be themselves collected, but new secondary ions could be unequivocally identified. Further, by varying the potential on the anode, it was possible to obtain an appearance potential for the secondary ions and from this to deduce the identity of its precursor.

A large number of reactions of ions with neutrals have now been identified and typical examples of the various classes of such bimolecular reactions are given in tables 1 through 7.

Table 1

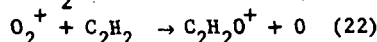
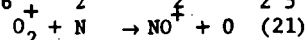
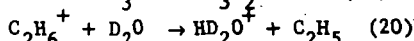
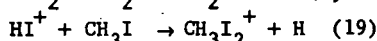
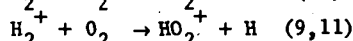
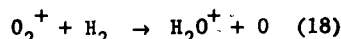
## Atom Transfer Reactions



- 
- (9) Schissler, D. O. and Stevenson, D. P., J. Chem. Phys., 24, 926 (1956)  
 (10) Field, F. H., Franklin, J. L., J. Am. Chem. Soc., 83, 4509 (1961)  
 (11) Stevenson, D. P., J. Phys. Chem., 61, 1453 (1957)  
 (12) Frankevich, E. L. and Tal'roze, V. L., Dokl. Akad. Nauk SSSR 119, 1174 (1958)  
 (13) Lampe, F. W., Field, F. H. and Franklin, J. L., J. Amer. Chem. Soc., 79, 6132 (1957)  
 (14) Potter, R. F., J. Chem. Phys., 23, 2462 (1955)  
 (15) Fehsenfeld, F. C., Schmeltekopf, A. L. and Ferguson, E. E., Planet. Space Science 13, 219 (1965)  
 (16) Fehsenfeld, F. C., Ferguson, E. E. and Schmeltekopf, A. L., J. Chem. Phys., 44, 3022 (1966)  
 (17) Pottie, R. F., Barker, R. and Hamill, W. H., Radiation Research 10, 664 (1940)
- 

Table 2

## Positive Atomic Ion Transfer Reactions

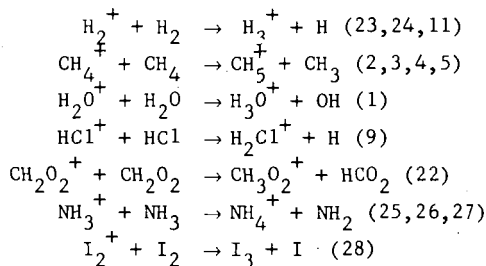


- 
- (18) Hutchinson, D. A., Paper presented at American Chemical Society Meeting, Minneapolis, Minnesota, September, 1955  
 (19) Pottie, R. F., Barker, R. and Hamill, W. H., Radiation Research 10, 664 (1959)  
 (20) Lampe, F. W., Field, F. H. and Franklin, J. L., J. Amer. Chem. Soc., 79, 6132 (1957)  
 (21) Goldan, P. D., Schmeltekopf, A. L., Fehsenfeld, F. C., Schiff, H. I., and Ferguson, E. E., J. Chem. Phys., 44, 4095 (1966)

- (22) Franklin, J. L., Munson, M.S.B., Tenth Symposium (International) on Combustion, The Combustion Institute, 1965, p. 561

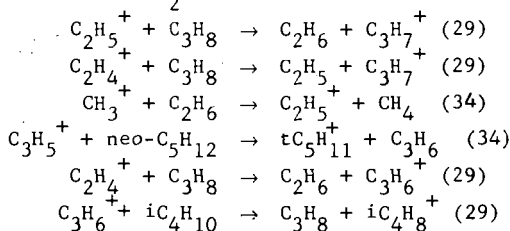
Table 3

## Symmetrical Transfer Reactions



- (23) Eyring, H., Hirschfelder, J. O. and Taylor, H. S., J. Chem. Phys. **4**, 479 (1936)  
 (24) Stevenson, D. P. and Schissler, D. O., J. Chem. Phys. **23**, 1353 (1955)  
 (25) Lampe, F. W. and Field, F. H., Tetrahedron **7**, 189 (1959)  
 (26) Dorfman, L. M. and Noble, P. C., J. Phys. Chem. **63**, 980 (1959)  
 (27) Derwish, G. A. W., Galli, A., Giardini-Guidoni, A., and Volpi, G. G., J. Chem. Phys. **39**, 1599 (1963)  
 (28) Hogness, T. R. and Harkness, R. W., Phys. Rev. **32**, 784 (1928)

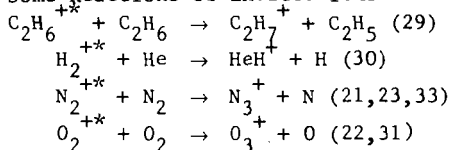
Table 4

H<sup>-</sup> and H<sub>2</sub><sup>-</sup> Transfer Reactions

- (29) M.S.B. Munson, J. L. Franklin and F. H. Field, J. Phys. Chem. **68**, 3098 (1964)

Table 5

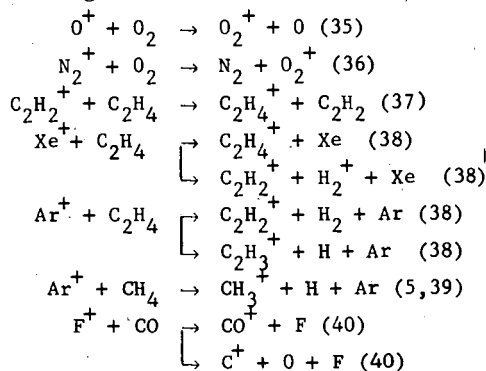
## Some Reactions of Excited Ions



- (30) H. von Koch and L. Friedman, J. Chem. Phys. **38**, 115 (1963)  
 (31) R. K. Curran, J. Chem. Phys. **38**, 2974 (1963)  
 (32) M.S.B. Munson, F. H. Field and J. L. Franklin, J. Chem. Phys. **37**, 1790 (1962)  
 (33) M. Saporoschenko, Phys. Rev. **111**, 1550 (1958)  
 (34) Field, F. H. and Lampe, F. W., J. Amer. Chem. Soc., **80**, 5587 (1958)

Table 6

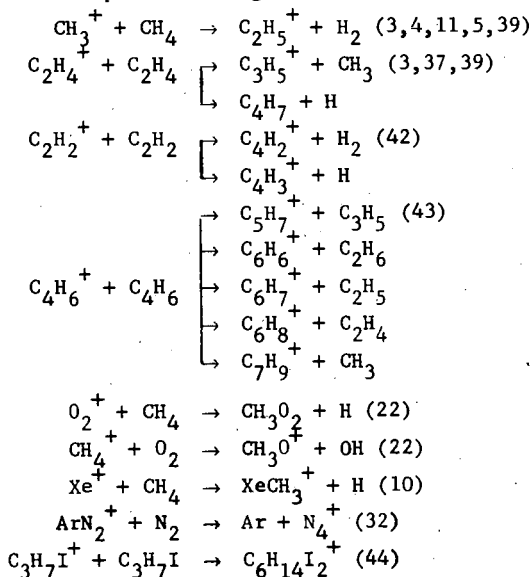
## Charge Transfer Reactions



- (35) F. C. Fehsenfeld, P. D. Goldan, A. L. Schmeltekopf and E. E. Ferguson, Planet. Space Sci. **13**, 579 (1965)
- (36) F. C. Fehsenfeld, A. L. Schmeltekopf and E. E. Ferguson, Planet. Space Sci. **13**, 919 (1965)
- (37) F. H. Field, J. Am. Chem. Soc. **83**, 1523 (1961)
- (38) J. L. Franklin and F. H. Field, J. Am. Chem. Soc. **83**, 3555 (1961)
- (39) G. G. Meisels, W. H. Hamill and R. R. Williams, Jr., J. Phys. Chem. **61**, 1456 (1957)
- (40) E. Lindholm, Arkiv Fysik **8**, 433 (1954)

Table 7

## Complex Rearrangements



- (44) Pottie, R. F. and Hamill, W. H., J. Phys. Chem. **63**, 877 (1959)
- (42) Field, F. H., Franklin, J. L. and Lampe, F. W., J. Amer. Chem. Soc., **79**, 2665
- (43) Barker, R., Williams, R. R., Jr. and Hamill, W. H., presented at meeting of ASTM Committee E-14 on Mass Spectrometry, New Orleans, Louisiana, June 2-6, 1959

Tables 1-6 present examples of relatively simple reactions. However, reactions involving quite profound changes in structure and bond reorganizations have been observed by a number of investigators. Table 7 shows several of these, which are given as typical examples. Certain of the reactions shown result in more than one set of products, all of which apparently occur at the same appearance potential and thus involve the same precursor. Of course, the intensities of the product ions will, in most instances, not be the same. One would expect that reactions of this kind would involve the formation of a relatively stable complex, which breaks up in ways dictated by the energy content of the complex. Unfortunately, no quantitative treatment of the break up of the complex has yet been published, so it is not now possible to predict the ratios of product ions where more than one product arises from a single reactant. It has, however, been observed by Lampe, et al. (41) that the ratios of secondary ions from a collision complex will often be very similar to those of the same fragment ions in the primary mass spectrum of a compound having the same composition as the complex. Thus, they pointed out that the ratio of  $C_3H_5^+$ / $C_2H_7^+$  in the reaction of  $C_2H_4$  with  $C_2H_4$  was about the same as that observed in the mass spectra of the butenes. The literature contains

---

(41) F. W. Lampe, J. L. Franklin and F. H. Field, "Progress in Reaction Kinetics," Vol. 1, Pergamon Press, New York, 1961, p. 69.

---

only a few examples of simple condensation reactions. This is not surprising in view of the fact that every complex is formed with enough energy to break up in either the forward or reverse direction. Since most complexes can break up very rapidly they will generally do so in a time short compared to that required to collect the ion. In a few instances such complexes have been observed to survive long enough to be measured. One example of this is given in Table 7. It might be mentioned that several apparently long lived complexes were observed by Field (37) in his study of ethylene, but these in all cases turned out to depend upon the third or higher power of the pressure, and thus were in fact complexes that had been stabilized by collision or had resulted from the decomposition of a complex of higher molecular weight.

Although the preceding discussion has largely been devoted to ions formed as bimolecular reaction products, in the last few years, many examples of ions formed with much higher pressure dependence have been observed. One of the earliest studies carried out at such elevated pressures, i.e., above 100 microns, was the study of Field (37) of ion-molecule reactions in ethylene. In this study he observed ions with pressure dependencies as high as about 6, although those exhibiting the highest pressure dependence were of such low intensity that the nature of the reactions involved could not be ascertained. Indeed, above about 3rd order the method of appearance potentials becomes completely useless, and the identification of precursors to a given product becomes very tenuous indeed. To form ions at high pressures in a region from which they can be collected it is usually necessary to employ electrons of several hundred volts rather than the usual 60-70 volts employed in most mass spectrometric problems. Indeed, because of this problem, Kebarle and Hogg (45) have employed alpha particles of high energy to provide primary ions.

---

(45) P. Kebarle and A. M. Hogg, *J. Chem. Phys.* 42, 668 (1965); 43, 449 (1965)

---

When ions are formed by high energy massive particles it is possible to operate at much higher pressures and Kebarle (45), Wexler et al. (46) and others have

---

(46) S. Wexler, Assa Lifshitz and A. Guattrochi, "Ion-Molecule Reactions in the Gas Phase," *Adv. in Chem. Series*, Amer. Chem. Soc., Washington, D. C. 1966 p. 193

---

studied the ions formed at pressures up to about one atmosphere. Naturally, they have observed ions with a very high pressure dependence, although they have not been able to establish the order of reaction. With such a system, Kebarle et al. (49,50)

have observed ions having the general formula,  $H^+(H_2O)_n$ , with  $n$  varying from 1 to 7, and Wexler, et al. (46) have observed polymer ions from acetylene having up to 12 carbon atoms.

Recently, studies have been carried out in mass spectrometry sources at pressures up to several torr. Under these conditions, any primary ions formed will undergo many collisions and will have ample opportunity to react if they are capable of doing so. Field and Munson (47,48) have taken advantage of this to carry out some very interesting studies of reactions of higher order. They observed that in very pure methane, the principal secondary ions  $CH_5^+$  and  $C_2H_5^+$  reached a plateau and re-

(47) M.S.B. Munson and F. H. Field, J. Am. Chem. Soc. 88, 2621 (1966)

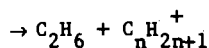
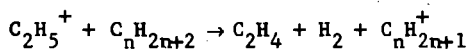
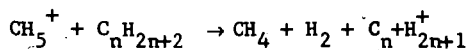
(48) F. K. Field, M. S. B. Munson and D. A. Becker, "Ion Molecule Reactions in the Gas Phase," Adv. in Chem. Series, Amer. Chem. Soc., Washington, D. C. (1966), p. 167

(49) P. Kebarle and A. M. Hogg, J. Chem. Phys. 42, 798 (1965)

(50) A. M. Hogg and P. Kebarle, J. Chem. Phys. 43, 498 (1965)

mained constant with increases in pressure beyond about 0.5 torr. They observed also that if there were any small amount of impurities in the methane the intensities of these ions passed through a maximum around a few .10ths torr and then declined steadily with further increases in pressure. The primary ions had very small probability of colliding with anything but methane and consequently the disappearance of the secondaries must be due to their reaction with the impurities, since it is demonstrated that they did not react with methane itself. It was a simple step from this to the addition of small amounts of a variety of materials to the methane plasma, with results that proved extremely interesting. When, for example, small amounts of long chain paraffin hydrocarbons, such as dodecane, were added to the methane plasma, the spectrum of ions from the high molecular weight paraffin was quite different from that obtained by electron impact. Such high molecular weight paraffins give only small intensities of ions above about the  $C_5$  range under electron impact. However, in the methane plasma, ions of the general composition  $C_nH_{2n+1}^+$  formed at each carbon number from the parent down to  $C_4$ . No doubt ions of smaller mass are also formed, but these are not observable because of the interference from secondary and ternary ions from methane. Further, the largest of these ions is the one corresponding to the parent molecules; i.e., with dodecane,  $C_{12}H_{25}^+$ .

Field and Munson have studied a number of compounds by this method, and in many instances have obtained profound changes in the mass spectrum, produced by "Chemical Ionization," the term which they have given the processes. (47,48) They have concluded that in the case of the methane the principal reactions are probably as follows:



Although the previous discussion has been devoted entirely to reactions of positive ions, negative ions are also known to undergo reactions on collision. Relatively few of these reactions have been studied, however, largely because negative ions present some rather serious difficulties to the investigator. Some reactions of negative ions, however, have been carried out by Melton, Henglein and others, and several typical reactions are given in table 9.

Table 8

Some Ions Formed by Processes of Order Higher than 2

Reactant	Ionic Product	Reference
H <sub>2</sub> O	H <sup>+</sup> (H <sub>2</sub> O) <sub>n</sub> (1 < n < 8)	(49)
NH <sub>3</sub>	H <sup>+</sup> (NH <sub>3</sub> ) <sub>n</sub> (1 < n < 5)	(50)
CH <sub>4</sub>	C <sub>3</sub> H <sub>5</sub> <sup>+</sup> , C <sub>3</sub> H <sub>7</sub> <sup>+</sup>	(51)
C <sub>2</sub> H <sub>4</sub>	C <sub>4</sub> H <sub>8</sub> <sup>+</sup> , C <sub>4</sub> H <sub>6</sub> <sup>+</sup>	(37)

(51) F. H. Field, J. L. Franklin and M.S.B. Munson, J. Am. Chem. Soc. 85, 3575 (1963)

Table 9

Negative Ion-Molecule Reactions

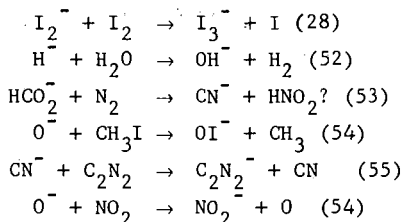
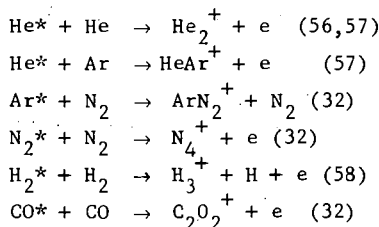
(52) E. E. Muschlitz, J. Appl. Phys. 28, 1414 (1957)(53) C. E. Melton and G. A. Ropp, J. Am. Chem. Soc. 80, 5573 (1958)(54) A. Henglein and G. A. Muccini, J. Chem. Phys. 31, 1426 (1959)(55) C. E. Melton and P. S. Rudolph, J. Chem. Phys. 33, 1594 (1960)

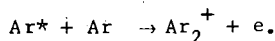
Table 10

Chemi-Ionization

(56) J. A. Hornbeck and J. P. Molnar, Phys. Rev. 84, 621 (1951)(57) M.S.B. Munson, J. L. Franklin and F. H. Field, J. Phys. Chem. 67, 1541 (1963)

(58) D. J. Keenan and E. M. Clarke, Fourteenth Annual Conference on Mass Spectrometry, Dallas, Texas, May 22-27, 1966, p. 42

Somewhat akin to ion-molecule reactions is a process first identified by Hornbeck and Molnar (56) for the formation of the rare gas diatomic ions. Hornbeck and Molnar observed diatomic ions of all the rare gases when the pressure in the ion source of their mass spectrometer was raised sufficiently. The appearance potentials of the diatomics proved to be 0.7 to 1.5 eV below the ionization potentials of the corresponding atom, and hence the diatomic ions were not derived from atomic ions. As a consequence, they proposed that excited atoms formed by electron impact reacted upon collision with a neutral atom to form a molecular ion and eject an electron, thus:



A number of investigators have subsequently studied this chemi-ionization reaction of the rare gas ions and have confirmed and extended Hornbeck and Molnar's observation. It has now been observed that all of the rare gases react with each other to form the hetero-nuclear diatomic ions (57). In addition, a number of ionic compounds of the rare gases with nitrogen, CO, O<sub>2</sub>, methane, acetylene and others have been reported. Chemi-ionization reactions are not necessarily limited to rare gases, however. Chemi-ionization products of excited mercury atoms with a number of compounds have been observed (59) and nitrogen and CO are known to undergo chemi-ionization with their own ground state species, forming respectively N<sub>4</sub><sup>+</sup> and C<sub>2</sub>O<sub>2</sub><sup>+</sup> (32).

(59) P. Cermak and Z. Herman, Tenth Annual Conference on Mass Spectrometry, New Orleans, La., 1962, p. 358.

It is natural that when both reactants and products are readily measurable consideration should early be given to the rate of the reaction. With the reaction  $A^+ + M \rightarrow B^+ + S$ , if M is much larger than A<sup>+</sup>, the reaction rate is pseudo first order and the equation expressing the concentration of A<sup>+</sup> and B<sup>+</sup> is as follows:

$$\frac{A^+}{A_0^+} = e^{-kMt} \quad (1)$$

$$\frac{B^+}{A_0^+} = 1 - e^{-kMt} \quad (2)$$

At relatively low pressures, (a few microns),

$$\frac{B^+}{A^+ + B^+} = kMt \quad (3)$$

A plot of  $\frac{B^+}{A^+ + B^+}$  against  $M^{-1}$  will yield a straight line whose slope is  $kt$ . If a continuous ion withdrawal is employed, the retention time in the source will be the time required for the primary ion to drift from the point of formation in the electron beam to the exit slit under the influence of the repeller potential. The time is thus:

$$\left( \frac{2md}{eE} \right)^{1/2}$$

where E is the field strength, m is the mass of the ion, and d the distance from the center of the electron beam to the ion exit slit. With the slope known, k can be calculated and a large number of rate constants have been determined in this way.

Lampe, Franklin and Field (41) discussed this problem of rates of ion molecule reactions at some length, and surveyed the known data at that time. A few typical rate constants for second order ion-molecule reactions are given in table 11. It will be observed that many of them are in the order of 10<sup>-9</sup> cc/molecule/sec. However, values as small as 10<sup>-13</sup> cc/molecule/sec have been reported for some reactions. The values in the neighborhood of 10<sup>-9</sup> cc/molecule/sec represent reactions that must occur at essentially every collision in that they have cross sections considerably larger than ordinary collision cross sections. The values around 10<sup>-13</sup> represent about the limit at which secondary ions can be measured with sufficient confidence to justify calculation. It is obvious that reactions of this kind occurring at relatively low pressures and in times of the order of a micro-second must be very fast reactions, and in fact, so fast that the activation energy must be either 0 or very small. As was mentioned before, ion-molecule reactions to be observable must not involve appreciable energy of activation. Stevenson and Schissler (4,11) have confirmed this experimentally for a few reactions and the very fact that a reaction is observed precludes this possibility. It should be mentioned, however, that certain endo-thermic reactions can be forced to take place if the relative

velocity of the reacting partners is sufficiently great. Giese and Maier (60) have shown that for the reaction  $\text{Ar}^+ + \text{CO} \rightarrow \text{Ar} + \text{C}^+ + \text{O}$ , which is endothermic by 6.62 eV for the  $2P_{3/2}$  state and 6.44 eV for the  $2P_{1/2}$  state of  $\text{Ar}^+$ , the threshold for the appearance of  $\text{C}^+$  is:

$$\frac{6.44 \times (M_{\text{Ar}^+} + M_{\text{CO}})}{M_{\text{CO}}} \text{ or } 15.65 \text{ eV.}$$

Their measured values were in agreement with this relation.

(60) C. F. Giese and W. B. Maier, *J. Chem. Phys.* 39, 197 (1963)

Table II  
Some Second-Order Rate Constants

Reaction	$10^{10} k$ , cc/molecule sec	Reference
$\text{D}_2^+ + \text{D}_2 \rightarrow \text{D}_3 + \text{D}$	14.5	4,11
$\text{CH}_4^+ + \text{CH}_4 \rightarrow \text{CH}_5^+ + \text{CH}_3$	10	61,62,63
$\text{H}_2\text{O} + \text{H}_2\text{O} \rightarrow \text{H}_3\text{O}^+ + \text{OH}$	12.7	1,2,13
$\text{C}_2\text{H}_3^+ + \text{C}_2\text{H}_6 \rightarrow \text{C}_3\text{H}_5^+ + \text{CH}_4$	14.5	9
$\text{O}_2^+ + \text{CH}_4 \rightarrow \text{CH}_3\text{O}_2^+ + \text{H}$	0.126	22
$\text{CH}_4^+ + \text{O}_2 \rightarrow \text{CH}_3\text{O}^+ + \text{OH}$	0.257	22

(61) V. L. Tal'roze and E. L. Frankevich, *J. Phys. Chem. USSR* 34, 1275 (1960)

(62) C. W. Hand and H. von Weissenhoff, *Can. J. Chem.*, 42, 195, 2385 (1964)

(63) J. L. Franklin, Y. Wada, P. Natalis and P. M. Hierl, *J. Phys. Chem.* 70, 2353 (1966)

All reaction rate studies have not been limited to extremely low pressures. When the pressure in the ion source becomes sufficiently great the reactions follow the pseudo first order rate laws over rather wide ranges of pressure, unless subsequent reactions interfere. Thus, Field et al. (51) found the disappearance of  $\text{CH}_4^+$  in methane to obey first law kinetics over a pressure range of about 0.1 to 400 Torr. However, as the pressure is raised, in certain systems, reactions of a higher order do occur. Field, (37) studying ethylene, has reported some reactions having apparent orders as high as about 6. These, of course, are not truly 6th order reactions, but simply represent a succession of perhaps five secondary reactions which show dependence upon the 6th power of the pressure. Rates of reactions of such high order do not yield satisfactory rate constants, but it has been possible to determine rate constants for reactions of 3rd order, and Field and several others have made approximate measurements of the rate constants for such third order processes. As is the case with the second order processes, these reaction rates are relatively high. For example, in ethylene, Field determined several third order rate constants to be in the order of  $10^{-27}$  cc molecule<sup>-2</sup> sec<sup>-1</sup>.

Although most of the measurements of rate constants in the literature were obtained with the source operating in a continuous mode employing a variation in pressure to establish the rate, some studies have been made in which retention time in the source was varied. Such measurements were originally made by Tal'roze and Frankevitch (61), but subsequent measurements have been made by Hand and von Weissenhoff (62) and Franklin, Natalis, Wada, and Hierl (63). In order to obtain a satisfactory variation of time, a pulsed mode is employed. In such an operation a pulse of electrons is fired through the gas. After it is stopped, the resulting ions can be retained in the source for a controlled period of time and then rapidly extracted by a pulse of high energy. By varying the delay time, the time of retention in the source is varied, and rate constants determined in the manner more usually employed by chemists in rate studies. Results obtained in this way generally agree

rather well with those obtained by the pressure method, although some differences have been observed. One difference that may be of significance is that the ions in the pulsed mode will generally have approximately thermal energies, whereas those reacting in the continuous mode will have variable energies, depending upon the point of their reaction in travelling from the electron beam to the exit slit.

The question of the effect of ionic energy on reaction rate has been one of considerable interest and the subject of a number of investigations, both theoretical and experimental. In their early work on ion-molecule reactions, Franklin, Field and Lampe (3) observed that when they varied the field strength in the ion source in order to vary the retention time, the rate constants that they calculated for their ion-molecule reactions varied considerably. In general, they seemed to drop as the field strength increased, suggesting that the reaction rate constant decreased with the relative velocity of ions and neutrals. Other investigators have made similar observations. However, it appears that not all reactions show such reduction in rate constants with increasing relative velocity. Attempts to explain this have been made by a number of investigators. Field, Franklin and Lampe (3) attempted to obtain the theoretical relations based upon a balance of polarization and centrifugal forces. Gioumouisis and Stevenson (64) derived a more precise expression

(64) Gioumouisis, G. and Stevenson, D. P., J. Chem. Phys., 29, 294 (1958)

(65) P. Langevin, Ann. Chim. Phys. 5, 245 (1905)

for the collision rate based upon Langevin's (65) treatment for polarizable systems. Gioumouisis and Stevenson found the collision cross section to be:

$$\sigma = \frac{2e\pi}{v_i} \left(\frac{\alpha}{\mu}\right)^{1/2} \quad (4)$$

where  $\alpha$  is the polarizability of the neutral,  $v_i$  is the velocity of the ion,  $\mu$  is the reduced mass and  $e$  the charge on the electron. Since

$$v_i = \left(\frac{2E}{m_i}\right)^{1/2}$$

$\sigma$  will vary as  $E^{-1/2}$ . Further, since  $k = \sigma v$

$$k = 2e\pi \left(\frac{\alpha}{\mu}\right)^{1/2} \quad (5)$$

and thus is independent of velocity or energy. This, unfortunately, did not agree with the observed rate behavior of a number of reactions, although it appears to hold for some. In fact, Field, et al. (3) studied the effect of field strength upon rate constant and found that for several reactions  $k$  decreased with increasing field strength. Hamill and his associates (66,67) have shown that ion-molecule reactions cannot be accurately treated as involving point particles. By considering the de-

(66) N. Boelrijk and W. H. Hamill, J. Am. Chem. Soc. 84, 730, (1962)

(67) D. A. Kubose and W. H. Hamill, J. Am. Chem. Soc. 85, 125 (1963)

formable neutral to exhibit a hard core to high energy collisions while being deformable in low energy collisions, these workers showed that for small ion energies  $\sigma$  obeyed the Gioumouisis-Stevenson relation (equation 5), but for large energy  $\sigma \propto E^{-1}$  which agrees with experimental results. Theard and Hamill (68) and Moran and Hamill (69) have extended their treatment to ion-molecule reactions involving

(68) L. P. Theard and W. H. Hamill, J. Am. Chem. Soc. 84, 1134 (1962)

(69) T. F. Moran and W. H. Hamill, J. Chem. Phys. 39, 1413 (1963)

neutrals with permanent dipoles. They showed that at low relative velocities a cross section for the ion-permanent dipole interaction,

$$\sigma_D = \frac{\pi e \mu}{E_t}$$

must be added to the Langevin cross section. Here  $\mu$  is dipole moment and  $E_t$  is the translational energy of the reacting system in center of mass coordinates.

No attempt will be made here to review all of the studies of the effect of energy upon the rates of ion-molecule reactions. However, several investigators who have made especially important contributions should be mentioned. In addition to the work of Hamill discussed above, important studies have been made by Futrell and Abramson (70), Giese and Maier (71), Friedman (72,73) and Light and Horrocks(74).

- 
- (70) J. H. Futrell and F. P. Abramson, "Ion-Molecule Reactions in the Gas Phase," Adv. in Chem. Series 58, Amer. Chem. Soc., 1966, p. 107.  
 (71) C. F. Giese and W. B. Maier, J. Chem. Phys. 39, 197, 739 (1963)  
 (72) T. F. Moran and L. Friedman, J. Chem. Phys. 39, 2491 (1963); 42, 2391 (1965)  
 (73) F. S. Klein and L. Friedman, J. Chem. Phys. 41, 1789 (1964)  
 (74) J. C. Light and J. Horrocks, Proc. Phys. Soc. 84, 527 (1964)
- 

It should be pointed out that if the relative velocities of ions and neutrals become sufficiently high other reactions begin to occur as a result of the different forces coming into play. Thus a fast moving ion passing a molecule with sufficient velocity may simply strip off a peripheral atom, leaving the partially denuded entity behind. Such stripping reactions have been studied by Henglein (75) and Koski (76), who found that they obey quite different rules from those above. It thus

- 
- (75) A. Henglein, "Ion Molecule Reactions in the Gas Phase," Adv. in Chem. Series 58, Amer. Chem. Soc., Washington, D. C., p. 63  
 (76) M. A. Berta, B. Y. Ellis and W. S. Koski, *ibid.*, p. 80
- 

appears that a complete theory of the rates of ion-molecule reactions has not been developed, but there is little doubt that to a first approximation the equation of Gioumousis and Stevenson gives fairly good results. It is also true that the reactions tend to be quite fast, and this becomes a matter of overriding importance in many processes involving ions. Thus it has been shown by Lampe (77,78) and by Futrell (79) that ion-molecule reactions are the controlling factor in certain

- 
- (77) F. W. Lampe, Radiation Research 10, 671 (1959)  
 (78) F. W. Lampe, J. Am. Chem. Soc., 82, 1551 (1960)  
 (79) J. H. Futrell, J. Am. Chem. Soc. 81, 5921 (1959)
- 

radiation induced processes involving paraffin and olefin hydrocarbons.

An electric discharge of course involves ions and electrons and the ions present can be sampled and analyzed by mass spectrometry. Such studies have been undertaken by a number of investigators and some progress is being made toward understanding the chemical behavior of ions in various discharges. The problem is complicated by the fact that there are several kinds of electric discharge, each of which has its own physical and chemical characteristics. Of these, the type most often studied is the direct current glow discharge, but corona and high frequency and micro-wave discharges have also received some attention.

In order to analyze the ionic content of a discharge it is necessary to transfer the ions from the discharge into the mass analyzer. While this is not a particularly serious problem at pressures below 10 microns, the difficulty becomes more acute as the pressure increases. This is attributable to the fact that electrons and ions diffuse to the walls at different rates, so that an electric gradient is established which alters the distribution of energy of the various charged species. Ordinarily a sheath of ions is formed at any surface, including that of a sampling probe and ions or electrons must have, or be given enough energy to pass through this sheath in order to be sampled. However, if the energy is sufficiently high some ions may be decomposed by collision. The result then is that there is often

considerable uncertainty as to the quantitative correspondence of the ion distribution reported by the mass spectrometer with the actual distribution in the discharge. Further, while there is little doubt that the ions observed were actually present, there is always some question as to the presence of ions that might be expected, but that are not observed.

An added complication that must be taken into account, especially in glow discharges, is that different portions of the discharge have different characteristics. Thus the negative glow and positive column have quite different electric fields, the ions and electrons present have different energies and the distribution of ions in the two regions is different.

In spite of these reservations, considerable information has been obtained concerning the ions present in certain discharges and some understanding of the reactions occurring is beginning to develop.

In the glow discharge, the regions most studied have been the negative glow and the positive column. Both are regions of nearly equal positive and negative ion concentration, although the ion concentration in the negative glow is usually greater (often 10-100 times) than that in the positive column. Further, the electric field in the negative glow is considerably greater than that of the positive column, through which the ions drift with relatively small energies.

Discharges in the rare gases, of course, always contain atomic ions and, at sufficiently high pressures, diatomic ions as well. This latter can be produced by two possible reactions, typified by helium:



Since the formation of  $\text{He}^*$  is an excitation process it will occur over a relatively small energy range with electrons of energy close to the ionization potential of He. Thus, it would be expected to predominate in the positive column of a glow discharge. This has been observed by Morris (80) and by Pahl (81,82).

---

(80) D. Morris, Proc. Phys. Soc. (London) A68, 11 (1955)

(81) M. Pahl and U. Weimer, Z. Naturforsch 13a, 753 (1958)

(82) M. Pahl, Z. Naturforsch, 14a, 239 (1959)

---

In order for reaction 7 to be observed relatively high pressures are required. The third order rate constant will probably not exceed  $10^{-30}$  cc<sup>2</sup>/molecule<sup>2</sup> second and the time of the ion in the plasma will probably not exceed  $10^{-9}$  seconds. Thus, for  $\text{He}_2^+/\text{He}^+$  to be approximately 0.1 by reaction 7 the pressure must be approximately 5 Torr. Thus the formation of the diatomic ion by the three-body process will decrease very rapidly with decreasing pressures and will be negligible below 0.1 Torr. Knewstubb and Tickner (83) have studied the ions of the rare gases in both the negative

---

(83) P. F. Knewstubb and A. W. Tickner, J. Chem. Phys. 36, 674, 684 (1962)

---

glow and the positive column of a dc glow discharge. They find the ratio  $\text{Ar}_2^+/\text{Ar}^+$  to be much less in the negative glow than in the positive column, and conclude that the diatomic ion is formed principally by the three body process in the negative glow, but that the chemi-ionization reaction predominates in the positive column. Similar considerations apply to the other rare gases.

In our laboratory a microwave discharge was generated in helium by a 100 watt Raytheon microtherm generator and sampled through a pinhole leak at the apex of a conical probe into a quadrupole mass filter. The intensity of the  $\text{He}^+$  ion dropped exponentially in the range studied from a relative intensity of unity at 0.1 Torr to about .002 at 0.5 Torr.

In the same pressure range  $\text{He}_2^+$  increased in intensity from 0.002 at 0.1 Torr to a broad maximum around 0.3 Torr and then declined rapidly at higher pressures. If the  $\text{He}_2^+$  is formed by the three-body process (equation 7) the rate constant would have to be about  $10^{-28}$  cc<sup>2</sup>/molecule<sup>2</sup>/sec. which seems excessive. We conclude then that the diatomic ion is probably formed principally by the chemi-ionization process. (equation 6).

Of perhaps greater interest are the ionic processes occurring in more complex gases. Thus, glow discharges in hydrogen (84,85) and in  $\text{H}_2$ - $\text{D}_2$  mixtures (86) showed

(84) C. J. Braesfield, Phys. Rev. 31, 52 (1928)

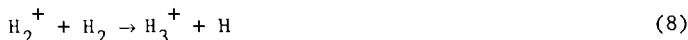
(85) O. Luhr, J. Chem. Phys. 3, 146 (1935)

(86) H. D. Beckey and H. Dreeskamp, Z. Naturforsch 9a, 735 (1954)

the formation of  $\text{H}_3^+$  or  $\text{H}_3^+$  -  $\text{D}_3^+$  mixtures, which increased in concentration with pressure at the expense of the diatomic ion. In an effort to interpret the behavior of the discharge in hydrogen, Eyring, Hirschfelder and Taylor (87) considered the

(87) H. Eyring, J. O. Hirschfelder and H. S. Taylor, J. Chem. Phys. 4, 479 (1936)

reaction forming  $\text{H}_3^+$  to be:



They took the activation energy for the reaction to arise from the balance of centrifugal force and polarization attraction acting in opposite directions. The resulting rate constant for the reaction is:

$$k = 2 \pi e \left( \frac{\alpha}{\mu} \right)^{1/2}$$

i.e., the same as equation 5. Subsequent studies of this reaction in a mass spectrometer ion source (4) have established this reaction beyond doubt, and have shown that the reaction rate is given approximately by the above relation of Eyring, et al. Recent studies by Ortenburger et al. (88) employing a high frequency discharge have

(88) I. B. Ortenburger, M. Hertzberg and R. A. Ogg, J. Chem. Phys. 33, 579 (1960)

shown that reaction 8 occurs under these conditions as well.

Studies of ions in the negative glow and Faraday dark space of a glow discharge in water vapor at 0.4 Torr have been made by Knewstubb and Tickner (89). They

(89) P. F. Knewstubb and A. W. Tickner, J. Chem. Phys. 38, 464 (1963)

found the maximum ion intensity to occur in the negative glow. There was little  $\text{H}_2\text{O}$  present, but a series of solvated protons was observed having the general composition  $\text{H}^+(\text{H}_2\text{O})_n$  with n varying from one to five. Mass spectrometer studies have established the reaction: (1,2,13)



and more recent studies have detected the more highly solvated species. (49,50) The results of the discharge studies showed the first four water molecules to be more strongly bonded to the proton than succeeding molecules and this has been substantiated by the work of Kebarle (49,50) previously discussed.

Similar studies have been made of ions in a glow discharge in ammonia (90)

(90) P. H. Dawson and A. W. Tickner, J. Chem. Phys. 40, 3745 (1964)

with similar results. The negative glow at 0.4 Torr was found to contain the ions  $H^+(NH_3)_n$  with n from 1 to 5, with  $NH_4^+$  being formed in highest concentration in the negative glow, but with  $H^+(NH_3)_4$  predominating in the Faraday dark space. The multiply solvated proton has also been observed in the ion source of a mass spectrometer at elevated pressure. (91, 92)

(91) A. M. Hogg and P. Kebarle, J. Chem. Phys. 43, 449 (1965)

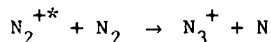
(92) A. M. Hogg, R. M. Haynes and P. Kebarle, J. Am. Chem. Soc. 88, 28 (1966)

Knewstubb (93) also mentions the observation of ions in a glow discharge in

(93) P. F. Knewstubb, "Mass Spectrometry of Organic Ions," Academic Press, New York, 1963, p. 284

methane in which the ions  $C_2H_5^+$  and  $CH_5^+$  predominated, and in which some 40% of the ions present contained three or more carbon atoms. This is quite different from the results obtained by Munson and Field (47, 48) for studies of methane at elevated pressures. They found that with quite pure methane at pressures above about 1 Torr the  $CH_5^+$  and  $C_2H_5^+$  ions were present in the same ratio as  $CH_4^+$  and  $CH_3^+$  (the precursors) in the primary mass spectrum of methane, and that ions having more than two carbon atoms were present in only minor proportions. This suggests that the ions of higher mass reported by Knewstubb (93) originated either from impurities in the methane employed or, more probably, from molecules such as acetylene or ethylene formed by the action of the discharge on methane.

Nitrogen has been the subject of several investigations employing both mass spectrometer ionization chambers and discharges for the production of ions. The ions of greatest interest are  $N_3^+$  and  $N_4^+$ . The mass spectrometer studies have shown  $N_3^+$  to be formed by the reaction:



where  $N_2^{+*}$  implies an excited ion having an appearance potential of about 21-22 eV. (31,32,33)  $N_4^+$  has been found to result from the reaction: (94)



(94) G. Junk and H. J. Svec, J. Am. Chem. Soc. 80, 2908 (1958)

In addition, Munson et al. (32) showed that under certain conditions  $N_4^+$  is formed by the chemi-ionization reaction:



Both ions have been observed in electric discharges in nitrogen. Luhr (95) and Dreeskamp (96) found  $N_3^+$ , but it appeared to be formed only in the drift space

(95) O. Luhr, Phys. Rev. 44, 459 (1933)

(96) H. Dreeskamp, Z. Naturforsch 12a, 876 (1958)

following the discharge. It was thought to result from the reaction



Shahin (97) has reported  $N_3^+$  formed in a glow discharge at 0.3 Torr in nitrogen

(97) M. M. Shahin, "Ion-Molecule Reactions in Gases," Advances in Chemistry Series No. 58, American Chemical Society, Washington, D. C., 1966 p. 315

as well as  $N_4^+$  in a corona discharge in a mixture of nitrogen and water vapor. The relative intensity of  $N_4^+$  passed through a maximum at about 10 Torr, then slowly declined at higher pressures. Shahin attributed the formation of the ion to the reaction:



In the same system he observed  $H_2O^+$ ,  $H_3O^+$ ,  $H_5O_2^+$  and  $N_2H^+$  ions, all apparently resulting, at least in part, from reaction of  $N_2^+$  with water.

In this laboratory nitrogen has been passed through a microwave discharge at pressures of 0.01 to 0.3 Torr and the plasma sampled into a quadrupole mass filter where the ions were separated and analyzed.  $N_4^+$  was not observed at any condition studied.  $N_3^+$  was formed in very small concentrations (about 1% of  $N_2^+$ ) at 0.01 Torr, but increased rapidly in intensity, passing through a broad maximum at about 0.15 - 0.20 Torr, and then decreasing at higher pressures. In the same pressure range the intensity of  $N_2^+$  dropped precipitously from 90 to 1.5, and that of  $N^+$  remained constant at about 9, all in arbitrary units. At the  $N_3^+$  maximum all of the ions were of nearly equal intensity. A brief study of the variation of the intensities of these ions with nominal power input at a pressure of 0.15 Torr showed  $N_2^+$  and  $N^+$  to decrease in intensity with decreasing power until the discharge was extinguished at about 40% of maximum. These curves were reminiscent of an ionization efficiency curve, and strongly suggest the average electron energy decreased with decreasing power input. The  $N_3^+$  ion increased in intensity with decreasing power input up to a broad maximum between 75 and 65% of maximum power, after which it again decreased. This suggests that an excited state is formed by electron impact with electrons of broad energy spread. Such an energy spread has been found in our studies, and will be reported separately. Further, we find that the electrons possess an approximately Maxwell-Boltzmann distribution of energy, and that the average energy decreases as the pressure increases, in accordance with our observation of the variation of  $N_3^+$  with pressure. This also accounts in part for the decrease in  $N_2^+$  with pressure.

The near constancy of  $N^+$  with increasing pressure is difficult to understand. The number of  $N^+$  ions formed by direct electron impact upon  $N_2$  or  $N$  must be relatively small and can hardly account for the intensity of the  $N^+$  observed. It is possible that at the higher pressures most  $N^+$  is formed by the reaction:



but this is, of course, speculative.

The absence of  $N_4^+$  is puzzling, since it has been observed in some discharges. It is possible the ion is destroyed in passing through the sampling probe. This seems unlikely, however, since  $N_4^+$  is held together by a bond of about 1.5 eV energy. This is about the same strength as the bond in  $He_2^+$ , which we observe. Conceivably, the ion may appear at higher pressures, but some alterations in our sampling probe will be necessary to achieve this.

Several investigations of ions in glow discharges in oxygen have been reported.  $O^+$  and  $O_2^+$  were reported by Knewstubb (93), Luhr (98) and Dickenson and Sayers (99).

(98) Luhr, O., *Phys. Rev.* **38**, 1730 (1931)

(99) P. H. G. Dickenson and J. Sayers, *Proc. Phys. Soc. (London)* **A76**, 137 (1960)

In addition,  $O_3^+$  and  $O_4^+$  (99) have been reported.

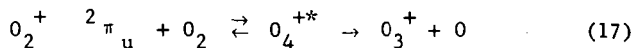
In our studies of oxygen in the pressure range 0.01-0.3 Torr, using a microwave discharge only  $O^+$  and  $O_2^+$  were found. Both ions dropped in intensity exponentially with increasing pressure, but the  $O^+$  dropped slightly less rapidly than did  $O_2^+$

The drop in  $O^+$  with increasing pressure may be due to the fact that  $O^+$  can react with  $O_2$  by charge exchange.



This would account for the drop in  $O^+$  intensity at conditions at which  $N^+$  (which cannot undergo loss by charge exchange) remains constant. In the same pressure range,  $O_2^+$  drops in intensity to about the same extent as does  $N_2^+$ , which can disappear by charge exchange with N.

In a mass spectrometer ion chamber  $O_3^+$  and  $O_4^+$  are found in rather small intensities, apparently formed by the reactions:



The latter is very faint, however. The ionization potential of  $O_3$  is slightly greater than that of  $O_2$  (100,101), so  $O_3^+$  can react with  $O_2$  as follows:



(100) J. T. Herron and H. I. Schiff, J. Chem. Phys. 24, 1266 (1956)

(101) R. K. Curran, J. Chem. Phys. 35, 1849 (1961)

No doubt this accounts for the failure to observe  $O_3^+$ . The absence of  $O_4^+$  may be merely a matter of sensitivity.

In our laboratory we have also studied the ions formed in a microwave discharge in a mixture of nitrogen and oxygen at a constant pressure of about 0.1 Torr. As might be expected, the intensities of  $N_2^+$  and  $N^+$  decreased and those of  $O_2^+$  and  $O^+$  increased as the proportion of nitrogen decreased and that of oxygen increased.  $NO^+$  was very intense over the range of 10% to 75% oxygen in the mixture. This is not surprising, since  $N^+$ ,  $N_2^+$  and  $N_3^+$  reacting with  $O_2$  or O and  $O^+$  and  $O_2^+$  reacting with N or  $N_2$  are capable of producing  $NO^+$ . Further,  $NO$  is produced in the discharge and no doubt is ionized by electron impact.

Small amounts of  $NO_2^+$  ions were observed in all of the mixtures studied, and small amounts of  $N_2O^+$  were found in the nitrogen rich mixtures, but disappeared when the proportion of nitrogen in the mixture dropped below 75%. The manner of their formation is not known, but from their very small intensity we infer that they are probably formed by third order processes. It is surprising that no  $N_3^+$  ion was observed when oxygen was present. Presumably it is capable of reacting in several ways with  $O_2$  or O, and so is destroyed as fast as it is formed. The system  $O_2-N_2$  is of great interest and will be studied further.

This research was supported by Project SQUID of the Navy, under Grant NONR 3623 S-21, which we acknowledge with gratitude.

## ION-MOLECULE REACTION RATES MEASURED IN A DISCHARGE AFTERGLOW

E. E. Ferguson, F. C. Fehsenfeld, and A. L. Schmeltekopf

Institute for Telecommunication Sciences and Aeronomy

Environmental Science Services Administration

Boulder, Colorado

## ABSTRACT

The application of a flowing afterglow reaction technique to the measurement of thermal energy ion-molecule reactions is briefly described. The flowing afterglow system allows the measurement of reactions of ions with such unstable neutrals as O, H, N, and O<sub>3</sub>. The reaction  $O^+ + CO_2 \rightarrow O_2^+ + CO$  appears to be important in CO<sub>2</sub> discharges, as O<sub>2</sub><sup>+</sup> has been found to be a dominant ion in this case. The O<sup>+</sup>, C<sup>+</sup>, and CO<sup>+</sup> ions rapidly react to produce either O<sub>2</sub><sup>+</sup> or CO<sub>2</sub><sup>+</sup>, the dominant ions observed in a CO<sub>2</sub> discharge. In an argon-hydrogen discharge, H<sub>3</sub><sup>+</sup> would be an important ion, since it is the most stable ion in that system and a reaction sequence leading to H<sub>3</sub><sup>+</sup> production is fast. Several associative-detachment reactions such as  $O^- + O \rightarrow O_2 + e$  and  $H^- + H \rightarrow H_2 + e$  have been found to have large rate constants and such reactions may be important in determining the negative ion concentrations in discharges.

## I. Introduction and Experimental

A flowing afterglow system has been utilized for the past several years in the ESSA Laboratories in Boulder, Colorado, for the measurement of reaction rate constants at 300° K for both positive and negative ions reacting with both stable and unstable neutral species<sup>1,2</sup>. Figure 1 illustrates one version of the flowing afterglow tube which has been utilized. A tube of about 1 m length and 8 cm diameter serves as the reaction vessel. A gas, usually helium, is introduced at one end of the tube and exhausted at the other end at a rate of around 100 atm cc/sec, the helium pressure being typically ~ 0.3 torr. The helium is ionized by a pulsed dc discharge producing about 10<sup>10</sup> He<sup>+</sup> ions and He(2<sup>3</sup>S) metastable atoms per cc. Positive ions are produced in most cases by adding a relatively small concentration of neutral gas into the helium afterglow by means of a small nozzle. The positive ions are products of He<sup>+</sup> and He(2<sup>3</sup>S) reactions with the added neutral. The reactions of these ions with a second neutral added at a second downstream nozzle are then measured. The ion composition of the afterglow is monitored by means of a frequency scanned quadrupole mass spectrometer covering the mass range 1 - 100 amu. The rate of disappearance of a reactant ion with neutral reactant addition leads directly to a reaction rate constant. Our estimate of the reliability of the rate constants so determined is ± 30% in favorable cases. Our experience in comparing our rate constants with other measured rate constants generally supports this estimate.

This experimental scheme has many variations. We have, for example, successfully used pyrex and quartz reaction tubes as well as stainless steel, and microwave and electron beam ionization as well as the dc discharge. We sometimes find it desirable to produce reactant ions by adding a suitable gas through the discharge with the helium rather than downstream in the afterglow, particularly in the case of certain negative ions such as O<sup>-</sup> and H<sup>-</sup>, which are readily created by dissociative attachment by fast electrons in the discharge. We sometimes use carrier gases other than helium, particularly argon.

Some of the important features of the flowing afterglow experimental technique are the following: (1) The reactant ions in many cases are known to be in their ground states, either because of the reaction which produces them or by virtue of superelastic electron collisions in the plasma prior to neutral reactant addition. Stable neutral reactant species are added without being subjected to discharge or

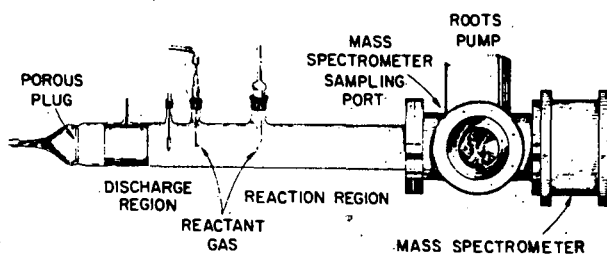
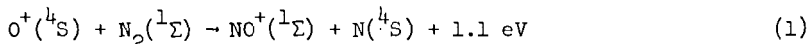


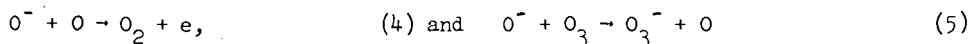
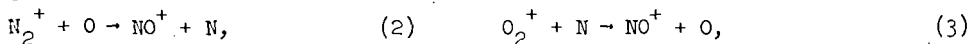
Figure 1. Flowing Afterglow Reaction System.

excitation conditions so that they can be assumed to be neither vibrationally nor electronically excited. On the other hand, some selective excitation is possible. For example, the reaction



has been measured<sup>3</sup> as a function of vibrational temperature from 300 - 5000°K.

(2) It is possible to add chemically unstable neutral reactants into the afterglow so that reactions such as



have been studied in this system.

(3) The difficulty of resolving concurrent reactions does not arise, as it does in mass spectrometer ion sources, and we have measured the reaction



without complication from the reaction



since  $\text{H}_2$  is not ionized in the flowing afterglow arrangement.

## II. Thermal Energy Charge-Transfer Reactions

The flowing afterglow system is well suited to exothermic charge-transfer reaction measurements, since the neutral reactant, necessarily of lower ionization potential, does not go through the ionization region and hence is not selectively ionized as would be the case in some experimental arrangements used for ion-molecule reaction studies. For positive ions, either atomic or molecular, charge-transfer to molecular neutrals is usually fast (barring occurrence of a competitive exothermic rearrangement reaction). Very many such examples (several dozen) have been observed and very few exceptions, notably the reaction between  $\text{He}^+ + \text{H}_2$ , which is observed not to have a rate constant as large as  $10^{-13} \text{ cm}^3/\text{sec}$ . For example,  $\text{Ar}^+$ ,  $\text{CO}^+$ ,  $\text{CO}_2^+$ ,  $\text{N}_2^+$ ,  $\text{N}^+$ , and  $\text{H}_2\text{O}^+$  all charge-transfer with  $\text{O}_2$  to produce  $\text{O}_2^+$  with rate constants greater than  $10^{-10} \text{ cm}^3/\text{sec}$  (or cross sections greater than  $20 \text{ \AA}^2$ ).

This result contradicts most theoretical predictions which had assumed that charge-transfer would be slow except in unusual cases involving fortuitous energy resonances.

The situation appears the same for negative ion charge-transfer although much less data is available in this case. We have found that the reactions



and several other negative ion charge-transfer reactions have rate constants greater than  $10^{-10} \text{ cm}^3/\text{sec}$  at 300°K and previously Curran<sup>4</sup> had observed a number of fast negative ion charge-transfers to  $\text{NO}_2$ , and Henglein and Muccini<sup>5</sup> observed a fast negative ion charge-transfer with  $\text{SO}_2$ . In the absence of experimental data one would certainly predict that exothermic charge-transfer to a molecular neutral will be fairly efficient.

## III. Ion-Atom Interchange Reactions

The most commonly studied ion-molecule reactions have involved changes in molecular configuration. Typical examples are



whose rate constant,  $1.1 \times 10^{-9} \text{ cm}^3/\text{sec}$ , from flowing afterglow experiments<sup>2</sup> agrees with an earlier value  $9 \times 10^{-10} \text{ cm}^3/\text{sec}$  measured in a mass spectrometer ion source by Franklin and Munson<sup>6</sup>; the reaction



with a rate constant of  $1.2 \times 10^{-9} \text{ cm}^3/\text{sec}$  from both flowing afterglow<sup>2</sup> and mass spectrometer ion source measurements<sup>7</sup>; and



with a rate constant  $1.9 \times 10^{-9} \text{ cm}^3/\text{sec}$ .

Such reactions are more often fast than slow. One of the slowest exothermic ion-molecule reactions (again barring cases where charge-transfer competes) is



with a rate constant  $\sim 10^{-12} \text{ cm}^3/\text{sec}^3$ . This rate constant increases<sup>3</sup> to about  $3 \times 10^{-11} \text{ cm}^3/\text{sec}$  for an  $\text{N}_2$  vibrational temperature of  $5000^\circ \text{K}$  and also increases with  $\text{O}^+$  kinetic energy<sup>8,9</sup>.

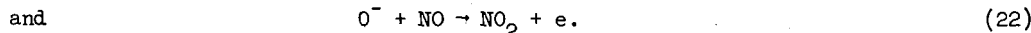
No case of a fast ion-atom interchange reaction involving the breaking of two bonds has so far been reported. The exothermic reaction



has a rate constant less than  $10^{-15} \text{ cm}^3/\text{sec}$ , for example.

#### IV. Associative Detachment Reactions

A number of associative detachment reactions have been recently measured to be fast in the flowing afterglow system (i.e.  $k > 10^{-10} \text{ cm}^3/\text{sec}$ ), including:



Phelps and Moruzzi<sup>10</sup> have been making similar measurements in drift tube experiments at Westinghouse and have measured reactions, (20), (21), and (22). The flowing afterglow and drift tube results agree within better than a factor of two in each case. Several exothermic associative detachment reactions do not occur at measurable rates ( $k < 10^{-12} \text{ cm}^3/\text{sec}$ ), an example being



#### V. Ion-Molecule Reactions in Discharges

One obvious application of measured rate constants to the qualitative interpretation of the ion composition of a gas discharge is the case of the  $\text{CO}_2$  discharge ion composition studied by Dawson and Tickner<sup>11</sup>. Dawson and Tickner observed the dominant ions in a glow discharge in  $\text{CO}_2$  to be  $\text{O}_2^+$  and  $\text{CO}_2^+$ . This is quite reasonable in view of the known occurrence of reactions (11), (12), and (13) above, together with the fast charge-transfer of  $\text{CO}^+$  with  $\text{CO}_2$  to produce  $\text{CO}_2^+$ . The results of these reactions are graphically illustrated in Fig. 2 (from Fehsenfeld, et al., J. Chem. Phys. 45, 23 (1966)), which shows that all of the ions,  $\text{C}^+$ ,  $\text{O}^+$ , and  $\text{CO}^+$ , do convert to  $\text{O}_2^+$  and  $\text{CO}_2^+$  by reaction with  $\text{CO}_2$  in the  $\sim 6$  milliseconds reaction time in the flowing afterglow. If molecular oxygen were added, one would expect the dominant ion to become  $\text{O}_2^+$  alone, since  $\text{CO}_2^+$  is known to charge-transfer rapidly with  $\text{O}_2$ <sup>12</sup>.

In a like manner Fig. 3, showing ion composition in an Argon-H<sub>2</sub> afterglow<sup>13</sup>, suggests that the ion-molecule chemistry is such that the dominant ion is H<sub>3</sub><sup>+</sup>, and this would very likely be true for certain active discharge conditions as well.

An example of the possible importance of associative detachment reactions in discharges was noted by Massey<sup>4</sup>, who speculated that the low negative ion density in oxygen discharges (relative to iodine discharges for example) might be due to electron detachment by reaction (16). In iodine the analogous reaction, I<sup>-</sup> + I → I<sub>2</sub> + e is endothermic. In view of the subsequent finding that reaction (16) is indeed fast ( $k_{16} = 1.9 \times 10^{-10}$  cm<sup>3</sup>/sec), Massey's suggestion takes on renewed interest. The same argument could be applied to H<sub>2</sub> discharges in view of the rapidity of reaction (17),  $k_{17} \sim 10^{-22}$  cm<sup>3</sup>/sec.

## VI. Conclusions

The growing body of quantitative ion-molecule reaction rate data now available should allow in favorable cases prediction and in many cases correlation of observed ion compositions of gas discharges with known ion-molecule chemistry.

Acknowledgement: This work has been supported in part by the Defense Atomic Support Agency.

## REFERENCES

1. F. C. Fehsenfeld, P. D. Goldan, A. L. Schmeltekopf, H. I. Schiff, and E. E. Ferguson, *J. Chem. Phys.* **44**, 4087, 4095 (1966).
2. F. C. Fehsenfeld, A. L. Schmeltekopf, and E. E. Ferguson, *J. Chem. Phys.* **44**, 3022, 4537 (1966); **45**, 23, 404, 1844 (1966).
3. A. L. Schmeltekopf, F. C. Fehsenfeld, G. I. Gilman, and E. E. Ferguson, *Planet. Space Sci.* in press; *J. Chem. Phys.*, to be published.
4. R. K. Curran, *Phys. Rev.* **125**, 910 (1962).
5. A. Henglein and G. A. Muccini, *J. Chem. Phys.* **31**, 1426 (1959).
6. J. L. Franklin and M. S. B. Munson, 10th Combustion Symposium, The Combustion Institute, Pittsburgh, Pa. (1965) p. 561.
7. J. L. Paulson, R. L. Mosher, and F. Dale, *J. Chem. Phys.* **44**, 3025 (1966).
8. R. F. Stebbings, B. R. Turner, and J. A. Rutherford, *J. Geophys. Res.* **71**, 771 (1966).
9. C. F. Giese, 152 Am. Chem. Soc. Meeting, New York, 1966.
10. J. L. Moruzzi and A. V. Phelps, *J. Chem. Phys.*, in press.
11. P. H. Dawson and A. W. Tickner, *Proc. Sixth Int. Conf. on Ionization Phenomena in Gases*, Vol. **2**, p. 79 (1963) Paris.
12. R. B. Norton, E. E. Ferguson, F. C. Fehsenfeld, and A. L. Schmeltekopf, *Planet. Space Sci.* **14**, 969 (1966).
13. F. C. Fehsenfeld, A. L. Schmeltekopf, and E. E. Ferguson, *J. Chem. Phys.* in press.
14. H. S. W. Massey, "Negative Ions", Second ed., Cambridge Univ. Press, Cambridge (1950).

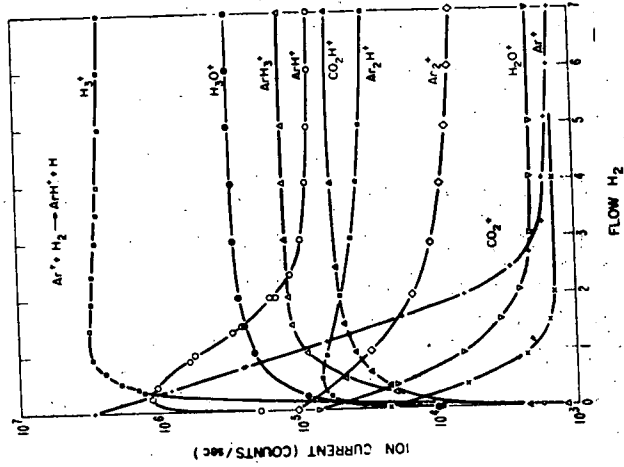


Figure 3. Ion Reactions in an Ar-H<sub>2</sub> System.

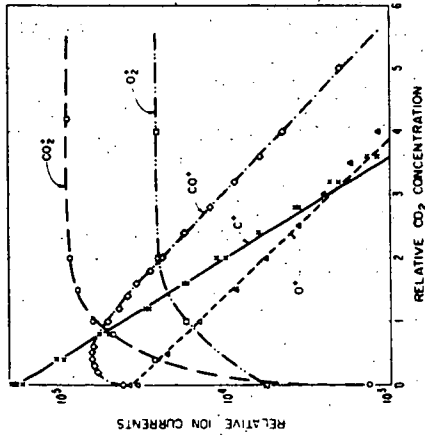


Figure 2. Ion Reactions with CO<sub>2</sub>.

Absorption Spectra of Transient Species  
in a Single-Pulse Microwave-Discharge

by A.B. Callear

Department of Physical Chemistry,  
University of Cambridge, Lensfield Road, Cambridge.

ABSTRACT

An apparatus was described for production of an intense and short duration microwave pulse discharge in various gases. At power levels in the 50 kw range, the microwave energy was coupled to the gas with a high Q tuned cavity. For higher power levels up to 1 mw peak, a glass tube containing the gas was placed inside a wave guide, in the central region of maximum field. Thereby intense discharges were produced in metre long columns of gas, to provide ideal conditions for kinetic absorption spectroscopy. Some simple applications of the technique were described, including measurement of energy transfer from He( $2^3S_1$ ) to atomic neon, exchange of vibrational energy from nitric oxide to D<sub>2</sub>S, and the production of diatomic free radicals in various gases.

Flash photolysis is proving to be of considerable value in the study of structure and kinetics. Our first object in developing the microwave technique, in which the photolytic flash is replaced by a powerful microwave pulse, was to explore alternative means of achieving substantial electronic excitation of gases. It was believed that the method would complement flash photolysis and would also extend the direct techniques of flash spectroscopy to more diverse systems, for example gases which only absorb light in the extreme vacuum ultraviolet<sup>1</sup>. Thus to mention a few as yet unattained and perhaps ambitious objects, we hope to follow dimer formation in pure helium and the other inert gases, to study N<sub>2</sub> A<sup>3</sup>Σ<sup>+</sup> by absorption spectroscopy, to investigate CH formation<sup>2</sup> in CH<sub>4</sub> (which has now been achieved by vacuum ultraviolet flash photolysis<sup>2</sup>), and to detect both positive and negative ions by absorption spectroscopy.

A microwave field will couple only with free electrons, and direct change of translational energy of gases is unimportant (because of the mass restriction) compared to the energy appearing as electronic and vibrational excitation. Described here are results obtained with a microwave-pulse generator of peak power ~50 kw, and also the development of a more powerful apparatus with a capability to deliver power to a gas at just under 1 mw. Results from the second machine will be available by the early spring of 1967.

Experimental and Discussion

The first apparatus was constructed to establish the feasibility

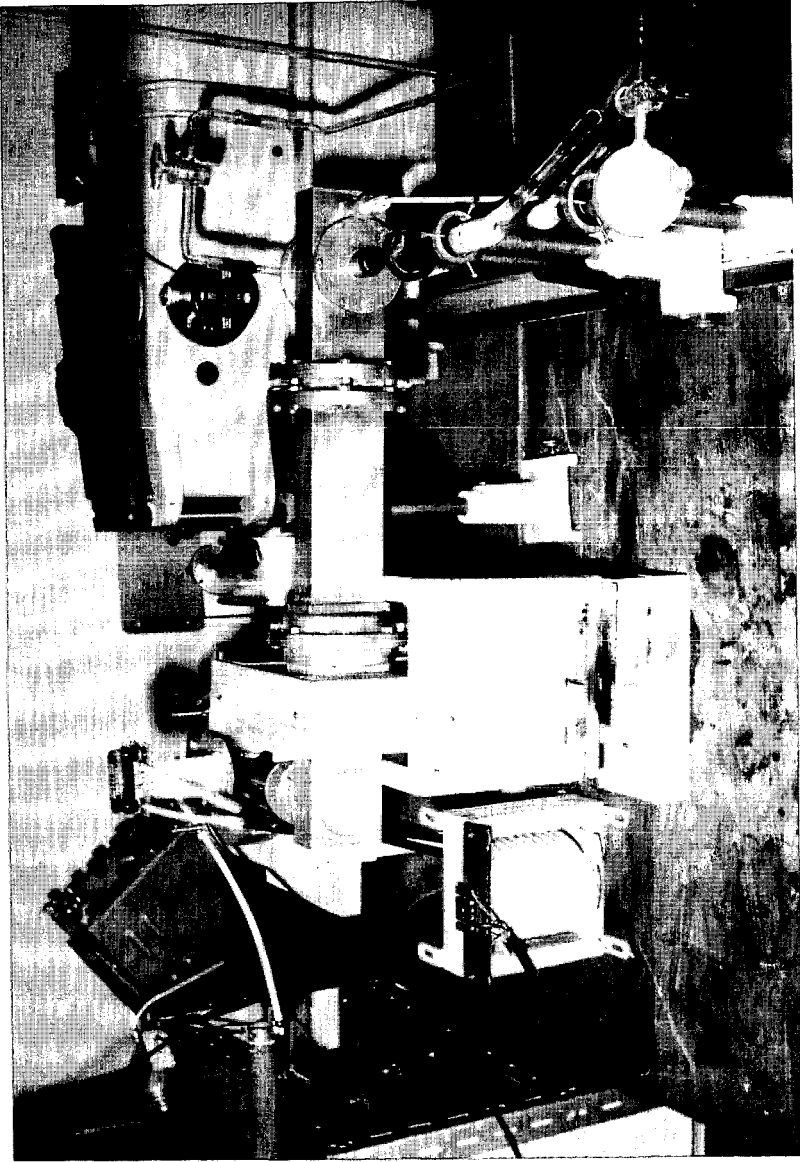


FIG. 1 Prototype equipment for microwave-pulse flash-spectroscopy.

of producing transients at concentrations detectable by absorption spectroscopy. An English Electric M561 Magnetron (3046 Mc/sec) was powered with a  $1 \mu\text{F}$  capacitor charged to  $\sim 15 \text{ kV}$ , and the pulse duration could be varied in the range 2 - 50  $\mu\text{sec}$  with English Electric FX290 thyratrons. Via a conventional 'door-knob' coupler and waveguide section (without an isolator), the power was transmitted to a cylindrical cavity with a  $Q$  of 380. This is illustrated by the photograph shown in figure 1, and the main details have already been described. Although a 10  $\mu\text{sec}$  pulse corresponds to 0.8 joules, only a minute fraction of this was successfully delivered to the gas. However, a number of encouraging observations were made, and some energy transfer rate coefficients were measured, as described below.

More recently, R.E.M.Hedges, J.G.Guttridge and I have completed the construction of a powerful microwave generator, which incorporates the English Electric M578 magnetron, with a rated peak-power of 900 kw. Into a 'matched load', we have produced single pulses at 500 kw, duration 5  $\mu\text{sec}$ ., which is close to the maximum power available per pulse. The H.T. arrangement is similar to that employed in the prototype equipment, with two thyratrons delivering a potential up to 30 kV. This particular magnetron turns out to be rather susceptible to arcing on single pulse operation, and in this respect is especially sensitive to reflected power. This has necessitated the inclusion of an isolator between the magnetron and the load; to obtain satisfactory functioning up to 25 kV (as evidenced by the profile of the current pulse), it is necessary to condition the magnetron cathode by somewhat laboriously pulsing with the applied potential increased by small increments from 20 kV upwards.

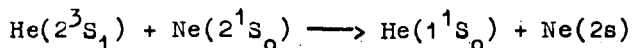
It was anticipated that the same cavity that had been employed in the early experiments would also be suitable for the high energy equipment. With the assistance of Mr. F.J.Weaver of the English Electric Valve Company, the size of the hole coupling the cavity to the waveguide was carefully optimised to give a standing-wave ratio of 1.2 and a  $Q$  of about 800. With such a tuned cavity, a discharge can be produced in helium at 1 atmos. pressure; however, the discharge was still quite feeble and it was obvious that only a minute fraction of the total energy was being coupled to the gas. Although the tuning and matching was near perfect under low power test conditions, for various reasons the cavity detunes as soon as the gas strikes.

Although a study of the cavity discharge may prove to be of some value, interest was directed at the problem of achieving ~~more~~ more efficient coupling of the microwave pulse to the experimental gas. In fact we have now achieved conditions under which it appears that practically the entire pulse may be absorbed by the gas. This innovation is a very simple one; a thin walled glass tube containing the gas is placed inside the waveguide in the region of

maximum field. In this manner, an intense discharge can be produced in metre long columns of gas, to provide ideal conditions for absorption spectroscopy. R.E.M.Hedges is presently assembling the optical components to carry out spectroscopic studies under these conditions. The beauty of this discovery lies in its inherent simplicity; power is coupled to the gas at low Q and matching problems are virtually eliminated.

### Results

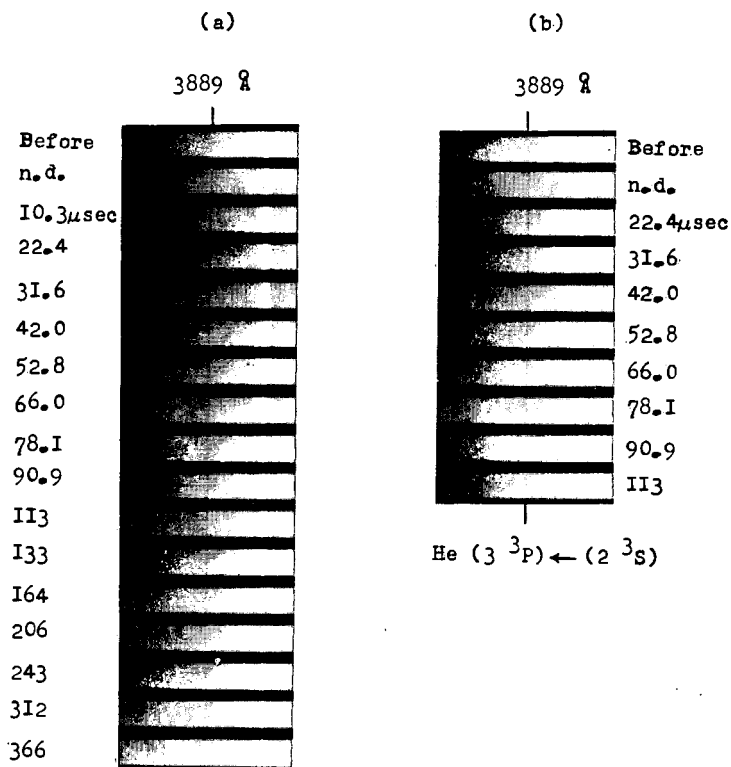
This section relates only to the low power equipment, with a tuned cavity discharge. Figure 2(a) shows the formation of  $\text{He}(2^3\text{S}_1)$  in a single pulse of 10  $\mu\text{sec}$  duration, and its decay following the pulse. Also observed in pulsed helium were the comparatively short lived  $2^3\text{P}_1$  and  $2^1\text{S}_0$  states. A simple quantitative application shown in figure 2(b), is the enhanced rate of decay of  $\text{He}(2^3\text{S}_1)$  in the presence of a trace of neon. By means of photometry of plates similar to that illustrated in figure 2, the rate of the energy transfer process



was recorded as  $0.35 \pm 0.02 \text{ \AA}^2$ , in agreement with  $0.37 \text{ \AA}^2$  reported by Javan, Bennett and Herriott<sup>3</sup>. The helium system is perhaps the simplest of all electric discharges and, as mentioned above, we hope to make more detailed observations of the formation of diatomic helium. All four of the 1s metastables were observed in pulsed neon<sup>1</sup>.

Figure 3 illustrates vibrational excitation of nitric oxide, and its decay following the pulse. It was concluded that excitation occurs by direct collision of nitric oxide molecules with electrons, because of the extreme weakness of fluorescence from electronically excited molecules<sup>4</sup>. The total yield of vibrationally excited NO produced with a microwave pulse, is about 10 - 100 fold higher than the yield of electronically excited species or free radicals, in all the systems which have thus far been investigated. The technique may therefore prove to be generally applicable to the study of vibrational energy transfer. Figure 3(b) shows the catalysis of the NO relaxation, by a trace of  $\text{D}_2\text{S}$ , which has a vibrational frequency close to that of NO. A number of rate coefficients for V-V processes of this type have recently been published.

Finally we mention the formation of chemical intermediates, produced by microwave pulses in polyatomic gases. Thus far, these aspects of the chemistry of electric discharges have only been investigated in  $\text{CS}_2$ ,  $(\text{CN})_2$ ,  $\text{H}_2\text{O}$  and  $\text{H}_2\text{S}$ . In each case, diatomic free radical intermediates were observed. Some of these are included in figure 4.



(a) Formation and decay of He ( $2\ ^3S$ ) in 5 mm of He.  
 (b) Decay of He ( $2\ ^3S$ ) in 5 mm He +  $1.2 \times 10^{-2}$  mm Ne.

Figure 2

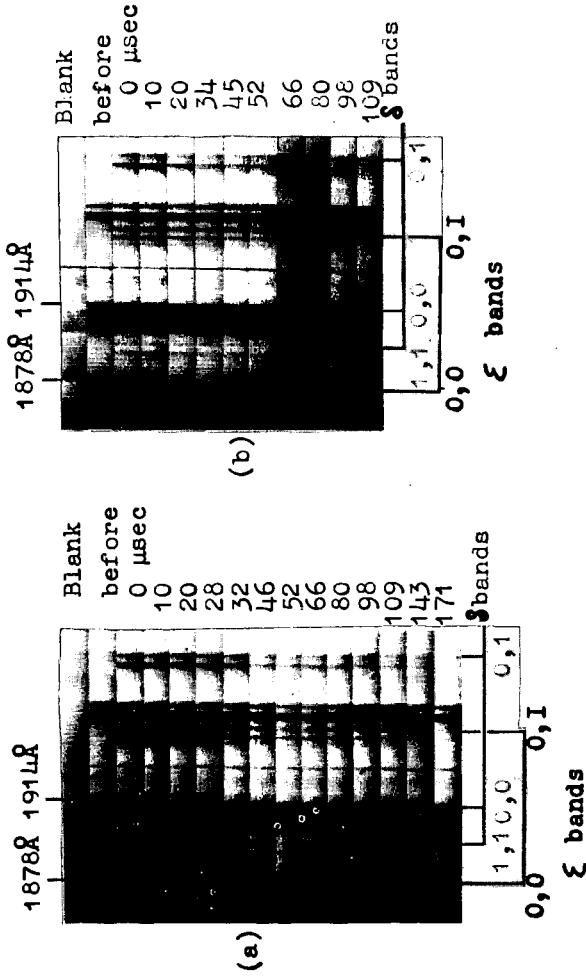


Fig. 3 Formation and decay of  $\text{NO X } 2 \Pi(v=1)$  in pulsed He / NO mixtures.

(a) 6mm NO + 300mm He

(b) 3mm NO + 0.06mm  $\text{D}_2\text{S}$  + 300mm He

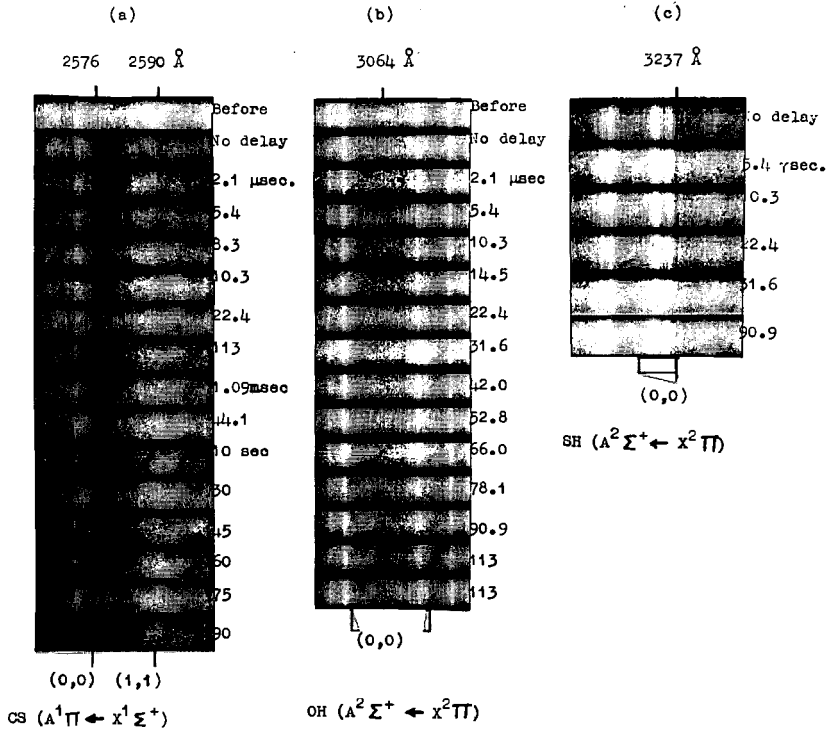


Fig 4 Formation and decay of (a) CS : 2mm CS<sub>2</sub> + 60 mm He;

(b) OH : 5 mm H<sub>2</sub>O + 35 mm He; (c) SH : 20 mm H<sub>2</sub>S + 100 mm He.

References

1. A.B.Callear, J.A.Green and G.J.Williams, Trans.Faraday Soc., (1965), 61, 1831.
2. W.Braun, K.H.Welge and A.M.Bass, J.Chem.Phys., (1966), 45, 2650.
3. A.Javan, W.R.Bennet and D.R.Herriott, Phys.Rev.Let., (1961), 6, 106.
4. A.B.Callear and G.J. Williams, Trans.Faraday Soc., (1966), 62, 2030.

55  
The Collection of Positive Ions and Electrons by a  
Screened Probe in the Neon Negative Glow\*

M.J. Vasile<sup>†</sup> and R.F. Pottie,  
Division of Applied Chemistry,  
National Research Council,  
Ottawa, Canada.

### INTRODUCTION

The collection of ions and electrons by small probes placed within the plasma of a gas discharge has received considerable attention over the past four decades. A major advance in measurement technique was reported by Boyd<sup>1</sup> in 1950 with the introduction of a small screened flat probe. The new technique made it possible to separate the collected currents into the ion and electron components. As a result it became possible to measure their concentrations separately and to extend the range of measured electron velocities to beyond the ionization potential of the discharged gas with no interference from positive ion current. The method was extended by Boyd and co-workers<sup>2</sup> and by Pringle and Farvis<sup>3</sup> to the measurement of ions and electrons in both the positive column and negative glow in various gases. Despite the apparent success of these studies, little or no use has been made of this technique by other workers in the field.

Previous work in this laboratory<sup>4,5</sup> had established the usefulness of a mass spectrometer to obtain relative ion concentrations in the various regions of glow discharges. The work reported here is an extension of these earlier studies and represents an attempt to (a) measure the absolute concentrations of ions and electrons in conjunction with the mass spectrometric studies and (b) to determine the electron energy distributions, particularly in the negative glow to assist in the interpretation of processes that result in the production of ions.

### EXPERIMENTAL

#### 1. Apparatus

In order to reduce undue disturbance of the discharge, an essential characteristic of a probe is small size. The probe consisted of a fine wire grid that was spot welded to a 5 × 5 mm platinum frame which was mounted on a Pyrex plate. A 1/8" circular hole in the glass plate defined the current reaching the platinum collector (.010" thick) mounted below it. A mica insulator shielded the collector from the discharge. The glass plate was 1 mm thick, and the grid was a stainless steel mesh (0.001" diameter wires) with an optical transparency of 42%. The effective area of the collector was computed to be  $3.33 \times 10^{-6} \text{ m}^2$ . The probe parts were cemented together with "Gevac" and the platinum leads (.01" diam.) from the electrodes were supported and insulated by means of a ceramic rod with two channels for the leads. The ceramic rod extended through a side-arm of the discharge tube so that it could be rotated or moved radially by means of a magnetic slug. Impedance measurements showed that the resistance between the collector and grid was greater than  $10^{13}$  ohms.

The Pyrex discharge tube<sup>56</sup> was 50 cm long and 5.5 cm in diameter. The electrodes were polished stainless steel discs, 5 cm in diameter and the cathode could be moved magnetically over a distance of 30 cm. The entire discharge tube, including side-arms, could be baked to greater than 350°C. Metal bellows valves were used for all openings into the discharge tube and the normal background pressure of  $2 \times 10^{-7}$  Torr was achieved with a silicone oil diffusion pump.

The gases were of assayed research grade and periodic checks were made for impurities by mass spectrometry. The operating gas was admitted to the discharge tube via a Granville-Phillips variable leak valve, the pressure being measured with a Decker diaphragm gauge. A small flow was maintained through the discharge tube during operations by means of a needle valve to the pumps. The exit pressure was about  $10^{-2}$  Torr. Preliminary discharges of about one hour duration were always carried out before measurements were taken. The tube was then evacuated and a fresh gas sample was admitted for the experiment.

All results reported here were taken with a gas pressure of 0.28 Torr and a discharge current of 0.250 ma.

A schematic diagram of the discharge tube and electrical circuit is given in Fig. 1. The potentials of the grid and collector relative to the grounded anode could be controlled independently so that either one could be positive or negative with respect to the anode. The collector current passing through precision resistors (0.05%) was measured with a 1 megohm impedance nanovoltmeter which was isolated from ground. The minimum detectable current was  $10^{-10}$ A. The potential of the collector was measured with a vacuum tube voltmeter, while a digital voltmeter was used for measurement of the grid potential. Grid and discharge currents were monitored by dc microammeters. Discharge power was provided by a commercial dc power supply.

## B. Results

(1) Collection of low energy electrons. Fig. 2(a) is a typical semi-logarithmic plot of the electron current, showing two straight line segments for the thermal and secondary electrons respectively. The space potential was obtained from extrapolation of the saturation current to the rising portion of the curve. The gas was pure neon and the probe was near the position of maximum electron intensity in the negative glow. The electron temperatures of the Maxwellian distributions were 0.271 and 3.67 eV for the thermal and secondary electrons, and their concentrations were  $158 \times 10^{13}/\text{m}^3$  and  $2.9 \times 10^{13}/\text{m}^3$  respectively, assuming collection of the random current at the space potential<sup>6,7</sup>. The small electron residual current that was always observed at higher retardation potentials was subtracted from the total electron currents. The collector potential was +70 V with respect to the anode.

(2) Collection of positive ions. The collector potential was maintained at -70 V and the grid voltage was varied from -70 V to well above the space potential for the collection of positive ions. The method of calculation of the random positive ion current differed somewhat from previous approaches and is given briefly below. We assume that positive ions are accelerated from the sheath to the grid and are further accelerated by the full potential between the collector and the grid. The current rises until all the random ion current arriving at the sheath edge has been collected. Further collection of ion current is the result of sheath expansion, edge effects and potential penetration of the sheath. If we treat the ion currents

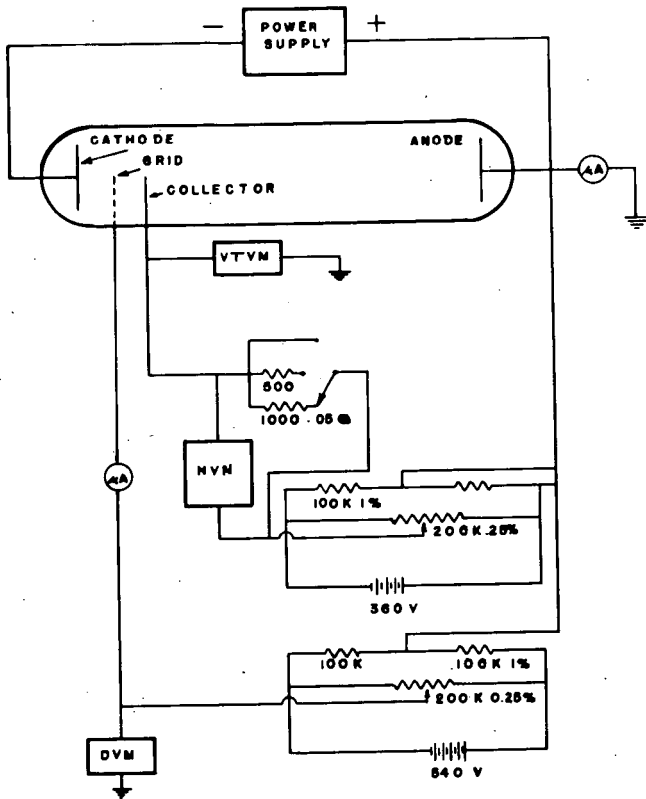


FIG. 1 Apparatus and schematic circuit diagram.

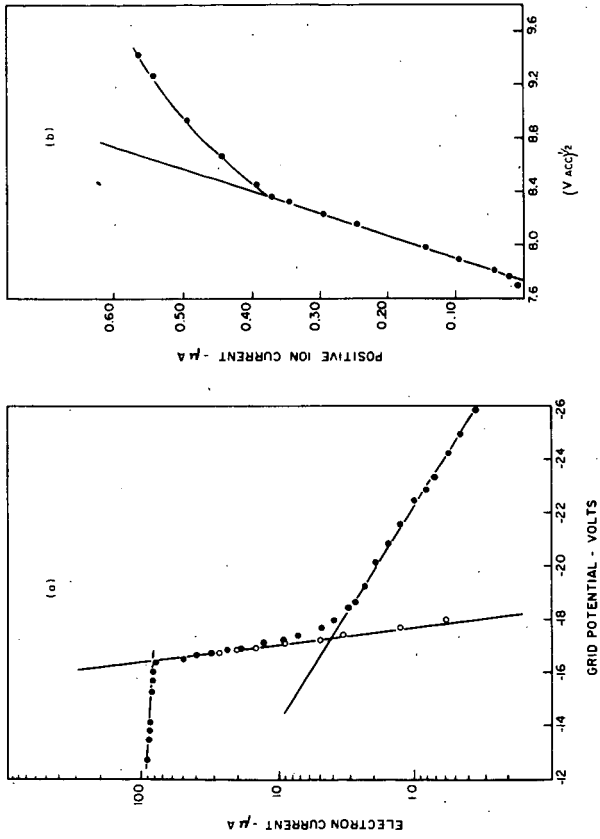


FIG. 2 Collection of ions and electrons in pure neon, distance from grid to cathode = 2.55 cm, probe faces anode. Fig. 2(a) - electron curve, Fig. 2(b) - ion collection curve.

below the saturation limit we find<sup>59</sup>

$$i_+ = A \times \frac{1}{4} n_p q V_f \quad (1)$$

in which  $n_p$  is the random ion density,  $q$  the electronic charge and  $V_f$  the velocity of the ions arriving at the collector. This is given by:

$$V_f = V_o + \left( \frac{2qV_{acc}}{m} \right)^{1/2} \quad (2)$$

in which  $V_o$  is the initial ion velocity and  $V_{acc}$  is the potential difference between the plasma and the collector. Thus:

$$i_+ = A \times \frac{1}{4} n_p q \left( V_o + \left( \frac{2q}{m} \right)^{1/2} V_{acc}^{1/2} \right) \quad (3)$$

Therefore, a plot of  $i_+$  versus  $V_{acc}^{1/2}$  should yield a straight line whose slope is

$$\frac{A}{4} n_p q \left( \frac{2q}{m} \right)^{1/2} .$$

The positive ion currents, plotted in this manner always yielded a straight line to a break point which was assumed to be the saturation limit. A plot of this type is shown in Fig. 2 (b); the small residual ion current has been subtracted from the experimental points. From this slope we calculate  $n_p = 145 \times 10^{13}/m^3$  in good agreement with the electron concentration of Fig. 2 (a) for the same probe position.

(3) Axial variation of ions and low energy electrons. The observed ion and electron concentrations as a function of axial distance from the cathode are given in Fig. 3 for the probe facing the anode. There is a slight displacement between the maxima for the two distributions and this may reflect a slight penetration of the field from the cathode dark space. However the results show that a true plasma is present in the negative glow, since to a good approximation  $n_e = n_p$ . The secondary electron current was relatively insensitive to position of the probe and gave an average concentration of  $3 \pm 1 \times 10^{13}/m^3$  with electron temperatures in the range of 3.5 - 4.0 eV. The rising portion of the secondary electron curve marks the anode edge of the negative glow. At this point the electric field begins to accelerate thermal electrons to the secondary electron velocities. For example at  $d = 7.2$  cm, the secondaries account for almost 50% of the total electron current.

(4) Residual electron current. Small residual electron currents were observed for all probe positions and orientations. These are summarized in Fig. 4 for pure neon. These minimum currents were constant for a range of -35 to -50 V in grid potential. For grid voltages in excess of -50 V there was a gradual rise in the current, presumably as a result of grid emission by the bombardment of positive ions. We find in Fig. 4 that the residual current decreases exponentially throughout the negative glow with increasing distance from the cathode for both orientations of the probe surface. Additionally, there is a reduction by almost a factor of 5 for the probe facing the anode versus cathode position. We have also observed no variation in the residual current as a function of radial position from the center to a point only 0.6 cm from the wall. The current increases slowly with axial distance in the Faraday dark space ( $d > 5$  cm) and reaches a plateau in the positive column.

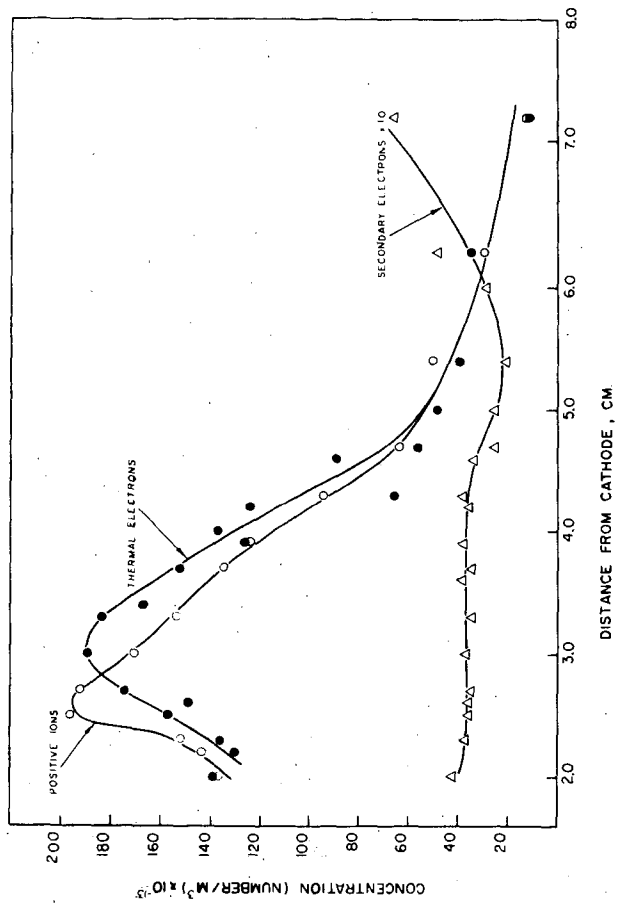


FIG. 3 Distribution of ions and low energy electrons vs. distance between grid and cathode, probe facing anode for pure neon.

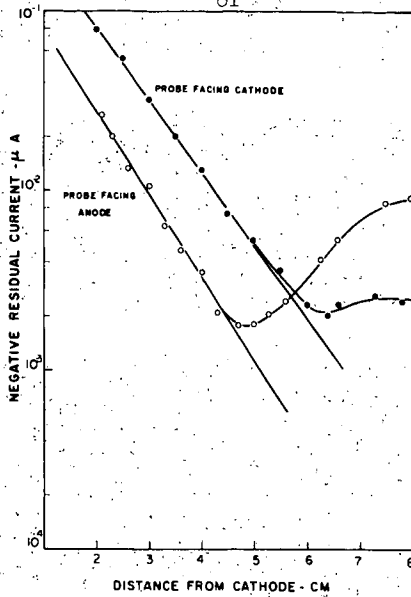


FIG. 4 Variation in residual negative current vs. distance between grid and cathode for pure neon.

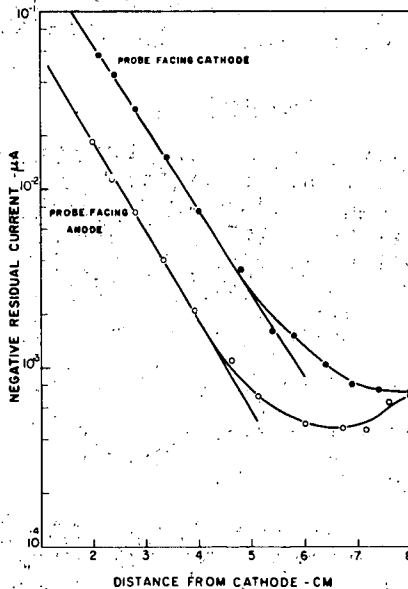


FIG. 5 Variation in residual negative current vs. distance between grid and cathode for 0.07% Xenon in neon.

The effect of adding 0.07% xenon to neon is seen in Fig. 5. The residual current drops and there is a steeper slope to the exponential part of the curve. In addition a smaller increase is observed in the Faraday dark space.

(5) Energy distribution of secondary electrons. From Fig. 2 (a) we see that the energy distribution of secondary electrons is essentially Maxwellian at the indicated position of the probe. However, as the axial distance is increased we find a successively greater loss of electrons whose energies exceed about 10 eV, although the distribution is not radically altered from Maxwellian. The addition of 0.07% xenon results in almost complete depletion of electrons above 12 eV and there are considerable deficiencies beginning only 5 eV above the space potential.

The data are summarized in Fig. 6. The distribution curves for the mixture were calculated from the experimental measurements according to the method of Medicus<sup>8</sup>, and comparison plots of the ideal Maxwellian distribution are given. The two curves in each case were normalized to those regions along the potential axis which gave a straight line on the semi-logarithmic plot. The fluctuations in the curves for the mixture were reproducible and are similar in appearance to the structural features that were observed by Twiddy<sup>9</sup> in the cathode region of rare gas discharges. It is apparent that xenon effectively reduces the higher energy secondary electrons, even at 0.07% concentration. Twiddy<sup>10</sup> has shown that there is a similar loss of energetic electrons in the positive column of an argon-neon mixture.

(6) Residual positive ion current. The ratio of residual currents for  $i_e \text{ min}/i_+ \text{ min}$  was 5:1 with the probe facing the cathode and about 10:1 with the probe facing the anode. These ratios were constant for all axial positions of the probe in the negative glow and in the Faraday dark space. The ratios for the 0.07% xenon-neon mixture were the same as for pure neon.

## DISCUSSION

Since the production of ions and low energy electrons in the negative glow is governed largely by the rate of arrival of high energy electrons from the cathode dark space it is obvious that the direct observation of these high energy electrons offers an important method for interpreting the processes of ionization in the negative glow. A possible means of making such a measurement is to consider the negative residual currents collected by the screened probe when it faces the cathode. These currents could arise from several processes:

- (a) Direct collection of high energy electrons.
- (b) Grid emission by high energy electrons.
- (c) Grid emission by bombardment of positive ions.
- (d) Grid emission by metastable atom impact.
- (e) Grid emission by photon impact.

Rotation of the probe to face the anode caused a 2/3 reduction in the residual current. One would not expect processes (c), (d), and (e) to depend markedly on probe orientation so that these processes probably account for less than 1/3 of the total residual negative current when the probe faces the cathode. Since neither the positive ion density nor the visible photon intensity decays exponentially, processes (c) and (e) are similarly rejected as a major source of current for the anode orientation. We conclude that the major causes of the negative residual current in the negative glow are processes (a) and (b).

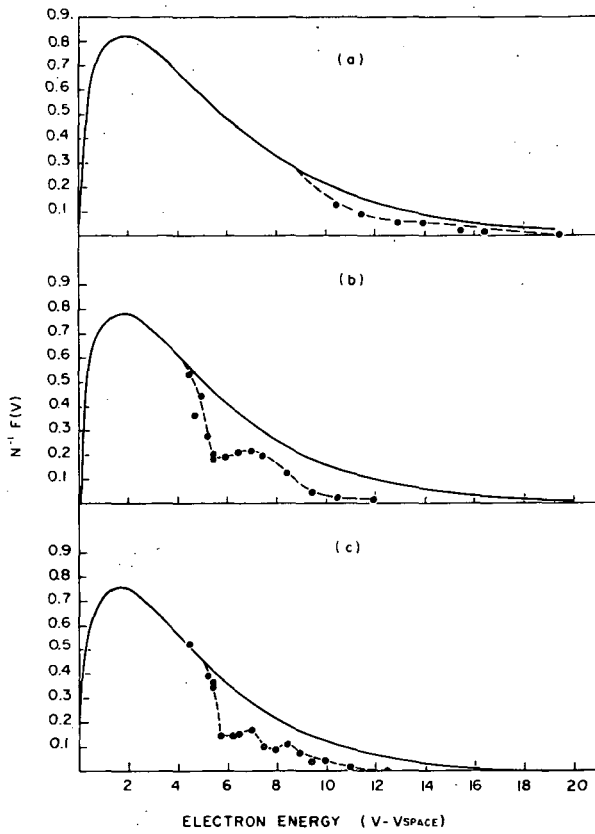


FIG. 6 Energy distribution function of secondary electrons compared with the Maxwellian distribution. (a) pure neon,  $d = 2.3$  cm (b) mixture .07% Xenon in neon,  $d = 2.2$  cm (c) mixture,  $d = 3.0$  cm. Probe facing anode.

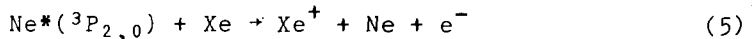
for the probe facing the cathode. We cannot distinguish between (a) and (b), nor is it possible to calculate the density of such high energy electrons without knowledge of their velocities.

The observed exponential decrease in  $i_e$  min through the negative glow of pure neon (Fig. 4) can be written as:

$$i_d = i_0 \exp(-\sigma n(d-d_0)) \quad (4)$$

in which  $i_0$  is the residual current at  $d_0$  cm from the cathode,  $d$  is the distance of the probe surface from  $d_0$  and  $n$  is the concentration of neon atoms per unit volume. Thus  $\sigma$  has the dimensions of  $\text{cm}^2$  and is an experimental cross section for loss of high energy electrons, as a first approximation. From the slope of the exponential curve in Fig. 4 we calculate that  $\sigma = 8.7 \times 10^{-17} \text{ cm}^2$ . This is a reasonable value since the cross section for ionization of neon<sup>11</sup> by 100 eV electrons is  $7.58 \times 10^{-17} \text{ cm}^2$ .

The addition of 0.07% xenon brings about a 30% reduction in the negative residual current and the exponential slope increases so that the experimental  $\sigma = 1.03 \times 10^{-16} \text{ cm}^2$ . This cannot be accounted for by assuming that the only additional loss is that arising from the ionization of xenon. At a concentration of only  $7 \times 10^{-2}$  atom %, this would imply a cross section for ionization of xenon equal to  $228 \times 10^{-16} \text{ cm}^2$  - about a factor of 40 higher than the known  $\sigma_i$  of xenon<sup>11</sup> for 100 eV electrons. A more reasonable inference is that the loss of neon metastables by the Penning reaction:



is responsible for the lower values of  $i_e$  min, and that the change in slope more nearly reflects the actual stopping power of neon for high energy electrons. Since excitation as well as ionization can result from impact of a high energy electron, a cross section of the order of  $1 \times 10^{-16} \text{ cm}^2$  is of the expected magnitude for an electron of approximately 100 eV.

It would be expected that the addition of a small amount of xenon would not significantly change either the cathode fall or the number of directed high energy electrons passing into the negative glow. Thus, if one assumes that the reduction in the residual electron current is caused by reaction (5) it is possible to obtain an approximate value for the concentration of metastables in the beginning of the negative glow.

Referring to Fig. 4, for  $d = 2 \text{ cm}$ ,  $-\Delta i$ , the reduction in the residual current is  $0.02 \mu\text{A}$ . If the neon metastables have thermal velocities, and if one considers a reasonable yield of about 0.03 for the grid emission (geometric factor  $\times$  efficiency), then a minimum concentration of  $1 \times 10^{13}/\text{m}^3$  is obtained for the metastables. It is then possible to calculate the reactive collision frequency between  $\text{Ne}^*$  and  $\text{Xe}$  by assuming the same cross section for deactivation as Sholette and Muschlitz<sup>12</sup> observed for the  $\text{He}^* - \text{Xe}$  Penning reaction, namely  $12 \times 10^{-16} \text{ cm}^2$ . This results in a calculated lifetime for the neon metastables of 0.5 m sec. This is somewhat shorter than the lifetime of 0.875 m sec measured by Blevis et al.<sup>13</sup> for the decay of  $\text{Ne}(^3\text{P}_2)$  in pure neon. We conclude that xenon can intercept the metastable neon atoms in the required time and that our assignment of the Penning reaction is reasonably justified as a major contributing

cause of the reduction in the residual negative current. Similar arguments can be used to account for the decrease in the residual current when the probe faces the anode. The effect is even more marked in this case, particularly at the beginning of the positive column.

The treatment of the positive ion residual current is not as straightforward, since there arises the additional complication of electron impact ionization in the space between the grid and the collector. To a rough approximation we can account for about 60% of the current with the probe facing the cathode by this process, but the remainder can be a combination of secondary emission from the collector by photons, by metastable atoms and by energetic electrons. The very small currents observed for the probe facing the anode suggest that the release of electrons by metastable impact is much less than would be expected for the metastable density obtained above. Apparently the impact of metastables with the platinum surface produces secondary electrons with a much lower efficiency than does the stainless steel grid. The reason is not clear, but a contributing cause may be due to the higher work function of platinum.

#### REFERENCES

- \* N.R.C. No. ...., †N.R.C. Postdoctorate Fellow.
1. R.L.F. Boyd, Proc. Roy. Soc. A201, 329 (1950).
  2. R.L.F. Boyd and N.D. Twiddy, Nature 173, 633 (1954).
  3. D.H. Pringle and W.E.J. Farvis, Proc. Phys. Soc. B68, 836 (1955).
  4. P.F. Knewstubb and A.W. Tickner, J. Chem. Phys. 36, 674 (1962).
  5. P.F. Knewstubb and A.W. Tickner, J. Chem. Phys. 36, 684 (1962).
  6. I. Langmuir and H. Mott-Smith, Jr., G.E. Review 27, 449 (1924).
  7. H. Mott-Smith and I. Langmuir, Phys. Rev. 28, 727 (1956).
  8. G. Medicus, J. Applied Phys. 27, 1242 (1956).
  9. N.D. Twiddy, Proc. Roy. Soc. A262, 379 (1961).
  10. N.D. Twiddy, Proc. Roy. Soc. A275, 338 (1963).
  11. D. Rapp and P. Englander-Golden, J. Chem. Phys. 43, 1464 (1965).
  12. W.P. Sholette and E.E. Muschlitz, Jr., J. Chem. Phys. 36, 3368 (1962).
  13. B.C. Blevis, J.M. Anderson, and R.W. McKay, Can. J. Phys. 35, 941 (1957).

ATTACHMENT OF MOLECULES WITH HIGH PERMANENT AND INDUCED  
DIPOLE MOMENT TO IONS IN GASES

P. Kebarle, G.J. Collins, R.M. Haynes and J. Scarborough

Department of Chemistry, University of Alberta, Edmonton, Canada

## ABSTRACT

The mass spectrometric study of clustered ions in function of polar gas pressure, temperature and electric field strength provides information not only on what ionic species might be present, but also on the strength of the ion-dipole interactions. Studies of the reaction  $H_3O^+ \cdot (n-1)H_2O + H_2O = H_3O^+ \cdot nH_2O$  in a Nier type ion source with a 100 keV proton beam are compared with earlier work on an alpha particle mass spectrometer. The residence time of the ions in the two sources are a few  $\mu$ sec and a few msec resp. Similarity of results shows that clustering equilibrium is established within  $\mu$ sec for water clusters above 0.5 torr. The presence of electric fields reduces the cluster size. 50 Volts/cm (at 1 torr) strip the clusters to  $H_3O^+$ . Experiments on the comparative attachment of different molecules show that the stability of the attachment increases in the order  $H_2O$ ,  $NH_3$ ,  $CH_3OH$ ,  $CH_3NO_2$  for first shell attachment. At larger distances from the ion (second shell) water becomes the strongest attaching. These results are explained by differences of dipole moments and polarizabilities.

## INTRODUCTION

Attachment of polar molecules to ions in the gas phase occurs in a number of systems: gases under high energy irradiation, gas discharges, flames, etc. The polar molecules may be present as an accidental impurity or as a deliberate admixture. The attachment has a number of important effects such as change of mobility, change of reactivity with regard to ion-molecule reactions, change of the positive (negative) ion (electron) recombination coefficient and change in the nature of the products resulting from the positive negative ion recombination. The study of ion-polar molecule interactions in the gas phase can also provide information on ionic solvation since the formation of ion clusters constitutes the first and most important step in the solvation of an ion.

A systematic mass spectrometric study of ion-polar molecule interactions was started in this laboratory some five years ago.<sup>8-12</sup>

The mass spectrometric gas phase studies are based on measurement of the relative concentrations of the clustered ionic species:  $A^+.nS$ ,  $A^+.(n+1)S$ , etc. The measurement of the relative concentrations is obtained by bleeding a probe of the gas into an ion mass analysis system, i.e. a vacuum chamber attached to a mass spectrometer. In the vacuum chamber the gas is pumped out while the ions are captured by electric fields, accelerated and focused and then mass analysed by some conventional means (magnetic separation quadrupole filter, etc.). After mass analysis, the ion beam intensities are detected as electrical currents.

Several types of solvation studies can be undertaken if the relative concentrations of the ionic species are known.

### 1. Solvation Enthalpies and Entropies of Individual Solvent Mole-

ule Additions Steps: Consider the ion  $A^+$  produced in the gas phase by some form of ionizing radiation or thermal means. If the atmosphere surrounding the ion contains the vapor of a polar molecule (solvent S), a number of clustering reactions will occur.



At equilibrium the following relations will hold

$$\Delta F^\circ_{0,n} = \Delta F^\circ_{0,1} + \Delta F^\circ_{1,2} + \dots + \Delta F^\circ_{n-1,n} \quad (I)$$

$$\Delta F^\circ_{n-1,n} = -RT \ln \frac{P_{A^+.nS}}{P_{A^+} \cdot (n-1)S \cdot P_S} = -RT \ln K_{n-1,n} \quad (II)$$

where  $P_x$  is the partial pressure of X.

Thus knowledge of the equilibrium concentrations of the clustered species  $A^+.nS$  obtained from experiments at different pressures of S will allow the determination of  $K_{n-1,n}$  and  $\Delta F_{n-1,n}$ . Such measurements done at different temperatures will lead to the evaluation of  $\Delta H_{n-1,n}$  and  $\Delta S_{n-1,n}$ . The availability of such detailed information will, for instance, reveal the shell structure since a discontinuous change of the  $H_{n-1,n}$  and  $\Delta S_{n-1,n}$  values will occur whenever a shell is completed. Finally, the total heat of solvation of the ion can also be obtained from the expression III, with equations of the same form holding for the

$$\Delta H_{\text{solv}} = \sum_{n=0}^{\infty} [\Delta H_{n-1,n} - \Delta H_{\text{evap}}(S)] \quad (III)$$

free energy and entropy change of solvation.

It is evident from equation II that only the relative concentrations of the ionic species are required. Thus  $\Delta F^\circ_{n-1,n}$  and  $K_p$  can be obtained from equation II by assuming that the mass spectrometrically measured ion intensities are proportional to the equilibrium partial pressures of the ions in the ion source. The solvation of  $\text{NH}_4^+$  by  $\text{NH}_3$ <sup>9</sup> and  $\text{H}_3\text{O}^+$  by  $\text{H}_2\text{O}$ <sup>12</sup> represent examples of studies of this type.

## 2. Comparative Solvation of Two Different Ions by the Same Solvent:

There are three variants of this type of study.

### (a) Comparative solvation of ions $A^+$ , $C^+$ by solvent S.

The two ions are produced in the same system which also contains vapor of the solvent S. In general, depending on the effective radius and structure of the ion, the relative concentration of clusters  $A^+_nS$  will be different from that of  $C^+_mS$ . Thus, for example, in the average  $n$  may be larger by 1 or 2 units than  $m$ . This will reveal a stronger interaction of  $A^+$  with S. Comparison of  $n$  and  $m$  can be done at different temperatures and pressures (of S) so as to compare the interactions in the inner shell or in the outer shells. An example of this type of study is the system  $\text{H}_3\text{O}^+$ ,  $\text{NH}_4^+$  and  $\text{Na}^+$  in  $\text{H}_2\text{O}$  vapor which is described in a forthcoming publication.<sup>13</sup>

### (b) Comparative solvation of ions $A^+$ and $B^-$ by solvent S.

An example of this type of study would be the system  $\text{K}^+$  and  $\text{Cl}^-$  with  $\text{H}_2\text{O}$ . Since the orientation of the water dipoles is reversed in the solvation of positive and negative ions, such a comparative study is of great interest, particularly for isoelectronic pairs as the one quoted above. We have not yet done studies on such isoelectronic pairs. However, such studies are perfectly possible. The pair  $\text{K}^+$  and  $\text{Cl}^-$  could be produced in water vapor. By reversing the mass spectrometer controls, measurements on the positive and negative ions in the system could be done within minutes of each other.

### (c) Comparative solvation of two negative ions by S.

An example of this type of study for the ions  $\text{Cl}^-$ ,  $\text{BCl}^-$ , and  $\text{B}_2\text{Cl}^-$  by  $\text{H}_2\text{O}$  is given in a forthcoming publication.<sup>13</sup>

## 3. Competitive Solvation of Ion $A^+$ (or $B^-$ ) by Solvent Molecules of

Solvents  $S_1$  and  $S_2$ : A comparison of the solvating power of two different solvents can be obtained by measuring the composition of ion clusters when two different solvents are present at known partial pressures. An example of this type of study is the competitive solvation of  $\text{NH}_4^+$  by  $\text{H}_2\text{O}$  and  $\text{NH}_3$  which has been reported on elsewhere.<sup>8</sup> Some more recent studies will be described in the present paper. These concern the competitive solvation of the proton by water and methanol. The water-methanol system is of interest since the dipole moment of water is slightly higher than that of methanol while the polarizability of methanol is considerably larger than that of water. Thus it might be expected that at close range to the central ion methanol might be preferentially solvating.

EXPERIMENTAL

The mass spectrometric study of ion solvent molecule interactions requires mass spectrometric apparatus which can sample ions originating in ion sources at relatively high pressures. Three somewhat different arrangements are presently in use in this laboratory.

1. Alpha particle mass spectrometer<sup>11</sup>

A recent version of this apparatus has been described elsewhere<sup>13</sup> in detail. The gas, supplied from a conventional gas handling system, is irradiated in the ionization chamber. The radiation is supplied from an enclosed 200 mc polonium alpha source. The irradiated gas bleeds through a leak into the evacuated electrode chamber. There the ions carried by the gas are captured by the electric fields while the gas is pumped away. The ions are focused, accelerated and then subjected to mass analysis and electron multiplier detection in a 90° sector field analyzer tube.

2. Electron beam mass spectrometer<sup>6</sup>

In a more recent apparatus an electron beam is used as ionizing medium. The ion source is identical to that used with the alpha source with the exception that the former alpha source port contains only one very thin nickel foil ( $10^{-5}$  inches) window through which the electrons enter the source. The electrons are created by an ordinary electron gun housed in a sidearm of the vacuum chamber opposite the nickel window. The electron filament is kept at some -25000 volts while the ion source is near ground potential. Absence of radioactive contamination, high intensity (~ 10 microamps) and possibilities for pulsing (for determination of ionic lifetimes) are some of the advantages of the electron beam source. A disadvantage is the much greater scattering of electrons at high ion source pressures which makes beam collimation a problem. A quadrupole mass analyzer is used with this instrument.

3. Proton beam mass spectrometer<sup>5</sup>

A 100 kev proton beam obtained from a Walton-Cockroft accelerator is used as ionizing medium. The ion source is not like the previous ones but of the conventional design, i.e. a rectangular box with repeller and narrowed-down ion exit slit. The proton beam enters and exits the ion source through very thin nickel foil windows ( $10^{-5}$  inches). The ion optics are of the conventional Nier type and magnetic analysis is used. A proton beam (preferably of even higher energy than used by us since at energies below 100 kev charge exchange converts appreciable fractions of the proton beam into an H atom beam) seems to be the most convenient ionizing medium for high ion source pressures since it provides high intensity, possibility for pulsing, and little scattering at high pressure. The proton beam can also be deflected electrostatically before entering the ion source. This permits variation of the proton beam - exit slit distance in the ion source. The cost of Walton-Cockroft accelerators is relatively low.

A high pressure mass spectrometer using Mev protons from a Van de Graaff accelerator has been described by Wexler.<sup>15</sup>

## RESULTS AND DISCUSSION

1. Competitive solvation of  $\text{CH}_3\text{OH}_2^+$  by water and methanol

A study of the ions in methanol vapor in the pressure range 1-10 torr showed that most of the ions belonged to the series  $\text{CH}_3\text{OH}_2^+ \cdot n\text{CH}_3\text{OH}$ . This suggested the possibility of observing the competitive solvation of  $\text{CH}_3\text{OH}_2^+$  by water and methanol molecules. Figure 2 shows the relative intensities of the mixed clusters obtained when irradiating mixtures of 5% methanol: 95% water and 20% methanol: 80% water, both at 5 torr total pressure and 50°C ion source temperature. In the mixed methanol-water clusters the question of the structural assignment arises. Thus the ion of mass 119 could be assigned as  $\text{H}^+ \cdot 2\text{CH}_3\text{OH} \cdot 3\text{H}_2\text{O}$  or  $\text{CH}_3\text{OH}_2^+ \cdot \text{CH}_3\text{OH} \cdot 3\text{H}_2\text{O}$  or  $\text{H}_3\text{O}^+ \cdot 2\text{CH}_3\text{OH} \cdot 2\text{H}_2\text{O}$ . We have selected the notation  $\text{CH}_3\text{OH}_2^+ \cdot \text{CH}_3\text{OH} \cdot 3\text{H}_2\text{O}$  (or  $\text{CH}_3\text{OH}_2^+ \cdot m\text{M} \cdot w\text{W}$ , for the general cluster where M and W stand for  $\text{CH}_3\text{OH}$  and  $\text{H}_2\text{O}$  and m and w for the number of methanol and water molecules). The proton was assigned to the methanol oxygen ion since the proton affinity of methanol is some 10-20 kcal/mole<sup>13</sup> higher than that of water. This assignment is also consistent with the observation that even in mixtures where water predominates, i.e. 5% methanol, the pure hydrate  $\text{H}_3\text{O}^+ \cdot w\text{W}$  was not observed, while the pure methanol cluster  $\text{CH}_3\text{OH}_2^+ \cdot m\text{M}$  was observed.

The clusters obtained with 5% methanol (Figure 1) contain, on the average, considerably more methanol than water even though the partial pressure ratio of water to methanol is 19:1. Thus methanol is the stronger solvent in the observed clusters, i.e. clusters containing up to six solvent molecules. We shall be able to understand the meaning of this result better after a more detailed treatment of the data. It can be shown that the distribution of water and methanol in the observed clusters follows quite closely a probability distribution. Calling the probabilities for inclusion of water and methanol  $\omega$  and  $\mu$ , for a cluster with a total of  $\ell$  solvent molecules the probability distribution will be given by the binomial expansion of the term  $(\omega + \mu)^\ell$ . For example if a probability distribution is followed, the cluster containing three solvating molecules  $\text{CH}_3\text{OH}_2^+ \cdot m\text{M} \cdot w\text{W}$ , where  $\ell = m + w = 3$ , should show the following relative intensities:  $\text{CH}_3\text{OH}_2^+ \cdot 3\text{W} : \text{CH}_3\text{OH}_2^+ \cdot 2\text{W} \cdot \text{M} : \text{CH}_3\text{OH}_2^+ \cdot \text{M} \cdot 2\text{W} : \text{CH}_3\text{OH}_2^+ \cdot 3\text{M} = \omega^3 : 3\omega^2\mu : 3\omega\mu^2 : \mu^3$ . We have obtained values for  $\omega$  and  $\mu$  by fitting binomial expansions to the experimentally observed distribution. The calculated intensities shown in Figure 2 demonstrate that a relatively good fit of the experimental data can be obtained. In order to express the preference for inclusion of methanol and water per unit methanol and water pressure we define  $\gamma = (\mu/P_M)/(\omega/P_W)$  as the factor for preferential take up of methanol,  $P_M$  and  $P_W$  being the partial pressures of methanol and water present in the ion source. The  $\gamma$ 's calculated in this manner are given in Figure 1. The results at 5 and 20% methanol show that the  $\gamma$ 's for a cluster of a fixed size (i.e.  $\ell = \text{const}$ ) are approximately independent of the methanol-water pressure ratio. This independence was confirmed in a number of other runs with 2, 4, 5, 8, 20, 50% methanol at 2 and 5 torr total pressure. The  $\gamma$ 's are found to decrease as  $\ell$  increases. Thus methanol is taken up preferentially by a factor of 55, 21 and 8 for clusters containing 3, 4 and 5 solvent molecules. Figure 2 shows a log  $\gamma$  plot versus the number of solvating molecules. The plot is almost linear and allows an extrapolation to log  $\gamma = 0$  or  $\gamma = 1$ . This occurs when the cluster contains seven solvating molecules. For  $\ell > 7$ ,  $\gamma$  becomes less than unity, i.e. water begins to take precedence. Figure 2 also shows results obtained with the proton beam mass spectrometer. The total pressure in these runs was much lower (0.6 torr) and the reaction time much shorter (a few microseconds versus a few milliseconds in the alpha particle ion source).

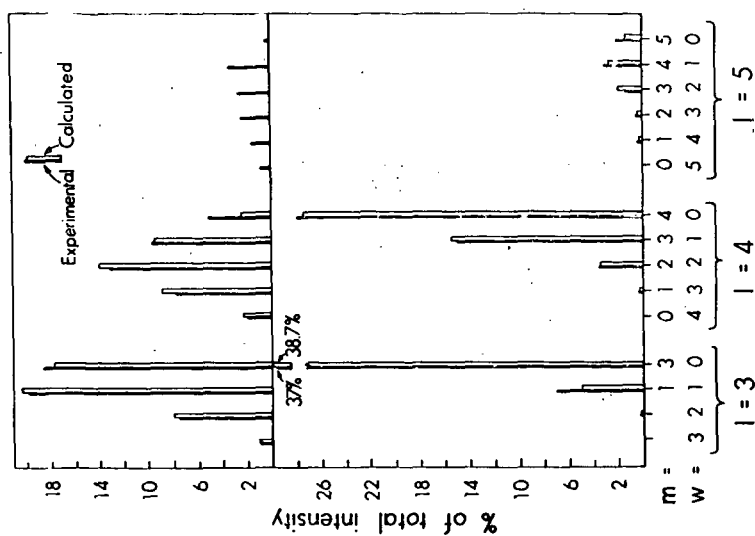


Figure 1 Mixed water and methanol content in  $\text{CH}_3\text{OH}_2^+ \cdot m\text{CH}_3\text{OH} \cdot w\text{H}_2\text{O}$  clusters. Ion source temperature  $50^\circ\text{C}$ .

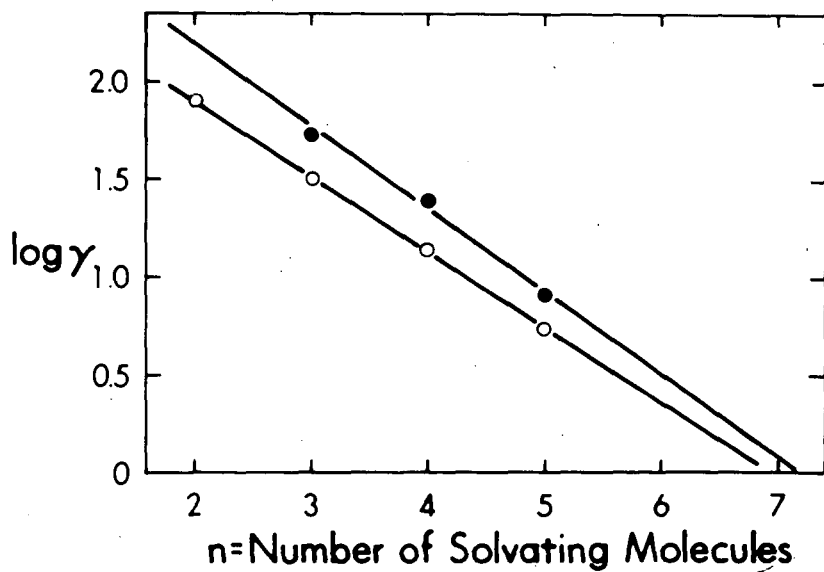


Figure 2 Plot of  $\log \gamma$  versus number of solvating molecules.

$\gamma$  is factor for preferential take up of methanol over water into ion  $\text{CH}_3\text{OH}_2^+ \cdot m\text{CH}_3\text{OH} \cdot w\text{H}_2\text{O}$ , where  $m + w = n$ .

One might suspect that under these conditions clustering equilibrium might not be achieved. However the results are, on the whole, quite similar to those obtained with the alpha ion source. This might be taken to mean that clustering equilibrium establishes very rapidly and that the proton beam results approach equilibrium.

In the interpretation of the present results considerable help can be obtained from the "electrostatic theory" for metal-ion coordination complexes.<sup>2</sup> It is recalled that this theory, using simple electrostatic concepts, allows the calculation of the binding energies of metal complexes in the gas phase and that the results of such calculations have been in many cases very successful. In general, the potential energy of a complex ion is built up of four terms. These are due to the attraction between the ion and the permanent and induced dipole of the ligands, the mutual repulsion of the dipoles, the energy required to form the induced dipoles and the van der Waals repulsions between the ligands and the central ion. Comparing the potential energies of an ion having water or methanol molecules as ligands, it is found that the first term is the decisive one. The first term contains the sum of the permanent dipole and the polarizability. The dipole moments of water and methanol are 1.85 and 1.69 D while the polarizabilities are 1.48 and 3.23 Å.<sup>3</sup> The potential energy of an ion dipole interaction varies inversely with the square of the distance while the polarizability interaction depends on the fourth power. It follows that the methanol molecules with their slightly lower dipole but considerably higher polarizability will be more strongly solvating than water at close range to the ion. The experimentally observed preference for methanol is thus to be understood as resulting from the higher methanol polarizability.

It can be shown that the possibility of fitting the observed clusters with a given  $\ell$  by a probability distribution suggests that for  $\ell < 6$  all solvent molecules belong to an inner solvation shell. Suppose that for  $\ell = 5$  some of the molecules went into an inner shell (fully occupied) and the rest into an outer shell. The preference for methanol over water in the inner shell will be very different from that in the outer shell. It might even be expected that water will be preferentially taken up in the outer shell. It follows that the water-methanol distribution in a cluster containing inner and outer shell molecules could not be fitted by a single probability distribution of the type  $(\omega + \mu)^\ell$  but that the inner and outer shell would have to be fitted separately. Such a case is in fact observed in the competitive solvation of  $\text{NH}_4^+$  by  $\text{H}_2\text{O}$  and  $\text{NH}_3$  which was studied earlier.<sup>12</sup> Since the water-methanol clusters of  $\ell = 3, 4, 5$  can each be fitted with a probability distribution we can conclude that these clusters do not contain molecules which occupy a distinct outer shell, i.e. that the inner shell contains at least five solvent molecules.

The ability to fit a cluster of constant  $\ell$  with a probability distribution is, to a certain extent, surprising even if all molecules belong to the same solvation shell. A probability distribution means, for example, that in the five cluster the preference for methanol over water is the same whether all the remaining four ligands are water or methanol or a mixture of them. Obviously this can not be strictly true. The meaning of the experimental result must be that the nature of the other occupants is, in the first approximation, not important.

While  $\gamma$  remains approximately constant for a cluster distribution with  $\ell = \text{const}$ , it was observed that  $\gamma_{\ell=\text{const}}$  decreases from  $\ell = 3$  to  $\ell = 5$ . This can be understood if one assumes that whenever  $\ell$  is increased by one unit the effective radius of the (inner) shell increases. This causes the polarizability to become less important and leads to a decrease of the preference for methanol. An increase of the effective

radius might be expected because of the mutual repulsion due to dipole and van der Waals' forces between the ligands.

Experiments on the competitive solvation of  $\text{CH}_3\text{NO}_2$  and  $\text{H}_2\text{O}$  have also been made but this work is not yet completed. The available results show that  $\text{CH}_3\text{NO}_2$  is taken up preferentially at close range of the central ion ( $\text{NH}_4^+$  and  $\text{H}_3\text{O}^+$  gave similar results). Thus at room temperature the preference factor is  $\sim 200$  for three ligands, 60 for four ligands, 40 for five, etc. The results also seemed to show that nitromethane is always taken up preferentially in an incomplete shell (inner or outer) but that it is ultimately expelled from inner shells.

## 2. Effect of electric fields on cluster size

One may expect that the presence of electric fields will lead to a decrease of the average cluster size. This effect is illustrated in Figure 3. The data were obtained with the proton beam mass spectrometer which has a Nier type ion source, i.e. ion exit slit and repeller. The distance from proton beam to ion exit slit was  $\approx 0.4$  cm.  $E_r$  is the repeller field strength. In preliminary experiments at very low repeller fields it could be shown that at  $\text{H}_2\text{O}$  pressures higher than about 0.3 torr the cluster composition obtained with the proton mass spectrometer was very similar to that obtained with the alpha particle instrument. Since the estimated ion residence times are  $\sim 10$  micron for the proton mass spectrometer and  $\sim 1$  millisecon for the alpha instrument these results were taken to mean that in both instruments clustering equilibrium or near equilibrium is achieved. Figure 3 shows that increase of the electric field decreases the cluster size. This is a gradual process as shown by the succession of maxima. The maximum composition shifting successively from four water to zero water content of the  $\text{H}_3\text{O}^+$  ion. Possibly plots of the type given in Figure 3 could be used for determination of the enthalpy of attachment, i.e.  $\Delta H_{n-1,n}$ .

### LITERATURE CITED

1. A.P. Altshuller, J. Am. Chem. Soc. 77, 3480 (1955).
2. F. Basolo and R.G. Pearson, Mechanisms of Inorganic Reactions, p.64 (John Wiley & Sons, New York, 1958).
3. R.P. Bell, The Proton in Chemistry (Cornell University Press, Ithaca, New York, 1959).
4. M. Born, Z. Physik, 1, 45 (1920).
5. G.J. Collins and P. Kebarle, to be published.
6. D.A. Durden and P. Kebarle, to be published.
7. W.J. Hamer (Edit.) "The Structure of Electrolytic Solutions" Chapter 5 (John Wiley & Sons, New York, 1959).
8. A.M. Hogg and P. Kebarle, J. Chem. Phys. 43, 449 (1965).
9. A.M. Hogg, R.M. Haynes and P. Kebarle, J. Am. Chem. Soc. 80, 28 (1965).
10. P. Kebarle and E.W. Godbole, J. Chem. Phys. 39, 1131 (1963).
11. P. Kebarle, R.M. Haynes and S.K. Searles, Advances in Chemistry, 58, 210 (1966).
12. P. Kebarle and A.M. Hogg, J. Chem. Phys. 42, 798 (1965).
13. P. Kebarle, Advances in Chemistry: Applications of Mass Spectrometry to Inorganic Chemistry (to be published) (American Chemical Society).
14. M.S.B. Munson, J. Am. Chem. Soc. 87, 2332 (1965).
15. S. Wexler, Advances in Chemistry, 58, 193 (1966).

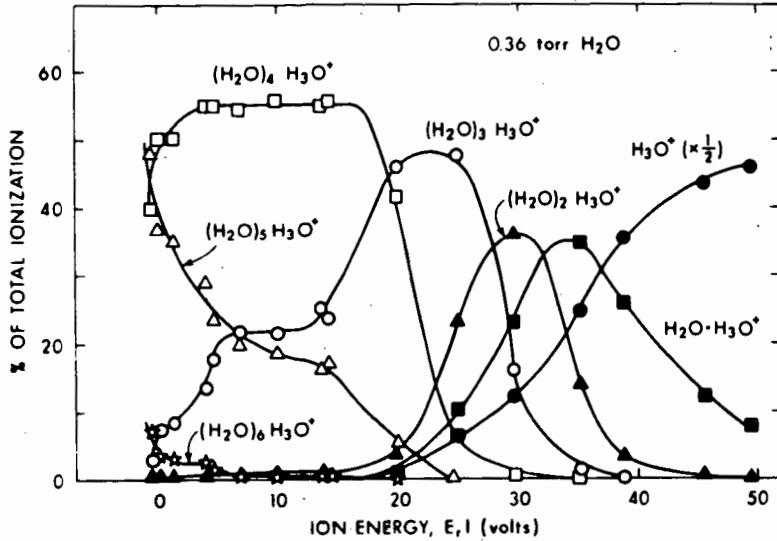


Figure 3 Effect of electric field on cluster composition.  $E_{rl}$  equals voltage between repeller and ion source exit slit. Temperature of ion source 30°C. Water pressure 0.36 torr. Experiments taken with 100 keV proton beam mass spectrometer.

D. F. Munro, J. E. Ahnell, and W. S. Koski

Department of Chemistry, The Johns Hopkins University, Baltimore, Maryland 21218

## Abstract

Questions of the role of negative boron hydride ions frequently arise in problems concerning energetics of electron impact processes, discharge tube reactions, and radiation chemistry. In view of the fact that the boron hydrides are electron deficient compounds, it might be expected that they are more prone to negative ion formation than hydrocarbons; however, very few studies of such ions have appeared in the literature. This paper gives some qualitative results obtained on boron hydride negative ions produced by electron bombardment of diborane, tetraborane, and pentaborane-9. A pulsed electron beam, a quadrupole mass analyzer, and an electron multiplier were used for this work. In diborane, the most intense ions observed were  $B_2H_3^-$  and  $BH_4^-$ . Lower and varying intensities of  $B_2H_4^-$ ,  $B_2H_3^-$ ,  $B_2H_2^-$ ,  $B_2H^-$ ,  $B_2^-$ ,  $BH_3^-$ ,  $BH_2^-$ ,  $BH^-$ , and  $B^-$  were also readily detectable. Similarly, the negative ions observed in tetraborane included the relatively high intensity  $B_3H_7^-$  and lower intensities of  $B_2H_5^-$ ,  $B_2H_4^-$ ,  $BH_4^-$ , etc. In addition, indications were obtained for  $B_4H_9^-$ . Similar results were obtained with pentaborane-9.

## Introduction

For many years, mass spectroscopists have dealt almost exclusively with processes involving positive ions; ionization, fragmentation, and ion-molecule reactions. Recently, however, despite problems of low intensity, an increasing amount of work has been done on negative ions. A number of species have been characterized,<sup>1</sup> and a few reactions have been studied.<sup>2,3</sup> In addition, at least one investigation on the role of negative ions in flames has been carried out, using mass spectroscopic techniques.<sup>4</sup>

The boron hydrides are traditionally classified among the electron deficient compounds, and might well be expected to form negative ions. Furthermore, some work has been done with the boron hydrides in gaseous discharges and in radiation chemistry where these ions might conceivably play a role.<sup>5</sup> Thus, it was of interest to us to study the negative ions of the boron hydrides with the eventual hope of providing information to permit the evaluation of the role these ions might play in discharges and other associated phenomena.

We have under construction in our laboratory a tandem mass spectrometer for the study of ion-molecule reactions. In the course of testing the first stage of the instrument, it became apparent that the spectrometer might be suited for the observation of negative ions. The ions from  $SF_6$  and  $O_2$  were detected with relative ease. It was decided to investigate what negative ions could be observed in the simpler boron hydrides; diborane, tetraborane, and pentaborane.

Because the spectrometer is still in the construction stage, some of the refinements normally found on conventional instruments are lacking, so that the results obtained are necessarily of a qualitative nature. Nevertheless, it was felt that the observations were sufficiently interesting to warrant reporting.

## Experimental

The important features of the basic experimental arrangement are shown diagrammatically in Fig. 1. The gas to be analyzed flows from a bulb at room temperature into the ion source through a Granville-Phillips leak. The ion source, which is similar in design to one described by Von Zahn,<sup>6</sup> has an electron beam energy

variable from 0 - 100 volts. There are no provisions for measuring pressure, temperature, or ionizing current in the ion source. The ions are focused and accelerated to 50 - 100 volts, and mass analyzed by a quadrupole mass filter with a length of 10.0 inches and an  $r_0$  of 0.27 inches. Mass scanning is accomplished by varying the RF and DC voltages to the quadrupole. The resolution of the quadrupole is electronically variable. The ions are then accelerated to 600 volts and detected by a Bendix Channeltron continuous electron multiplier.

Because of the absence of slits in the mass spectrometer, the relatively open nature of the ion source, and the high sensitivity of the detector, it is necessary to reduce the background from scattered electrons reaching the detector. This is accomplished in two ways: first, by establishing a weak magnetic field to deflect the electrons but not the ions; and second, by pulsing the electron beam. The ionizing beam is pulsed at 10 kc by applying a 40 volt pulse to the first lens of the electron beam. The beam "on" time is 10 microseconds. After a delay of 5 microseconds, the second pulser sends a one volt pulse to turn on the transistorized "AND" gate for 20 - 30 microseconds. Only those pulses which arrive at the gate during this interval are sent on to the ratemeter. At the voltages used, most of the electrons arrive at the detector within one or two microseconds; the flight time of the negative ions, however, is of the order of 10 - 20 microseconds. Thus, the signal to the ratemeter is primarily due to ions, with a drastic reduction in the electron background. The output of the ratemeter is plotted versus the DC voltage on the quadrupole with an XY recorder. A signal of five ions per second can readily be observed. A typical plot, shown in Fig. 2, is the lower portion of the mass spectrum of the negative ions of pentaborane.

All the boron hydride samples were purified by distillation in a vacuum system. The diborane was trapped out at  $-154^\circ\text{C}$ . The tetraborane was purified in three steps: pumping off hydrogen and diborane while trapped at  $-130$ , passing through a trap at  $-95$  to condense the pentaborane and the higher boron hydrides, and finally condensing at  $-196$ . The pentaborane was similarly purified: pumping off diborane and tetraborane at  $-98$ , passing through a trap at  $-79$ , and final trapping at  $-196$ .

#### Results and Discussion

The results are shown in the bar graph in Fig. 3. The narrow bars represent peaks which have been multiplied by a factor of ten. All measurements are for 70 volt ionizing electrons. The monoisotopic mass spectrum was computed assuming the natural  $B_{10}/B_{11}$  distribution of 20/80, and also assuming that there was no isotope effect in loss of hydrogen from  $B_{10}$  versus  $B_{11}$ . In nearly all cases, the peak heights from which the monoisotopic spectra were calculated were an average of at least three measurements, with separate measurements in agreement within 10%. In calculating the monoisotopic spectrum, the system is "over-determined," i.e., there are more equations than there are unknowns. This provides a means of checking the internal consistency of the results. For every case except two, the self-consistency deviation was less than 2%, and in all cases less than 10%. On the basis of these considerations, relative intensities within a group of peaks, e.g.,  $B_5H_9$ ,  $B_5H_8^-$ ,  $B_5H_7^-$ , etc., should be accurate to  $\pm 10\%$ . In comparing peaks between different groups, however, it is more difficult to assign limits of error, for the spectrometer may favor the observation of low masses over high masses in certain cases. One can observe this "discrimination" in the positive ion spectra, and it appears to be primarily a function of the resolution of the quadrupole. It is possible, however, that the continuous electron multiplier and the ion source also mass discriminate, perhaps differently for positive and negative ions. Since the signal from the multiplier is analyzed as pulses rather than current, mass discrimination by the detector should be minimized. The exit holes in our ion source are rather large, and it would be expected that discrimination here would also be negligible. Thus, if it is assumed that the discrimination effects are the same

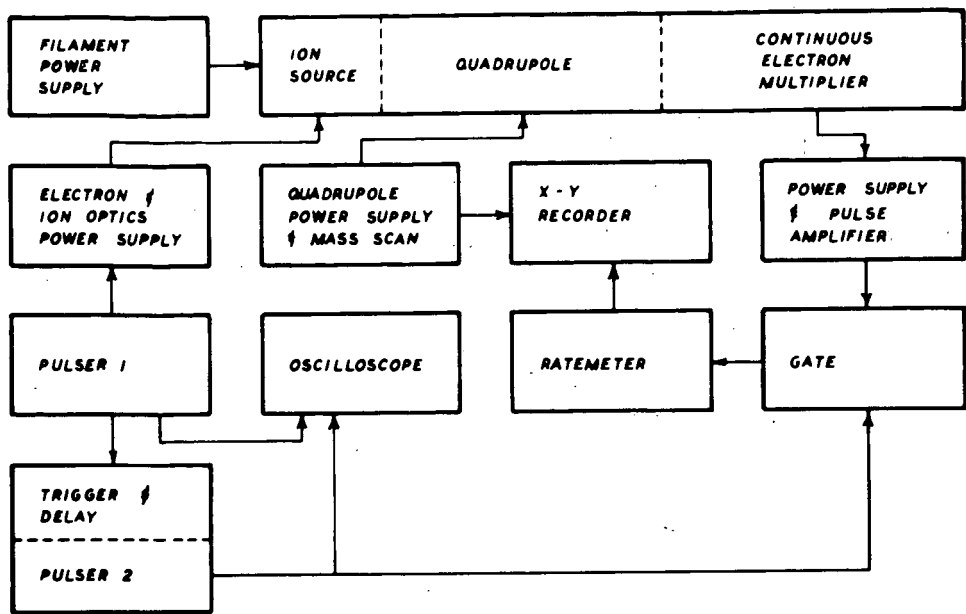


FIGURE 1

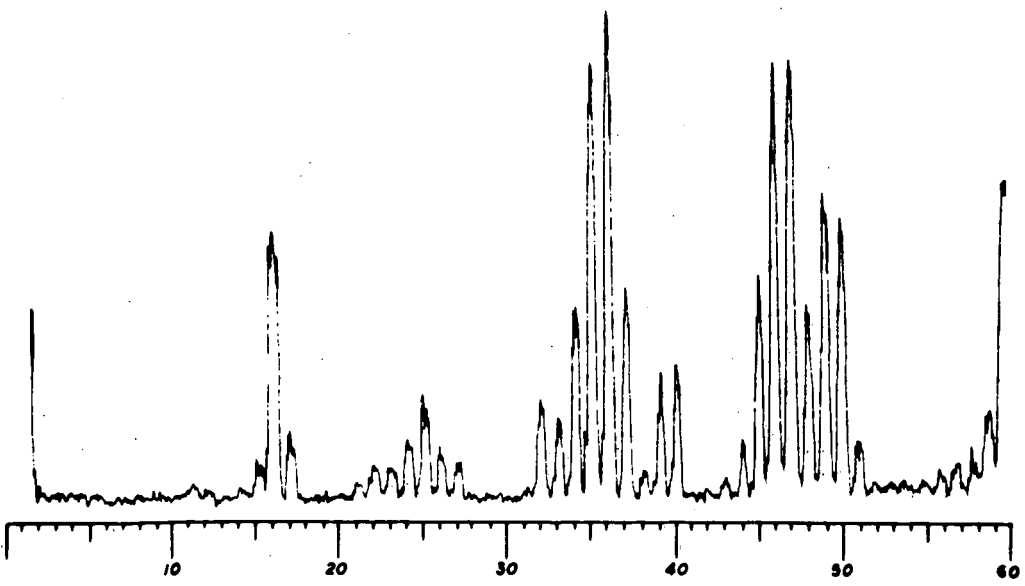


FIGURE 2

NEGATIVE IONS OF BORON HYDRIDES  
MONOISOTOPIC RELATIVE INTENSITIES

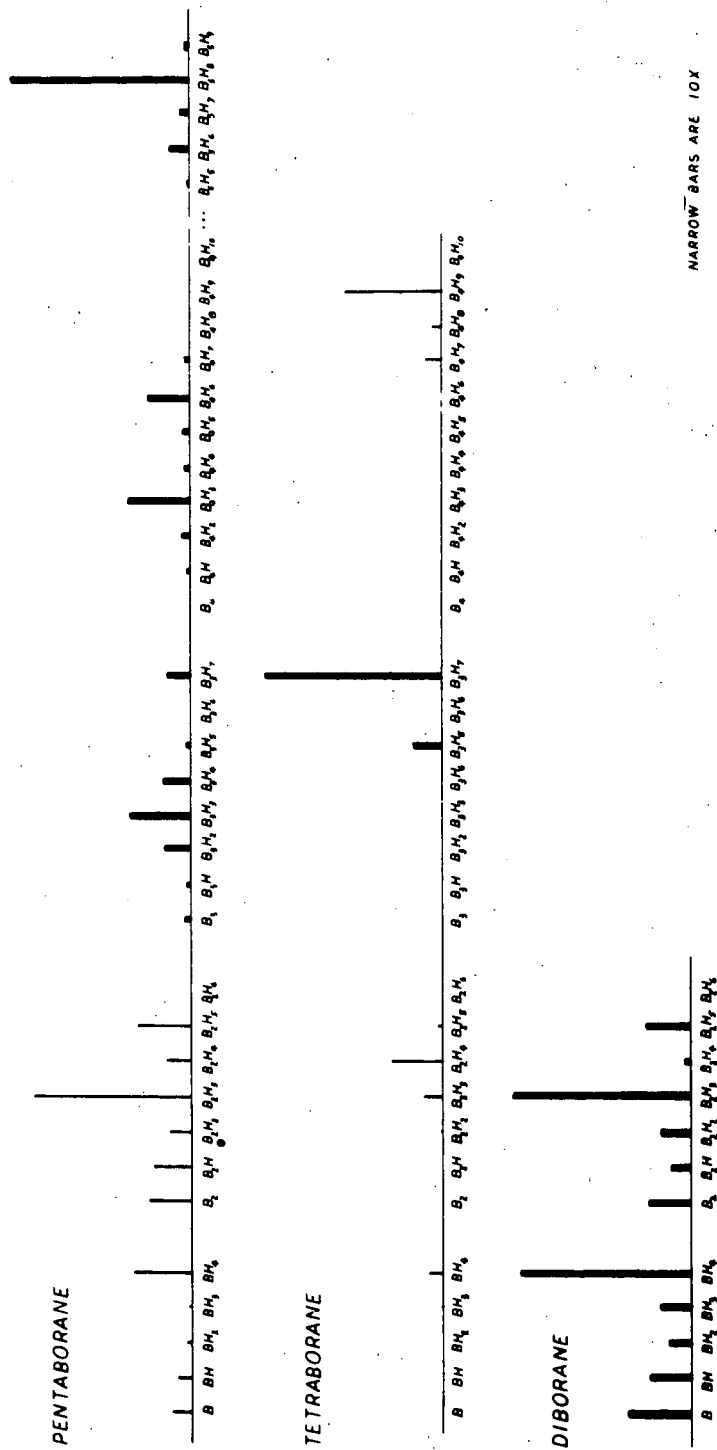


FIGURE 3

for positive and negative ions, approximate corrections can be made. At worst, the relative intensities throughout the whole spectra are probably correct within  $\pm 25\%$ .

Although reasonable precautions were taken to assure the purity of the sample in the diborane spectrum, peaks corresponding to  $B_3H_7^-$  and  $B_4H_9^-$  were observed. These could have arisen either from ion-molecule reactions, from pyrolysis of the diborane as the sample flowed into the source, or from impurities in the diborane. The latter is improbable, for in a positive ion spectrum of the same sample in the same spectrometer, the tetraborane peaks could be observed only with difficulty. It was estimated on the basis of the positive ion spectrum that the tetraborane impurity could be no greater than one part in five hundred. In the negative ion spectrum the peaks corresponding to  $B_3H_7^-$  and  $B_2H_3^-$  were of almost equal intensity. It should be noted, however, that in comparing the diborane and tetraborane samples, it was much easier to observe the negative ion peaks from tetraborane, which were larger by about two orders of magnitude.

There are several mechanisms by which negative ions can be formed. The traditional processes are as follows:

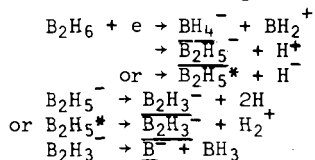
1. Ion pair formation:  $XY + e \rightarrow X^+ + Y^- + e$
2. Resonance attachment:  $XY + e \rightarrow XY^-$
3. Resonance attachment with dissociation:  $XY + e \rightarrow X + Y^-$

In addition, a process somewhat like the third mentioned above can be imagined, in which the neutral species is left in an excited state which in turn decays to an ion pair. Also, a negative ion may fragment, giving rise to a neutral species and a new negative ion.

4. Excited state decay:  $XYZ + e \rightarrow XY^* + Z^-$   
 $XY^* \rightarrow X^+ + Y^-$
5. Fragmentation:  $XY^- \rightarrow X + Y^-$

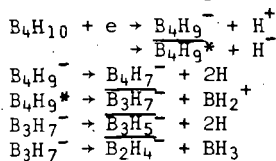
Using the above scheme, and assuming that the fragments most easily lost are  $BH_2^+$ ,  $BH_3$ , and hydrogens, most of the more intense peaks in the negative ion boron hydride spectra can be accounted for rather well in the following manner.

#### Possible Modes of Fragmentation of Diborane



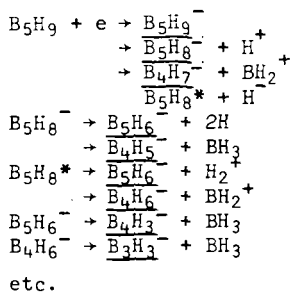
The underlined peaks are the four most intense in the diborane mass spectrum. The other peaks come from loss of hydrogens, either singly or in pairs, from the above species.

#### Possible Modes of Fragmentation of Tetraborane



This scheme accounts for all of the peaks with an observed intensity of greater than 1%, except for the  $B_2H_3$  peak, whose intensity is 1.1%, and which could be due to a diborane impurity.

## Possible Modes of Fragmentation of Pentaborane



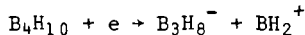
In support of the above mechanism, the data in Table 1 can be cited.

	Diborane <sup>7</sup>	Tetraborane <sup>8</sup>	Pentaborane <sup>9</sup>
$\text{BH}_2^+$	19.1	7.0	12.2
$\text{BH}_3^+$	.59	.6	--

(These ion intensities were obtained with 70 volt electrons, and are given in percent relative to the most intense peak in the mass spectrum for the compound in question.)

Thus, it can be argued that the loss of  $\text{BH}_2^+$  is much more likely than the loss of  $\text{BH}_3^+$ . The loss of  $\text{BH}_3$ , however, at least from neutral species, is fairly well established in a number of reactions.<sup>10</sup> It should not be too surprising if  $\text{BH}_3$  can also be readily fragmented from negative ions.

It is tempting to question the necessity of invoking the excited state decay process (4) described above. For example, can the formation of the  $\text{B}_3\text{H}_7^-$  not be simply written as a resonant attachment process with the dissociation of  $\text{BH}_3$ ? Although this is certainly possible, one or two points argue against this mechanism. First, at the electron energies used, a resonant process of this type would not be expected to be of primary importance. Secondly, one might inquire why the pair ionization process,



is not observed, especially in view of the fact that the analogous process seems to be the predominant one in diborane. Indeed, the pair ionization process is the one which is expected; it is disturbing that it is not seen in view of the stability of  $\text{B}_3\text{H}_8^-$  in solution and in the solid phase. The structure of  $\text{B}_3\text{H}_8^-$  is known from x-ray work, and there is ample theoretical and experimental justification for its existence.<sup>11</sup> On the other hand, we have found no evidence in the literature for  $\text{B}_3\text{H}_7^-$ . The question arises as to whether an error can be made in the mass assignments. The marker compounds used were  $\text{O}_2$  and  $\text{H}_2\text{O}$ , giving rise to the  $\text{O}_2^-$ ,  $\text{OH}^-$ , and  $\text{O}^-$  peaks, which were always present in the background. Considerable care was taken in making the mass assignments, so that unless some unknown instrumental or chemical processes were occurring of which we are unaware, the given assignments are correct. Therefore, granting that the reported observations are valid, and accepting the notion that pair ionization should be the dominant process at higher electron energies, and further noting that the  $\text{BH}_2^+$  ion is much more predominant than the  $\text{BH}_3^+$  in the positive ion spectrum, it seems necessary to invoke some mechanism analogous to (4). Perhaps further weight can be given to this argument by noting that the parent peak is not observed in tetraborane, suggesting that a loss of hydrogen is a strongly favored process in the electron impact situation.

The present work suggests several further experiments which should be carried

out to answer some of the questions which have been raised here. An investigation of metastable negative ions on a magnetic sector instrument should prove useful in confirming or negating the fragmentation scheme postulated above. A careful study of the diborane spectrum, either in a tandem instrument, or with an ion source in which one could be sure that pyrolysis is not taking place would be necessary to remove the ambiguity in the observation of tetraborane—in the diborane sample; whether the peaks above diborane are due to impurities, or whether they do in fact result from ion-molecule reactions. Perhaps most useful initially would be an investigation of the boron hydride spectra at low electron energies, where resonance attachment becomes the dominant process. Ideally, one should study the spectra as a function of energy; the clastogram technique<sup>12</sup> might prove valuable in sorting out the various processes occurring. We made some attempt to work at low electron energies, but largely without success. Since we are unable to measure the ionizing current, i.e., keep it constant as a function of energy, we would have little confidence in an appearance potential measurement, particularly since the background from electrons again becomes a problem at low electron energies, when they can be pushed out of the ionization chamber by the repeller.

Reese, Dibeler, and Mohler have reported on the spectrum of pentaborane, in which they observed the resonant attachment process in the parent ion.<sup>13</sup> Although their relative intensities are different from those which we observed, this is probably not surprising, in view of the different energies of the ionizing electrons in the two cases. Curiously, however, Dibeler does not report any of the lower fragments for pentaborane.

In conclusion, it is evident that the lower boron hydrides do form negative ions. In certain circumstances, the abundance of these ions may be great enough so that they would have to be taken into consideration in mass spectral, radiation, or gaseous discharge phenomena. It is also clear, however, that more than a mere qualitative study of these negative ions will be necessary for the complete understanding of their roles in these situations.

Acknowledgment— This work was done under the auspices of the United States Atomic Energy Commission.

#### Figure Captions

- Fig. 1. Block diagram of the mass spectrometer.  
 Fig. 2. Lower portion of the mass spectrum of the negative ions from pentaborane.  
 Fig. 3. The monoisotopic relative abundances for the negative ions from diborane, tetraborane, and pentaborane.

#### References

1. F. Fiquet-Fayard, *Actions Chimiques et Biologiques des Radiations* II, p. 44 (1965).
2. J. F. Paulson, *Ion Molecule Reactions in the Gas Phase*, p. 28, American Chemical Society Publications (1966).
3. G. Jacobs and A. Henglein, *Advances in Mass Spectroscopy* 3, p. 28, The Institute of Petroleum (1966).
4. M. F. Calcote and D. E. Jensen, *Ion Molecule Reactions in the Gas Phase*, p. 291, American Chemical Society Publications (1966).
5. V. V. Subbanna, L. H. Hall, and W. S. Koski, *J. Am. Chem. Soc.* 86, 1304 (1964).
6. V. Von Zahn, *Rev. Sci. Inst.* 34, 1 (1963).
7. NBS No. 333 Mass Spectra Data, American Petroleum Institute Project 44 (1949).
8. T. P. Fehlner and W. S. Koski, *J. Am. Chem. Soc.* 85, 1905 (1963).
9. NBS No. 334 Mass Spectra Data, American Petroleum Institute Project 44 (1949).
10. T. P. Fehlner and W. S. Koski, *J. Am. Chem. Soc.*, 86, 2733 (1964).
11. W. N. Lipscomb, *Boron Hydrides*, W. A. Benjamin, Inc. (1963).

12. R. W. Kiser, Introduction to Mass Spectrometry and Its Applications, p. 191, Prentice-Hall, Inc. (1965).
13. R. M. Reese, V. H. Dibeler, and F. L. Mohler, J. Research NBS 57, 367 (1956).

## INTERACTIONS OF EXCITED SPECIES AND ATOMS IN DISCHARGES\*\*

Robert A. Young\* and Gilbert A. St. John

Stanford Research Institute  
Menlo Park, California

## ABSTRACT

The influence of atomic nitrogen on the concentration of  $N_2(A^3\Sigma_u^+)$  excited in nitrogen by a weak discharge has been studied. It was found that (1) a high-order process involving atomic nitrogen destroys  $N_2(A^3\Sigma_u^+)$ , (2) a process utilizing species, other than atomic nitrogen, created in the discharge removes  $N_2(A^3\Sigma_u^+)$ , and (3) a process involving atomic nitrogen and another excited species produces  $N_2(A^3\Sigma_u^+)$ .

It was also found that NO rapidly quenches  $N_2(A^3\Sigma_u^+)$  with a rate coefficient of  $3 \times 10^{-11}$  cm<sup>3</sup>/sec. A quarter of the  $N_2(A^3\Sigma_u^+)$  destroyed excites NO to the  $A^2\Sigma^+ v' = 0$  level.

## INTRODUCTION

Nitrogen subjected to an electrical discharge at low pressure has been a subject of study for over 70 years. In general, phenomena occurring in the discharge itself have been studied in static systems, while phenomena caused by long-lived species generated by a discharge have been studied in fast-flow apparatus.

In all these phenomena there are apparently two classes of reactants involved, atomic species and excited molecules. Recombination of atoms accounts for most of the long-lived afterglow phenomena, while the latter are necessary for much that occurs during the discharge and shortly ( $\sim 10$  m sec) after its termination.

In both the discharge and the long-lived afterglow, molecular nitrogen in the  $A^3\Sigma_u^+$  state is suspected of playing an important role. This is because it is metastable, it is the lowest electronic state of  $N_2$ , it is supposedly easily excited in a discharge, and it is a necessary result of atom recombination. However, emission from this state of  $N_2$ , the Vegard-Kaplan bands, is exceedingly difficult to observe in these phenomena. In fact the Vegard-Kaplan bands have never been observed in the long-lived afterglow, and only under very special circumstances in the discharge or in the short afterglow.

Recently<sup>1</sup> we attempted to observe the Vegard-Kaplan bands in the long-lived (Lewis-Rayleigh) nitrogen afterglow. This afterglow is almost entirely due to the first positive bands of  $N_2$  which terminate on the  $A^3\Sigma_u^+$  state. The flux of this radiation represents a minimum rate of production of  $N_2(A^3\Sigma_u^+)$ . From our failure to observe the Vegard-Kaplan bands, from the radiative lifetime of the  $A^3\Sigma_u^+$  state ( $\sim 10$  sec) and from the sensitivity of detection, an upper limit to the actual lifetime of  $N_2(A^3\Sigma_u^+)$  in the afterglow of  $5 \times 10^{-4}$  sec was derived.

This result implied that collision processes were removing  $N_2(A^3\Sigma_u^+)$ . However, it is known that  $N_2$  does not quench  $N_2(A^3\Sigma_u^+)$ . Aside from  $N_2$ , atomic nitrogen is the largest constituent present, and we conjectured that it was responsible for the short lifetime of  $N_2(A^3\Sigma_u^+)$ .

\*\* This work was done under Contract DA-31-124-ARO-D-434.

\* Visiting Fellow, Joint Institute for Laboratory Astrophysics, 1966-67.

This paper describes experiments aimed at investigating the hypothesis that atomic nitrogen, as well as several other compounds ( $\text{NO}$ ,  $\text{CO}$ ,  $\text{NH}_3$ ,  $\text{H}_2$ ), effectively destroy  $\text{N}_2(\text{A}^3\Sigma_u^+)$ .

#### EXPERIMENTAL - ATOMIC NITROGEN INTERACTION

Nitrogen was excited by a pulsed or continuous 150 kc, 10 kV oscillator (of the type used in high-voltage supplies) in a 5-liter quartz bulb with simple one-eighth inch tungsten rod electrodes separated by the diameter of the bulb. A one-half-meter Jarrel-Ash Seya-Namioka monochromator was used to scan the discharge spectrum or to isolate bands for decay measurements. Signal levels were very low, and an Enhancetron signal integration unit<sup>2</sup> was used to abstract the decaying signal from the noise.

Prepurified nitrogen was passed through a liquid nitrogen trap, then through heated titanium-zirconium and two additional liquid nitrogen traps, past a microwave excitation section, an NO titration inlet, and finally into the 5-liter observation bulb, from which it was exhausted by a mechanical vacuum pump at approximately 100  $\text{cm}^3/\text{sec}$ . A filtered photomultiplier downstream from the bulb observed the  $\text{N}_2$  first positive bands resulting from atom recombination.<sup>3</sup> This permitted the atom concentration to be computed after calibration against an NO titration.

#### RESULTS INVOLVING ATOMIC NITROGEN

Figure 1 shows spectrometer scans of the discharge. In Fig. 1a the  $\text{N}_2$  second positive and NO  $\gamma$  bands predominate below 3000 A. The  $\beta$  bands were the only other system of NO detected, and these were very weak. If the microwave discharge is adjusted to produce a small quantity of atomic nitrogen, the NO bands can be suppressed almost entirely (Fig. 1b). Although the Vegard-Kaplan bands are also reduced, the second positive bands remain relatively unchanged. Addition of NO causes a large increase in the intensity of the NO  $\gamma$  bands (Fig. 1c).

Figure 2 shows the decay of the (0,5) Vegard-Kaplan band and the (0,3) NO band with the addition of atoms, *i.e.*, when the upstream microwave discharge was on. The decay of the NO  $\gamma$  bands is identical to that of the Vegard-Kaplan bands.

Figure 3 demonstrates the buildup and decay of the (0,5) Vegard-Kaplan band when the 150 kc discharge is turned on and off; the rise and fall of this band involved the same exponential.

Figure 4 indicates the rate of decay of the Vegard-Kaplan bands as a function of pressure without added nitrogen atoms.

Figure 5 shows the dependence of the Vegard-Kaplan decay rate on  $[\text{N}]^2$  derived from the downstream photomultiplier.

Figure 6 illustrates the pressure dependence of the rate coefficient for de-excitation of  $\text{N}_2(\text{A}^3\Sigma_u^+)$  by atomic nitrogen.

Figure 7 is a plot of the growth rate constant of the Vegard-Kaplan bands, after the discharge is turned on, as a function of  $[\text{N}]^2$ .

Figure 8 shows  $(I_0/I)_{vk}$  as a function of atomic nitrogen, where  $I_{ovk}$  is the intensity without added atoms and where  $I_{vk}$  is the intensity with atoms.

Figure 9 indicates the decreased number of nitrogen atoms leaving the quartz bulb due to the discharge.

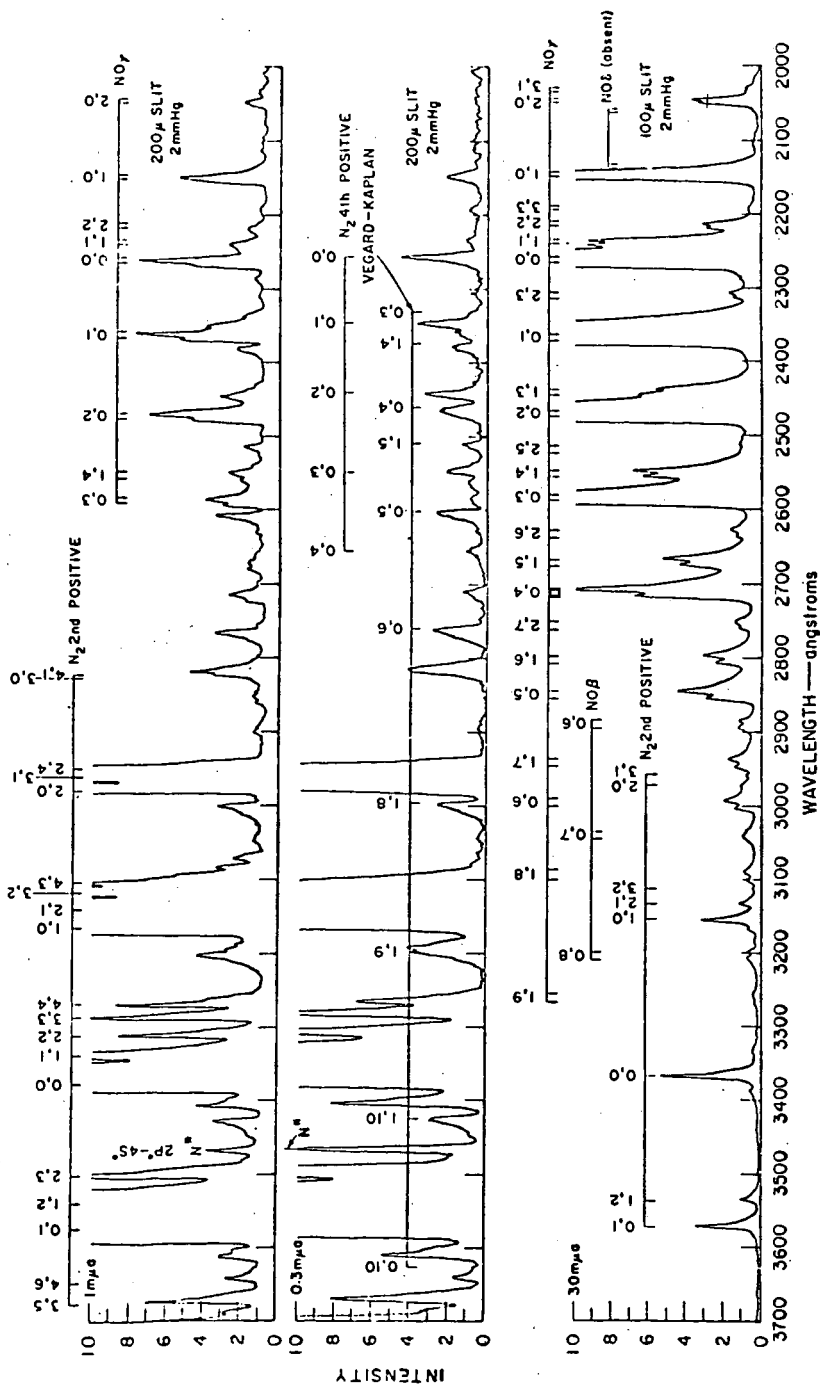
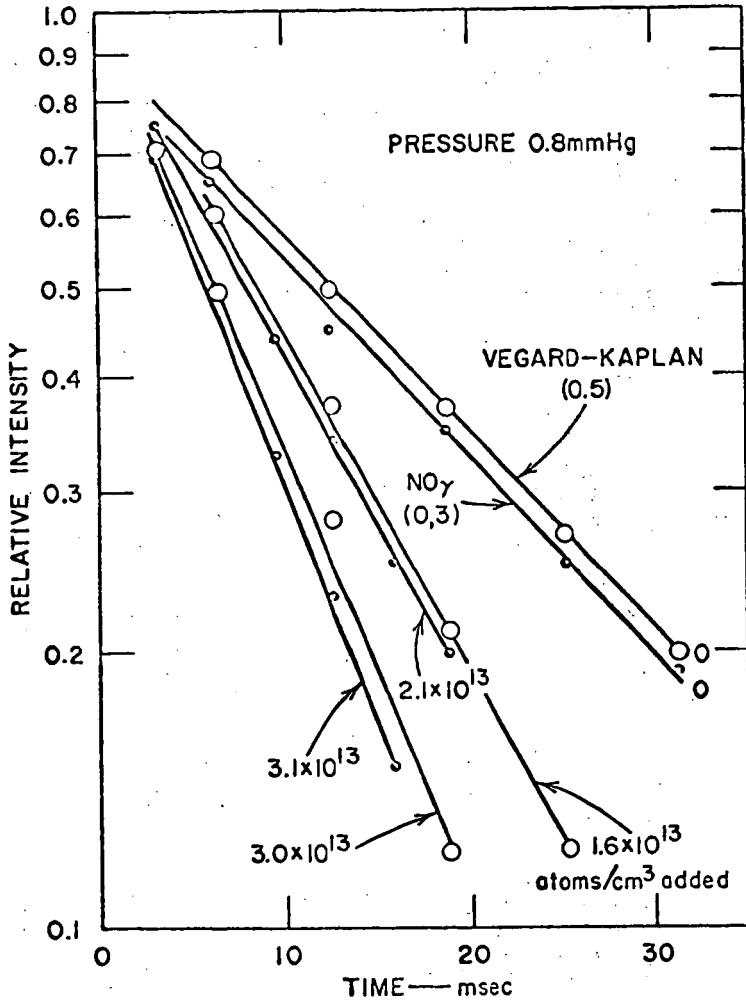


Fig. 1a A characteristic spectrum excited in purified nitrogen by a Tesla-type discharge at 2 mm Hg.

Fig. 1b A spectrum characteristic of purified nitrogen excited by a Tesla-type discharge with a small amount of nitrogen atom added from an upstream microwave discharge. Note how weak the NO bands have become.

Fig. 1c The characteristic spectrum of purified nitrogen with  $\sim 40$  ppm added NO excited by a Tesla-type discharge. Note change in scale from Figs. 1a and 1b.



TB-452522-40

Fig. 2

The intensity of the (0,5) Vegard-Kaplan band and the (0,3)  $\gamma$  band as a function of time for various amounts of added atomic nitrogen.

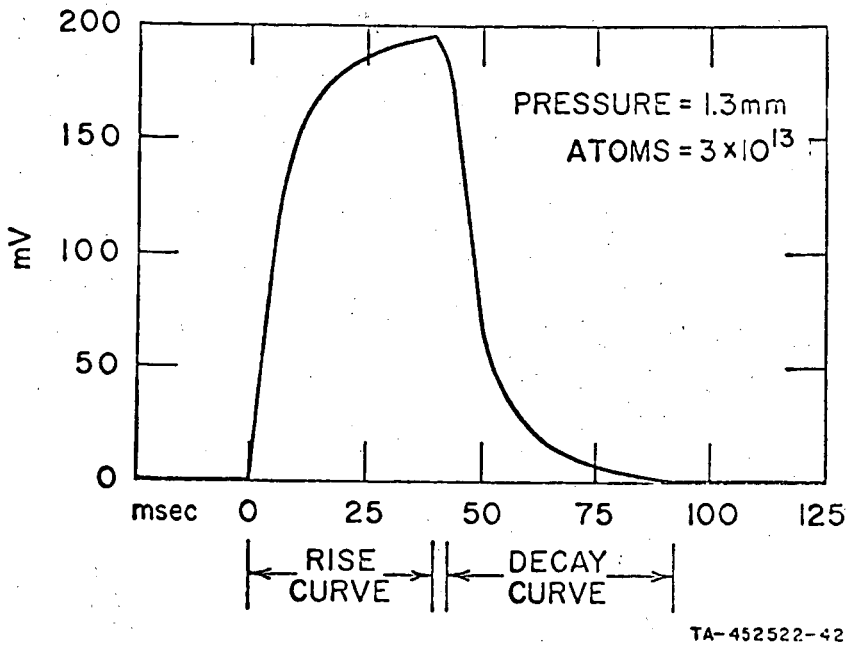


Fig. 3 Buildup and decay of the (0,5) Vegard-Kaplan band when the 150-kc discharge is turned on and off. The curve represents integration of approximately 1000 cycles.

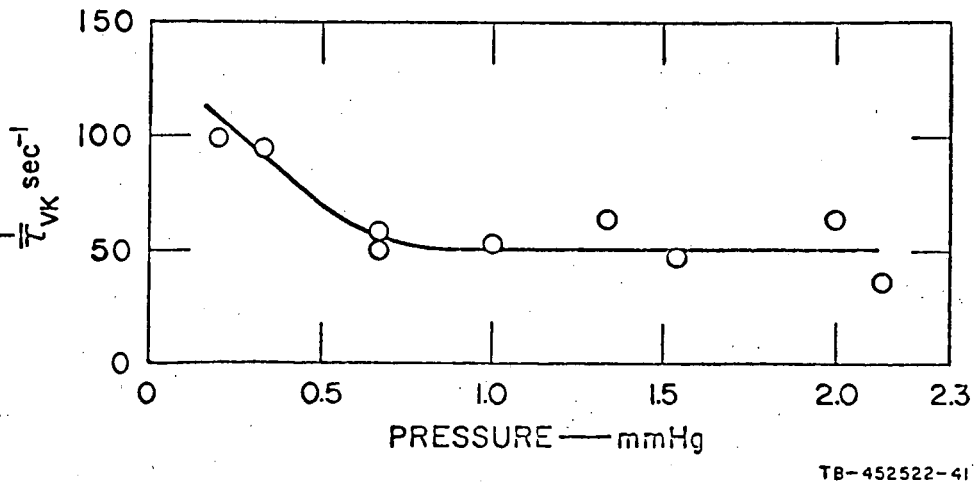
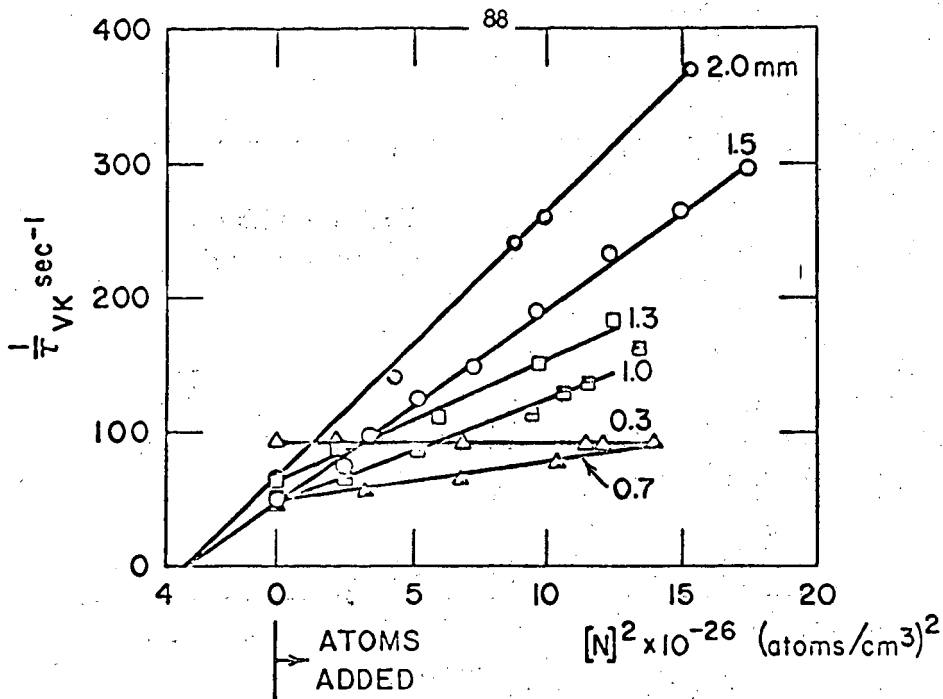
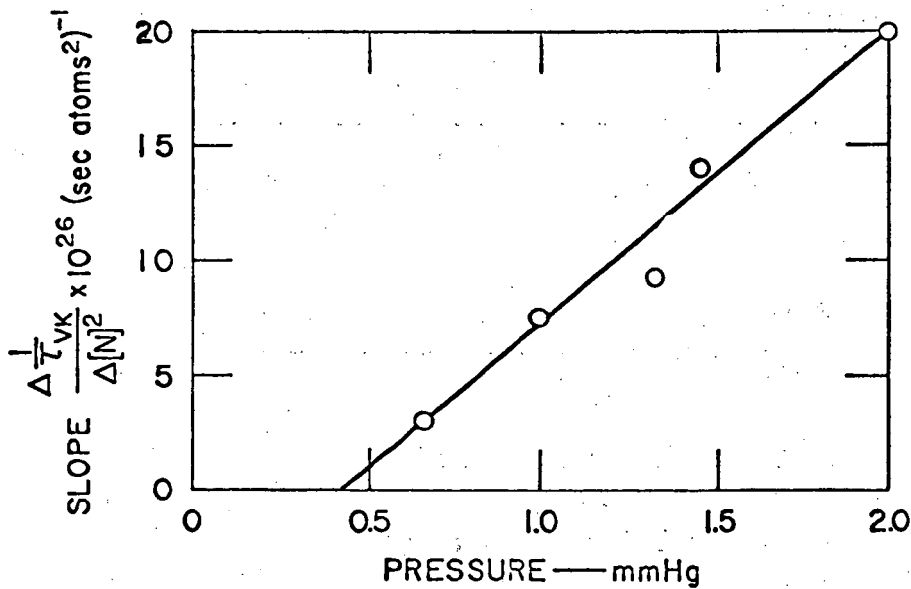


Fig. 4 The dependence of the rate of decay of the Vegard-Kaplan bands as a function of pressure without added nitrogen atoms.



TB-452522-47

Fig. 5 The rate of decay of the Vegard-Kaplan bands as a function of the square of the nitrogen atom concentration.



TA-452522-44

Fig. 6 The pressure dependence of the rate coefficient for atom destruction of the  $N_2(A^3\Pi_u^+)$  state.

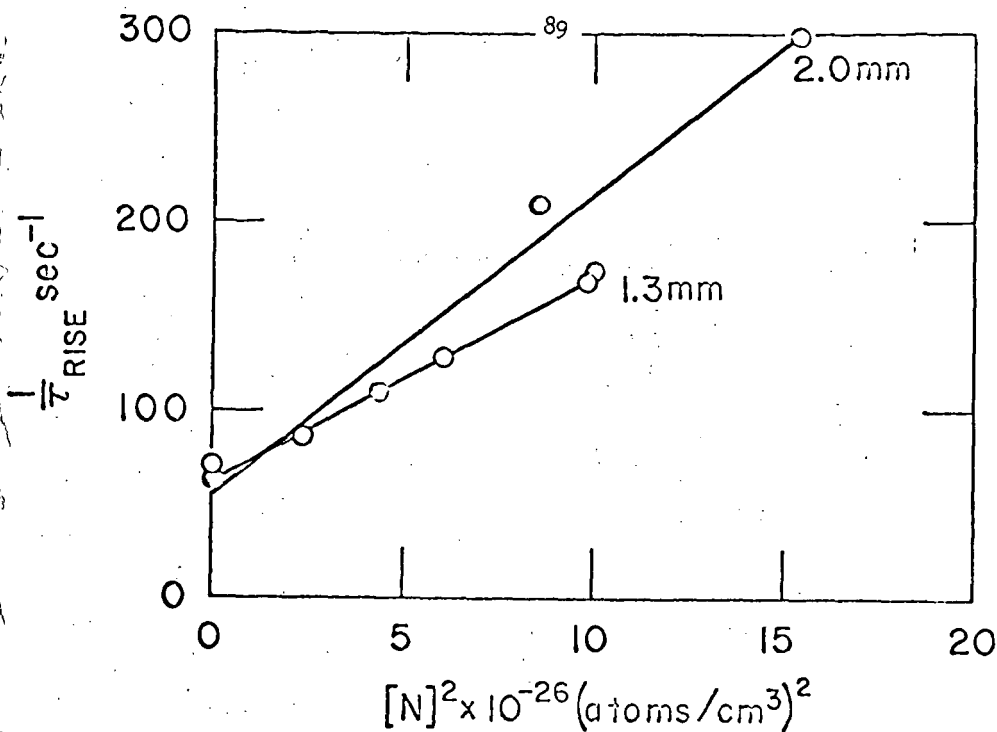


Fig. 7 The buildup rate of the Vegard-Kaplan bands during the excitation discharge as a function of the square of the atomic nitrogen concentration.

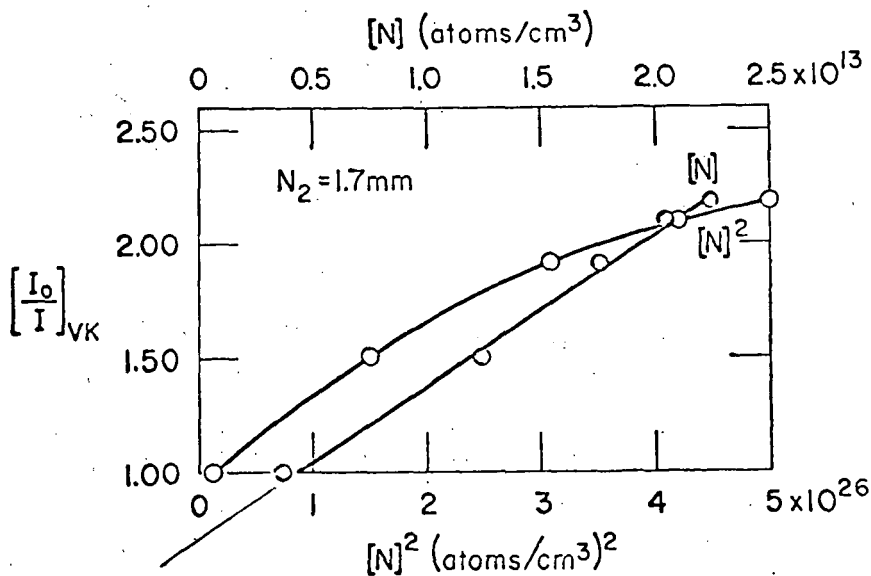
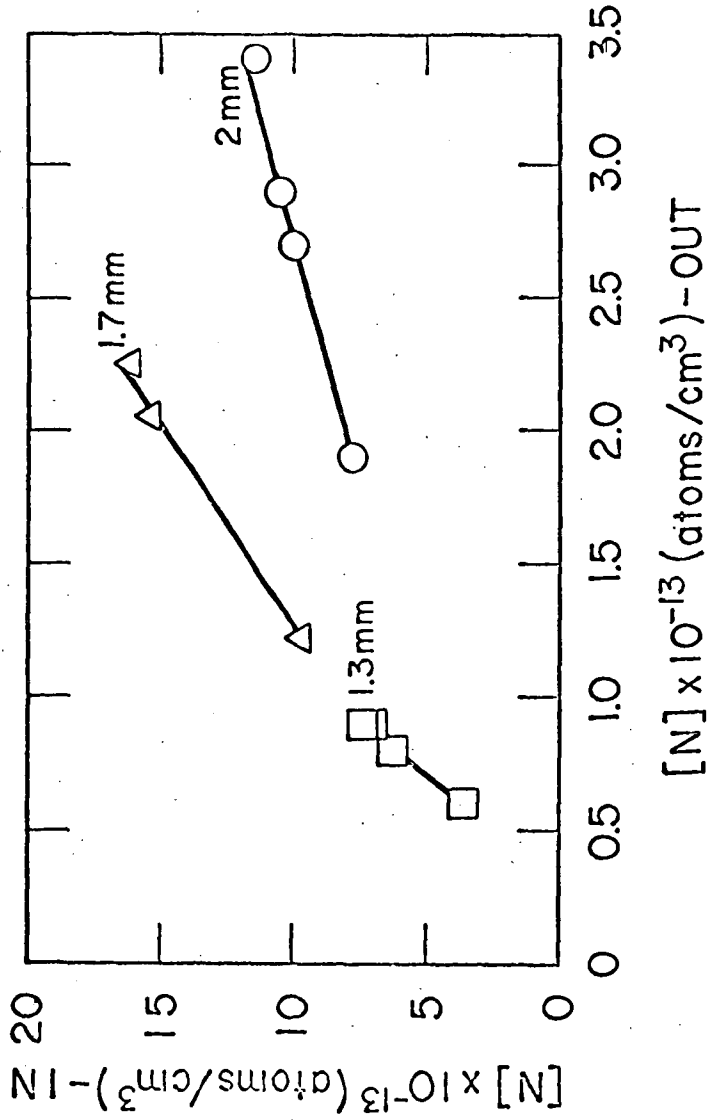


Fig. 8 The normalized inverse intensity of the Vegard-Kaplan bands during the excitation discharge as a function of added atomic nitrogen. The discharge was run continuously.

TB-452522-49



TB-452522-46

Fig. 9 The reduction in the atom concentration produced by the excitation discharge as a function of the atom concentration leaving the excitation bulb. The discharge was run continuously.

## DISCUSSION OF RESULTS PERTAINING TO ATOMIC NITROGEN

The observations indicate that during decay

$$[N_2(A^3\Sigma_u^+)] = [N_2(A^3\Sigma_u^+)]_0 e^{-t/\tau_a} \quad (1)$$

where

$$\frac{1}{\tau_a} = \frac{1}{\tau_0} + K[N]^2 [M] \quad (2)$$

with  $K \approx 4 \times 10^{-42}$  cm<sup>9</sup>/sec. Neither  $\tau_a$  or  $\tau_0$  can be the radiative lifetime of  $N_2(A^3\Sigma_u^+)$  which is  $\approx 10$  sec.

The differential equation describing the time dependence of  $[N_2(A^3\Sigma_u^+)]$  is

$$\frac{d[N_2(A^3\Sigma_u^+)]}{dt} = P - L[N_2(A^3\Sigma_u^+)] \quad (3)$$

where  $L$  contains all factors other than  $[N_2(A^3\Sigma_u^+)]$  such as collision partner concentrations, rates of radiation or diffusion, etc., that are involved in processes removing  $N_2(A^3\Sigma_u^+)$ , and where  $P$  is the rate of production. Substituting Eq. (1) in Eq. (3) gives

$$[N_2(A^3\Sigma_u^+)]_0 e^{-t/\tau_0} (L - \frac{1}{\tau_a}) = P \quad (4)$$

Then either

$$L = \frac{1}{\tau_a} \quad \text{and} \quad P = 0 \quad (5)$$

or

$$\frac{P}{(L - \frac{1}{\tau_a}) [N_2(A^3\Sigma_u^+)]_0} = e^{-t/\tau_a} \quad (6)$$

In the latter eventuality  $L > 1/\tau_a$ , since neither  $P$  nor  $e^{-t/\tau_a}$  can be negative. If  $L$  is comparable to  $1/\tau_a$ , it must be essentially constant in time, while if it is large compared to  $1/\tau_a$ ,

$$\frac{P}{L [N_2(A^3\Sigma_u^+)]_0} = e^{-t/\tau_a} \quad (7)$$

Since all constituents of the system probably decay when the power input is stopped,  $\tau_a$  would be characteristic of the decay of a reactant concentration involved in  $P$  to a higher power than in  $L$ , while other reactant concentrations are either constant or common to both  $P$  and  $L$ . The previous statement would be true if a product of reactant concentrations replaces a single reactant concentration.

Since  $1/\tau_a$  changes by almost a factor of 10 over the range of  $[N]$  used, either  $L \gg 1/\tau_a$  for small  $[N]$  and hence  $P/L [N_2(A^3\Sigma_u^+)]_0 = e^{-t/\tau_a}$ , or  $L$

closely follows  $1/\tau_a$  in dependence on  $[N]$ , *i.e.*,  $L \propto 1/\tau_a$ . Discussion of the last possibility will be deferred. In the former case  $L$  must be very large indeed and  $[N_2(A^3\Sigma_u^+)]$  must be essentially in a quasi-steady state with its production rate, *i.e.*,  $\tau_a$  refers to the decay of  $P$ . Since  $[N_2(A^3\Sigma_u^+)]$  is not strongly deactivated by pure  $N_2$ ,  $L$  would certainly not increase when the energy of the system dissipates as would be necessary if  $P$  did not decay. Because the decay of  $[N_2(A^3\Sigma_u^+)]$  appears to remain exponential for all values of  $[N]$  and because  $\tau_a$  is a smooth function of  $[N]$ , then  $L > 1/\tau_a(\max)$  if the data are interpreted as the decay of  $P$  with  $[N_2(A^3\Sigma_u^+)]$  in a quasi-steady state. For this to be true some species capable of deactivating  $N_2(A^3\Sigma_u^+)$  must be generated in the discharge and remain constant for times long compared to those where  $[N_2(A^3\Sigma_u^+)]$  is detectable. The most abundant chemical species generated by the discharge is  $N$ ; the most abundant excited molecule is  $N_2(A^3\Sigma_u^+)$  -- except possibly for the  $^3\Delta$  state of  $N_2$  which has not yet been directly detected. Only atomic nitrogen appears to be a realistic choice for the species which decays slowly and would keep  $L \gg 1/\tau_a$ .

However, a difficulty arises in the interpretation with  $L \gg 1/\tau_a$  if we consider the observed behavior of  $[N_2(A^3\Sigma_u^+)]$  when the discharge is turned on. The rise of  $[N_2(A^3\Sigma_u^+)]$  to a steady state is describable by

$$[N_2(A^3\Sigma_u^+)] = [N_2(A^3\Sigma_u^+)]_0 (1 - e^{-t/\tau_a}) \quad (8)$$

If this is substituted into Eq. (3), we obtain

$$[N_2(A^3\Sigma_u^+)]_0 ((1/\tau_a) - L) e^{-t/\tau_a} = P - L [N_2(A^3\Sigma_u^+)]_0 \quad (9)$$

If  $1/\tau_a = L$ , then  $P = L [N_2(A^3\Sigma_u^+)]_0 = P_0$ , a constant in time. When  $t = 0$ ,  $P = P_0 = ([N_2(A^3\Sigma_u^+)]_0/\tau_a)$  if  $L \neq (1/\tau_a)$ ; and if  $P = P_0 + P'$ , we obtain

$$P' = [N_2(A^3\Sigma_u^+)]_0 (1/\tau_a - L) (e^{-t/\tau_a} - 1) \quad (10)$$

If  $L \gg 1/\tau_a$ ,  $P'$  is positive; and if  $L \ll 1/\tau_a$ ,  $P'$  is negative and  $P$  ranges from  $P_0$  to 0. A decrease of  $P$  from  $P_0$  is not expected during the discharge and certainly not with an exponential behavior identical to that which occurs when the discharge is turned off. Hence of the two possibilities, when  $L \neq 1/\tau_a$ ,  $L \gg 1/\tau_a$  is the only one tenable during the excitation discharge.

Since  $P_0$  follows the discharge transients, it must become zero when the discharge is turned off, so that  $P$  changes rapidly compared with  $\tau_a$  from  $P_0 + P'$  to  $P'$ . But this is inconsistent with the interpretation of the decay of  $[N_2(A^3\Sigma_u^+)]$  previously given on the assumption that  $L \gg 1/\tau_a$  because this rapid fall in  $P$  would be reflected in a rapid fall of  $[N_2(A^3\Sigma_u^+)]$  which is not observed. Hence this contradiction forces  $L = 1/\tau_a$  and  $P = P_0$ , a constant, during the discharge and  $L = 1/\tau_a$  and  $P = 0$  after the discharge.

During the excitation discharge a steady state is reached, and

$$\bar{P} = \bar{L} [N_2(A^3\Sigma_u^+)] \quad (11)$$

where the bar indicates values constant in time. Then indexing all quantities with a subscript 1 when atoms are not added and with N when they are added, we obtain

$$\frac{I_1(\text{VK})}{I_N(\text{VK})} = \frac{\bar{P}_1}{\bar{P}_N} \frac{\bar{L}_N}{\bar{L}_1} = 0.75 + \alpha[N] \quad (12)$$

where the last equality uses the results of Fig. 8. Hence  $\bar{L}_N$  involves  $[N]$  to a higher power than does  $\bar{P}_N$ . Thus  $\tau_a$  cannot refer to the decay of  $[N]$ . This is consistent with the usual slow decay of  $[N]$ .

Since  $\bar{L}_N$  is essentially proportional to  $[N]^2$ , these results imply that  $\bar{P}_N$  is proportional to  $[N]$ . If this additional production of  $N_2(A^3\Sigma_u^+)$  utilizes nitrogen atoms on a one-for-one basis,  $[N]$  must decrease in passing through the discharge, i.e.,

$$[N]_{\text{in}} - L[N]_{\text{out}} \Delta t = [N]_{\text{out}} \quad (13)$$

where  $\Delta t$  is an average residence time, where  $L[N]_{\text{out}}$  represents the rate of atom removal, and where mixing is rapid compared with reaction. This leads to

$$[N]_{\text{in}} = [N]_{\text{out}} (1 + L\Delta t) \quad (14)$$

or

$$[N] = [N]_{\text{out}} L\Delta t \quad (15)$$

which is the general form observed.

From Fig. 9 we can obtain  $L$  (using  $\Delta t \approx 50$  sec), and from Fig. 8 with a slope of  $(K\tau_0 P_0 [N_2]/L)$ , we can also obtain  $L$  if  $K\tau_0 P_0 [N_2]$  can be found. A comparison of  $L$  derived from Fig. 9 and Fig. 8 is then possible. Since  $P = [N_2(A^3\Sigma_u^+)]/\tau_0$ , absolute measurements of  $[N_2(A^3\Sigma_u^+)]$  derived from  $I(\text{VK}) = ([N_2(A^3\Sigma_u^+) ]/\tau_r)$  where  $\tau_r$  is the radiative lifetime of the excited state give  $\tau_0 P$ .

The absolute intensity of the 0,5 Vegard-Kaplan band in the discharge bulb can be roughly obtained by measuring its signal and calibrating the spectrometer response using the NO  $\gamma(0,3)$  band excited by the chemiluminescent association of N and O in conjunction with measurements of  $[N]$  and  $[O]$  and the known rate coefficient for these processes.<sup>4</sup> In general, the comparisons of  $L$  derived from Figs. 8 and 9 show that if nitrogen atoms are consumed in the excitation of  $N_2(A^3\Sigma_u^+)$ , then several hundred times more atoms need to disappear than in fact are destroyed. This implies that nitrogen atoms are not consumed but catalyze the production of  $N_2(A^3\Sigma_u^+)$  in conjunction with other species generated in the discharge.

A similar argument can be used to show that atomic nitrogen is not consumed in destroying  $N_2(A^3\Sigma_u^+)$ . For example, there are often as many  $N_2(A^3\Sigma_u^+)$  molecules as N atoms; these would be seriously depleted during the decay of  $N_2(A^3\Sigma_u^+)$  and thus would lead to a nonexponential behavior.

The short lifetime of  $N_2(A^3\Sigma_u^+)$  in the discharge (Fig. 4) cannot be due to atoms because their concentration, as inferred from downstream chemiluminescence measurement, is too small. Furthermore, the pressure dependence of  $\tau_0$  is incompatible with atom

deactivation. Hence, some species is produced in the discharge in addition to atomic nitrogen which is capable of rapidly deactivating  $N_2(A^3\Sigma_u^+)$ . This species persists for times long compared to  $\tau_0$ .

The results of these experiments indicate that several unusual processes are occurring: (1) a high-order process destroying  $N_2(A^3\Sigma_u^+)$  which involves atomic nitrogen; (2) a process utilizing species, created in a discharge other than atomic nitrogen, which removes  $N_2(A^3\Sigma_u^+)$ ; and (3) a process involving atomic nitrogen and another species generated in the discharge which produces  $N_2(A^3\Sigma_u^+)$ . These processes are in addition to electron excitation and radiative destruction of  $N_2(A^3\Sigma_u^+)$ . Several possible reaction schemes can be constructed which are consistent with our observations. However, without positive identification of all the species created in the discharge and the intermediaries necessarily involved in high-order processes, these reaction schemes are speculative. It seems best to postpone discussions of these until more experimental information is available.

#### EXPERIMENTAL REACTIONS INVOLVING NO

For experiments on the effect of NO on  $N_2(A^3\Sigma_u^+)$ , three photomultipliers were installed downstream from the RF excitation bulb to observe chemiluminescence. One photomultiplier had an interference filter centered on the strong bands of  $N_2$  at 5800 Å, a second (called the yellow detector) observed radiation at wave lengths longer than 5200 Å, and a third (called the ultraviolet detector) observed emission between 3800 Å and the pyrex cutoff. The first two photomultipliers are sensitive to the  $N_2$  first positive bands excited by recombination of atomic nitrogen and to the  $NO_2$  continuum excited by reactions of O with NO, while the ultraviolet photomultiplier is mainly sensitive to the NO,  $\beta$  bands excited in the association of atomic nitrogen and oxygen.<sup>4</sup> These photomultipliers were calibrated by generating nitrogen atoms in the microwave discharge and titrating them with NO. It should be remembered that all emission observed in the downstream bulb is of chemiluminescent origin.

#### RESULTS

Figure 10 shows the decay rate when the exciting discharge is turned off from the 0,3 NO  $\gamma$  band, and the 0,5 Vegard-Kaplan band as a function of atomic nitrogen added by the upstream microwave discharge.

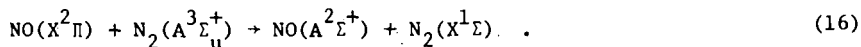
Figures 11 and 12 show the intensity of the 0,5 Vegard-Kaplan band, the 0,3 NO  $\gamma$  band and the 0,6 NO  $\beta$  band in the discharge bulb as a function of the NO concentration that would have existed in the stream if no destruction of NO occurred. Also shown are the responses of the yellow photomultiplier and the ultraviolet photomultiplier, both of which are located at the downstream bulb.

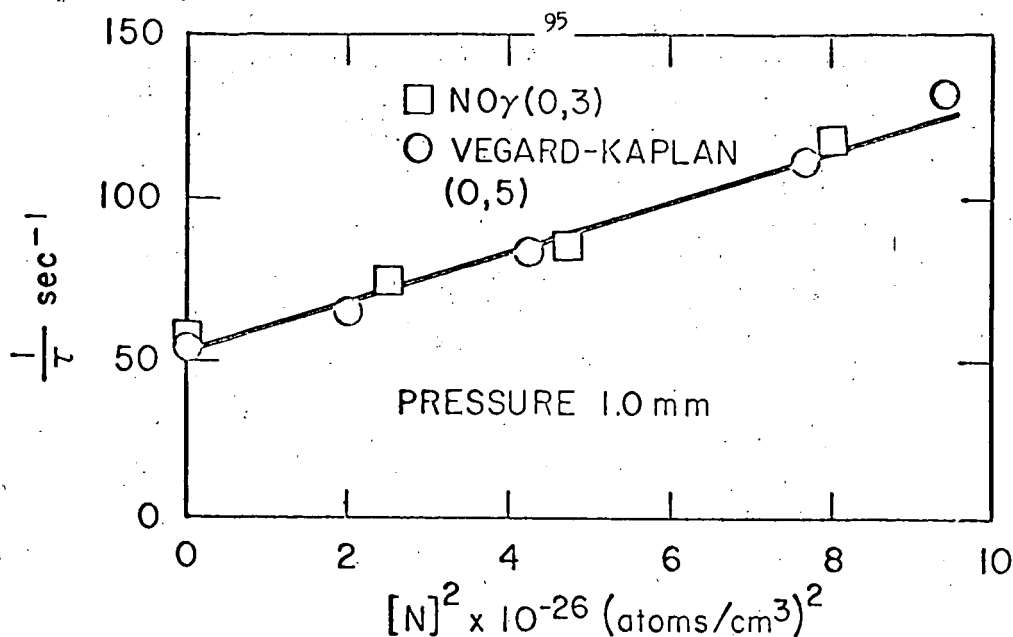
Spectrometer scans of the discharge without adding NO and on the plateau of Figs. 11 and 12 are shown in Fig. 1.

Figure 13 is a plot of the area intensity ratio of 0,3 NO  $\gamma$ /0,5 Vegard-Kaplan bands as a function of NO added beyond the null and as a function of the relative response of the yellow phototube to the  $NO_2$  continuum. Figure 14 is similar to Fig. 13 but involves the 1,10 Vegard-Kaplan band and the 3,0 NO  $\gamma$  band.

#### DISCUSSION

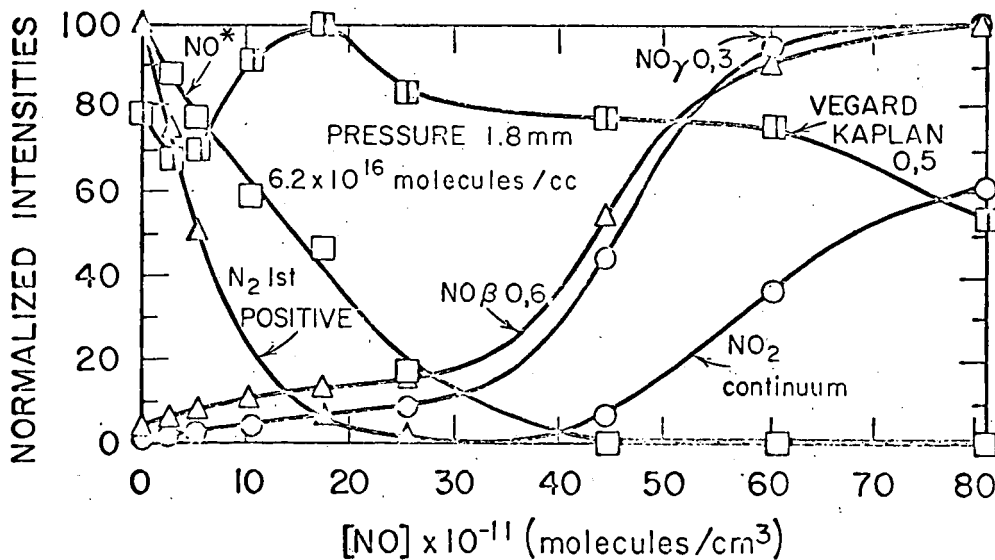
The simultaneous decay of  $N_2(A^3\Sigma_u^+)$  and  $I_\gamma$ , the intensity of the NO  $\gamma$  bands, suggests that NO is excited in the process<sup>5</sup>





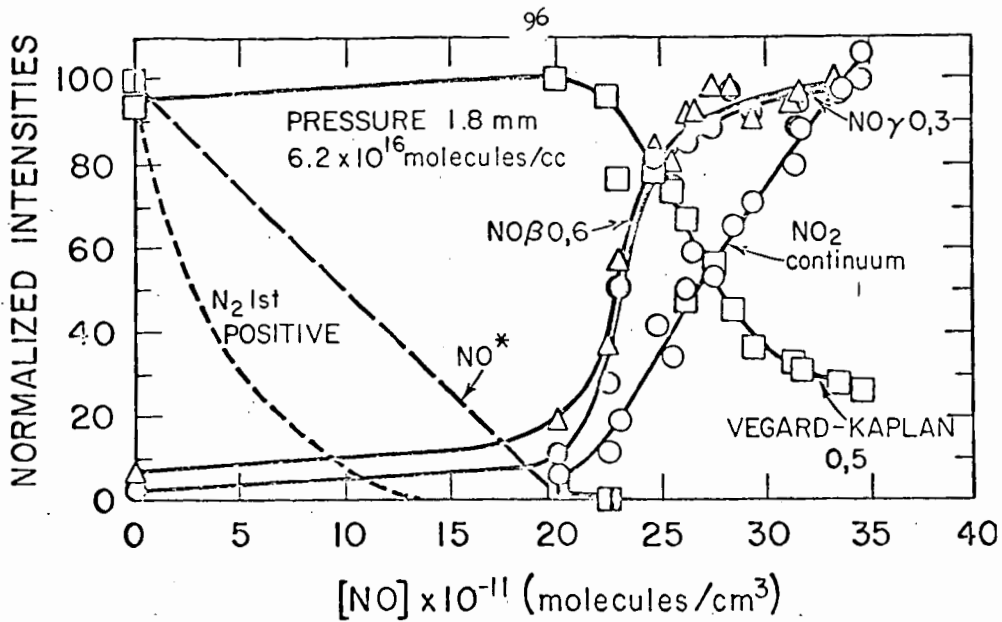
TB-452522-37

Fig. 10 The dependence of the rate of decay of  $N_2(A^3\Sigma_u^+)$  and  $NO(A^2\Sigma^+)$  as a function of the square of the atomic nitrogen concentration.



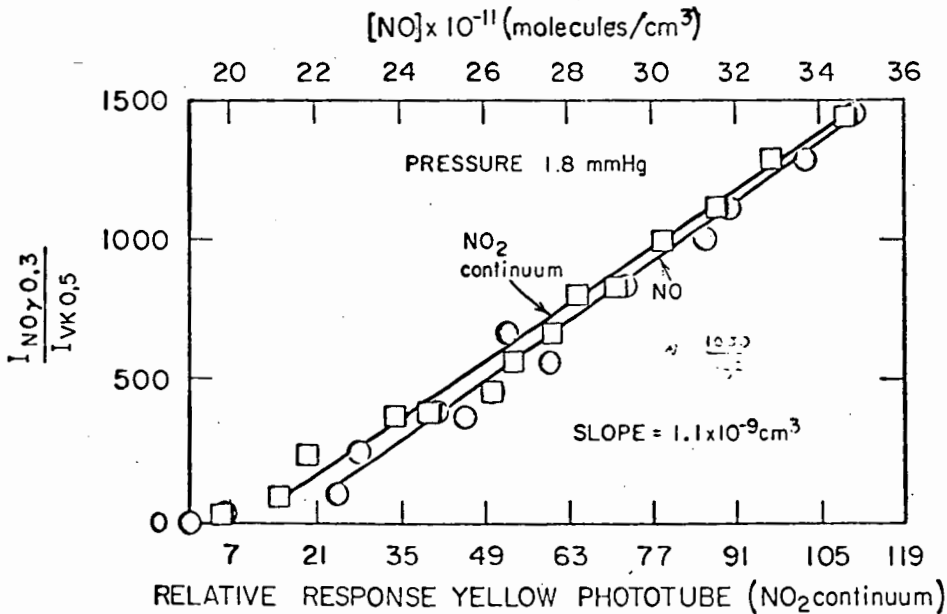
TB-452522-39

Fig. 11 The dependence of emission intensities on NO concentration:  $\square$  - the  $NO \beta$  bands,  $\Delta$  - the  $N_2$  first positive bands,  $\circ$  - the  $NO_2$  continuum -- all excited in the downstream observation bulb;  $\circ$  - the 0,3  $NO \gamma$  band,  $\Delta$  - the 0,6  $NO \beta$  band, and  $\square$  - the 0,5 Vegard-Kaplan band excited in the Tesla discharge bulb.



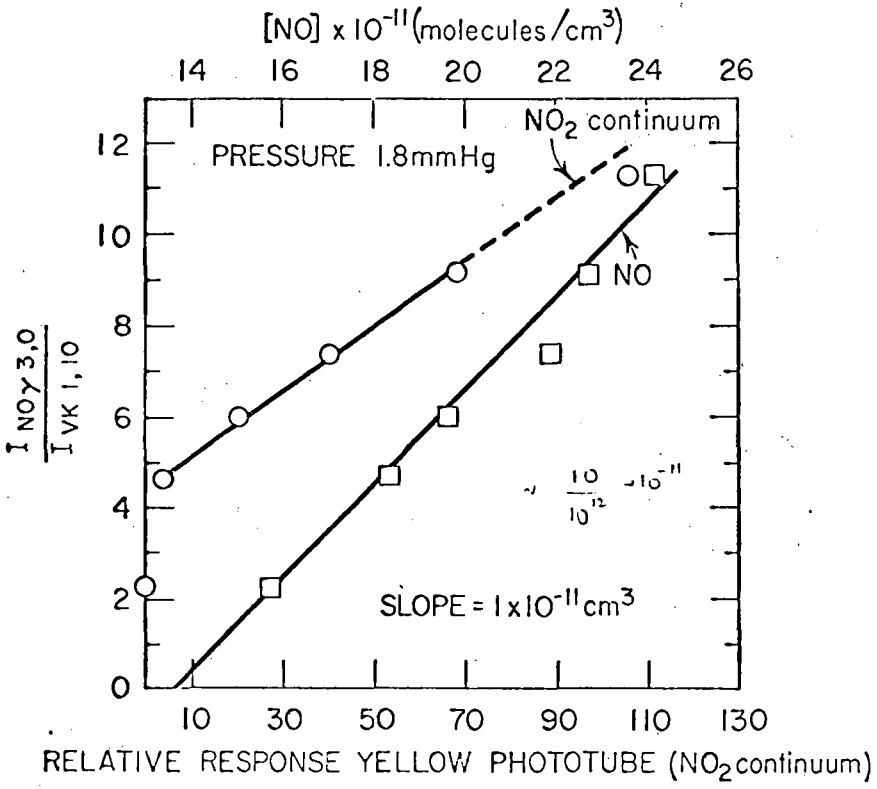
TB-452522-48

Fig. 12 The dependence of emission intensities on NO concentration:  $\square$  - the NO  $\beta$  bands,  $\circ$  - the NO<sub>2</sub> continuum -- both excited in the downstream observation bulb;  $\circ$  - the 0,3 NO  $\gamma$  band,  $\Delta$  - the 0,6 NO  $\beta$  band; and  $\square$  - the 0,5 Vegard-Kaplan band excited in the Tesla discharge bulb.



TB-452522-36

Fig. 13 The relative photomultiplier response to the NO  $\gamma$  (0,3) and N<sub>2</sub> (0,5) Vegard-Kaplan bands as a function of both [NO] and the response of the yellow photomultiplier.



TB-452522-51

Fig. 14 The relative photomultiplier response to the  $NO \gamma (3,0)$  and  $N_2(1,10)$  Vegard-Kaplan bands as a function of both  $[NO]$  and the response of the yellow photomultiplier.

The initial decrease of the signals from the yellow downstream photomultiplier is due to NO titration of nitrogen atoms produced in the exciting discharge, i.e.,



The null point represents the complete conversion of nitrogen atoms to oxygen atoms. The concentration of these atoms derived from the amount of NO added to reach this null is consistent with the intensity of the first positive bands before NO addition. The linear rise of the yellow sensitive photomultiplier after null is due to



and indicates that O is essentially constant.

There is a slow increase of the NO  $\gamma$  and  $\beta$  bands in the excitation bulb because of the slow increase in the actual steady-state concentration of NO which is maintained by



and reaction (16), i.e.,

$$[NO] = \frac{k_{19}}{k_{17}} [O] [M] \quad (22)$$

When [N] goes to zero, this steady state cannot be maintained, and NO in the stream increases as expected for no reaction of NO. In the reaction time available reaction (20) does not significantly alter either [O] or [NO].

As [NO] increases sharply after the removal of N, the NO  $\gamma$  and  $\beta$  bands increase sharply in the discharge and the  $N_2$  Vegard-Kaplan bands decrease rapidly. Since

$$I_{vk} = [N_2(A^3\Sigma_u^+)]/\tau_{vk} \quad (23)$$

$$I_{\gamma} = [NO(A^2\Sigma^+)]/\tau_{\gamma} \quad (24)$$

for excitation in the discharge bulb, and since

$$I_{NO_2} = K_{NO_2} [NO] [O] \quad (25)$$

for chemiluminescent excitation in the downstream bulb, reaction (16) implies

$$I_Y = k_{16} [\text{NO}] [\text{N}_2(\text{A}^3\Sigma_u^+)] = k_{16} [\text{NO}] I_{\text{vk}\tau_{\text{vk}}} = \frac{k_{16} I_{\text{NO}_2} I_{\text{vk}\tau_{\text{vk}}}}{[\text{O}]K_{\text{NO}_2}} \quad (26)$$

if  $\text{NO}(\text{A}^2\Sigma^+)$  is only deactivated by emission.

Since  $\text{O}$  is constant,

$$\frac{I_Y}{I_{\text{vk}}} \propto I_{\text{NO}_2} \quad (27)$$

This is true, as Figs. 13 and 14 show. In these graphs intensities are not absolute, but relative.

To obtain  $k_{16}$  from Eq. (26), we must experimentally relate the emission intensities more directly to the concentration of the emitting state. If  $I_Y(0,3)$  represents the absolute intensity of the 0,3  $\gamma$  band of NO and similarly for the Vegard-Kaplan bands, then Eq. (11) becomes

$$\frac{I_Y(0,3)}{f_Y(0,3)} = \frac{k_{16} [\text{NO}] \tau_{\text{vk}} I_{\text{vk}}(0,5)}{f_{\text{vk}}(0,5) \beta} \quad (28)$$

where  $f_Y(0,3)$  is the fraction of all emission from the  $v' = 0$  level which terminates on the  $v'' = 3$  level and similarly for  $f_{\text{vk}}(0,5)$  and where  $\tau_{\text{vk}}$  is the radiative lifetime of the  $\text{A}^3\Sigma_u^+$  state<sup>6</sup> and  $\beta$  represents the fraction of all  $\text{N}_2(\text{A}^3\Sigma_u^+)$  which are in  $v' = 0$ . Only  $v' = 1$  and 0 are detected by their emission, and  $\beta$  is found to be one half and constant. Then

$$k_{16} = \left( \frac{f_{\text{vk}}(0,5)}{f_Y(0,3) \tau_{\text{vk}}} \right) \frac{\beta I_Y(0,3)}{I_{\text{vk}}(0,5) [\text{NO}]} \quad (29)$$

The parameters in parentheses depend only on the internal characteristics of the molecules and have previously been measured<sup>6</sup> as  $\tau_{\text{vk}} = 20$  sec,  $f_{\text{vk}}(0,5) = 0.17$ , and  $f_Y(0,3) = 0.14$ . Hence

$$k_{16} = \frac{0.03 I_Y(0,3)}{[\text{NO}] I_{\text{vk}}(0,5)} \quad (30)$$

To obtain  $k_{16}$ , only the relative intensity of  $I_Y(0,3)$  and  $I_{\text{vk}}(0,5)$  are required. Since these bands occur very near each other in the spectra of the discharge, their relative intensity is equal to their relative signal level. Hence  $k_{16}$  is 0.03 times the slope of the line in Fig. 13, i.e.,

$$k_{16} = 0.03 (1.1 \times 10^{-9}) = 3 \times 10^{-11} \text{ cm}^3/\text{sec} \quad (31)$$

This rate is much larger than that reported by Dugan.<sup>7</sup>

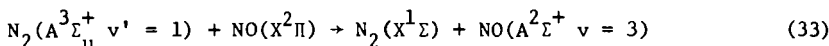
The existence of the  $\beta$  bands and emission from higher vibrational levels of the  $\text{NO}(A^2\Sigma^+)$  state indicate that this rate is a lower bound to the rate of energy transfer from  $\text{N}_2(A^3\Sigma_u^+)$  to  $\text{NO}(X^2\Pi)$ . There are several states of NO accessible in an energy exchange involving  $\text{N}_2(A^3\Sigma_u^+)$  -- the  $a^4\Pi$ ,  $b^4\Pi$ ,  $b^4\Sigma^-$ , as well as the  $A^2\Sigma^+$  and  $B^2\Pi$  which are revealed by their emission.

The total rate of de-excitation of  $\text{N}_2(A^3\Sigma_u^+)$  can be estimated, since we know, in the absence of NO, its deactivation rate is  $1/\tau = 50/\text{sec}$ , and the intensity of the Vegard-Kaplan bands is reduced by half when  $[\text{NO}] \approx 7 \times 10^{11}$  molecules/cm<sup>3</sup>, i.e.,  $50 = k'_{16}(7 \times 10^{11})$ ; in other words

$$k'_{16} = 7 \times 10^{-11} \text{ cm}^3/\text{sec} \quad (32)$$

or essentially a quarter of all the  $\text{N}_2(A^3\Sigma_u^+)$  deactivated leads to excitation of the  $v' = 0$  level of the  $\text{NO}(A^2\Sigma^+)$ .

It is apparent from the spectra that excitation of the  $A^2\Sigma$  state of NO by  $\text{N}_2(A^3\Sigma_u^+)$  decreases in efficiency as  $v'$  increases in the NO molecule, becoming very small for  $v' = 3$  which is the highest level observed. This level can only be excited by  $\text{N}_2(A^3\Sigma_u^+ v = 1)$ , while the  $v' = 2, 1$ , and 0 levels of the  $\text{NO}(A^2\Sigma^+)$  state can be excited by  $\text{N}_2(A^3\Sigma_u^+ v = 0, 1)$ . Using the data in Fig. 14, we can obtain the rate coefficient of



as  $k_{16}(1,3) = 10^{-13} \text{ cm}^3/\text{sec}$ .

#### REFERENCES

1. R. A. Young, *Canad. J. Chem.* **44**, 1171 (1966). This paper contains additional references. K. Wray independently arrived at similar conclusions in *J. Chem. Phys.* **44**, 623 (1966).
2. Enhancetron Nuclear Data Inc.
3. R. A. Young and G. Black, *J. Chem. Phys.* **44**, 3741 (1966). This paper has references leading back to the description of most of the phenomenon associated with discharged nitrogen.
4. R. A. Young and R. L. Sharpless, *Discussions Faraday Soc.* **33**, 228 (1962).
5. A. B. Collear and I. W. M. Smith, *Trans. Faraday Soc.* **61**, 2383 (1965).
6. W. R. Brennan, *Studies in active nitrogen*, Ph. D. Thesis, Dept. of Chemistry, Harvard University, Sept. 1964, and references quoted here; R. W. Nicholls, *J. Res. Natl. Bureau Std. (U.S.)* **65A**, 451 (1961); R. A. Young and R. L. Sharpless, *J. Chem. Phys.* **39**, 1071 (1963); R. A. Young and R. L. Sharpless, *J. Chem. Phys.* **39**, 1971 (1963); R. A. Young and G. Black, *J. Chem. Phys.* (in press). These references contain an extensive review of the pertinent chemiluminescent reactions.
7. C. H. Dugan, *An experimental study of metastable atoms and molecules*, Thesis, Division of Engineering and Applied Physics, Harvard University, June 1963; C. H. Dugan and N. P. Carleton (in press).

## Chemiluminescent Reactions of Excited Helium with Nitrogen and Oxygen

Mark Cher

North American Aviation Science Center, Thousand Oaks, California 91360

## Abstract

Active species created in a fast flow of helium by a microwave discharge react outside the discharge with nitrogen or oxygen causing the emission of visible bands of  $N_2$  and  $O_2$ . The emission intensity of these bands decays exponentially with distance, and the decay coefficient depends on both the flow rate of helium and the flow rate of nitrogen or oxygen. At constant flow rate of helium the decay coefficient increases with increasing flow rate of added gas, but the dependence is less than linear. A theoretical analysis of the flow system predicts the exponential decay and a linear dependence between the decay coefficient and the flow rate of added gas. Comparison of the experimental and theoretical results permits the calculation of approximate values of the rate constants for the reactions populating the emitting states and the diffusion coefficients of the excited helium species. A plausible explanation and a means for removing the discrepancy between the experimental and theoretical results are suggested.

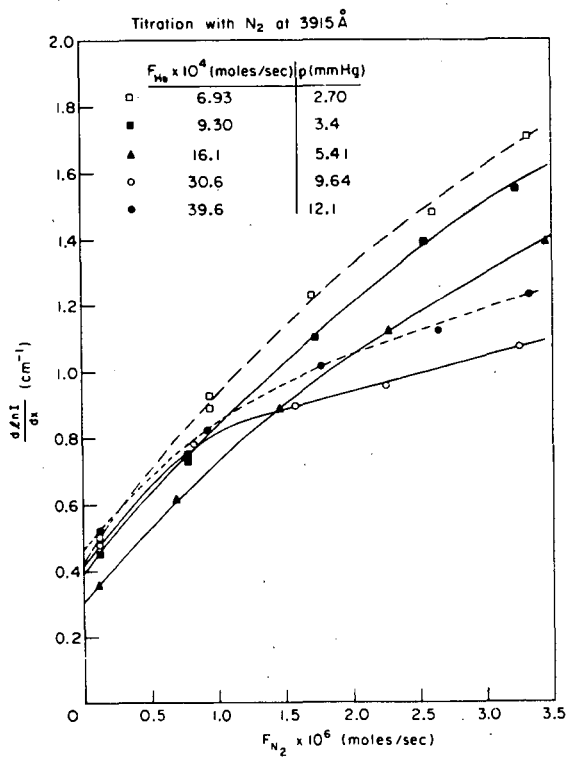
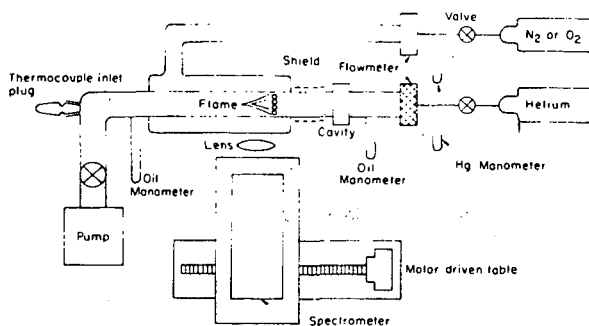
## Introduction

Long lived reactive species, produced when helium gas is subjected to an electrical discharge, react with many other gases and generate characteristic emissions of visible light. The nature of some of these chemiluminescent reactions has been discussed recently in a number of papers.<sup>1,2</sup> The reaction with nitrogen gas produces an intense bright blue flame consisting of the first negative system of  $N_2^+(B^2\Sigma^+ \rightarrow X^2\Sigma^+)$ . With oxygen a bright yellow-green flame is observed due to the excitation of both the first negative system of  $O_2^+(b^4\Sigma^- \rightarrow a^4\Pi)$  and the second negative system of  $O_2^+(A^2\Pi \rightarrow X^2\Pi)$ . In this paper we report the results of our measurements of the spectral variation of the emission intensity in a fast flow system for various flow conditions, and show how these measurements can be used to evaluate the rate constants for the reactions populating the emitting states.

**Apparatus.** The reaction cell and associated equipment are shown schematically in Fig. 1. The reaction cell consisted of a pair of concentric pyrex tubes 13 and 25 mm o.d. Helium flowed through the inner tube. The titrating gas was introduced into the helium stream via the outer tube through eight 1 mm diameter holes located symmetrically in the wall of the inner tube. High velocity flows of about  $10^4$  cm/sec were maintained by a mechanical vacuum pump rated at 425 liters/sec. The flow rates of the gases were measured using a pair of calibrated critical velocity orifice flowmeters described by Andersen and Friedman.<sup>3</sup> The pressure in the reaction cell was taken as the average value measured by two oil manometers located approximately 20 cm upstream and downstream from the flame zone. The temperature was determined in separate experiments by means of a fine wire thermocouple sealed from the outside with black wax. The observed temperature was determined primarily by the pressure of helium in the discharge, and was nearly independent of the nature and flow rate of the added gas.

The discharge in the helium stream was excited by a 2450 Mc/sec cavity of the Evenson type<sup>4</sup> powered by a 125 W Raytheon diathermy unit. The cavity was located 85 mm upstream of the injection holes. A metal shield excluded the active discharge from extending into the flame zone.

Spectra and intensity measurements were made with a 500 mm Jarrell-Ash Ebert spectrophotometer using an RCA 1P21 photomultiplier tube. A pair of large condensing lenses served to focus the image of a cross-section of the flame on the entrance slit. The spectrophotometer was mounted on a table which could be moved at constant speed parallel to the axis of the tube. In this way the intensity of the flame was recorded as a function of distance along the tube.



All gases were taken directly from the commercially available high pressure cylinders. The stated concentration of impurities in the helium tanks was 50 ppm, with  $N_2$  being the major contaminant.

#### Interpretation of Data

We assume that an excited helium species  $X^*$  reacts with  $N_2$  or  $O_2$  to give the electronically excited  $N_2^+$  or  $O_2^+$ , and the latter immediately decays by emitting a quantum of light, as indicated by reactions (1) and (2)



At this point the identity of  $X^*$  remains unspecified.  $X^*$  could be for example metastable  $2^3S$  helium atom, in which case  $X$  represents a ground state He atom plus an electron. Alternatively  $X$  could be the  $He_2^+$  molecule, and  $X$  would then represent two ground state helium atoms. For simplicity we assume that under any one set of conditions only one excited helium species is dominant, although we can expect several processes occurring simultaneously. The natural lifetime of  $N_2^+$  or  $O_2^+$  is short compared with the time scale of the experiment, and thus the emission intensity is proportional to the rate of reaction (1). If the concentration of nitrogen is uniform and constant along the tube, which should be the case after some distance of travel to effect complete mixing, the decay in intensity with distance should parallel the decay in concentration of  $X^*$ . We therefore need to derive an expression for the concentration of  $X^*$  as a function of position.

We consider a semi-infinite cylinder of radius  $r_0$ . Let  $n$  be the concentration of  $X^*$  and  $N$  the concentration of the added gas, say  $N_2$ . We assume that the two major mechanisms responsible for the decay of  $n$  are diffusion of  $X^*$  to the walls where  $n=0$  and the chemical reaction represented by Eq. (1). Under these conditions the rate of change of  $n$  is given by

$$u \frac{dn}{dx} = D \nabla^2 n - kNn \quad (3)$$

where  $u$  is the stream flow velocity,  $x$  is the axial coordinate,  $D$  is the diffusion coefficient of  $X^*$ , and  $k$  is the specific rate constant for reaction (1). Since transport along the axial direction by convection is much greater than by diffusion, we need only consider radial diffusion, and for this case the solution of the axial part of Eq. (3) is

$$\bar{n}(x) = n_0 \exp\left[-\left(\frac{D}{\Lambda^2} + kN\right)\frac{x}{u}\right] \quad (4)$$

$\Lambda$ , the characteristic diffusion length given by  $\Lambda = r_0/2.405$ , is obtained from the solution of the radial part of Eq. (3) using the assumed boundary condition  $n=0$  at the walls. The radial dependence of  $\bar{n}(x)$  is taken care by the experimental arrangement, since the photomultiplier tube views an entire cross-section of the flame, and its response is proportional to the average intensity. The flow velocity  $u$  and the concentration  $N$  are calculated by Eqs. (5) and (6)

$$u = RT\Sigma F/p\pi r_0^2 \quad (5)$$

$$N = (F_N/\Sigma F)(p/RT) \quad (6)$$

where  $p$  is the pressure,  $T$  is the temperature,  $F_N$  is the flow rate of the added gas in moles/sec, and  $\Sigma F$  is the total flow rate, which in these experiments is essentially equal to the flow rate of helium. If the emitted intensity  $I(x)$  is proportional to  $\bar{n}(x)$ , it follows that a plot of  $\ln I$  vs.  $x$  should be a straight line with slope

$$-\frac{d \ln I}{dx} = S = \frac{(D_0 p_0)(2.405)^2 \pi}{760 \Sigma F RT} + k\pi \left(\frac{p r_0}{\Sigma F RT}\right)^2 F_N \quad (7)$$

In Eq (7) we make use of the fact that  $D$  is inversely proportional to pressure and  $(D_0 p_0)$  is the diffusion coefficient at pressure 1 mm Hg. Using Eq (8) it

should be possible to evaluate  $k$  and  $D_{O_2}$  from the variation of  $S$  with flow rate of added gas.

#### Results

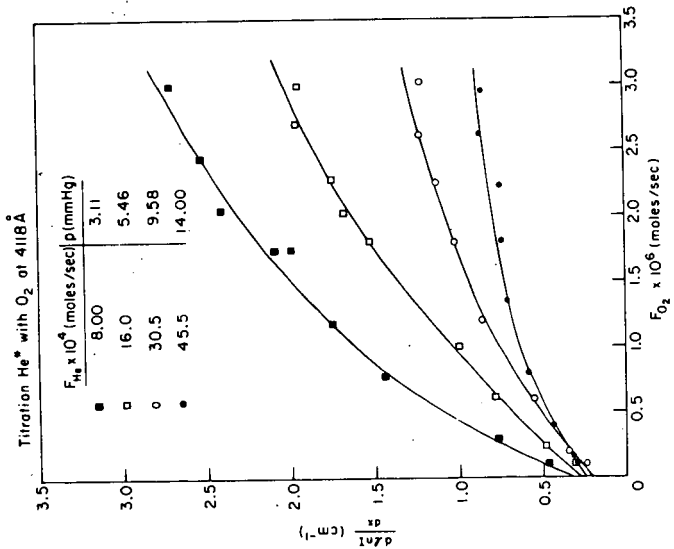
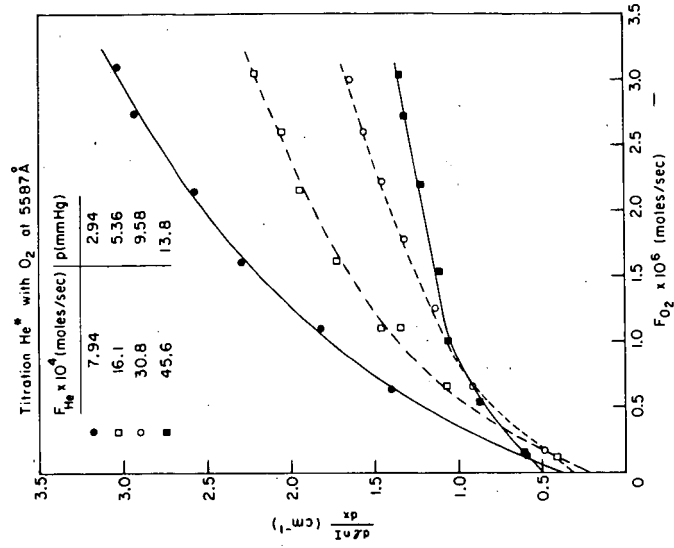
Measurements of intensity vs. distance were recorded for nitrogen at 3915 Å and for oxygen at 5587 Å and 4116 Å. These wave lengths are the heads of intense vibrational bands of the first negative system of  $N_2^+$  and the first and second negative systems of  $O_2^+$ . Typical flames were 2-10 cm in length, and over this distance the intensity varied by nearly a factor of 100. Plots of the logarithm of intensity vs. distance demonstrated a linear behavior over a 50 fold change in intensity, as predicted from Eq (7). Negative deviations from linearity occurred in the region within 0.5-1.0 cm from the injection ports, this no doubt resulting from incomplete mixing of the reactive gases. The slopes of the linear portions were plotted against the flow rate of the added gas, and the results are shown in Figs. 2-4. It is evident that these curves are not linear over the range of flow rates covered, as expected from Eq. 8, but rather show a pronounced downward curvature. We have provisionally taken the extrapolated intercepts and the initial slopes and used them together with Eq. (7) to compute the reaction rate constant as well as the diffusion coefficient of the excited species  $X$ . The results are shown in Table I. The magnitude of the rate constants for the nitrogen and oxygen reactions are comparable and in the range of  $10^{13}$  cc mole<sup>-1</sup> sec<sup>-1</sup>. These rate constants are very fast indeed being of the order of the collision frequency. The diffusion coefficients are of the right order of magnitude for any one of the excited helium species, but the observed temperature dependence is clearly too steep.

#### Discussion

The procedure of using initial slopes to evaluate the rate constants in Table I is admittedly questionable in view of the fact that the curves in Figs. 2-4 do not fit well the model embodied in Eq. (8). Although the intensity of the flames does decay exponentially with distance, and the decay coefficient increases with increasing flow rate of added gas, the increase is not linear. Deviations from linearity appear to be more pronounced at higher pressures (i.e. higher flow rates of helium), presumably because of slower mixing of the reactive streams. This suggests that incomplete mixing and non-uniform concentration of added gas may be responsible for the breakdown of the model, even though the method of injecting the second gas into the helium stream with an initial radial component of velocity should encourage fast mixing. At the lower flow rates of added gas the intensity of the flame decays less rapidly, and consequently intensity measurements are made farther away from the inlet of the second gas. Under these conditions we expect mixing to be more nearly complete and this is in fact the rationale for using the initial part of the curves for evaluating the rate constants. We can check whether incomplete mixing is indeed the source of our difficulties by changing the size of the inlet holes and seeing whether the intensity profiles are affected. We are currently carrying out these experiments.

We have not considered so far the identity of the excited helium species  $X$ . Collins and Robertson have shown that the upper state of  $N_2^+$  giving rise to the blue emission is populated by reaction of  $N_2$  with both metastable  $2^3S$  He and  $He_2^+$ . Similarly they have shown that the upper states of both band systems of  $O_2^+$  are populated by reaction of  $O_2$  with  $2^3S$  He, and in addition the upper state of the 5587 Å system is also populated by  $He_2^+$ . Differences in the  $O_2$  titration curves for the two band systems, particularly with regard to the diffusion coefficients at high pressures when  $He_2^+$  is dominant, may result from the fact that different species give rise to the emission. More accurate measurements of the diffusion coefficient are necessary to resolve this point.

There are very few measurements of the rate constants for these reactions with which we may compare our results. Fehsenfeld and co-workers report a rate constant of  $4 \times 10^{14}$  cc mole<sup>-1</sup> sec for reaction (8)





while Sholette and Muschlitz<sup>9</sup> give values of  $5 \times 10^{13}$  and  $11 \times 10^{13}$  cc mole<sup>-1</sup> sec<sup>-1</sup> for the reactions (1) and (10)



Our preliminary results are in quite reasonable agreement.

#### References

1. C. B. Collins and W. W. Robertson, *J. Chem. Phys.* **40**, 701 (1964); **40**, 202 (1964); **40**, 2208 (1964).
2. A. L. Schmeltekopf and H. P. Broida, *J. Chem. Phys.* **39**, 1261 (1963).
3. E. E. Ferguson, F. C. Fehsenfeld, P. D. Goldan, A. L. Schmeltekopf, and H. I. Schiff, *Planetary Space Sci.* **13**, 823 (1965).
4. J. W. Andersen and R. Friedman, *Rev. Sci. Just.* **20**, 61 (1949).
5. F. C. Fehsenfeld, K. M. Evenson, and H. P. Broida, *Rev. Sci. Just.* **36**, 294 (1965).
6. E. W. McDaniel, *Collision Processes in Ionized Gases* (John Wiley & Sons, Inc., New York, 1964), p. 503.
7. *Ibid*, p. 516.
8. F. C. Fehsenfeld, A. L. Schmeltekopf, P. D. Goldan, H. I. Schiff, and E. E. Ferguson, *J. Chem. Phys.* **44**, 4087 (1966).
9. W. P. Sholette and E. E. Muschlitz, *J. Chem. Phys.* **36**, 3368 (1965).

Table I

Run	$F_{\text{He}} \times 10^4$ moles/sec	p mm Hg	T °K	$k \times 10^{-13}$ cc mole <sup>-1</sup> sec <sup>-1</sup>	$\frac{D P}{\rho}$ (cm <sup>2</sup> sec <sup>-1</sup> )(mm Hg)
a. Titration with N <sub>2</sub> at 3915 Å					
1	6.93	2.70	363	2.1	374
2	9.30	3.46	376	2.0	480
3	16.1	5.41	413	2.8	696
4	30.6	9.64	480	4.2	2140
5	39.6	12.1	508	4.4	3310
b. Titration with O <sub>2</sub> at 5587 (First negative system of O <sub>2</sub> <sup>+</sup> )					
6	7.94	2.99	370	6.7	403
7	16.1	5.36	409	8.4	543
8	30.8	9.58	475	9.0	1660
9	45.6	13.8	515	8.3	4030
c. Titration with O <sub>2</sub> at 4118 (Second negative system of O <sub>2</sub> <sup>+</sup> )					
10	8.00	3.11	366	5.7	331
11	16.1	5.40	418	5.3	643
12	30.5	9.58	488	6.4	1020
13	45.5	14.0	526	5.1	2140

THE MATHEMATICS OF STEADY-STATE DIFFUSION AND FLOW TUBE SYSTEMS  
II. Measurement of Discharge-Zone Rate Parameters

Peter R. Rony

Central Research Department  
Monsanto Company  
St. Louis, Missouri

I. INTRODUCTION

The techniques used to measure the rate of a chemical reaction or to determine the physical characteristics of a chemical compound are dictated by the physical and chemical properties of the compound, particularly by its lifetime and reactivity in relation to its chemical environment. This environment can be chosen to maximize the interactions between the compound and other materials (a reaction environment) or else to minimize such interactions (an isolation environment). Progress in chemistry has been dependent upon the skill chemists have shown in selecting the appropriate reaction or isolation environments.

The problem of developing suitable isolation environments has been a difficult one in the study of flames, shock waves, explosions, and electrical discharges, where the chemical intermediates -- ions, electrons, atoms, free radicals, excited atoms, excited molecules, excited ions, and metastable molecules -- are highly reactive and have extremely short lifetimes. Notable advances along these lines have been the matrix isolation technique developed by Pimentel and co-workers, contacting the intermediates with a very cold surface, and the use of materials that deactivate surfaces against the recombination of atoms and free radicals.<sup>1-7</sup> None of these techniques have yet been successful in significantly prolonging the lifetime of an ion.

This problem can be circumvented by the expedient of placing a source of the chemical intermediates in close proximity to a sink and optimizing the rates of loss and transport of the highly reactive species between these two regions. The most popular source-sink system for the study of gas-phase kinetics of neutral molecules is the diffusion or flow tube, which usually employs an electrodeless discharge as the source.<sup>9,10</sup> Such systems have also been used with considerable success in the field of plasma chemistry for the experimental measurement of associative detachment and ion-neutral reaction rates.<sup>11,12</sup>

The simplicity of these systems is deceptive -- they are usually quite complex. To illustrate this point, Table I gives a non-exhaustive list of rate processes occurring within the system shown in Fig. 1.<sup>24</sup> It is clear that a comprehensive mathematical description of such systems is desirable not only to aid in the choice of experimental conditions and assessment of experimental data, but also to guide those who use diffusion or flow tubes or the measured rate parameters.

Most theoretical descriptions of a diffusion or flow tube have ignored the source of reactive species -- the electrical discharge -- by the assumption of a specified value for the reactive specie concentration at the discharge-zone boundary.<sup>13-17</sup> Tsu and Boudart were the first to incorporate the discharge zone in the derivation and the author has elaborated upon this type of theoretical

description for both diffusion and flow tubes.<sup>18-20</sup>

In the present paper, it is shown that these new equations provide the missing link between the theoretical expressions characterizing the electron and ion concentration distributions within a discharge zone and the expressions typically used for describing the gas-kinetic reactions of the discharge products.<sup>21-23,30</sup> Suggestions are given on how averaged first-order rate constants for the production of discharge products can be measured and how they can be used to calculate the steady-state concentrations of neutral species at any point within the reaction tube. In certain cases, relatively modest equipment can be used to perform such measurements.

The numbering of equations in the present paper continues a previous sequence.<sup>19</sup>

## II. RATE EXPRESSIONS

### A. Neutral Species

Consider a binary system of atoms and the parent molecules present within a long cylindrical tube that has two zones -- a discharge zone and a reactor zone (Fig. 1). If the walls of the tube are not too active, if there are no three-body recombination reactions, and if the atom concentration is less than 15%, the mass-balance equations for the atoms become<sup>19</sup>

$$D_{12} \frac{d^2 c_1'}{dz^2} - v_z \frac{dc_1'}{dz} + k_0'(c - c_1') - k_1' c_1' = 0 \quad (1)$$

diffusion                  convection                  atom production                  first-order  
atom loss

for the discharge zone and

$$D_{12} \frac{d^2 c_1}{dz^2} - v_z \frac{dc_1}{dz} - k_1 c_1 = 0 \quad (2)$$

diffusion                  convection                  first-order  
atom loss

for the reactor zone. These equations can be rewritten in dimensionless form,

$$\frac{d^2 \eta}{d\lambda^2} + \beta \frac{d\eta}{d\lambda} + \sigma^2(1 - \eta) - \frac{\eta}{\delta'^2} = 0 \quad (6)$$

and

$$\frac{d^2 \psi}{d\lambda^2} + \beta \frac{d\psi}{d\lambda} - \frac{\psi}{\mu^2} = 0 \quad (7)$$

In a previous paper, a total of 36 equations summarized the operation of a flow or diffusion tube, with or without a first-order atom loss process in the reactor zone, for three different discharge-zone boundary conditions and three different end-plate boundary conditions.<sup>19</sup> The solutions to Eq. (7) were sub-

divided into four cases:

- Case I. Diffusion tube ( $\beta = 0$ ) with inactive reactor zone walls ( $1/\mu^2 = 0$ );  
 Case II. Diffusion tube ( $\beta = 0$ ) with active reactor-zone walls ( $1/\mu^2 \neq 0$ );  
 Case III. Flow tube ( $\beta \neq 0$ ) with inactive reactor-zone walls ( $1/\mu^2 = 0$ ); and  
 Case IV. Flow tube ( $\beta \neq 0$ ) with active reactor-zone walls ( $1/\mu^2 \neq 0$ ).

The eight most useful solutions are listed in Table II. The most general solution for the reactor zone, from which the 35 others can be obtained by appropriate simplifications, is Eq. (60). The original paper should be consulted for further information concerning the derivation of the mass-balance equations, the boundary conditions, or the other theoretical solutions. Definitions of dimensionless groups are given in the Appendix.

TABLE II. Pertinent Solutions to Equation (7).

End-plate Boundary Conditions:	Discharge-zone boundary condition: $\frac{d\eta}{d\lambda} = 0$ at $\lambda = \frac{L+M}{R}$			
	Case I.	Case II.	Case III.	Case IV.
$\frac{d\psi}{d\lambda} = 0$ at $\lambda = -\infty$	Eq. (27)	Eq. (36)	Eq. (27)	Eq. (54)
$\frac{d\psi}{d\lambda} = \frac{\psi}{\xi'}$ at $\lambda = 0$	Eq. (33)	Eq. (42)	Eq. (51)	Eq. (60)

$$\psi = \sigma^2 \delta^2 \quad (27)$$

$$\psi = \sigma^2 \delta^2 \frac{\lambda + \xi'}{L/R + \xi' + \delta \coth(M/\delta R)} \quad (33)$$

$$\psi = \sigma^2 \delta^2 \frac{e^{-z/\mu R}}{1 + \delta/\mu \coth(M/\delta R)} \quad (36)$$

$$\psi = \sigma^2 \delta^2 \frac{H e^{\lambda/\mu} + e^{-\lambda/\mu}}{(1 + \delta/\mu \coth M/\delta R) H e^{L/\mu R} + (1 - \delta/\mu \coth M/\delta R) e^{-L/\mu R}} \quad (42)$$

$$\psi = \sigma^2 \delta^2 \frac{(\beta \xi' + 1) - e^{-\beta \lambda}}{(\beta \xi' + 1) - \left[ \frac{(X-\beta) - (X+\beta)P}{(X+\beta) - (X-\beta)P} \right] e^{-\beta L/R}} \quad (51)$$

$$\psi = \sigma^2 \delta^2 \frac{e^{-(\Omega-\beta)z/2R}}{\frac{P(X-\Omega) - (X+\Omega)}{P(X-\beta) - (X+\beta)}} \quad (54)$$

$$\psi = \sigma_+^2 \delta^2 \frac{T e^{(\Omega-\beta)\lambda/2} + e^{-(\Omega+\beta)\lambda/2}}{\left[ \frac{P(X-\Omega) - (X+\Omega)}{P(X-\beta) - (X+\beta)} \right] T e^{(\Omega-\beta)L/2R} + \left[ \frac{P(X+\Omega) - (X-\Omega)}{P(X-\beta) - (X+\beta)} \right] e^{-(\Omega+\beta)L/2R}} \quad (60)$$

### B. Ions and Electrons

Consider a ternary system of electrons and two different positive ions present within the discharge zone shown in Fig. 1. If it is assumed that

$$c_1^+ \ll c_2^+ \approx c_e + c_e' \quad (108)$$

the mass balance equation for the minor ionic specie can be linearized to give

$$D_a \nabla^2 c_1^+ + \underset{\text{ambipolar diffusion}}{k_i c_e c_m} - \underset{\text{ion-electron recombination}}{k_r c_e' c_1^+} = 0 \quad (109)$$

where  $c_e$  and  $c_e'$  refer to the concentrations of electrons of different energies. Equation (109) can be put in dimensionless form,

$$\frac{d^2 \eta_+}{d\rho^2} + \frac{1}{\rho} \frac{d\eta_+}{d\rho} + \frac{d^2 \eta_+}{dT^2} - \frac{\eta_+}{\delta_+^2} + \sigma_+^2 = 0 \quad (110)$$

where the dimensionless groups are defined in the Appendix. It should be noted that a transformation of coordinates from Fig. 1 has been made,

$$T = \lambda + \frac{\frac{M}{2} - L}{R} \quad (111)$$

The boundary conditions are

$$\eta_+ = 0 \quad \text{at } T = 0 \text{ and } T = M/2R \text{ at all } \rho \quad (112)$$

$$\eta_+ = 0 \quad \text{at } \rho = 1 \text{ and all } T \quad (113)$$

$$\frac{d\eta_+}{d\rho} = 0 \quad \text{at } \rho = 0 \text{ and all } T \quad (114)$$

and the solution is

$$\eta_+ = \sigma_+^2 \delta_+^2 \left[ 1 - \frac{\cosh T/\delta_+}{\cosh M/2\delta_+ R} \right] - \frac{4\sigma_+^2}{\pi} \sum_{n=0}^{\infty} \frac{(-1)^n I_0(\beta_n \rho) \cos \alpha_n T}{\beta_n^2 (2n+1) I_0(\beta_n)} \quad (115)$$

Equation (115) can be progressively simplified to

$$I. \quad \eta_+ = \frac{\sigma_+^2}{2} \left[ \left( \frac{M}{2R} \right)^2 - T^2 \right] - \frac{4\sigma_+^2 M^2}{R^2 \pi^3} \sum_{n=0}^{\infty} \frac{(-1)^n I_0(\alpha_n \rho) \cos \alpha_n T}{(2n+1)^3 I_0(\alpha_n)} \quad (116)$$

$$\text{II. } \eta_+ = \sigma_+^2 \delta_+^2 \left[ 1 - \frac{\cosh \tau / \delta_+}{\cosh M / 2\delta_+ R} \right] - \frac{4\sigma_+^2}{\pi} \left[ \frac{I_0(\beta_0 \rho) \cos \alpha_0 \tau}{\beta_0^2 I_0(\beta_0)} \right] \quad (117)$$

$$\text{III. } \eta_+ = \frac{\sigma_+^2}{2} \left[ \left( \frac{M}{2R} \right)^2 - \tau^2 \right] - \frac{4\sigma_+^2 M^2}{\pi^2 R^2} \left[ \frac{I_0(\alpha_0 \rho) \cos \alpha_0 \tau}{I_0(\alpha_0)} \right] \quad (118)$$

$$\text{IV. } \eta_+ = \frac{\sigma_+^2 M^2}{8R^2} \quad (119)$$

$$\text{V. } \eta_+ = \sigma_+^2 \delta_+^2 \left[ 1 - \frac{I_0(\rho / \delta_+)}{I_0(1 / \delta_+)} \right] \quad (120)$$

$$\text{VI. } \eta_+ = \frac{\sigma_+^2}{4} \left[ 1 - \rho^2 \right] \quad (121)$$

$$\text{VII. } \eta_+ = \sigma_+^2 \delta_+^2 \quad (122)$$

when: I.  $1/\delta_+^2 = 0$ ; II. the first root of Eq. (115) is dominant; III. the first root of Eq. (115) is dominant; IV.  $\rho = 0$ ,  $\tau = 0$ , and  $I_0(\alpha_0)$  is large in Eq. (118); V.  $\frac{\partial^2 \eta_+}{\partial \tau^2} = 0$ ; VI.  $\frac{\partial^2 \eta_+}{\partial \tau^2} = 0$  and  $1/\delta_+^2 = 0$ ; and VII.  $\rho = 0$  and  $I_0(1/\delta_+)$  is large in Eq. (120). Carslaw and Jaeger should be consulted for other solutions to these types of equations.<sup>25</sup>

An average value for the concentration of the minor ionic specie,  $\bar{\eta}_+$ , can be obtained by the following integration,

$$\bar{\eta}_+ = \frac{\int_0^{M/2R} \int_0^1 \eta_+ d\rho d\tau}{\int_0^{M/2R} \int_0^1 d\rho d\tau} \quad (123)$$

Unfortunately, the integral  $\int_0^1 I_0(\alpha_n \rho) d\rho$  cannot be evaluated explicitly.

### III. CONSEQUENCES

#### A. Previous Results

For the sake of brevity, a number of topics pertaining to the discharge zone given previously will not be repeated here. The reader is referred to the following sub-sections of Sec. VI in reference (19): A. Choice of Steady-State Systems; B. Complexity of Solutions; C. Velocity and Mass Flux; D. Residence Time; E. Radial Concentration Gradients; F. Comparison of Rate Processes; I. Back Diffusion; and M. Surface Reaction vs Atom Production.

#### B. Measurement of $k_0$

##### 1. Comparison of Rate Processes

The behavior of atoms in the system shown in Fig. 1 is characterized by eight different rate processes: convection, radial diffusion to the walls,

axial diffusion through the discharge zone, axial diffusion through the reactor zone, production, recombination on the end plate, recombination in the discharge zone, and recombination in the reactor zone. Thus, the interaction between the rate of production and the other rate processes can be conveniently characterized by seven dimensionless groups:

$$\sigma^2 = \frac{\text{rate of atom production in the discharge zone}}{\text{rate of radial diffusion to the wall}} = \frac{k_0' R^2}{D_{12}}$$

$$\frac{\sigma^2}{1/\delta'^2} = \frac{\text{rate of atom production in the discharge zone}}{\text{rate of atom recombination within the discharge zone}} = \frac{k_0'}{k_1'} \text{ or } \frac{2k_0' R}{\gamma v_1}$$

$$\frac{\sigma^2}{1/\mu^2} = \frac{\text{rate of atom production in the discharge zone}}{\text{rate of atom recombination within the reactor zone}} = \frac{k_0'}{k_1'} \text{ or } \frac{2k_0' R}{\gamma v_1}$$

$$\frac{\sigma^2}{1/\xi'} = \frac{\text{rate of atom production in the discharge zone}}{\text{rate of atom recombination on the end plate}} = \frac{4k_0' R}{\gamma' v_1}$$

$$\frac{\sigma^2}{\beta} = \frac{\text{rate of atom production in the discharge zone}}{\text{rate of axial convection}} = \frac{k_0' R}{v_z}$$

$$\frac{\sigma^2}{R/M} = \frac{\text{rate of atom production in the discharge zone}}{\text{rate of axial diffusion through the discharge zone}} = \frac{k_0' R M}{D_{12}}$$

$$\frac{\sigma^2}{R/L} = \frac{\text{rate of atom production in the discharge zone}}{\text{rate of axial diffusion through the reactor zone}} = \frac{k_0' R L}{D_{12}}$$

These dimensionless groups can be further condensed to yield just two groups relating the overall rates of atom production, transport, and loss:

$$\frac{\phi_{\text{prod}}}{\phi_{\text{loss}}} = \frac{\text{rate of atom production}}{\text{rate of atom loss}} = \frac{\sigma^2}{1/\xi' + 1/\delta'^2 + 1/\mu^2} \quad (124)$$

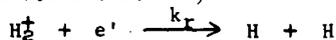
$$\frac{\phi_{\text{loss}}}{\phi_{\text{transport}}} = \frac{\text{rate of atom loss}}{\text{rate of atom transport}} = \frac{1/\xi' + 1/\delta'^2 + 1/\mu^2}{R/L + R/M + \beta + 1} \quad (125)$$

In a steady-state experiment, there must be a competition between two rate processes -- a source and a sink. If the source and sink are spatially separated, then a transport process may further complicate the results. In the present case, the rate of atom production can be measured only if

$\frac{\phi_{\text{prod}}}{\phi_{\text{loss}}} < 1$ , for if the source is much greater than the sink, no concentration gradient can exist.

## 2. Significance of $k_0'$

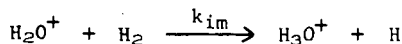
For purposes of discussion, assume that the rate parameter  $k_0'$  represents the rate of production of atomic hydrogen ( $c_1'$ ) via the following ion-electron recombination reaction,



Thus,

$$k'_0(c - c_1) = \frac{dc_1}{dt} = 2k_r(H_2^+)(e') \quad (126)$$

defines the parameter  $k'_0$ . If atomic hydrogen is also produced when water is present via an ion-molecule reaction,



$k'_0$  changes to

$$k'_0(c - c_1) = \frac{dc_1}{dt} = 2k_r(H_2^+)(e') + k_{im}(c - c_1)(H_2O^+) \quad (127)$$

It is clear from the above that  $k'_0$  is a composite parameter which rarely can be subdivided into its component parameters from discharge product measurements alone. Furthermore, as shown in Sec. II. B., the ion and electron concentrations are not uniform throughout the discharge zone, so an average value,  $\bar{k}'_0$ , is observed,

$$\bar{k}'_0(c - c_1) = 2k_r(H_2^+)_{AV}(e')_{AV} + k_{im}(c - c_1)(H_2O^+)_{AV} \quad (128)$$

Thus, the measurement of absolute yields of discharge products is not a fruitful technique for studying discharge-zone kinetics. An exception to this statement occurs when the discharge is initially well characterized and perturbations are made on this initial state. For example, in the absence and presence of water, the ratio of the above rate parameters  $\bar{k}'_0$  becomes

$$\frac{\bar{k}'_0(c - c_1)|_{\text{with } H_2O}}{\bar{k}'_0(c - c_1)|_{\text{no } H_2O}} = 1 + \frac{k_{im}(c - c_1)(H_2O^+)_{AV}}{2k_r(H_2^+)_{AV}(e')_{AV}} \quad (129)$$

The quantity  $k_{im}(H_2O^+)_{AV}$  can be determined provided that the ratio of  $\bar{k}'_0$  values is measurable and the other quantities are known.

### 3. Interaction Between Discharge and Reactor Zones

The activity of the reactor-zone walls and the location of the catalytic end plate have a measurable influence upon the atom concentration within the discharge zone and at the discharge-zone boundary. This phenomenon can be used to advantage for the measurement of absolute or relative values of the rate constant of atom production  $k'_0$ .

In the absence of reactor-zone sinks, Eqs. (27) and (45) apply,

$$\psi = \sigma^2 \delta^2 = \frac{k'_0}{k'_0 + k_1} \quad \text{or} \quad \frac{k'_0}{k'_0 + \frac{\gamma \bar{v}_1}{2R}} \quad (130)$$

The atom production rate constant  $k'_0$  can be determined from Eq. (130) provided that (a) the amount of atom recombination on the discharge-zone walls is known, (b) it remains constant during the measurement process, and (c) it is the dominant atom loss process. In an electrode discharge, metal sputtering on

the tube walls occurs continuously and the above conditions are not fulfilled. With other types of discharges, a period of wall aging may be required.

If an end plate is present, the concentration of atoms at the discharge boundary ( $\lambda = L/R$ ) is given by Eq. (33),

$$\psi = \sigma^2 \delta^2 \frac{\frac{L}{R} + \xi'}{\frac{L}{R} + \xi' + \frac{\delta^2 R}{M}} \quad \left( \frac{M}{\delta R} \leq 1/4 \right) \quad (131)$$

When  $L/R + \xi' \gg \frac{\delta^2 R}{M}$ , then  $\psi = \sigma^2 \delta^2$  as previously. However, if  $\frac{\delta^2 R}{M} \gg L/R + \xi'$ , then

$$\psi = \frac{M}{R} \sigma^2 \left( \frac{L}{R} + \xi' \right) = \frac{M k_0'}{D_{12}} \left( L + \frac{4 D_{12}}{\gamma_1 v_1} \right) \quad (132)$$

The rate constant  $k_0'$  can be determined if the recombination coefficient of the end plate or the diffusion coefficient of the atoms is known.

If only the reactor-zone walls are active, Eq. (36) applies at the discharge-zone boundary ( $z = 0$ ),

$$\psi = \sigma^2 \delta^2 \frac{1}{1 + \frac{\delta^2 R}{\mu M}} \quad \left( \frac{M}{\delta R} \leq 1/4 \right) \quad (133)$$

The only new result occurs when  $\frac{\delta^2 R}{\mu M} \gg 1$ , and leads to

$$\psi = \sigma^2 \frac{M}{R} \mu = k_0' M \left( \frac{2R}{D_{12} \gamma_1 v_1} \right)^{1/2} \quad (134)$$

which is no improvement over Eq. (132). Equations (42), (51), (54), and (60) lead to progressively more complicated solutions.

In the preceding paragraphs we have been preoccupied with the measurement of  $k_0'$ . The equations derived above are equally applicable if  $k_0'$  is already known and show how such data can be used to predict steady-state atom concentration levels in diffusion and flow tubes.

As an example, consider the effect of an end plate on the atom concentration within the discharge zone. In the absence of the end plate, the concentration throughout the reaction tube is given by Eq. (130). When the end plate is present, either Eq. (33) or Eq. (131) applies for the reactor zone and Eq. (135) applies for the discharge zone ( $z$  assumes negative values only between 0 and  $-M$ ).

$$\eta = \sigma^2 \delta^2 \left[ 1 - \frac{\delta \frac{\cosh \left( \frac{z+M}{\delta R} \right)}{\sinh M/\delta R}}{\frac{L}{R} + \xi' + \delta \coth \frac{M}{\delta R}} \right] \quad (135)$$

With  $R = 2$  cm,  $D_{12} = 1.25 \cdot 10^4$  cm<sup>2</sup>/sec (atomic hydrogen at 100 mTorr and 25°C),  $L = 10$  cm,  $v_1 = 2.5 \cdot 10^5$  cm/sec (atomic hydrogen),  $M = 8$  cm,  $v_2 = 0$  cm/sec,

$\gamma_{\text{walls}} = 10^{-5}$ ,  $\gamma'_{\text{end plate}} = 10^{-2}$ , and  $k_0' = 0.100 \text{ sec}^{-1}$ , the average atom concentration in the discharge zone is reduced from 14% to 0.19%. It is assumed here that the end plate has no effect on the electron and ion concentration levels within the discharge.

#### 4. Mass-Flux Devices

As shown above, the measurement of the absolute value of  $k_0'$  requires a knowledge of either  $\gamma$ ,  $M$  and  $D_{12}$ , or  $M$  and  $\gamma'$ . A simpler procedure applicable to the study of atoms requires the use of a mass-flux device such as an isothermal calorimeter, which measures the atom flux at a given point within the reactor zone.<sup>19</sup> Equation (131) becomes

$$\begin{aligned} J_{1s} \text{ (atoms/cm}^2 \text{ sec)} &= - D_{12} \left. \frac{\partial c_1}{\partial z} \right]_{z=L} = \left. \frac{c D_{12}}{R} \frac{\partial \psi}{\partial \lambda} \right]_{\lambda=0} \\ &= \sigma^2 \delta^2 \frac{c D_{12} / R}{\frac{L}{R} + \xi' + \frac{\delta^2 R}{M}} \approx \frac{M}{R} \sigma^2 \frac{c D_{12}}{R} = k_0' M c \end{aligned} \quad (136)$$

when  $\frac{\delta^2 R}{M} \gg \left( \frac{L}{R} + \xi' \right)$ . Thus, the rate of atom production can be determined by a mass-flux measurement provided that the value of  $M$  is known and the calorimeter is the dominant atom sink.

#### 5. Relative Measurements

Provided that certain parameters remain constant and the appropriate inequality relationships hold, the measurement of relative values of  $k_0'$  is the easiest measurement to perform in diffusion or flow tubes. The most important requirement is that  $\frac{\Phi_{\text{prod}}}{\Phi_{\text{loss}}} \ll 1$ , as discussed in Sec. III. B. 1. The desired relationship

$$\psi = \text{constant} \cdot k_0' \quad (137)$$

is rigorously correct for any of the following cases:

- I.  $\sigma^2 \delta^2 \ll 1$  in Eq. (130);
- II.  $\left( \frac{L}{R} + \xi' \right) \gg \frac{\delta^2 R}{M}$  and  $\sigma^2 \delta^2 \ll 1$  in Eq. (131);
- III.  $\frac{\delta^2 R}{M} \gg \left( \frac{L}{R} + \xi' \right)$ ,  $M = \text{constant}$ ,  $L = \text{constant}$ , and  $\xi' = \text{constant}$  in Eq. (131);
- IV.  $\frac{\delta^2 R}{\mu M} \ll 1$  and  $\sigma^2 \delta^2 \ll 1$  in Eq. (133);
- V.  $\frac{\delta^2 R}{\mu M} \gg 1$ ,  $M = \text{constant}$ , and  $\mu = \text{constant}$  in Eq. (133);
- VI.  $\frac{\delta^2 R}{M} \gg \left( \frac{L}{R} + \xi' \right)$  and  $M = \text{constant}$  in Eq. (136); and

$$\text{VII. } \left( \frac{L}{R} + \xi' \right) \gg \frac{\delta^2 R}{M}, \quad \sigma^2 \delta^2 \ll 1, \quad L = \text{constant}, \quad \text{and } \xi' = \text{constant in Eq. (136).}$$

The above list is not exhaustive, since any of the solutions in Sec. II. A. can be used if the proper conditions are fulfilled.

#### 6. Multiple Discharge Products

When more than one discharge product is formed, the simplest mass-balance equations and boundary conditions become

$$\frac{d^2 \eta_i}{d\lambda^2} + \sigma_i^2 (1 - \sum_{j=1}^n \eta_j) - \frac{\eta_i}{\delta_i^2} = 0 \quad \text{and} \quad \frac{d^2 \psi_i}{d\lambda^2} = 0 \quad (138)$$

$$\frac{d\eta_i}{d\lambda} = 0 \quad \text{at} \quad \lambda = \infty \quad \text{and} \quad \frac{d\psi_i}{d\lambda} = 0 \quad \text{at} \quad \lambda = -\infty \quad (139)$$

The solution is of the form

$$\psi_i = \eta_i = \sigma_i^2 \delta_i^2 \left[ \frac{1 - \sum_{\substack{j=1 \\ j \neq i}}^n \frac{1}{\sigma_j^2 \delta_j^2}}{\sigma_i^2 \delta_i^2 - \sum_{\substack{j=1 \\ j \neq i}}^n \frac{1}{\sigma_j^2 \delta_j^2}} \right] \quad (140)$$

which, if the total amount of product is small, simplifies to

$$\psi_i = \eta_i \approx \sigma_i^2 \delta_i^2 \quad (141)$$

If there are no sinks, a discharge product will not disappear once it has been formed. For moderately stable molecules, such sinks include decomposition on the walls of the reaction tube and reaction with other gas-phase components. Conditions can be adjusted to minimize these loss processes, a fact which accounts for the variety of novel chemical species that can be produced from chemical discharge systems.<sup>26-29</sup>

#### IV. SUMMARY AND CONCLUSIONS

The rate of production of a given chemical intermediate in a diffusion or flow tube is characterized by  $k_0'$ , a composite parameter incorporating the rates of ionization, ion-electron recombination, ion-molecule reactions, electron attachment, wall recombination, ion-ion recombination, ambipolar diffusion, and other kinetic processes occurring within the discharge zone. The measurement of the absolute value of  $k_0'$  requires a knowledge of either  $\gamma$ ,  $M$ ,  $M$  and  $D_{12}$ , or  $M$  and  $\gamma'$ . Relative measurements of  $k_0'$  are possible under a wide variety of conditions. Many novel chemical species can be produced from such systems if all homogeneous and heterogeneous sinks are minimized.

## V. NOTATION

$\nabla$	Del operator (vector)
$\infty$	Infinity
{ }	Braces indicating molar concentration of enclosed species
$c$	Total molar concentration of gaseous species
$c_1$	Molar concentration of atoms in reactor zone
$c_1^+$	Molar concentration of atoms in discharge zone
$c_2^+$	Molar concentration of minor positive ionic specie
$c_2^-$	Molar concentration of major positive ionic specie
$c_e$	Molar concentration of high-energy electrons
$c_e'$	Molar concentration of low-energy electrons
$D_{12}$	Binary diffusion coefficient for atom-molecule system
$D_a$	Ambipolar diffusion coefficient
$e$	Exponential
$i$	Represents quantity related to specie $i$
$I_0( )$	Modified Bessel function
$j$	Represents quantity related to specie $j$
$J_{1s}$	Molar flux of atoms to end plate
$k_1$	First-order rate constant for loss of atoms in reactor zone
$k_1^+$	First-order rate constant for loss of atoms in discharge zone
$k_0^+$	First-order rate constant for production of atoms in discharge zone
$\bar{k}_0^+$	Averaged first-order rate constant $k_0^+$
$k_i$	Second-order ionization rate constant
$k_r$	Second-order ion-electron recombination rate constant
$k_{im}$	Second-order ion-molecule reaction rate constant
$L$	Length of reactor zone to end plate
$M$	Length of discharge zone (or half the length for a symmetrical system)
$R$	Radius of reaction tube
$\frac{v_z}{v_1}$	Mass-average velocity in $z$ direction (axial direction)
$\frac{v_z}{v_1}$	Velocity of an atom
$z$	Distance from discharge-reactor zone boundary to end plate (+ direction)

## REFERENCES

1. Whittle, E., Dows, D. A., and Pimentel, G. C., *J. Chem. Phys.* 22, 1943 (1954).
2. Norman, I., and Porter, G., *Nature* 174, 508 (1954).
3. Pimentel, G. C., in Formation and Trapping of Free Radicals, (Academic Press, New York, 1960), p. 69.
4. Rice, F. J., and Frearno, M. J., *J. Am. Chem. Soc.* 73, 5529 (1951).
5. Rice, F. J., and Frearno, M. J., *J. Am. Chem. Soc.* 75, 548 (1953).
6. Goldenberg, H. M., Kleppner, D., and Ramsey, N. F., *Phys. Rev.* 123, 530 (1961).
7. Berg, H. C., and Kleppner, D., *Rev. Sci. Instr.* 33, 248 (1962).
8. Shaw, T. M., in Formation and Trapping of Free Radicals, (Academic Press, New York, 1960), p. 47.
9. Dickens, P. G., Linnett, J. W., and Palczewska, W., *J. Catalysis* 4, 140 (1965).
10. Evenson, K. M., and Burch, D. S., *J. Chem. Phys.* 45, 2450 (1966).
11. Fehsenfeld, F. C., Schmeltekopf, A. L., and Ferguson, E. E., *J. Chem. Phys.* 44, 4537 (1966).
12. Fehsenfeld, F. C., Ferguson, E. E., and Schmeltekopf, A. L., *J. Chem. Phys.* 45, 1844 (1966).
13. Wise, H., and Ablow, C. M., *J. Chem. Phys.* 29, 634 (1958).
14. Wise, H., and Ablow, C. M., *J. Chem. Phys.* 35, 10 (1963).
15. Dickens, P. G., Schofield, D., and Walsh, J., *Trans. Far. Soc.* 56, 1338 (1959).
16. Schulz, W. R., and Le Roy, D. J., *Can. J. Chem.* 40, 2413 (1962).
17. Morgan, J. E., and Schiff, H. I., *J. Chem. Phys.* 38, 2631 (1963).
18. Tsu, K., and Boudart, M., *Can. J. Chem.* 39, 1239 (1961).
19. Rony, P. R., "The Mathematics of Steady-State Diffusion and Flow Tubes. Factors Affecting Rate Measurements," 32nd Annual Chemical Engineering Symposium, Stanford, California, 1965. (Copies are available).
20. Rony, P. R., I. & E. C. (to be submitted).
21. Biondi, M. A., and Brown, S. C., *Phys. Rev.* 75, 1700 (1949).
22. Phelps, A. V., and Brown, S. C., *Phys. Rev.* 86, 102 (1952).
23. Gray, E. P., and Kerr, D. E., *Ann. Phys.* 17, 276 (1959).
24. McDaniel, E. W., Collision Phenomena in Ionized Gases (John Wiley & Sons, Inc., New York, 1964).
25. Carslaw, H. S., and Jaeger, J. C., Conduction of Heat in Solids (Clarendon Press, Oxford, England, 1959), Section 8.3, p. 217.
26. Jolly, W. L., "The Use of Electric Discharges in Chemical Synthesis," Lawrence Radiation Laboratory UCRL-9501 (1960). (unpublished).
27. Gould, R. F., Free Radicals in Inorganic Chemistry (Amer. Chem. Soc., Washington, D.C., 1962).
28. Kondrat'ev, V. N., Chemical Kinetics of Gas Reactions (Addison-Wesley Publishing Company, Ind., Reading, Massachusetts, 1964), p. 467.
29. Kana'an, A. S., and Margrave, J. L., Advances in Inorganic Chemistry and Radiochemistry 6, (Academic Press, New York, 1964), p. 143.
30. Hurt, W. B., *J. Chem. Phys.* 45, 3439 (1966).

## APPENDIX

$$\lambda = \frac{L - z}{R}$$

$$T = \lambda + \frac{M/2 - L}{R}$$

$$\rho = \frac{r}{R}$$

$$\psi = \frac{c_1}{c}$$

$$\eta = \frac{c_1'}{c}$$

$$\beta = \frac{v_2 R}{D_{12}}$$

$$\sigma^2 = \frac{k_0' R^2}{D_{12}}$$

$$\delta_{12}^2 = \frac{2D_{12}(1 - \gamma/2)}{R\gamma\bar{v}_1} \quad (\text{surface phase})$$

$$\delta_{12}^2 = \frac{D_{12}}{k_1' R^2} \quad (\text{gas phase})$$

$$\mu^2 = \frac{2D_{12}(1 - \gamma/2)}{R\gamma\bar{v}_1} \quad (\text{surface phase})$$

$$\mu^2 = \frac{D_{12}}{k_1' R^2} \quad (\text{gas phase})$$

$$\eta_+ = \frac{c_1^+}{c}$$

$$\bar{\eta}_+ = \frac{c_1^+}{c}$$

$$\xi_1' = \frac{4D_{12}(1 - \gamma'/2)}{R\gamma_1'\bar{v}_1}$$

$$\gamma = \frac{2k_1 R}{\bar{v}_1}$$

$$\frac{1}{\delta^2} = \sigma^2 + \frac{1}{\delta_{12}^2}$$

$$\frac{\Omega}{2} = \left[ \frac{\beta^2}{4} + \frac{1}{\mu^2} \right]^{\frac{1}{2}}$$

$$\frac{X}{2} = \left[ \frac{\beta^2}{4} + \frac{1}{\delta^2} \right]^{\frac{1}{2}}$$

$$H = \frac{\xi_1' + \mu}{\xi_1' - \mu}$$

$$P = \left( \frac{X + \beta}{X - \beta} \right) e^{-MX/R}$$

$$T = \frac{\Omega\xi_1' + \beta\xi_1' + 2}{\Omega\xi_1' - \beta\xi_1' - 2}$$

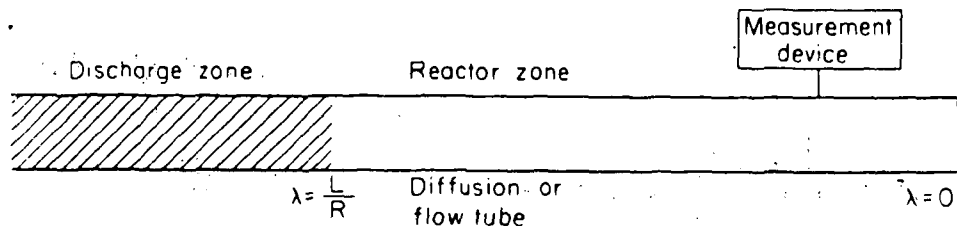
$$\sigma_+^2 = \frac{k_1 c_e R^2}{D_a}$$

$$\delta_+^2 = \frac{k_r c_e' R^2}{D_a}$$

$$\alpha_n = \frac{\pi R(2n + 1)}{M}$$

$$\beta_n^2 = \alpha_n^2 + \frac{1}{\delta_+^2}$$

$$\frac{1}{\delta_1^2} = \sigma_1^2 + \frac{1}{\delta_+^2}$$



MU. 35708

Fig. 1. Schematic drawing of a typical "reaction tube," showing the location of the discharge zone, the reactor zone, the discharge-zone boundary (at  $\lambda = L/R$ ), and the end plate (at  $\lambda = 0$ ).

Table 1. Rate processes occurring within a typical reaction tube.<sup>24</sup>

<u>Ions and Electrons in Discharge Zone</u>		<u>Neutral Species in Discharge and Reactor Zones</u>
<b>PRODUCTION:</b>	Ionization Photoionization Ion-molecule Reactions Electron Attachment Charge Transfer Metastable Atom Reactions	Ion-electron Recombination Ion-ion Recombination Ion-molecule Reactions Electron Attachment Wall Recombination of Ions
<b>LOSS:</b>	Ion-electron Recombination Ion-ion Recombination Wall Recombination Loss to Measurement Device Electron Detachment	Gas-kinetic Reactions Recombination on Walls Recombination on End Plate Loss to Measurement Device
<b>TRANSPORT:</b>	Convection Diffusion Ambipolar Diffusion Drift Cyclotron Resonance	Convection Diffusion

Radiation Chemistry and Electric Discharge Chemistry:  
Comparison and Contrast.

Milton Burton and Koichi Funabashi

Department of Chemistry and the Radiation Laboratory\*  
University of Notre Dame, Notre Dame, Indiana 46556

\* The Radiation Laboratory of the University of Notre Dame is operated under contract with the U. S. Atomic Energy Commission. This is AEC document number COO-38-511.

In radiation chemistry the customary situation is that a charged particle with energy in the MeV range is slowed down in matter and, in the course of such deceleration, excites some molecules and ionizes others. The ultimate fate of the initial charged particle is of little consequence compared to the many processes which it initiates but that initial particle is actually responsible for initial excitations and ionizations which amount to about one-quarter of the total number of such processes. The corollary statement is that about three-quarters of all the effects observed are attributable to the action of secondary (and, to a very small extent, tertiary) charged particles. Roughly, these particles have initial energy,  $\epsilon_i$ , averaging about 75 eV.

The secondary charged particles can cause further ionizations (in addition to excitations) only so long as they have energy,  $\epsilon$ , in excess of the ionization potential,  $I$ , of the species which they traverse. A convenient value for  $I$  is about 10 eV. When  $\epsilon$  becomes  $< I$ , the only processes which can occur significant for radiation chemistry are electronic excitations to singlet or triplet states. When  $\epsilon$  becomes  $< 5$  eV the major portion of the excitations are optically disallowed (i. e., mainly triplet). For radiation chemistry about  $\frac{3}{4} \times \frac{5}{75}$  or 5% of all the phenomena are initiated by particles with about that amount of energy.

In electric discharge processes, irrespective of the voltage employed the electrons start with about zero energy and rarely attain an energy in excess of 5 eV and much more rarely in excess of the ionization potential. It has been one of the important problems of electric discharge chemistry to determine how molecules are excited to chemically active levels and how ionized species are produced. According to some theoretical views most of the electrons cause optically forbidden excitations on the first opportunity and it might appear that chemical effects simply could not be observed. Nevertheless, they are observed and the fact must be that a significant number of molecules are excited to sufficiently high states so that chemistry results. Furthermore, some of them, in number adequate for maintenance of the discharge, are excited up to ionization potentials. Thus, in this case,  $\epsilon_i$  is initially approximately zero and might appear not to exceed very low energies; e. g.,  $\epsilon_t$ , corresponding to the lowest triplet state. Yet, high excitations and ionizations do occur.

Two views may be employed to account for this dilemma. The theory presented is oversimplified and electrons in significant quantity attain energies in excess of 7 eV. Alternatively, it was suggested initially by Magee and Burton<sup>1</sup> that electric discharge chemistry is characterized by a series of successive excitations by low-energy electrons in optically forbidden steps to higher and higher levels with ultimate attainment of levels adequate for production of a chemical effect - or even of ionization.

The role of thermal energy is somewhat different in the two fields. In discharge chemistry a local temperature may be raised as high as 1000°C, whereas the usual dosage level used in the basic research of radiation chemistry is so low that the temperature increase can be of the order of a few degrees C even if the entire energy input is converted to thermal energy. This difference is not a trivial one, because thermal

energy and electronic energy (in the forms of excitation or ionization) do not exist as independent sources of energy for chemical reactions; the effect arising from a combination of the two forms of energy is not a simple sum of the two effects when each source acts alone. The detail of the interaction between thermal and electronic energies is not known. The qualitative picture, however, is fairly well understood. Namely, the rate of energy conversion from the electronic to the thermal form (radiationless transition or energy degradation) increases as the temperature increases. Thus, the process has the characteristics of an explosive chain reaction.

The main reason for this difference is attributable to the difference in the spacial distribution of excited and ionized species initially formed in each field. In radiation chemistry the distribution is more or less uniform as a natural consequence of the high penetrating power of the impinging radiation and highly random nature of the energy loss processes. The local inhomogeneities of energy deposition are submicroscopic in size and cannot be conveniently conceived as local regions of abnormal temperature. The "hot spot" idea has little significance in modern theories of the usual radiation chemistry. On the other hand, in a discharge tube, electronic excitation and ionization are somewhat confined to certain parts of the tube (negative glow and positive column). Since electronic excitation processes are generally accompanied by vibrational excitation (because of the Franck-Condon principle), the temperatures of these regions are also expected to be higher than those of the rest of the system. The direct transfer of electron energy to vibrational or translational motions of molecules can be ignored.

On the other hand, the coexistence of high temperature and high density of excitation is not really unique to electric-discharge chemistry. Under extremely high dose rate with certain charged species (particularly heavy particles such as fission fragments), it is probable that a similar situation has significance in the radiation chemistry of unusual systems.

A rather obvious feature of radiation chemistry, which cannot be found in discharge chemistry is the fact that the impinging energy is theoretically sufficient to excite the molecule to a level where multiple-bond dissociation and multiple ionization are possible. These effects have indeed been observed, but their contribution to the total chemical effect of high-energy radiation turns out to be negligible. The role of highly excited states or excited ionized states in the physical aspect of radiation chemistry (energy or charge transfer processes) is far from being negligible. By contrast, it would appear that lower excited states alone are the initial products of excitation in electric-discharge chemistry. In the latter case higher states appear to result from successive excitation exclusively and, under certain conditions of chemical reactivity, any presumptive substantial role of such states in the chemistry of discharge processes can be completely excluded - at least, on a speculative basis.

Radiation chemistry may be studied in systems of any degree of aggregation from highly attenuated matter (as in interstellar space) to liquids or solids under high compression. Studies in electric-discharge

chemistry seem limited essentially to gases or to interfaces involving gaseous systems. In radiation chemistry a major question is why, in spite of the initially high energies involved, the chemical effects are as specific as observed. In electric-discharge chemistry, by contrast, a very important question is why chemical effects are at all observed and why they are observed in the high yields reported.

#### References

1. Milton Burton and John L. Magee, *J. Chem. Phys.*, 23, 2194 (1955).
2. F. Dessauer, *Z. Physik*, 20, 288 (1923).

Inorganic Synthesis with Electric Discharges

William L. Jolly

Department of Chemistry of the  
University of California and the  
Inorganic Materials Research Division of the  
Lawrence Radiation Laboratory  
Berkeley, California 94720

Electric discharge reactions which yield thermodynamically unstable products are of interest to synthetic chemists because such products are often difficult to prepare by other methods. Many fascinating compounds of unusual structure have been isolated from discharge reactions. Although such syntheses usually have low efficiencies, the general techniques are nevertheless of interest to chemists who hope to discover new types of compounds. In this paper, we shall consider some important types of reactions which can be effected with the aid of electric discharges, together with some recent examples of these reactions.

Conversion of Simple Molecules into  
Higher Homologs

When simple volatile hydrides are passed through an ozonizer-type discharge tube near atmospheric pressure or through a glow discharge at low pressure, fairly good yields are obtained of the higher homologs of the hydrides. For example, both silane and germane can be converted to their respective higher hydrides; silanes as high as  $\text{Si}_8\text{H}_{18}$  and germanes as high as  $\text{Ge}_9\text{H}_{20}$  are formed. Similarly, arsine may be converted to diarsine. A wide variety of boron hydrides, including  $\text{B}_9\text{H}_{15}$ ,  $\text{B}_{10}\text{H}_{16}$ ,  $\text{B}_{20}\text{H}_{16}$ ,  $\text{B}_6\text{H}_{12}$  and  $\text{B}_8\text{H}_{12}$ , has been prepared in electric discharges. In all these reactions, hydrogen is a by-product, and there is no tendency for back-reaction of the hydrogen with the product molecules.

When the volatile halides,  $\text{SiCl}_4$ ,  $\text{GeCl}_4$ , and  $\text{BCl}_3$ , are passed through a glow discharge at low pressure, small yields of the higher homologs,  $\text{Si}_2\text{Cl}_6$ ,  $\text{Ge}_2\text{Cl}_6$  and  $\text{B}_2\text{Cl}_4$ , are obtained if provision is made to separate the products from the by-product chlorine by fractional condensation. (Chlorine reacts readily with the product molecules to reform the starting materials.) However, the yields are much improved if a reducing agent which can react with chlorine is included in the discharge zone or immediately after the discharge zone. Mercury and copper wool have been found to be very effective reducing agents for this purpose. In fact,  $\text{P}_2\text{Cl}_4$  can be obtained from a discharge in  $\text{H}_2 + \text{PCl}_3$  or from a  $\text{PCl}_3$  discharge followed by copper wool, whereas no  $\text{P}_2\text{Cl}_4$  has been obtained in the absence of the reducing agents.

Conversion of Mixtures into  
More Complicated Molecules

When mixtures of relatively simple hydrides are passed through an electric discharge, higher molecular weight ternary hydrides are formed. Thus by using appropriate mixtures of  $\text{SiH}_4$ ,  $\text{GeH}_4$ ,  $\text{PH}_3$ , and  $\text{AsH}_3$ , it has been possible to prepare, among other things,  $\text{SiH}_3\text{GeH}_3$ ,  $\text{SiH}_3\text{PH}_2$ ,  $\text{SiH}_3\text{AsH}_2$ ,  $\text{GeH}_3\text{PH}_2$ , and  $\text{GeH}_3\text{AsH}_2$ . By using a silent electric discharge, which does not cause drastic fragmentation and rearrangement, it is possible, within limits, to tailor-make molecules. Thus a mixture of  $\text{SiH}_3\text{PH}_2$  and  $\text{SiH}_4$  yields  $(\text{SiH}_3)_2\text{PH}$ , and a mixture of  $\text{Si}_2\text{H}_6$  and  $\text{PH}_3$  yields  $\text{Si}_2\text{H}_5\text{PH}_2$ .

Passage of diborane-acetylene mixtures through an electric discharge yields carboranes as the major volatile products, including 1,5- $\text{C}_2\text{B}_3\text{H}_5$ , 1,6- $\text{C}_2\text{B}_4\text{H}_6$ , 2,4- $\text{C}_2\text{B}_5\text{H}_7$ , and at least six B-methylated derivatives of these plus C,3- $(\text{CH}_3)_2$ -1,2- $\text{C}_2\text{B}_3\text{H}_3$ . The reaction of  $\text{SiH}_4$  and  $(\text{CH}_3)_2\text{O}$  in a silent electric discharge yields mainly a series of inseparable mixtures, but a fair yield of  $\text{Si}_2\text{H}_5\text{CH}_3$  can be isolated.

A fascinating series of oxygen fluorides ( $\text{O}_2\text{F}_2$ ,  $\text{O}_3\text{F}_2$ ,  $\text{O}_4\text{F}_2$ ,  $\text{O}_5\text{F}_2$  and  $\text{O}_6\text{F}_2$ ) has been prepared by subjecting mixtures of oxygen and fluorine to electric discharge at very low temperatures. All these compounds are very unstable, and, on warming, they decompose to oxygen and fluorine. Nitrogen trifluoride,  $\text{AsF}_5$ , and  $\text{F}_2$  when subjected to a glow discharge at low temperatures yields  $\text{NF}_4\text{AsF}_6$ . This material is a relatively stable material which is fairly well characterized.

The only reported method for the preparation of a xenon compound that does not involve the use of elementary fluorine or some fluorinating agent almost as difficult to handle as fluorine, is the electric discharge synthesis of  $\text{XeF}_2$  from Xe and  $\text{CF}_4$ . The carbon-containing by-products of the reaction were not identified.

Controlled Reactions of Atoms and Radicals  
with Other Species

In the discharge methods discussed above, all the reactant species are passed through an electric discharge. However many synthetically useful reactions can be carried out in the absence of a discharge by allowing a stream of atoms or radicals (prepared in an electric discharge) to impinge on various compounds. For example, atomic hydrogen is a very reactive species which has been used for the preparation of hydrides and for carrying out reductions. A promising field of study is the reaction of atomic hydrogen with aqueous solutions. In basic solutions, the hydrogen atoms yield electrons, and the method furnishes a convenient method for studying the reducing effects of the aqueous electron.

Atoms and radicals act as electrophilic reagents. The atoms O, Cl, Br, I, and N favor attack at polarizable donor atoms. Thus atomic nitrogen reacts with divalent sulfur compounds ( $\text{H}_2\text{S}$ ,  $\text{CS}_2$ ,  $\text{OCS}$ ,  $\text{S}_8$ ,  $\text{S}_2\text{Cl}_2$  and  $\text{SCL}_2$ ) to yield sulfur-nitrogen compounds, whereas no sulfur-nitrogen compounds are formed in the reaction of N atoms with  $\text{SO}_2$ ,  $\text{SOCl}_2$ , and  $\text{SO}_3$ . The reaction with  $\text{S}_2\text{Cl}_2$  gives fair yields of the interesting molecule  $\text{NSCl}$ .

#### Equipment

Most of the readily-available laboratory equipment for producing electric discharges is suitable only for relatively small-scale operation, involving only a gram or two of material. Such equipment, and the corresponding low yields, is satisfactory for the preparation of new compounds in amounts satisfactory for identification purposes. But in order for electric discharge syntheses to be useful for the preparation of mole quantities of materials, as are the usual synthetic methods, it will be necessary to have a marked break-through in the development and marketing of these instruments.

## Hydrazine Synthesis in A Silent Electrical Discharge.

Thornton J.D., Charlton W.D., Spedding P.L.

Department of Chemical Engineering,  
University of Newcastle-upon-Tyne, Merz  
Court, Claremont Road, Newcastle-upon-  
Tyne 2. England.

### INTRODUCTION.

The synthesis of hydrazine from ammonia using the silent electric discharge was first demonstrated by Besson in 1911 (1). Subsequent investigation showed that both the electrical energy yield and percentage conversion obtained were very low (2,3) and interest in the process waned. Further work was introduced in the early 1950's enabling substantial improvements in yields to be obtained in certain circumstances and a better understanding of the kinetic mechanisms in the discharge to emerge. Devins and Burton (4) showed that significant hydrazine formation only took place in the positive column of a D.C. discharge. Moreover, they found that yields could be substantially increased if the atomic hydrogen concentration in the discharge could be reduced by recombination. These general observations were later confirmed by Rath sack (5). As a result mechanisms were proposed for hydrazine synthesis based on the underlying premise that the hydrazine was first formed in the discharge and then degraded by back reactions. Ouchi (6) showed that yields could be increased by reducing the residence time of the hydrazine in the discharge in agreement with the general premise of hydrazine degradation in the discharge. Subsequent work has not been at variance with this finding (7,8).

Recently, I.C.I. of the U.K. have reported (9) that removal of product hydrazine in a liquid absorbent gives a substantial increase in yield and an improvement in percentage conversion. This is, of course, a modification of the general premise of hydrazine degradation in the discharge proposed by Devins and Burton (4) and Ouchi (6). Furthermore, following on the pioneering work of Ouchi (6), and others (10), I.C.I. apparently were able to achieve even better yields by suitable modification of the waveform characteristics of the discharge. In order to confirm their claim and to help clarify the mechanisms taking place in the discharge, work was commenced on this system at the University of Newcastle-upon-Tyne in 1965. This is a preliminary statement of the results obtained to date.

### EXPERIMENTAL.

The main aim of this work was to attempt to increase hydrazine yields by reducing the residence time of the product in the discharge. A concentric barrier discharge reactor was employed with and without the use of a liquid absorbent. Reactant flow rate was increased up to the

maximum pumping capacity of the apparatus after which the discharge voltage was reduced by changing the electrode area in order to give a further reduction in product residence time. Finally a D.C. parallel electrode reactor was used in which the discharge waveform characteristics were altered so that only a short activating pulse was supplied to the reactant in the electrode gap as it passed through the reactor.

The apparatus consisted essentially of a discharge reactor set between measuring and analysing sections in a flowing gas train. Commercially pure ammonia was fed into the measuring section of the apparatus via a reduction valve and a regulating needle valve. The flow rate was measured on a rotameter which had been previously calibrated under operating conditions by using a soap film manometer. Gas temperatures and pressures also were measured before the discharge reactor. The hydrazine formed in the discharge was absorbed in ethylene glycol either in situ or in a separate absorption train. Hydrazine was determined using the spectrophotometric method of Watt and Crisp (11). Vacuum control was achieved by a cartesian manostat located before the vacuum pump.

The A.C. radio frequency power (1.2 meg c/s) to the A- and B-type reactors was supplied by a modified C-12 Radyne generator of 1KW rated output. Measurement of the power dissipated in the discharge was achieved by firstly determining the power factor directly on a suitable oscilloscope. This value in conjunction with the direct readings of an R.M.S. voltmeter (Airmec 314) and a radio frequency ammeter (Cambridge Unipivot) enabled a reasonably accurate determination of the power in the discharge to be achieved. The D.C. power for the C-type reactor was provided by a specially engineered SKW generator. Measurement of the actual discharge power was made using a combination of an oscilloscope trace and the appropriate meter readings.

The various types of discharge reactors used in this work are illustrated schematically in Fig.1. Other essential geometric details of these reactors and their operating data are given in Table 1. The A-type series of reactors consisted of a precision silica tube (which acted as the capacitive barrier) with the high tension electrode attached around the outside. The inner electrode was a spinning cylinder so constructed that absorbent liquid could be sprayed onto the inside of the tube to flow down through the annular discharge gap. Co-current gas and liquid flow was employed.

The B-type series of reactors were of similar construction except that a central wire electrode was used and the absorbent liquid was fed into the incoming gas as a spray. Dispersion of the liquid was achieved ultrasonically using a vibratory generator. The spray was fed into the gas stream through an annular orifice placed at a sufficient distance

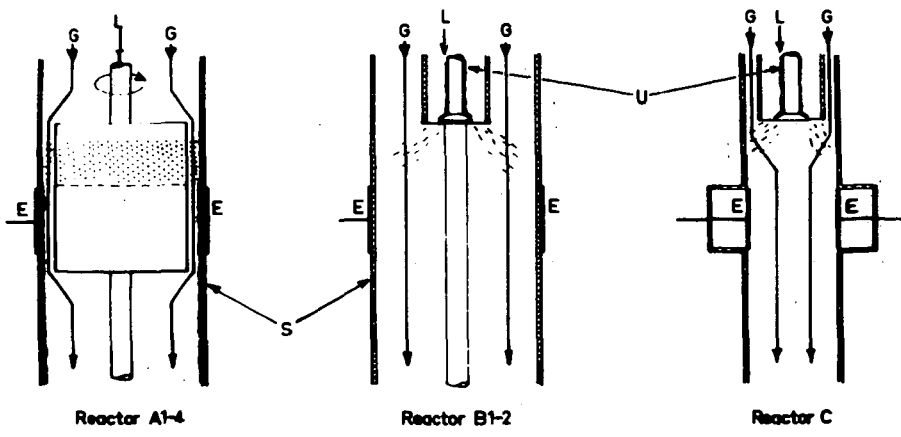


Fig.1 Schematic diagram of reactors used for hydrazine synthesis  
 E = Electrodes      L = Liquid Inlet      G = Gas Flow  
 S = Silica Barrier      U = Ultrasonic Vibrator

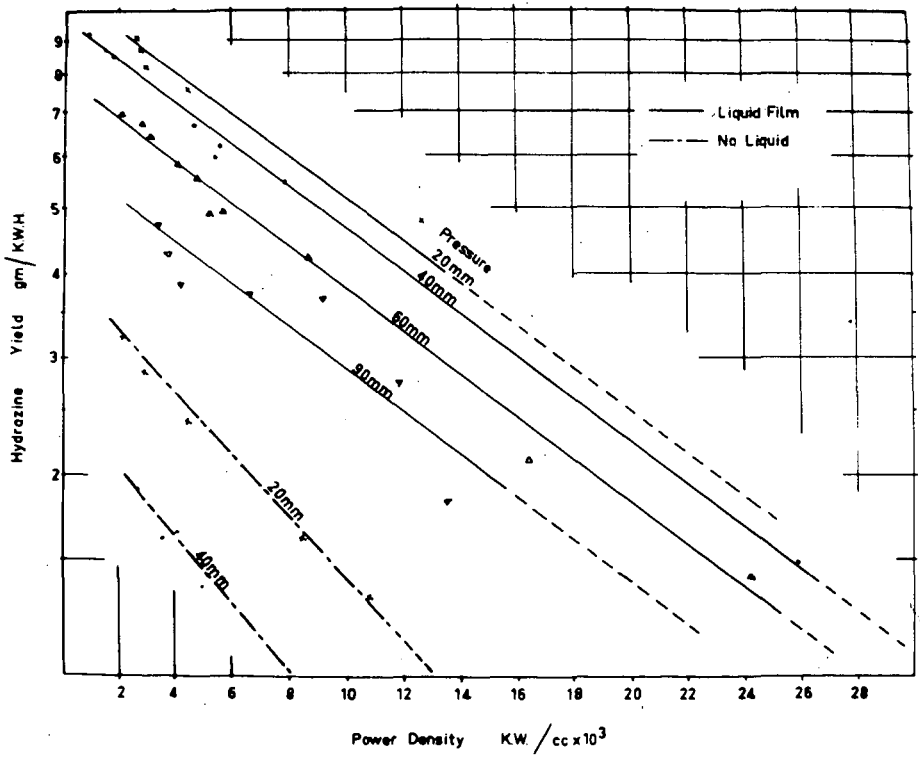


Fig. 2 Hydrazine yield for the co-axial reactor A1 with & without Liquid film

downstream from the discharge to ensure proper dispersal of spray in the electrode gap. The C-type reactor employed a pair of rectangular electrodes so set in the gas flow as to avoid reactant by-passing. The use of D.C. power necessitated stabilization of the discharge by means of a resistive load in the electrical circuit. Provision was made to admit liquid spray into the inlet gas stream using the same aerosol generator used in the type-B reactors.

Table 1.  
Reactor units employed.

Type	Reactor Code	Flow Area cm <sup>2</sup>	Discharge Width cm	Discharge Volume cm <sup>3</sup>	Dilectic Barrier Thickness cm
Tubular	A1	2.203	1.270	2.798	0.15875
Centrifugal	A2	"	0.254	0.560	"
Film Reactor	A3	"	0.127	0.280	"
	A4	"	0.040	0.089	"
Tubular	B1	1.089	1.270	1.383	"
Spray Reactor	B2	"	0.254	0.277	"
Pulsed Reactor	C1	1.411	0.635	0.896	0

#### RESULTS.

Hydrazine yields for the various reactor geometries and the operating variables employed are given in Figs. 2 to 6. From the data presented in Fig 2 to 4, it is evident that the yield varies inversely as an exponential function of the power density at pressures under 100mm of mercury. The effect of pressure also follows a negative exponential variation therefore a general equation of the form

$$Y = a \exp(-bP - c\pi)$$

adequately describes the results. Of course this correlation of the results does not in any sense give a complete description of the underlying physical chemistry involved in the synthesis. Ideally, it would have been preferable to develop separate rate equations in terms of the partial pressures of the various components in the overall hydrazine synthesis. This would have necessitated a complete product analysis and since, in the present case, these data are lacking the phenomenological approach had to be used. The constants in the equation for the various reactors and operating conditions used were evaluated using the method of least squares (12). These are tabulated in Table 2. It should be noted in this Table that certain pressure exponential values were bracketed. Here the relevant data were lacking for calculation and, therefore, the dependence of energy yield upon pressure for reactors A2 to A4 and B2 were assumed to be the same as those found experimentally for Reactors A1 and B1.

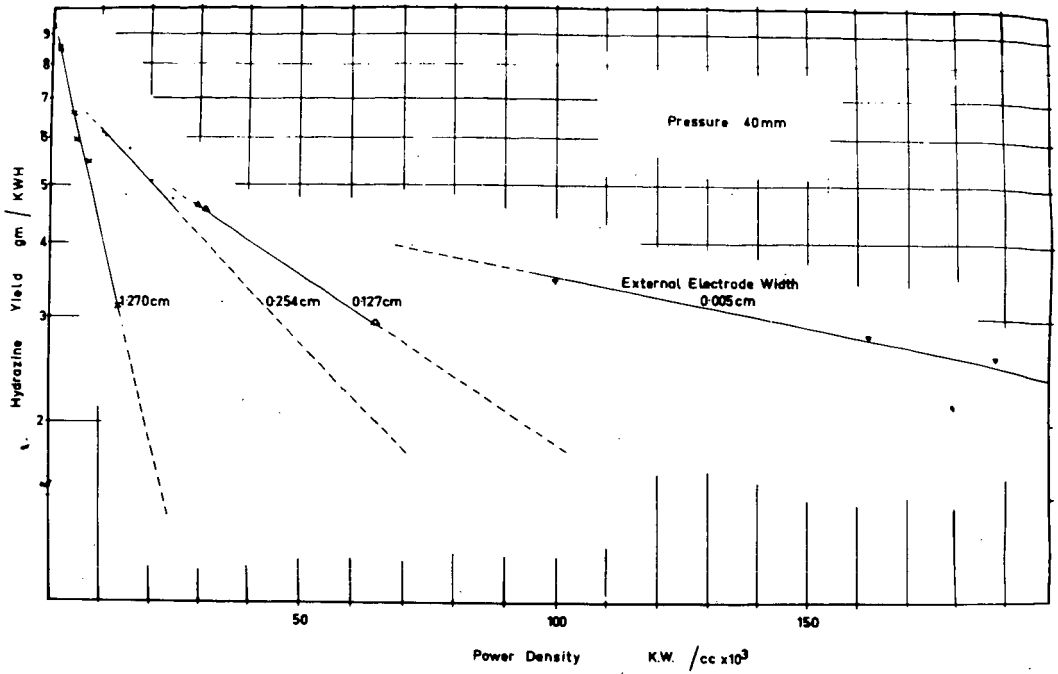


Fig. 3 Hydrazine yield for the liquid film co-axial reactors A1-4

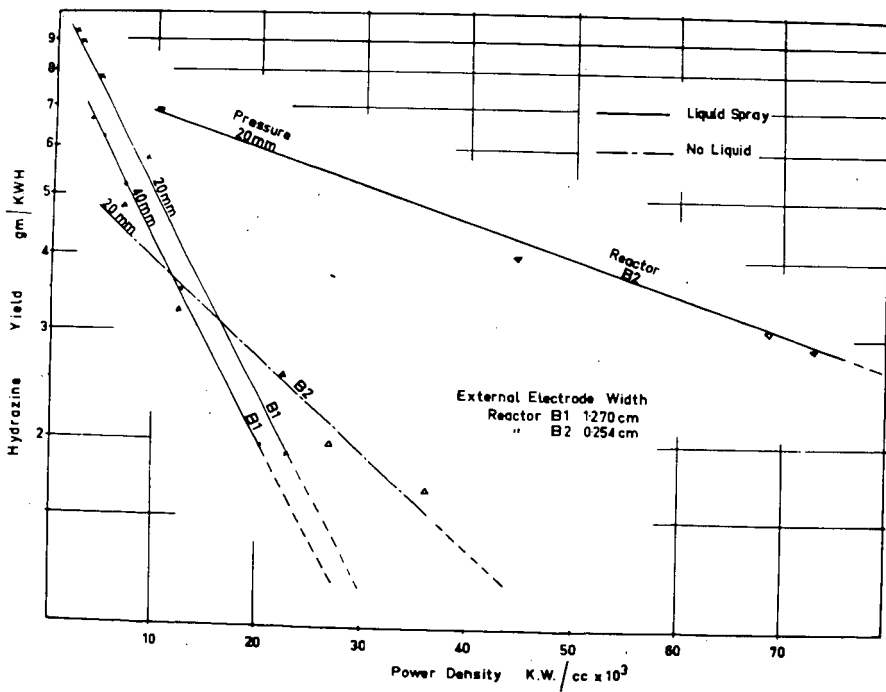


Fig. 4 Hydrazine yield for the co-axial reactors B1-2 with & without liquid spray

Table 2.  
Derived constants for the equation  $Y = a \exp(-bF - cT)$

Reactor	a gm/KWH	b mmHg <sup>-1</sup>	c cc/Kwatt	liquid absorbent
A1	13.14	0.0087	73.81	film
A1	6.35	0.0236	118.74	none
A2	10.70	(0.0087)	19.43	film
A3	9.56	"	12.93	"
A4	7.28	"	3.73	"
B1	12.99	0.0098	73.58	spray
B2	9.26	(0.0098)	13.69	"
B2	8.88	(0.0236)	35.15	none

This is a reasonable procedure within any one particular series of reactors such as A1 to 4, but it is only approximate with differing reactor series (e.g. Reactor series A and B) due to dissimilarities in discharge geometries.

#### DISCUSSION.

The most notable overall feature of the results is the progressive increase in hydrazine yield obtained by the use of a liquid absorbent and by pulsing the discharge. The highest average yield was obtained with the pulsing technique with or without liquid absorbent and was approximately 15 gms  $N_2H_4$ /KWH. Isolated values as high as 20 gms/KWH were obtained but further experimental work is required before these values can be made reproducible. It is noteworthy that a yield of 15 gms/KWH is beginning to look commercially attractive although it must be remembered that the final product cost will depend to a great extent on the cost of the product purification process downstream of the reactor.

There are several interesting features shown by this work which bear discussion. From the results set out in Fig. 2 to 4 it is evident that the hydrazine yield decreases with increasing discharge power intensity despite a corresponding increase in the decomposition of ammonia. The only reasonable explanation for this which has been advanced is that hydrazine is formed in the discharge by a complex reaction mechanism and is subsequently decomposed by electron bombardment or other collision phenomena (4,6).

The use of a liquid absorbent results in a decrease in the slope of the energy yield-power density plot. This is well illustrated in both Fig. 2 and Fig. 4 by comparing the slope of the plots with and without the use of liquid absorbent. This indicates that hydrazine is being removed from the discharge by the liquid absorbent instead of being degraded. If the hydrazine were completely removed so that degradation did not occur the slope of this plot would be either independent of discharge power or possibly positive. The very

fact that the slope is still negative with the use of liquid absorbent may indicate that a significant amount of hydrazine is still being degraded in the discharge in this case. Therefore, the use of a more efficient absorption process would reasonably be expected to recover more of the hydrazine being degraded and thus increase yields still further. Moreover, the observed decreasing effect of pressure on the yield with the use of liquid absorbent (shown in Fig.2) adds weight to this suggestion.

As the pressure was decreased below 100mm of mercury the yield of hydrazine increased steadily while the slope of the yield-power density curve remained constant for similar reactor operating conditions such as the use of a liquid absorbent. A reasonable explanation for this behaviour is that at the lower pressures the electrons passing into the discharge are less likely to suffer collisions in the immediate vicinity of the electrode so that the average energy of the electrons will be high just prior to the required activating collisions. Therefore, activating collisions are more likely to occur and yields to increase correspondingly. Degradation of product by electrons is, by the same argument, more likely under these conditions but other product degrading discharge collisional phenomena e.g. the reaction with hydrogen atoms, are reduced because of the greater mean free path at the lower operating pressure. The overall result is that hydrazine yields increase. Secondary effects become increasingly important at higher pressures and it is likely that other variations in the effect of pressure on yield may well occur. One such variation is reported to occur at about 5mm pressure where the energy yield passes through a maximum (8).

Product yields were increased by removing hydrazine in a liquid absorbent and it was considered that a more efficient absorption technique should lead to even greater yields. In order to obtain a more intimate gas liquid dispersion a spray reactor was used of the general design shown for Reactors B1 and 2 in Fig.1. The results (Fig.4) show that yields were slightly below that of the film reactor. In practice there were difficulties caused by dissimilarities in the construction of Reactors A and B which led to radically different discharge conditions being obtained. The film reactor (A1) had a more uniform discharge density because it was of an annular construction where the annulus width was small compared to the reactor diameter. The spray reactor, on the other hand, employed a central wire electrode and consequently there was a non-uniform field in the discharge gap with a higher local discharge density in the vicinity of the wire electrode. Because the yield is known to depend on an inverse function of the power density, it is only reasonable to expect that the reactor design B1 would give somewhat lower yield than the Reactor design A1 under similar operating conditions. This means that the more intimate gas-liquid contact in the spray reactor had no measurable effect on the product yield.

On the other hand, if hydrazine is formed and degraded uniformly in the activating section of the discharge this result is difficult to explain. It is suggested from this that, under these conditions, the absorption process is no longer the controlling factor since an increase in the overall potential absorption rate, through an increase in the interfacial area, produces no corresponding rise in hydrazine yields. It may be that liquid surface activation phenomena are taking place and the increased hydrazine yield which is observed with the use of an absorbent liquid is caused by hydrazine formed by other mechanisms in which the liquid surface plays an important role. If this were the case the liquid film, which presents a complete barrier to the discharge, would naturally give maximal yield and the spray reactor would only tend to this value in the limit.

It was found experimentally that a decrease in the residence time of the reactant in the discharge is accompanied by an increase in energy yield of hydrazine and a corresponding fall in percentage conversion. The results are detailed in Fig. 5 and appear to be in general agreement with those of Ouchi (6). When a liquid absorbent is used the change of yield and percent conversion is steady but without the use of an absorbent the effect becomes very marked at low residence times. Ouchi (6) has concluded from his results that some of the hydrazine formed in the discharge is preserved from degradation by rapid physical removal out of the discharge. This would adequately explain, in general terms, the increase in energy yield with reduced residence time. The degree of activation of species in the discharge must fall as the reactant throughput is increased. This would result in a decrease in percent conversion as residence time was reduced. Furthermore, as the concentration of hydrazine governs the rate of the degrading reaction the smaller percent conversion achieved at high flow rates will result in a higher overall energy yield being achieved. With the use of a liquid absorbent some effect on the yield may well arise because of changes in the absorption rates due to increased turbulence and a decrease in the gas liquid contact time.

Another point which must be borne in mind is that physical removal of the product or even, for that matter, the use of the pulsed discharge technique cannot give better conversions than that dictated by the equilibrium concentration of hydrazine for the basic reactions taking place in the discharge. The use of the liquid absorbent, on the other hand, permits higher conversion to be achieved because of the inability of the discharge reaction to reach equilibrium as hydrazine is being continuously removed after it is formed in the discharge.

The negative slope of the energy yield-residence time plot (Fig. 5), when liquid absorbent was used, implies that it is possible to increase yields still further by some other suitable modification of technique.

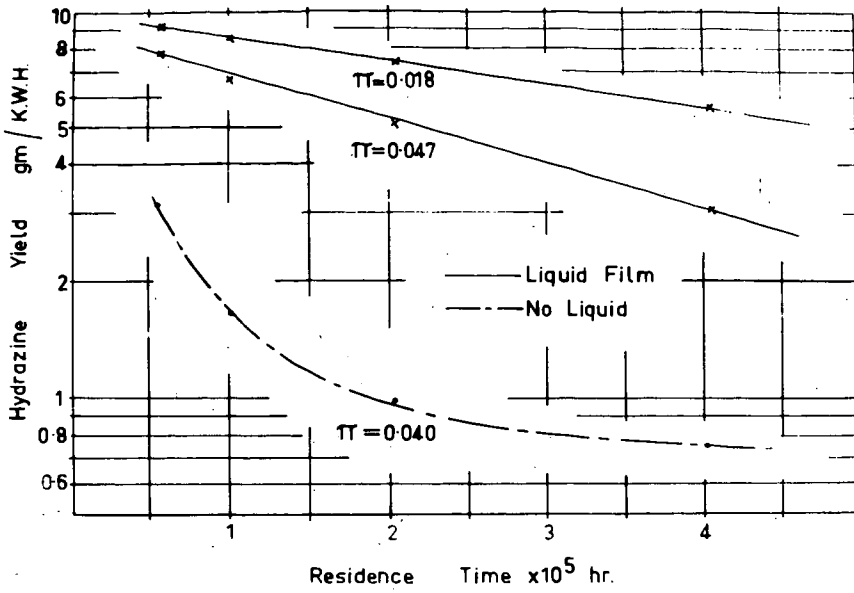


Fig.5 Variation of hydrazine yield with flow rate for reactor A1

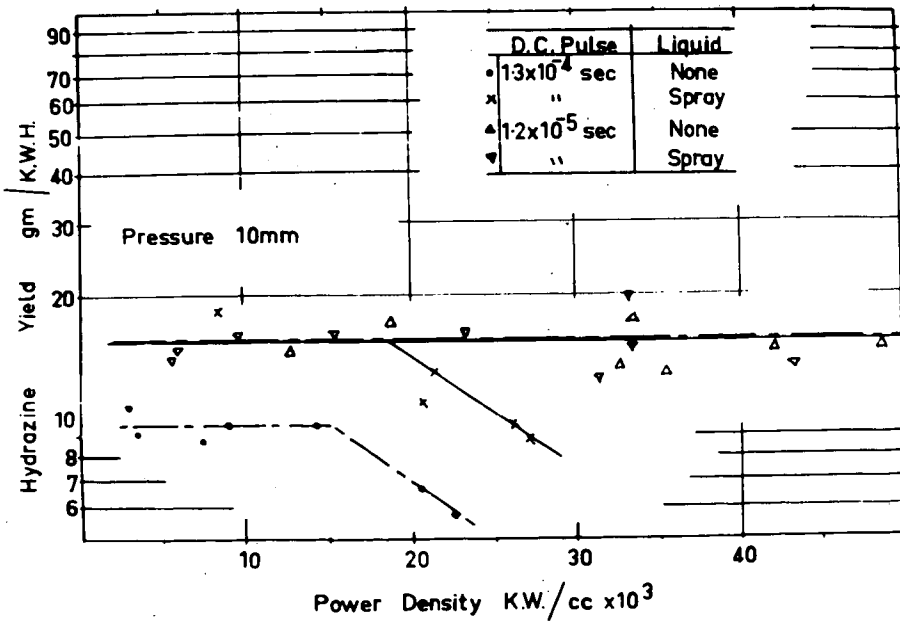


Fig.6 Hydrazine yield for pulsed D.C. reactor C1

The results, for the case when liquid absorbent was not used, show a very marked increase in yield with reduction of residence time. This abnormal behaviour suggests that the process resulting in increased hydrazine yields is not just the physical removal of product alone but a change may also be occurring in the basic reaction mechanisms.

In an endeavour to reduce the residence time below the level dictated by the capacity of the vacuum system the electrode area was steadily reduced (Reactors A1 to 4). The results obtained (Fig. 3) show that the yield fell and the discharge itself altered radically due to the increased influence of electrode edge effects.

Discharge pulsing gave a substantial increase in yields over the other methods employed. As the duration of the discharge pulse was shortened the yield was found to rise and become independent of power density. Furthermore, the yield was not affected by the use of a liquid absorbent. Up to this point the usual variations with these two variables were observed. Indications are that hydrazine yields can be increased well beyond 15 gms/KWH by suitable modification of the pulsed discharge technique.

It is clear from these results that the yield of hydrazine from ammonia using the silent discharge can be increased if the residence time of the product in the discharge is reduced by the use of liquid absorbent, physical flow rate of reactant or discharge pulsing. Several aspects of the results seem to imply that the underlying mechanism involved is not entirely that of physical removal of product but other factors, such as changes in the basic reaction mechanisms, are also involved.

#### REFERENCES.

1. Besson A. Compt.rend. 152 1850 1911
2. Bredig G. Koenig A. Wagner O.H. Z.Phys.Chem. 139A 211 1928
3. Koenig A. Wagner O.H. Z Phys. Chem. 144A 213 1929
4. Devins J.C. Burton M.J. J.Am.Chem.Soc. 76 2618 1954
5. Rathsack H.A. Z Phys. Chem.(Leipzig) 214 101 1960
6. Ouchi K. J.Electrochem Soc. Japan 17 285 1949  
" " " " 20 164,168,378 1952
7. Andersen W.H. Zwolinsk B.J. Parlin R.B. I.E.C. 51 527 1959
8. Skorokhodov I.I.et.al. Russ.J.Phys.Chem. 35 503 1961
9. British Patent 948,772; 958,776-8; 966,406 1964
10. Jogarao A. Shastri B.S.R. J.Sci.Ind. Research (India) 18B 38 1959
11. Watt G.W. Chrisp J.D. Anal.Chem. 24 2006 1952
12. Margenan H. Murphy G.M. The mathematics of physics and chemistry Van Nostrand N.J. 2nd Ed. 1957 P519.

#### ACKNOWLEDGEMENT

Financial support for this work was provided by the Science Research Council of the U.K.

M. M. Shahin

Xerox Corporation, Rochester, New York 14603

### INTRODUCTION

Mass spectrometric studies of electrical discharges have been carried out during the past decade by several workers (1-6) in an attempt to identify the ionic precursors of a variety of neutral by-products which are formed in these systems. Such studies are expected to reveal the detailed chemistry of the many reactions that follow the formation of primary ions through the impact of energetic electrons on the neutral gas molecules, and end with the neutralization of the final form of the ion either in the gas-phase or at the electrodes or the walls of the discharge tube. Thus, the identification of these ionic reactions will, in many cases, demonstrate the mechanism of the production of the free-radicals which are the source of the neutral by-products. Further, such studies would be expected to provide information on the mechanisms of catalytic or inhibitory effects of trace quantities of certain compounds (e.g. water vapor) on the formation of these products. Processes such as charge-exchange or ion-molecule reactions which occur with large cross-sections and have been suspected to be responsible for such effects will thus be easily identified.

The complexity of electrical discharges however, often makes the interpretation of mass spectrometric data very difficult. Specifically, the variations of electric field along and across the discharge tube in certain commonly used discharges (e.g. glows) often affect the abundance distribution of the various ionic species which are observed at the mass spectrometer (2,3). This is mainly due to the complex dependence of the cross-sections of both charge-exchange and ion-molecule reactions on ion energy as determined by the electric field within the discharge tube. Further complication arises from the formation of ion-sheaths around the walls of the discharge tube, through ambipolar diffusion. These may strongly influence the sampling of the discharge by the mass spectrometer. It is therefore essential that the system under investigation be well understood before the interpretation of the data is attempted.

In this paper, the results of mass spectrometric investigations on low pressure positive corona discharges established between two coaxially placed electrodes will be discussed. This form of discharge has been chosen primarily because its electrical properties are relatively simple and well understood. Further, the ion-sheath effects at the point of sampling are minimized because of the low level of ionization in these systems.

### EXPERIMENTAL

Detailed description of the apparatus has already been given (6). Figure 1 shows the schematic diagram of the apparatus. Briefly, a coaxial discharge tube is operated through a high-voltage d.c. power supply and the current is stabilized through the use of an external current limiting resistor, R. Electrons moving through the high field region present only at very close distances to the anode wire will gain energy from the field and cause ionization of the gas molecules in this region. Because of the symmetry of the electrodes, therefore, the system closely behaves as a line source of positive ions which are continuously regenerated. These ions will then move through the gas, perpendicular to the axis, undergoing various interactions before reaching the cathode. A small sampling port (10 to 100 microns in diameter) at the cathode allows a small portion of the ions to escape the discharge tube and be analyzed by a quadrupole mass spectrometer.

The form of the electric field within the discharge tube is rectangular hyperbolic before the discharge is established. As the discharge is formed, however, the presence of the positive space charge distorts this initial field, causing the

latter to attain a constant value for the major distance between the electrodes (7).

Differential pumping of the sampling region and the mass spectrometer allows operation of the discharge tube between pressures ranging from less than 1 torr to atmospheric. An electron gun placed before the mass spectrometer serves as an independent ionizing source for monitoring the composition of the neutral discharge gas when no ions are extracted from the discharge tube. For such analysis, calibration curves made on prepared gas mixtures, showing mass discrimination due to the specific flow condition are used. A rapid flow of gas is maintained through the discharge tube in order to avoid appreciable accumulation of neutral by-products of the discharge. For this purpose a linear flow velocity is maintained such as to completely renew the gas within the tube in two seconds. In systems where the concentration of the electro-negative gas (e.g. oxygen) is low, an external source of ionization through the use of a weak radioactive source (e.g.  $\text{Po}^{210}$ ) is used to stabilize the discharge.

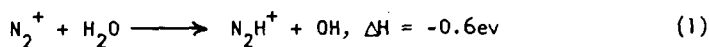
The general problem of mass spectrometric sampling from high pressure sources has recently been discussed by several workers (8). In systems where condensable gases are present, the temperature drop following the adiabatic expansion of the gas through the sampling nozzle may cause condensation if such gaseous components are present in sufficient concentrations. In the present experiments, the water content of the gases under investigation has been chosen below  $5 \times 10^{-2}$  mole %. Under these conditions, it can be demonstrated\* that such condensations make negligible contribution to the results.

### RESULTS AND DISCUSSIONS

Earlier experiments (6) on corona discharges in air at atmospheric pressure clearly demonstrated the important role of trace quantities of water vapor in these systems. In nitrogen, oxygen and their mixtures, where the water content exceeded 4 to  $5 \times 10^{-2}$  mole %, the dominant ionic species observed at the mass spectrometer were those corresponding to hydrated proton clusters,  $(\text{H}_2\text{O})_n\text{H}^+$ . These species were apparently formed from the interaction of the primary ions with the water molecules in the system as they passed through the gas to the cathode. In order to determine the role of various reactions which lead to such clusters, low pressure experiments were designed with individual gaseous components (e.g.  $\text{O}_2$ ,  $\text{N}_2$ ) and their corresponding mixtures with various quantities of water vapor. These experiments were expected to reveal the formation of intermediate species and their final conversion to hydrated protons.

#### Discharge in Nitrogen:

Experiments with nitrogen at low pressures, containing various concentrations of water vapor show several intermediates which are formed through the reactions of nitrogen ions with water. The results of a typical experiment showing the relative abundances of various species reaching the mass spectrometer as the pressure of the discharge is varied, are shown in Fig. 2. In this experiment, it can be observed that as the pressure is increased, the abundance of the primary ion,  $\text{N}_2^+$ , is sharply reduced while those of the intermediate ions, namely,  $\text{N}_4^+$ ,  $\text{N}_2\text{H}^+$  and  $\text{H}_2\text{O}^+$  rise to a maximum and then decrease as the tertiary ion  $\text{H}_3\text{O}^+$  begins to appear. This latter ion also rises to a maximum at higher pressures as its more highly hydrated forms appear. Thus the two reactions:



and

---

\*Calculations based on the maximum number of collisions of an ion with water molecules present up to  $10^{-1}$  mole % in an expanding gas, assuming cross-sections of  $10^{-13}\text{cm}^2$ , show negligible contribution to the total collisions that such an ion and molecule will undergo within the discharge system. These calculations will be published elsewhere.

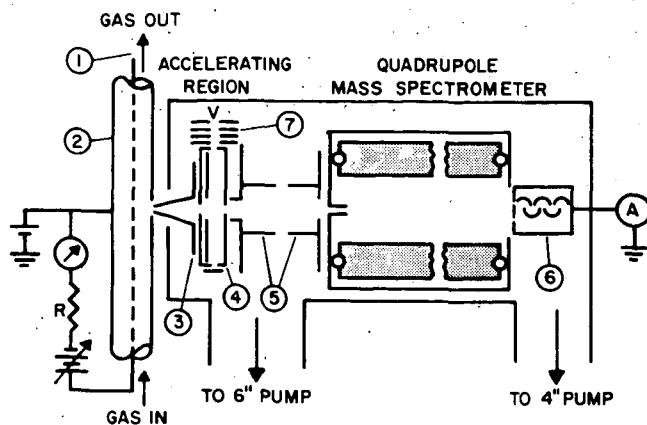


Fig. 1. Schematic diagram of the discharge tube and mass spectrometer; 1, platinum wire anode; 2, cylindrical discharge tube; 3, extraction electrode; 4, mass spectrometer ionization chamber; 5, focussing electrodes; 6, electron multiplier; 7, electron-gun assembly.

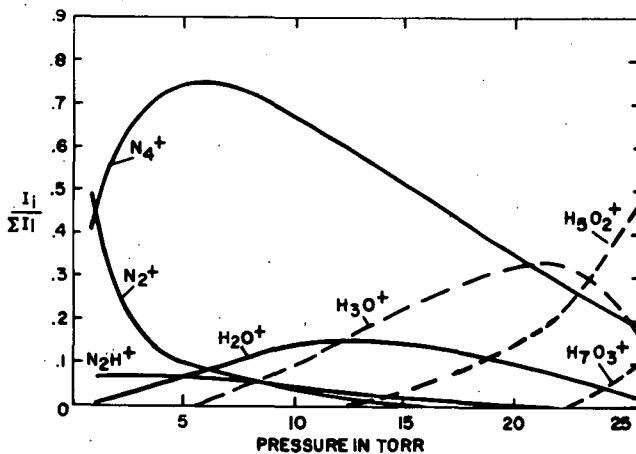
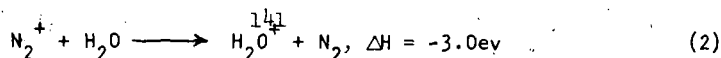
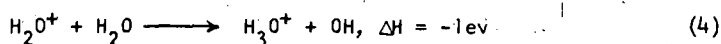
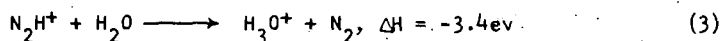


Fig. 2. Variation of the relative abundance of different ions with pressure in a positive corona discharge in nitrogen containing  $2.2 \times 10^{-2}$  mole % of water vapor.



appear to provide species which can further react with water through reactions (3) and (4) to form the hydrated proton:



The third and the major intermediate, namely  $\text{N}_4^+$  which is formed through reaction of  $\text{N}_2^+$  with neutral nitrogen molecule (9) apparently also undergoes reactions with water similar to reactions (1) and (2) to form  $\text{N}_2\text{H}^+$  and  $\text{H}_2\text{O}^+$  ion. These reactions are also expected to be exothermic. The relative abundance of  $\text{N}_4^+$  ion is found to be strongly dependent on the field strength within the discharge tube. Specifically, the formation of a space-charge around the corona wire is found to strongly influence the relative abundance of  $\text{N}_4^+$  and  $\text{N}_2^+$  ions in the system as this space-charge substantially reduces the field strength within the discharge tube. In the experiments shown in Fig. 2, the magnitude of E/P, the pressure reduced electric field for the major distance between the two electrodes, was calculated to be about 7 volt/cm. mm Hg.

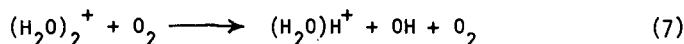
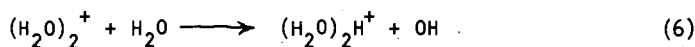
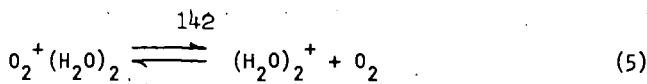
Two other intermediate species have been observed in this system. These ions, not shown in Fig. 2, are  $\text{N}_4\text{H}^+$  and  $\text{N}_3\text{H}^+$ . They apparently arise as a result of ion-molecule reactions involving  $\text{N}_4^+$  and  $\text{N}_3^+$  ions in the system with water molecules and are expected to undergo proton transfer reactions similar to reaction 3, to yield  $\text{H}_3\text{O}^+$ .

Other ions observed were at  $m/e = 32$  and  $46$ . These ions are believed to arise from trace quantity of oxygen which is inevitably present in this system as a result of the decomposition of water. The ion of  $m/e = 32$  is apparently  $\text{O}_2^+$  while that of  $m/e = 46$  is  $\text{NO}_2^+$ .

In a system of pure nitrogen where the water concentration was kept below  $5 \times 10^{-3}$  mole %, under similar discharge conditions as those presented in Fig. 2, it was observed that the intensity of  $\text{N}_4^+$  ion rapidly increased as the gas pressure was increased, reaching a plateau after a few mm Hg pressure. This plateau corresponded to 95% of total ion intensity, with the remaining 5% being mainly due to  $\text{N}_3^+$  ion. This result supports the earlier reference to the presence of a low E/P between the two electrodes (9) and the lack of any appreciable ion-sheath near the cathode.

#### Discharge in Oxygen:

Figure 3 shows the pressure dependence of the relative abundance of various ionic species in a corona discharge in oxygen. This experiment shows several marked differences from those shown for nitrogen in Fig. 2. The most striking feature is the presence of large abundances of hydrated forms of the primary ion, namely  $\text{O}_2^+(\text{H}_2\text{O})_{1,2}$  and their dependence on pressure. That the abundances of these ions appear to rise to a maximum and then decrease at higher pressures with the formation of hydrated protons strongly suggests their role in the intermediate processes. This evidence together with the appearance of  $(\text{H}_2\text{O})_2^+$  ions in the system, and the variation of its abundance with pressure, i.e. rising to a maximum and then reducing at higher pressures, indicates the operation of an entirely new mechanism in this system for the formation of hydrated protons. Moreover, the appearance of  $m/e = 37$ ,  $(\text{H}_2\text{O})_2\text{H}^+$  before the first member of the series suggests that a reaction other than the hydration of  $\text{H}_3\text{O}^+$ , is responsible for the formation of this species. Since the ionization potential (I.P.) of oxygen (12.07ev) is lower than that of water (I.P. = 12.56ev), a charge-exchange reaction similar to reaction 2, for nitrogen does not appear probable. Nor is it likely that a reaction similar to that of reaction 1, to form  $\text{O}_2\text{H}^+$  would occur, as it appears to be endothermic. It is therefore probable that the hydrated form of the primary ion, especially the species containing two water molecule may be a precursor in the formation of the hydrated proton through the reactions:



Reaction 5 is expected to be exothermic owing to the heat of hydration of  $H_2O^+$  ion. It may also be possible, though unlikely, that any required energy for the reaction be supplied through the electric field in the discharge.

One other ionic species which may play a role in this system is  $O^+$ . However, since the I.P. of atomic oxygen (13.61eV) is greater than that of oxygen, this species is not observed in this system as it most probably undergoes charge exchange with molecular oxygen at pressures used in these experiments. The reaction of  $O^+$  with  $O_2$  to give rise to  $O_3^+$ , if it occurs at all, is not observed in these experiments since ozone has also a higher I.P. (12.8eV) than that of oxygen and therefore  $O_3^+$  is similarly expected to undergo a charge-exchange reaction with  $O_2$ .

Three other ions were observed in minor relative abundance in this system. These ions are  $OH^+$ ,  $H_2O^+$  and  $H_2O_2^+$ . The relative yield of the  $OH^+$  ion is shown in Fig. 3 while the yields of  $H_2O^+$  and  $H_2O_2^+$ , being somewhat smaller, are not indicated. It is believed that the first two of these ions arise from an ion-molecule reaction and a charge-exchange process between  $O^+$  and water molecule respectively, and are detected only at higher discharge pressures where such reactions compete with direct charge transfer of  $O^+$  to oxygen molecules.  $H_2O_2^+$  ion, however, may appear as a result of an efficient charge transfer process between  $O_2^+$  ion and the trace quantities of  $H_2O_2$ , apparently formed in the system by the recombination of hydroxyl free radicals, or the reaction,  $HO_2 + H_2 \longrightarrow H_2O_2 + H$ , hydrogen being supplied through the decomposition of water.

In a system of pure oxygen, where the water content was kept below  $5 \times 10^{-3}$  mole %, only two ions,  $O_2^+$  and  $O_4^+$  were observed within the pressure range investigated. The abundance of  $O_4^+$  ion rises sharply as the pressure is increased while that of  $O_2^+$  decreases and both reach a plateau beyond a pressure of 20 Torr in the discharge tube. The relative abundance of  $O_4^+$  in this plateau region was found to be about 62%.

#### Discharge in Nitrogen Containing 0.12 mole % Oxygen:

In order to determine the role of oxygen in air discharges in the absence of water vapor, a number of experiments were carried out in nitrogen containing 0.12 mole % of oxygen. The lower limit of water vapor in these experiments was  $5 \times 10^{-3}$  mole %. Fig. 4 shows the results of the relative abundance of various ionic species which are detected at the cathode as the pressure of the discharge is increased. These experiments clearly trace the history of the primary ionic species, namely  $N_2^+$  as it is converted to  $N_4^+$  and the latter undergoes charge-exchange with the trace quantity of oxygen present in this system. Thus, beyond a pressure of 20 Torr in the discharge tube the charge carriers in this system are almost all  $O_2^+$ . The trace amount of  $N_3^+$  observed in the system is also all removed beyond a pressure of 15 Torr.

It is significant to note that no nitric oxide ion is observed in this system, indicating that neither the reaction  $N_4^+ + O_2 \longrightarrow NO^+ + NO + N_2$ , nor  $O_2^+ + N_2 \longrightarrow NO^+ + NO$ , occur to any appreciable extent, in spite of the fact that both these reactions are expected to be exothermic.

Experiments in which water was not excluded showed the appearance of many ionic intermediates of both pure oxygen and nitrogen and their mixtures. All these ions could be traced and their final conversion to hydrated protons followed.

#### Discharge in Air:

Experiments in air in the absence of water vapor (less than  $5 \times 10^{-3}$  mole %) were carried out in order to determine the importance of ionic species of oxides of nitrogen in these systems. The results of these experiments are shown in Figure 5.

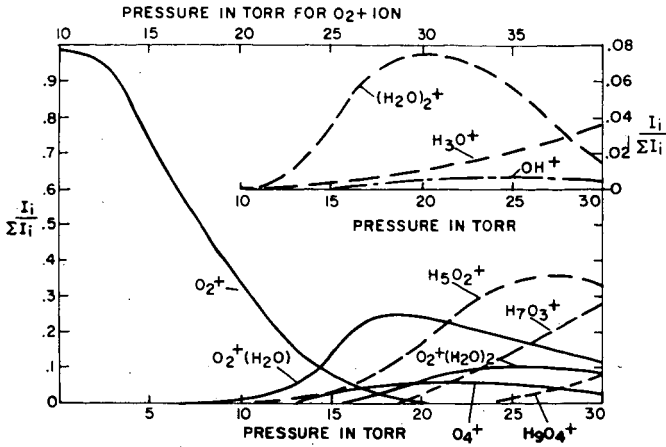


Fig. 3. Variation of the relative abundance of different ions with pressure in a positive corona discharge in oxygen containing  $2.0 \times 10^{-2}$  mole % of water vapor. The pressure scale for  $O_2^+$  ion is shown on the top of the figure.

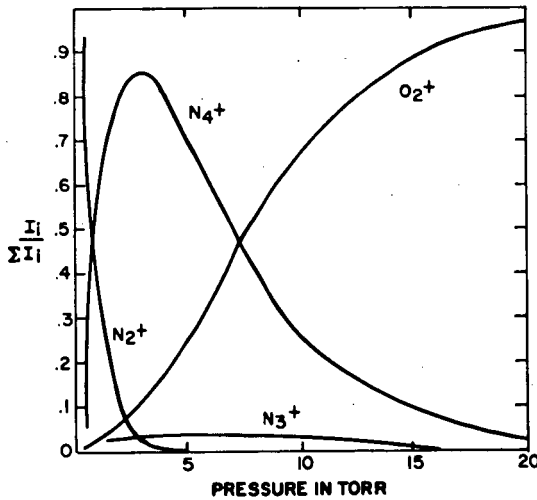


Fig. 4. Variation of the relative abundance of different ions with pressure in a positive corona discharge in nitrogen containing  $1.2 \times 10^{-1}$  mole % of oxygen and less than  $5 \times 10^{-3}$  mole % of water vapor.

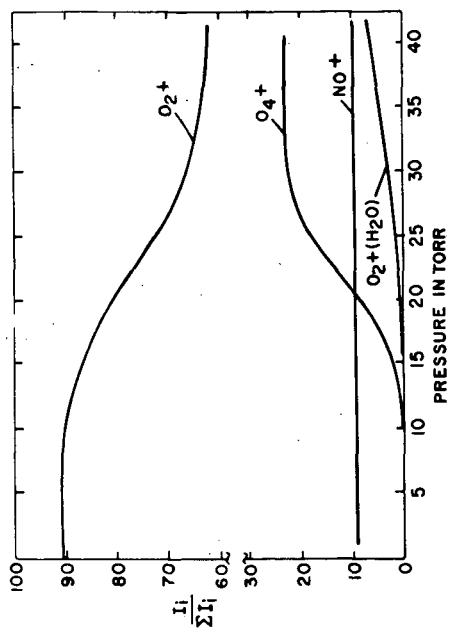
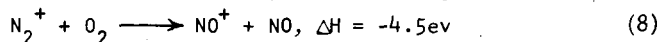


Fig. 5. Variation of the relative abundance of different ions with pressure in a positive corona discharge in air with water concentration below  $5 \times 10^{-3}$  mole %.

As expected from the previous sections,  $O_2^{145+}$  ion appears as the most abundant ion in this system. Also as expected,  $O_4^+$  ion appears in the system and as the pressure is increased, it becomes an important charge carrier and its relative abundance eventually reaches a plateau. The appearance of the ion  $O_2^+(H_2O)$ , hydrated form of molecular oxygen ion, in this system, indicates the high affinity of this ion for hydration as the gas contained less than  $5 \times 10^{-3}$  mole % water in the discharge tube.

Nitric oxide ion was the only oxide of nitrogen found in the system under the experimental conditions used here. Its relative abundance remained constant as the discharge pressure was varied between 2 to 40 Torr. The presence of  $NO^+$  in these experiments and its absence in experiments carried out in nitrogen containing 0.1 mole % of oxygen, indicates that these ions are probably formed through the reaction



Assuming that  $O_2^+$  arises either through charge-exchange with  $N_2^+$  ion or by direct electron impact on neutral oxygen molecule, one can use the data in these experiments to obtain a relative ratio of the rate-constants for the charge-exchange reaction of  $N_2^+$  with oxygen to that of ion-molecule reaction (8). This ratio is found to be equal to 8, a value which is lower than the ratio of the published values of these rate-constants (10). This indicates that possibly other reactions such as  $N^+ + O_2 \longrightarrow NO^+ + O$  and  $O^+ + N_2 \longrightarrow NO^+ + N$  or others involving neutral atomic species also contribute to the total yield of  $NO^+$  ion.

#### CONCLUSIONS

Mass spectrometric studies of low pressure positive d.c. corona discharges in atmospheric gases containing trace quantities of water vapor show a complex series of reactions with each component leading to the formation of hydrated protons in the system. In the case of nitrogen, intermediate species  $N_2H^+$  and  $H_2O^+$  are presumably formed through ion-molecule reaction and charge-exchange of  $N_2^+$  and  $N_4^+$  with water molecules. These species later form the hydrated proton through proton transfer reactions in subsequent collisions with water molecules. In moist gaseous oxygen, it appears that the hydrated form of the primary ion  $O_2^+(H_2O)_2$ , plays an important role in the conversion of the charge carriers to hydrated protons. It is suggested that this transformation may occur through the formation of the intermediate  $(H_2O)_2^+$  which has been found in this system. In experiments where water vapor is excluded from the system, a concentration of  $1.2 \times 10^{-1}$  mole % oxygen can transform, through charge-exchange reactions, all ionic species of nitrogen to  $O_2^+$  at a discharge pressure of 20 Torr, and that ion-molecule reactions leading to the formation of oxides of nitrogen are by far less probable within the pressure range investigated.

#### ACKNOWLEDGMENTS

The author is indebted to Dr. W. Roth for his invaluable comments during the course of this work and to A. Friske for his assistance in experimental work.

#### References

- 1) Knewstubb, P. F., Tickner, A. W., J. Chem. Phys. 36, 684 (1962).
- 2) Knewstubb, P. F., Tickner, A. W., J. Chem. Phys. 36, 674 (1962).
- 3) Knewstubb, P. F., Tickner, A. W., J. Chem. Phys. 37, 2941 (1962).
- 4) Shahin, M. M., J. Chem. Phys. 43, 1798 (1965).
- 5) Shahin, M. M., Advances in Chemistry Series, No. 58, Ion-Molecule Reactions in the Gas Phase, p. 315 (1966).
- 6) Shahin, M. M., J. Chem. Phys. 45, 2600 (1966).
- 7) vonEngel, Ionized Gases (Oxford University Press, London, 1965).
- 8) Green, F. T., Miln, T. A., J. Chem. Phys. 39, 3150 (1963); Leckenby, R. E., Robbins, E. J., Trevalion, P. A., Proc. Roy. Soc. (London) A280, 409 (1964); Anderson, J. B., Anders, R. P., Fenn, J. B., Advances in Atomic and Molecular Physics, p. 345; edited by D. R. Bates, Academic Press, New York 1965.
- 9) Varney, R. N., J. Chem. Phys. 31, 1314 (1959).
- 10) Ferguson, E. E., Fehsenfeld, F. C., Goldan, P. D., Schmeltekoff, A. L., J. Geophys. Res. 70, 4323 (1965).

SYNTHESIS OF ORGANIC COMPOUNDS BY THE ACTION OF ELECTRIC  
DISCHARGES IN SIMULATED PRIMITIVE ATMOSPHERES

C. Ponnampetuma, F. Woeller, J. Flores, M. Romiez, and W. Allen

Exobiology Division  
National Aeronautics and Space Administration  
Ames Research Center  
Moffett Field, California

In the study of chemical evolution we are interested in the path by which molecules of biological significance could have been formed on the primitive earth in the absence of life. It is generally accepted that the primitive atmosphere of the earth consisted mainly of methane, ammonia, and water. Various forms of energy such as ultraviolet light from the sun, electrical discharges, heat, and ionizing radiation acting on this atmosphere must have given rise to a wide variety of organic substances.

Table I gives a summary of the sources of energy on the earth's surface today. (1) It is probable, therefore, that solar energy must have made the principal contribution to the synthesis of organic compounds in primordial times. Next in importance are electric discharges, such as lightning and corona discharges from pointed objects. These occur closer to the earth's surface and, hence, would have more effectively transferred the organic matter synthesized to the primitive oceans. This paper describes attempts to simulate some of the reactions which may have taken place on the prebiotic earth, through the action of electric discharges.

While extensive work has been done on the effect of electric discharges on various organic molecules, relatively few experiments have been performed to elucidate its role in chemical evolution. Some of the earliest such investigations were carried out by the chemist Haber. Beutner, in his book entitled "Life's Beginning on the Earth," recalls how Haber performed numerous experiments in which electrical discharges were sent through carbon containing gases like methane, carbon dioxide, etc., with the aim of obtaining sugars. (2) Although traces of some sugars were formed, a large number of various other substances were also synthesized. Haber thus came to the conclusion that by means of electrical discharges through carbon containing gases, "practically any substance known to organic chemistry can be found."

Perhaps the most celebrated experiment in this field was performed by Stanley Miller in Urey's laboratory in 1953. (3) Miller submitted a mixture of methane, ammonia, and water in the presence of hydrogen to electrical discharges from tesla coils. A large number of organic compounds were formed. Among these, four amino acids were identified. Miller postulated two alternative possibilities for the mechanism of synthesis of amino acids. According to the first, aldehydes and hydrogen cyanide are synthesized in the gas phase by the spark. These aldehydes and hydrogen cyanide react in the aqueous phase to give amino and hydroxynitriles. These nitriles are, in turn, hydrolyzed to amino and hydroxy acids. The mechanism is essentially a Strecker synthesis. A second suggestion made was that the amino and hydroxy acids were synthesized in the gas phase by ions and radicals produced in the electrical discharge. Miller's subsequent work has shown that the first mechanism is the one most likely to have produced the amino acids. (4) The rate of production of aldehydes and hydrogen cyanide by the spark and the rate of hydrolysis of the aminonitriles were sufficient to account for the total yield of amino acids.

In our experimental work, we have endeavored to study the mechanism by which various molecules of biological interest could have been formed by the action of electrical discharges. A series of experiments was outlined in which the starting materials were varied. Four different classes of experiments have been performed: with methane; with methane and ammonia; with methane, ammonia, and water; and with methane and water.

The effect of a semi-corona discharge, a low intensity arc discharge, and a high intensity arc discharge on gaseous methane was first investigated. The current through the discharge was measured by the voltage drop across a resistor with the cell. For the semi-corona discharge, the cell current was 0.4 m. amp, 0.5 m. amp for the low arc, and 10 m. amp for the high arc discharge. Gas chromatography and mass spectrometry were used for the analysis of the end products. Comparative results of the analysis of hydrocarbons up to  $C_5$  are shown in Table II. In the semi-corona most of the methane remained unreacted after a 24-hour discharge. Some ethane and propane were formed. There were small amounts of ethene, propene, and substituted paraffins. In the case of the low and high arcs, ethylene and acetylene were also present.

The analysis of the hydrocarbons from  $C_6 - C_9$  reveals that the semi-corona gave unsaturated substances while the arc discharge gave rise to aromatic compounds. The semi-corona cell yielded a colorless distillate, the gas chromatogram of which was poorly resolved. The high intensity arc gave a yellow fluid, the chromatogram of which had well spaced peaks. Benzene was the most abundant with toluene next in order of magnitude. The peaks from the semi-corona chromatogram were identified by the use of mass spectrometry as: 2,2-dimethyl butane, 2-methyl pentane, 3-methyl pentane, 2,4-dimethyl hexane, 3,4-dimethyl hexane. In figure 1 the chromatogram of the semi-corona discharge products (low) has been superimposed on that from the high intensity arc (high). The results presented here show that the character of compounds in the range of interest appears to be determined by the type of discharge more than by any factor. (5)

We have also examined the composition of the hydrocarbons above  $C_9$  in the products of the semi-corona discharge. The gas chromatogram is very unresolved (Fig. 2). No normals or branched-chain isoprenoid hydrocarbons were identified. Analysis of the mixture by mass spectrometry shows that the compounds are possibly cyclic in structure. (6)

The effect of an arc discharge on anhydrous methane and ammonia was next investigated for two reasons. Firstly, such a study would help us to understand the pathways by which some organic compounds such as amino acids can be synthesized. Secondly, reactions of this type would simulate, to some extent, conditions which may exist on the planet Jupiter.

In this investigation, we have used reaction vessels of about a liter in volume containing an equimolar mixture anhydrous methane and ammonia up to a pressure of 0.5. The electrodes consisted of gold wires about 1 cm apart. A typical reaction lasted for about 15 hours. The current passing through the system was about 0.5 mA. The end products consisted of: (1) gases, (2) a colorless distillate, and (3) a ruby colored residue.

In the present study, our attention was primarily directed to the colorless distillate. The volatile products were vacuum distilled into a U-trap at  $-78^\circ\text{C}$  and analyzed by gas chromatography (Fig. 3). The fractions corresponding to each peak were collected for subsequent mass spectrometric analysis. The GLC retention time, the mass spectrometric fragmentation pattern, and the NMR spectrum established the

GAS CHROMATOGRAMS  
LOW-INTENSITY CELL VS HIGH-INTENSITY CELL

AEROGRAPH A90-P

12' COLUMN 10% OCTOIL-S ON  
60-80 MESH CHROMOSORB-W

COLUMN: 130°      INJECTOR: 155°  
DETECTOR: 160°      He = 40cc/min

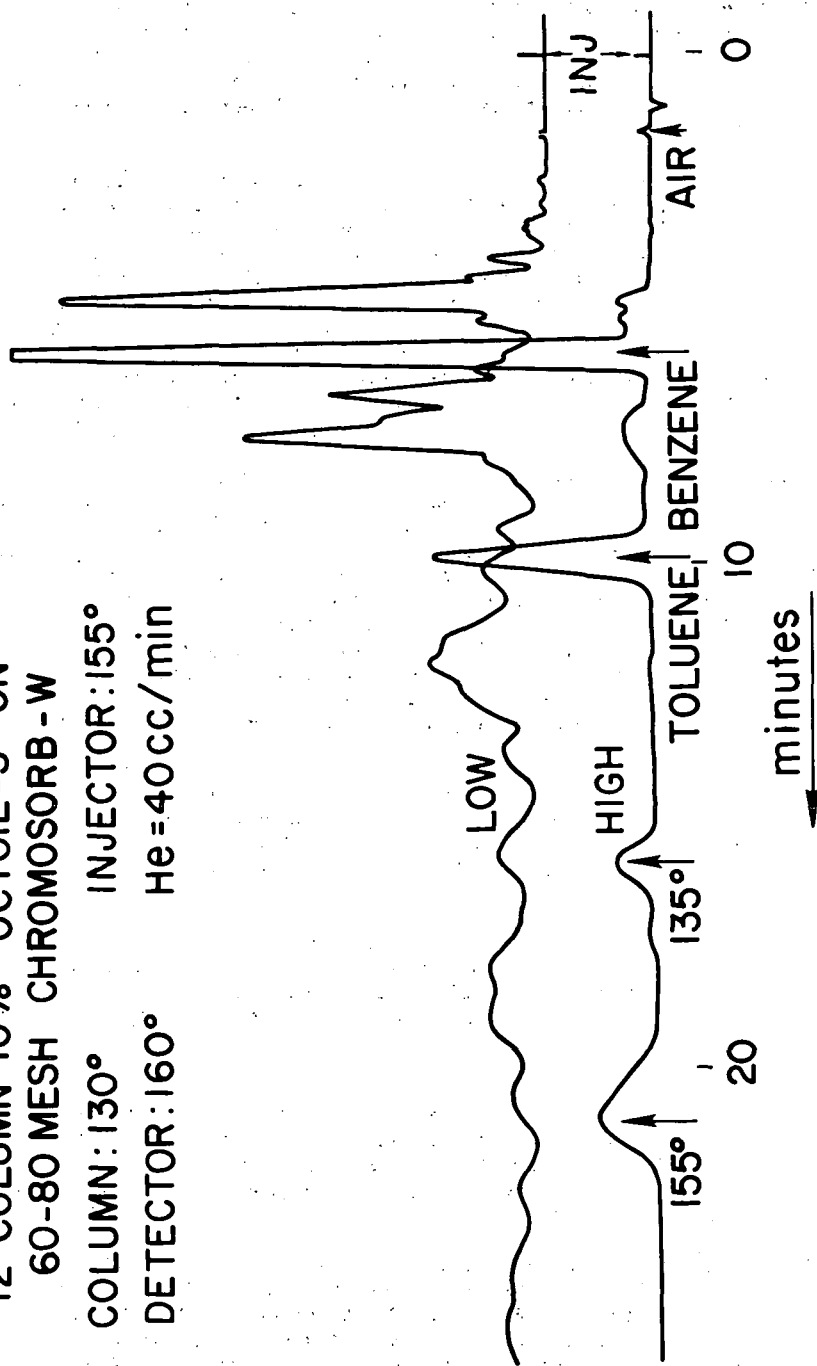


Fig. 1 - Gas chromatograms of semi-corona and arc discharge products C<sub>6</sub> - C<sub>9</sub>

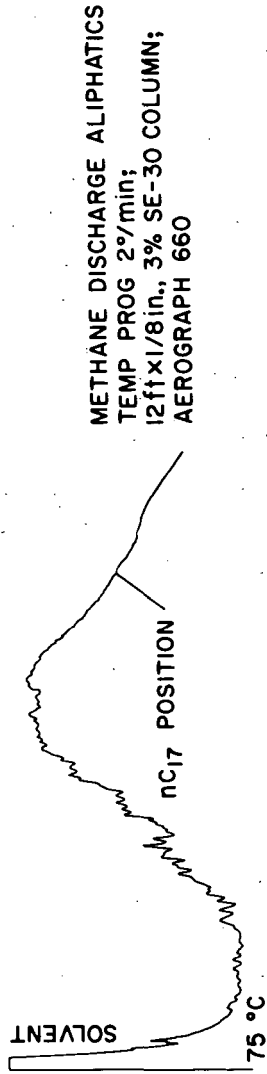


Fig. 2 - Gas chromatogram of semi-corona discharge products above C<sub>9</sub>

NATIONAL AERONAUTICS AND SPACE ADMINISTRATION  
AMES RESEARCH CENTER, MOFETI FIELD, CALIFORNIA

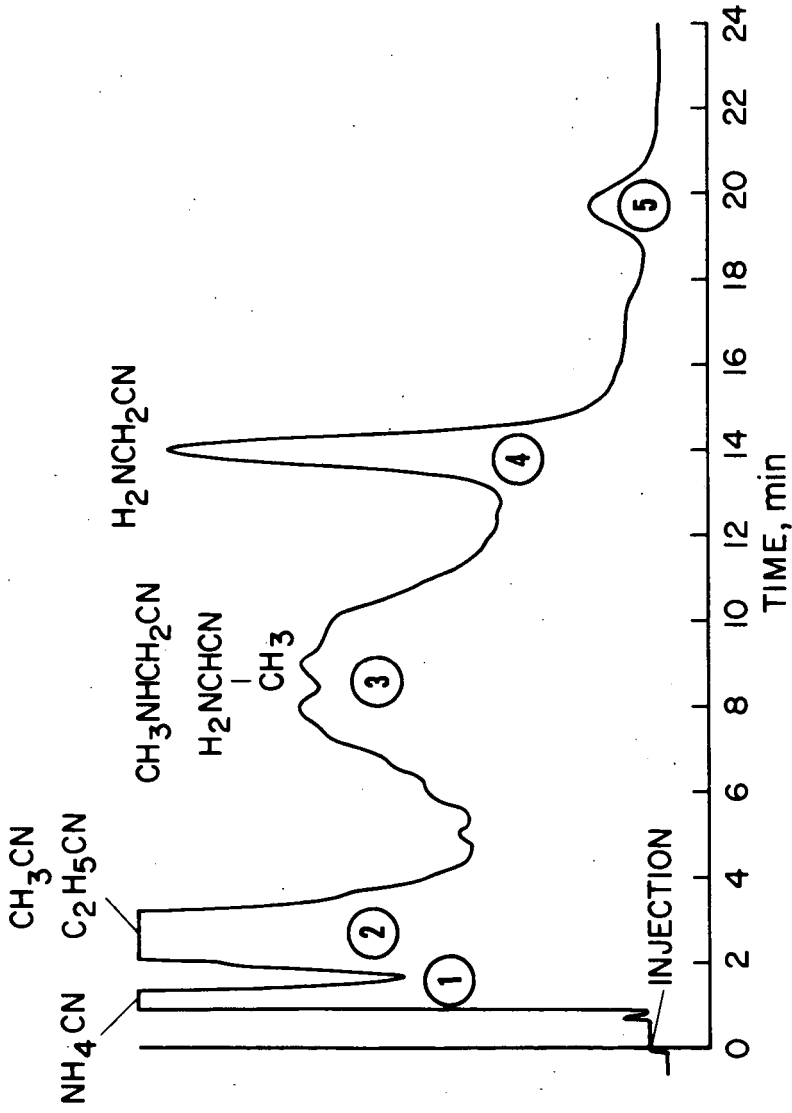


Fig. 3 - Gas chromatogram of colorless distillate from arc discharge through methane and ammonia

identity of each of the fractions separated by gas chromatography. Ammonium cyanide, methyl cyanide, ethyl cyanide,  $\alpha$ -aminoacetonitrile and its C-methyl and N-methyl homologues were identified. The  $\alpha$ -aminonitriles on hydrolysis give rise to  $\alpha$ -amino acids. These nitriles may provide a reasonable pathway for the origin of amino acids under prebiological conditions.

In some of our discharge experiments, we turned to the question of the origin of monocarboxylic acids under prebiotic conditions. If we assume that pre-existing abiotically synthesized fatty acids were necessary for the functioning of selective membranes, some mechanism must have existed for their formation. The reaction between methane and ammonia appears to provide such a pathway. When a mixture of methane and water exposed to a semi-corona discharge and the end products examined after saponification, the monocarboxylic acids from  $C_2 - C_{12}$  were identified. (7)

The volatile acids  $C_1 - C_8$  were examined as their free acids by gas chromatography. A resulting chromatogram is illustrated in Figure 4. The individual peaks were then trapped and their identity confirmed by mass spectrometry. Acids containing seven or more carbon atoms were analyzed as methyl esters. The methyl esters, after chromatography, were examined by mass spectrometry. Of eleven major peaks obtained by gas chromatography (Fig. 5) only one appears as the normal methyl ester. Presumably, the remaining peaks represented branched-chain isomers.

While it is clear that in the case of the longer chain fatty acids several isomers have been produced, only a few of the innumerable possible compounds are realized. A preferential synthesis of some type appears to be favored. Theoretically, the branching of carbon chains, which is favored in free radical reactions, may be repressed by steric restrictions when the lengthening carbon chains are absorbed on monolayers. An attempt to favor the formation of straight chain acids by placing the aqueous phase in close proximity with the discharge zone did not produce any change in our results.

In the study of prebiotic organic synthesis, perhaps the most relevant experiments involve the use of all the main constituents of the presumed primitive earth atmosphere. We have therefore exposed a mixture of methane, ammonia, and water to a discharge from tesla coils simulating lightning on the primitive earth. At the end of a 24-hour discharge, the gas phase analysis has shown that over 90% of the starting methane has been converted into organic compounds. Of this, about 45% is found in the water fraction. 18% of the water soluble material is in the form of cyanide. The formation of cyanide in this reaction is significant in the light of the multiple role played by hydrogen cyanide in organic synthesis. (8)

The analysis of the end products of this reaction by paper chromatography reveals that a large number of organic compounds were formed but none of these corresponded to the commonly occurring amino acids. A certain amount of material appeared at the origin. However, when the reaction products were hydrolyzed with 6N HCl for 24 hours and then analyzed, a large number of amino acids were formed (Fig. 6). Among those identified are nine which are commonly found in biological materials: glycine, alanine, aspartic, glutamic, threonine, serine, isoleucine, leucine, and phenylalanine. The results obtained by ion exchange analysis were confirmed by gas chromatography. The evidence, thus, points to the fact that the amino acids were already polymerized in the solution of end products. Separation by the use of a biogel-P column gave us a fraction having a molecular weight in the range 186 to about 2,000 and whose 1-dimethylaminonaphthalene-5 sulphonyl chloride (DNS) derivative showed a single band on electrophoresis. When this fraction was hydrolyzed, the amino acids aspartic, serine, glutamic, glycine, and alanine were obtained.

# VOLATILE FATTY ACIDS

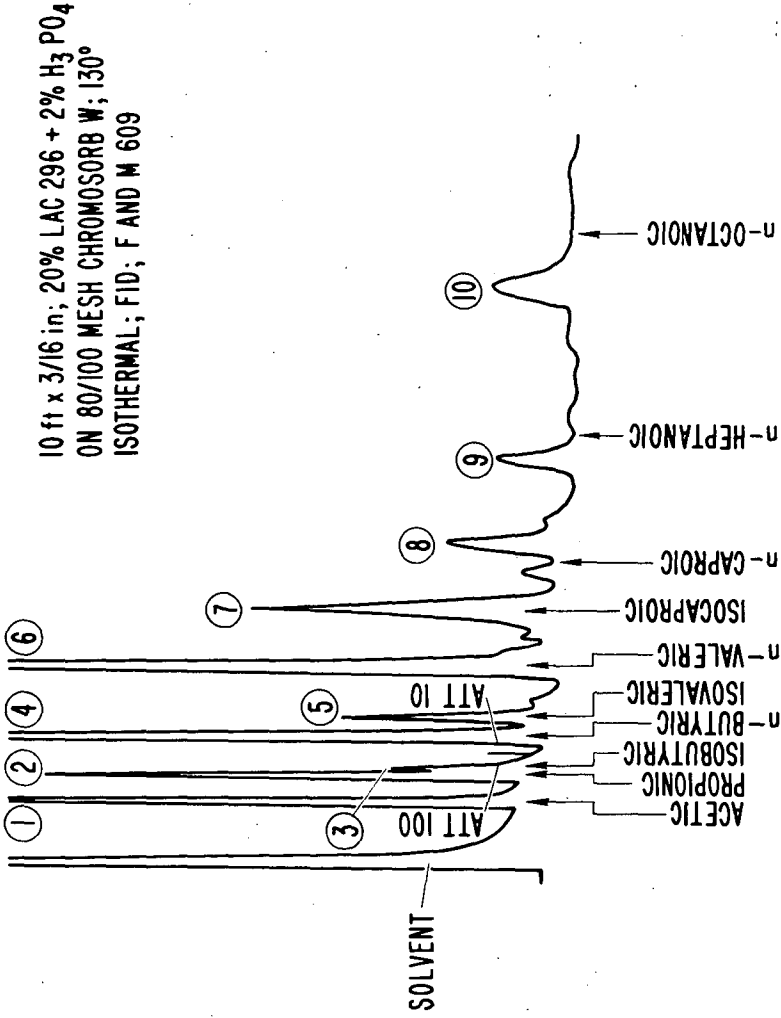


Fig. 4 - Gas chromatogram of volatile fatty acids from a semi-corona discharge through methane and water.

## METHYL ESTERS

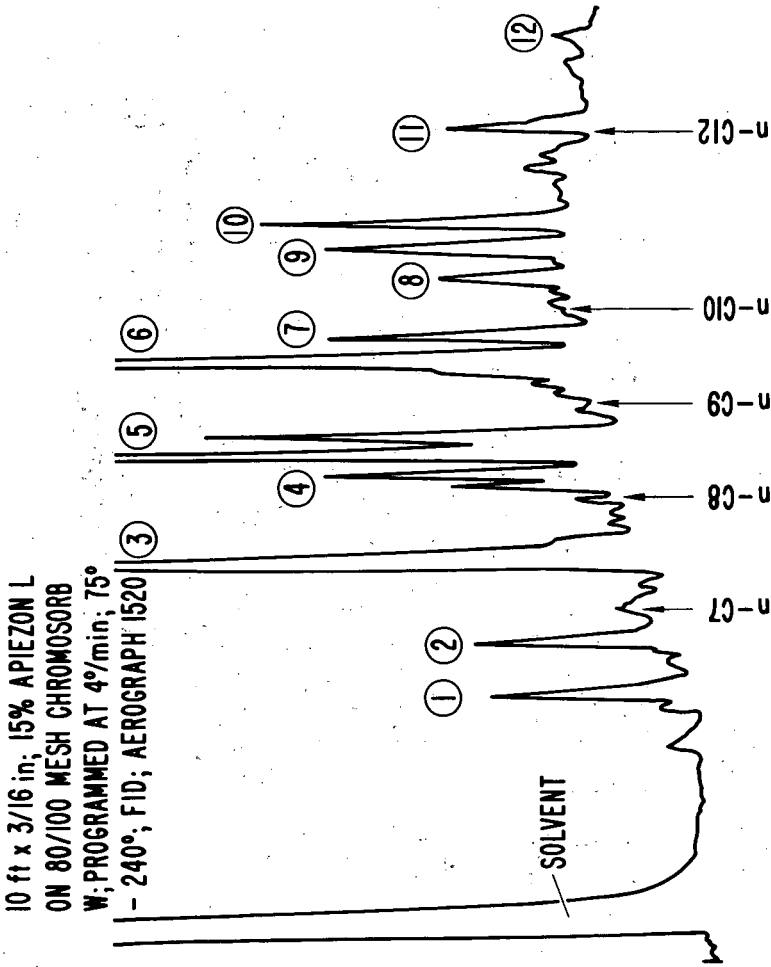


Fig. 5 - Gas chromatogram of methyl esters of higher fatty acids from a semi-corona discharge through methane and water.

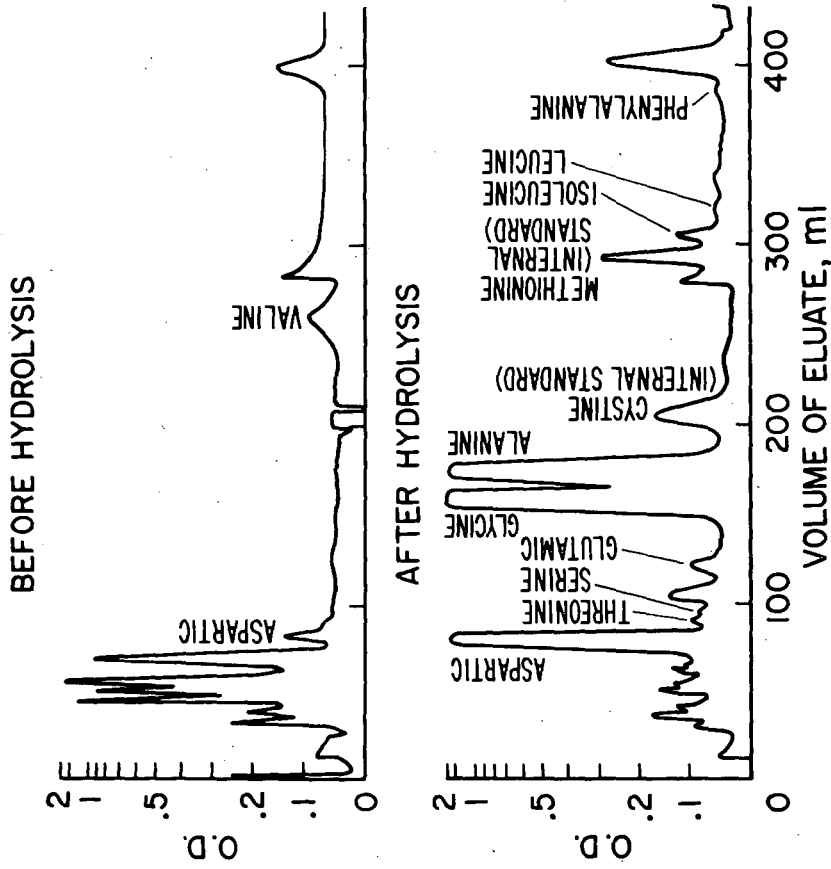
AMINO ACIDS FROM A SPARK DISCHARGE ON CH<sub>4</sub>, NH<sub>3</sub> AND H<sub>2</sub>O

Fig. 6 - Ion exchange separation of amino acids from a spark discharge through methane, ammonia, and water.

This result is significant in the context of chemical evolution. It has generally been thought, that amino acids had first to be synthesized and then condensed together into a polymer. The synthesis of a polypeptide in an electric discharge experiment reveals that such a sequence of reactions may not have been necessary. If a suitable condensation agent is present the polymer appears to be formed as soon as the acids are synthesized. In our case, the condensation agent is probably hydrogen cyanide. The presence of 18% hydrogen cyanide in the reaction mixture combined with the fact that in previous experiments we have been able to condense bases and sugars with cyanide support this hypothesis.

The different experiments that have been described so far reveal that important biological molecules can be synthesized by the use of a form of energy which existed on the primitive earth. These conditions may be considered to be genuinely abiotic since the materials used are the constituents of the presumed primitive earth atmosphere, the conditions are aqueous, and the form of energy is one that is likely to have occurred on the earth before the appearance of life.

## References

1. S. L. Miller and H. C. Urey, *Science* 130, 245 (1959)
2. R. Beutner, *Life's Beginning on The Earth*, Williams and Wilkins, Baltimore, 1938
3. S. L. Miller, *J. Am. Chem. Soc.* 77, 2351 (1955)
4. S. L. Miller, *Biochim. et Biophys. Acta* 23, 480 (1957)
5. C. Ponnampertuma and F. Woeller, *Nature* 203, 272 (1964)
6. C. Ponnampertuma and K. Pering, *Nature* 209, 979 (1966)
7. W. A. Allen and C. Ponnampertuma, *Currents in Modern Biology* (in press) (1967)
8. R. Sanchez, J. Ferris, and L. E. Orgel, *Science* 153, 72 (1966)

TABLE I

SOURCE	ENERGY (in cal cm <sup>-2</sup> yr <sup>-1</sup> )
Ultraviolet light ( 2500 Å )	570
Electric discharges	4
Radio activity	0.8
Volcanoes	0.13

TABLE II

	High Arc	Low Arc	Semi-Corona
Total hours of current flow	1.5	40	48
Electrode voltage	1400	2500	9400
Cell current (m. amp)	4.0	0.5	0.3
% Loss CH <sub>4</sub> /h	6.6	1.1	0.6
End products (%)			
Ethane	32	20	58.8
Propane	2	5.2	36.8
Ethene	32	2.4	1.5
Propene	--	1.9	0.6
Acetylene	27	42.5	0.0

## The Dissociation of Metal Halides in Electrical Discharges

F. K. McTaggart

Division of Mineral Chemistry, C.S.I.R.O. Box 124, Fort  
Melbourne, Victoria, Australia.

Introduction. The effect of the energetic electrons produced in electrical discharges in dissociating gas molecules is well known, and is the basis of the chemical reactions that are observed in plasma systems. Since gases such as  $O_2$ ,  $N_2$ ,  $N_2O$  and  $Cl_2$ , as well as vapours of organic and other compounds have been dissociated to atoms and/or radicals, it appears logical to suppose that many other molecules would behave similarly. This paper describes the dissociation of the halides of the Group I, II and III, and rare earth metals.

Experimental. Ideally, the halides should be introduced into the discharge tube in the form of vapours at suitable pressures. Due to the wide range of volatilities occurring in the above compounds and to other experimental difficulties it proved more convenient to use carrier gases, and to volatilize the halides from small boats contained within the reaction tube by heating these boats to suitable temperatures. It was usually possible to make use of the heat generated in the plasma itself for this purpose. Samples were placed upstream from, or within the central plasma region, in positions where heat sufficient to give the desired rate of volatilization was produced. Since heating of solids due to atomic recombination is largely a surface effect it was also possible to vary the sublimation rate of samples by changing the surface area exposed to the plasma.

Both inert gases (in particular He and  $N_2$ ) and hydrogen have been used and certain reactions which are discussed below appear to involve H atoms as well as dissociative effects. These gases were of commercial purity, the He and  $H_2$  being purified by passing them over zirconium powder heated to  $800^\circ C$ ; although no essential differences between the cylinder gases and the purified gases were observed. Pressures of the carrier gases were varied between 0.5 and 2.3 mm. Halides used were of A.R. grade, but in certain cases impure compounds were deliberately used in order to determine the effects of impurities on the dissociation and on the purity of the metal obtained.

Extensive use was made of a 2450 mC magnetron generator (Mullard JN2/2.5A) which although capable of an output in excess of 2 kW continuous wave power, was seldom operated at inputs higher than 600 watts. Radio-frequency energy from the magnetron was fed via a 50 ohm air dielectric coaxial line, to a section of waveguide operated as a resonant cavity by means of a sliding plunger inserted into the open end. The discharge tube passed transversely through the guide at a point of maximum electrostatic field. Some investigations, involving the chlorides of Li, Be, and Al, which dissociate very readily, were made using an "rf" generator consisting of a 4-125A vacuum tube at a frequency of 30 mC, the power of which could be varied from close to zero to about 400 watts. In these

cases the reaction tube passed through the "tank coil" of the output circuit.

Conventional methods of analysis were used to determine a/ the amount of metal deposited, b/ the undissociated halide sublimed onto the reaction tube, and c/ the halogen or hydrogen halide collected in the liquid air trap which followed the reaction tube in the flow system.

**Results.** From all the halides studied it was possible to separate metals, often in good yields.

The lithium group compounds<sup>1</sup> dissociated in both inert carrier gases and in  $H_2$  to give metals and the relative reaction rates were determined for the iodides, bromides, chlorides and fluorides of Li, Na, K and Cs. Some of these are shown in Table 1. It will be noted that for any one metal

Table 1

Relative Reaction Rates for the Halides of Li and Na

Compound	Bond Energy	Rel. React. Rate	Compound	Bond Energy	Rel. React. Rate
LiI	82	232.5	NaI	72	26.0
LiBr	102	101.5	NaBr	89	15.0
LiCl	115	66.5	NaCl	99	10.0
LiF	138	19.0	NaF	108	5.0

the rate is greatest for the iodide and least for the fluoride as might be expected from the bond energies (also quoted). However in going from one metal to another it is seen that bond energy is not the main factor involved since, for example, the rates for LiI and NaI are 232.5 and 26.0 while the bond energies are 82 and 72 respectively. The rates presumably depend largely on the energy levels to which the molecules must be raised before dissociation will occur. Not a great deal is known about these energies and they appear to depend more on the nature of the metal atom present than on the halogen.

The effect of variation of sublimation rate (partial pressure) for NaCl is shown in Figure 1 for several input powers. All the Group I halides gave curves of similar shape. As the sublimation rate decreased the percentage dissociation increased to a maximum beyond which there were insufficient halide molecules to "use up" the electrons having sufficient energy to dissociate them. For any one power the amount of halide dissociated was almost independent of sublimation rate (see Table 2). As expected, an increase in power resulted in increased dissociation and an empirical relationship  $\text{Rate} = KP^{1.7}$  was found to apply throughout. The highest yield of metal obtained during the experiments was 70% lithium from LiI.

1. McTaggart, F. K. Aust. J. Chem. 18, 936, 949 (1965).

Table 2

Dissociation of NaCl in H<sub>2</sub> at 1.0 mm for Various Input Powers

Sublm. Rate mmole/hour	mmole/hour Na produced			
	168W	220W	270W	320W
0.5	0.11	0.160	-	-
1.0	0.11	0.158	0.225	0.280
1.5	0.105	0.145	0.223	0.255
2.0	0.12	0.156	0.230	0.270
2.5	-	0.175	0.250	0.287
3.0	-	-	0.264	0.291
4.0	-	-	0.240	0.280
Mean	0.111	0.159	0.239	0.277

Figure 2 shows the effect of carrier gas pressure at constant power. A maximum in metal production occurred at about 1.5 mm pressure. For H<sub>2</sub> this pressure coincides closely with the highest concentration of H atoms, and is probably related to the concentration of electrons having sufficient energy to cause dissociation. The reaction rates appeared to be substantially independent of the nature of the carrier gas.

The fact that considerable quantities of highly reactive metals are deposited in atmospheres of even more highly reactive gases, namely halogen atoms, suggests that these halogen species may be in the form of negatively charged ions. Such ions, having a complete outer shell of eight electrons, would be non-reactive chemically, and if neutralization of their charges is delayed until they are swept clear of the metal deposit, an explanation of the apparent absence of appreciable back reaction would be afforded. Mass spectroscopic studies are being made on the nature of the species in these discharges to elucidate this matter.

The Group II compounds. The majority of the halides of Be, Mg, Ca, Sr and Ba were investigated. Rates of dissociation did not appear to vary as widely as those of Group I. As optimum conditions were approached for each compound, all the halide vapourized was dissociated and deposits were formed on the walls of the reaction tube in which metals and dihalides were found in equi-molar proportions. This points strongly to the formation of unstable monohalide molecules in the discharge, which disproportionate to yield the observed products. Again the dissociations were not dependent on the carrier gas employed. BeCl<sub>2</sub>, one of the more volatile halides in this group, and one of the most easily dissociated of all the compounds studied, may be broken down in the lower frequency apparatus mentioned previously.

Metals could be separated from the dihalides in the deposits by means of suitable solvents for the latter, or in some cases by vacuum sublimation of the dihalide.

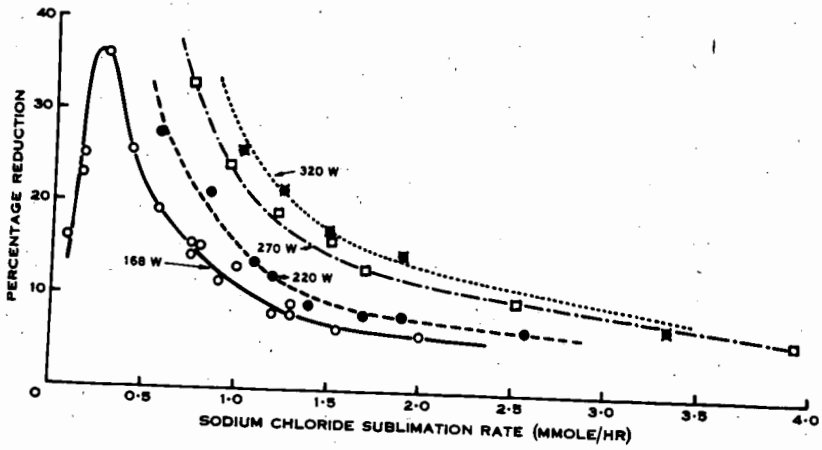


Figure 1

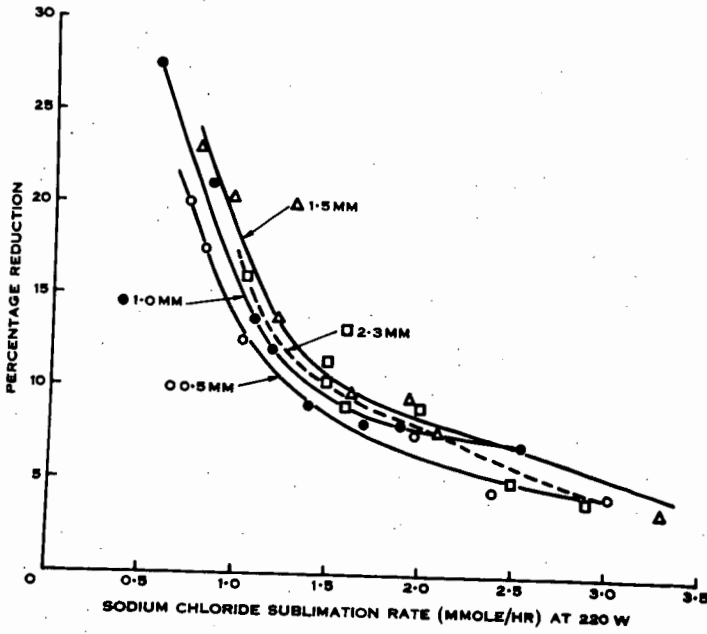


Figure 2

Group III compounds. No investigations have been made on the compounds of boron. Markovskii et al.<sup>2</sup> reported in 1958 that  $\text{BCl}_3$  was reduced to elemental boron by H atoms, and the present work on aluminium halides supports this claim.

When inert carrier gases were used there was a very limited deposition of metal from Al and Sc halides amounting to only a few per cent of the vapour passed through the discharge, but when hydrogen was employed much higher yields of metals were obtained. It would appear, therefore, that at least one step in the decomposition involves a H atom reaction, and the process may well be, for  $\text{AlCl}_3$ :— initial dissociation of  $\text{AlCl}_3$  to  $\text{AlCl}_2$ ; H atom reduction of  $\text{AlCl}_2$  to  $\text{AlCl}$ ; disproportionation of  $\text{AlCl}$  to Al and  $\text{AlCl}_3$ . A mass spectrometric examination of the species present in the discharge revealed  $\text{AlCl}$  in readily detectable quantities but no  $\text{AlCl}_2$  was observed. Yields of up to 55% Al metal have been obtained from  $\text{AlCl}_3$  in a single pass through a 2450 mC plasma, and if a second discharge was produced downstream more Al deposited. The rate at which  $\text{AlCl}_3$  decomposes, with comparatively low power, and with its intense blue plasma makes this reaction one of the most spectacular of those studied. The relatively involatile  $\text{AlF}_3$  also dissociated quite readily to give the metal, although it is not easily handled in the experimental apparatus described. The chloride and fluoride of scandium behaved in a similar manner to the corresponding aluminium compounds.

$\text{AlCl}_3$  also dissociated readily in the lower frequency apparatus. It should be mentioned here that the chief difference between the waveguide and the coil-coupled apparatus appears to be that in the former the electrons are accelerated to higher energies since the electrostatic field is concentrated between the resonator walls where a high potential gradient exists in a direction axial to the discharge tube. By comparison the E field in a coil is much more randomly distributed.

Rare Earth Compounds. We have not as yet had an opportunity of studying these halides systematically, but preliminary experiments have shown that they behave in a manner similar to  $\text{AlCl}_3$ . That is, there is only limited dissociation to metal in an inert carrier gas, but with hydrogen satisfactory yields of metals are obtained. Thus Ce and La result from  $\text{CeF}_3$ ,  $\text{CeCl}_3$ ,  $\text{LaF}_3$  and  $\text{LaCl}_3$ . If, for example, chlorides containing appreciable quantities of oxychloride are used for the dissociation this impurity is left in the sample boat and a highly pure metal is deposited. Such reactions may therefore prove of use in the preparation of certain metals.

2. Markovskii, L. V., Lvova, V. I., Kondrashev, Y. D., Ber. Tr. Konf. po Khim. Bora i Ego Svedin, 36 (1958).

## THE GLOW DISCHARGE DEPOSITION OF BORON

A. E. Hultquist and M. E. Sibert

Materials Sciences Laboratory  
Lockheed Palo Alto Research Laboratory  
Palo Alto, California

## INTRODUCTION

Many new materials concepts are evolving out of aerospace materials technology. One of the most promising of these is that of boron filament-reinforced composite structures. Incorporation of continuous boron filament in a suitable matrix could yield a structure with the strength of high-strength steel, the rigidity of beryllium, and the density of magnesium. A large-scale development effort is currently concerned with fabrication of such structures. Once this has been achieved, large amounts of filament must be made available at reasonable cost to make large-scale usage practical. Present techniques for filament production are based on scaled-up laboratory chemical vapor deposition procedures, and major technological development is required to result in large-scale production. As a result, many other new and novel techniques for filament preparation have been investigated with the intent of developing alternate approaches.

This study is concerned with investigation of one such approach, that of deposition in an electrodeless glow discharge. Basically a high-voltage, low-amperage, high-frequency rf current is imposed across a boron-containing gas, resulting in a high degree of ionization/activation of the ions present. Boron then deposits out in elemental form on all surfaces within the glow discharge area. Use of proper deposition conditions confines the glow largely to the filament substrate. By passage of the filamentary substrate continuously through the discharge, the approach is potentially capable of high rate filament formation with excellent uniformity and reliability. Variation of current input can result in deposition at any point from room temperature up to 800-1000°C. Both metallic and non-metallic substrates can be employed. Deposition is achieved at low pressures of the order of a few mm.

The bulk of the work described has been carried out using a fixed filament system in order to study the effects of operating parameters. Work has also been confined to the hydrogen-boron trichloride system. The approach has been studied with respect to ratio of reactants, total system pressure, voltage, current, and type of substrate. The most recent work is concerned with development of a continuous system and adjustment of parameters to produce desired deposition characteristics.

Literature in the area of glow discharges is very extensive, but work on chemical reactions in discharges, such as are of concern to this work, is very limited. Some work has been done on effects of discharges on boron compounds together with a small amount of work on deposition of boron as amorphous powders.

Holzman and Morris (Ref. 1) have reported formation of  $B_2Cl_4$  from  $BCl_3$  in an electrodeless glow discharge.  $BCl$  was the principal intermediate in the course of the reaction. Kotlensky and Schaeffer (Ref. 2) have described decomposition of diborane in a low-pressure glow discharge to give higher hydrides of boron. Rosenberg (Ref. 3) has studied the reaction of boron halides with nonmetal oxides under the influence of electrical discharges. Markovskii et al. (Ref. 4) claim to have prepared elemental boron of 99.9% purity through reaction of boron trichloride and hydrogen in a glow discharge. However, efforts to duplicate this work indicate that the conditions employed lead to effects more like an arc than a glow discharge. Related, although distinctly thermally rather than electrically initiated processes, are the original arc preparations of pure boron as carried out by Weintraub (Ref. 5) and Kroll (Ref. 6). Other references to behavior of boron compounds in electrical discharges are given in the report of the International Symposium on Electrical Discharges in Gases (Ref. 7).

## EXPERIMENTAL WORK

**Apparatus.** The basic apparatus utilized for parametric studies employing a fixed substrate is shown in Fig. 1. The reaction vessel is a simple pyrex tube with the substrate filament suspended down the central axis and suitably sealed at each end. The reactant gases are admitted at one end of the tube and exit at the opposite end. Electrodes are simple concentric copper strips which may be moved along the tube for optimum positioning. The glow discharge then forms between these electrodes. Both horizontal and vertical reactor configurations have been employed; the vertical system is preferred since substrate alignment is better controlled. The vertical arrangement is also more amenable to moving filament systems for continuous filament preparation. Both air and water cooled reaction vessels have been evaluated. Water cooling was originally instituted to minimize sidewall deposition; later work demonstrated that this could be accomplished by regulation of gas composition and current input so as to confine the glow area to the central area of the reaction tube. A three compartment chamber was used so that these experiments could be performed before the system was opened for examination.

The balance of the system is largely a gas flow system. Hydrogen is passed through a catalytic cartridge and a liquid nitrogen trap for removal of oxygen and water impurities. Boron trichloride is fed into the hydrogen stream. Both lines have appropriate flowmeter devices. The boron trichloride is controlled at the cylinder valve; satisfactory control with respect to potential condensation is obtained by bleeding the gas into a section of tubing at operating pressures and heated to 35°C. Hydrogen flow is regulated by a stainless steel needle valve just downstream from the flowmeter. The combined hydrogen-boron trichloride stream then passes into the reaction chamber. Exit gases from the reactor pass successively through a trap for condensation of unused boron trichloride, past a manometer, through a Cartesian manostat, and thence to a mechanical vacuum pump.

The power supply is a Lockheed-designed 3 Mc oscillator capable of about 30 W output; however, only a portion of this output is available as rf power, about 20 W at 1400–1500 V. The first 20 turns of the large coil (Fig. 1), and the capacitance connected across them, act as the tank. The tank is a resonance combination wherein the energy is alternately stored in the condensers and in the field of the coil, with interchange occurring at a frequency determined by the coil inductance and capacitance of the condensers. A variable condenser included in the tank allows its frequency to be matched to that of the secondary. When such matching occurs, the coils are efficiently coupled, and rf power is drawn from the secondary. This power is fed into the primary by a 6146A transmitter tube activated at proper frequency by feedback from the tank. This is done through a condenser and a resistor wound with a coil, serving as a low-Q resonance circuit to suppress high frequency parasitic oscillation. A 47K resistor allows the grid to be self-biased. An rf choke prevents loss of power into the backup power supply. Two 10K resistors and a 7500  $\Omega$  resistors serve as a voltage divider for the screen grid.

**Materials.** The boron trichloride used was electronic grade supplied by American Potash and Chemical Co. Hydrogen was a high purity laboratory grade (BB-H-886) supplied by Air Reduction Co. Quartz monofilament utilized as a substrate for most of the work was obtained from the General Electric Co. Glass filaments were drawn from pyrex glass rods by the LMSC glass shop.

**General Procedure.** Experiments were started by evacuating the assembled apparatus to 1 mm Hg pressure. The leak rate was determined by turning off the pump and noting the increase in pressure over extended time periods. A leak rate of less than 0.05 mm Hg/min is necessary to avoid boron oxide formation. When the system was determined to be essentially leak free, a flow of hydrogen was introduced and allowed to sweep through the apparatus for 15 to 30 min. The desired gas pressures and flow rates of hydrogen and boron trichloride were established, the power supply for the oscillator turned on, and the flow was initiated by adjusting the variable capacitor. At the end of the experiment, the flow discharge and the boron trichloride flow were turned off and hydrogen allowed to sweep through the

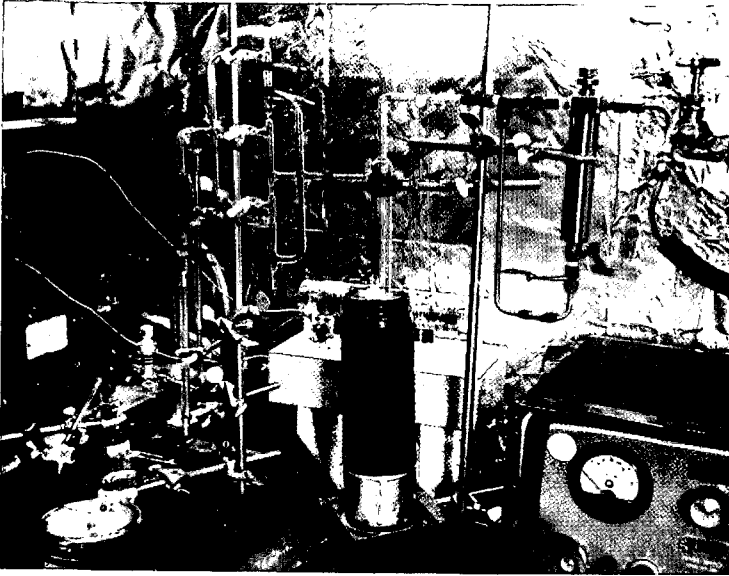
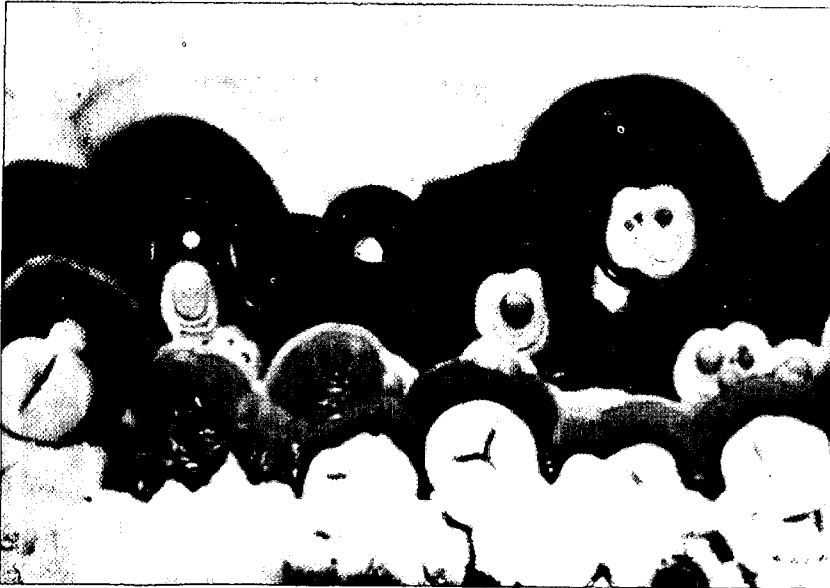


Fig. 1 Process Apparatus



Boron

$B_2O_3$

Oxygen  
Enriched  
or  
Oriented  
Material

Boron

Fig. 2 Boron on Glass, Longitudinal Section (3000x)

apparatus for 10 min to remove unreacted boron trichloride. The pump was turned off and the apparatus returned to ambient pressure using hydrogen. The apparatus was then dismounted and the sample removed.

## RESULTS

**Preliminary Experiments.** Initial experiments were made to observe operating characteristics while exciting hydrogen gas in a glow discharge. Glow discharges were initiated in hydrogen at pressures of 6, 15, 36, 40, 60, and 81 mm Hg and at flow rates of about 40 to 100 cc/min. Electrode separations of 0.75, 1.0, 2.0, 3.5, and 4.5 cm were used. The glow was initiated by tuning the capacitor at maximum voltage to obtain an input current of 105 mA. The effect of power input to the oscillator on the glow discharge was determined by varying the voltage. The change in glow is reflected in the current drawn by the oscillator at any particular voltage and capacity setting. The following characteristics were observed:

- Increasing gas-flow rates reduces the glow intensity.
- Increasing pressure reduces the glow intensity.
- In general, glow intensity is reduced as the electrode distance is increased.

Glow was maintained in the presence of a dielectric and a conductor filament to determine their effect on glow characteristics. The presence of a strand of quartz, QFY-150 to 204 end, 1/0, with oil starch finish,  $d = 0.004$  in., did not affect the operating characteristics of the glow. However, the presence of a 5-mil tungsten wire resulted in considerable changes in the glow. The tungsten wire acted as a ground connection, and the ground lead from the oscillator could be disconnected without affecting the glow. The glow was concentrated at and spread out along the wire. This system used much higher currents and, as a result, considerable heat was generated. A mirror was deposited on the reaction tube walls.

A series of experiments were performed using glass and quartz substrates to determine approximate conditions necessary for the deposition of boron. A qualitative description of the process was obtained from these observations. The data shown in Table I describes the experimental conditions along with pertinent observations. The results have been summarized in the following qualitative statements:

- Wall deposition is favored by high hydrogen and low  $BCl_3$  flow rates.
- Deposition on the filament substrate is more pronounced at higher flow rates of  $BCl_3$ .
- Use of a water cooled reactor lowers wall deposition.
- Small leaks of air result in the formation of the oxide rather than the metal (see experiment 07-18A and Fig. 2).
- Under certain conditions of power input and gas flow, a brown deposit is formed that hydrolyzes on exposure to air and evolves a gas (see experiment 07-20A and 07-21A).
- Thick deposits of boron can be produced in reasonable times and conditions (see Fig. 3).

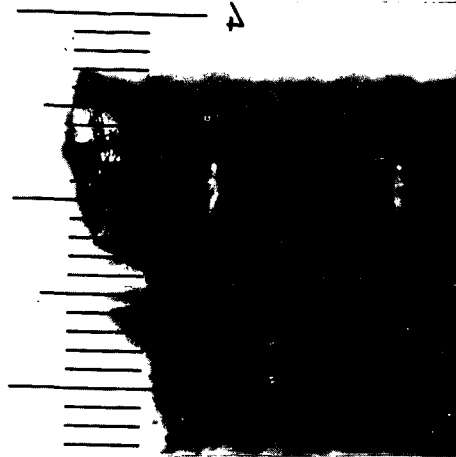
Following these preliminary experiments, flowmeters were calibrated and the quartz monofilament substrate was characterized in terms of physical and mechanical properties. A study was then initiated on effects of the various process parameters.

**Parametric Study.** A study of the effect of process parameters on the deposition of boron using the static filament apparatus was conducted. The parameters studied include system pressure, reactant gas flows and ratios, electrode separation and configurations, and field strengths. The evaluation of certain parameters has been quantitative and was based on the weight of boron deposited or on the thickness of the deposit at the midpoint of the filament. Other parameters were evaluated by a qualitative description of the deposit.

Table I

## DEPOSITION OF BORON IN GLASS AND QUARTZ SUBSTRATES

Experiment	Manometer pressure (mm Hg)	BCl <sub>3</sub> flow reading (mm)	H <sub>2</sub> flow reading (mm)	Direct current to oscillator (mA)	Reaction time (min)	Results
07-13A	2.0	6-7	5-8	75	75	Medium deposit at electrodes; light deposit between electrodes.
07-13B	2.0	6-7	3.5	95 75	15 15	Heavy deposit on walls.
07-13C	2.0	6.5	6.5	75 90	60 30	Heavy deposit on walls near electrodes.
07-13D	2.0	14	2.5	75 90	100 20	Very heavy deposit on walls.
07-13E	2.0	14	7	90	75	Medium deposit on walls.
07-13F	2.0	3.5	14	90	25	Glass filament heated; light deposit on walls.
07-13G	2.0	(Initial) 1.0	10	-	15	As H <sub>2</sub> is depleted, glow turns white, then green, then goes out.
07-17A	40	2.0	2.0	150	40	Water-cooled reactor; smooth thin coating.
07-18A	25	1.5	9.0	110	25	Rough thick metallic appearing (see Fig. 2), leak developed during run, was repaired and run completed.
07-20C	25	1	4	80	30	Brown non-metallic deposit which hydrolyzes in air.
07-21A	25	4.0	9.5	80	10	Metallic (see Fig. 3).



(a) Filament Emerging From Broken End (220 $\times$ )



(b) Surface of Deposit at Broken End (220 $\times$ )

Fig. 3 Boron on Quartz

This study is only an approximation of the moving filament system. The movement of the filament in a continuous system averages the effects of all the parameters so that the filament sample is prepared in a uniform manner. The edge effects noted on the filament situated under the electrodes would not be evident in a continuous system.

Material efficiencies are based on the amount of boron produced from the total amount of boron passed through the reactor. The electrical efficiency is based on the amount of boron produced divided by the theoretical amount that could be produced by the total charge passed using the reduction equation  $B^{+3} \rightarrow B^0 + 3e$ . The current was measured by an rf ammeter placed in the electrical circuit.

### (1) Electrode Configuration

The experiments performed previously have used electrodes made from copper foil. The electrodes are shown in Fig. 4. It was the purpose of one of the series of experiments conducted to determine if other electrode configurations would be desirable. The configurations shown in Figs. 4b, 4c, 4d, and 4e were used. The following qualitative observations were sufficient for determining the best design at this time:

- The plate electrodes parallel to the gas flow shown in Fig. 4 produce a glow but no boron deposition with gas flows and reactant concentrations known to deposit boron when ring electrodes are used.
- The large sheet electrodes shown in Fig. 4d encourage the deposition of boron on the side walls between the electrodes.
- Electrodes, using No. 16 copper wire, hooked up as in Fig. 4a produce a minimal amount of sidewall deposition, and influence of the electrodes on the deposit underneath is also reduced.
- Electrodes, using No. 16 copper wire, hooked up as in Figs. 4b and 4c produce uneven glows and deposits. The glow will be intense between two of the electrodes while the glow between the other electrodes is very faint. The conductivity of the gas phases, electrode separation, and limitation of the current output of the oscillator are probably important factors.

On the basis of the results observed, copper wire electrodes wound around the reactor tube as in Fig. 4a have been used in the process study.

### (2) Electrode Separation

The effect of electrode separation on the deposition of boron is shown in Table II. The gas flow, reactor pressure, and electrical parameters were the same in all cases. The data show a rise in efficiency as the electrode separation is increased to 2.54 cm.

Table II

EFFECT OF ELECTRODE SEPARATION

Electrode distance (cm)	Deposit length (cm)	Deposit weight ( $\mu\text{gm}/\text{cm}$ )	Total thickness (mils)	Material efficiency	Electrical efficiency
0.62	0.85	35.3	1.8	0.34	0.76
2.22	2.15	23.4	1.67	0.59	1.52
3.16	2.22	25.3	1.72	0.66	1.41
2.54(a)	2.15	46.5	2.22	1.15	2.55

(a) Reactor walls grooved at electrode positions.

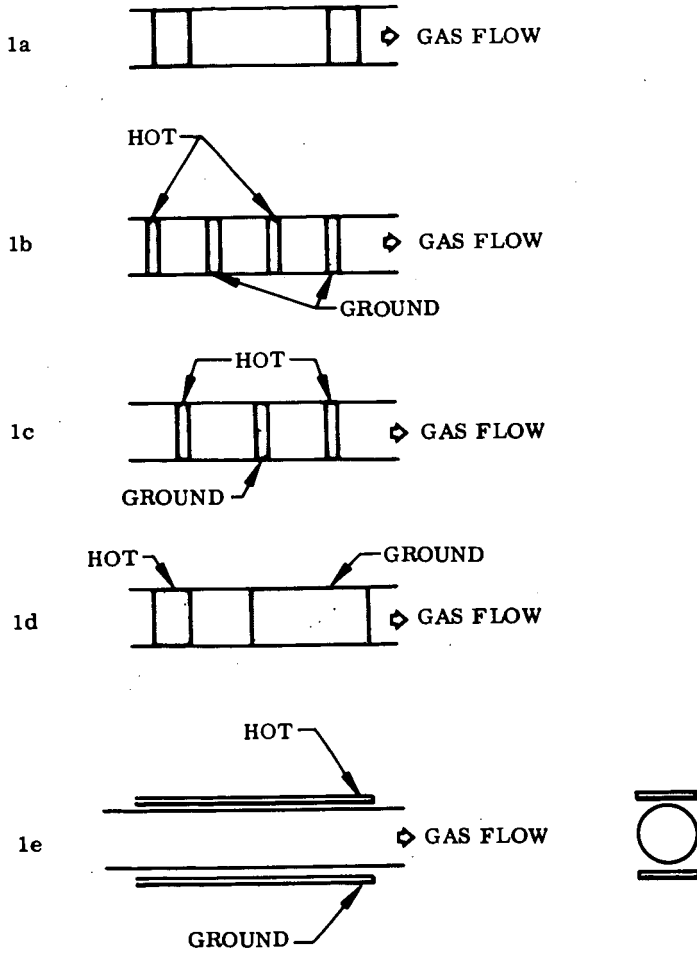


Fig. 4 Electrode Configuration

Increasing the distance beyond this does not increase the efficiencies or the length of substrate upon which deposition occurs. The last experiment shown in this table indicates considerable improvement in efficiencies at 1-in. electrode distances. The reactor is pinched at the electrode positions in this experiment so that the gas stream is forced closer to the substrate. This results in considerable improvement in efficiencies.

### (3) Ratio of $\text{BCl}_3$ to Hydrogen

The ratio of  $\text{BCl}_3$  to hydrogen has very little effect on the efficiency of the reaction. This is shown in Table III. The increase in efficiency at the very low ratio is probably due to the use of the pinched electrode positions in the reactor walls. The efficiencies are so low, the quantities measured are quite small and the material efficiencies shown are not significantly different. In keeping with this observation, the electrical efficiency remains constant over this flow ratio range and indicates that the electrical energy is primarily used in activating atoms or molecules and producing electrons which then react with the other gases. Since hydrogen is the predominate gas it can be presumed that the particular frequency employed in the system results in ionization of the hydrogen.

Table III

#### EFFECT OF FLOW RATIO

Mole ratio $\text{BCl}_3/\text{H}_2$	Reaction time (min)	Material efficiency (% per pass)	Electrical efficiency (% per pass)
0.22	7.80	0.046	1.2
0.19	5.0	0.044	1.1
0.12	10.0	0.06	1.1
0.08	20.0	0.14	1.2

As the mole ratio of  $\text{BCl}_3$  to hydrogen is increased from 0.22 to 0.66 (near stoichiometric) and by reducing the hydrogen gas flow, the appearance of the glow and the character of the deposit are changed significantly. The hydrogen flow rate is an estimated value because the calibration curve does not extend to these low flowmeter readings. However by cutting the hydrogen flow rate in half, making the flow rate near stoichiometric for the reaction, the glow is intensified around the filament substrate and will migrate along the substrate beyond the rf electrodes. The deposit character produced by this procedure is shown in Fig. 40. These pictures show the types of deposits that are formed at different points on the substrate.

The deposition rate is significantly affected by the flow ratio as shown in Table IV.

Table IV

#### EFFECT OF FLOW RATIO ON DEPOSITION RATE

Mole flow ratio $\text{BCl}_3/\text{H}_2$	Deposition rate (mils/min)
0.22	0.05
0.33	0.04
0.66 (est.)	0.19

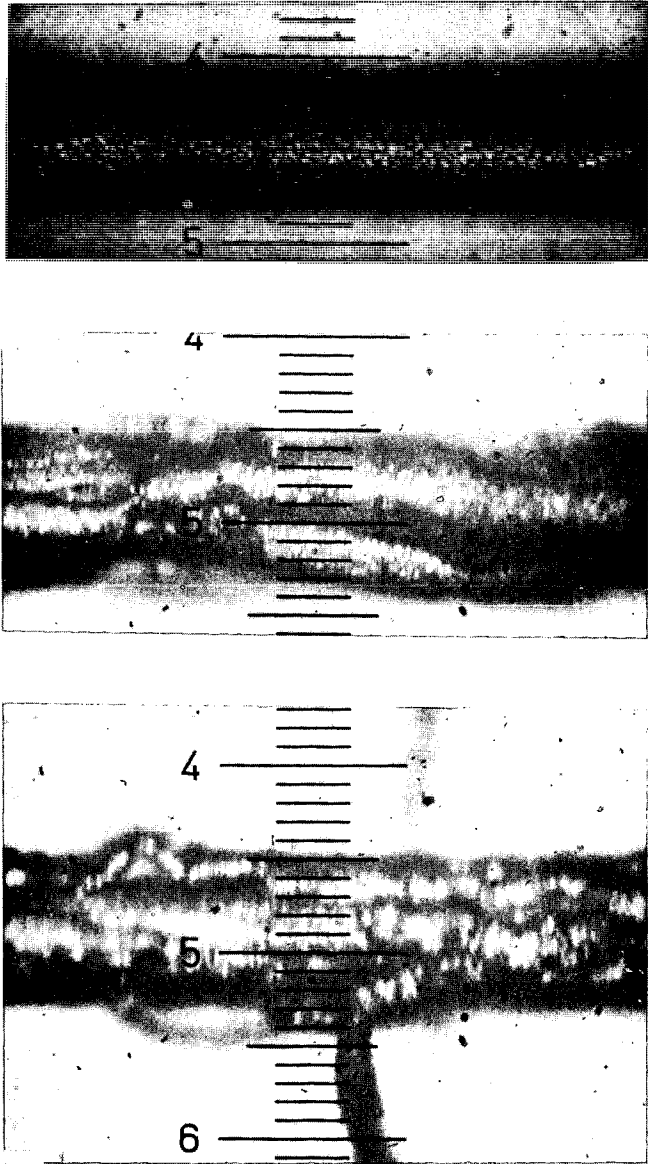


Fig. 5 Filaments Produced at Near Stoichiometric Flow Ratios (220 $\times$ )

#### (4) Effect of System Pressure

The effect of system pressure on deposit characteristics is shown in Table V.

Table V  
EFFECTS OF SYSTEM PRESSURE

Pressure (mm Hg)	Type of deposit
5	Needles, trees, and dendrites. Exploded from substrate if run was long
20	Thick, fairly uniform, some craters or knobs
30	Thick, small mounds, no craters

#### (5) Effect of Power Input

At all pressures and flow rates employed, a reduction in rf current by capacitance control, or a reduction in dc voltage results in a non-metallic, hydrolyzable material which is clear white in appearance.

#### (6) Interaction of Parameters

The gas phase being ionized is an integral part of the electrical circuit. Thus as gas composition, pressure, or electrode spacing is varied, the impedance of the gas phase is also changed. The necessary voltage and rf currents are thus changed. These changes are reflected in the type of deposit obtained.

### DISCUSSION

**General.** The results of these experiments show that boron can be deposited on a dielectric substrate in a glow discharge. There is no limit on the coating thickness inherent in the process. Complete control of the process parameters has not been achieved, but there is no reason to believe that control cannot be achieved. The results obtained so far indicate that gas purity, gas composition, and rf power input are among the most important factors.

**Gas Purity.** The deposit obtained can be considered to be in chemical equilibrium with the gas composition. The introduction of certain impurities such as oxygen or water will result in certain amounts of oxygen in the deposit. The solid solubility of oxygen in boron is probably not great, and its effect in the mechanical properties of the deposit is unknown. However, if a certain concentration of oxygen or water is present, the equilibrium solid phase resulting from the processing will be the oxide and not the element. Experimental experience has shown that this concentration value is probably not very great, and a tight process system must be used with the reduced pressure process.

**Gas Composition.** The effect of gas composition, i. e., the ratio of hydrogen to boron trichloride, will influence the type of reaction that occurs and the type of product formed. It has been observed that the amount of (1) sidewall deposition; and (2) fine particles that fall out of the gas downstream of the glow, increase with increasing hydrogen concentrations. This indicates that reduction in the gas phase increases with the higher hydrogen to boron trichloride ratios. With increasing hydrogen ratios, the glow is more uniform over the space and the formation of fine particles is encouraged.

Increasing the ratio of boron trichloride to hydrogen causes the glow to concentrate toward the center around the substrate. This concentration of the glow toward the center discourages

the formation of small particles by the boron atoms and encourages the growth of the coating by deposition of the boron atoms directly on the substrate. As the flow ratio approaches the stoichiometric value of 1.5 moles of  $H_2$  per mole  $BCl_3$ , the glow concentrates very close to the substrate and is observed to migrate along the filament beyond the electrode rings. At the same time the rate of deposition increases about fourfold or more.

The resistance of the filament decreases as the boron coating is formed, which allows more current to flow. This increases the temperature of the filament, which encourages more rapid deposition of boron. Under these conditions, the reaction goes out of control and the filament heats to a general red-orange glow with brighter spots and finally breaks.

Careful adjustment of the reactant gas concentration and the rf power input to the coil will minimize the gas-phase reaction, sidewall deposition, and fine-particle formation.

The gas composition also obviously influences the nature of the material deposited. The glow discharge of boron trichloride has been studied by several workers (Refs. 1, 5, and 8 to 16) in the field, and their results should indicate the deposit to be expected at high ratios of boron trichloride to hydrogen. Holzmann and Morris (Ref. 1) analyzed the light from glows of boron trichloride at 1 mm of Hg pressure. The glow discharges were caused by a  $2.4$  to  $2.5 \times 10^9$  Hz (2,400 to 2,500 Mc). They observed bands due to boron monochloride and lines due to atomic boron and atomic chlorine. Frazer and Holzmann (Ref. 9) have used this technique to prepare laboratory quantities of  $B_2Cl_4$ , which is the primary product under these conditions.

The compound  $B_2Cl_4$  can be decomposed under a variety of conditions. Rosenberg (Ref. 8) used 60-Hz 10-kV discharges in  $B_2Cl_4$  and obtained  $BCl_3(g)$  and  $(BCl)_n$ , which he described as a light brown or yellow film which is hydrolyzed by water to form  $B_2O_3$ , hydrochloric acid, and hydrogen. From the rather incomplete data on this system and from other authors, it appears that a  $(BCl)_n$  phase can be obtained at compositions down to  $(BCl_{0.9})_n$ , and a material which analyzes as  $BCl_{0.6}$  has been reported. At the present time the  $(BCl)_n$  material is considered to be a polymer, and a series of higher unit structures other than  $B_2Cl_4$ , (such as  $B_4Cl_4$ ) can also be obtained.

In addition to these considerations, experiments have shown that, by operating at reduced rf currents, a deposit possessing the reported properties of  $(BCl)_n$  can be obtained with gas compositions that would normally deposit elemental boron.

In summarizing the results and literature survey, it is possible by glow-discharge techniques to obtain a variety of products from boron trichloride and hydrogen gas streams. These products can range from a polymer-type  $(BCl)_n$ , a liquid  $B_2Cl_4$ , or a solid  $BCl_{0.6}$  to the boranes. In between these gas compositions that will give the foregoing products is the gas-composition range that will give boron as a product. In addition to the gas composition, the amount of rf power used will also determine the product. It is fortunate that the gas composition obtainable with our experimental apparatus is in the range for boron deposition, otherwise selection of gas composition from present information would be impossible.

Power Input. The power input to the glow is of great importance in determining the product and character of the product. The rf voltage at any gas composition and electrode geometry must be a value greater than the breakdown potential of the gases at that pressure. The rf current is a direct measurement of the ionization of the gases to produce electrons and positive ions. In electrochemical processing, these terms are or can be considered analogs of the redox potentials and current density, respectively. At higher currents, a faster coating rate will be attained, but changes in deposit characteristics will occur as a result of such changes in plating rate. Perhaps part of the nonuniformity of the deposit can be attributed to a nonuniform plating rate. The uniformity should be improved by moving the filament substrate through the glow.

**Pressure.** Since pressure is a concentration function, it may be expected to influence the type of deposit and the rate of deposition. At low pressures, needle-like deposits are observed. As the pressure is increased, the type of deposit changes and a coating or continuous layer is formed. Increasing the pressure further provides a smoother deposit. However as the pressure is increased the voltage necessary to maintain a glow discharge is increased.

**Post-Deposition Treatment.** One sample prepared at 30 mm Hg pressure, and at flow ratios and electrical conditions which normally provide a typical coating, was exposed to a hydrogen glow discharge before removal from the system. This was done to explore possible methods of reducing the brown, glassy material observed near the end of filaments. The treatment was done in 30 mm Hg  $H_2$  pressure and at low flow rates  $\sim 25$  cc/min. The rf current and dc voltage were 250 mA and 480 V respectively.

The glow was normal in every respect except that just outside the electrode on the downstream side a faint green fluorescence or glow was observed. The end areas of the sample did show some evidence of reduction. The most interesting part of the sample is shown in Fig. 6. This is a longitudinal cross section of a fracture. A very thin (less than 0.187-mil) layer is much darker than the bulk of the deposit. This has not been observed in any samples prepared during this process study.

#### FILAMENT EVALUATION

**Density.** The density of filaments produced by this process has been measured by two techniques. A direct measurement was made by dropping a boron-coated pyrex rod in a density gradient tube. The average density was 2.24 gm/cc, which agrees satisfactorily with the value estimated from the density of boron, 2.35 gm/cc, and pyrex, 2.24 gm/cc.

An alternate indirect measurement has been performed during the process study by comparing the observed thickness of samples with that calculated-from-weight measurements. It was anticipated that the optically-measured value would be higher than the value calculated from weight measurements, which is an average value, since it is measured near the center of the filament.

This is observed in the data for samples 07-42 26A and B. The total thickness measured by optical methods are 2.2 and 2.4 mils, and calculated by weight the thicknesses are 1.45 and 1.72 mils. The results illustrate the nonuniformity of the static filament samples. However, the data is sufficiently in agreement to indicate that the filaments produced possess a density in accordance with the relative amounts of boron deposit and quartz substrate.

**X-Ray Identification.** A typical x-ray analysis is shown in Table VI. The diffuse lines observed in the x-ray pattern correspond to the alpha rhombohedral structure. This is the low-temperature form of boron. However, the structure is not well developed as indicated by the broad lines. The boron may have been in the process of changing from an amorphous structure to a crystalline structure at the time the experiment was terminated, or the crystalline boron was mixed with a matrix of amorphous boron.

Other samples of boron-coated 1.0-mil quartz filament show only two broad diffuse halos. No lines indicating  $B_2O_3$  were seen. No positive identification of the material was possible from the data.

**Tensile Strengths.** Several sample filaments of boron-coated 1-mil quartz substrate have been tested for ultimate strengths. No attempts have been made to obtain an elastic modulus since the samples prepared in the static apparatus are not of sufficient length. These data are presented in Table VII. The coating cracked and in some cases completely exfoliated. Thus, the values reported here basically represent breaking strengths of quartz rather than composite filament of boron-coated quartz monofilaments.

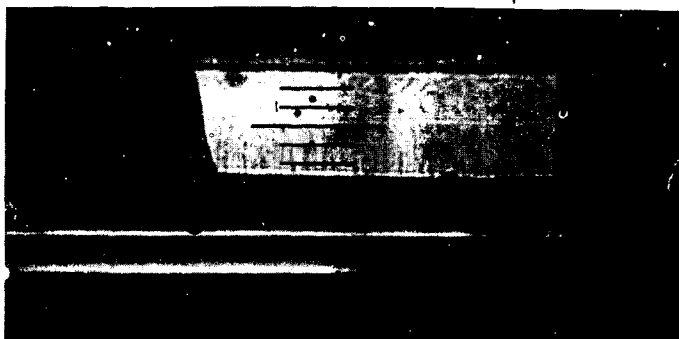
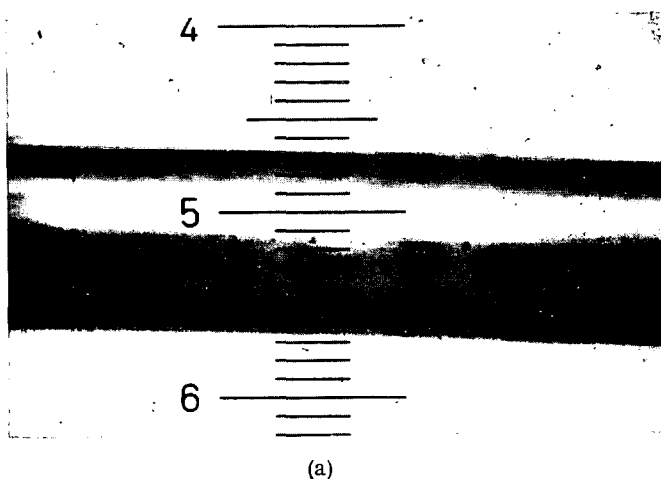
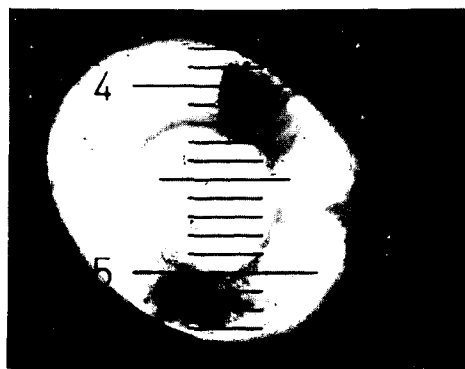


Fig. 6 Longitudinal Cross Section of Deposit After Exposure to  $H_2$  Glow Discharge



(a)



(b)

Fig. 7 (a) Longitudinal and (b) Cross Section of Boron-Coated Quartz Monofilament (220 $\times$ )

Table VI

## X-RAY DATA OF DEPOSIT

X-ray data		Deposited boron coating			
d	Unknown intensity	B <sub>2</sub> O <sub>3</sub>		Boron (a)	
		d	I/I <sub>o</sub>	d	I/I <sub>o</sub>
6.0	Medium	6.08	35	4.07	100
4.1	Strong (broad)	3.21	100		
3.2	Medium			1.98	8
2.55	Strong (broad)				
1.95	Weak				
1.40	Very weak (broad)				

(a) Alpha rhombohedral form.

Table VII

## BREAKING WEIGHT OF SELECTED SAMPLES

Sample Number	Sample condition prior to test	Breaking weight (lb)	Filament diameter (mils)
07-40-24	Not observed	0.07	1.5
07-42-26	Not observed	0.07	1.5
07-52-36	Longitudinal cracks	0.11	2.0
07-53-36	Coating missing near tab	0.033	2.0

Coating Evaluation. A typical sample cross section prepared during the process study is shown in Fig. 7, demonstrating that a continuous coating can be successfully deposited. In the longitudinal cross section two mounds are fortuitously shown and it can be seen that the growth extends to the substrate. This indicates that the cause of this different growth originates at the substrate surface, possibly as a microcrack or particle of dust. The problem of handling the filament and its contamination would be minimized with use of a continuous system.

The bond between the coating and the substrate is essentially mechanical in nature. It would be very desirable to improve this by effecting some sort of reaction between the two materials to improve the overall properties of the filament. It would perhaps be undesirable to clean the organic or silicone finish from the substrate as has been done.

Microscopic examination of one of the filaments has revealed a possible explanation of the reduced strength of boron-coated quartz filaments. The pictures in Fig. 8 are typical of what is occasionally seen on samples. The chip and hole in the top and middle picture were not measured, but the rather deep cut made indicates that the quartz monofilament possesses weak portions that may separate before the bond between the boron and the quartz ruptures. These weak volumes contribute to the spread of the strength values observed earlier since they are probably randomly distributed. The hole and ball shown in the bottom figure have been measured during the microscopic examination. The ball was about 1.0 mil in diameter, the hole was observed to 0.8 mil, while the filament cross section averaged 1.8 mils. The coating thickness can be only 0.4 mil, so that the hole must have been formed by the loss of 0.4 mil of the quartz substrate.

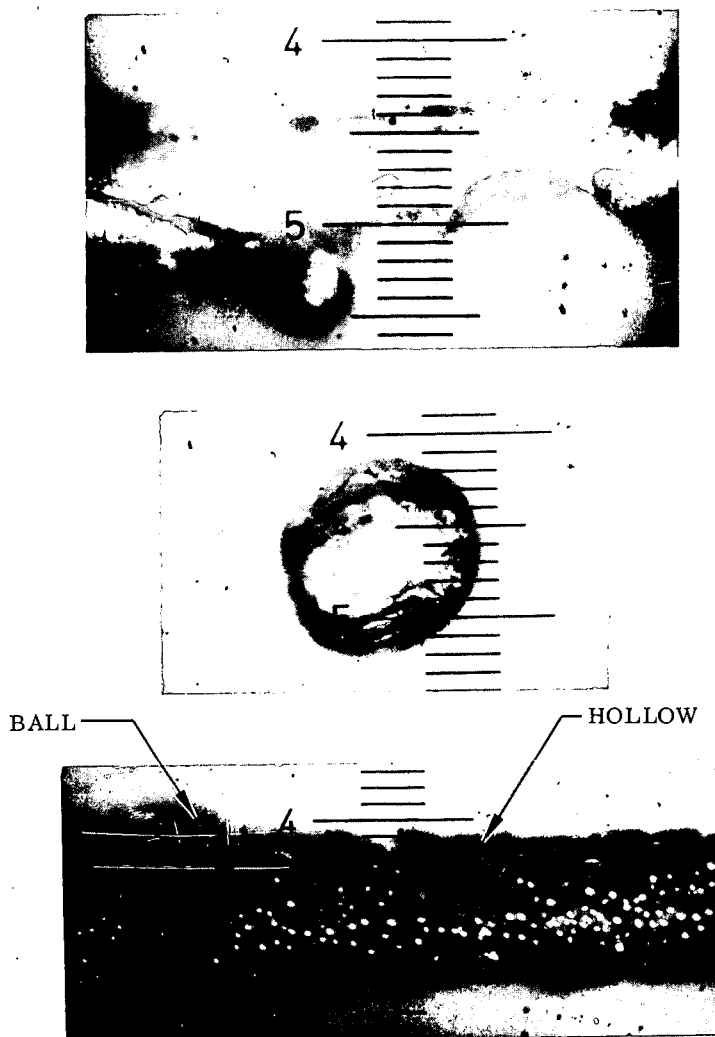


Fig. 8 Boron-Coated Quartz Monofilament ( $\times 340$ )

Top - Hollow in Boron-Coated Quartz Monofilament  
 Middle - Material From Hole  
 Bottom - Ball and Hollow in Thick Coating on Quartz Monofilament

Another source of weakness is the cracking and peeling. Many of these cracks and breaks are the result of handling during removal from the static apparatus. Use of a continuous filament moving through the apparatus and improvement in the adhesion of the coating to the substrate would possibly eliminate this problem.

### CONCLUSIONS

This paper basically represents a feasibility study of the deposition of boron from a glow discharge system produced in a boron trichloride-hydrogen medium. Feasibility of the basic concept has been conclusively demonstrated for dielectric or insulating substrates. It is probable that conditions can be adjusted to provide for deposition on metallic or conductive substrates as well. The following secondary conclusions can also be drawn from this work:

- Glow discharges can be initiated and sustained in hydrogen-boron trichloride mixtures at pressures of 50-100 mm.
- There is no apparent limit on coating thickness which can be deposited.
- The deposited boron is amorphous with a partial alpha rhombohedral crystalline character.
- Deposition rate is of the order of  $5 \times 10^{-5}$  gm/sec.
- Filament resistance increases with thickness; temperature in turn increases resulting in a higher deposition rate; this also results in increased bonding to the substrate by chemical or diffusive action.
- The process is quite sensitive to small amounts of impurities in the gas stream, particularly oxygen and moisture.
- The ratio of hydrogen to boron trichloride has a major effect on nature of the deposit; both sidewall deposition and downstream particle fallout increase with hydrogen concentration. However, the glow is more uniform at high hydrogen values, so these factors must be balanced for optimum performance.
- An increase in the boron trichloride to hydrogen ratio tends to concentrate the glow around the substrate, promoting efficiency and minimizing extraneous deposition.
- High hydrogen to boron trichloride ratios tend to produce boranes; operation at reduced rf currents tends to yield  $(BCl)_n$  polymers.

Current investigations are concerned with further development of the glow discharge deposition procedure to operate on a continuous basis utilizing moving filament techniques. Indications are that the technique may be used to prepare a high-quality boron filament at reasonable processing rates.

### ACKNOWLEDGMENT

This work was sponsored by the U.S. Air Force under Contract AF 33(615)-2130. Acknowledgement is given to J. G. Bjeletich, W. C. Coons, J. Robinson, B. A. Traina, R. N. Varney, and R. D. Wales for assistance on photographic and experimental portions of the program. All are members of the Lockheed Palo Alto Research Laboratory. Further acknowledgment is made to R. M. Neff of the Air Force Materials Laboratory for continuing consultation on progress of the program.

### REFERENCES

1. R. T. Holzmann and W. F. Morris, *J. Chem. Phys.*, Vol. 29, 1958, p. 677
2. W. V. Kotlensky and R. Schaeffer, *J. Am. Chem. Soc.*, Vol. 80, 1958, p. 4517
3. R. M. Rosenberg, Univ. Microfilms (Ann Arbor, Mich.) L.C. Card No. MIL-59-2911, 160 pp; *Dissertation Abst.*, Vol. 20, 1959, p. 526
4. L. Ya. Markovskii, V. I. L'viva, and Yu D. Kondrashev, "Obtaining Elementary Boron in a Glow Discharge," *Bor. Trudy Konf. Khim, Bora; Ego Soedineni*, pp. 36-45 (1958); cf. FTD-MT-64-427, Foreign Technol. Division, AF System Command, 1965

5. F. Weintraub, Trans. Am. Electrochem. Soc., Vol. 21, 1909, pp. 165-184
6. W. Kroll, Z. Anorg. Allgem. Chem., Vol. 101, 1918, p. 1
7. "Report of the International Symposium on Electrical Discharges in Gases," Delft, Netherlands, April 1955; The Hague, 1955
8. R. M. Rosenberg, PhD Thesis, Pennsylvania State University, 1959
9. J. W. Frazer and R. T. Holzmann, J. Am. Chem. Soc., Vol. 80, 1958, pp. 2907-2908
10. T. Wartik, R. Moore, and H. I. Schlesinger, J. Am. Chem. Soc., Vol. 71, 1949, p. 3265
11. G. Urry, T. Wartik, and H. I. Schlesinger, J. Am. Chem. Soc., Vol. 76, 1954, p. 4293
12. A. Stock, A. Brandt, and H. Fischer, Ber. Deut. Chem. Ges., Vol. 58B, 1925, p. 653
13. H. I. Schlesinger and A. B. Bing, J. Am. Chem. Soc., Vol. 53, 1931, p. 4321
14. A. Stock, H. Martin, and W. Sutterlin, Ber. Deut. Chem. Ges., Vol. 67, 1934, p. 396
15. F. F. Apple, PhD Thesis, Pennsylvania State University, 1955
16. H. I. Schlesinger, H. C. Brown, B. Abraham, N. Davidson, A. E. Finholt, R. A. Lad, J. Knight, and A. M. Schwartz, J. Am. Chem. Soc., Vol. 75, 1953, p. 191

## PLATING IN A CORONA DISCHARGE

R. D. Wales

Materials Sciences Laboratory  
Lockheed Palo Alto Research Laboratory  
Palo Alto, California

## ABSTRACT

It has been demonstrated that boron can be deposited on a suitable substrate in a corona discharge. Application of high-voltage electrical energy across a gaseous hydrogen-boron halide mixture forms ionized/activated states, resulting in the deposition of metallic boron. The deposition process is electrochemical in nature, the boron being deposited cathodically.

## INTRODUCTION

Literature on electric discharges is quite extensive. However, most of this literature concerns the nature and properties of discharges taking place in stable gas systems. Detailed discussions of electrical discharges are presented in several books<sup>(1, 2, 3, 4)</sup>. Relatively little information is available concerning chemical reactions initiated and sustained by electrical discharges. Arc reactions are basically thermally initiated reactions deriving their thermal energy from the arc and thus are not applicable in the present sense. Glow discharges have been utilized for the polymerization of organic materials and the deposition of oxide films. The formation of pure boron powder<sup>(5)</sup> and the decomposition of diborane<sup>(6)</sup> and boron trichloride<sup>(7)</sup> have been studied in a glow discharge. No references have been located concerning chemical reactions initiated and sustained by a corona discharge.

Those references<sup>(8, 9, 10)</sup> which refer to the utilization of a corona discharge to catalyze, or cause, a chemical reaction do not in fact utilize a corona discharge. The discharge utilized in these references has an odd resemblance to a glow discharge, but is actually a suppressed spark. Thus, the discharge goes through the phenomena of spark buildup without, however, generating a spark. Direct current cannot be used in these systems since the buildup of charge at the insulated electrodes quenches the discharge, and a reverse cycle is necessary to remove this charge and reinitiate the discharge.

A corona discharge is, essentially, intermediate between a glow and an arc discharge being, however, a low current phenomenon. Glow discharges are generally generated at low pressures while an arc is generally a high-pressure phenomenon. The gas is ionized more or less uniformly throughout the system in a glow discharge. An arc is obtained when a narrow path of ionized particles is generated between two electrodes, resulting in a low resistance path which further aggravates the situation until extremely energetic particles exist in the narrow path. A corona discharge is not as pressure-dependent and is obtained at a small electrode which is opposed by a much larger electrode. There is a very large

change in field through the corona, but very little change over the remaining distance to the opposing electrode. Most studies of corona discharges have been in inert gas systems, and have been generated at a point electrode.

This study has been directed toward the determination of the feasibility for depositing a coating, e.g., boron, on a suitable substrate in a corona discharge. A further object has been to determine some of the critical parameters and a possible indication of the mechanism and characteristics of this technique for coating the substrate material.

#### EXPERIMENTAL WORK

A schematic diagram of the system used in this study is indicated in Fig. 1. The system pressure was controlled with a Cartesian Manostat 6A (Manostat Corporation) and a Welch mechanical pump Model 1402 (W. M. Welch Manufacturing Company). The discharge was initiated and sustained with a 7,000/12,000 V Jefferson luminous tube outdoor-type transformer (Jefferson Electric Company) connected to 60-cps 110-V power source through a Variac variable transformer.

To determine the effect of alternating and direct current, an RCA CR 212 half-wave rectifier was added to the circuit. At the same time a resistance bridge, a current measuring resistor, and an ammeter were added to the circuit. A schematic of the circuit is presented in Fig. 2. The resistance bridge consisted of six 2-W 2-megohm resistors ( $R_2$ ) and one 2-W 1,000-ohm resistor ( $R_1$ ), all in series; the total voltage being 11,775 times the voltage across the 1,000-ohm resistor. The current measuring resistor was a 2-W 10.075-ohm resistor. The voltage measurements were made with a Hewlett-Packard Model 130B oscilloscope, and alternating current measurements were made with a Simpson Model 378 milliammeter.

The reactants utilized in this study were hydrogen, helium, or argon, and boron tribromide. The hydrogen was passed through a "De-oxo" unit (Engelhard), through a drying column of magnesium perchlorate, and then through a flowmeter. After the flowmeter, the hydrogen was split into two streams, one of which was bubbled through the boron tribromide, and then recombined into one stream before entering the reaction chamber or cell.

The temperature of the bubbler, and of the cell, was controlled by wrapping each (and the associated gas lines) with heating tape and controlling the power input with a Variac variable transformer.

The system was maintained at or below atmospheric pressure for this study, with most of the data being obtained at 2 to 3 in. of mercury below atmospheric pressure.

Tungsten wire was chosen as the substrate material. This wire was cleaned by passing it successively through a train consisting of concentrated nitric acid, a distilled water rinse, and an acetone rinse.

Using the hydrogen-boron tribromide reactant system and 60-cps alternating current to develop a corona, approximately a dozen cell designs were tried. The cell design which appears to be the most satisfactory is pictured in Fig. 3. This cell consists of a 2-in.-long pyrex glass tube with a neoprene o-ring inside each end and wrapped with eight turns of 3-mil tungsten wire along the tube length such that the wire is parallel and concentric to the axis of the tube. The wire is 0.9 cm from the axis. This assembly is then inserted in a 5-in.-long pyrex glass tube 1.5-in. in diameter and supported such that the tubes are concentric. A tungsten wire lead is then extended out of the tube, and neoprene rubber stoppers inserted in each end. Each stopper has a capillary tube through its center such that there are approximately 3 in. between the capillaries, and the filament enters and leaves the cell through these capillaries. The reactants also enter (and leave) the cell through the stoppers.

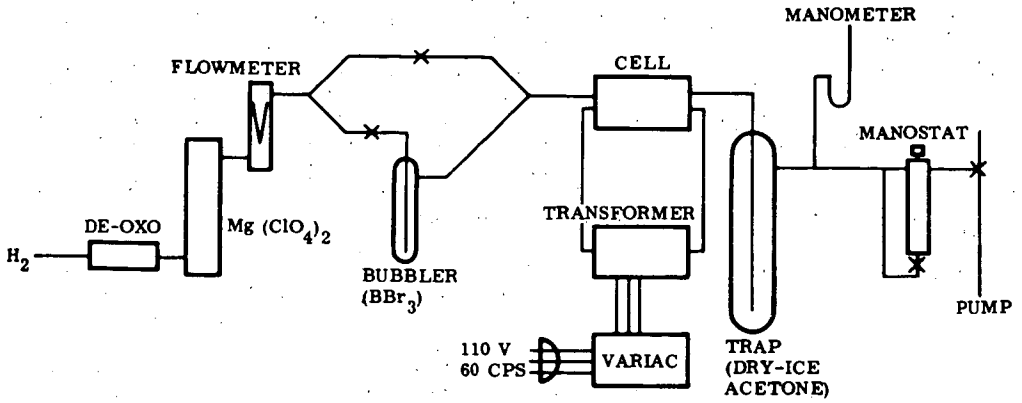


Fig. 1 Schematic of System Utilized for Plating in a Corona Discharge

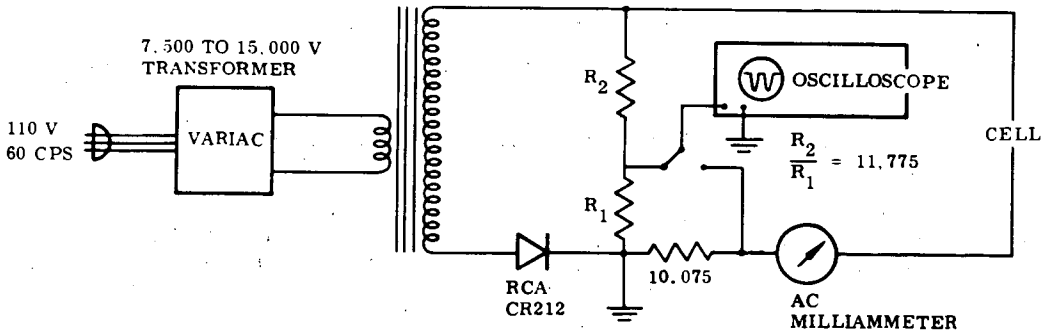


Fig. 2 Schematic of Power Input and Measuring Circuit Used With the Corona Discharge Plating Apparatus

## PRIMARY VARIABLE CONSIDERATIONS

Deposition Utilizing Alternating Current

Hydrogen and boron tribromide vapors were used to obtain a coating of boron on 1-mil tungsten wire in a corona developed with 60-cps alternating current. It was determined that, at about 70 and 350 mA/cm<sup>2</sup>, no coating is obtained when the cell (and reactants) are at room temperature, while a coating of boron is obtained if the temperature is raised to approximately 100° C. At higher current densities, the coating is concentrated in nodules. If enough power is supplied to heat the filament to a dull red glow, a good coating is obtained in the hot zone. At lower current densities, a more uniform coating is obtained, depending upon the reactant ratios and flow rates. Thus, hydrogen was bubbled through boron tribromide at a rate of approximately 400 ml/min, and the system was maintained at approximately atmospheric pressure. When the boron tribromide was maintained at about room temperature and at a total hydrogen flow rate of about 1.5 liter/min, the corona was discontinuous along the wire and boron deposited in the area of the coronas to give discrete coated and uncoated areas. With a hydrogen flow rate of about 400 ml/min and a plating time of about 10 min, a much smoother coating was obtained. There was some tendency for the corona to break into discontinuous sections, which resulted in a nonuniform buildup of boron.

When the boron tribromide was heated to about 30° C and the hydrogen flow rate was maintained at 400 ml/min, the corona was somewhat more continuous and the coating nearly uniform. However, the coating was not nearly as smooth as in the previous example.

There was also a tendency for the formation of corona points on the opposing electrode system with a resulting deposition of boron under the corona.

Deposition Utilizing Direct Current

Using hydrogen and boron tribromide as reactants to obtain a deposit of boron on 1-mil tungsten wire in a corona developed with half-wave rectified 60-cps alternating current, no deposit was obtained when the 1-mil wire was the anode. However, a coating was obtained when the 1-mil wire was the cathode. Good, continuous corona and boron deposits were obtained when the corona was initiated in a large excess of hydrogen (the hydrogen flow was then decreased to the desired amount after about 5 min).

The coating is quite uniform and has an orange peel appearance at 2,000X magnification. Some of the morphology of the substrate is apparent at high magnification (e.g., die marks). The voltage requirements for a particular current increased as the hydrogen flow decreased, increasing from more than 1,000 V peak to about 7,000 V peak as the excess hydrogen was decreased in these runs.

Attempts to utilize pure dc power were unsuccessful. The power supplies available were designed to deliver several hundred milliamperes and had relatively coarse controls. Thus, as the corona was initiated, the power supplies did not allow sufficient control, resulting in "runaway" or burning in two of the substrate wire.

Deposition Utilizing Argon and Helium

Using helium instead of hydrogen, a coating was obtained, but arcing was much easier and thus lower current (and lower flow rates) were necessary. Peak voltages of 7,000 to 8,000 V were used.

Using argon instead of hydrogen required higher voltage (with lower currents) and resulted in the formation of corona points under which boron was deposited to give whiskers. Peak voltages of about 9,000 V were used. Whiskers greater than 6 mils long and about 0.5 mil in diameter were obtained before discontinuing these experiments.

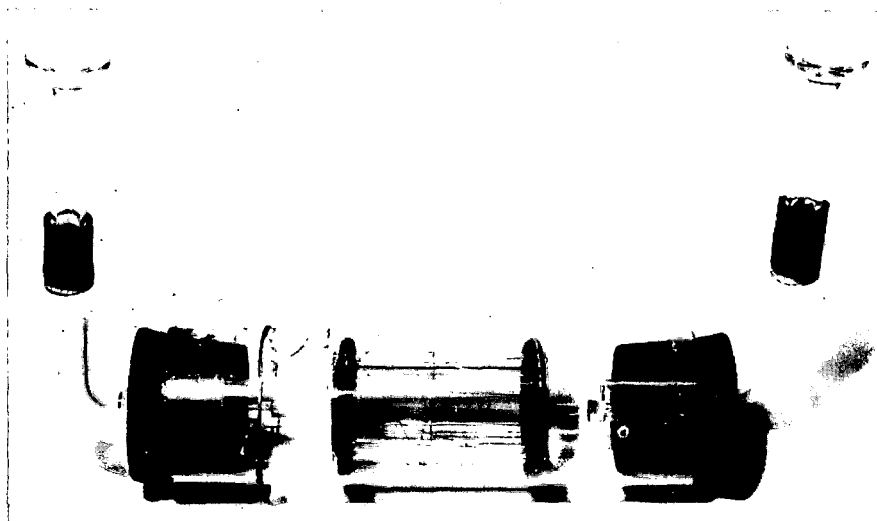


**Fig. 3** Reaction Cell Used for Plating in a Corona Discharge

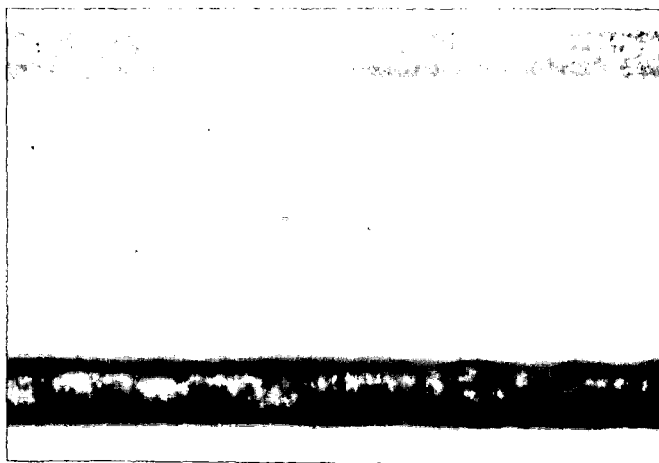


**Fig. 4** Boron Deposit on 1-mil Tungsten Wire, Run 28-1,  
Tungsten Substrate Material at Top (340 $\times$ )



**Fig. 5** Boron Deposit on 0.5-mil Tungsten Wire,  
Run 35-1 (450 $\times$ )

Bromine was a product when helium or argon was used while hydrogen caused the formation of hydrogen bromide.

### Discussion

(1) Cell Design. The reaction cell should be designed so that the concentration of reactants and products is essentially constant throughout the cell to give a more uniform corona and deposit. The electrode geometry and separation are to some extent dependent upon the power requirements, which are in turn dependent upon the resistance heating effects in the filament and upon the arcing probability. Thus, in practice, the current in the filament should not be great enough to heat the filament excessively. With this current limitation, the electrode separation is dependent upon the arcing probability and should be great enough to level out any small variations in electrode separation which could cause the current to concentrate in a small region. Furthermore, to obtain a uniform corona around the filament, the opposing electrode should be concentric around the filament. If the power input is not pure direct current, a "motoring" effect results if the opposing electrode is a wire coiled around the filament. That is, a vibration or circular oscillation will be induced on the filament. Therefore, the opposing electrode has been made up of a group of connected electrodes arranged concentrically around the filament and parallel to it in order to minimize the "motoring" effect. The opposing electrode could also have been a metal cylinder or screen, but in order both to observe the filament and be able to operate at reasonable electrode separations (reasonable voltages), interconnected parallel wire electrodes were selected.

(2) Mechanism of Deposition. The results obtained indicate that the mechanism of boron deposition in a corona discharge is cathodic. In this type system, electrons are generated and repelled from the cathode while positive ions are drawn to it. At the anode, positive ions are generated or electrons are drawn to it. Thus, the boron radical is positively charged and drawn to the cathode where it is deposited as elemental boron.

Helium and argon were used to determine if the boron tribromide was ionized directly, or if its ionization was a secondary reaction. Table I indicates some of the ionization levels for these gases. Helium in a corona discharge has only one or two potential (or ionization) levels, and these are quite high. However, helium is ionized at lower applied voltages than most gases because the electrons generated at the cathode have only elastic collisions with helium atoms until they acquire enough kinetic energy from the field to ionize the helium. Argon has a potential (or ionization) level which is relatively low (about half that of helium) but higher than the ionization levels for hydrogen. In helium the system was very susceptible to arcing, while in argon higher voltages were required with some susceptibility to arcing. In hydrogen arcing was not such a problem because of the many types of inelastic collisions possible and the consequent tendency to decrease the electron energy and concentration. Boron was deposited in all three systems. However, in hydrogen, hydrogen bromide was obtained while bromine was obtained in both argon and helium. Deposition was slightly easier and there was a slightly increased rate of deposition of boron with an increased tendency to arcing in helium and argon. The difference, however, was not sufficient to be due to direct reaction with the free electron, and indicates that the boron tribromide is ionized by collision with ionized particles rather than electrons or the field. Thus, the mechanism includes: (a) the ionization (or activation) of the hydrogen (helium or argon), (b) the collision or exchange of energy of the ionized particle with boron tribromide to result in (c) the formation of a positively charged boron radical and hydrogen bromide (or bromine), (d) the transport of the charged boron radical to the cathode in the field, and (e) the electrochemical deposition of boron on the cathode.

It is apparently necessary to add a small amount of kinetic (thermal) energy to aid the deposition in hydrogen. However, this reactant system offers certain advantages over helium or argon systems. That is, with hydrogen, there are apparently more ionized or activated particles with fewer electrons and consequently less likelihood of creating conditions conducive to arcing.

Table 1. Ionization Levels for Helium, Argon, and Hydrogen(2, 11)

Gas	First Excitation Potential (eV)	Ionization Potential (eV)			Metastable Level (eV)
		I	II	III	
He	20.5	24.5	54.1		19.7
A	11.6	15.7	27.7	40.7	11.5
H <sub>2</sub>	11.5	15.4			11.9
H	10.2	13.5			10.15

(3) The Corona. In the high-field region near the substrate wire, positive ions can attain high energies and the secondary electron emission process is quite efficient. These secondary electrons will start electron avalanches, which will in turn produce many positive ions, which produce more avalanches, etc. At low pressures, diffusion of the electron avalanches spreads the glow and distributes the positive space charge so that the discharge is not quenched. Diffusion does not take place at higher pressure, and a localized dense space charge extinguishes the corona. The extinction lasts until the positive space charge diffuses to the electrode and the last ions reinitiate the discharge, resulting in a periodic corona with a frequency dependent upon the field and the velocity of the positive ions.

With the negative wire (cathode), the ionization increases first with distance from the wire, reaches a peak, then drops sharply. That is, the electrons move out from the wire and produce relatively stationary positive ions between themselves and the wire, thus weakening the field at greater distances. The maximum ionization occurs at several ionizing free paths from the wire, and there is a dark space between the wire and the luminous glow. Furthermore, as mentioned, at low pressures the lateral diffusion of electron avalanches spreads the corona over the wire surface. Because the value of the coefficient of electron emission is important, and because the glow will not be uniform if the coefficient of electron emission varies over the surface of the wire, the glow may settle in patches of greater or lesser luminosity and at high pressures will appear as a single small area of corona. The corona may exhibit a marked flickering near threshold because the positive ion bombardment may change the effective coefficient of electron emission by denuding the surface of its gas film. The discharge thus decreases or ceases in that region, resuming again when the surface has recovered. At low pressures and voltages well above the threshold value, the corona is fairly steady.

In this work it was necessary to clean the substrate wire so that there were no variations in the coefficient of electron emission along the wire, and thus a localization of the corona into points. During deposition the corona was distributed over the substrate wire in a uniform manner. However, the discharge was periodic as indicated in the above discussion. That is, the sheath (of light) along the wire was not of a uniform brightness, but consisted of brighter and darker areas which seemed to move along the wire in a somewhat random manner, but which appeared periodic in nature at a given point on the wire.

## SECONDARY VARIABLE CONSIDERATIONS

### Experimental Work

The deposition system was that previously described. The tungsten wire was cleaned as before, then placed in the cell. The corona was then initiated in excess hydrogen and maintained for about 5 min, or until the corona was continuous or nearly continuous along the substrate electrode, before the conditions were changed to give boron deposition. This initial "cleaning" process was effected with hydrogen flowing at about 160cc/min through the boron tribromide at about 26° C and with hydrogen flowing through the bypass line at about 270cc/min. The electrical input during this time was about 17 mA peak and about 4,700 V peak for 1-mil tungsten wire and about 5,600 V peak and 4.5 and 11.0 mA peak for 0.5-mil tungsten wire.

### Results

(1) Deposition on 1-mil Tungsten Wire. Some of the results obtained are presented in Table 2. The corona was maintained continuously in all runs. A picture of the filament obtained in Run 28-1 is shown in Fig. 4. In Run 28-1 the current fell from an approximate initial value of 12.3 mA peak to about 3.5 mA peak in about 9 min, after which it was nearly constant. The peak voltage changed from 6,900 to 13,190 V. The filament obtained in this run is apparently the desired type, although not of optimum thickness.

Table 2. Some Effects of Varying Process Conditions With 1-mil Tungsten Wire Substrate

Run	Vacuum (in. Hg)	H <sub>2</sub> flow bubbler (cc/min)	H <sub>2</sub> flow bypass (cc/min)	Current peak (mA)	Voltage peak (V)	Time (min)	Temp. BBr-3 (°C)	Comments
17-3	2.3	160	—	14.2	6,800	40	26	Corona uniform for about 6 min then broke up. Coating not uniform, large nodules formed, due to discontinuous corona.
23-1	1.2	40	35	16	6,700	30	26	Corona fairly uniform, substrate etched, no coating.
23-3	1.4	80	—	13.6	8,100	58	26	Corona fairly uniform, coating fairly uniform, final diameter of about 1.2 mil.
25-1	2.3	50 50	40 —	14.2 13	6,100 7,900	7 42	— 47	To attain 47° C. Overheated substrate in areas. Coating thick and mostly rough.
28-1	2.6	50 50	40 —	12.3 3.5	6,900 13,200	5 78	— 70	To attain 70° C. Good coating, final diameter 1.33 mil.

The data obtained in the experiments presented, and in other similar experiments, indicate that:

- (a) the voltage requirements increase as the boron tribromide to hydrogen ratio increases.
- (b) The voltage requirements increase as the system pressure increases.
- (c) The substrate is etched with little or no boron deposited as the boron tri-bromide to hydrogen ratio decreases.
- (d) The corona tends to break up into points at high flow rates, resulting in nonuniform boron deposits.

Good coatings were obtained at high boron tribromide to hydrogen ratios and relatively low currents.

(2) Deposition on 0.5-mil Tungsten Wire. Some of the results obtained are given in Table 3. The corona was maintained continuously in Runs 30-1 and 30-2. The power input was discontinued in all remaining runs until the boron tribromide and the cell has attained the desired temperature. The currents and voltages indicated for all runs below 35 are approximate since no adjustments were made once the run had begun.

The effects of operating conditions are similar to those observed for deposition on 1.0-mil tungsten wire. However, the decreased heating effects of the 0.5-mil wire necessitate heating the cell to about 200°C to prevent condensation of the boron tribromide.

In Run 31-1, an apparently desirable coating was obtained at the ends of the reaction zone while the central portion of the filament was quite nodular. In Run 31-1 the peak current was 6.2 mA, falling to about 1.8 mA at the end of the run. During this time the peak voltage changed from 12,480 V to about 15,780 V.

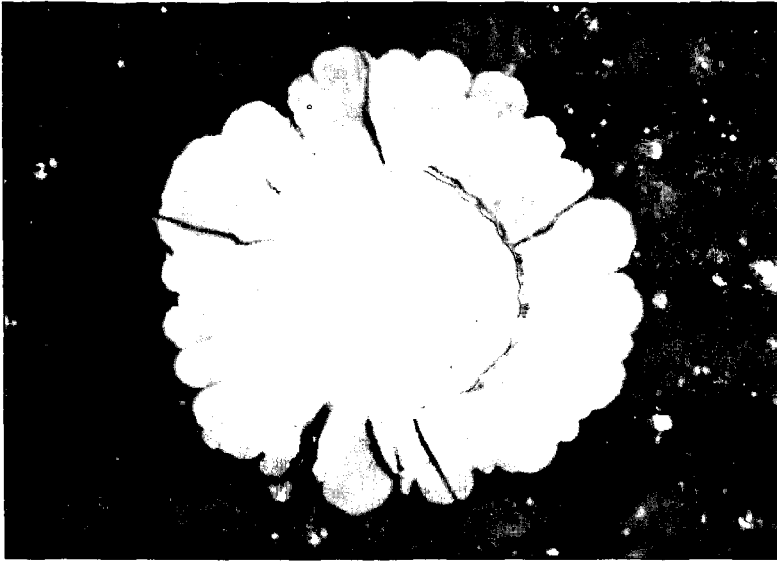
Runs 35-1 and 35-2 yielded filaments having uniform coatings of boron. The coating, as shown in Fig. 5, had ridges along its surface resembling die marks on wire. Figure 6 shows a cross section of filament from Run 35-1 in normal and in polarized light. The higher magnifications indicate that the markings on the surface are reflections of the markings on the substrate in almost a one-to-one ratio. Furthermore, there is no indication of boride formation. However, polarized light indicates some anisotropic properties similar to pyrolytic graphite. The material seems softer and much darker than that grown by gas plating techniques. Although there are some unidentified lines, x-ray data indicate that the coating is amorphous boron with no borides in the filament.

Cursory examination of the surface for a few of the substrates has indicated surface finishes varying from the ridged (die marks) through smooth to an orange-peel-type finish, while the filaments obtained have had surface finishes ranging from ridged through smooth to nodular. Therefore, the substrate surface is a critical factor in determining the appearance and surface of the final filament.

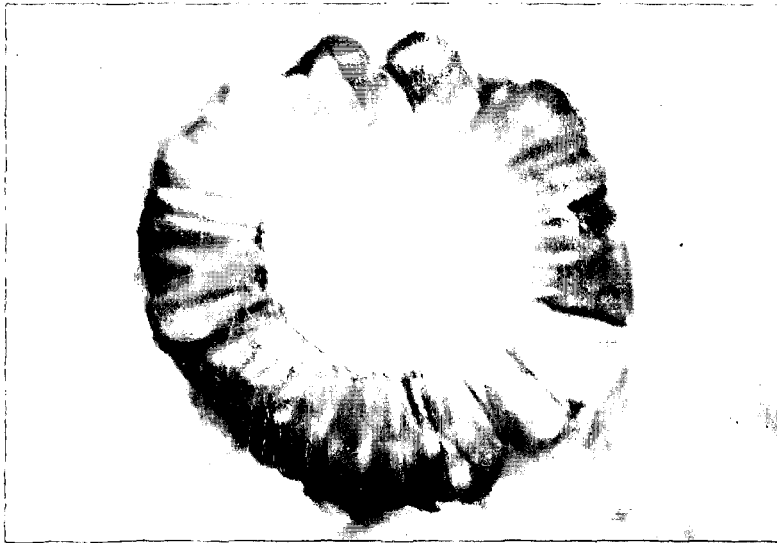
(3) Effect of Morphology of the Substrate. The 0.5-mil tungsten substrate wire has been examined after various stages in the process. Some of the results are presented in Table 4.

It has been determined that the liquid cleaning train cleans and slightly etches the wire, and the high hydrogen corona etches the wire as indicated in Table 4. At low peak currents the die marks were etched away, but the surface has a very rough orange peel finish. Using both high and low currents consecutively, a much smoother orange peel finish is obtained.

Boron deposited on wire etched to an orange peel finish gives a coating similar to that pictured in Fig. 7. The morphology of boron deposited on variously etched wire verifies the hypothesis previously presented in that the coating morphology and growth structure are directly dependent upon the morphology of the substrate.



(a) Normal



(b) Polarized Light

Fig. 6 Cross Section of Filament Obtained by Plating in a Corona Discharge, cf. Fig. 5 (3,000 $\times$ )

Table 3. Some Effects of Varying Process Conditions With 0.5-mil Tungsten Wire Substrate

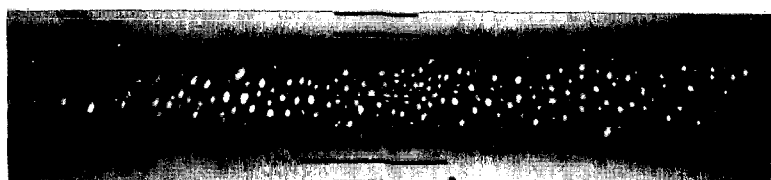
Run	Vacuum (in. Hg)	H <sub>2</sub> flow bubbler (cc/min)	Current peak (mA)	Voltage peak (V)	Time (min)	Temp. BBr <sub>3</sub> (°C)	Temp. cell (°C)	Approx. flow rate BBr <sub>3</sub> (ml/hr liq)	Comments
30-1	2.7	50	4.0	12,200	19	64	-	7.0	Final thickness - 0.94 mil, substrate - 1/4 mil, coating appears porous, flakes off fairly easily, BBr <sub>3</sub> condensed in cell.
30-2	3.0	50	1.0	13,000	30	67	111	6.8	Final thickness - 0.68 mil, substrate - 0.3 mil, coating a little better than Run 30-1, BBr <sub>3</sub> condensed in cell.
31-1	2.6	50	1.8	15,780	27	58	175	-	Final thickness on ends 1.2 mils, in center - 1.7 mils, coating as desired on ends, uniform and nodular in center, BBr <sub>3</sub> condensed in cell.
33-1	2.7	50	3.0	8,830	20	48	215	3.5	Final thickness - 0.8 mils uniform coating, somewhat nodular, mostly as ridges or "wrinkles." No BBr <sub>3</sub> condensed in cell.
34-1	2.5	50	1.0	11,770	22	63	210	4.0	Final thickness on ends 0.9 mil, in center - 0.7-2 mil, substrate 0.4 mil on ends. Coating on ends about like Run 30-2, coating in center nonuniform with large nodules separating short lengths of uniform ridged or "wrinkled" coating.

Table 3. (cont'd)

Run	Vacuum (in. Hg)	H <sub>2</sub> flow bubbler (cc/min)	Current peak (V)	Voltage peak (V)	Time (min)	Temp. BBr <sub>3</sub> (°C)	Temp. cell (°C)	Approx. flow rate BBr <sub>3</sub> (ml/hr liq)	Comments
35-1	2.5	50	2.0	Start 6,120 End 9,420	20	52	205	4.9	Final thickness 0.9 mil, substrate thickness 0.5 mil, coating uniform with ridges which have the appearance of die marks on drawn wire. Coating coherent but appears to be poorly bonded to substrate.
35-2	2.6	50	4.0	Start 6,950 End 7,770	8	53	204	4.9	Coating about same as in Run 35-1.
36-3	2.5	50	8.0	Start 7,800 End 8,420	20	54	236	4.0	Rough, nodular coating, thickness > 1 mil.
39-2	2.5	50	2.0	Start 6,690 End 7,680	24	52	225	3.5	Final thickness approx. 1 mil. Coating uniform, very small nodules with some "nodes."



(a) 604x



(b) 1,230x

Fig. 7 Boron Deposit on 0.5-mil Tungsten Wire, Run 52-1,  
cf. Table 4

Table 4. Some Effects of Various Process Conditions Upon Morphology

Run	H <sub>2</sub> flow bubbler (cc/min)	H <sub>2</sub> flow bypass (cc/min)	Temp. BBr <sub>3</sub> (°C)	Temp. cell (°C)	Current peak (mA)	Voltage peak (V)	Time (min)	Comments
-	0.5 mil tungsten wire untreated							
46-1	0.5 mil tungsten wire after cleaning train only							
46-2	160	270	-	-	4.6	6,450	5	Dirty, not too smooth, die marks. Clean, some etching; die-marks plainly visible microscopically.
46-3	160	270	-	-	7.6	6,190	5-1/2	Corona not uniform for first 3 min, some pitting, die-marks faintly visible.
46-4	160	270	-	-	7.6	6,190	4	Corona good from beginning; outside visible corona apparently no change, in corona surface uniformly etched quite rough with no die marks.
47-1	160	270	-	-	7.5	6,190	2	Corona not uniform for first 2 min. surface has orange-peel finish, no die marks.
47-2	95	270	-	-	7.8	5,010	5	No apparent surface change.
	95	270	-	-	3.0	4,830	3	Corona fair.
48-1	95	270	-	-	7.6	5,200	5	Corona nonuniform, surface fairly smooth, die mark visible.
	95	270	-	-	2.0	4,460	3	Corona fair
48-3	95	270	-	-	7.0	4,950	4	Surface has orange peel finish, smoother than 46-4.
	95	270	-	-	2.0	4,460	5	Corona fair
52-1	160	270	-	-	7.6	6,320	3	Surface about like 48-1, die marks faintly visible.
	95	95	to heat cell and BBr <sub>3</sub> ; power left on; at temperature in 3 min; made no power adjustments					
	50	0	53	235	Final 0.4	Final 11,580	18	Coating uniform except for a couple of areas, coating of approximately 0.05-mil nodules, final diameter approximately 0.8 mil.

Table 5. Some Effects of Various Process Conditions

Run	H <sub>2</sub> flow bubbler (cc/min)	H <sub>2</sub> flow bypass (cc/min)	Temp. BBr <sub>3</sub> (°C)	Temp. cell (°C)	Current peak (mA)	Voltage peak (V)	Time (min)	Comments	
61-1	160	270	-	-	7.6	6,190	2	Coating mostly uniform. Final diameter 1.1 mil.	
	Started heating cell and BBr <sub>3</sub> ; power left on; made no power adjustments								
	95	95	32	H <sub>2</sub> flow constant for 2 min					
69-2	50	0	51	H <sub>2</sub> flow and temperature constant				Coating on inlet side good. Final diameter 1.1 mil. Outlet side had many large nodules.	
	at end of run								
	160	270	-	235	0.4	11,520	21		
		Shutdown for 11 min		-	7.6	6,870	3		
71-1	Started heating cell and BBr <sub>3</sub> ; power left on; made no power adjustments								
	95	95	37	95	6.5	7,620	2		
	50	0	55	230	4.9	8,540			
					Final	9,970	15		
	160	270	24	26	7.6	7,180	4		
Started heating cell and BBr <sub>3</sub> ; power left on; made no power adjustments									
95	95	-	-	-	-	-	3	Coating even and uniform. Final diameter 0.79 mil.	
50	0	53	230	4.8	8,930	10			
				Final	10,400				

Table 5 (Continued)

Run	H <sub>2</sub> flow bubbler (cc/min)	H <sub>2</sub> flow bypass (cc/min)	Temp. BBr <sub>3</sub> (°C)	Temp. cell (°C)	Current peak (mA)	Voltage peak (V)	Time (min)	Comments	
71-2	160	270	25	-	7.6	7,060	4	Coating even and uniform. Final diameter 0.60 mil.	
	Started heating cell and BBr <sub>3</sub> ; power left on; made no power adjustments								
	95	95	34	-	6.3	7,430	3		
73-1	50	0	54	235	-	-	6	Coating uniform. Final diameter 0.75 mil.	
	Final								
	3.0								
	7.6								
74-1	Varied conditions as in Run 61-1 except final BBr <sub>3</sub> temperature 71° C and current not allowed below 2.0 mA								
	At end of run								
	160	270	24	220	2.0	20,800	16	Coating uniform and even except for one area. Final diameter 1.0 mil.	
	Started heating cell and BBr <sub>3</sub> ; power left on; made no power adjustments								
	95	95	38	215	6.2	7,800	2		
50	0	71	235	5.0	8,540	5			
Current maintained at 2.0 mA									
Final									
27,860									

(4) Variation of Plating Conditions. Combining the information obtained in the previous tests, several runs were made using variations of the plating conditions. Some of the results obtained are presented in Table 5 and in Fig. 8.

The current-time and voltage-time characteristics for two runs are indicated in Fig. 8. The filament obtained in Run 73-1 (Table 5) was evenly and uniformly coated similar to the filament pictured in Fig. 7. Except for one defect, the filament obtained from Run 74-1 (Table 5) was evenly and uniformly coated similar to the filament pictured in Fig. 7. As indicated in Fig. 8, the defect probably occurred after an elapsed time of about 21 min at a cell voltage of about 23,600 V.

The results obtained indicate that the best process conditions and plating procedure for boron deposition on a stationary 0.5-mil tungsten wire are as indicated in Fig. 8.

### Discussion

The morphology of the deposit obtained reflects, in general, the morphology of the substrate. The coating is essentially amorphous in nature although there is indication of anisotropy.

One set of operating conditions giving a satisfactory coating of boron on tungsten is presented graphically in Fig. 8. In general, good coatings have been obtained at high boron tribromide-to-hydrogen ratios and relatively low currents. Furthermore, if the flowrate is too great, the corona tends to break up into points, resulting in nonuniform deposits.

Other effects of varying operation conditions which suggest limitations for deposition, and which also tend to verify the mechanism for deposition presented previously, include:

- (a) The voltage requirements increase as the boron tribromide to hydrogen ratio increases.
- (b) The voltage requirements increase as the system pressure increases.
- (c) The substrate is etched with little or no boron deposited as the boron tribromide-to-hydrogen ratio decreases.

## CONTINUOUS BORON DEPOSITION ON A MOVING FILAMENT

### Experimental Work

A system was designed, assembled, and tested for continuous boron deposition on a moving filament. Figure 9 is a schematic of the apparatus. The design resembles that for the batch plating process (Fig. 1). The filament is pulled through the system with a Graham constant speed motor. The spool is mounted on a shaft and suspended in such a manner as to offer minimum friction. The seal and electrical contact between cells is a unique arrangement such that the filament moves through the seal in a vertical direction without breaking the seal.

The power for the cells has been obtained in a manner similar to that used for the batch plating process (Fig. 2). There has been a considerable problem with 60-cycle pickup in the measurement system. Shielding and grounding at various critical positions were necessary to eliminate this problem.

Hydrogen-boron trichloride was chosen as the reactant system. The reactant mixture has been obtained by bubbling hydrogen through boron trichloride maintained at about  $-20^{\circ}\text{C}$ . The reaction cells have not been heated externally, and the vapor flow was split between all three cells.

The etching cell was not utilized as such, and was eventually converted to use for cleaning the substrate filament by the hot-wire technique. Thus, the chemical cleaning train was eliminated. Hydrogen only was passed through the cleaning cell and the substrate heated to

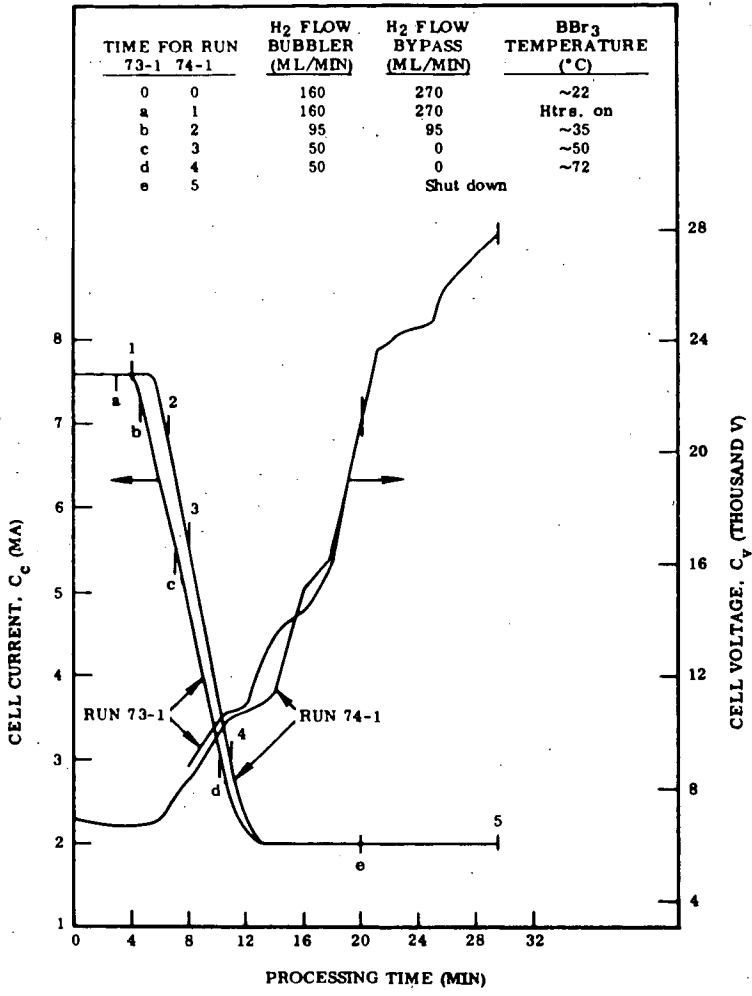


Fig. 8 Electrical Characteristics During Deposition of Boron on 0.5-mil Tungsten Wire in a Corona Discharge

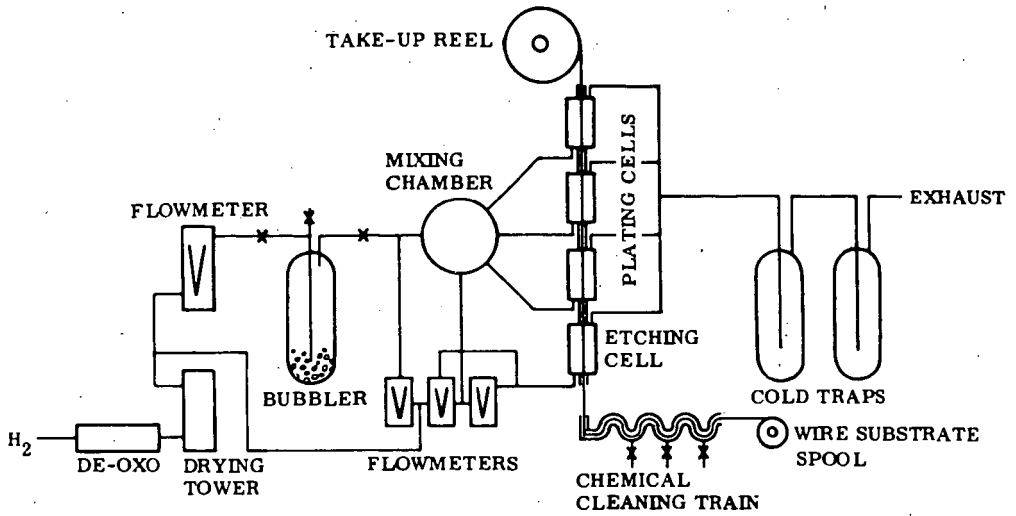


Fig. 9 Schematic of Continuous System for Plating in a Corona Discharge

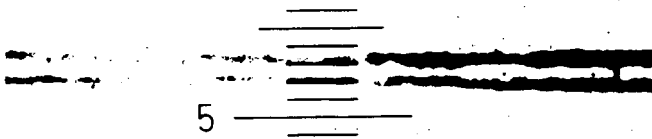


Fig. 10 Boron Deposit on 0.15-mil Tungsten Wire, Continuous System (600 $\times$ )

a red heat in this cell using dc power. Tests performed in this system have utilized both 0.5-mil and 0.15-mil tungsten substrate.

## Results

(1) AC Pickup. The use of shielded leads and wire cages around the transformers has, with the use of 1,000 ohm current measuring resistors, virtually eliminated the ac pickup.

(2) Deposition on 0.5-mil Tungsten Wire. Satisfactory results have been obtained at a hydrogen flow rate through the bubbler of about 100 cc/min and additional hydrogen at a flow rate of about 350 cc/min. Hydrogen is flowing through the cleaning cell at about 140 cc/min and the wire is cleaned by resistance heating at a dc voltage of about 70 V and a DC current of about 320 milliamperes. Some of the results obtained are indicated in Table 6.

Using only one cell, at a filament speed of about 3.6 in./min a coating about 0.25-mil thick was obtained; at a filament speed of about 14.4 in./min, a coating about 0.05-mil thick was obtained.

Using two cells, there was some problem in maintaining the corona in the second cell. At a filament speed of about 3.6 in./min a coating about 0.7-mil thick was obtained in the areas where a good corona was maintained. At a filament speed of about 14.4 in./min and a current input to the second cell of about half that to the first cell, a coating about 0.07-mil thick was obtained.

(3) Deposition on 0.15-mil Tungsten Wire. The 0.15-mil tungsten substrate wire was cleaned by the hot-wire technique at hydrogen flow rate of about 140 cc/min and at a dc power input of about 208 V and 90 mA. While the input vapors were split between the three plating cells, only one cell was utilized for plating studies. Some of the results are indicated in Table 7.

The best results were obtained at a filament speed of about 5 in./min with a hydrogen flow rate through the bubbler of about 70 cc/min, and additional hydrogen at a flow rate of about 350 cc/min. To maintain a uniform corona, it was necessary to switch the power on and off relatively slowly during the run. Under these conditions a coating thickness of about 0.17 mil was obtained.

There is apparently some difference in either the morphology of the 0.15-mil substrate as compared to the 0.5-mil material, or less effect by this substrate upon the morphology of the deposit. Although the morphology of the material deposited on 0.5-mil tungsten appeared similar to that indicated in Fig. 5, the morphology of the deposit on the 0.15-mil tungsten appeared more like that indicated in Fig. 4. Figure 10 indicates the morphology usually obtained on 0.15-mil tungsten substrate. The total diameter of this sample is 0.4 mil.

## Discussion

An apparatus has been presented, and tests performed, indicating the feasibility of depositing boron on a continuously moving substrate in a corona discharge.

Although no tests were made for verification, the results obtained with the 0.15-mil substrate indicate that the substrate diameter also effects the operating conditions, probably through buildup of the positive ion sheath to such an extent that the corona cannot recover after being quenched. This effect is possibly related to the similar effect of high flowrates on larger substrates noted in the previous section. The effects might be explained by postulating a higher concentration of boron radicals around the smaller substrate simply through volume considerations, and around the larger substrate through an increased concentration resulting from increased availability due to higher flowrates. The charged species would tend to remain in the volume near the substrate because of the greater effects of the electrical field.

Table 6. Some Effects of Varying Process Conditions With 0.5 Mil Tungsten Substrate in a Continuous System

Run	Filament Speed (in./min)	H <sub>2</sub> flow (cc/min)			Cell no. 1		Cell no. 2		Comments
		Cleaning	Bubbler	Bypass	Voltage peak (V)	Current peak (mA)	Voltage peak (V)	Current peak (mA)	
85-4	3.6	140	100	350	7,000	16	-	-	Good corona, final diameter - 1 mil.
85-5	3.6	140	100	350	7,000	17	7,200	18	Corona not good in 2nd cell, final diameter in uniform portions - 1.9 mils.
87-1	14.1	140	100	350	6,600	5.8	-	-	Apparently very faint but good corona.
					6,000	12.5	-	-	Corona broke up as power increased, then formed good corona, final diameter 0.6 mil.
87-2	14.4	140	100	350	6,000	12.5	6,720	6.4	Corona good in Cell 1, weak but apparently good in Cell 2. Final diameter 0.64 mil.
					6,000	12.5	6,960	17.5	Cell 2; Corona broke up with increasing power and did not improve before heating occurred.

Table 7. Some Effects of Varying Process Conditions With 0.15 mil Tungsten Substrate in a Continuous System

Run	Filament Speed (in./min)	H <sub>2</sub> flow (cc/min)			Cell no. 0		Cell no. 1		Comments
		Cleaning	Bubbler	Bypass	Voltage dc (V)	Current dc (mA)	Voltage peak (V)	Current peak (mA)	
88-3	0.8	140	100	350	218	85	6,000	12	Corona as discontinuous 1/8 in. strips, some heating of substrate, could get good corona by switching on full power, but new wire had breaks in the corona, in good corona areas total thickness 0.6 mil.
88-5	5.1	140	70	350	208	90	5,200	-	Maintained good corona by switching power on and off slowly, total thickness 0.5 mil.
89-2	5.1	140	120	350	208	90	7,100	14.6	Corona poor with some heating of wire.
89-3	5.1	140	120	350	208	90	7,200	14.0	Corona good, after short time wire began to heat.
90-4	5.1	140	120	350	208	90	7,400	14	Could get good corona by switching on full power, but new wire had breaks in the corona.

## CONCLUSIONS

Chemical reactions can be initiated and sustained by a corona discharge. Boron has been deposited on a tungsten wire substrate in a corona discharge at relatively low temperatures. The deposition process is electrochemical in nature, the boron being deposited cathodically, and the mechanism for the reaction is indicated to be of the form:

- (a) Emission of electrons from the cathode
- (b) Ionization (or activation) of hydrogen, argon, or helium, and production of secondary electrons which in turn ionize more hydrogen, etc.
- (c) Collision of ionized hydrogen, argon, or helium with boron tribromide and exchange of energy
- (d) Formation of positive boron radicals and hydrogen bromide or bromine
- (e) Transfer of the positive boron radical to the cathode
- (f) Electrochemical reaction of the boron radical to form an essentially amorphous deposit of boron

The morphology of the deposit is essentially the same as the morphology of the substrate. There is no interaction of the boron with the tungsten and there is apparently some anisotropy of the deposit.

The corona discharge during deposition is not essentially different from a corona discharge developed in an inert gas system, and the same criteria and properties are extant. Like a corona discharge in an inert gas, the coefficient of electron emission and the ability of the electrons to diffuse along the wire are most important in obtaining a uniform corona, and thus a uniform deposit, on the substrate. Furthermore, if the sheath of positively charged boron radicals becomes too dense, the corona is quenched and will not recover fast enough to prevent the breakup of the corona into points.

## ACKNOWLEDGEMENT

This work was supported by the U. S. Air Force Contract AF 33(615)-2130, and was based upon an idea presented by J. B. Story. The filament cross-sections were prepared by W. C. Coons and the continuous system was operated by Barbara Traina. Grateful acknowledgement is also made to R. N. Varney, M. E. Sibert, and A. E. Hultquist for many helpful discussions of gas discharges in general and of corona discharges in particular.

## REFERENCES

1. N. A. Kapzow, "Elelstrische Vorgange in Gasen und in Vakuum," Veb Deutscher Verlag der Wissenschaften, Berlin, 1955
2. S. C. Brown, "Basic Data of Plasma Physics," The Technology Press of MIT and John Wiley and Sons, Inc., New York, 1959
3. E. J. Helland, The Plasma State, Reinhold Publishing Corporation, New York, 1961
4. L. B. Loeb, Electrical Coronas, Univ. of Calif. Press, 1965
5. L. Ya. Markovskii, V. I. L'vova, Yu. D. Kondrashev, Bor. Trudy Konf. Khim, Bora; Ego Soedineii, 36-45 (1958) cf. FTD-MT-64-427, Foreign Technology Division, A. F. Systems Command, 1965
6. W. V. Kotlensky and R. Schaeffer, *J. Am. Chem. Soc.* **80**, 4517 (1958)
7. R. T. Holzmann and W. F. Morris, *J. Chem. Phys.* **29**, 677 (1958)
8. N. R. Dibelius, J. C. Fraser, M. Kawahata, and C. D. Doyle, *Chem. Engr. Progress*, **60**, No. 6, 41-44 (June 1964)
9. S. J. Lawrence, *Chem. Engr. Progress*, **60**, No. 6, 45-51 (June, 1964)
10. J. A. Coffman and W. R. Browne, *Scientific American*, **212**, No. 6, 90-98 (June 1965)
11. N. A. Lange, Editor, Handbook of Chemistry, 10th Ed., 111, McGraw-Hill Book Company, Inc., N. Y. 1961

## VAPOR PHASE FORMATION OF NONCRYSTALLINE FILMS BY A MICROWAVE DISCHARGE TECHNIQUE

D. R. Secrist and J. D. Mackenzie

International Business Machines Corporation, Poughkeepsie,<sup>1</sup> New York  
Rensselaer Polytechnic Institute, Troy, New York

### ABSTRACT

Numerous variations of the microwave discharge method have been employed to prepare thin films. In this study, non-crystalline films were deposited at low temperatures and pressures by the vapor phase reaction of suitable compounds with the energetic gaseous species generated in a discharge operated at 2,450 megacycles/sec. The major part of the investigation concerned the decomposition of metal-organic compounds of the type  $(R)_xM$  or  $(RO)_xM$ , where R may be  $C_2H_5$ ,  $C_3H_7$ , etc. Amorphous oxide films of silicon, germanium, boron, tin, and titanium were readily formed when an oxygen plasma was maintained. Silica films were also grown via an argon plasma. These films were deposited on metallic and non-metallic substrates positioned outside the discharge region. Conversely, the oxidation of silicon tetrafluoride to yield a fluorsiloxane polymer of composition  $SiO_{1.5}F$  was found to occur only within the confines of the plasma. It is shown that the films are free from decomposition products when deposited above a certain critical temperature, which is dependent on the reactant flow rate. The effects of temperature, pressure, flow rate, and hygroscopic nature of the substrate on the deposition rate are examined. Optical properties are presented. The utilization of a nitrogen or nitrogen oxide plasma to generate nitride or oxynitride films is discussed.

### INTRODUCTION

Extensive studies have been conducted with crystalline films in regard to film structure, epitaxy, and property variations as a function of the history of a particular deposition process. The nature of glassy films, however, has not been investigated with the same thoroughness. This is due, in part, to the inability of most materials to form in the glassy state. In general, the approach to film formation has been from the vapor phase. Some methods from the vapor include evaporation, vapor phase hydrolysis, thermal decomposition, and "sputtering". All of these techniques will yield non-crystalline films with the proper conditions. However, with the exception of the latter method, relatively high temperatures are required. As a result, most films invariably crystallize immediately after being deposited. The non-crystalline films prepared by these techniques are usually materials which readily form a glass by the conventional cooling of a melt; e. g.,  $SiO_2$ . The method of sputtering, on the other hand, occasionally leads to the formation of uncommon non-crystalline films when the substrates are maintained at low temperatures<sup>(1)</sup>. In this paper, the low temperature preparation of a wide variety of non-crystalline films is discussed utilizing a microwave discharge method as an alternative to sputtering. With this technique, the rate of film deposition can be carefully controlled by regulation of the reactant flow rates. The quality of any particular film is shown to be a sensitive function of (1) the concentration

and type of reaction products, (2) the chemical nature of the substrate, and (3) the reactor (substrate) temperature.

### APPARATUS

A schematic drawing of the main flow system employed in this work is shown in Figure 1. A gaseous plasma, in this instance oxygen, could be maintained in a 1" O. D. pyrex tube when the system pressure was less than 800 microns. The electrodeless discharge was produced with a Raytheon PGM-10 Microwave Generator. This unit could supply 100 watts of microwave energy at a fixed frequency of 2,450 mc/sec. The energized species were allowed to flow into the bell jar through a 0.5" dia. pyrex tube. The metal-organic compounds selected for this work were liquids with a vapor pressure of about 0.5 mm. near-room temperature and were contained in a graduate cylinder immersed in a constant temperature bath. The metal-organic evaporation rate (flow rate) at any temperature could be altered by adjusting a 1 mm. dia. Teflon stopcock. The ultimate vacuum achieved in the system was 240 microns pressure with a gas flow rate of 176 cm<sup>3</sup>/minute. The majority of the studies were performed inside an aluminum furnace 2 1/4" in dia. x 4" long. A fused silica cylinder 1 3/8" in dia. x 2 1/2" long served as a second furnace core. The constant temperature zones for these furnaces extended one cm. above and below the gas inlet port with a maximum radial temperature variation of  $\pm 5^{\circ}\text{C}$  for points one cm. from the cylinder axes. A fused silica balance having a sensitivity of 1 cm/mg. was employed to determine the rate of film deposition. Details of this apparatus have been previously reported<sup>(2)</sup>. In order to provide a secondary working geometry, the basic apparatus was modified as illustrated in Figure 2. This adaption was used to study the oxidation of silicon tetrafluoride.

### FILM DEPOSITION AND EVALUATION

The substrates were positioned in the furnace reaction vessel with their wide dimension perpendicular to the gas inlet tube. The general cleaning procedure consisted of dipping the specimens into a 48% solution of hydrofluoric acid, followed by a rinse in distilled water. During the period when the furnace temperature was increasing the system was purged with the gas selected to form the plasma. In all work, the microwave generator was operated at 90% of its rated power output.

The films were deposited onto NaCl or KBr discs to facilitate examination by infrared transmission. Substrates of platinum, aluminum, Al<sub>2</sub>O<sub>3</sub>, and fused SiO<sub>2</sub> approximately one cm. in diameter were prepared for the rate studies. The index of refraction and isotropic character of film specimens obtained from the substrates and/or gas inlet tube were determined with a petrographic microscope. Debye-Scherrer x-ray diffraction powder patterns were made to establish whether the films were amorphous or crystalline.

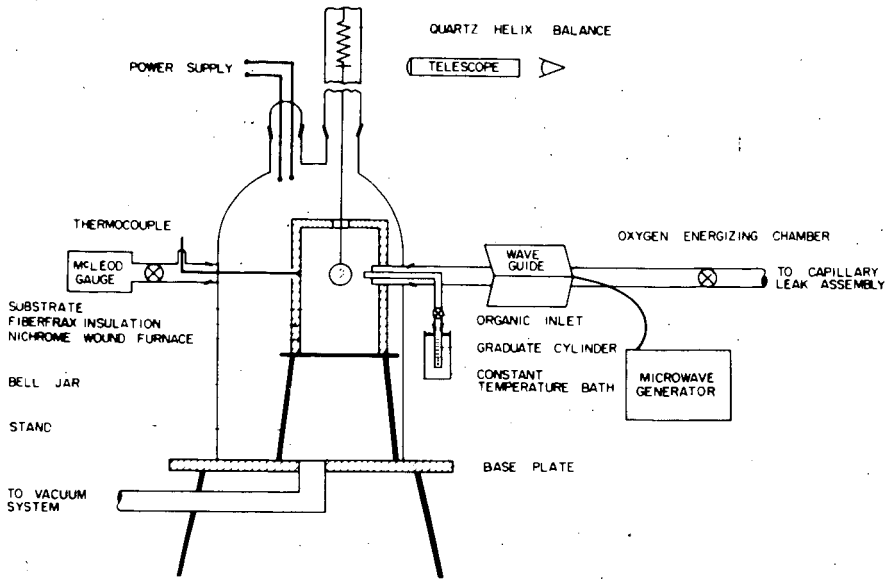


Figure 1: Schematic Drawing of Microwave Discharge Apparatus.

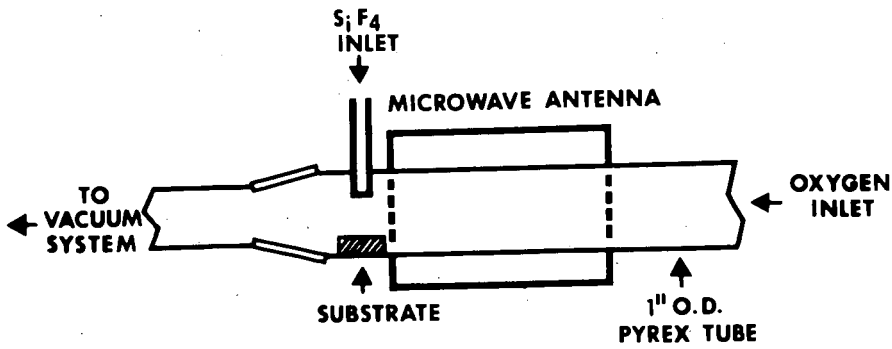


Figure 2: Modified Microwave Discharge System.

## RESULTS AND DISCUSSION

Preliminary studies indicated that extensive water was formed as a reaction product when the metal-organic compounds were decomposed via an oxygen discharge. This water could be chemically incorporated into the oxide films when the substrates were held below a certain temperature which depended on the organic evaporation rate and the hygroscopic nature of the substrate. For instance, with NaCl substrates, the silica films were found to be free of water above 180°C with a tetraethoxysilane evaporation rate of 0.015 cm<sup>3</sup>/hour.<sup>(3)</sup> The presence of silicic acid was detected below 180°C by infrared transmission studies. Conversely, with a KBr substrate and similar conditions of temperature and evaporation rate, extensive water was incorporated into the silica film.

The majority of the films prepared in this study were formed with low deposition rates of about 20 Å/minute on NaCl substrates heated to a temperature of 200°C. The optical properties of some of the films are presented in Table 1.

TABLE 1

COMPARISON OF THE OPTICAL PROPERTIES OF  
VAPOR-FORMED FILMS AND THEIR RESPECTIVE  
GLASSY OR CRYSTALLINE OXIDES

Material	Principal Infrared Frequency (CM <sup>-1</sup> )	Index of Refraction	
SiO <sub>2</sub> :	vapor-formed film	1,045;800	1.458+ .002
	fusion-formed glass	1,080;800	1.458+ .002
GeO <sub>2</sub> :	vapor-formed film	850	1.582+ .002
	fusion-formed glass	860	1.534-1.607
B <sub>2</sub> O <sub>3</sub> :	vapor-formed film	1,350	1.470+ .002
	fusion-formed glass	1,370	1.464 <sup>(4)</sup>
Ti <sub>x</sub> O <sub>y</sub> :	vapor-formed film	950-700	>1.7
TiO <sub>2</sub> :	anatase	1,200-500	>1.7
Sn <sub>x</sub> O <sub>y</sub> :	vapor-formed film	1,425	1.536+ .002
SnO <sub>2</sub> :	cassiterite	850-500	>1.7

All of the films were isotropic when examined with polarized light and were amorphous by x-ray diffraction. The silica films were formed by (1) decomposing tetraethoxysilane, (C<sub>2</sub>H<sub>5</sub>O)<sub>4</sub>Si, in either an oxygen or argon plasma or (2) decomposing tetraethylsilane in an oxygen plasma. The germania and boron oxide films were prepared by decomposing tetraethoxygermane and triethylborate via an oxygen discharge. The infrared absorption frequencies and refractive indices of the latter three vapor-formed films are similar to those of the respective fusion-formed glasses, which suggests that a random network structure can be achieved by methods other than the conventional cooling of the melt. The spread in the index of refraction for germania glass was realized by slowing cooling one specimen and quenching another from 1100°C; the slow-cooled specimen had the larger refractive index. With the exception

of the boron oxide film, the films listed in Table 1 adhered well to the NaCl substrates. The  $B_2O_3$  film was immediately coated with mineral oil after removal from the glow discharge apparatus because of its extreme moisture sensitivity and was only partially adherent.

The non-crystalline titanium oxide films were prepared from titanium tetraisopropylate while maintaining an oxygen discharge. Since titanium oxide is not a common glass-forming system, one may inquire as to whether or not the viscosity of such a film would be similar to that of a glass near its transition region, e. i.  $10^{13}$ - $10^{14}$  poises. For many undercooled systems, the growth rate can be described in terms of the reciprocal viscosity<sup>(5)</sup> as:

$$u = \frac{\Delta H_f (T_f - T)}{3 T_f \pi \lambda^2 \eta N}$$

where  $u$  is the rate of growth (cm/sec),  $T$  is the undercooled temperature,  $\eta$  is the viscosity (poises),  $T_f$  is the fusion temperature,  $\lambda$  is the mean jump distance (cm),  $H_f$  is the latent heat of fusion (ergs), and  $N$  is Avogadro's number. If this relationship is valid for a system, then an approximate estimation of the viscosity at the crystallization temperature can be made if the rate of growth (crystallization) is known. In this study, the titanium oxide film exhibited birefringence (crystallized) after 45 minutes at  $325^\circ\text{C}$ . An approximate rate of crystallization can be calculated for the film if it is assumed that the particles grew from some arbitrary value, for example,  $10 \text{ \AA}$  to  $110 \text{ \AA}$ , before crystallinity was detected. The jump distance  $\lambda$  was taken as  $2 \text{ \AA}$  units. Although  $TiO_2$  dissociates, the heat of fusion has been reported as  $15.5 \text{ kcal/mole}$  at a melting point of  $1840^\circ\text{C}$ <sup>(6)</sup>. The growth rate determined from the rate of crystallization is about  $3.7 \times 10^{-10} \text{ cm/sec}$ . The corresponding viscosity at  $598^\circ\text{K}$  is  $5.5 \times 10^{11}$  poises, which would classify the film as a highly viscous supercooled liquid since the viscosity value is slightly below  $10^{13}$ - $10^{14}$  poises. Since viscosity is approximately an exponential function of temperature, it is reasonable to conclude that at some slightly lower temperature the viscosity of the film is characteristic of a solid glass, e. i.  $10^{13}$ - $10^{14}$  poises.

An amorphous tin oxide film was formed by decomposing dibutyltin-diacetate via an oxygen plasma. Preliminary measurements indicated that the electrical resistivity of the film near room temperature was greater than  $10^7 \text{ ohm-cm}$ . Comparing the I. R. spectra of the film and  $SnO_2$ , it is seen in Table 1 that the main absorption mode for the amorphous film occurs at a much higher frequency than that of the crystalline modification. This shift can probably be attributed to a large structural variation such as a change in coordination number.

The basic apparatus shown in Figure 1 was modified as illustrated in Figure 2 in order to study the oxidation of  $SiF_4$  via an oxygen discharge. Research grade  $SiF_4$  gas was metered into the pyrex chamber at a rate of  $1.8 \text{ cm}^3/\text{minute}$ . Simultaneously, dry oxygen was admitted at the rate of  $5 \text{ cm}^3/\text{minute}$ . The electrodeless discharge was maintained at  $800 \text{ u}$  total pressure. Under these conditions, a thick non-adherent film was deposited onto the walls of the pyrex

chamber within the boundaries of the plasma in about one hour. The wall temperature in this region was approximately  $100^{\circ}\text{C}$ . The film can be described as a translucent blue-white gel which was amorphous by x-ray diffraction and isotropic when observed with polarized light. The index of refraction of the gel was estimated to be considerably less than 1.400; infrared absorption bands were evidenced at 1080, 920, and  $750\text{ cm}^{-1}$ . A microchemical analysis of the film indicated that its composition could be represented as  $(\text{SiO}_{1.5}\text{F})_n$ . It is interesting to note that the film formed only within the confines of the plasma, which suggests that thermal and/or microwave energy are required for the oxidation and/or polymerization processes.

Effect of Pressure, Temperature, and Substrate - An extensive study was made with the silica films with respect to the mechanism and kinetics of film formation<sup>(2)</sup>. It is reasonable to suspect that the general conclusions formulated in this work with respect to pressure, temperature, and nature of the substrate are applicable to most of the other oxide films discussed in this manuscript. Support for this viewpoint is also documented in regards to the incorporation of water into the films<sup>(3)</sup>.

Basically, the effect of minor pressure fluctuations on the rate of deposition of silica films was found to be negligible. However, above 500 microns pressure, the rate of deposition was rapidly decreased due to (1) an increased atomic oxygen recombination and (2) poisoning effects from the reaction products. The films discussed in the present work were deposited near 240 u pressure. Typical rates of deposition for the silica films ranged from 10 to 80 Å/min. by variation of (1) the organic evaporation rate or (2) the substrate temperature. The rate of deposition was constant with time. The relationship between logarithm of the deposition rate and reciprocal temperature is depicted in Figure 3 for various substrates. The data have been spread to show the temperature dependence of deposition with each substrate. With a tetraethoxysilane evaporation rate of  $0.15\text{ cm}^3/\text{hour}$ , the silica films were free of water and/or organic inclusions (by infrared transmission studies) above  $\sim 290^{\circ}\text{C}$ . At higher temperatures, the rate of deposition decreased with increasing temperature and was ascribed to a process of physical adsorption. The apparent heat of adsorption of silica glass on the fused silica, NaCl, and platinum substrates was calculated to be  $12.7 \pm 0.2\text{ kcal/mole}$ . For the aluminum or  $\text{Al}_2\text{O}_3$  substrates, the apparent heat of adsorption of silica was calculated to be  $9.5 \pm 0.3\text{ kcal/mole}$ . It was concluded that the hygroscopic nature of the  $\text{Al}_2\text{O}_3$  surface was responsible for the lower heat of adsorption observed. It was postulated that a hydrated surface tends to incorporate further hydroxyl groups into the film structure. With this reasoning, one might expect that the hygroscopic nature of the KBr substrate discussed earlier would also lead to a decreased heat of adsorption. In conclusion, it is postulated that the rate of deposition of an oxide film with a moisture sensitivity similar to that of silica is most likely affected in the same manner, e. i. physical adsorption controlled below  $410^{\circ}\text{C}$ . The apparent heat of adsorption of the oxide films on the various substrates, is of course, dependent on the molecular structure of the films and the hygroscopic nature of the substrate.

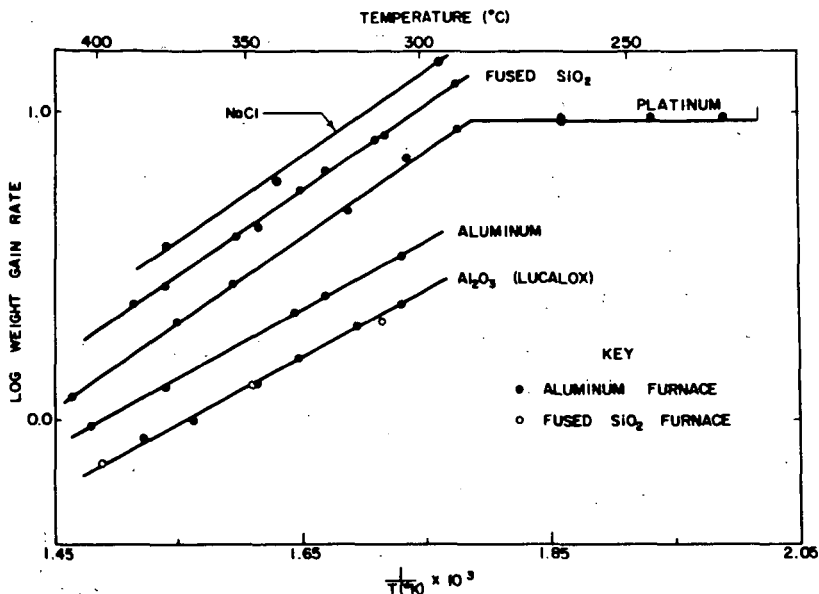


Figure 3: Relationship of Logarithm Silica Deposition Rate and Reciprocal Temperature for Deposition on Various Substrates.

**Other Systems** - The microwave discharge technique can be employed to deposit a variety of thin films at low temperatures. One obvious variation of the technique utilizes gaseous plasmas other than oxygen. For instance, in the work with silica films it was found that  $(C_2H_5O)_4Si$  contained sufficient oxygen to facilitate the formation of  $SiO_2$  when the compound was decomposed with energetic argon species. Sterling and Swann<sup>(7)</sup> have recently deposited amorphous  $Si_3N_4$  films by the reaction of silane and anhydrous ammonia in an RF discharge. Non-crystalline silicon nitride films have also been prepared at Rensselaer Polytechnic Institute by the decomposition of  $(C_2H_5)_4Si$  via a nitrogen discharge. The use of a  $N_2O$  plasma to form  $Si_2ON_2$  poses another equally interesting possibility. Success to date with the latter reactions has been complicated by the ease of formation of silica. Since metal-organic compounds are now available for a large number of metals, it would seem that the microwave discharge technique could lead to many new and unusual films by a simple variation of the reactant and/or plasma compositions.

References

1. R. A. Mickelson, "Electrical and Optical Properties of Amorphous Zinc Oxide Films", Sc. D. Thesis, M. I. T., 1963.
2. D. R. Secrist and J. D. Mackenzie, "Deposition of Silica Films by the Glow Discharge Technique", J. Electrochem. Soc. 113 (9), 914-920, (1966).
3. D. R. Secrist and J. D. Mackenzie, "Incorporation of Water Into Vapor Deposited Oxide Films", Solid State Electronics, 9, 180 (1966).
4. G. W. Morey, "The Properties of Glass", 2nd Edition, Chap. XVI, p. 370, Reinhold Publishing Corp., New York, 1954.
5. David Turnbull, p. 225 in Solid State Physics, Vol. 3, edited by F. Seitz & D. Turnbull, Academic Press, Inc., N. Y. 1956.
6. Q. Kubachewski and E. Evans, Metallurgical Thermodynamics, p. 306, Pergamon Press, N. Y. 1958.
7. H. F. Sterling and R. C. G. Swann, "Chemical Vapor Deposition Promoted by R. F. Discharge", Solid State Electronics 8, (8) p. 653-54 (1965).

Acknowledgements

The authors are grateful to the Pittsburgh Plate Glass Company for the support of a fellowship. (D. R. S.).

The Reaction of Oxygen with Carbonaceous Compounds  
in the Electrodeless Ring Discharge

Chester E. Gleit

Department of Chemistry, North Carolina State University, Raleigh, North Carolina, 27607

Abstract

The electrodeless ring discharge has recently found use in chemical analysis as a means of removing carbon from graphitic and organic compounds preceding elemental analysis and determination of microstructure. To determine appropriate reaction conditions, the relationship between oxidation rate and sample temperature was studied. Samples were immersed in a plasma produced by passing molecular oxygen through a radiofrequency field. An inductively coupled, 13.56-MHz generator producing 95 watts was utilized. Gas pressure was 1.2 torr, and flow 150 cc/min. The apparent activation energy of pure graphite was found to be 6.5 Kcal/mol in the temperature range 100 to 300°C, and zero at higher temperatures. The activation energy of both impure graphite and sucrose were slightly lower. These values are consistent with those of atomic oxygen. The reaction of graphite with CO<sub>2</sub> did not occur below 120°C and yielded an apparent activation energy of 3.2 Kcal/mol in the temperature range 150 to 300°C. Oxidation rate was observed to depend on electrical field configuration. Increasing the temperature of the reaction tube's walls decreased the rate of carbon oxidation. Trace ions, such as Fe(II), Se(IV), Os(IV), and iodide, were converted to higher oxidation states. Neither oxidation nor volatility was observed to be strongly temperature dependent.

Introduction

In 1962 a method was reported for the decomposition of organic substances based on reaction with an oxygen plasma, produced by passing molecular gas through a radiofrequency electrodeless discharge (5). This method has found use in a variety of chemical studies. Loss of trace elements through volatilization and diffusion is less than that in conventional dry ashing. Destruction of mineral structure is reduced. As a small quantity of purified oxygen is the only reagent, the possibility of chemical contamination is diminished. Applications of this method include: microincineration of biological specimens (13), the ashing of coal (6) and filter paper (4), and the recovery of mineral fibers from tissue (1). Several reviews of analytical applications have been published (9)(14).

In conventional ashing both reaction rate and retention of volatile components are strongly temperature dependent. However, disagreement exists as to the effect of temperature in plasma ashing. In part, this is due to difficulty in applying conventional temperature measuring techniques to solids immersed in a strong radiofrequency field. The question is further complicated by the fact that a single temperature cannot be assigned to the system. Electrons in the low pressure plasma are not in thermal equilibrium with the ions and neutral species. Furthermore, the temperature of the specimen and the surrounding vessel may differ considerably. In this study the effects of temperature on oxidation rate, recombination of active gaseous species, and volatility of inorganic reaction products are considered.

Experimental

The reaction system employed in these studies (figure 1) consisted of a 100-cm long, 3.5-cm I.D., borosilicate cylinder (Pyrex No. 7740). Specimens were placed on

the principal axis 43 cm from the gas inlet. A 0.6-cm tube, C, passed diametrically through the cylinder and held the specimen on a central projection. Sample temperature was regulated, in part, by circulating liquids between this tube and a constant temperature bath. Radiofrequency excitation was supplied from a 250-watt, crystal controlled 13.56-MHz generator, described previously (3). Except as otherwise noted, an output of 115 watts was employed. Power was transferred to the gas by means of an impedance matching network terminating in a 10-turn coil of  $\frac{1}{4}$ -inch O.D. copper tubing tapped 2 turns from ground. The coil, B, which had an inside diameter of 4.5 cm and was 12.5 cm long, was coaxial with the reaction tube and placed 10 cm from the gas inlet.

After passage through a rotometer, molecular gas entered the reaction system through a capillary orifice, A. Pressure was monitored by a McCloud gauge attached to side arm E, located 50 cm beyond the gas inlet. Pressure was maintained at 1.2 torr; and flow rates at 150 cc per minute, S.T.P. U.S.P. grade oxygen and instrument grade carbon dioxide were used.

The temperature of solid specimens in the plasma was determined by means of an infrared radiation thermometer (Infrascopes Model 3-1000, Huggins Laboratories Inc., Sunnyvale, Calif.) attached to a chart recorder. This device employs a lead sulfide detector and suitable filters to permit remote measurement of 1.2 to 2.5  $\mu$  radiation emitted by the specimen. To compensate for variations in emissivity and inhomogeneity in the optical field, empirical calibration curves were constructed. Thermocouples were employed to determine cylinder-wall temperatures. To eliminate interaction with the radiofrequency field, the transmitter was inactivated during the latter measurements.

High purity graphite rods (National Carbon Co., Grade AGKSP) were employed as standard specimens. These rods were 0.61 cm in diameter and had a cavity machined into their base to affix them to the cooling tube. Pellets of sucrose and carbon containing small quantities of cupric acetate were also employed. The latter were produced by heating and then pressing a slurry of the salt solution and 200-mesh graphite powder.

## Results and Discussion

**Sample Temperature:** The temperature variation of oxidation rate of graphite exposed to the oxygen plasma is shown in figure 2. Over the range 120 to 300°C, the Arrhenius equation,  $K = Ce^{-E_a/RT}$ , fits the data well and yields a value of 6.5 Kcal/mol for the apparent activation energy,  $E_a$ . Between 300 and 450°C, the highest temperature studied, oxidation rate is not dependent on temperature. The oxidation of graphite by molecular oxygen at high temperature is strongly dependent on the purity of the graphite. To determine if a similar effect occurs in plasma oxidation, pellets composed of pure graphite powder and inorganic salts were utilized. The results of the addition of 0.01 M cupric acetate are shown in figure 2. At low temperature the change in oxidation rate of pure and impure graphite with temperature is similar. However, the rate of oxidation of the impure graphite becomes independent of temperature at a lower temperature. Measurements performed with specimens containing lower concentrations of cupric acetate led to results which fell between the illustrated curves.

The gas in the low pressure electrodeless discharge is chemically similar to that in the positive column of a low pressure arc. Molecule-molecule and ion-molecule collisions are frequent. The ions and neutral species are, therefore, nearly in thermal equilibrium. Elastic collisions between these species and electrons are less frequent. At low pressure electron temperatures are quite high. In the oxygen discharge atomic oxygen ( $O^2P$ ) is believed to be the most abundant active species. Higher energy states of atomic oxygen, positive and negative ions, and electronically excited

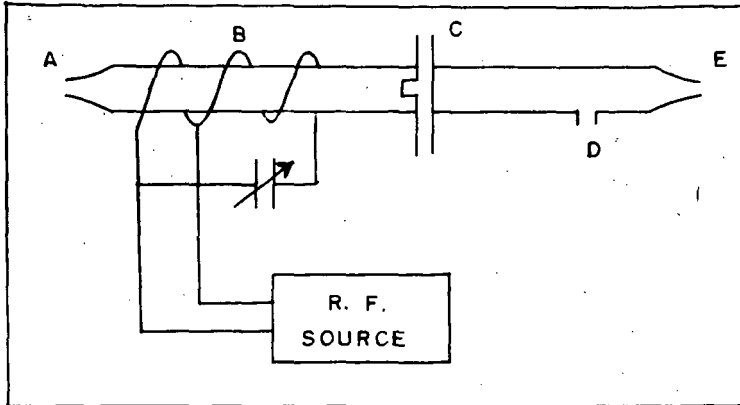


Fig. 1. Experimental apparatus: capillary inlet, A; power coil, B; specimen mounting tube, C; sidearm to manometer, D; outlet to vacuum pump, E.

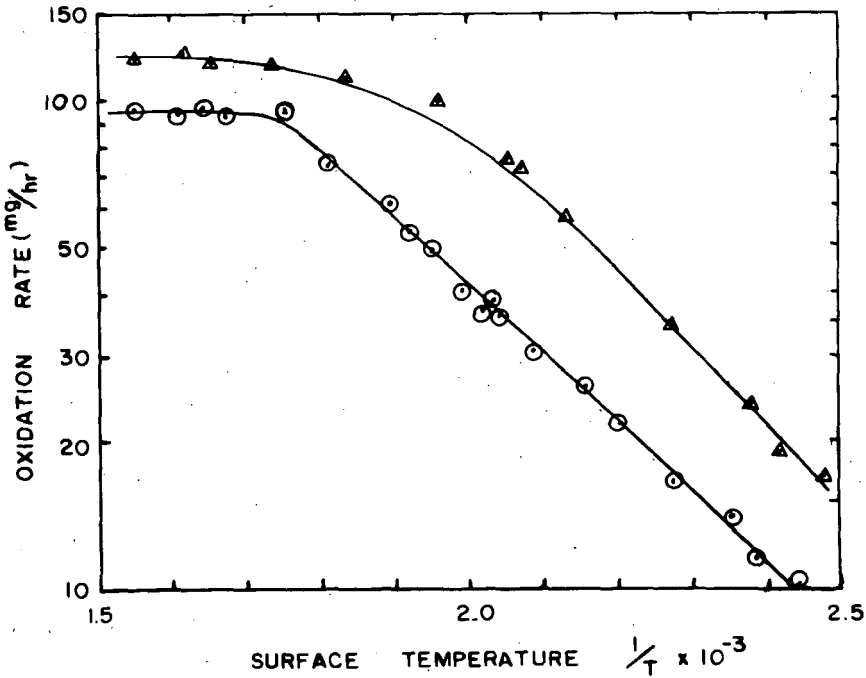


Fig. 2. Rate of oxidation vs. surface temperature for graphite rods, ○, and graphite pellets containing 0.01 M cupric acetate, △.

states of molecular oxygen are also present.

It is instructive to compare these results with measurements of the activation energy of graphite with atomic oxygen removed from the luminous discharge. In several early studies a value of zero was reported (2) (16). Hennig (8) observed no dependence on temperature at a pressure of 1.0 torr and a value of 7 Kcal/mol at 10 torr. This difference was attributed to ozone formation. In a recent detailed study of the atomic oxygen-graphite reaction, Marsh et al. (11) reported an activation energy of 10 Kcal/mol between 14 and 200°C, which approached zero at 350°C. Although the rate of oxidation in these studies was considerably lower than that obtained in the plasma, their values are consistent with the belief that atomic oxygen is a major reactant within the discharge.

Of a variety of specimens, only graphite exhibited an abrupt change in activation energy near 300°C. For example, the apparent activation energy in the decomposition of sucrose is approximately 4 Kcal/mol over the entire measurement range. The independence of oxidation rate for graphite at high temperatures is ascribed to the formation of surface oxides. Numerous studies of graphite combustion have shown that such surface compounds control rate at elevated temperatures in excess oxygen. As anticipated, increasing radiofrequency power to the discharge does not measurably increase the rate of graphite oxidation at high sample temperature.

The exhaust gas of the oxygen-graphite reaction contains both carbon monoxide and carbon dioxide, with the latter predominating. In the luminous discharge region these gases react with graphite. The results of measurements in which carbon dioxide was passed through the radiofrequency field and then exposed to graphite rods activated are shown in figure 3. Between 150 and 400°C the Arrhenius equation fits well, yielding an apparent activation energy of 3.2 Kcal/mol. Below 120°C less than one mg per hour of carbon was removed. This small weight loss is attributed to ion and electron bombardment.

Wall Conditions: In a number of experiments, increasing power beyond an optimum value led to the anomolous result of reducing ashing rate. Earlier it was noted that placing a dry ice-acetone trap in the exhaust stream extended the length of the luminous discharge (5). To study this effect, wall temperatures were varied while the carbon rod was maintained at 200°C. The results of a series of measurements are shown in figure 4. Assuming that the decrease in oxidation rate at increased wall temperature is due to recombination of active species at the wall, the overall activation energy at low temperatures for this process is approximately 2 Kcal/mol.

The major sources leading to loss of active oxygen species are recombination of atomic oxygen and ions at the walls of the vessel. The recombination of discharged oxygen on glass surfaces has been investigated. Linnett and Marsden (10) reported that the recombination coefficient of atomic oxygen on clean borosilicate glass (Pyrex) was independent of temperature. However, positive values were observed on contaminated surfaces. In a later series of papers Greaves and Linnett (7) studied a number of oxide surfaces, in all cases the recombination coefficient was temperature dependent. For silica apparent activation energies were 1 to 13 Kcal/mol over the temperature range 15 to 300°C. The exceptional nature of Pyrex was noted.

The second major source of loss of active species results from electron-ion recombination at the chamber walls. The electric field restricts the drift of ions to the chamber walls. Rate of recombination is controlled by ambipolar diffusion, but is limited by the presence of negatively charged oxygen ions in the discharge (15). Although diffusion is not dependent on wall temperature, a distortion of the axially symmetric electrical field will enhance wall recombination, producing an increase in wall temperature and a reduction of oxidation rate. This effect is noted in table I. The presence of a 6-cm long metallic ring on the exterior wall of the reaction vessel reduced oxidation rate by more than ten per cent. Grounding the ring in common with

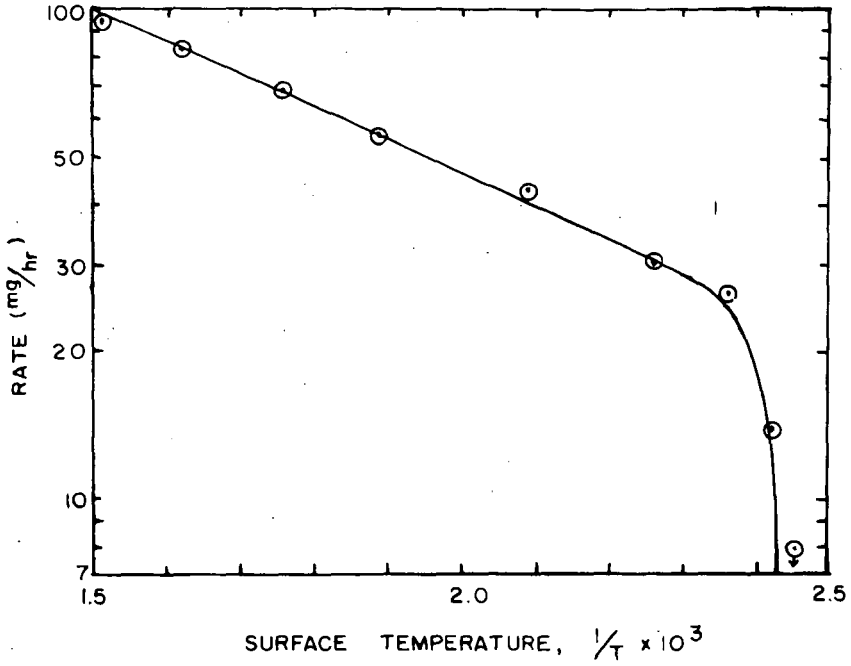


Fig. 3. Rate of gassification vs. temperature for graphite rods exposed to carbon dioxide discharge.

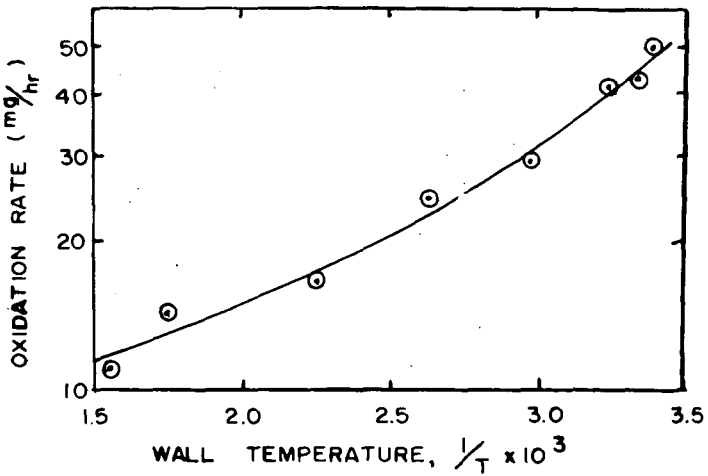


Fig. 4. Effect of wall temperature on the oxidation rate of graphite.

the output coil further reduced the oxidation rate. This is a local effect, in that oxidation rate beyond the ring was not greatly reduced. Distortion of the field can also be introduced by changing the angle between the end of the output coil and the reaction tube. Variations from axial symmetry led to reduced rates and decreased the length of the luminous discharge. Similar effects have been observed in electrodeless discharges at higher pressure (12).

Table I

## Effect of Field Distortion on Carbon Oxidation Rate

	Angle	Oxidation Rate mg/hr
Pyrex tube	0°	79
Pyrex tube and ungrounded copper ring	0°	70
Pyrex tube and grounded copper ring	0°	62
Pyrex tube	1.°	71
Pyrex tube	3.°	63

**Effect on Mineral Constituents:** It has been reported that there is no appreciable loss of a number of metal ions in plasma oxidation (4,5). Nonvolatile species include: Na(I), Cs(II), Cu(II), Zn(II), Mn(II), Pb(II), Cd(II), Co(II), Ho(III), Er(III), Fe(III), Cr(III), As(III), Sb(III), and Mo(VI). The effect of ashing temperature, the reason for the surprisingly low volatility, and the final oxidation state of the product were not previously explored. As part of the present study, 20 to 100 mg of compounds containing radioactive tracers were deposited on Whatman cellulose filters. After exposure to ashing for a sufficient period to remove the filter paper, generally 30 minutes, the activity of the ash was measured and the oxidation state of the element determined. Specimen temperature was adjusted during ashing by altering input power.

These measurements are summarized in table II. In general, temperature has little effect on retention. These results and earlier observations indicating complete retention of metals in compounds such as arsenic chloride and metalloporphyrins (5) are believed to be due to competition between volatilization and oxidation to less volatile compounds. Unlike the other elements studied, the highest valence oxide of osmium, OsO<sub>4</sub>, is the most volatile. Therefore, this element is volatilized in the plasma oxidation process.

The volatility of iodide, shown in figure 5, is also consistent with the hypothesis of competition between volatilization and oxidation. During these measurements, ashing was stopped at 5 minute intervals. It is seen that loss of I<sup>131</sup> closely follows the curve for filter paper gassification. No loss of I<sup>131</sup> occurs after the filter paper is removed. Loss of I<sup>131</sup> varied between 15 and 35 per cent. However, none of the residual I<sup>131</sup> could be precipitated with silver nitrate, indicating that the iodide had been oxidized. When the I<sup>131</sup> tracer was converted to NaIO<sub>3</sub> before ashing all of the iodine activity was retained.

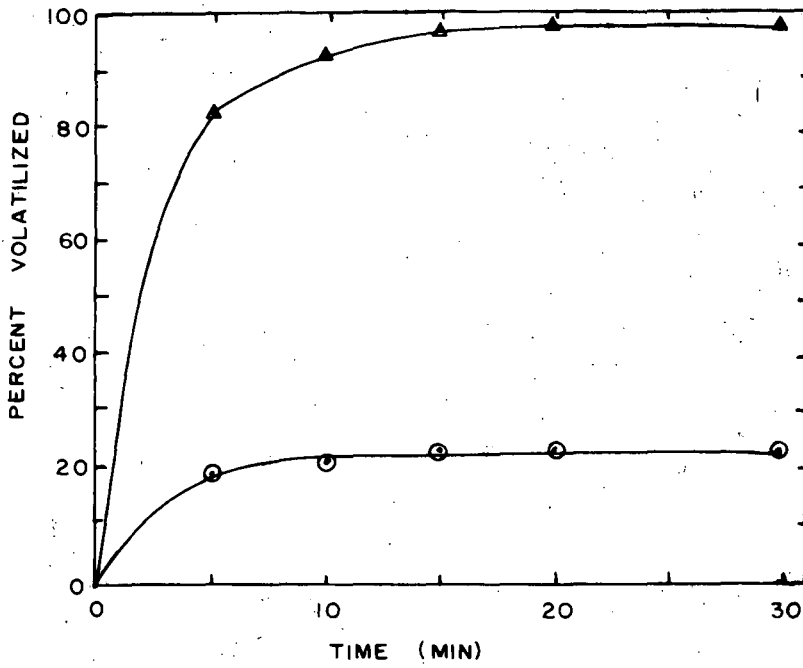


Fig. 5. Loss of sample weight,  $\Delta$ ; and loss of  $I^{131}$  tracer,  $\odot$ , during ashing of filter paper in an oxygen plasma.

Table II

## Recovery of Trace Elements from Ashed Filter Paper

<u>Tracer</u>	<u>Compound</u>	<u>Max. sample Temperature</u>	<u>Percent Recovered</u>	<u>Highest Oxidation State</u>	<u>Percent in Highest Oxidation State</u>
Fe <sup>59</sup>	Fe(OH) <sub>2</sub>	120	100	III	95
Fe <sup>59</sup>	Fe(OH) <sub>3</sub>	120	100	III	100
Se <sup>75</sup>	Na <sub>2</sub> SeO <sub>3</sub>	110	99	V	91
Se <sup>75</sup>	Na <sub>2</sub> SeO <sub>3</sub>	250	100	V	93
Se <sup>75</sup>	Na <sub>2</sub> SeO <sub>4</sub>	110	100	V	100
Se <sup>75</sup>	Na <sub>2</sub> SeO <sub>4</sub>	250	100	V	100
Ag <sup>110m</sup>	AgCl	110	89(99)*	I	--
Ag <sup>110m</sup>	AgCl	250	79(100)*	I	--
Os <sup>191</sup>	OsO <sub>2</sub>	120	<1	VIII	--
Os <sup>191</sup>	Na <sub>2</sub> OsO <sub>4</sub>	150	<1	VIII	--

\* Recovered after rinsing tube with HF-HNO<sub>3</sub>

The behavior of silver ion represents a different type of ashing loss. As opposed to the other metals in this study, only 75 to 90 per cent of the Ag<sup>110m</sup> could be recovered from the borosilicate sample holder by rinsing with dilute nitric acid. To recover the remainder of the Ag<sup>110m</sup>, the glassware had to be repeatedly rinsed with a warm mixture of nitric and hydrofluoric acids. By maintaining the system at low temperature this difficulty was ameliorated, but not eliminated.

**Conclusion:** A number of active species are known to be present in the luminous electrodeless discharge. Although a similarity between reactions in the plasma and those of discharged oxygen is noted, it cannot be concluded that within the plasma only the reactions of atomic oxygen are significant. The present study indicates appropriate conditions for the application of the electrodeless discharge to decompose carbonaceous materials prior to elemental analysis. Specifically, increasing sample temperature to 200-300°C leads to an improvement in ashing rate without appreciably increasing volatility losses.

## Acknowledgement

The electrical apparatus used in this study was constructed by James Breitmeier. The assistance of Juan Wong and Daniel Silvers is appreciated. Walter Holland, Harvey Beaudry and Robert Reinhart assisted in preliminary studies performed under a contract between Union Carbide Chemical Corporation and the Laboratory for Electronics. This study was supported by grants from the North Carolina Engineering Foundation and North Carolina State University Professional Development Fund.

## Literature Cited

1. Berkley, C., Churg, J., Selikoff, I. J., and Smith, W. E., Ann. New York Acad. Sci., 132, 48 (1965).
2. Blackwood, J. D., and McTaggart, F. K., Austral. J. Chem., 12, 114 (1959).
3. Gleit, C. E., Microchem. J., 10, 7 (1966).
4. Gleit, C. E., Benson, P. A., Holland, W. D., and Russell, I. J., Anal. Chem., 36, 2067 (1964).
5. Gleit, C. E., and Holland, W. D., Anal. Chem., 34, 1454 (1962).
6. Gluskoter, H. J., Fuel, 44, 285 (1965).
7. Greaves, J. C., and Linnett, J. W., Trans. Farad. Soc., 54, 1355 (1958).
8. Hennig, G. R., Dienes, G. J., and Kosiba, W., Proc. Second Intern. Conf. Peaceful Uses At. Energy, Geneva, 7, 301 (1958).
9. Hollahan, J. R., J. Chem. Educ., 43, A401, A497, 392 (1966).
10. Linnett, J. W., and Marsden, D. G. H., Proc. Roy. Soc. (London) Ser. A, 234, 489 (1956).
11. Marsh, H., O'Hair, T. E., and Wynne-Jones, W.F.K., Trans. Farad. Soc., 61, 274 (1965).
12. Mitin, R. V., and Pryadkin, K. K., Zh. Tekhn. Fiz., 35, 1205 (1965).
13. Thomas, R. S., J. Cell Biol., 23, 113 (1964).
14. Thomas, R. S., "Techniques of Electron Microscopy: Microincineration for the Fine Localization of Mineral Constituents" in "Subcellular Pathology" ed. by Steiner, J. W., Morat, H. Z., and Ritchie, A. C., Harper and Row, New York (in press).
15. Thompson, J. B., Proc. Phys. Soc. (London), 73, 818 (1959).
16. Turkevich, J., and Streznewski, T., Revue L'Inst. Fran. du Petrole, 13, 686 (1958).

## THE EFFECT OF CORONA ON THE REACTION OF CARBON MONOXIDE AND STEAM

T.C. Ruppel, P.F. Mossbauer, and D. Bienstock

U.S. Department of the Interior, Bureau of Mines,  
Pittsburgh Coal Research Center, Pittsburgh, Pa.

## SUMMARY

The water-gas shift reaction was chosen for study in a corona discharge with the aim of establishing the important variables associated with the production of hydrogen.

The reaction was carried out in a quartz Siemen's type ozonizer having an electrode length of 12 inches and an electrode separation of 8 mm. The electrodes consisted of fired-silver paint--one electrode coating the inside of the inner (high voltage) tube, and the other coating the outside of the outer (ground) tube.

The reaction was studied by means of a four-factor, two-level, factorially designed set of experiments. This consisted of input power levels of 60 and 90 watts, pressures of  $\frac{1}{2}$  and 1 atmosphere, hourly space velocities of 200 and 800, and reactor temperatures of 127 and 527°C (400 and 800°K). Although voltage was not a factor, the voltage ranged from 3100 to 11,000 rms volts.

The prediction equation resulting from the statistical analysis of the data indicates that more hydrogen is produced at higher pressures, temperatures, and power inputs, and lower space velocities. Practically no hydrogen is produced in the absence of a discharge, regardless of the values of space velocity, temperature, pressure, or power dissipated.

The highest yield of hydrogen within the factorial region studied was 4.5 percent. An extra-factorial region, which was indicated by the prediction equation to be fruitful, was explored and 11.5 percent hydrogen was obtained.

It was found that the water-gas shift reaction in a corona discharge is kinetically, rather than thermodynamically controlled.

## INTRODUCTION

Novel techniques are being investigated at the Bureau of Mines to introduce energy into coal and coal products in an effort to find new uses for coal. One technique under study involves chemical reactions in a corona discharge. Initially the gas-phase reaction of carbon monoxide and steam to produce carbon dioxide and hydrogen will be investigated.

The immediate aim of this study is to establish the important variables associated with the production of hydrogen in the water-gas shift reaction in the presence of a corona discharge. A more general goal is to determine the dependence of product yield on the important variables in a corona discharge for several gas-phase reactions. As knowledge is gained on the effect of corona discharge in chemical reactions, more complex reactions involving coal and its products will be studied.

The water-gas shift reaction, which is usually carried out industrially over an  $\text{Fe}_2\text{O}_3\text{-Cr}_2\text{O}_3$  catalyst at 300-500°C and 100-300 psig, has been discussed at great length in the literature. Summary articles are available.<sup>1-4</sup> It is almost certainly a surface reaction<sup>5</sup> as opposed to the apparent homogeneous nature of the reaction in the corona discharge. Experiments with the quartz Siemen's type ozonizer to be described have shown that no reaction occurs between water and carbon monoxide at

600°C and 1 atmosphere pressure in the absence of a corona. This suggests that the reaction is homogeneous when it does occur with a corona. That is, the reactor walls probably do not enter into the reaction by acting as a catalyst or as a third body.

The physics<sup>6-8</sup> and chemistry<sup>9-11</sup> of corona discharge have been surveyed by several authors. A bibliography of chemical reactions in electrical discharges over a thirty-year period, 1920-1950, has been compiled.<sup>12</sup>

#### PROCEDURE

The corona discharge unit is shown in figure 1. The operational scheme can be seen in the flow diagram, figure 2. Carbon monoxide from a compressed gas cylinder (1) is passed through an activated carbon adsorption trap (5). The metered flow (7) passes through a flow control valve (9); a second stream of gas may be blended here if desired. The carbon monoxide at the pressure of the system passes through a steam generator (11). The thermocouple immediately above the reflux condenser (17) controls the steam flow rate via a time-proportionating temperature controller (not shown). The carbon monoxide and water flow rates may be individually varied between 0.2 and 3 ft.<sup>3</sup>/hr. by adjusting the flow controller (9) and temperature controller settings. The carbon monoxide-steam mixture then enters the Siemen's-type reactor through preheaters (18) and (21). The reactor is enclosed in a tube furnace (23). The product gases pass through a series of three cold traps (25, one shown) at -80°C. Bypass cold traps (26) are available if required. The non-condensable gases pass through a sample train (28,29) and then through a flow meter (30) which is at system pressure. On leaving the flow meter the non-condensable gases pass through the system-pressure regulator (32), vacuum pump (34), and finally a wet test meter (35). The system is designed to operate from 0.5 to 2.0 atmospheres.

The Siemen's type reactor, shown in figures 3 and 4, consists of two concentric quartz tubes, 45 and 33 mm. OD, having a 4 mm. annular space. The electrode length is 12 inches and there is an 8 mm. electrode-to-electrode separation. The electrodes consist of fired-silver paint--one electrode coating the inside of the inner (high voltage) quartz tube, and the other coating the outside of the outer (ground) tube. Tungsten (or optionally copper) wires are attached to the outside and inside of the reactor with two or three coatings of fired-silver paint. The capacitance of the reactor was measured as 86-89 pfd using an impedance bridge.

The average wall temperature was used as a measure of the temperature of the system. Three thermocouples were equally spaced vertically along the inside wall of the reactor (fig. 2) and three along the outside wall. The inside wall thermocouples were at the corona potential and thus were isolated from ground. A millivoltmeter was connected in series to each of the inside wall couples, and thus was similarly "floated". To simplify the electrically hot thermocouple circuits, no compensating ice junction was included; the room temperature correction was added to each millivoltmeter reading. The corona potential had a positive effect on the millivoltmeter readings in the hot circuit. Therefore the millivoltmeters were read before the corona potential was impressed on the system. The system temperature was taken as the average of all six thermocouple measurements.

The study was made according to a factorially designed set of experiments to determine the effect of pressure, space velocity, temperature, and input electrical power on the yield of hydrogen.

This was a four factor, two level set of experiments as shown in Table 1.

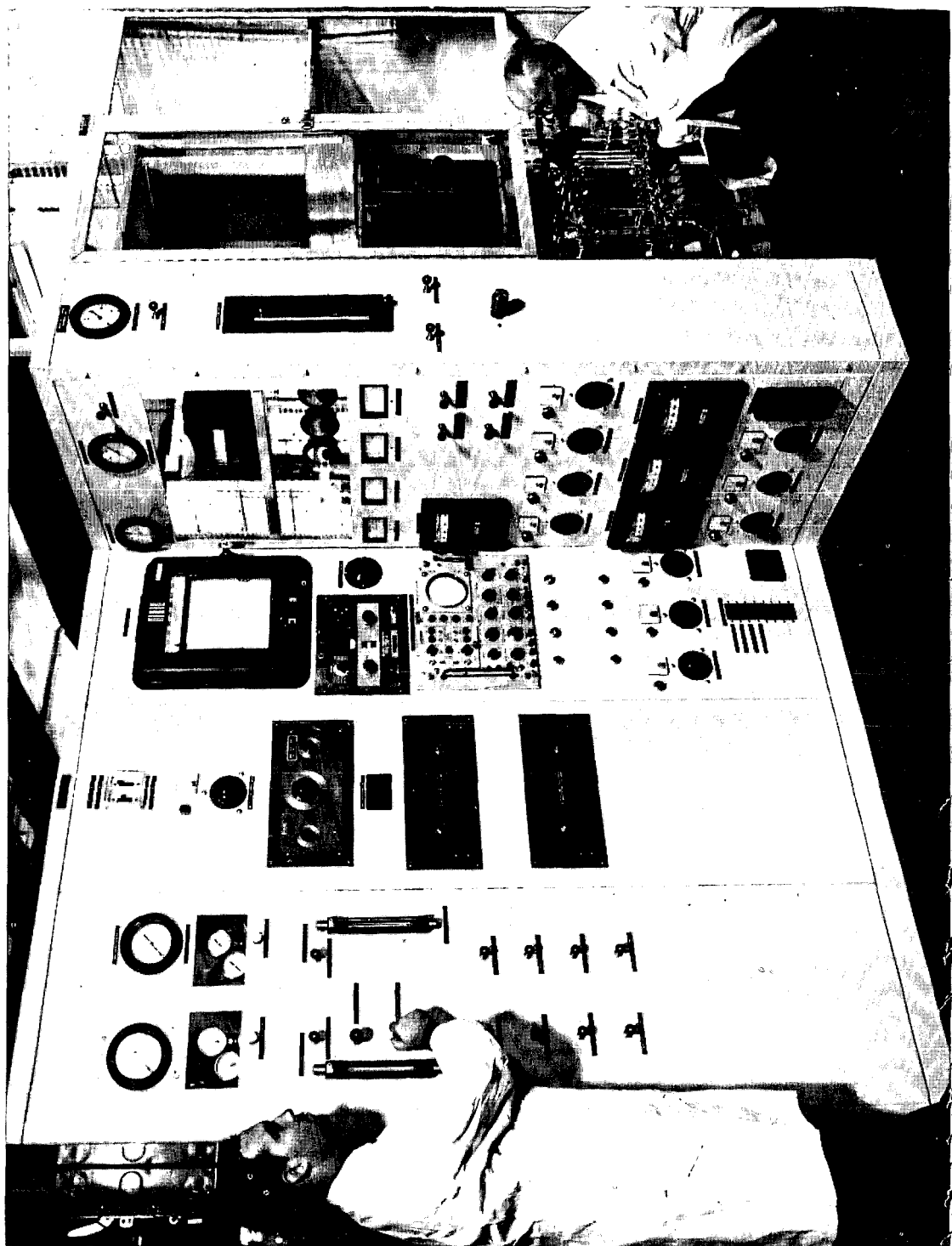
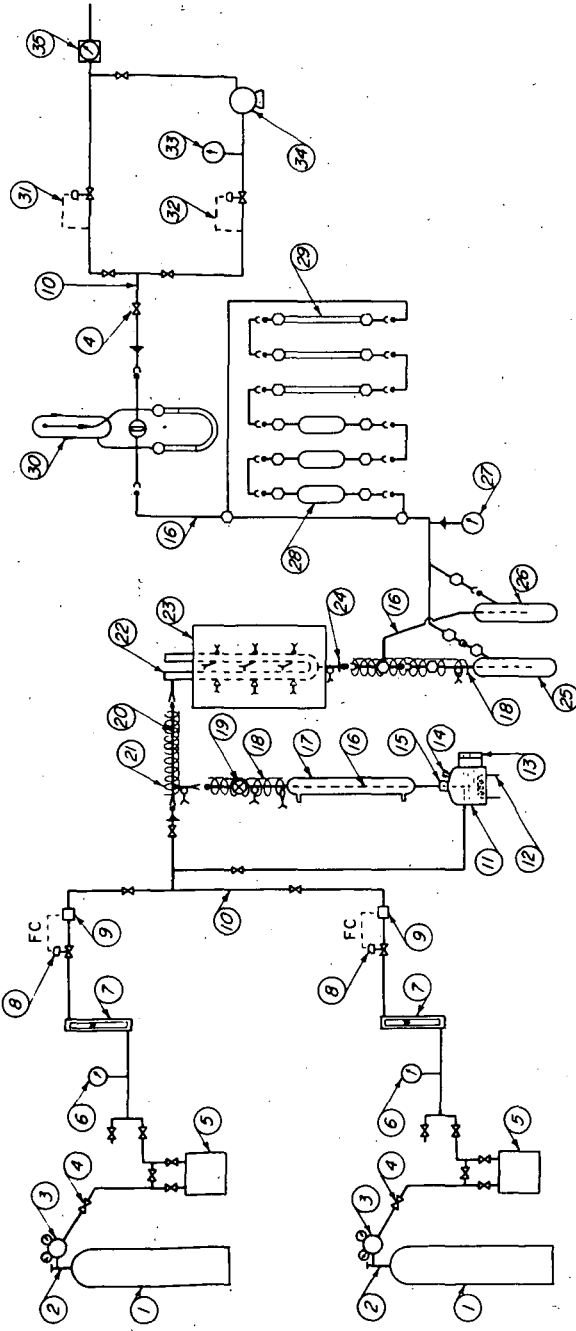


Figure 1.- Unit for studying chemical reactions in a corona discharge.



- (1) FEED GAS (2)
- (2) VALVES (2)
- (3) REDUCING REGULATORS (2)
- (4) VALVES, 1/8 IN. BALLS, ALLOY STEEL TIPPED STEEL, MAKE NO. 2611538 (24)
- (5) ACTIVATED CARBON TRAP, FOR HYDROGEN GAS USE ONLY (2)
- (6) GAUGES, 0-30 PSIG, AIRCRAFT DISBURGANCE (2)
- (7) FLOWMETER, 0.1-1.5 SCFM, WITH INTERCHANGIBLE TUBES, FISCOR & PONTRE NO. 104333A (2)
- (8) VALVES, 1/8 IN. BALLS, BRASS, MAKE NO. 262266 (2)
- (9) FLOW CONTROLLERS, 0.015-11 SCFM, MODEL NO. 6380-L (2)
- (10) TUBING, SOFT COPPER, 1/4 IN.
- (11) STEAM GENERATOR
- (12) INTERNAL WATER HEATER
- (13) DISTILLED WATER LEVEL SIGHT GLASS
- (14) WATER FILLER CAP
- (15) O-RING COMPRESSION SEAL
- (16) TUBING, PEXEL, 7 MM.
- (17) REFLECT CONDENSER, FOR CONDENSAT TEMPERATURE OIL CIRCULATOR
- (18) HEATING TAPS, ELECTRICAL (2)
- (19) STYROFOAM, BALL, PEXEL, WITH TEFLOM O-RINGS, SIZE 1275, WEST NO. W-1531-T (20)
- (20) JOINT, BALL, VITON, SIZE 1275, CORNING NO. 18762
- (21) JOINTS, SOCKET, PEXEL, SIZE 1275, WEST NO. W-1540 (18)
- (22) JOINTS, SOCKET, VITON, SIZE 1275, CORNING NO. 18764 (1)
- (23) SEALS, PEXEL-SEALS (3)
- (24) STYROFOAM, NONSILICATE GLASS, 3 MM DIAM., 3 MAT, EXCEL-CELLO NO. 3035 (3)
- (25) STYROFOAM, NONSILICATE GLASS, 3 MM DIAM., 3 MAT, EXCEL-CELLO NO. 3000 (16)
- (26) THERMOCOUPLES, TO FEEDING MILLIVOLTMETER NO. 1 (3)
- (27) THERMOCOUPLES, TO FEEDING MILLIVOLTMETER NO. 2 (2)
- (28) THERMOCOUPLES, FOR INTERNAL WATER HEATER CONTROL (2)
- (29) THERMOCOUPLES, FOR INTERNAL WATER HEATER CONTROL (2)
- (30) THERMOCOUPLES, TO MULTIPROUT RECORDER (5)
- (31) TUBING, VITON, 7 MM.
- (32) CORONA CELL, QUARTZ, QUANT SCIENTIFIC CO., LANSING, MICH
- (33) FERRULE, CONDUCTION TUBE TYPE, WIPAC, 2 ELEMENT, 25-1000°C. ELECTRO-APPLICATIONS, INC., WASHINGTON, PA.
- (34) SEAL, BRASS, QUARTZ-PEXEL
- (35) COLD TRAP
- (36) BYPASS COLD TRAP
- (37) GAUGE, 30 IN. HG VACUUM TO 15 PSIG, AIRCRAFT DISBURGANCE
- (38) GAS SAMPLING TUBES, 250 CC, FISCOR NO. 10-235 (1)
- (39) GAS SAMPLING TUBES, 10 CC, 3 MM I.D., PEXEL TUBING (3)
- (40) FLOWMETER, PEXEL, CAPILLARY-TYPE, FOR 0.1-5 CFM AT 15 IN. HG VACUUM
- (41) REGULATORS, PRESSURE, 0-15 PSIG, MODIFIED CONDUON
- (42) REGULATORS, VACUUM, 1-30 IN. HG CONDUON NO. V10
- (43) GAUGE, 0-30 IN. HG VACUUM, AIRCRAFT DISBURGANCE
- (44) PUMP, VACUUM, 0-25 IN. HG, EXPUSION PUMP MOTOR, ALIGHT CHURCH, UNCOMPENSATED GAUGE
- (45) METER, NET TEST, 0.1 CU.FT. PER REVOLUTION, 0.1-20 SCFM, AMERICAN METER CO.

Figure 2.- Flow diagram for corona discharge.

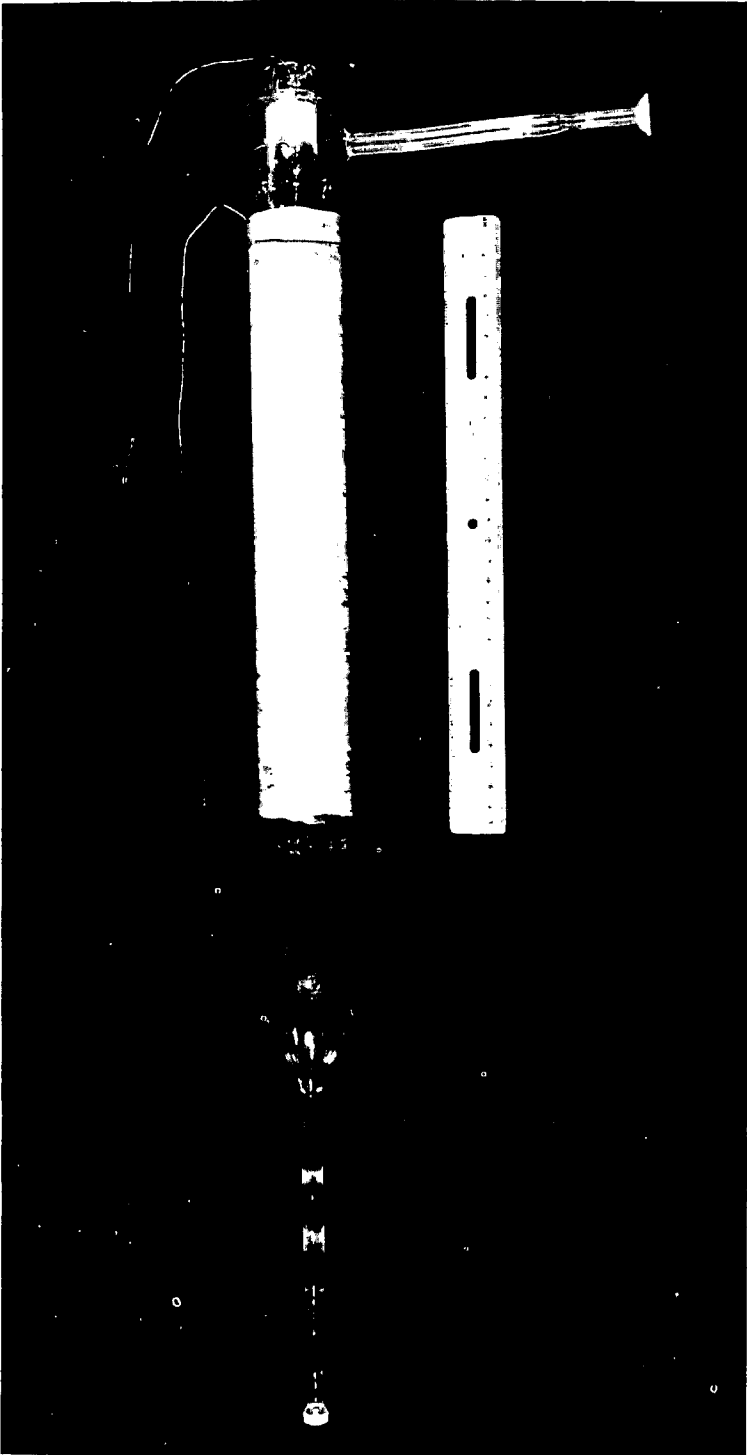


Figure 3.- Siemen's type reactor.

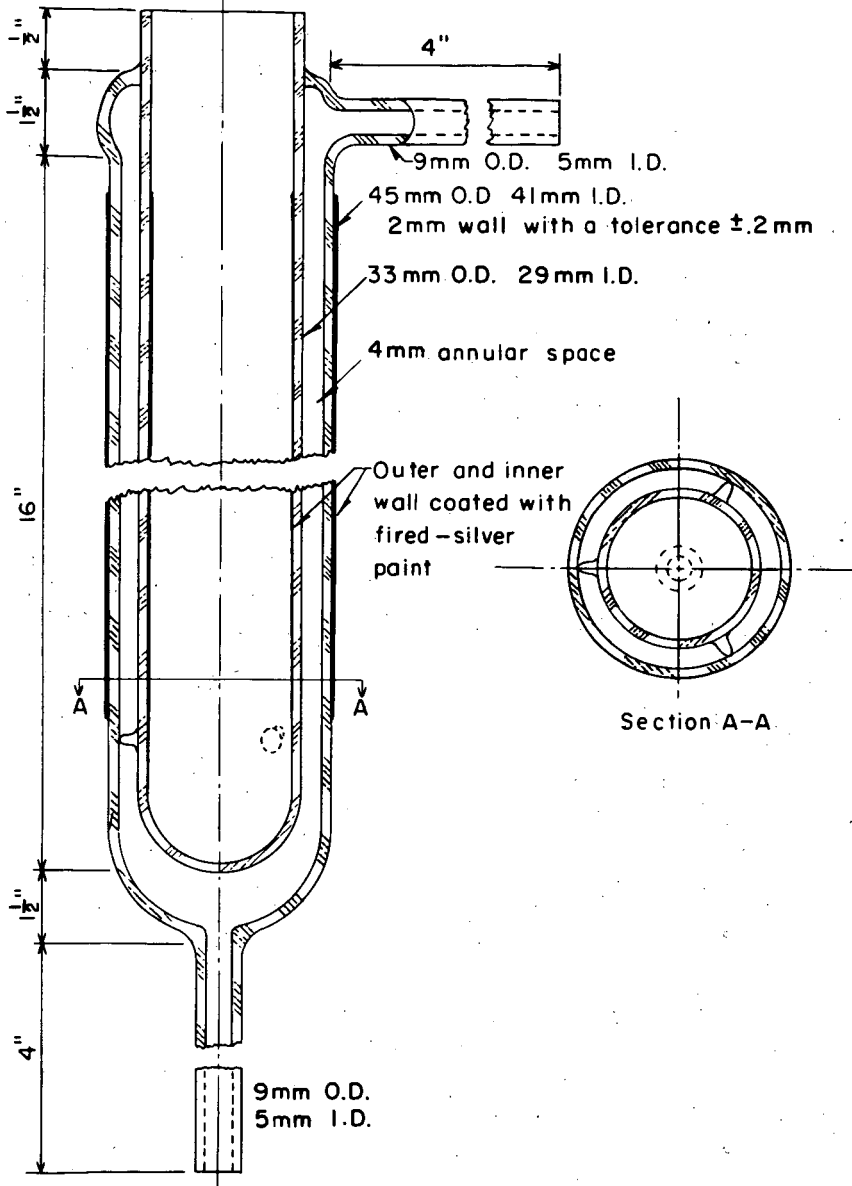


Figure 4. Siemen's type reactor.

Table 1.- Factorial design of the experiments

2 level, 4 factor, full factorial

 $2^4 = 16$  experiments1:1 molar mixture, H<sub>2</sub>:CO

Factor	Level	
	Low	High
Pressure, atm.	0.5	1.0
Space velocity, hr. <sup>-1</sup>	200	800
Temperature, °K	400	800
Input power, watts	60	90

It was found that no hydrogen was produced in the absence of a discharge, no matter what the potential impressed on the high voltage electrode. Thus Paschen's law curves, discharge-initiating potential vs. the product of pressure and electrode separation, were developed for the reactor. These are shown in figure 5. A second reactor with 12 mm. electrode separation was also used to obtain these curves.

Initially it was intended to factorialize secondary voltage, rather than input power. However, it was not possible to factorialize voltage (set a high and low level) without losing the discharge at low temperatures or drawing too high a current at high temperatures. At high currents the arc would puncture the quartz reactor. Maintaining a discharge in some cases and not others would introduce a very significant unfactorialized (uncontrolled) qualitative variable, discharge vs. no discharge, into the design. While it might be possible to factorialize discharge vs. no discharge, it was known that no hydrogen would be produced with no discharge, regardless of the power level.

Input power was factorialized since the voltage and amperage required for a chosen power level are determined by the discharge and therefore need not meet set requirements of a factorial design.

Although the voltage was not a factor, the voltage ranged from 3100 to 11,000 rms volts.

The above factors were chosen intuitively. Other factors, such as AC frequency, distance between reactor electrodes, and electrical current, may also have an effect. Future experiments using a frequency of 10,000 cps are planned to detect any frequency effect on hydrogen production.

The factorial design form of experimentation has the advantages of 1) obtaining an empirical regression equation with minimum effort, 2) isolating the magnitudes of the effects of each variable and its interaction with other variables (synergism) on the dependent variable, 3) allowing optimization of the dependent variable within the levels of the factors studied, and 4) suggesting the direction to be taken outside the region studied for further optimization.

After the desired carbon monoxide and steam flow rates were obtained and stabilized at  $\frac{1}{2}$  or 1 atmosphere, the discharge was initiated. It was monitored with an oscilloscope (Tektronix Model RM 35A), typical oscillographs of which are shown in figure 6. The waveforms on the left show the voltage trace above the current trace. The area enclosed by the Lissajous figure on the right is a measure of the true power used by the discharge.

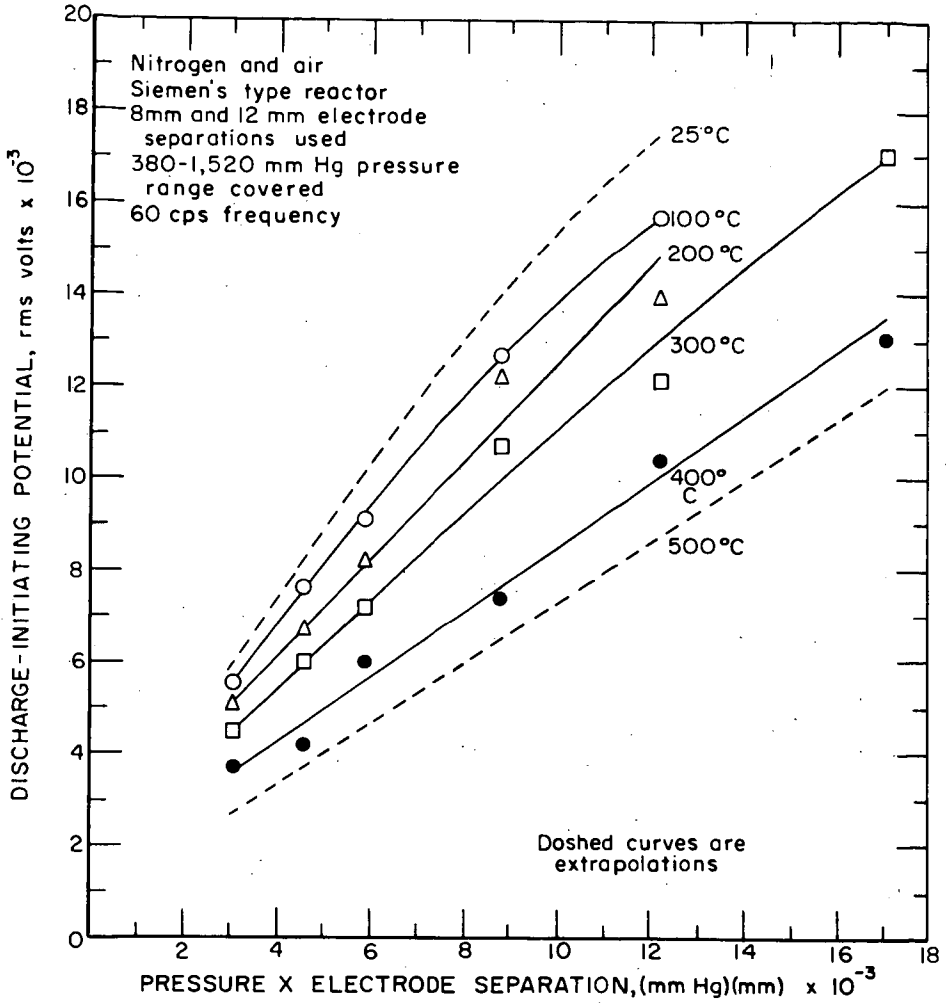
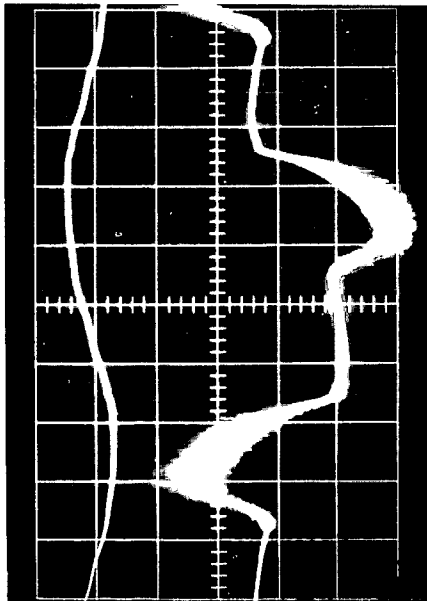
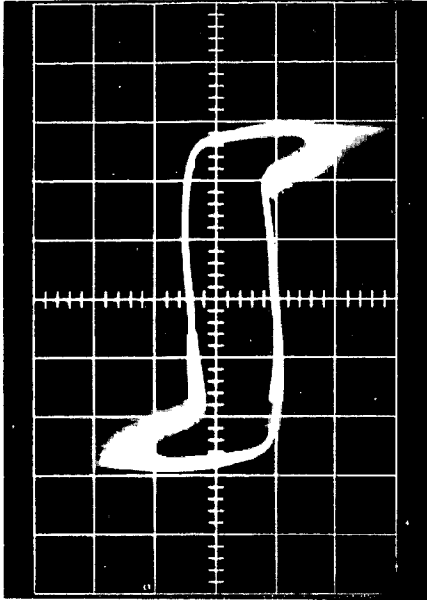


Figure 5.—Paschen's law curves.

2-15-67



Voltage (above) and current waveforms



Lissajous figure

Figure 6.- Typical oscillographs of same corona discharge.

The water-free product gases were analyzed by gas chromatography. However the hydrogen yields are reported with water present.

### RESULTS AND DISCUSSION

The data were analyzed according to the linear hypothesis statistical model resulting in the following empirical prediction equation for the percent hydrogen (water included):

$$\begin{aligned} \text{Pct. H}_2 = & -1.885 \pm 0.762 - (1.946 \pm 0.499)P + (0.00402 \pm 0.00042)SV \\ & + (0.00486 \pm 0.00121)T - (0.0106 \pm 0.00830)W \\ & + (0.00470 \pm 0.000791)(P \cdot T) - (0.0000103 \pm 0.0000006)(T \cdot SV) \\ & + (0.0000288 \pm 0.0000132)(T \cdot W) \end{aligned}$$

where P = pressure, atmospheres  
SV = space velocity, hr.<sup>-1</sup>  
T = temperature, °K  
W = input power, watts.

An inspection of the terms in the equation, after numerical values are inserted, shows that temperature has the largest effect on the production of hydrogen, with space velocity being the least important.

The coefficient with the largest error associated with it is in the input power term. Since the factorial levels were maintained quite closely, the inference which can be drawn is that the yield of hydrogen tends to be least correlatable with input power. The reverse is also true, that hydrogen production tends to correlate best with the interaction term T·SV.

The coefficients were determined with an IBM 7090 digital computer available at the University of Pittsburgh, using a program for a regression equation previously developed by Bureau personnel.

According to the equation, maximum production of hydrogen, within the range studied, was found to be at 1 atmosphere, 200 hourly space velocity, 800°K, and 90 watts input. At these levels the percentage of hydrogen was 4.5, compared with the figure 4.1 calculated by the equation. The extra-factorial region of interest suggested by the equation would be higher pressures, temperatures, and inputs, and lower space velocities. Within the limitations of our equipment, and operating on a flow basis, this was P=2, SV=100, T=800, and W=100. The hydrogen percentage increased to 8.6. By stopping the gas flow, 11.6% H<sub>2</sub> was obtained in the product.

Extrapolating an empirical equation is always dangerous. There is no guarantee that an indicated extra-factorial region will yield good results. In the present case, the extra-factorial region proved to be more fruitful than predicted. The advantage of an empirical equation is the ease in which it is obtained while representing the data well in a compact form within the region in which the data were taken.

If one could define the reaction temperature in a corona discharge, it would be possible to discuss the thermodynamics of the system. However it is difficult, if not impossible, to define an equilibrium with respect to the corona reaction. While there are methods available for obtaining measurements of the average (translational) temperature of the gas or plasma, there is a valid question as to the "local temperature" at the reaction site of the activated species. However it was attempted in this study to correlate the average wall temperature of the system with hydrogen production and thus to define the system sufficiently for design purposes. The prediction equation strongly indicates that this approach is satisfactory.

The decrease in equilibrium constant of the water-gas-shift reaction with temperature is shown in figure 7. As the prediction equation indicates a positive temperature effect on the production of hydrogen, the water-gas-shift reaction in an electrical discharge must be kinetically rather than thermodynamically controlled.

The yields of hydrogen shown here are less than the yields achieved industrially<sup>13</sup> by catalytic means. What is of more interest to us is the empirical determination, for several reactions, of the functional dependence of the yield of a given product on the several independent variables in a corona discharge. This information is a prelude to future experiments where powdered coal or coal volatiles will be treated with certain gases in a corona discharge.

#### CONCLUSIONS

The conclusions that can be drawn from this study are:

- (1) No hydrogen is produced in the absence of a discharge, regardless of the values of space velocity, pressure, temperature, or power dissipated.
- (2) The prediction equation arising from the statistical analysis of the data indicates that more hydrogen is produced at higher pressures, temperatures, and power inputs, and lower space velocities.
- (3) Within the range of variables studied, temperature has the largest relative effect on the production of hydrogen, while space velocity has the least relative effect.
- (4) Of the four factors chosen, input power is the least correlatable with the production of hydrogen, while the first order interaction: (temperature) X (space velocity) is the most correlatable.
- (5) The water-gas-shift reaction in a corona discharge is kinetically, rather than thermodynamically controlled.

#### REFERENCES

1. Morgan, J.J. Water Gas. Ch. in Chemistry of Coal Utilization. Vol. 2, H.H. Lowry, ed., John Wiley & Sons, Inc., New York, N.Y., 1945.
2. Fredersdorff, C.G. von, and M.A. Elliott. Coal Gasification. Ch. in Chemistry of Coal Utilization, Supplementary Volume, H.H. Lowry, ed., John Wiley & Sons, Inc., New York, N.Y., 1963.
3. Blackwood, J.D. Kinetics of Carbon Gasification. *Ind. Chem.* 36, 55-60, 129-133, 171-175 (1960).
4. Sherwood, P.W. Water Gas Conversion. *Petroleum (London)* 24, 338-340 (1961).
5. Reference 1, p. 1704.
6. Loeb, L.B. Electrical Coronas, Their Basic Physical Mechanisms, Univ. of Calif. Press, Berkeley & Los Angeles, 1965, 694 pp.
7. Brown, S.C. Basic Data of Plasma Physics, Mass. Inst. of Tech. and John Wiley & Sons, Inc., New York, N.Y., 1959, pp. 258-273.
8. Meek, J.M., and J.D. Craggs. Electrical Breakdown in Gases. Oxford Univ. Press, 1953, pp. 148-176.

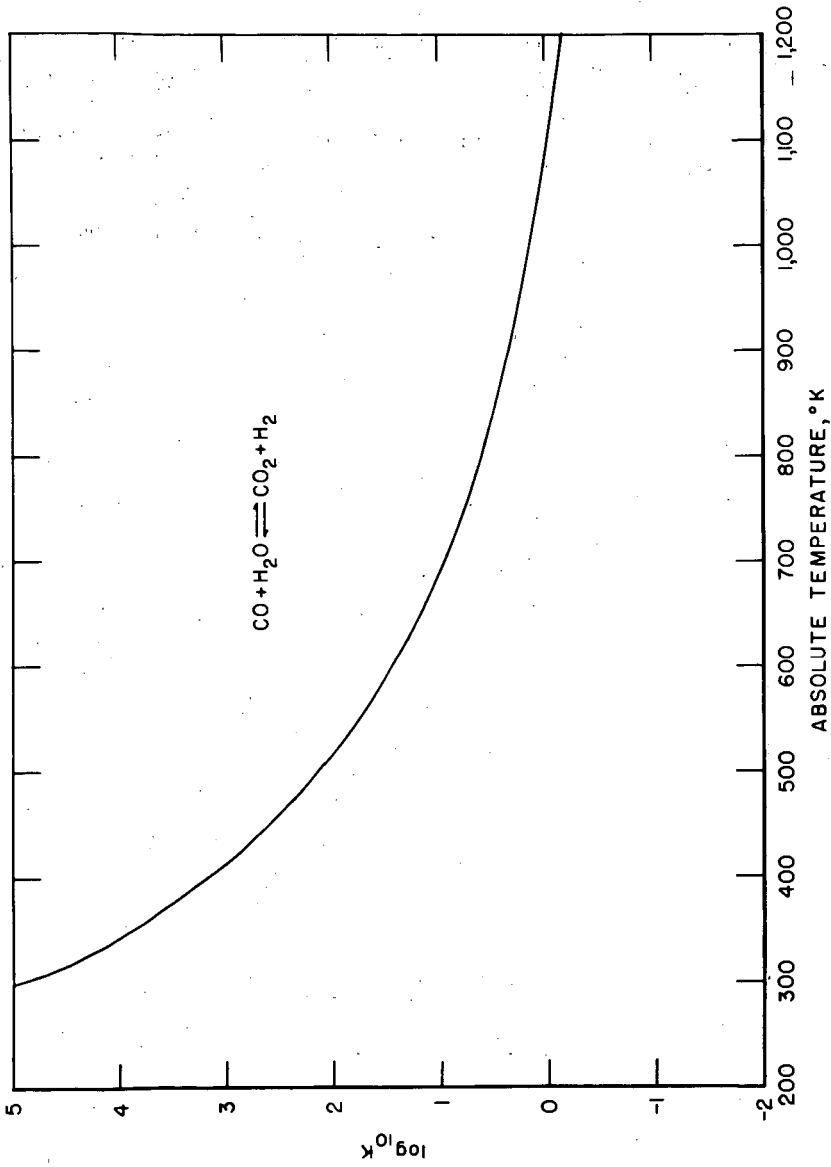


Figure 7. Change in equilibrium constant of the water-gas shift reaction with temperature.

9. Glockler, G., and S.C. Lind. *The Electrochemistry of Gases and Other Dielectrics*, John Wiley & Sons, Inc., New York, N.Y., 1939.
10. Thomas, C.L., G. Egloff, and J.C. Morrell. Reactions of Hydrocarbons in Electrical Discharges. *Chem. Rev.* 28, No. 1, 1-70 (1940).
11. Jolly, W.L. The Use of Electrical Discharges in Chemical Syntheses. Ch. in *Technique of Inorganic Chemistry*, ed. by H.B. Jonassen and A. Weissberger, v. 1, Interscience Div. of John Wiley & Sons, Inc., New York, N.Y., 1963, pp. 179-208.
12. Akerlof, G.C., and E. Wills. Bibliography of Chemical Reactions in Electric Discharges, Aug. 1951, Office of Technical Services, Dept. of Commerce, Washington, D.C.
13. Christain, D.C., and P.B. Boyd, Jr. What to Look for in CO Conversion Catalysts. *Chem. Eng.* 56, No. 5, 148-150 (1949).

## SOME PROBLEMS OF THE KINETICS OF DISCHARGE REACTIONS

Robert Lunt

Department of Physics  
University College, London

This essay is concerned with the kinetics of reactions in electrical discharges through gases that are either effected by, or initiated by, the charged particles present in the gas.

The principal experimental investigations on the kinetics of such reactions which have led to the development of the statistical theory of discharge reaction are recalled briefly before stating some elaborations of the formal analysis that are now seen to be pertinent and which have not been summarized hitherto.

The present state of the theory is then illuminated by outlining some examples of:

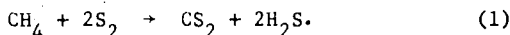
- (1) the achievements of the theory in providing a detailed and quantitative interpretation of the values found from experiment for the empirical reaction rate coefficients considered as functions of the discharge parameters,
- (2) the apparent inadequacy of the theory to account for the results of experiment in two gases, and
- (3) the lacunae in the experimental data hitherto available that impede the interpretation of the data in terms of statistical theory: the recognition of these lacunae may pave the way to the better design of experiment and to a more precise understanding of the mechanism of discharge reaction and of the usefulness of electrical discharges in chemical and in electrical engineering.

## The Plasma Induced Reaction of Hydrogen Sulfide with Hydrocarbons

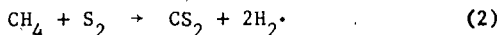
F. J. Vastola and W. O. Stacy

Department of Fuel Science  
The Pennsylvania State University, University Park, Pa.Introduction

The interaction of sulfur with hydrocarbons under a range of experimental conditions has been investigated by various workers. Knight and co-workers<sup>1</sup> reacted excited sulfur atoms, produced by 'in situ' photolysis of COS at 250°C, with a range of paraffinic hydrocarbons and found as primary products only the corresponding mercaptans. Bryce and Hinselwood<sup>2</sup> studied the reaction of sulfur vapor with paraffinic hydrocarbons in the temperature range 320°C to 349°C and observed that the primary products were hydrogen sulfide and unsaturated hydrocarbons. Study of the reaction of sulfur and methane<sup>3-7</sup> over a catalyst at 500°C to 700°C has shown the products to be carbon disulfide and hydrogen sulfide according to the reaction



Thomas and Strickland-Constable<sup>8</sup> studied the interaction of sulfur and hydrocarbons at temperatures 1200°K to 1500°K and in the absence of a catalyst observed no carbon disulfide formation. With a catalyst, however, the reaction proceeded yielding carbon disulfide, hydrogen sulfide, and hydrogen; reactions similar to (1) for methane, above 1200°K, being increasingly superseded by those similar to (2):



Reported now are some results of a study of the reactions of excited atomic species, generated by the dissociation of hydrogen sulfide in a plasma jet, with methane and neopentane.

This study was suggested by an earlier investigation of Vastola and co-workers<sup>9</sup> into the reaction between carbon and the products of water vapor microwave discharge, where it was observed that the presence of carbon downstream inhibited the recombination, to either oxygen or water, of the active atomic species. Instead, the active oxygen reacted preferentially with carbon.

Experimental Procedure

The plasma reactor is shown in Figure 1. The reactor consists of a 10 x 0.75 inch fused quartz tube. The gas to be brought to the plasma state is introduced tangentially upstream from the output coil of a 1.2 KW, 120 MHz RF induction heater. The spiraling motion imparted by the tangential input increases the dwell time of the gas in the plasma zone. The hydrocarbon gases to be reacted with the plasma dissociation products are introduced down stream from the plasma flame. By moving the hydrocarbon feed tube the distance between the plasma flame and the point of hydrocarbon introduction can be varied.

To initiate the plasma discharge argon is passed through the reactor (0.5 cu ft/hr, 1 Atm) and a graphite rod is placed in the induction field. After the heated graphite rod starts the discharge it is removed and the gas feed is switched to the desired H<sub>2</sub>S-Ar mixture. Mass spectrometric gas analyses were made before and after the reaction.

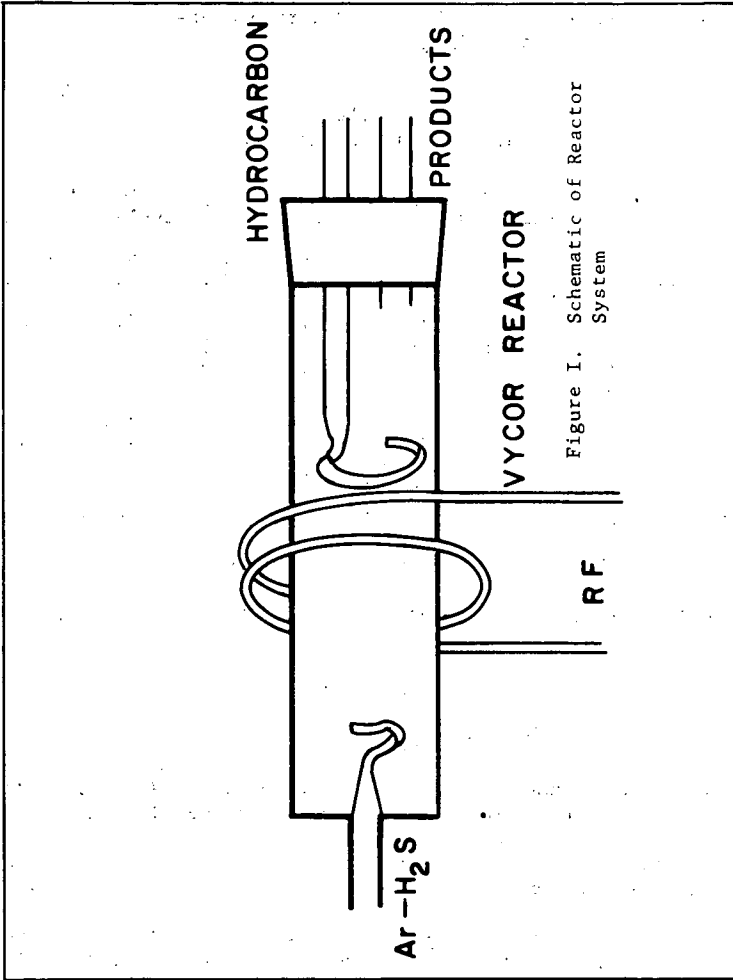


Figure I. Schematic of Reactor System

Results and Discussion

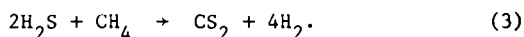
When hydrogen sulfide is introduced into an argon plasma condensing elemental sulfur produces a dense fog downstream from the plasma flame. As the amount of hydrocarbon that is introduced into this region is increased the elemental sulfur production decreases to a point where it can no longer be observed. With large excesses of hydrocarbon the color of the plasma flame changes from blue to orange due to back diffusion of the hydrocarbon.

Table 1 gives the reactant and product concentrations for reactions of dissociated hydrogen sulfide with methane and neopentane. With the exception of run number 3 the only gaseous products detected were hydrogen sulfide, unreacted hydrocarbon, carbon disulfide, and hydrogen.

Table 1  
Reactant and Product Analyses

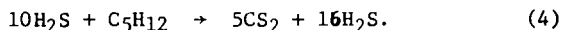
Run No.	Reactants	Reactant Mixture Composition Mole %			Products Composition Mole %					
		HC	H <sub>2</sub> S	Ar	HC	H <sub>2</sub> S	H <sub>2</sub>	CS <sub>2</sub>	C <sub>2</sub> H <sub>2</sub>	Ar
1	H <sub>2</sub> S, CH <sub>4</sub>	6.4	17.6	76.5	2.2	4.5	18.5	3.8	0	70.1
2	"	6.4	17.6	76.5	4.3	6.7	13.4	1.6	0	71.1
3	"	25.5	9.9	64.7	13.0	1.3	21.9	3.5	3.0	57.8
4	H <sub>2</sub> S, C <sub>5</sub> H <sub>12</sub>	15.3	14.9	70.2	11.0	0.7	18.1	3.9	0	69.7
5	"	15.3	14.9	70.2	13.4	4.8	12.9	2.8	0	70.0

The following stoichiometry would be expected for the reaction of methane:



In run number 3 the acetylene was produced by the back diffusion of methane into the plasma region.

The stoichiometry for the neopentane reaction would be



The reactions of neopentane were performed with a large excess of hydrocarbon with the hope of detecting sulfur insertion compounds or reaction intermediates. However, hydrogen and carbon disulfide were the only gaseous species produced. This indicates that once the neopentane reacts with one sulfur atom its resistance to further reaction is lowered.

Table 2 shows the variation of reactant decomposition with changes of hydrogen sulfide to hydrocarbon flow ratio and plasma-hydrocarbon injection distance. From Table 2 it can be seen that the extent of hydrogen sulfide decomposition is a function of the amount of hydrocarbon present downstream from the plasma flame and the distance from the flame that the hydrocarbon is introduced, the highest decomposition, 95 per cent, occurring in run number 4 with an approximately ten fold excess of neopentane introduced 1/4 inch from the flame. The figures for the decomposition of hydrogen sulfide tend to be misleading, the hydrocarbon addition does not change the degree of dissociation of the hydrogen sulfide but rather it reacts with the atomic sulfur minimizing formation of hydrogen sulfide by the recombination of the

Table 2  
Experimental Variables and Reaction Conversion Efficiencies

Run No.	Reactants	Flow rate (total) c. f. h. *	H <sub>2</sub> S/HC	HC inlet distance from plasma inches	Reactant decomposition		Conversion of decomposed reactants to:		
					H <sub>2</sub> S %	HC %	CS <sub>2</sub>		H <sub>2</sub>
							H <sub>2</sub> S %	HC %	H <sub>2</sub> S + HC %
1	H <sub>2</sub> S, CH <sub>4</sub>	0.14	2.75	1/4	72	63	65	~100	~100
2	"	0.14	2.75	1	59	28	33	~100	~100
3	"	0.33	0.39	1/4	85	43	93	36	81
4	H <sub>2</sub> S, C <sub>5</sub> H <sub>12</sub>	0.25	1.03	1/4	95	28	55	19	46
5	"	0.25	1.03	1	68	12	56	30	61

\* cu ft/hr.

atomic hydrogen and sulfur. The data on extent of conversion to hydrogen and carbon disulfide in Table 2 show that in runs 1 and 2 essentially all of the carbon from the decomposed methane is converted into carbon disulfide and the hydrogen into molecular hydrogen. In run number 3 the acetylene produced accounts for the missing carbon and hydrogen. In runs number 4 and 5 a large fraction of the neopentane that was decomposed was converted into a solid product.

Table 2 also shows the percentage of the sulfur, resulting from the decomposition of the hydrogen sulfide, that is converted into carbon disulfide; the remainder of the sulfur appears as elemental sulfur (runs 1-3) or can be incorporated with the carbon-hydrogen polymeric solid that is produced in the runs using neopentane.

These results indicate that hydrogen sulfide can be completely dissociated by an electric discharge and the excited atomic hydrogen and sulfur generated can be reacted with hydrocarbons to produce molecular hydrogen and carbon disulfide. Under conditions which minimize back diffusion of the hydrocarbon into the electric discharge substantially complete conversion of the hydrogen sulfide and hydrocarbon to hydrogen and carbon disulfide can be effected.

#### References

1. Knight, A. R., Strausz, O. P. and Gunning, H. E., J. Am. Chem. Soc. 85, 2349, (1963).
2. Bryce, W. A. and Hinshelwood, C., J. Chem. Soc. 4, 3379, (1949).
3. Nabor, G. W. and Smith, J. M., Ind. Eng. Chem. 45, 1272, (1953).
4. Thacker, C. M. and Miller, E., Ind. Eng. Chem. 36, 182, (1944).
5. Folkins, H. O., Miller, E. and Hennig, H., Ind. Eng. Chem. 42, 2201, (1950).
6. Fisher, R. A. and Smith, J. M., Ind. Eng. Chem. 42, 704, (1950).
7. Forney, R. C. and Smith, J. M., Ind. Eng. Chem. 43, 1841, (1951).
8. Thomas, W. J. and Strickland-Constable, R. F., Trans. Farad. Soc. 53, 972, (1957).
9. Vastola, F. J., Walker, P. L., Jr. and Wightman, J. T., Carbon 1, 11, (1963).

Competition of Ethylene and Propane for  
"Active" Nitrogen<sup>1</sup>

by P. Terence Hinde and Norman N. Lichtin

Dept. of Chemistry, Boston University, Boston, Mass., 02215.

The extensive literature of "active" nitrogen chemistry does not appear to record any study of competition between organic substrates. This paper reports an investigation of consumption of hydrocarbon in the competition between an olefin, ethylene, and a paraffin, propane. Reaction probably went to completion under most, if not all, experimental conditions.<sup>2</sup> Consumption of hydrocarbon as a result of both primary attack by one or more components of "active" nitrogen and of secondary attack by reactive intermediates must be considered possible.

### Experimental

Apparatus and methods are described more completely elsewhere,<sup>3,4</sup>. Active nitrogen was generated by electrodeless glow discharge supported by 2450MHz microwaves at a total pressure of 311 Torr. Transport rates were 230cm. sec.<sup>-1</sup>, 150 $\mu$  mole sec.<sup>-1</sup> and 1.3 $\pm$ 0.2 $\mu$  mole sec.<sup>-1</sup> for linear flow, N<sub>2</sub> flow and N(<sup>4</sup>S) flow, respectively. The latter was measured by nitric oxide "emission" titration.<sup>5</sup> Hydrocarbon substrate was introduced countercurrent<sup>3</sup> into the active nitrogen stream at autogenous temperature (approx. 50°C) 20cm. (.087 sec.) downstream from the glow discharge. The gas stream passed through liquid nitrogen traps 50cm. (.22 sec.) downstream from the substrate inlet. Amounts of recovered reactants were determined by gas chromatography on silica gel.<sup>4</sup> Relative activities of <sup>14</sup>C-labeled compounds were determined<sup>4</sup> by proportional counting of CO<sub>2</sub> obtained by combustion of the gas chromatographically purified compounds in O<sub>2</sub> over CuO at 450°. Propane and labeled ethylene were Matheson products. Cold ethylene was Phillips Research Grade.

### Data

Table I summarizes percent consumption of ethylene consequent upon reaction of the pure substrate and three of its mixtures with propane with six different ratios of N(<sup>4</sup>S). Table II summarizes analogous data for propane. The data for mixtures given in the two Tables are derived from the same sets of experiments. Table III summarizes apparent relative specific rates of consumption, " $k_{C_2H_4}/k_{C_3H_8}$ ". These ratios were calculated by means of eq. 1, the expression which would be appropriate " $k_{C_2H_4}/k_{C_3H_8} = \log[(C_2H_4)_f/(C_2H_4)_t] / \log[(C_3H_8)_f/(C_3H_8)_t]$ " (1) if the relative rates of consumption depended entirely on the bimolecular reaction of each of the substrates with the same reagent. Table IV summarizes molar radioactivities of recovered reactants or product ethane relative to that of reactant ethylene for the reaction of equimolar mixtures of <sup>14</sup>C-labeled ethylene and ordinary propane.

Table I

## Percent Consumption of Ethylene

<u>(Total Hydrocarbon)</u> (N) <sup>a</sup>	Average Percent Consumption (C <sub>2</sub> H <sub>4</sub> ) <sub>0</sub> /(C <sub>3</sub> H <sub>8</sub> ) <sub>0</sub>			
	Pure C <sub>2</sub> H <sub>4</sub> n <sup>b</sup>	3.0 n <sup>b</sup>	1.0 n <sup>b</sup>	0.33 n <sup>b</sup>
4	19 3	18 3	28* 10	-
2	24* 3	27 3	37* 10	51 6
1	39* 4	45 4	47 <sup>x</sup> 16	56 9
2/3	45 2	59 1	-	73° 2
1/2	78 <sup>x</sup> 3	87 3	93 10	90 7
1/6	93° 2	-	93 7	84 3

- a. Flow rate of N(<sup>4</sup>S) is  $1.3 \pm 0.2 \mu$  mole sec.<sup>-1</sup> throughout.  
 b. Number of independent determinations averaged to give the tabulated figure.

Table II

## Percent Consumption of Propane

<u>(Total Hydrocarbon)</u> (N) <sup>a</sup>	Average Percent Consumption (C <sub>2</sub> H <sub>4</sub> ) <sub>0</sub> /(C <sub>3</sub> H <sub>8</sub> ) <sub>0</sub>			
	Pure C <sub>3</sub> H <sub>8</sub> n <sup>b</sup>	3.0 n <sup>b</sup>	1.0 n <sup>b</sup>	0.33 n <sup>b</sup>
4	-	25 3	27* 10	-
2	29* 1	32 3	32* 10	22 6
1	35* 2	34 4	32 <sup>x</sup> 16	30 9
2/3	-	36° 1	-	32 2
1/2	41 <sup>x</sup> 2	39 3	39 10	37 7
1/6	48° 2	-	45 7	44 3

- a. Flow rate of N(<sup>4</sup>S) is  $1.3 \pm 0.2 \mu$  mole sec.<sup>-1</sup> throughout.  
 b. Number of independent determinations averaged to give the tabulated figure.

Table III

## Apparent Relative Reactivities

<u>(Total Hydrocarbon)</u> (N)	"k <sub>C<sub>2</sub>H<sub>4</sub></sub> /k <sub>C<sub>3</sub>H<sub>8</sub></sub> "			
	Separate <sup>a</sup>	(C <sub>2</sub> H <sub>4</sub> ) <sub>0</sub> /(C <sub>3</sub> H <sub>8</sub> ) <sub>0</sub>		
		3.0	1.0	0.33
		0.69	1.1	-
2	(0.30)	0.83	1.2	2.9
1	(1.2)	1.5	1.7	2.3
2/3	-	2.0	-	3.5
1/2	(2.9)	4.1	5.4	5.2
1/6	(6.0)	-	4.5	3.1

- a. Numbers in this column are calculated from the data for pure substrates. (Total Hydrocarbon) is taken arbitrarily as the concentration of one of the pure hydrocarbons. Values are based on data for identical concentrations of pure hydrocarbons.

Table IV

Relative Molar Activities of Recovered Reactants and Product Ethane<sup>a</sup>

<u>(Total Hydrocarbon)</u> (N) <sup>d</sup>	Relative Molar Activity					
	C <sub>2</sub> H <sub>4</sub>		C <sub>2</sub> H <sub>6</sub>		C <sub>3</sub> H <sub>8</sub>	
	n <sup>b</sup>	n <sup>b</sup>	n <sup>b</sup>	n <sup>b</sup>	n <sup>b</sup>	n <sup>b</sup>
2	0.98	7	-	-	0.01 <sup>c</sup>	1
1	0.98	4	-	-	-	-
1/2	-	-	0.8	1	0.01 <sup>c</sup>	1
1/6	0.89	2	0.5	1	0.01 <sup>c</sup>	1

- a. Compared to unreacted ethylene; hydrocarbon reactants equimolar.  
 b. The number of independent experiments.  
 c. Indistinguishable from the value found for unreacted propane.  
 d. Flow rate of N(<sup>4</sup>S) was  $1.3 \pm 0.2 \mu$  mole sec.<sup>-1</sup> throughout.

## Discussion

The systematic variation of the ratio " $k_{C_2H_4}/k_{C_3H_8}$ " over the range of concentration parameters summarized in Table III demonstrates that relative consumption of competing hydrocarbons is not determined simply by the relative rates of attack of  $N(^4S)$  (or any set of reactive species) on ethylene and propane since such determination would lead to constancy of the ratio. A similar conclusion can be drawn from the data of Tables I and II by comparison of the consumption of a given substrate at a fixed concentration upon reaction with a fixed proportion of  $N(^4S)$  in the presence and absence of the competing substrate. Such matched points are designated in Tables I and II by identical superscripts. If the simple model of the competition from which eq. 1 is derived were correct, and keeping in mind the similar degrees of consumption of the two substrates, addition of the second substrate should always substantially suppress the consumption of the first and should have the largest effect when substrate is in excess over reagent. In fact, with (reactant hydrocarbon)/(N)  $\geq 1$  such suppression is absent or negligible. It becomes significant only when  $N(^4S)$  is in excess. The complexity of the reaction is also indicated by the shallow dependence of percent consumption of pure hydrocarbon on the ratio, (pure hydrocarbon)/(N), particularly with propane for which a twelvefold decrease in the ratio is associated with increase in percent consumption by a factor of only 1.65. Such behaviour is consistent with destruction of the substrate by both attacking reagent and reactive intermediates arising from the primary attack if, as the proportion of  $N(^4S)$  is raised, these intermediates are increasingly consumed by the reagent before they can attack the substrate. This feature is also present with ethylene but to a smaller extent.

Except with the largest excess of  $N(^4S)$ , the value of " $k_{C_2H_4}/k_{C_3H_8}$ " (Table III) increases with decrease in the ratio  $(C_2H_4)_0/(C_3H_8)_0$  at constant values of (total hydrocarbon)/(N). This systematic change is consistent with occurrence of competition between the two substrates with respect to their destruction by reactive intermediates arising from primary attack of the reagent. More specifically, (cf. Tables I and II) ethylene appears to be more sensitive to consumption by intermediates arising from propane than vice versa. Presumably, the effect of attack by reactive intermediates can be reduced or eliminated by using sufficiently large excesses of  $N(^4S)$  that the intermediates react with the latter rather than with hydrocarbon. This analysis suggests that the values of " $k_{C_2H_4}/k_{C_3H_8}$ " obtained with the largest excess of  $N(^4S)$  most closely approximate the true value of this ratio for primary attack and indicates that this true value is at least 5. (See further discussion of the data at (hydrocarbon)/(N) = 1/6 below.)

The above discussion tacitly assumes that  $N(^4S)$  is the only component of "active" nitrogen which is significantly involved. That this is so for ethylene is widely accepted. The work of Jones and Winkler<sup>6</sup> suggests that it is probably also the case for propane. The latter study provides a value of  $1.0 \times 10^6 M^{-1} sec^{-1}$  for the specific rate of reaction of  $C_3H_8$  at  $50^\circ C$ . Since nitrogen atom concentrations were determined from HCN yields produced by reaction with ethylene, this constant should be adjusted downward 30 to 50%, e.g. to  $7 \times 10^5 M^{-1} sec^{-1}$ . Since the constant was apparently evaluated from experiments in which propane was in molar excess over propane it may also be significantly high because it does not correct for the consequences of attack by reactive intermediates arising from initial attack by  $N(^4S)$ . Herron has estimated from his elegant mass spectrometric study<sup>7</sup> of the reaction of  $N(^4S)$  with ethylene that the rate of primary attack in the (virtually temperature independent) reaction of  $N(^4S)$  with ethylene is equal to or less than  $7 \times 10^6 M^{-1} sec^{-1}$ . A value of the ratio of specific rates of primary attack by  $N(^4S)$  on ethylene and propane, respectively, in the vicinity of 10 is thus indicated by earlier work. Agreement with the present

result is well within the range of the mutual uncertainties. Herron's work further establishes that hydrogen atoms produced in the reaction of  $N(^4S)$  with ethylene compete with the reagent for the substrate and, in fact, provides the model upon which interpretation of the present data is based.

The data of Table IV establish that even with a sixfold excess of  $N(^4S)$ , synthesis of propane<sup>4</sup> in the reaction mixture at least in part from fragments originating in ethylene is not detectable. Production of ethylene either by degradation of propane or synthesis at least in part from fragments originating in propane occurs to a detectable extent with a sixfold excess of  $N(^4S)$  and equal initial concentrations of the hydrocarbons. Presumably such processes are more important with propane in excess over ethylene. The values of " $k_{C_2H_4}/k_{C_3H_8}$ " obtained with a sixfold excess of  $N(^4S)$  are, accordingly, reduced by such replacement of consumed ethylene, the reduction being greatest with excess propane. This effect results in reversal of the trend to higher values of " $k_{C_2H_4}/k_{C_3H_8}$ " with increasing excess of  $N(^4S)$  which is apparent in the data of Table III. It can also account for the unusual sequence of values of this ratio with increasing proportion of propane observed with (hydrocarbon)/(N) = 6 and to a lesser extent when this ratio equals 2. The data of Table IV also establish that ethane is produced from both ethylene and propane.

#### Footnotes

1. Paper VI in the series, "Reactions of Active Nitrogen with Organic Substrates."
2. This statement is based on a study of the effect of trapping times on product yields in the reaction of "active" nitrogen with propylene by Dr. Y. Titani in these laboratories. Cf. N. N. Lichtin, Int. J. Radiation Biol., in press.
3. Y. Shinozaki, R. Shaw and N. N. Lichtin, J. Am. Chem. Soc., 86, 341 (1964).
4. P. T. Hinde, Y. Titani and N. N. Lichtin, ibid., in press.
5. P. Harteck, G. G. Mannella and R. R. Reeves, J. Chem. Phys., 29, 608 (1958).
6. W. E. Jones and C. A. Winkler, Can. J. Chem., 42, 1948 (1964).
7. J. T. Herron, J. Phys. Chem., 69, 2736 (1965).

FORMATION OF HYDROCARBONS FROM  $H_2 + CO$  IN  
MICROWAVE-GENERATED ELECTRODELESS DISCHARGES

Bernard D. Blaustein and Yuan C. Fu

U. S. Bureau of Mines, Pittsburgh Coal Research Center,  
4800 Forbes Avenue, Pittsburgh, Pennsylvania 15213

Formation of hydrocarbons from  $H_2 + CO$  over metal catalysts is of considerable interest and has been studied at length. Hydrocarbons can also be formed in electrical discharges,<sup>3, 5-9, 11-17/</sup> and this offers an interesting alternative for producing hydrocarbons from  $H_2 + CO$ . Fischer and Peters<sup>5/</sup> worked with a flow system where the gases at 10 torr pressure circulated through a discharge (50 Hz) between metal electrodes, then through a mercury vapor pump, a liquid air-cooled trap, and back to the discharge. Conversion of CO to hydrocarbons was very low for one pass through the discharge, but by recirculating the gases for 100 minutes, practically all of the CO would react.

Lunt<sup>9/</sup> and Epple and Apt<sup>3/</sup> worked with electrodeless radiofrequency (2-110 MHz) discharges in static reactors at pressures up to 300 torr. Conversions of  $H_2 + CO$  and  $H_2 + CO_2$  to  $CH_4$  were quite high for reaction times of several minutes; no other hydrocarbons were formed. McTaggart,<sup>11/</sup> and Vastola et al.<sup>16/</sup> working with electrodeless microwave (2450 MHz) discharges in flow systems at pressures of a few torr formed only traces of hydrocarbons from  $H_2 + CO$ . Here, the gas passed through the discharge only once, and the residence time was a fraction of a second. However, work in our laboratory has shown that in a static reactor, and with reaction times of the order of a minute, CO can be converted in high yields to hydrocarbons in an electrodeless microwave discharge in  $H_2 + CO$ , under conditions where essentially no polymers are formed.

## EXPERIMENTAL PROCEDURES

Reactions were carried out in 11-mm ID cylindrical Vycor reactors placed in a coaxial cavity (Ophthos Instruments, similar to type 2A described by Fehsenfeld et al.<sup>4/</sup>) connected by a coaxial cable to a Raytheon KV-104A CMD-10 2450 MHz generator. For a run, the reactors were evacuated to  $< 3 \mu$  and filled with either 5:1  $H_2$ -CO or various  $H_2$ -CO-Ar (typically 5.1:1.0:0.4) mixtures prepared from tank gases and stored in the vacuum system. Product analyses were made on a CEC 21-103C mass spectrometer. Net power into the discharge, measured with a Microwave Devices model 725.3 meter, was approximately 34 watts, although lower power levels could be used. Air was blown through the cavity to cool the reactor somewhat, but the estimated wall temperature in the discharge was still several hundred degrees C.

Runs with argon gave the same results as in the absence of Ar, and the ratio of total-carbon-to-argon in the product was usually a few percent lower in the product, but did not vary by more than  $\pm 10$  percent from its value in the original mixture, indicating that only negligible amounts of polymers were formed in the reaction. For  $H_2 + CO$  mixtures without Ar it was assumed that polymer formation was negligible, so long as reaction conditions were similar.

As a precaution against the gradual accumulation of small amounts of polymer in the reactors, they were cleaned before each run by maintaining a discharge in  $O_2$  at about 10 torr for 3 minutes to oxidize any carbonaceous material present. This was repeated twice, with fresh samples of  $O_2$ . A discharge in  $H_2$  (about 10 torr) was then maintained for 3 minutes in the reactor. This was also repeated twice, with fresh samples of  $H_2$ . Since the reactions to be studied were to be carried out in a reducing environment, this treatment with  $H_2$  was felt to be desirable after the  $O_2$  discharge.

## RESULTS

Figure 1 shows the results of experiments made at initial gas pressure of 12 + 1 torr in 36-cm long by 11-mm ID reactors. The percent of carbon present in the product as  $C_2H_2$  and as  $CH_4 + C_2H_2$  is plotted vs. reaction time. Figure 2 shows the percent of carbon present in the product as  $CH_4$  for the same runs. Water,  $CO_2$ , and occasionally slight traces of other hydrocarbons, were also present in the product. The conversion of CO to  $CH_4 + C_2H_2$  reaches a maximum of 17-18% for reaction times of 30-120 seconds. Figure 3 shows the results of experiments made at initial gas pressures of 50 + 3 torr in 20-cm long by 11-mm ID reactors. Here, the percent of carbon present as  $CH_4 + C_2H_2$  is at a maximum of 24-25% for reaction times of 3-4 minutes. There is considerable scatter in the data; the dashed curves are intended to show only the general trend.

These data show that conversion of CO to hydrocarbons in the discharge under these conditions is limited. The composition of the gases in the reactor approaches a stationary state, for reaction times of the order of 0.5 to 3 minutes, depending upon the pressure. Because of the geometry of the reactors, and the volume of a reactor relative to the volume occupied by the discharge, the time required to reach the stationary state appears to be longer than is actually so, due to the relatively long times required for diffusion of gases into and out of the discharge. (The 36-cm long reactors were used for the runs made at 12 torr; for the runs made at 50 torr, the shorter 20-cm long reactors were used. Preliminary experiments showed that the conversion of CO to  $CH_4 + C_2H_2$  at 50 torr in 36-cm long reactors was essentially the same as for the 20-cm long reactors, but took 1-2 minutes longer to achieve maximum conversions.)

High yields of gaseous hydrocarbons from  $H_2 + CO$  have now been shown to occur in low-frequency (50 Hz<sup>5/</sup> and 60 Hz<sup>17/</sup>) discharges, radiofrequency (2-110 MHz)<sup>2/</sup> and microwave (2450 MHz) discharges. However, in all of these cases, the reaction does not appear to be an extremely rapid one, such as is the case for dissociation of diatomic molecules in a discharge, for instance.

For reaction times longer than those needed to reach maximum conversions, the conversions appear to decrease. This is probably due to some polymer formation, but not enough to show up as a 10% decrease in the analytically determined C/Ar ratio. Several runs at 12 torr (not plotted) of 5 minutes duration, and some longer runs, including one at 50 torr for 10 minutes, gave values of the C/Ar ratio more than 10% below the initial value of the ratio, and this was considered evidence of polymer formation. Here, also, the yields of  $CH_4$  and  $C_2H_2$  were lower.

Conversions of CO could be increased by removing reaction products as they formed, by having a cold trap surround the bottom 5 cm of the reactor before and during the time that the discharge was maintained at a distance of 10 cm from the bottom. The discharge is localized and extends over a distance of about 2 cm. As shown in table 1, the conversion of CO increased markedly and the product distribution changed. Values for the C/Ar ratio indicated that polymers were not formed. Also, there is no indication that the product distribution is any different in the presence of Ar than in its absence. The first three columns in the table are for the 3-minute runs shown in figures 1 and 2. When the discharge was maintained for 3 minutes or longer, with Dry Ice ( $-78^\circ$ ) surrounding the end of the reactor, the percent of carbon present in the final product as  $CH_4$  is 51%;  $C_2H_2$ , 17%;  $C_2H_6$ , 10%. At this temperature, the only reaction product frozen out is  $H_2O$ . Apparently, the removal of this is sufficient to increase the conversion of CO to hydrocarbons to approximately 78%.

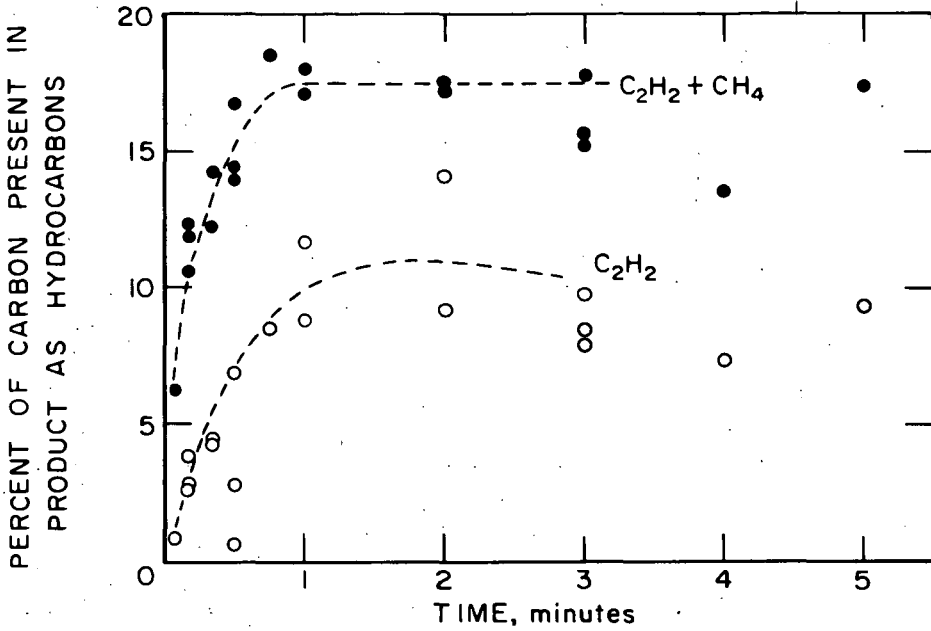


Figure 1.—Formation of hydrocarbons from  $H_2 + CO$  in microwave-generated discharge: acetylene  $\circ$ , acetylene + methane  $\bullet$ . Initial gas pressure =  $12 \pm 1$  torr.

11-30-66

L-9694

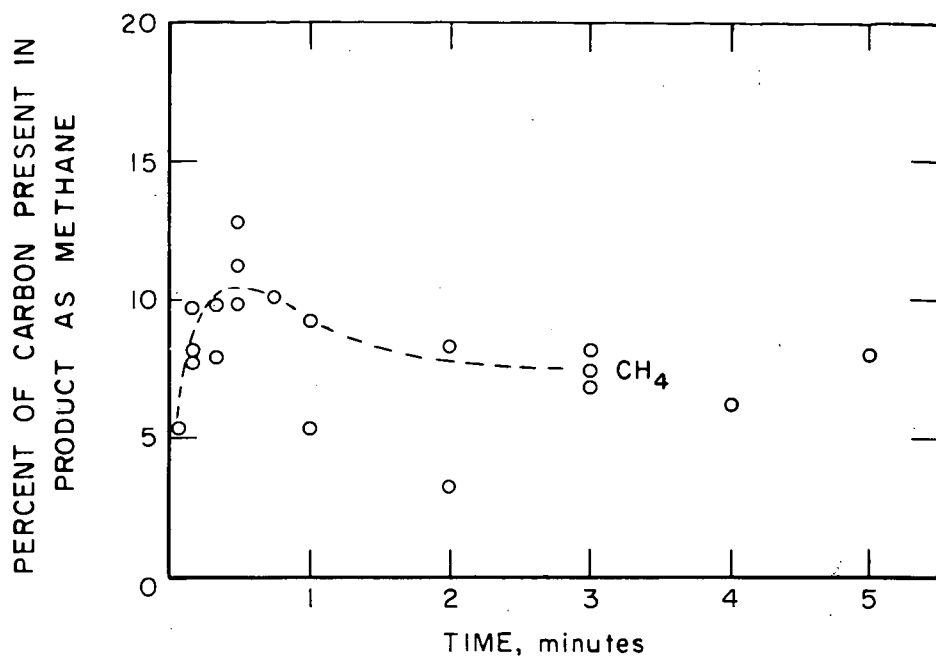


Figure 2.—Formation of  $\text{CH}_4$  from  $\text{H}_2 + \text{CO}$  in microwave-generated discharge. Initial gas pressure =  $12 \pm 1$  torr.

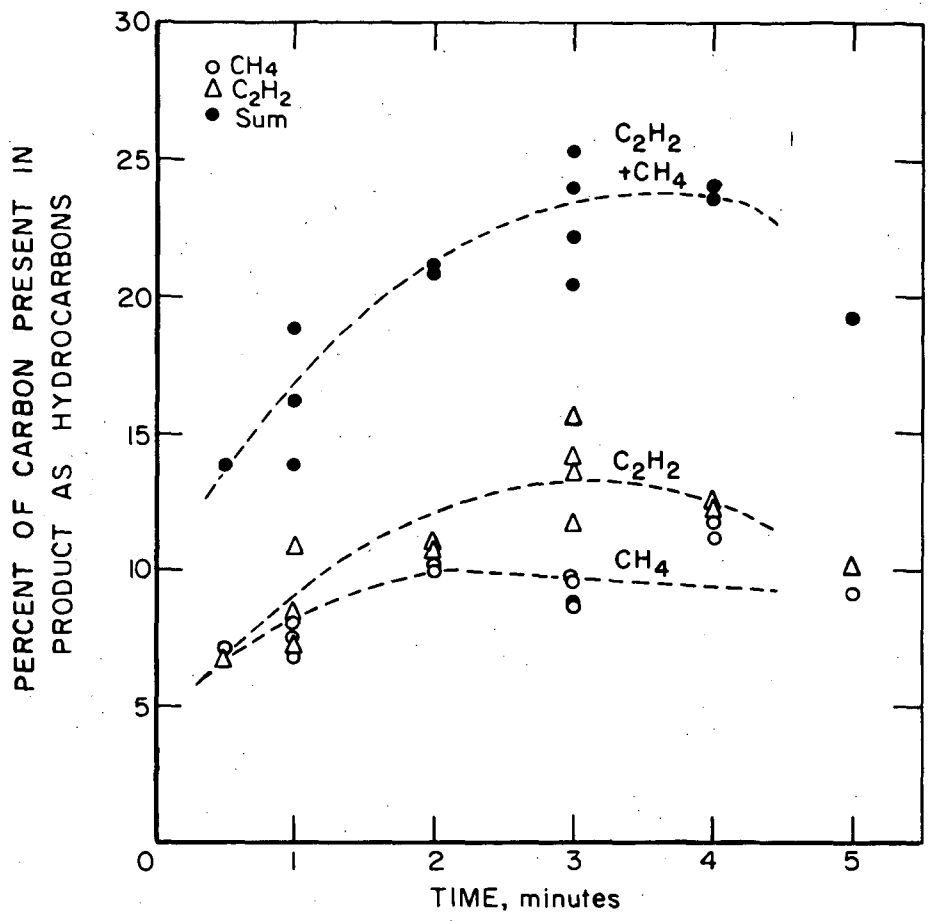


Figure 3.—Formation of hydrocarbons from H<sub>2</sub> + CO in microwave-generated discharge: methane ○, acetylene △, acetylene + methane ●. Initial gas pressure = 50 ± 3 torr.

TABLE 1. - Conversion of CO to hydrocarbons in a microwave discharge:  
No cooling vs. cooling the bottom of the reactor

Conditions	Run:	6294	10252	10253	9232	11012	7154	7153	8129	10213	11011	9233	9025	8192	10211	7071
Cooling bath, °C		None	None	None	-78	-78	-78	-196	-196	-196	-196	-196	-196	-196	-196	-196
Time, min		3	3	3	3	3	5	3	3	3	3	3	2	3	3	5
Pressure, torr		12.0	12.8	12.0	12.6	12.4	12.0	11.2	12.5	11.9	13.0	12.0	12.4	12.6	51	52
H <sub>2</sub> /CO		5.1	5.1	5.1	5.0	5.1	5.1	5.1	5.1	5.1	5.1	5.0	2.2	2.2	5.1	5.1
Argon		Yes	Yes	Yes	No	Yes	Yes	Yes	Yes	Yes	Yes	No	No	No	Yes	Yes
Percent carbon present in product as																
CH <sub>4</sub>		6.8	8.1	7.4	52.0	50	51.0	3.4	4.8	4.0	3.9	3.4	1.0	.6	3.9	3.7
C <sub>2</sub> H <sub>2</sub>		8.5	9.7	7.9	19.9	15	17.2	5.7	48.6	2.9	19.7	4.8	46.3	32.9	61.8	55.6
C <sub>2</sub> H <sub>6</sub>		-	-	-	7.8	9	12.6	79.2	31.0	75.7	63.6	75.8	35.6	46.6	.4	.5
C <sub>3</sub> + C <sub>4</sub>		-	-	-	trace	trace	trace	3.6	8.8	8.9	2.0	8.7	3.2	10.0	-	-
CO <sub>2</sub>		2.1	1.4	2.1	trace	+	-	4.2	4.0	4.1	5.3	4.3	9.4	9.6	2.4	2.5
Hydrocarbons		15	18	15	80	74	81	92	93	92	89	93	86	90	66	60

The next five columns in table 1 show that with liquid  $N_2$  cooling ( $-196^\circ$ ), the percent of carbon in the product as  $CH_4$  in only 4%;  $C_2H_2 + C_2H_6$  (with the latter predominating) 81%;  $C_3 + C_4$  hydrocarbons, 6%; more  $H_2O$  and  $CO_2$  are also formed. The mass spectrometric analyses indicated that traces of oxygenates were also present in the products of these runs, but in such small amounts that no identifications could be attempted. For some unknown reason,  $C_2H_4$  is not formed under these conditions. (Several runs were analyzed by gas chromatography for  $C_2H_4$  and none was found.) At a temperature of  $-196^\circ$ , the only non-condensables present in the mixture are  $H_2$ ,  $CO$ , and  $CH_4$ ; all the other products are frozen but. One can speculate that the high yield of  $C_2H_6$  is due either to a recombination of  $CH_3$  radicals at the cold surface, or hydrogenation of  $C_2H_2$ , but the mechanism of formation of any of the hydrocarbon products is not known.

The next-to-last pair of columns in table 1 show that very high conversions of  $CO$  to  $C_2$ - and higher hydrocarbons can be obtained using a 2.2:1  $H_2 + CO$  mixture. Here, also, the  $CO_2$  production is higher, and the  $CH_4$  lower, than compared with the more hydrogen-rich reactant mixture. The last pair of columns, giving data for runs made at 50 torr, indicate that  $C_2H_2$  was, by far, the predominant product in these runs.

The almost complete conversion of  $CO$  to hydrocarbons,  $H_2O$ , and  $CO_2$ , obtained by cooling the bottom of the reactor, is reversible. Several additional experiments (at 12 torr), where the gases were reacted for 3 minutes while the reactor was cooled, the bottom of the reactor then warmed to room temperature in a few seconds with a water bath, and the gases reacted for 2 more minutes, gave the same product compositions as for the runs shown in figures 1 and 2.

Table 2 gives the results of some preliminary experiments where water vapor was added to the  $H_2 + CO + Ar$  mixture before reaction. The water vapor was added to the previously evacuated reactor and a portion of the vacuum system connected to a Pace Engineering Co. Model P7 pressure transducer containing a  $\pm 1$  psi diaphragm. The output of this was indicated on a Pace Model CD25 transducer indicator. After the water vapor partial pressure was measured, the stopcock to the reactor was closed and the water frozen at the bottom of the reactor. The reactor was then filled with the  $H_2$ - $CO$ - $Ar$  mixture, the bottom of the reactor warmed slightly, and 3 minutes allowed for mixing of the gases before the discharge was initiated.

Even from these few experiments, it can be seen that adding water vapor to the initial reactant mixture has a strong inhibitory effect on the production of hydrocarbons. (The  $CO_2$  yield is increased due to the reaction  $H_2O + CO \rightarrow CO_2 + H_2$ .) Comparison of the second and third runs listed in the table shows that 3 minutes reaction time increases the yield of hydrocarbons only slightly as compared to one minute. The last two runs in the table show that when the water vapor partial pressure is equal to or greater than the  $CO$  partial pressure in the reactant gas mixture, no hydrocarbons are produced at all.

The pronounced inhibitory effect of  $H_2O$  vapor on hydrocarbon formation in this reaction may explain some of the scatter of the data shown in figures 1, 2, and 3. It is possible that small (and variable) amounts of  $H_2O$  vapor were adsorbed on the walls of the reactor tubes, and that this decreased the hydrocarbon yield in (some of) the runs by a varying amount which shows up as scatter in the data. Further experiments would have to be done to shed more light on this point. However, there are other, as yet unknown, sources of variability in the experimental conditions which also undoubtedly contribute to the scatter in the data.

TABLE 2. - Effect of adding water to the H<sub>2</sub>-CO-Ar mixture.  
Repression of hydrocarbon formation

	Run 11153	11151	11154	11152	11013
Initial H <sub>2</sub> -CO-Ar (5.1:1.0:0.4) pressure torr	10.8	12.6	13.9	11.8	12.7
Initial H <sub>2</sub> O pressure added, torr	.35	.85	.95	1.83	6
Time of discharge, min.	1	1	3	1	1
Percent of carbon present in product as					
CH <sub>4</sub>	4.0	1.9	1.7	0.0	0.0
C <sub>2</sub> H <sub>2</sub>	4.2	1.8	2.6	0.0	0.0
CO <sub>2</sub>	3.3	4.6	4.5	8.8	23.1
Hydrocarbons	8.2	3.7	4.3	0	0

#### DISCUSSION

The different conversions of CO can be explained by assuming that the reaction in the discharge, without cooling the bottom of the reactor, reaches a stationary state where the production of CH<sub>4</sub> and C<sub>2</sub>H<sub>2</sub> is limited by the back reaction of these hydrocarbons with H<sub>2</sub>O and/or CO<sub>2</sub> to form H<sub>2</sub> + CO. The data in figure 3, by comparison with the runs in figures 1 and 2, indicate that conversion of CO to hydrocarbons is increased at higher initial pressures, as would be expected for a reaction where the volume of the products is less than the reactants. When one or more of the reaction products are removed from the discharge zone by being frozen out, the stationary state shifts and more CO reacts to form hydrocarbons. When the frozen-out hydrocarbons are re-introduced into the discharge, they react very readily to re-form the initial stationary state composition. If, on the other hand, water vapor is added to the initial reactant gas mixture, the conversion of CO to hydrocarbons is repressed.

These experimental observations can be summed up by discussing the reaction  $H_2 + CO \rightarrow CH_4 + H_2O$  in terms of a stationary state in the discharge which can shift in the direction that would be predicted by applying Le Chatelier's principle. Actually, in this respect, the system behaves as if it were in chemical equilibrium. Qualitatively, this interpretation of the data is very reasonable. Fischer and Peters,<sup>5/</sup> Wendt and Evans,<sup>17/</sup> Lunt,<sup>9/</sup> and Epple and Apt<sup>3/</sup> have all discussed the production of hydrocarbons from H<sub>2</sub> + CO in terms of equilibria in the discharge. However, simple arguments show that any discussion of equilibria in discharges is not a straightforward one because of the absence of temperature equilibria among the various species - electrons, ions, and molecules - in the discharge.<sup>1/</sup>

Manes<sup>10/</sup> has pointed out that in the statistical mechanical derivation of the equilibrium constant in terms of the partition functions, the functional form of the equilibrium constant expression follows from the conservation of atoms in the system. This leads to the likelihood that the H<sub>2</sub>-CO-CH<sub>4</sub>-H<sub>2</sub>O-CO<sub>2</sub> system will conform to some equilibrium "constant" in an electrical discharge system, although the magnitude of this constant will not be derivable from equilibrium thermodynamic properties.

Given the existence of this equilibrium "constant" for (some) reactions occurring in a discharge, we would then expect Le Chatelier's principle to apply. In fact, the "constant" need be only approximately constant, as conditions change over a certain range, for the system to exhibit qualitative changes in accordance with Le Chatelier's principle.

For a preliminary inspection of the quantitative aspects of these equilibria "constants," from the data in table 2 and the two one-minute runs in figures 1 and 2, values were calculated for

$$K_1 = \frac{P_{CO} \times P_{H_2O}}{P_{CO_2} \times P_{H_2}}$$

and

$$K_2 = \frac{P_{CH_4} \times P_{H_2O}}{P_{CO} \times P_{H_2}^3}$$

These are given in table 3. If these equilibria had been established in an ordinary thermal system, the values for  $K_1$  and  $K_2$  would depend only on temperature. However, these "equilibria" were established in a reactor system where part of the gas was in an electrical discharge. Since we cannot define one temperature for the discharge, the experimental values obtained for  $K_1$  and  $K_2$  depend on the parameters which characterize the discharge, such as rate of energy input, geometry of the reactor, the volume of gas in the discharge relative to the volume of the reactor, and the electrical variables, such as field strength, etc.

The values obtained for  $K_1$  and  $K_2$  can be used to define a "chemically equivalent temperature" for the gases in the discharge. Thus, the average value for  $K_1$  corresponds to a "temperature" of 1300°K. This is very approximate, due to the small change of  $K$  with temperature for this reaction near 1300°K. The average value for  $K_2$  corresponds to a "temperature" of approximately 800°K. Pursuing much the same line of thought, Epple and Apt<sup>3/</sup> calculated "equivalent temperatures" of about 750°K from values of  $K_1$  and 850°K from values of  $K_2$  obtained from the data on the  $H_2$ -CO- $CH_4$ - $H_2O$ -CO<sub>2</sub> system in their static radiofrequency reactor experiments. The significance, if any, of these "temperatures" calculated from the discharge data, is unknown.

TABLE 3. - Values of equilibrium "constants" calculated from the data in table 2

Run	11153	11151	11154	11152	11013	2154	4272	"Temperature," °K
$K_1$	1.4	1.8	1.9	2.0	1.9	1.1	1.9	1300
$K_2$	21	12	9	<u>1/</u>	<u>1/</u>	22	33	800
$K_3 \times 10^3$	7.4	17	37	<u>1/</u>	<u>1/</u>	4.5	6.3	1300
$K_4$	3.2	2.5	3.2	<u>1/</u>	<u>1/</u>	2.1	6.9	-

<sup>1/</sup> Due to the large concentration of  $H_2O$  vapor, no hydrocarbons were produced in these runs.

One unusual finding of Epple and Apt is that  $\text{CH}_4$  was the sole hydrocarbon produced under their conditions. Even though  $\text{CH}_4$  was present in the discharge for minutes, no  $\text{C}_2\text{H}_2$  was produced. We have repeated their experiments (using a 400 KHz generator) and can confirm this finding, as well as their values for the amount of CO converted to  $\text{CH}_4$  in a radiofrequency discharge. On the other hand,  $\text{C}_2\text{H}_2$  is always produced in the reaction in a microwave discharge. In attempting to explain this difference in products in the two cases, perhaps some significance can be found in the approximate values of 1300°K calculated from  $K_1$  for our microwave discharge runs as contrasted with 750°K from  $K_1$  calculated by Epple and Apt. The difference in these "temperatures" may be another indication of what we feel intuitively - namely, that the microwave discharge is "hotter" than the radiofrequency discharge, because of the higher value of energy input per mole of gas in the discharge.

Values were also calculated for

$$K_3 = \frac{P_{\text{C}_2\text{H}_2} \times P_{\text{H}_2}^3}{P_{\text{CH}_4}^2}$$

and

$$K_4 = \frac{P_{\text{C}_2\text{H}_2} \times P_{\text{H}_2\text{O}}^2}{P_{\text{CO}}^2 \times P_{\text{H}_2}^3}$$

and are given in table 3. From the average value for  $K_3$ , one can calculate a "temperature" for this reaction of approximately 1300°K. The values for  $K_4$  ( $K_4 = K_2 \times K_3$ ) are much higher than there is any reason to expect, since for this reaction,  $\log K = -4.6$  at 300°K, and decreases with increasing temperature. The values calculated for  $K_4$  indicate that the reaction



is not even remotely near any sort of equilibrium in the discharge; the amount of  $\text{C}_2\text{H}_2$  formed is far greater than can be accounted for at equilibrium.

In summary, it is helpful to discuss qualitatively at least some reactions in discharges from the point of view of stationary states or equilibria, which can shift according to Le Chatelier's principle. Admittedly, this approach is speculative at the moment. Other workers<sup>2,7</sup> are also attempting to discuss discharge reactions in terms of equilibria, and it will be of interest to see how useful these ideas prove to be in interpreting chemical reactions in discharges.

The authors wish to thank Gus Pantages, Waldo A. Steiner, and Paul Golden for their technical assistance; A. G. Sharkey, Jr. and Janet L. Shultz for the mass-spectrometric analyses; and Drs. Irving Wender and Frederick Kaufman for their valuable discussions.

#### REFERENCES

1. Arzimovich, L. A. Elementary Plasma Physics. Blaisdell Pub. Co., New York, N. Y., 1965, pp. 5-6.
2. Eck, R. V., E. R. Lippincott, M. O. Dayhoff, and Y. T. Pratt. *Science*, **153**, August 5, 1966, pp. 628-633.

3. Epple, R. P. and C. M. Apt. The Formation of Methane from Synthesis Gas by High-Frequency Radiation. Gas Operations Research Project PF-27(ext.), Am. Gas Assoc. Catalog No. 59/OR, Am. Gas Assoc., Inc., July 1962, 47 pp.
4. Fehsenfeld, F. C., K. M. Evenson, and H. P. Broida. Rev. Sci. Instruments, 36, March 1965, pp. 294-298.
5. Fischer, F. and K. Peters. Brennstoff-Chem., 12, No. 14, 1931, pp. 268-273.
6. Lefebvre, H. and M. van Overbeke. Chimie et Industrie, Special No., April 1934, pp. 338-342.
7. Lefebvre, H. and M. van Overbeke. Compt. rend., 198, 1934, pp. 736-738.
8. Losanitsch and Jovitschitsch in Ch. IV of "The Conversion of Coal into Oils," by F. Fischer, E. Benn, Ltd., London, 1925
9. Lunt, R. W. Proc. Roy. Soc. (London), 108A, 1925, pp. 172-186.
10. Manes, M. Private Communication.
11. McTaggart, F. K. Austral. J. Chem., 17, 1964, pp. 1182-1187.
12. Sahasrabudhey, R. H. and S. M. Deshpande. Proc. Indian Acad. Sci., 31A, 1950, pp. 317-324.
13. Sahasrabudhey, R. H. and S. M. Deshpande. J. Indian Chem. Soc., 27, 1950, pp. 361-368.
14. Sahasrabudhey, R. H. and S. M. Deshpande. J. Indian Chem. Soc., 28, 1951, pp. 377-382.
15. Sahasrabudhey, R. H. and A. Kalyanasundaram. Proc. Indian Acad. Sci., 27A, 1948, pp. 366-374.
16. Vastola, F. J., P. L. Walker, Jr., and J. P. Wightman. Carbon, 1, No. 1, 1963, pp. 11-16.
17. Wendt, G. L. and G. M. Evans. J. Am. Chem. Soc., 50, 1928, pp. 2610-2621.

RADIOFREQUENCY ELECTRODELESS SYNTHESIS OF POLYMERS:  
REACTION OF CO, N<sub>2</sub> AND H<sub>2</sub>

John R. Hollahan  
Richard P. McKeever

Research and Development Department  
TRACERLAB, A Division of LFE  
2030 Wright Avenue  
Richmond, California 94804

### Introduction

A certain amount of the large literature concerning the synthesis of compounds in electrical discharges relates to the synthesis of polymeric materials, and many industrial patents exist in this category. Most of these syntheses have employed 1) hydrocarbon reactant(s) or 2) discharge apparatuses involving internal electrode configurations as the source of excitation, and the glow discharge or "cold plasma" was initiated by a. c. or d. c. fields of several hundred volts between the internal electrodes (1).

We wish to report an electrodeless discharge synthesis of a polymeric material involving the simple inorganic gases CO, N<sub>2</sub> and H<sub>2</sub>. The advantages of the electrodeless technique are principally avoidance of electrode erosion or kinetic interaction of the electrodes with the reacting gas mixtures, the capability of filling uniformly a plasma reactor with a volume of excited gas, and engineering advantages of radiofrequency excitation.

### Experimental

#### Run Procedure

An apparatus for precision metering of several gases into plasma reactors was designed and constructed for this work. Figure 1 shows the system design. Up to four different gases may be metered individually at known flowmeter pressures. Since the gases were non-corrosive, mercury manometers adequately served as the flowmeter pressure measurement device. Flows of gases in cm<sup>3</sup> min<sup>-1</sup> NTP were calculated from the gas viscosity at the operating temperature, the gas density at the operating pressure and temperature, and the flowmeter scale reading. The flowmeter operating pressure P<sub>FM</sub> was calculated from  $P_{FM} = \Delta P + P_{SYS}$  where P<sub>SYS</sub> is the system pressure measured at Point A and  $\Delta P$  is the differential pressure across the manometer.

The accuracy of flow rates are taken to be  $\pm 2\%$  to  $\pm 10\%$  depending on flow meter condition and flow rate. In nearly every case, the  $\pm 2\%$  accuracy was maintained. The reagent gases, sources, and statement of purity are as follows:

<u>Gas</u>	<u>Grade</u>	<u>Source</u>	<u>Purity</u>
CO	C. P.	Matheson	99.5%
N <sub>2</sub>	Extra Dry	"	99.7%
H <sub>2</sub>	Pre-Purified	"	99.95%
CO <sub>2</sub>	Coleman	"	99.99%

After calculations of the desired flow rates and consequent required flow conditions, the entire gas line is purged by alternate pumping and filling with the desired gases. The metering valve V(2) and the flow meter pressure regulating valve V(3) are adjusted to provide the conditions of flow meter pressure P<sub>FM</sub> and flow meter indication necessary to produce with accuracy the desired flow-rates. Leak checks

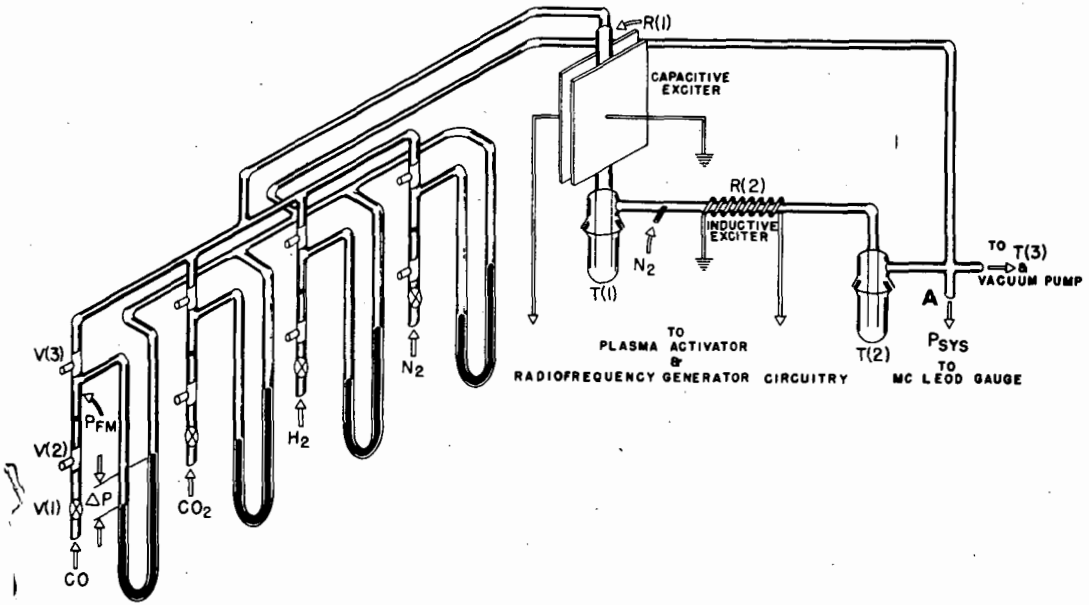


Fig. 1 Schematic of flow discharge apparatus and gas monitoring system.

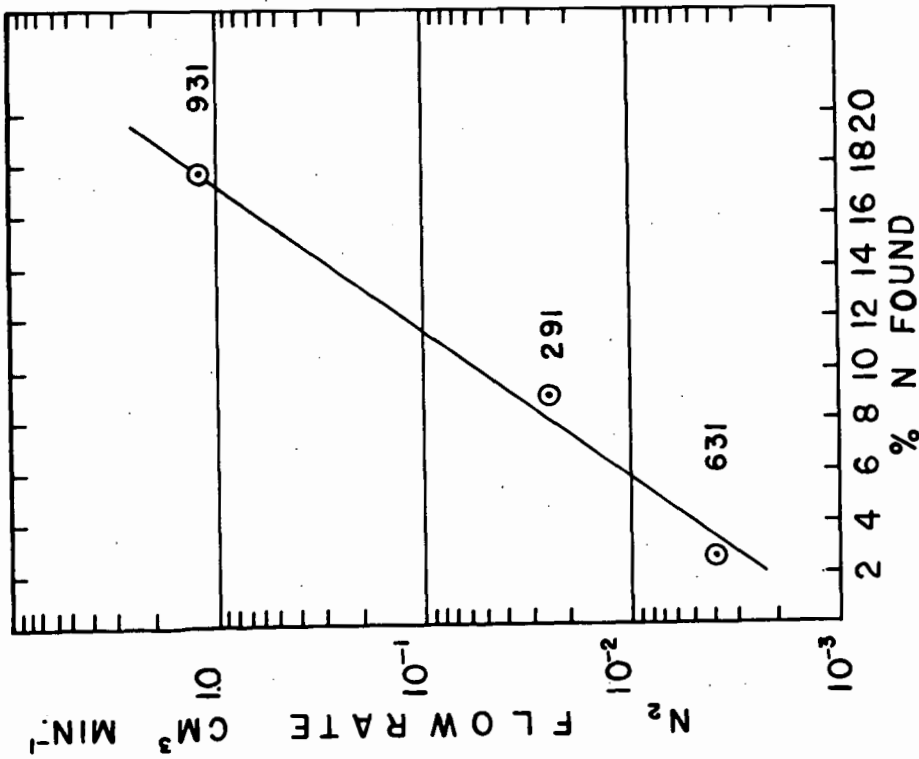


Fig. 2 Dependence of nitrogen found in polymer on nitrogen flow rate.

with a helium mass spectrometer leak detector are made before and after the experimental run. Valve V(1) is a gas flow on-off valve.

With the flow rates accurately adjusted, the RF Generator/RFG-600 (see below) connected to the capacitive exciter is energized and the activator tuned while bringing the generator to maximum power,  $\sim 300$  watts. Trap T(1) which is filled with 3 mm diameter glass beads and some pyrex wool to assure efficient trapping is chilled with liquid nitrogen. Traps T(2) and T(3) are chilled respectively with a dry ice/2-propanol slurry and liquid nitrogen. T(3) contains 5 mm glass beads again to assure efficient trapping and to assure non-interference from vapors originating from the pump. Next, the second RF generator/RFG-600 connected to the inductive exciter is energized and the activator tuned while bringing the generator to maximum power,  $\sim 300$  watts.

With the gases and flows selected for the experiment, the reaction proceeds and the polymer is allowed to accumulate along with the other products. After running a length of time, the generators and gas flows are turned off and the traps allowed to warm up. The pump is then valved off and the system let up to atmosphere with Argon. The polymer of interest is removed from the inner surface of the center tube of T(2) and retained for analysis.

### Radiofrequency Equipment

The two plasma reactors were each activated either capacitively or inductively with RF generators (RFG-600, Tracerlab, Inc.) with deliverable power from minimum up to 300 watts. The generators consist of an RF section composed of a two stage system utilizing a crystal controlled oscillator, and a Class C power amplifier stage. The second part is a power supply producing plate, screen, bias, and filament power. The details of the electronic requirements for generation and transmission of RF energy have been described elsewhere (2).

Energy from the generator is transmitted to the exciter plates R(1), or coil, R(2) via a plasma activator, the circuitry of which allows maximization of the RF energy to the gas load and minimization of the reflected power back to the generator. A great experimental advantage of this means of power delivery and measurement is the ability the operator realizes in being able to reproduce his discharge conditions for the different experiments or from run to run. The net power delivered by the generator is a function of gas type and concentrations, which in turn are related to system pressures and flow rates. Each time an excited gas parameter is changed, there is a concomitant change in the intrinsic impedance of the gas load, which must be rematched to the impedance of the secondary activator circuits. Thus, the convenience of simply being able to achieve this matching by the power meter on the generator, which reads forward and reflected power, is a decided advantage.

All experiments were carried out at a radiofrequency of  $13.56 \text{ MHz} \pm 6.87 \text{ KHz}$ , an FCC approved non-interference band. The choice of inductive vs. capacitive exciters for R(1) and R(2) was rather arbitrary, both were employed to test any significant differences in the reactions induced. The conclusion is that the chemistry is independent of the mode of excitation. There are, however, definite advantages either configuration offers in certain systems, such as gas-solid reactions. This has been described in Ref. (2).

## Observations and Discussion

### Synthesis

The polymers to be described below can be produced either of two ways: (1) the reaction directly of CO, H<sub>2</sub>, and N<sub>2</sub>; or (2) the reaction first of CO<sub>2</sub> and H<sub>2</sub> to produce CO, via the water gas reaction, and then subsequent reaction of the produced

CO, with excess H<sub>2</sub>, and N<sub>2</sub> admitted either downstream of T(1), as indicated in Fig. 1, or in the manifold system. The latter experiment was believed to be a purer source of CO and was employed for most of the preparations. The liquid nitrogen temperature of T(1) and its packing trapped all significant water produced in the water-gas reaction, as well as remaining CO<sub>2</sub>. It became apparent that if T(1) does not trap all the significant water, that no polymer forms at T(2), due either to a re-action of H<sub>2</sub>O or discharge products therefrom (3) with polymer precursors, or to the interference of water to the deposition of the polymer as a film on the cold inner tube of T(2).

The polymers at low N<sub>2</sub> flows are characterized by being transparent, yellow, tightly adherent films. At higher N<sub>2</sub> flows, the transparency decreases, and film strength appears to decrease, indicating perhaps lower molecular weight materials being formed.

The production of the polymer under the flow conditions listed in Table I appears critically dependent on the system pressure. In the experiments, the flows of CO or CO<sub>2</sub> and H<sub>2</sub> were maintained at nearly constant values while the nitrogen flow rate was varied. The very low flow rates of N<sub>2</sub> resulted from permeation through a very short segment of Tygon tubing initially connecting R(1) to the manifold outlet. These rates of permeation were measured by observing rates of system pressure increases with time, and checked by He permeation with the mass spectrometer at the same point. In Run 861, the uncertainty is probably an order of magnitude; in Runs 631 and 291, the uncertainties are half that. In any case, the low flows of N<sub>2</sub> in the initial experiments were much less than measured flow rates in subsequent experiments, which indicate (Table I) that less and less polymer is produced (other gases fixed) as the N<sub>2</sub> flow rate increases. At a very high N<sub>2</sub> flow, ca. 107 cm<sup>3</sup> min<sup>-1</sup>, no polymer was observed to form at all.

TABLE I. Flow Conditions for Several Sample Preparations

Run	Flow Rates, cm <sup>3</sup> min <sup>-1</sup>				P <sub>SYS</sub> , torr	Power, Watts		Run Time, Mins.
	CO <sub>2</sub>	CO	N <sub>2</sub>	H <sub>2</sub>		R(1)	R(2)	
861	1.18	---	~3.1x10 <sup>-6</sup>	3.65	.310	330	355	680
631	1.43	---	3.9x10 <sup>-3</sup>	3.95	.320	---	280	414
291	----	2.18	~2.5x10 <sup>-2</sup>	4.43	.36	300	---	720
931	1.25	---	1.26	3.60	.45	320	350	463
991	1.36	---	9.88	3.83	.75	320	410	460
890	1.36	---	107	3.74	2.47	320	360	273

Table II indicates elemental analyses for C, H, N, and O for several runs. The per cent nitrogen is found to increase as the flow of N<sub>2</sub> increases. This suggests, up to a certain point, that one can produce in this experiment tailored polymers containing a controllable amount of a given constituent by controlling its flow rate. The dependence of per cent nitrogen found in the polymer on flow rate is given in Figure 2.

Why no polymer forms at high system pressures, ca. 1.0 mm Hg pressure, is perhaps due to competing gas phase processes (4). The same types of polymers no doubt may be arrived at by substitution of ammonia for the N<sub>2</sub> - H<sub>2</sub> mixture, since one often achieves many similar results irrespective of whether one uses N<sub>2</sub> + H<sub>2</sub> or NH<sub>3</sub>. Little molecular or atomic oxygen, as such, should be produced in these

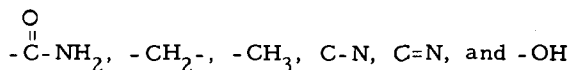
discharge reactions producing the polymer film. If any appreciable amount were present, this would readily oxidize the polymer, since we typically clean up our system of all organic products using an oxygen discharge.

TABLE II. Elemental Analysis for Several Typical Preparations

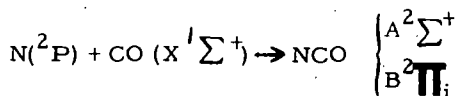
Run	% Element Found				Total
	C	H	O	N	
861	80.51	10.31	8.06	0.2	99.1
631	75.0	9.5	12.7	2.8	100.0
291	68.19	9.12	13.23	8.84	99.38
931	55.90	7.77	18.40	17.64	99.71
991	very little formed				
890	no polymer formed				

### Spectroscopy

The transmission infrared (Fig. 3) and internal reflectance, ATR (Fig. 4) spectra for samples 291 and 633, respectively, show very nearly identical features for the principal bands. Structural moieties such as



in organic compounds give the best comparative infrared spectral features to those observed for the synthesized polymer. Spectra of polyacrylamides, polyacrylonitriles and proteins (5) of some types, give quite similar spectra. Carbon-nitrogen double or single bonds may exist in the synthesized polymer, but there is no evidence for the strong  $-\text{C}\equiv\text{N}$  frequency at ca. 2240 - 2260  $\text{cm}^{-1}$  (5). Nicholls and Krishnamachari (6) found in microwave electrodeless discharges at 2450 MHz emission bands of NCO formed at cryogenic temperatures from the reaction



at the cold surface. Thus an NCO species may enter into the polymer as an important structural entity in the present case.

### Conclusions

Under the flow discharge conditions of this study, the RF electrodeless method appears to offer interesting synthetic possibilities with the simple inorganic gases. One might better understand the mechanism of origin of some polymers as a function of simple excited molecular, atomic or free radical precursors, generated in the discharge. The composition of the gas phase products formed in various reactions would be worth monitoring. Some of the gas products in the present study are being analyzed.

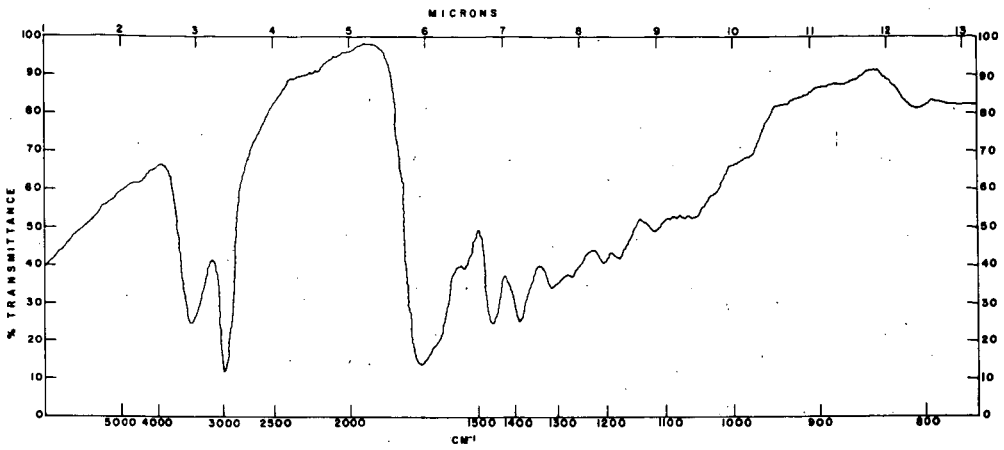


Fig. 3 Infrared transmission spectrum of polymer, Run 291.

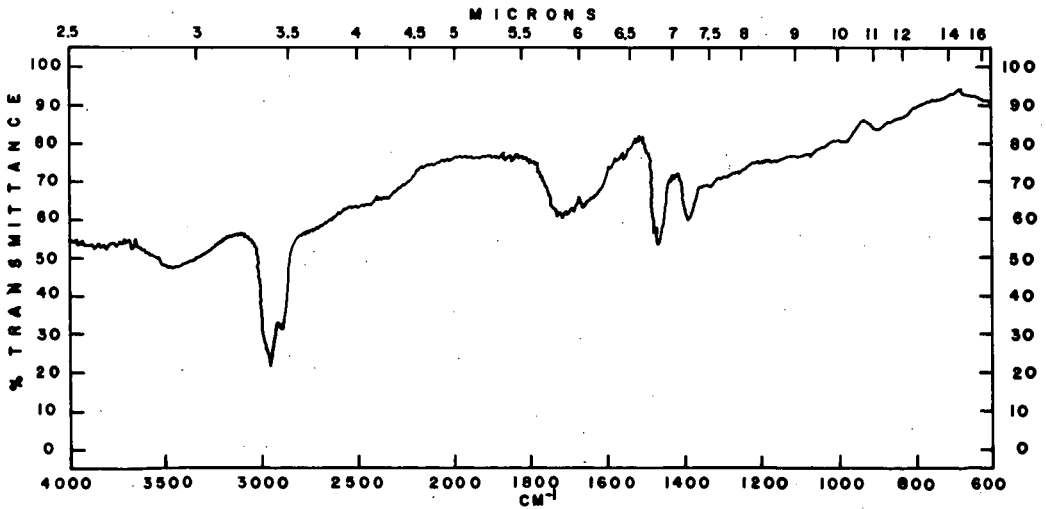


Fig. 4 Infrared ATR spectrum of polymer, Run 633.

Acknowledgement

The authors are pleased to acknowledge the analytical assistance of Dr. Robert Rinehart of Huffman Laboratories, of Wheatridge, Colorado. Mr. Jim Beaudry engineered all the RF generator and activator circuitry, and for whose assistance we are deeply indebted. Finally, technical discussions with Richard Bersin were most helpful.

Literature Cited

1. J. Goodman, J. Polymer. Sci. 44, 551 (1960); pertinent references to past works are located here.
2. J. R. Hollahan, J. Chem. Ed., 43, A401, A497 (1966).
3. N. Hata and P. A. Giguere, Can. J. Chem., 44, 869 (1966); F. Kaufman, Ann. de Géophys., 20 106 (1964).
4. B. D. Blaustein, U. S. Bureau of Mines, Pittsburgh, Pa., personal communication, has studied a system similar to ours at higher pressure, but has observed no polymer formation.
5. J. Schurz, H. Bayzer, and H. Sturcken, Makromol. Chem. 23, 152 (1957); P. A. Wilks and M. R. Iszard, "Identification of Fibers and Fabrics by Internal Reflection Spectroscopy", paper presented at Fifteenth Mid-America Spectroscopy Symposium, Chicago, Illinois, June 2-5, 1964.
6. R. W. Nicholls and S. L. N. G. Krishnamachari, Can. J. Chem., 38 1952 (1960).

## The Dissociation of Toluene Vapor in a Radiofrequency Discharge

Frank J. Dinan

Department of Chemistry, Canisius College, Buffalo, New York

The emission spectra resulting from the excitation of toluene vapor in electrode discharges have been investigated by Schuler as a part of his extensive work dealing with the behavior of molecules in discharges.<sup>(1)</sup> He found that two distinctly different spectra were emitted. One, the normal toluene emission spectrum, was centered in the 2600-3000 Å region and was related to the forbidden benzenoid absorption band of toluene in the crude minor image relationship which characterizes fluorescence emission. This spectrum, as it was obtained in the present study, is shown in figure 1. In addition to this ultraviolet emission, Schuler also observed a visible emission spectrum from toluene which appeared in the 4300 to 5000 Å region, the details of which were not published. This spectrum was designated the "blue spectrum" and was assigned to the benzyl radical without strong supporting evidence.

In a subsequent study of the reactions of toluene vapor in a high voltage electrode discharge, Kraaijeveld and Waterman<sup>(2)</sup> investigated the formation of the bibenzyl molecule from toluene and found that, under optimum conditions in a 2400 V arc, 40% of the toluene vapor could be converted to bibenzyl. The other products formed under these conditions were not investigated. This result, as well as those obtained by Schuler, imply the existence of benzyl radicals as the major species present in electrode induced toluene discharges.

More recently, Streitwieser and Ward conducted the first comprehensive study which was concerned with the range of products formed from the electrodeless microwave excitation of toluene vapor.<sup>(3)</sup> In this study, flowing toluene vapor in a helium carrier gas stream was excited by a 3 Mc microwave generator. The spectrum of the light emitted was not investigated, however the products were carefully determined. The composition of the mixture of products obtained is shown in figure 2.

The very minor amounts of dimer biaryls which were formed in this discharge suggested that radical intermediates were not of dominant importance. The lack of formation of the xylene isomers was also interpreted as supporting the absence of methyl radicals in the plasma.

Two other possibilities, the molecular cation and anion were considered as likely intermediates in the microwave discharge. Results obtained from labeling experiments ruled out consideration of the cation, and it was tentatively concluded that anion intermediates remained as the most likely possibility.

This result contrasted interestingly with the conclusions which had been previously drawn regarding the dominance of radicals in toluene discharges and cast some doubt on these conclusions. However, work which had been done in W. D. Cooke's laboratory at Cornell University suggested that very significant differences might be anticipated between the products resulting from the excitation of organic vapors in a microwave powered discharge and the excitation of these vapors with a radiofrequency source. It was, therefore, decided to investigate both the spectra and the products obtained when toluene vapor was excited in a 28 Mc. radiofrequency discharge.

The apparatus used in this study is shown in block diagram form in figure 3. Flowing toluene vapor was passed through a discharge powered by an R.F. transmitter operating at 28 megacycles and 100 watts output. The pressure of the vapor was maintained constant at 0.10 to 0.15 mm. Materials formed in the plasma were collected in traps maintained at 0° and 80° and were subsequently investigated by gas chromatographic and spectroscopic techniques. The light emitted from the discharge was focused into a scanning monochromator and detected by a IP-28 photomultiplier tube. The amplified output of the photomultiplier was recorded electronically. Under the conditions used in these experiments, toluene was converted to products in 12 to 16% yield with 75 to 82% of the toluene being recovered unchanged.

## TOLUENE ULTRAVIOLET EMISSION

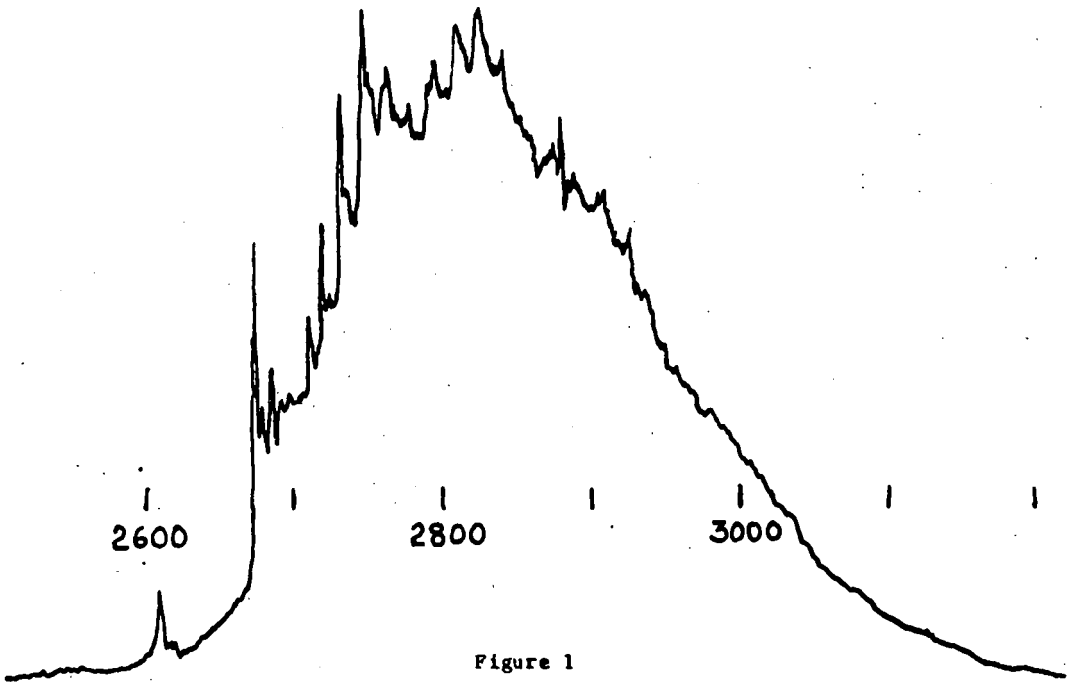


Figure 1

PRODUCTS FROM TOLUENE VAPOR  
IN A 3 KMc. POWERED DISCHARGE

	%
BENZENE	49
ETHYLBENZENE	30
PHENYLACETYLENE	8
STYRENE	3
XYLENE ISOMERS	TRACE
BIBENZYL	~0.5
DIPHENYLMETHANE	~0.2
BIPHENYL	~0.1

Figure 2

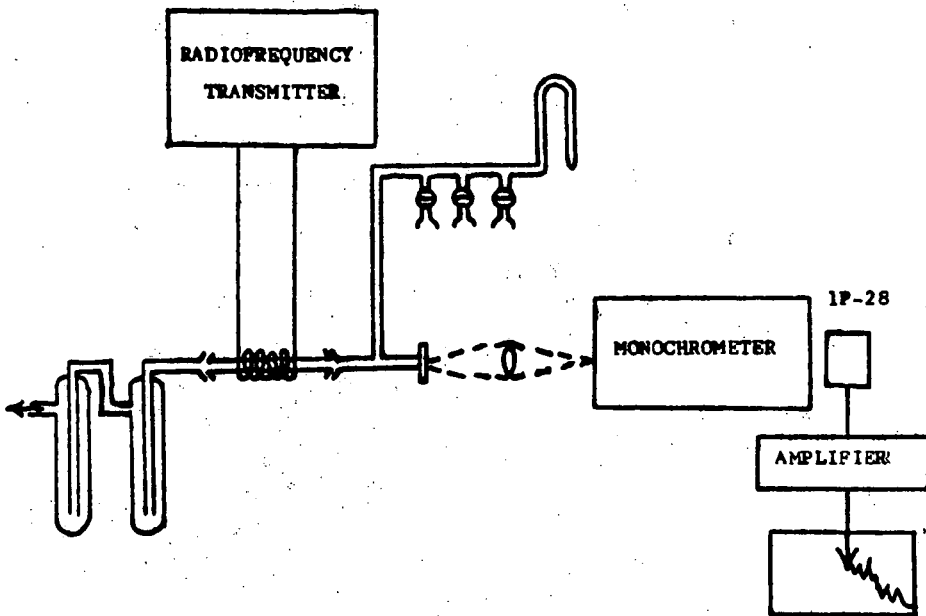


Figure 3

PRODUCTS FROM A 28 MC.  
DISCHARGE IN TOLUENE

<u>PRODUCT</u>	<u>%</u>
BENZENE	35
ETHYLBENZENE	41
BIBENZYL	16
DIPHENYLMETHANE	7
BIPHENYL	2
XYLENE ISOMERS	<1

Figure 4

A summary of the products formed in the R. F. powered discharge is presented in figure 4. It should be noted that these results are normalized to exclude recovered toluene, non-condensable gases and polymeric materials which in combination accounted for 3 to 6% of the original toluene vapor.

The formation of substantial amounts of dimer biaryls; bibenzyl, diphenylmethane and biphenyl is of particular significance since, as noted above, the formation of only trace amounts of dimer biaryls was observed in the microwave discharge. Additional experiments were conducted in which a helium carrier gas was used, and no substantial difference in the nature and amounts of products formed was noted. The change in product ratios, therefore, appears to reflect a change in mechanism which results from the use of an R. F. powered discharge.

The products formed in this study, in particular the large amounts of biaryls, indicate that free radicals are the major intermediates leading to the formation of products. The compounds formed can be readily explained by the series of radical combination and hydrogen abstraction reactions involving benzyl, phenyl and methyl radicals which are outlined in figure 5.

It should be noted that minor, but definite amounts of the three xylene isomers were formed in the radiofrequency discharge. The trace amounts of these isomers which were formed from the dissociation of toluene vapor in a microwave powered discharge has previously been used as an argument against the presence of methyl radicals in the microwave discharge. (3) As is shown in figure 6, however, it has been demonstrated that methyl radicals react with toluene vapor with a hundred fold preference for the side chain rather than the ring positions. (4) It is, therefore, entirely consistent with the presence of methyl radicals in the R. F. discharge that reaction should take place predominantly with the toluene side chain to form ethylbenzene rather than with the ring positions to yield xylene isomers, although the formation of small amounts of xylene should be anticipated.

Experiments in which specifically labeled deuteriotoluene was passed through the R.F. discharge afforded additional experimental data which supported the importance of radical intermediates. The products formed from the labeled toluene were collected, separated by chromatographic techniques, and the distribution of the deuterium label determined by infrared and nuclear magnetic resonance spectroscopy and mass spectrometry.

The side chain of the recovered ethylbenzene was found to be heavily deuterated. The partial mass spectrum of the recovered ethylbenzene compared to the mass spectrum of un-deuterated material is shown in figure 7. The parent peak of the recovered material is five mass units higher than the corresponding peak in the un-deuterated material, and demonstrates the inclusion of five deuterium atoms in the molecule. The base peak of the unlabeled ethylbenzene molecule results from a P-15 cleavage corresponding to the loss of a methyl group. In the spectrum of the recovered material, the base peak results from P-18 cleavage and clearly demonstrates the methyl group of the side chain to be fully deuterated. This molecule presumably forms from the combination of  $C_7H_5D_2$  radical with a  $CD_3$  radical.

The distribution of the deuterium label in the benzyl fragment can be demonstrated by considering the NMR spectrum of the recovered bibenzyl. In figure 8, the 100 Mc. proton magnetic resonance spectrum of un-deuterated bibenzyl and that of the recovered material are compared. It is important to note that the 5:2 ratio of aromatic to methylene protons observed in the non-deuterated material would also be observed with the partially deuterated molecule if the deuterium label were uniformly distributed. The greatly reduced methylene proton peak in the spectrum of the recovered material, however, clearly demonstrates that the label remains localized in the side chain of the benzyl fragment, and is not distributed throughout the ring.

This result is entirely consistent with the presence of free radical intermediates in the discharge since, as is shown in figure 9, it has been demonstrated that the un-ionized benzyl radical does not undergo any type of rearrangement which would result in the randomization of a label, such as the formation of the tropylium radical. (5) By contrast, the benzyl cation does undergo an immediate arrangement to the tropylium ion, which would result in uniform distribution of the deuterium label. (6) Since this is not observed, the benzyl cation can be ruled out as a

## PRODUCT FORMATION REACTIONS

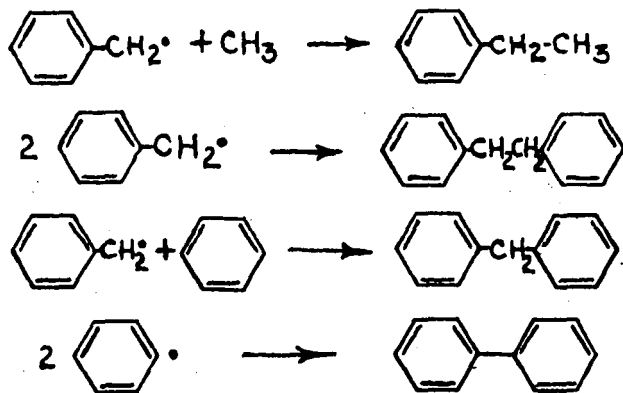
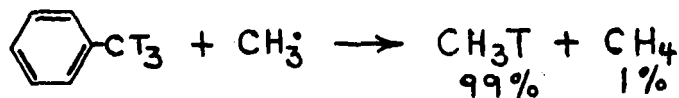


Figure 5

REACTION OF METHYL RADICALS  
WITH TRITIATED TOLUENERELATIVE RATE  
CONSTANTS AT 85°

o -	0.76
m -	0.26
p -	1.00
CH <sub>3</sub> <sup>-</sup>	156

I.V. BEREZIN, et al., ZHUR. OBSCHEI KHIM.,  
30, 4093 (1960). C.A., 55, 27153 b.

Figure 6

## PARTIAL MASS SPECTRA OF ETHYL BENZENE

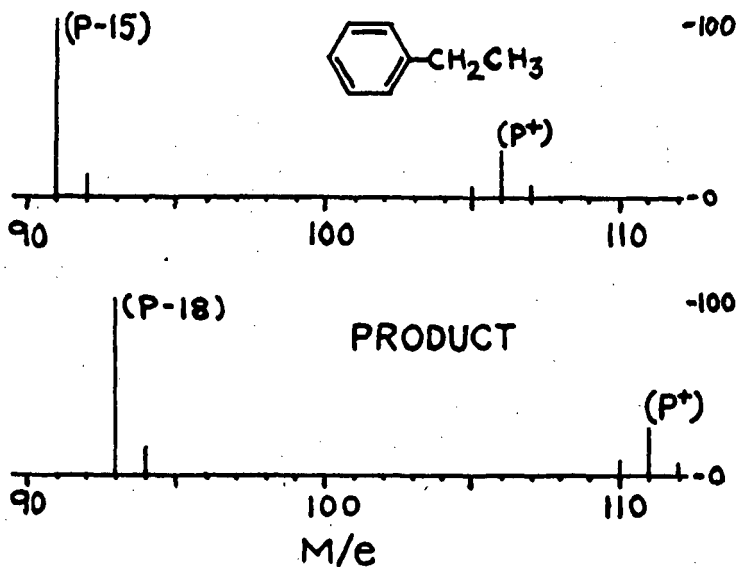


Figure 7

## PARTIAL NMR SPECTRA OF BIBENZYL

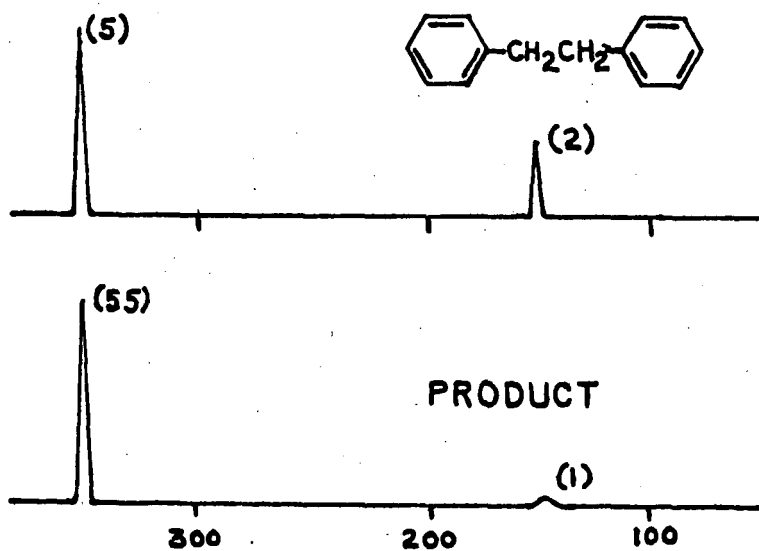


Figure 8

## BENZYL CATION AND RADICAL BEHAVIOR

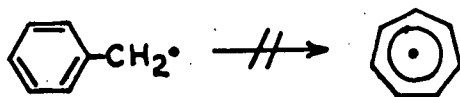
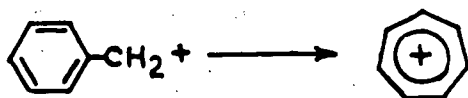


Figure 9

PRODUCTS FROM IODINE AND  
TOLUENE VAPOR IN A 28Mc. DISCHARGE

PRODUCT	%
BENZYL IODIDE	47
IODOBENZENE	14
ETHYLBENZENE	11
BENZENE	13
METHYL IODIDE	6
UNIDENTIFIED	9

Figure 10

significant reaction intermediate.

Additional experiments were conducted in which toluene and iodine vapors were passed through the R.F. discharge together. Figure 10 shows the composition of the products formed in this experiment. In view of the known affinity of iodine for free radicals, (7) the formation of benzyl iodide, iodobenzene and methyl iodide together with greatly reduced amounts of the previously observed products argues for the presence of benzyl, phenyl and methyl radicals in the discharge.

It should also be noted that the visible emission spectrum which is shown in figure 11 was observed with the toluene discharge. This spectrum is similar to that which Schuler had previously observed from electrode toluene discharges and assigned to the benzyl radical.

In summary, the different products and intermediates formed in this work as contrasted to Streitwieser and Ward's study indicates that significant differences are to be anticipated between R.F. and microwave powered discharges, and unequivocally establish the importance of radical intermediates in the toluene R.F. discharge. Additionally, the hazards involved in the generalization of data obtained in a specific type of discharge are readily apparent from these observations.

#### Literature Cited

1. H. Schuler and A. Michel, *A. Naturforsch.*, 10a, 495 (1955)
2. H.J. Kraaijveld and H.I. Waterman, *Brenstoff-Chem.*, 43, 33 (1962).  
*C.A.* 57, 10627f
3. A. Streitwieser and H.P. Ward, *J. Am. Chem. Soc.*, 85, 539 (1963).
4. I.V. Berezin, N.F. Kazankaya and K. Martinek, *Zhur. Obschei Khim.*, 30, 4093 (1960). *C.A.*, 55, 27153b.
5. R.F. Pottie and F.P. Lossing, *J. Am. Chem. Soc.*, 83, 2634 (1961)
6. P.N. Rylander, S. Meyerson and H.M. Grubb, *J. Am. Chem. Soc.* 79, 842 (1957).
7. J.F. Garst and R.S. Cole, *Tetrahedron Letters*, No. 11, 679 (1963).

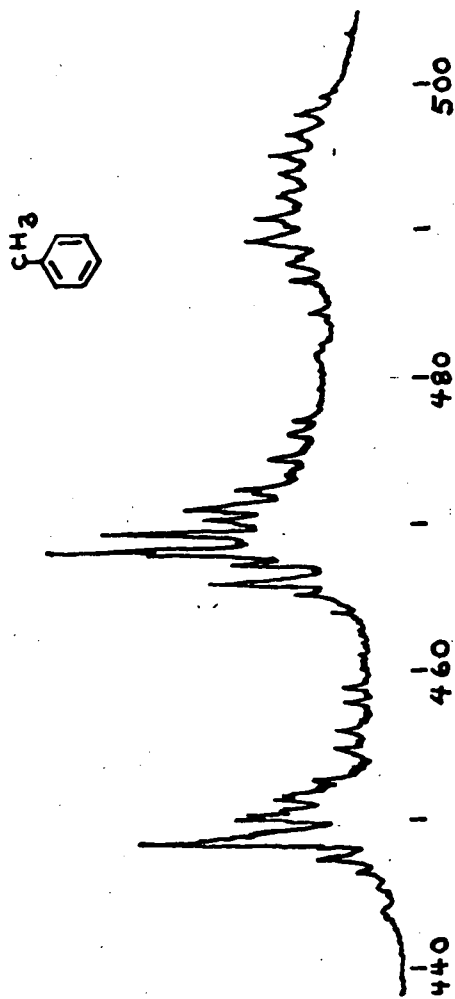


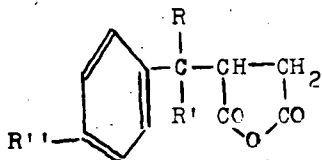
Figure 11  
Toluene Visible Emission

REACTION OF MALEIC ANHYDRIDE WITH AROMATIC HYDROCARBONS  
UNDER THE INFLUENCE OF SILENT ELECTRIC DISCHARGE  
AT ATMOSPHERIC PRESSURE.

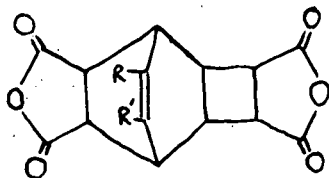
Stylios Sifniades, David Jerolamen, Robert Fuhrmann

Allied Chemical Corporation, Central Research Laboratory, Box 309,  
Morristown, N. J.

Maleic anhydride is known to form two classes of adducts with alkyl benzenes, depending on the conditions of excitation. At reflux temperatures and in the presence of catalytic amounts of peroxides adducts of type I are formed (1,2). A free radical chain reaction is assumed involving abstraction of a benzylic hydrogen. The chain length, based on the ratio of product to added peroxide, is 20 to 100.



I (R, R' = H or Me; R'' = Me, Et, i-Pr)



II (R, R' = H, Me, t-Bu, Cl)

At room or somewhat higher temperatures and in the presence of ultra-violet radiation adducts of type II are formed (3 to 8). Excited aromatic molecules or excited charge-transfer complexes of maleic anhydride with an aromatic molecule are claimed to be the reaction intermediates. The addition is sensitized by benzophenone, but the adduct can be formed in the absence of a sensitizer, although at a much lower rate. It appears that the presence of benzophenone is indispensable if sun light is used as the source of exciting radiation (9). It is interesting to note that in this case only benzene forms an adduct II with maleic anhydride, while alkylbenzenes are only partly incorporated in poly-anhydride chains which are formed.

Recently formation of the adduct II of benzene and maleic anhydride under the influence of gamma radiation was reported (10). The adduct is only a minor product of the reaction, corresponding to about 4% of the maleic anhydride spent. The main product is a mixture of poly-anhydrides. These can be considered to arise through a free radical chain similar to the one yielding adducts of type I.

It is then clear that in the system maleic anhydride-benzene (or alkylbenzene) two types of reactions are prevalent, one by free radical chain yielding adduct I or poly-anhydrides, the other by means of excited molecules or charge-transfer complexes yielding adduct II. It was thought of interest to investigate the influence of silent or corona discharge on this system. This type of discharge was chosen because it is easy to maintain at atmospheric pressure.

#### Experimental.

The discharge apparatus was essentially a modified Siemens ozonizer vertically mounted. It was made of Pyrex glass. A solution of sodium chloride in glycerol circulating in the jacket constituted the ground electrode, while a silver coating in the interior surface of the central

tube served as the high voltage electrode. The reaction mixture was circulated at a high rate from top to bottom through the reactor by means of a custom-made membrane pump constructed of Halon (registered mark of Allied Chemical Corporation). An inert gas, nitrogen or helium, was introduced at the top of the reactor and vented at the bottom through a condenser. The temperature of the reaction mixture was measured at the exit of the discharge. Temperature control was ensured by regulating the temperature of the circulating glycerol solution.

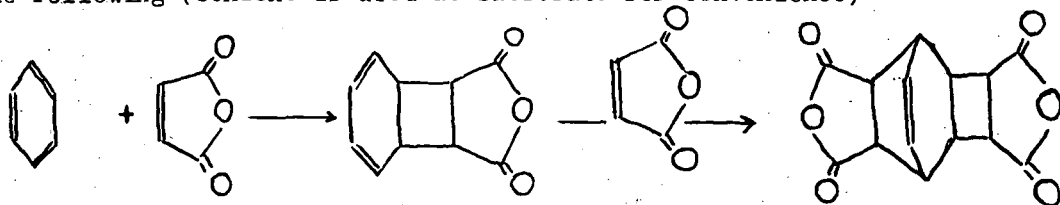
Current at the desired frequencies was produced by an audio-frequency generator (Heathkit Model I7-72) coupled with a 1000 VA custom-made amplifier. It was raised to high voltage by means of a 25 KV transformer. Lower voltages could be obtained by acting on the output of the amplifier. The power input to the system was monitored by means of a watt-meter (Westinghouse Type PY6, specially compensated for high frequency work) at the primary circuit of the transformer.

Eastman White Label chemicals were used without purification. In a typical experiment 29.4 grams of maleic anhydride in 416 ml of cumene were circulated for two hours in the apparatus while the discharge was maintained at a power level of 400 watts. Nitrogen was supplied at the rate of 50 ml/min. The temperature of the reaction mixture was 127° C. The reaction mixture was cooled to 20° C. and the resulting crystals were filtered and washed with 50 ml of cold benzene. Additional crystals were obtained after the mother liquor had been condensed to one third of its initial volume by flash evaporation. The combined product was dried at 50° C. in a vacuum oven. It weighed 5.18 grams and had melting point 255-7° C. Elementary analysis and neutralization equivalent were consistent with formula II ( $R = H$ ,  $R' = i\text{-Pr}$ ). The infra-red spectrum showed absence of aromatic character. Flash evaporation of the unreacted cumene and maleic anhydride left 23.0 grams of a viscous residue which had neutralization equivalent corresponding to a mixture of a 1:1 and 2:1 adduct of maleic anhydride and cumene. It was assumed that it contained adduct of formula I ( $R = R' = \text{Me}$ ) together with products of further condensation with maleic anhydride. Infra-red and NMR spectra were consistent with this assumption.

Similar results were obtained using benzene, toluene, and ethylbenzene as substrates. Chlorobenzene and nitrobenzene failed to yield a crystalline product. The experimental conditions and the results are summarized in table I.

#### Discussion.

It is apparent from the present results that maleic anhydride forms an adduct of type II with benzene and alkylbenzenes under the influence of silent discharge. The generally accepted path of formation of II in photochemical (3) or gamma-radiation induced (10) reaction is the following (benzene is used as substrate for convenience)



It is reasonable to expect that the same path is followed also in the present case of discharge excitation. Since the rate of formation of adduct II is independent of the concentration of maleic anhydride (experiments 2 and 4) it is concluded that the formation of the intermediate monoadduct is the rate-determining step. The same conclusion has been reached in the photochemical formation of adduct II (3,4).

Adduct II is not, however, the only product formed in the reaction; a considerably larger amount of resinous material (tabulated as adduct "Type I") is also formed in all cases. This material arises from a free radical reaction similar to the one giving rise to adduct I in peroxide-initiated reactions. The chain length of these reactions is about 20 to 100, as mentioned earlier. On the other hand it has been shown that the quantum yield of adduct II formed in photochemical reaction is about 0.1 (4). Since in the present experiments adduct II is formed in amounts about one quarter of the amount of "type I" adduct although about ten excited molecules, or charge-transfer complexes, are necessary to produce one molecule of II, while one free radical will produce 20 to 100 molecules of I, it must be concluded that the great majority of active species in the liquid phase in contact with the discharge are excited molecules and not free radicals. In fact it can be estimated that 98% to 99% of the active species are excited molecules. The absence of free radicals as important reaction intermediates has also been deduced by product analysis in the microwave glow discharge of aromatics in helium, (11).

In the photochemical reaction benzene forms an adduct II at a higher rate than the alkylbenzenes, which in turn react in relative rates indicative of steric hindrance. No such effect was observed in the present work, as shown by the power yields in the table. These yields are also measures of the rate of formation of adduct II since roughly equal power levels of discharge were maintained in all cases.

Comparison of runs 1 and 2 shows that formation of adduct II is favored at the lower frequency with a correspondingly higher potential difference applied across the electrodes. Although the electric field strength between the dielectric surfaces is not necessarily proportional to the externally measured potential difference (12), it appears that electrons of higher average energy favor the production of adduct II, as evidenced by the fact that the rate of formation of II is higher in a helium than in a nitrogen atmosphere (runs 4 and 5). It is known that the average electron energy for equal field strength is quite larger in the former gas (13). Of course the presence of organic vapors modifies the electron energy distribution but it is reasonable to expect that some difference still exists.

The mechanism of energy transfer cannot be deduced with certainty from the present data. Comparison of yields at two temperatures (runs 2 and 3) shows higher yield at the higher temperature, a fact which may be interpreted as meaning that benzene vapors in the discharge are excited by collision with electrons: at the higher temperature the concentration of benzene in the gas phase is higher. While this conclusion may be correct it is not unambiguous because of mechanical difficulties at the lower temperature, arising from the fact that adduct II was sparingly soluble in benzene at this temperature and quickly coated the dielectric surfaces where it was partly decomposed. Another way of excitation would involve bombardment of the liquid phase with electrons generated in the discharge. This method of excitation has been shown to prevail in the discharge-induced oxidation of acidified water and ferrous

ion (14). Excitation by collision with excited nitrogen or helium cannot be an important process, considering that the first excited state of helium contains 19.81 ev of energy (15). Collision with such a species would result in extensive fragmentation of an organic molecule, whereas the present results point to the fact that free radical initiation is very limited in this system.

Table I. Condensation of maleic anhydride with benzene and alkylbenzenes under the influence of silent electric discharge.

Number	Charge, gas	Frequ. Kc/sec	Potent. KV.	Temp. C.	Adduct, grams		Yield of II mmole/kw-hr	m.p. C.
					Type I	II		
1	350 ml benz. 50 g MA, N <sub>2</sub>	8.0	10.0	78	25.3	2.12	12.0	
2	350 ml benz. 51 g MA, N <sub>2</sub>	3.6	13.0	75	18.0	3.40	26.5	
3	350 ml benz. 49 g MA, N <sub>2</sub>	3.6	12.5	37	13.2	2.19(a)	15.6	
4	380 ml benz. 12 g MA, N <sub>2</sub>	3.6	13.0	74	14.5	2.77	26.2	
5	380 ml benz. 13 g MA, He	3.6	13.0	75	15.1	4.16	33.3	355-57
6	380 ml tolu. 13 g MA, He	3.6	13.0	82	30.0	4.79	30.4	245-60
7	268 ml etbz. 29 g MA, N <sub>2</sub>	3.6	13.0	121	25.1	7.35	36.0	260-61
8	416 ml cume. 29 g MA, N <sub>2</sub>	3.6	13.0	127	23.0	5.18	29.8	255-57

(a) The product was brown.

Abbreviations: MA, benz, tolu, etbz, cume denote correspondingly maleic anhydride, benzene, toluene, ethylbenzene and cumene.

#### References.

1. W.G. Bickford, G.S. Fisher, F.C. Doller and C.E. Swift, J. Am. Oil Chem. Soc. 1948, 251
2. E.M. Beavers to Rohm and Haas Co, U.S. Patent 2,692,270 (1954)
3. D. Bryce-Smith and A. Gilbert, J. Chem. Soc. 1965, 918
4. G.S. Hammond and W.M. Hardham, Proc. Chem. Soc. 1963, 63
5. D. Bryce-Smith and J.E. Lodge, J. Chem. Soc. 1962, 2675
6. E. Groveinstein, Jr, D.V. Rao and J.W. Taylor, J. Am. Chem. Soc. 83, 1705 (1961)
7. G.O. Schenck and R. Steinmetz, Tetr. Letters, No 21, 1 (1960)
8. H.J.F. Angus and D. Bryce-Smith, J. Chem. Soc. 1960, 4791
9. D. Bryce-Smith, A. Gilbert and B. Vickery, Chem. Ind 1962, 2060; British Patent 986,348 (1965)
10. Z. Raciszewski, Chem. Ind. 1966, 418
11. A. Streitwieser, Jr, and H.R. Ward, J. Am. Chem. Soc. 85, 539 (1963)
12. R. Bartnikas and J.H.E. Levi, Rev. Sci. Instr. 37, 1245 (1966)
13. L.B. Loeb, "Basic processes of Gaseous Electronics", University of California Press (1961)
14. A. Yokohata and S. Tsuda, Bull. Chem. Soc. Japan, 39, 46, 1640 (1966)
15. L.B. Loeb, "Electrical Coronas", University of California Press (1965)

## The Polymerization of Benzene in a Radio-Frequency Discharge

David D. Neiswender

Mobil Oil Corporation, Princeton, New Jersey

### INTRODUCTION

The reactions of benzene in various types of electrical discharges have been studied by a number of researchers over a span of nearly 70 years. Reported results vary widely. Several early workers (1-3), using ozonizer tubes, obtained a gummy, wax-like substance, along with hydrogen, acetylene and other light hydrocarbon gases. One of these researchers later obtained a liquid and a solid, both analyzing as  $C_{24}H_{25}$  compounds (4). In 1930 Austin and Black (5) found diphenyl and a solid which they suspected to be a polyphenylene containing phenol groups. Harkins and Gans (6), using an electrodeless discharge, got complete conversion to a red-brown insoluble solid analyzing for  $(CH)_x$ . Davis (7), on the other hand, obtained diphenyl, p-terphenyl, a resin  $(C_6H_4)_x$ , hydrogen, acetylene, ethylene and light paraffins. A 1935 U.S. patent (8) describes a discharge apparatus for preparing diphenyl from benzene. More recently, Streitwieser and Ward (9,10) obtained a 5% conversion of benzene in a microwave discharge, the products being low molecular weight gases, toluene, ethylbenzene and phenylacetylene. Stille and co-workers (11), using a radio-frequency discharge, got a 10% conversion to poly(p-phenylenes); diphenyl, fulvene, acetylene, allene, and methylacetylene. Vastola and Wightman (12) obtained a solid film and concluded from the infrared spectrum of the film that no aromaticity remained in the polymer. Jesch et al (13), on the other hand, also obtained a solid film, but interpreted its infrared spectrum as suggesting the presence of aromatic groups as well as olefinic and acetylenic unsaturation. The wide disparity of the results certainly indicates there is still much to be learned about the chemistry of benzene in electrical discharges. This disparity is probably due largely to widely varying reaction conditions. Especially important are considerations such as the power dissipated in the discharge, the pressure, etc.

The work described here is an attempt to systematize the study of benzene reactions in radio-frequency discharges. The only products isolated in these reactions were diphenyl, a liquid polymer and a solid polymer. The polymers appear to be polystyrenes.

## EXPERIMENTAL

Apparatus and Procedure

The apparatus consisted of a 3.69 MHz radio-frequency generator capacitively coupled to a cylindrical pyrex flow reactor by means of two external copper electrodes. An inductively coupled tank circuit was used to match the impedances of the generator and the reactor. An approximate measure of the power dissipated in the discharge was determined by measuring the voltage and current during the experiments and making a phase correction for the capacitive component of the reactor current. A simple schematic of the apparatus is shown in Figure 1.

The hydrocarbon or helium-hydrocarbon mixture was metered into the reactor at various rates. Reactor pressures from 1-20 torr were employed. In most cases the discharge established itself as soon as the r.f. signal was applied. If it did not, it was triggered with a Tesla coil. Products were collected in a series of traps, one at room temperature, one at  $-78^{\circ}\text{C}$  and one at  $-195^{\circ}\text{C}$ .

Chemicals

Reagent grade, thiophene free benzene (Baker) and vacuum distilled styrene (Matheson, Coleman and Bell) were used in the discharge experiments. The helium (Matheson) had a reported minimum purity of 99.995%.

## RESULTS

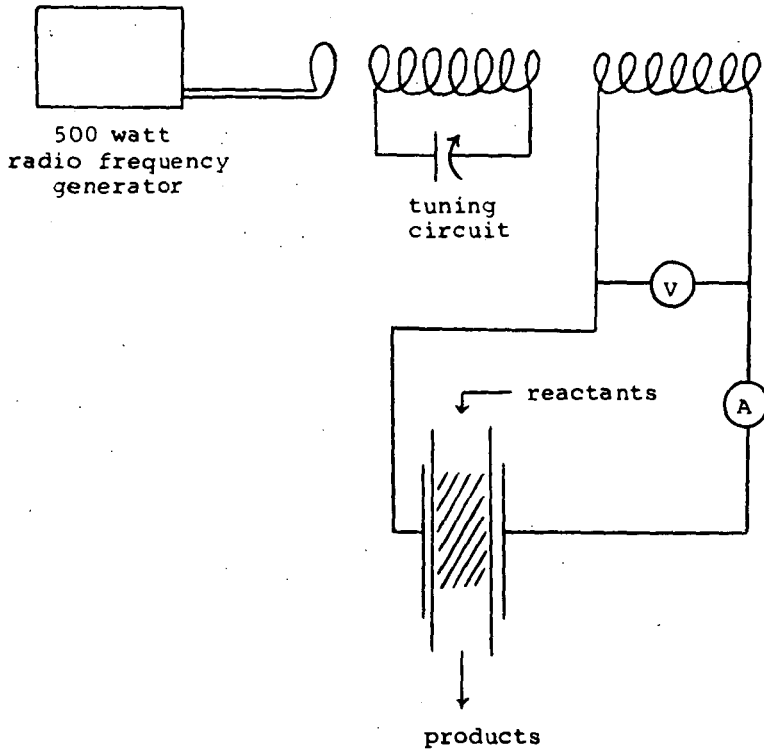
Depending on the conditions employed, the reaction of benzene in the r.f. discharge resulted in either a complete conversion to a solid polymer or a lower conversion to a liquid polymer and diphenyl. The solid tends to form under conditions of high power dissipation and/or low partial pressures of benzene in the reactor. Conversely, the liquid polymer and diphenyl result under low power dissipation and/or high partial pressures of benzene.

The solid polymer, which can sometimes be observed leaving the discharge zone as a fine smoke, deposits throughout the trap system, but principally in the dry ice trap. When collected, it is a very light, fluffy, nearly white powder which picks up a considerable static charge upon handling. Some of the substance's physical and chemical properties are as follows:

1. It is completely insoluble in water and in all organic solvents which were tested.
2. It does not melt up to  $435^{\circ}\text{C}$ .
3. Thermogravimetric analysis shows that the polymer undergoes a stepwise loss in weight, with the loss being complete at  $580^{\circ}\text{C}$ .
4. X-ray diffraction studies show it to be completely amorphous.
5. The density of a pressed pellet is 1.10 g/cc.

Figure 1

## Radio Frequency Discharge Reactor



6. A freshly prepared sample was found to have an electron spin density of  $2 \times 10^{17}$  spins/cc.
7. Its surface area (nitrogen adsorption) is  $42 \text{ m}^2/\text{g}$ , a rather high value for an organic substance.
8. It is neither thermosetting nor thermoplastic.
9. It chemisorbs oxygen from the air at room temperature, the adsorption continuing for extended periods of time.
10. Its carbon-hydrogen ratio is 1:1.

In those experiments which did not yield the solid polymer, the conversion of the benzene was of the order of 30%. About 5% of the benzene was converted to diphenyl; the other 25% was converted to a liquid polymer with an average molecular weight of 617. This polymer, a viscous amber liquid, was not characterized as completely as the solid, but infrared spectral data indicate it to be very similar structurally to the solid.

## DISCUSSION

### Polymer Structure

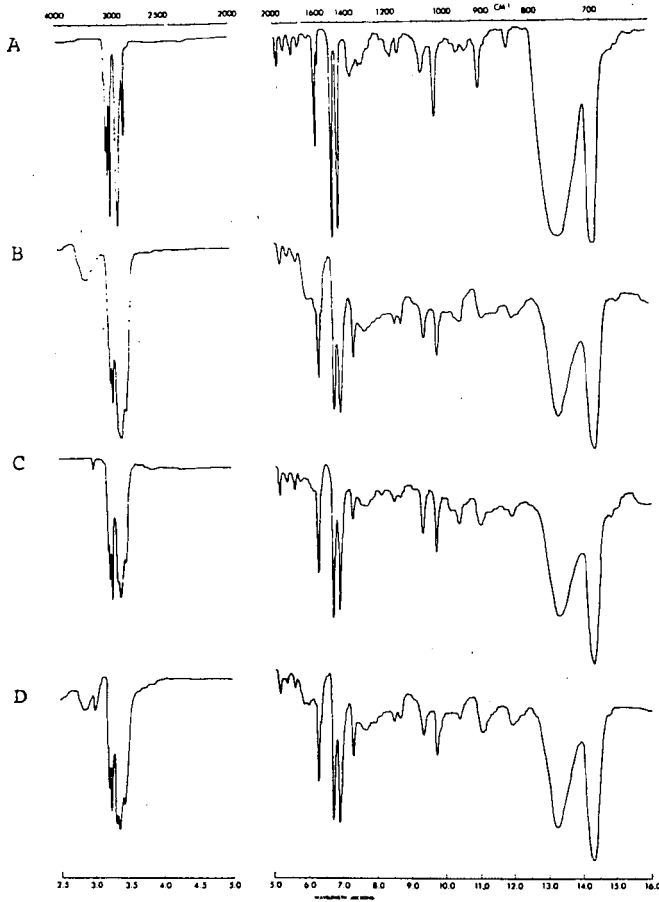
The physical properties of the solid suggest that it is a high molecular weight, highly cross-linked polymer with an irregular structure. The extreme insolubility precludes spectral studies requiring solutions. It was possible to obtain an infrared spectrum by preparing a KBr pellet containing 2% of the solid. The liquid polymer, which was soluble in organic solvents had an infrared spectrum very similar to the solid.

Of several structural possibilities considered, the one which agrees best with the infrared data and seems the most likely from a chemical viewpoint is a polystyrene type structure. In Figure 2, the infrared spectrum of a reference polystyrene film (A) is compared with the spectra of the solid (B), the liquid (C) and a solid polymer obtained when a styrene-helium mixture was passed through the discharge (D). The spectra are nearly identical, the only significant differences being the OH absorptions in the  $3300\text{--}3400 \text{ cm}^{-1}$  range and the carbonyl absorptions at about  $1700 \text{ cm}^{-1}$ . These bands in all three of the spectra from the discharge-derived polymers are due to rapid oxidation by molecular oxygen. These bands become quite pronounced if the polymers are allowed to stand in air for a few hours.

It is believed that the principal difference between the solid and liquid products is that the liquid is essentially a linear polymer, while the solid is highly cross-linked. Such a highly cross-linked polystyrene would be expected to have a lower ratio of aromatic C-H to aliphatic C-H bonds than would a linear polymer. Comparison of spectrum B or D with C in Figure 2 shows that the intensity of the C-H stretching vibrations agrees with this expectation.

Because the solid and liquid seem to be structurally similar, the NMR spectrum of the latter was examined and compared with that of an authentic polystyrene sample. As is generally true with polymeric materials, the resolution was quite poor and only broad bands were

Figure 2. Infrared Spectra

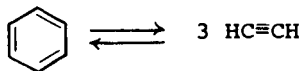


- A = Polystyrene film
- B = Solid polymer from benzene
- C = Liquid polymer from benzene
- D = Solid polymer from styrene

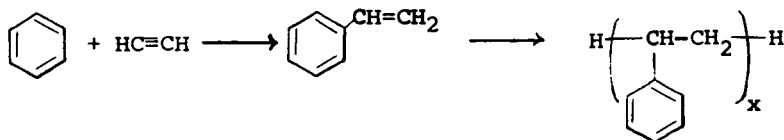
observed. The polystyrene (10% solution in  $\text{CCl}_4$ ) spectrum simply showed two broad peaks - one centered at  $\delta = 1.50$  due to aliphatic protons and one at  $\delta = 7.08$  (with a small companion peak at  $\delta = 6.58$ ) due to aromatic protons. The spectrum of the liquid polymer (10% solution in  $\text{CCl}_4$ ) was quite similar with the peaks appearing at  $\delta = 1.60$  and  $7.04$  (no peak at  $\delta = 6.58$ ). In addition, a very small peak at  $\delta = 5.70$  was observed. This is probably due to protons on olefinic double bonds, and suggests either that some unsaturation is present in the polymer backbone, or that some unpolymerized vinyl groups are present. An attempt was made to increase the resolution of the NMR spectra by using a time averaging computer on very dilute solutions of the polymers, but the resolution was unchanged. Though of limited value, the NMR data do support a polystyrene type structure. Coupled with the infrared data, it seems quite likely that the polymers are both polystyrenes.

#### Mode of Formation of Polymer

The most likely route from benzene to polystyrene involves several steps, the first of which is the establishment of an equilibrium between benzene and acetylene:

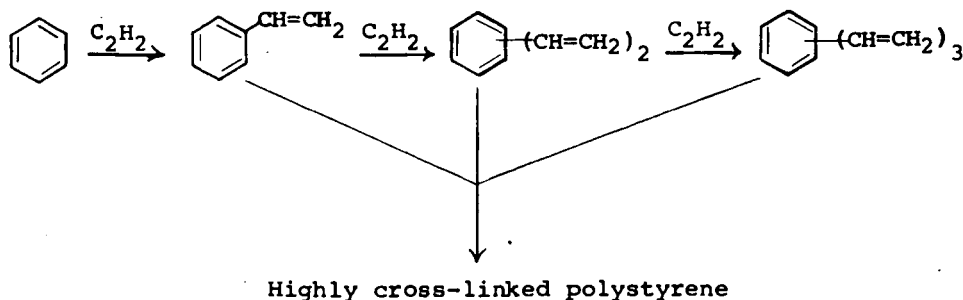


This interconversion has been observed in many high energy systems including electrical discharges. In the next step, the benzene and acetylene, one or both of which may be in a reactive state, combine to give styrene which then polymerizes:



The simple linear polymer thus formed, limited to small chains such as pentamers, hexamers, etc., would explain the liquid polymer product.

The formation of the highly cross-linked solid polymer can be explained by postulating the formation of polyvinylbenzenes which, when polymerized, would yield an extensive, irregular structure:



Both ionic and free radical mechanisms can be written to explain the foregoing reactions in more detail, but these would be strictly speculative, since no definitive experimental evidence has been obtained. Some sort of benzene ions must form as a result of inelastic collisions between the electrons and benzene molecules in the plasma, but whether these ions or some derivative species are the reactive intermediates is not known. Recently, Potter et al (14) have shown that styrene, when perfectly dry, does polymerize via an ionic mechanism when irradiated with gamma rays. One can picture a similar mechanism occurring in the electrical discharge.

On the other hand, the fact that the polymer has a high electron spin density suggests free radical involvement. However, it can be questioned whether the unpaired electrons arose during or after the polymerization reaction. An attempt was made to induce a spin signal in a finely divided polystyrene sample by passing the solid through a helium discharge. No signal was detected after this treatment.

The question of mechanism must await the results of more fundamental studies of the phenomena occurring within the discharge.

#### Effect of Reaction Variables

In an attempt to find a correlation between the reaction conditions and the type of polymer obtained, about 50 experiments were examined. The dependence of the nature of the product and the benzene conversion on r.f. power dissipated per mole of benzene was tested first. Those experiments which gave a complete conversion to solid polymer had an average dose of  $1.9 \times 10^7$  watt-sec/mole  $\phi H$ . Those which gave a low conversion to liquid polymer plus diphenyl had an average dose of only  $7.0 \times 10^6$  watt-sec/mole  $\phi H$ . This correlation with dose is reasonable since more energy would be required to furnish the additional acetylene required for cross-linking and to gain the complete conversion.

A number of experiments within the group examined were conducted with varying proportions of helium, neon and argon mixed with the benzene. The presence of these gases did not alter the correlation with dose provided that the r.f. power dissipated was considered as deposited in the benzene alone. This is a reasonable presumption because the ionization potential of these gases is well above that of benzene.

Within the group of experiments, some produced solid polymer at doses as low as  $4.9 \times 10^6$  watt-sec/mole  $\phi H$ , but with reduced conversions. This suggests that while the dose does correlate with the conversion obtained, it alone does not determine the product. It is evident that this system will require additional investigation to understand how the products form.

## LITERATURE CITED

- ( 1 ) Losanitsch, S. M. and Jovitschitsch, M. Z., Ber. 30, 135 (1897).
- ( 2 ) DeHemptinne, A., Bull. sci. acad. roy. Belg. (3) 34, 269 (1897).
- ( 3 ) DeHemptinne, A., Z. physik. Chem. 22, 360 (1897); 25, 284 (1898).
- ( 4 ) Losanitsch, S. M., Ber. 41, 2683 (1908).
- ( 5 ) Austin, J. B. and Black, I. A., J. Am. Chem. Soc. 52, 4552 (1930).
- ( 6 ) Harkins, W. D. and Gans, D. M. *ibid.* 52, 5165 (1930).
- ( 7 ) Davis, A. P., J. Phys. Chem. 35, 3330 (1931).
- ( 8 ) Kleinschmidt, R. V., U.S. 2,023,637 (1930).
- ( 9 ) Streitwieser, A. and Ward, H. R., J. Am. Chem. Soc. 84, 1066 (1962).
- (10) Streitwieser, A. and Ward, H. R., *ibid.* 85, 539 (1963).
- (11) Stille, J. K., Sung, R. L. and Vander Kooi, J., J. Org. Chem. 30, 3116 (1965).
- (12) Vastola, F. J. and Wightman, J. P., J. Appl. Chem. 14, 69 (1964).
- (13) Jesch, K., Bloor, J. E. and Kronick, P. L., J. Polymer Sci. 4, 1487 (1966).
- (14) Potter, R. C., Bretton, R. H., Metz, D. J., *ibid.* 4, 2295 (1966).

# Chemistry of Electrical <sup>282</sup>Discharge Polymerizations

Dr. Peter M. Hay

Central Research Laboratories, J. P. Stevens & Co.  
Garfield, N. J.

## INTRODUCTION

The conversion of volatile organic compounds into liquid and solid products by the action of a high-voltage gas discharge has been investigated by many people over the past 100 years and more (1). Recently some companies have been reported to be working on the application of this principle to the coating of containers (2), steel strip (3) or fabric (4). These references all have indicated that work was to be under low-pressure conditions where the only gases would be the volatile monomer. In this paper I will describe some results obtained under atmospheric-pressure conditions, with the electrical discharge taking place in a mixture of nitrogen and volatile organic compounds.

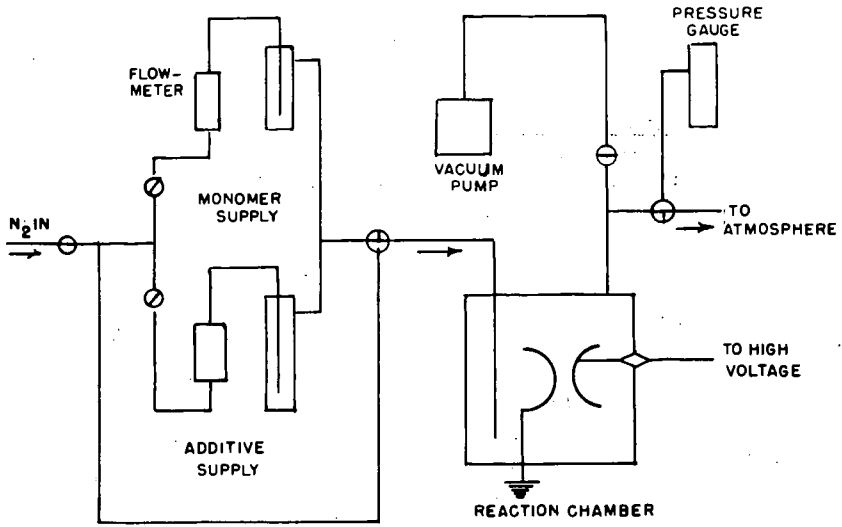
## EXPERIMENTAL METHODS

All polymerizations were carried out at room temperature in a mixture of organic vapors and nitrogen at a total pressure of one atmosphere. The gases were delivered to the reaction zone through the system shown schematically in Figure 1. Nitrogen passed through liquid monomer in one bubble tube and through additive in another tube. The nitrogen and entrained vapors entered the enclosed reaction chamber at one corner and exited to the atmosphere at the opposite corner. The ratio of monomer to additive was determined by weighing the tubes before and after the experiment.

Details of the reaction chamber are shown in Figure 2. Polymerization was initiated by corona discharge between two cylindrical, parallel, insulated electrodes (A) made by lining the inner surfaces of Pyrex glass tubing with aluminum foil. The glass tubing had a wall thickness of 2.5 mm. and an outside diameter of 63 mm. The two glass surfaces were separated by a gap of 4 mm. The alternating current high voltage was supplied by a Tesla generator, manufactured by Lepel High Frequency Laboratories, Inc. (Model HFSG-2). The peak voltage, as estimated by spark length in air, was about 20,000 volts.

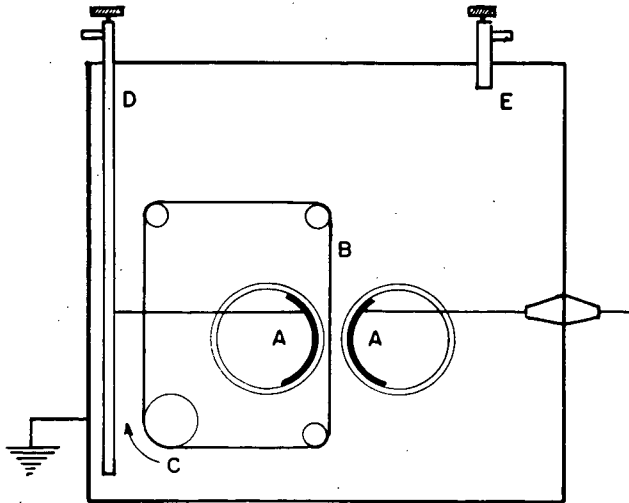
A moving strip of flexible substrate, (B) was positioned in the electrode gap. As shown in Figure 2, this substrate, which in most cases was 2-mil (50 microns) poly(ethylene terephthalate) film, was formed into a closed loop 47 cm. long and 5 cm. wide and was moved by the rotating roller, C. Vapors entered through D and exited through E.

Polymer which formed in the corona zone deposited both on the glass electrode coverings and on the moving substrates. The substrate strip was dried and weighed before and after the polymerization. The coated strips were also baked in a circulating air oven and reweighed. The final weight gain was taken as the yield. In some cases polymer was



VAPOR POLYMERIZATION - SCHEMATIC LAYOUT

Figure 1



VAPOR POLYMERIZATION ON MOVING SUBSTRATE

Figure 2

removed from the glass surfaces by solvent and recovered for infrared or chemical analysis.

## RESULTS

### Survey of Polymerizable Compounds

A number of volatile organic compounds were subjected to corona discharge with a wide variety of results. In almost all cases a deposit of oily or solid brown material formed on the substrate strip. The weight gain resulting from 15 minutes of corona polymerization ranged from tenths of a milligram to over 30 milligrams. When the coated strips were heated at 150°C for 10 minutes, part of the added weight was lost. Some of this is thought to be unreacted monomer which was absorbed by the substrate and coating. Another part of it could be very-low-molecular-weight products of the corona reaction. A third possibility is thermal decomposition of the coating.

The compounds which gave the heaviest coatings after heating, (taking into account the amount of monomer volatilized) included triallylamine, acrylonitrile, toluene and styrene. As the list in Table 1 shows it is not necessary for the monomer to be a vinyl compound in the strict sense of the word in order for a non-volatile polymer product to form in corona discharge. Toluene, benzene, benzotrifluoride and even acetone gave measurable yields. There seems to be no pattern of relationship between the structure of a monomer and its yield in corona polymerization.

TABLE 1

Corona-Polymerizable Compounds  
(Arranged in Order of Yield)

Triallylamine	Benzotrifluoride
Acrylonitrile	4-Vinyl cyclohexene
Toluene	Ethyl acrylate
Styrene	1-Octene
Acrylic Acid	Allyl amine
Benzene	Vinyl acetate
	Acetone

### Effect of Additives

It was found that many halogenated organic compounds, when added to the monomer being volatilized, had the effect of giving a higher yield. Chloroform, bromoform and iodoform were more effective with styrene than some other additives. The yields after oven heating are given in Table 2, expressed as milligrams of weight gain per gram of styrene vaporized. It is interesting to note that the yield is usually increased more by a moderate amount of additive and not so much by a larger amount. Bromine itself reacted immediately with the styrene in the bubble tube but produced the largest yield of all additives tested. Chlorine and iodine seemed to have the reverse or no effect.

TABLE 2

Effect of Halogenated Additives on Corona Polymerization of Styrene  
Yield in Milligrams per Gram of Styrene

<u>Additive</u>	<u>Percent Added</u>	<u>Yield</u>	<u>Additive</u>	<u>Percent Added</u>	<u>Yield</u>
Chloroform	0.5	22.4	Chlorine	7	5.6
Bromoform	0.5	11.6	Bromine	1	19.0
Bromoform	1.0	14.2	Bromine	5	32.0
Bromoform	2.5	19.7	Bromine	10	16.7
Bromoform	5.0	19.2	Iodine	5	9.7
Bromoform	10.0	12.0	None	0	10.7
Iodoform	5.0	21.2	-	-	-

Other additives that enhanced the yields of styrene polymer were carbon tetrachloride, 1,2-dibromo-1,1,2,2-tetrafluoroethane, 1-bromobutane and 2-bromobutane. Yields from monomers other than styrene were not all increased by halogenated additives; some even were decreased. It was impossible to develop any rational relationship between monomer structure and susceptibility of the monomer to yield enhancement by halogenated additive.

The results given above were all derived from experiments in which the additive and the monomer were mixed and volatilized from a single bubble tube. Thus, the exact composition of the vapor was not known. A new set of experiments was carried out using separate bubble tubes for monomer and additive. The weight changes of the tubes during a run were used to calculate mole ratios of additive to styrene. The results of experiments with four additives are shown in Figure 3. The conversion to polymer of styrene without additives was 0.75 to 0.9 percent. As increasing amounts of bromoform, 1-bromobutane or 2-bromobutane were added, the conversion increased and then fell off again. The pattern of points in the case of 1-bromobutane was widely scattered but most of the points lay well above the level for styrene itself. With 2-bromo-2-methylpropane as an additive there was no significant increase in conversion. The weight gain from the additives alone, with no styrene, were all low compared to styrene.

In considering chemical explanations for corona polymerization, both free radical and ionic intermediates are possibilities. Experiments were run with various additives to styrene that might be expected to inhibit each kind of reaction through combination with the active intermediate but no clear-cut reduction in yield was observed. Benzoquinone at 1 and 2 mole percent gave normal yields. Water and butyl amine were extensively studied but, as Figure 4 demonstrates, the tendency for these supposed cation scavengers to depress the conversion is slight and not clear-cut. Butyl amine alone gave a surprisingly high yield. Ammonia, triethylamine, acetone and carbon dioxide as additives had no substantial effect on yield.

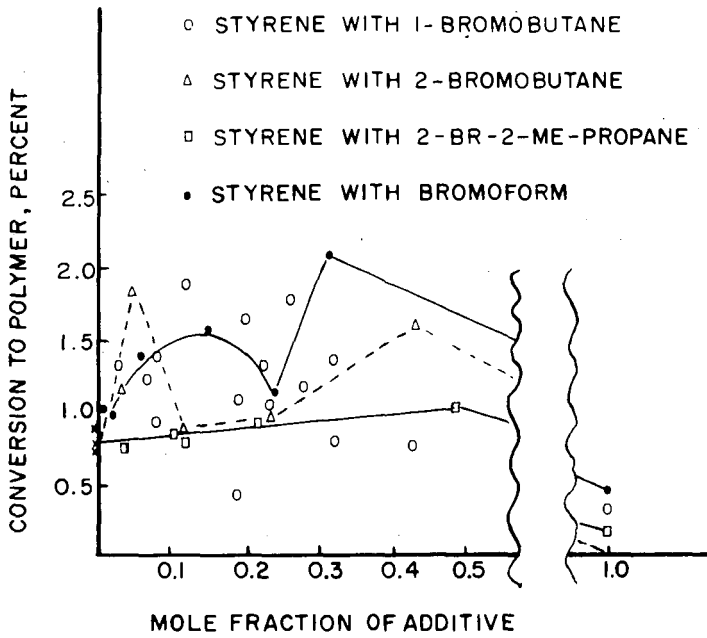


Figure 3

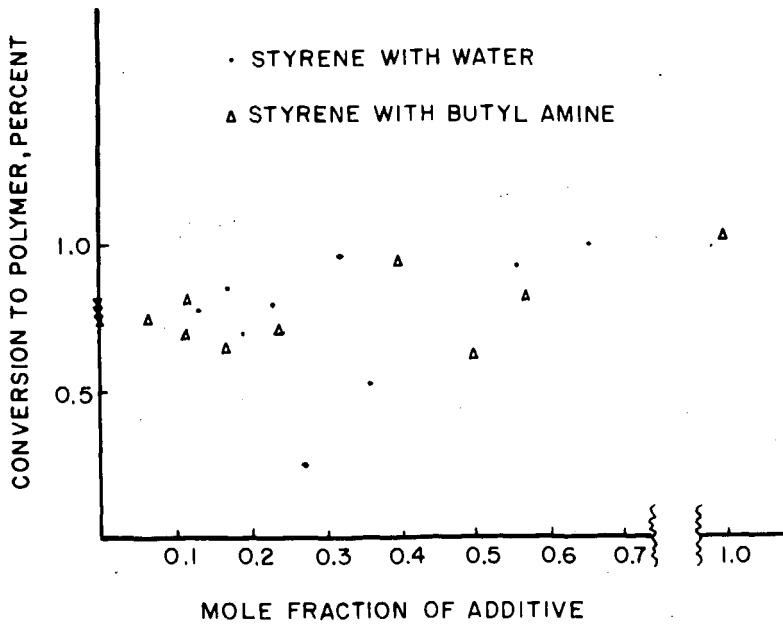


Figure 4

Some evidence was collected on the chemical nature of some of the products. The products deposited on the moving film and on the glass electrode covers were always easily dissolved in common solvents like acetone, chloroform and benzene, indicating low molecular weight and that there was little cross-linking.

Infrared spectra were obtained of polymers made from styrene, benzene and toluene by dissolving the deposit from the glass electrode cover with chloroform and evaporating the solution on a salt plate. The spectra were all similar and closely resembled conventional polystyrene. As Figure 5 shows, there were additional absorptions at 1050, 1220, 1720 and 3400 wave numbers indicating oxygenated products of various kinds including hydroxyl or amino, ester and probably ether. These spectra are very similar to those published by Jesch, Bloor and Kronick (5).

The infrared evidence of oxygen-containing groups was obtained on a styrene product which was prepared and transferred in a nitrogen atmosphere. The only contact with air was during the time the spectrum had been run. The sample was exposed to the atmosphere for 24 hours and it changed only slightly. As Figure 6 shows there was little further increase of bands attributed to oxygenated groups. The only noticeable change in the spectrum was in the relative peak heights at 700 and 760 wave numbers. The spectrum of a product made with 1-bromobutane mixed with the styrene was almost identical to the unmodified styrene product with a stronger absorption ascribed to ketone carbonyl at 1720 wave numbers.

The final evidence of chemical composition was elemental analysis. The styrene product had considerably less carbon than styrene itself, as seen in Table 3. It also contained a significant amount of nitrogen and, as determined by difference, a large amount of oxygen. Heating the polymer in air did not change the composition significantly. Styrene polymer made in the presence of 25 to 30 weight-percent 1-bromobutane had almost the same analysis plus a significant bromine content.

TABLE 3  
Elemental Analysis of Corona Polymers

<u>Monomer</u>	<u>C</u>	<u>H</u>	<u>N</u>	<u>Br</u>	<u>O (by difference)</u>
Styrene, unheated product	72.23	6.86	3.2	-	17.71
Styrene, oven-heated	73.46	6.68	3.39	-	16.47
Styrene plus bromobutane					
unheated product	73.74	6.95	3.59	6.08	9.64
oven-heated product	73.29	6.69	3.56	6.97	9.49
Styrene, calculated	92.26	7.74	-	-	-
Bromobutane, calculated	35.06	6.62	-	58.32	-

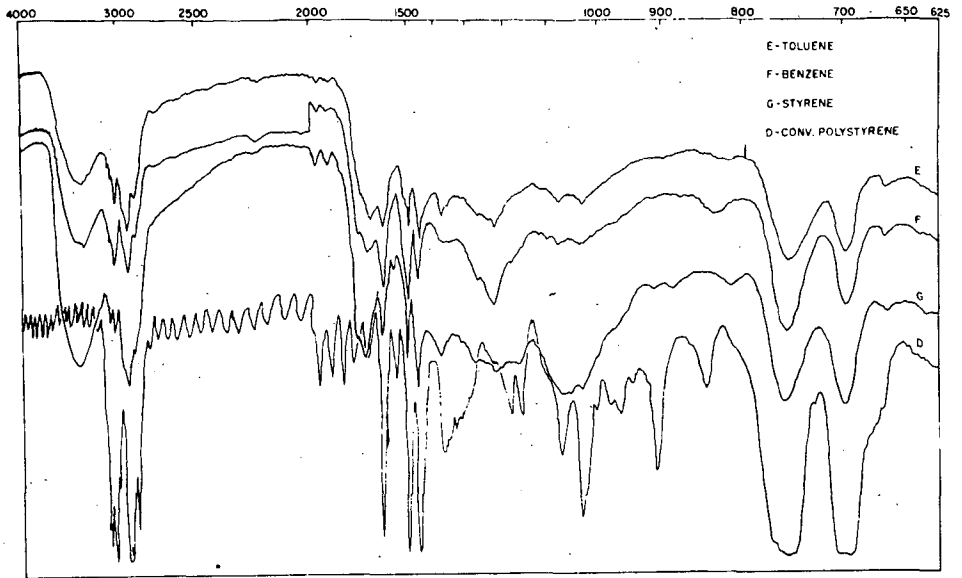


Figure 5

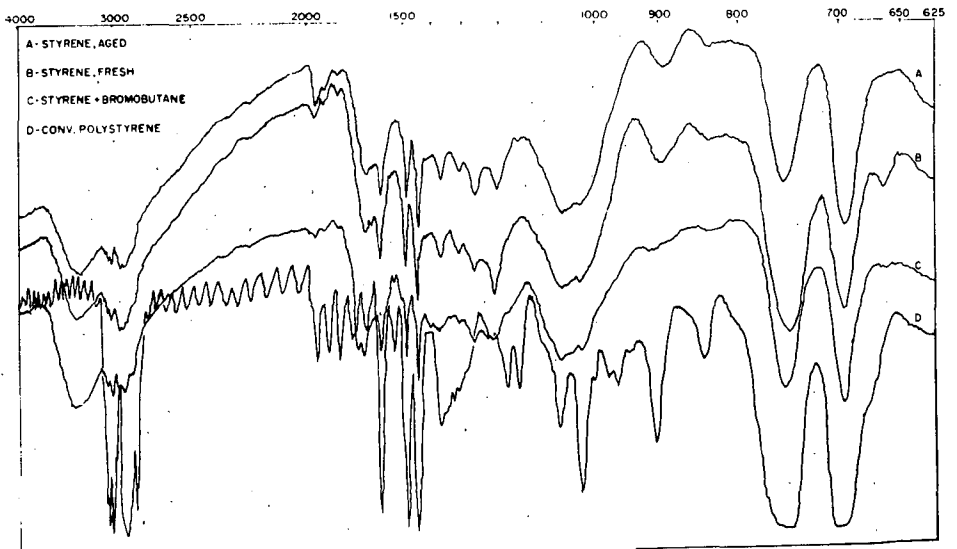
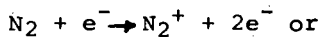


Figure 6

DISCUSSION

The salient features of the information presented above might be summarized as follows. In a mixture of organic vapor and nitrogen subjected to high-frequency, high-voltage, electrodeless discharge, the nitrogen, the organic compound and trace amounts of oxygen and water are activated and combine chemically to yield products of higher molecular weight than the starting materials. These products condense on any solid surface available and may even undergo further chemical reaction within themselves and with more monomeric material which is not electrically activated.

The chemical mechanism of this series of reactions must be complex, possibly produced by simple ionization through collision with a rapidly-moving electron followed by expulsion of two secondary electrons:



These are the products ordinarily found in mass spectrometry and on exposure to gamma or beta radiation. These activated cationic products may activate vinyl polymerization or undergo secondary reactions, yielding neutral free radicals or even anions, either of similar structure or in the form of fragments and combination or rearrangement products. In the present case there exists the further possibility that reaction products become reactivated, since they are formed in the presence of the high-voltage field, and undergo further reaction.

The simplest mechanism to consider would be polymerization of the vinyl monomers to long-chain products after initiation by some active species. The fact that non-vinyl compounds gave good yields may be explained through a mechanism involving some fragmentation of every monomer molecule and combination of the fragments to products of higher molecular weight. The vinyl monomers could be reacting through this non-vinyl mechanism also.

The action of halogenated additives suggests that the yield of reactive intermediates is increased by some of them and that these intermediates increase the initiation of vinyl polymerization. There is not enough data to establish this firmly. It may also be considered that, by changing the dielectric constant of the gas mixture, the additive can increase the efficiency of energy transfer from the electric field to the monomer.

The other additives had little or no effect, indicating that the situation is not very similar to bulk or solution polymerizations by free radical or ionic catalysis such as are now being actively studied by several laboratories (6,7). Certainly we do not have a simple vinyl polymerization. Otherwise some of the potential inhibitors would have shown an effect.

One of the unexpected results was <sup>290</sup>the fixation of nitrogen. This can be seen in retrospect to be related to work with discharge-activated nitrogen which has been reported from time-to-time (8,9,10).

No complete mechanistic explanation will be presented. More experiments are in process but it is not expected that a system which is as potentially complex as this can soon be completely explained.

#### ACKNOWLEDGEMENTS

The able assistance of Messrs. Roger Kolsky and Walter Miner and the helpful analytical interrelations of Mr. Elliot Baum are gratefully acknowledged.

#### REFERENCES

1. A. Charlesby, "Atomic Radiation and Polymers," Pergamon Press, Oxford, 1960, p.1.
2. R. M. Brick and J. R. Knox, Modern Packaging, January 1965, pp. 123-128.
3. T. Williams, J. Oil and Colour Chemist's Association 48, 936-951 (1965).
4. Manmade Textiles, July, 1965, pp. 58-9.
5. K. Jesch, J. E. Bloor and P. L. Kronick, J. Polymer Sci., A-1, 4, 1487-97 (1966).
6. R. C. Potter, R. H. Bretton, D. J. Metz, J. Polymer Sci. A-1, 2295-2306 (1966).
7. K. Ueno, K. Hayashi, S. Okamura, J. Polymer Sci. B3, 363-8, (1965).
8. L. B. Howard and G. E. Hilbert, J. Am. Chem. Soc. 60, 1918 (1938).
9. T. Hanafusa and N. N. Lichtin, J. Am. Chem. Soc. 82, 3798-9, (1960).
10. G. D. Steinman and H. A. Lillevik, Arch. Biochem. Biophys. 105, 303 (1964); CA 61, 4198 (1964).

## MEMBERSHIP IN THE DIVISION OF FUEL CHEMISTRY

The Fuel Chemistry Division of the American Chemical Society is an internationally recognized forum for scientists, engineers and technical economists concerned with the conversion of fuels to energy, chemicals, or other forms of fuel. Its interests center on the chemical problems, but definitely include the engineering and economic aspects as well.

Any chemist, chemical engineer, geologist, technical economist, or other scientists concerned with either the conventional fossil fuels, or the new high-energy fuels-- whether he be in government, industry or independent professional organizations-- would benefit greatly from participation in the progress of the Fuel Chemistry Division.

The Fuel Chemistry Division offers at least two annual programs of symposia and general papers, extending over several days, usually at National Meetings of the American Chemical Society. These include the results of research, development, and analysis in the many fields relating to fuels which are so vital in today's energy-dependent economy. Members of the Division have the opportunity to present papers of their own, or participate in discussions with experts in their field. Most important, the Fuel Chemistry Division provides a permanent record of all of this material in the form of complete preprints.

Starting in September 1959, the biennial Fuel Cell Symposia of the Division have been the most important technical meetings for chemists and chemical engineers active in this field. These symposia have all been published in book form. The recent landmark symposium on Advanced Propellant Chemistry has been published in book form also. Further, the Division is strengthening its coverage of areas of air and water pollution, gasification, and related areas.

In addition to receiving several volumes of preprints each year, as well as regular news of Division activities, benefits of membership include: (1) Reduced subscription rates for "Fuel" and "Combustion and Flame," (2) Reduced rates for volumes in the "Advances in Chemistry Series" based on Division symposia, and (3) The receipt card sent in acknowledgment of Division dues is good for \$1.00 toward a complete set of abstracts of all papers presented at each of the National Meetings.

To join the Fuel Chemistry Division as a regular member, one must also be or become a member of the American Chemical Society. Those not eligible for ACS membership because they are not practicing scientists, engineers or technical economists in areas related to chemistry, can become Division Affiliates. They receive all benefits of a regular member except that they cannot vote, hold office or present other than invited papers. Affiliate membership is of particular value to those in the informational and library sciences who must maintain awareness of the fuel area. Non-ACS scientists active in the fuel area and living outside of the United States are invited also to become Division Affiliates.

Membership in the Fuel Chemistry Division costs only \$4.00 per year, or \$11.00 for three years, in addition to ACS membership. The cost for a Division Affiliate, without joining ACS, is \$10.00 per year. For further information, write to:

Dr. Frank Rusinko, Jr.  
Secretary-Treasurer  
ACS Division of Fuel Chemistry  
c/o Speer Carbon Company  
St. Marys, Pennsylvania 15857  
Telephone: 814 - 834-2801

J.D. THORNTON.

Department of Chemical Engineering, The University,  
Newcastle upon Tyne, England.

---

### 1.0. Introduction.

Although numerous investigations have been published dealing with the effects of electrical discharges upon chemical reactions, most of the work is fragmentary in the sense that even now no clear picture has emerged of the relative importance of discharge characteristics and reactor geometry upon the reaction yield. This is largely because no systematic studies have been undertaken with a fixed reaction system covering a reasonably wide range of discharge conditions and reactor configurations. Furthermore most of the published work has been concerned with laboratory-scale investigations so that, with the possible exception of ozone synthesis, little or no attention has been paid to the chemical engineering problems involved in gas phase electrosynthesis. This is no doubt consequent upon the low yields obtained in many laboratory studies and is unfortunate in that a proper application of the engineering factors affecting the reactor efficiency could, in many cases, lead to considerably improved reaction yields.

Whereas physical chemistry is usually concerned with the individual kinetic steps contributing to a particular reaction scheme, chemical engineering is concerned with the translation of the laboratory reaction to a full scale continuous process wherein the desired reaction product is produced at the lowest capital and operating costs. In the case of gas discharge synthesis, these financial criteria imply that the reactor should have three highly desirable characteristics:

- (a) The energy yield (Gms. product per Kw.Hr.) should be high.
- (b) The conversion per pass should be high.
- (c) The reactor should be selective for the desired product, i.e. side reactions with their consequent wastage of material and energy should be minimised.

In practical terms, it is not necessary to have a detailed step by step knowledge of the reaction kinetics in order to design the reactor, so long as an empirically determined rate equation is available which adequately describes the influence of the operating variables upon the net rate of reaction. Clearly a more informed approach to the design problem is possible when fundamental data are available but this is seldom the case at the design stage.

Assuming that the electrons in a discharge are able to excite the reactant molecules, it is possible that many of the low product yields hithertoreported may be attributed to one or more of the following factors:

- (a) The use of unsuitable reactor geometries in which a sizeable fraction of the reactant by-passes the discharge zone.
- (b) The use of non-optimum discharge conditions in which the average activation cross-section for the desired reaction is low.
- (c) The use of inappropriate residence times or residence time distributions of the reactants and products.
- (d) The presence of parallel reactions which compete for the reactant and the occurrence of rapid reverse and degradation (or consecutive) reactions which destroy the primary product.

It is with these aspects of gaseous electrosynthesis that the present paper is concerned, since it is possible that many of these effects can be minimised by proper consideration at the reactor design stage.

### 2.0 Reactor Classification.

It is useful to consider initially the basic reactor geometries that can be employed in a continuous-flow reaction system. Although no formal reactor classification has hitherto been proposed, the electrode configuration and direction of

flow of the reactant gas stream can be made the basis of a convenient system of classification. Thus the electrodes may consist of parallel plates, co-axial cylinders or a pair of points whilst the gas flow may be parallel or at right angles to the plane of the discharge. Figure 1 shows in diagrammatic form the 4 various electrode and flow arrangements on the basis of this classification. Parallel flow in parallel plate and coaxial electrode reactors necessitates the use of porous electrodes through which the gas phase flows as shown in Figures 1.1 and 1.2. On the other hand, the commoner cross-flow arrangements shown in Figures 1.4, 1.5 and 1.6 usually employ impervious metal electrodes, there being no necessity for the reactants to flow through the electrodes themselves. The usual parallel/point and cross-flow/point reactors are depicted in Figures 1.3 and 1.7 respectively.

The distinction between parallel-flow and cross-flow is not an academic one by reason of the non-uniform nature of the electric field in many of these reactor arrangements. In most of the laboratory investigations reported in the literature, the areas of the electrodes are small and little or no attempt has been made to minimise edge effects by the use of suitable electrode profiles. The field intensity is therefore a function of position in the inter-electrode gap. Furthermore the use of coaxial geometries where the respective electrode radii are very different also gives rise to highly non-uniform fields in the vicinity of the central electrode. It follows therefore that the overall activation effects might well be different in the parallel/parallel and cross-flow/parallel systems in Figures 1.1, 1.4 and 1.5. In the former case, molecules traversing a centre-line path will encounter electrons of different energies to molecules following a peripheral path whilst, in a cross-flow reactor, all the molecules encounter electrons with a wide spectrum of energies. In coaxial reactors, the position is further complicated by virtue of the non-uniform field associated with the central electrode. Thus in Figures 1.2 and 1.6 not only is there a transverse field variation but there is also an axial variation as the molecules approach the bottom and top planes of the outer electrode.

Such considerations are purely speculative at the present time because no experimental data are available which would enable a direct comparison of reactant conversions for parallel and cross-flow systems to be made for the same reactants under similar conditions. Nevertheless these factors must be born in mind when interpreting the influence of reactor geometry on a quantitative basis.

Coaxial electrode systems in which the reactant flows through the annular space between the two electrodes have an advantage in that all the reactant molecules must pass through the discharge. There is therefore no by-passing and subject to suitable electron energies, there will be a high level of activation in the gas phase. Such conditions are difficult to achieve in parallel plate arrangements unless the reactant is introduced at the centre of one of the electrodes as in Figure 1.4. Much work has been reported with point electrode systems such as those illustrated in Figures 1.3 and 1.7 and here it is difficult to see how by-passing of the discharge can be avoided. Furthermore the flow pattern within the reactor is also dependent upon the turbulence level so that changes in the gas flowrate will almost certainly be accompanied by corresponding changes in the fraction of the gas stream by-passing the discharge zone.

All the reactor systems discussed so far can be described as homogeneous in the sense that only a single, gaseous, phase is present in the reactor. In many instances, however, it is advantageous to remove one or more products of reaction as rapidly as possible in order to minimise subsequent reactions which would adversely affect the primary reaction yield. A convenient method of achieving this involves the introduction of a second phase into the discharge zone in the form of a liquid adsorbent (6) or fluidised solid adsorbent (12). In principle a second phase can be introduced between any of the electrode arrangements shown in Figure 1. This modification gives rise to a second series of reactor systems which will be referred to subsequently as heterogeneous reactors.

### 3.0 Nature of the Electrical Discharge.

For optimum reactor performance it is necessary to ensure that the reactants

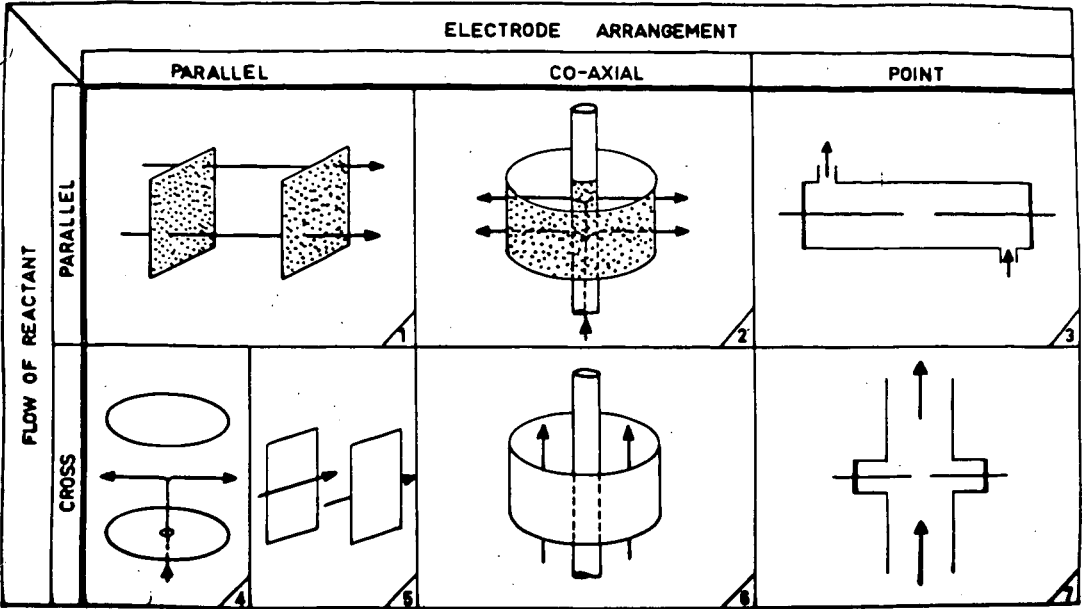


Fig.1. Basic reactor geometries.

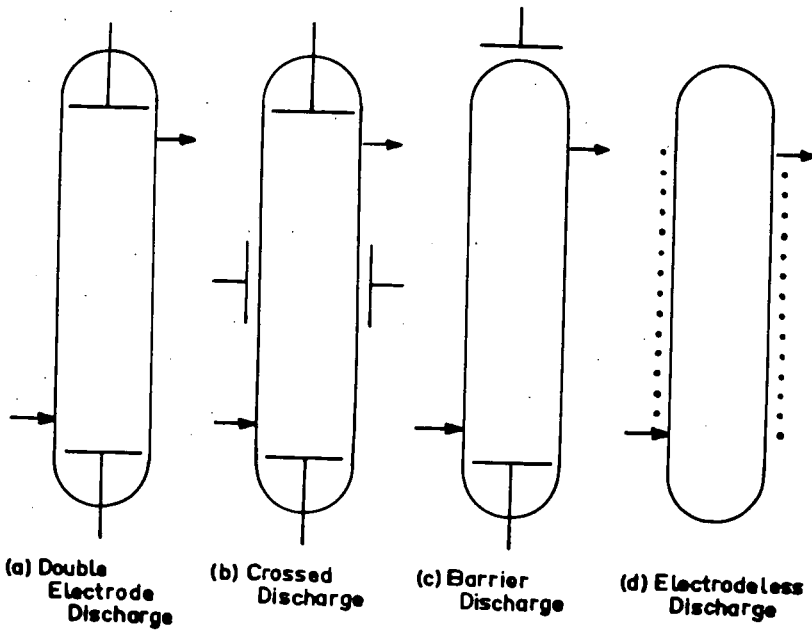


Fig.2. Diagrammatic electrode arrangements for various discharge conditions.

have suitable residence times in that part of the discharge zone where activation is most favoured. In this connection it will be recalled that the relative rate of ammonia synthesis from its elements has been shown to be greatest in the region of the cathode potential drop ( $\lambda$ ) whilst in the case of hydrazine synthesis from ammonia, the significant fraction of the discharge is the positive column region (4). In theory, it is desirable to be able to predict the discharge conditions necessary for optimum conversion in any particular reaction; in practice however, this is not yet possible. This is because in the past it has been customary to describe discharges in general terms such as glow, arc or silent discharges without regard to the local or point properties existing in different parts of the discharge zone. Since there is a gradual transition between our regime and the next, qualitative descriptions of this type are not of great value in interpreting reaction rate data. Any fundamental correlation of rate data with discharge characteristics would involve not only a knowledge of the concentrations and energy distributions of the various particle species present in the discharge space, including electrons, but also an understanding of the way in which the probability of excitation varied with electron energy. A typical example of the way in which the degree of excitation is dependent upon electron energy is shown in Figure 3 which depicts total cross-section curves for argon and neon (5). The cross-section for an  $m$ th type transition by electron collision is zero when the electron energy is less than the energy required to raise a valency electron of an atom from the  $m$ th to the  $n$ th level, but increases with electron energy to a maximum after which any further increase in electron energy is accompanied by a decrease in the value of the total cross-section. There is therefore an optimum value of the electron energy corresponding to the maximum cross section for the process under consideration. It is the lack of data of this type together with a knowledge of the reactive species present in the discharge that makes it difficult to correlate reaction rates with discharge parameters for systems of engineering interest.

Nevertheless despite the absence of fundamental information relating to the activation characteristics of discharges, one or two general observations can be made with regard to the nature of the discharges commonly employed. All the reactor geometries discussed so far, and illustrated diagrammatically in Figure 1, employ the same type of discharge in the sense that both electrodes are located within the reactor and are therefore in contact with the reactant gas. This class of discharge in which electrons pass freely between the two electrodes is represented schematically in Figure 2a. An alternative type of discharge which has been used frequently is the so called barrier discharge shown diagrammatically in Figure 2c. Here one of the electrodes is separated from the gas phase by means of a dielectric barrier such as quartz so that the reactor may be looked upon as a capacitive and resistive load in series. In practice a dielectric barrier may be employed in conjunction with any of the reactor geometries shown in Figure 1. This arrangement has the advantage of providing a more uniform type of discharge which is current limited so that the build up of spark or arc type discharges is avoided. If this principle is carried to its logical conclusion, both electrodes may be isolated from the reactant gas and molecular excitation set up by applying a high frequency potential to the external electrodes or by induction from an external conductor carrying a high frequency current. (Figure 2d.) This type of "electrodeless" reactor has not been mentioned in the classification discussed above but is of interest since in the absence of metal electrodes in the gas phase, the degree of dissociation of the gas and therefore the concentration of atoms would be expected to be high (10). The high concentration of atomic species in such discharges is evidenced by the afterglow phenomena frequently encountered in electrodeless systems.

One type of electrodeless system which might well prove of interest in electro-synthesis is the microwave discharge. Here the degree of activation can be high (9) and it has been reported that the atomic yields in hydrogen, nitrogen and oxygen are approximately ten times greater than the yields of atoms and radicals in low frequency and direct current discharges at the same field strength and pressures. From the engineering point of view, microwave systems have the added advantage

that they can be sustained at higher pressures but on the other hand the detailed economics still require evaluation.

The crossed discharge arrangement shown in Figure 2b comprises a low frequency discharge at right angles to one of high frequency. The discharge zone itself is said to be characterised by a low energy density and to result in unexpectedly high activation of the reactants and relatively high yields of the reaction products (3). These claims have not however been confirmed by recent work in these laboratories in which methane was subjected to a crossed discharge at 31 mm.Hg pressure. The reactor consisted of a 15 mm. internal diameter glass tube fitted with two pairs of 3 mm. diameter stainless steel electrodes arranged at right angles. The percentage decomposition of methane was observed using a 0.91 Mc/s high frequency discharge, a 50 c/s low frequency discharge and combinations of high and low frequency discharges simultaneously. Figure 4 shows some typical data plotted in the form % methane decomposed versus % H.F. power for a series of runs at constant total power. The methane flowrate was constant throughout at 93 cc/minute at N.T.P. These results confirm the general trend whereby an increase in discharge power is accompanied by an increase in the percentage decomposition of the methane but on the other hand do not substantiate the claim made for the higher activating effect of the crossed discharge. Had this been the case, the curves shown in Figure 4 would have exhibited maxima whereas, in fact, the observed methane decomposition at constant total power increased steadily with increasing percentage of H.F. power. In this particular case, there is therefore no advantage in the use of crossed discharges and the characteristics claimed by Cotton still remain to be confirmed.

#### 4.0 Product Selectivity and Residence Time Considerations.

In the simple plug flow reactor, the conversion (x) obtained is related to the residence time ( $\tau$ ) by the expression:

$$\tau = \int_0^x \frac{dx}{v_p \cdot r}$$

where  $v_p$  and  $r$  are the molal volume of the reacting mixture and the reaction rate respectively. If the reaction is one which can only take place under the influence of an electrical discharge, then the residence time refers to the time spent by the reactants in the discharge zone itself. If however subsequent reactions involving the primary reaction products are possible outside the discharge zone, these will usually proceed at a different rate and must be taken into account separately in analysing the overall performance of the reactor system.

If the reaction rate ( $r$ ) could be written in terms of the concentrations of the reactants and a rate constant ( $k$ ) which in turn was dependent upon the discharge characteristics, then in principle it would be possible to integrate the above expression for any set of discharge conditions and compute the residence time for any desired conversion. In practice however this is seldom possible because the functional relationship between the reaction rate and the discharge characteristics is unknown.

Discharge reactions are frequently complicated by reason of the interactions between the atomic, molecular, ionic and free radical species present. Moreover because of the wide range of species present, reactions are rarely simple in the sense that only one primary reaction product is produced. Competing parallel, consecutive and degradation reactions are often present, the net result of which is to produce a wide spectrum of reaction products. One of the key problems at the present time therefore is how to design reactors in which unwanted side reactions are reduced to a minimum. There is no clear-cut answer to this problem as yet, but an examination of some of the more elementary types of reactions such as those listed in Table I indicates a promising method of approach.

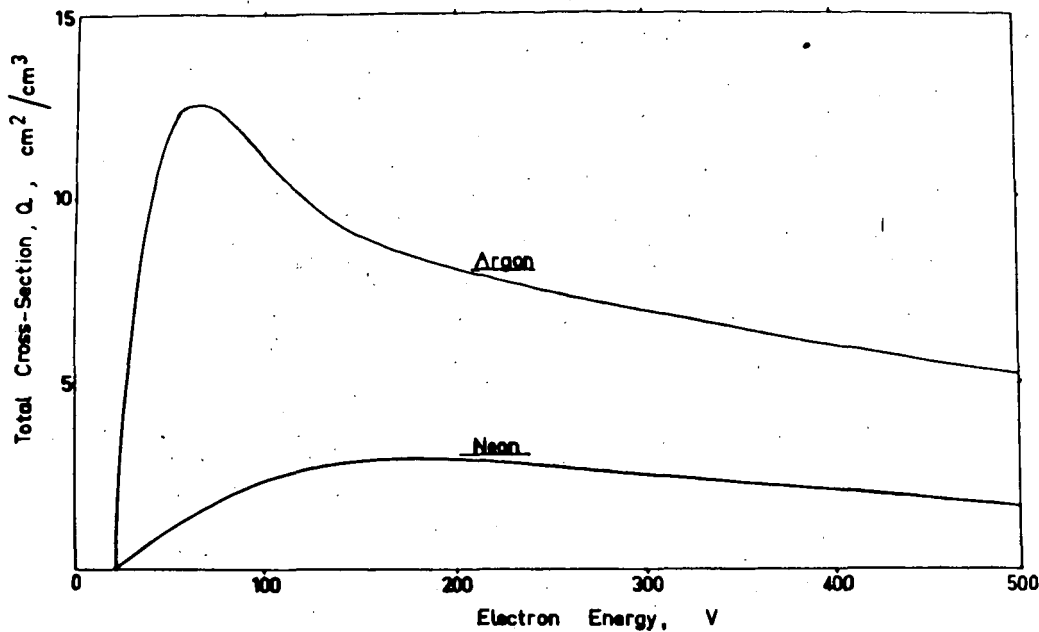


Fig.3. Typical Cross-Section versus Electron Energy Curves.

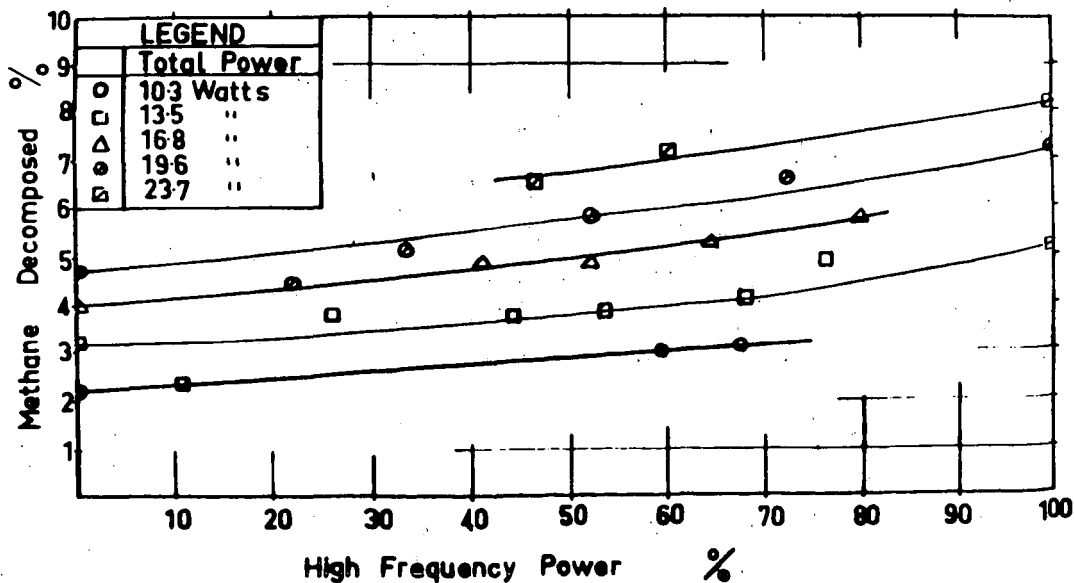


Fig.4. Effect of a Crossed Discharge on % Methane Decomposition.

TABLE I  
Examples of Elementary Reactions.

Consecutive Reactions	$A + B \rightarrow C$ $A + C \rightarrow D$
Polymerisation Reactions	$A + A \rightarrow B$ $A + B \rightarrow C$ $A + C \rightarrow D$
Parallel Reactions	$A + B \begin{matrix} \rightarrow C \\ \rightarrow D \end{matrix}$
Reversible Reactions	$A + B \rightleftharpoons C + D$
Degradative Reactions	$A + B \rightarrow C \rightarrow D \rightarrow E$

In all the reactions listed in Table I it is assumed that C is the preferred product. Intermediate steps involving excited species are omitted so that the equations merely represented the overall stoichiometry of the various situations. If therefore product C is being produced from reactants A and B and a second (consecutive) reaction is present which destroys C, then the rate of the second reaction can be reduced by maintaining the concentration of C at a low value. Since the primary reaction responsible for the formation of C should, on economic grounds, proceed as rapidly as possible, the only way of maintaining a low product concentration is to remove C from the discharge zone as rapidly as it is formed. The methods by which this can be achieved will be discussed further below.

The same principles apply to the other reactions in Table I. Thus in the case of polymerisation reactions, the molecular weight of the product can be controlled by selective removal of certain constituents from the discharge. If product B is preferred, then further polymerisation can be minimised by rapid removal of B. If on the other hand, the higher molecular weight product C is required, B is allowed to remain in the discharge and C is selectively removed. It frequently happens that the product yield is limited by reverse and parallel reactions. In the latter case, C can be produced in preference to D by selective removal of C. In the former instance, any yield limitations imposed by equilibrium considerations can be overcome by rapid removal of C so that the equilibrium is displaced almost entirely in favour of products.

Similar reasoning shows that in the case of degradative reactions, product C can be produced in preference to D or E provided that C is removed rapidly enough from the activating influence of the discharge.

A number of methods are available for the rapid removal of a particular component from the discharge zone, namely:

- (1) Quenching the reaction at low temperatures and freezing out the product (2)
- (2) Absorbing the desired product selectively in an inert liquid absorbant (6)
- (13)
- (3) Adsorbing the desired product in a fluidised bed of solid adsorbent (12).
- (4) By using a low residence time in the discharge zone. This may be achieved either by high gas flowrates or by using a pulsed discharge technique. These are all devices which reduce both the produce concentration and residence time in the gas phase and so minimise product losses through subsequent reactions.

Methods (1) - (3) are means of controlling selectively the residence time and concentrations of certain specific products in the discharge and a choice can only be made between them in the light of the physical properties of the various constituents of the gas phase. The fourth method, which does not discriminate between the concentrations or residence times of reactants and products, can only be evaluated when the relative rates of the competing reactions are known. Of the various techniques available, simultaneous reaction and absorption in a heterogeneous reactor (method 2) opens up interesting possibilities for producing economic

yields of many chemical products where hitherto the overall yield has been restricted by decomposition reactions. The theoretical analysis of such systems is however extremely complex and even if the kinetics of the process were fully understood, it is doubtful if the absorption rate into the liquid phase could be predicted with any degree of certainty because of complications arising from dielectrophoretic stirring of the liquid. If the liquid phase is polarizable the electrical forces in a non-homogeneous field will cause polar molecules to move towards regions of maximum non-homogeneity. Any turbulence thereby set up within the liquid phase will enhance the rate of gas absorption but at the same time render the prediction of mass transfer coefficients extremely uncertain. From a practical point of view, such effects are desirable insofar as it is important that the rate of absorption of the product should be high compared with its rate of production by synthesis.

Some illustrations of the factors discussed are of interest at this stage and Figs. 5 and 6 show how the molecular weight of the product is influenced by residence time in the case of consecutive type reactions involving methane as the reactant. Figure 5 shows how the higher molecular weight product, in this case propane, is favoured by longer residence times in the discharge (11). These data were obtained at 80 mm Hg pressure in a cross-flow/coaxial reactor with a 1.60 mm. thick quartz barrier adjacent to the inside surface of the outer electrode. The relevant electrode diameters were 17 mm and 3 mm respectively and the power density was 0.05 Kw/cc throughout. Figure 6 shows the effect of longer residence times on the higher molecular weight fraction from methane at a pressure of 10 mm Hg and again the molecular weight of the product is strongly dependent on residence time (7).

In the discharge synthesis of hydrazine from ammonia, it has been suggested (4)(1) that the hydrazine can be subsequently destroyed by further electron excitation or by reaction with atomic hydrogen produced in the primary electron bombardment of ammonia. If therefore the concentration and residence time of the hydrazine in the discharge be reduced, degradative reactions should be minimised and the yield increased correspondingly. That this is the case can be seen from Figures 7 and 8. The arrangement of the cross-flow/coaxial reactor employed in these runs is shown in Figure 9. The reactor tube was made from 1.60 mm. thick quartz tubing which constituted the dielectric barrier and was 28.6 mm. O.D. The inner electrode consisted of a perforated stainless steel drum 19 mm O.D. which was mounted on a coaxial shaft so that it could be rotated at high speed. A liquid absorbent, in this case ethylene glycol, was fed to the drum so that, as the latter rotated, the glycol was forced through the drum perforations into the discharge annulus in the form of a fine spray. The data shown in Figure 7 were obtained at an average power density of 0.044 Kw/cc and illustrate the fact that not only can the energy yield of hydrazine be increased by reducing the gas residence time but that a further substantial increase in yield can be obtained if the hydrazine is rapidly removed from the discharge by selective absorption (13).

The data shown in Figure 8 in which the energy yield is plotted versus the discharge duration for a constant gas flowrate were obtained in a cross-flow parallel plate reactor using a pair of electrodes each measuring 12.5 x 6.3 mm. and located 11 mm. apart. In these runs the average power density was 0.01 Kw/cc using a pulsed D.C. discharge, the pulse duration ranging from 12 to 130 microseconds. Under these conditions, the effective residence time of the reactant and products was no longer dictated by the gas flowrate but by the pulse duration. This technique is therefore a device for securing very low residence times without the inconvenience of high gas velocities. Again the data are in agreement with previous results in that the lower residence times favour higher energy yields because of the smaller loss of hydrazine through reverse and consecutive reactions. It is interesting to note that an alternative technique whereby atomic hydrogen is converted to less reactive molecular hydrogen through the agency of a platinum catalyst has also shown increased yields of hydrazine (4).

It has been assumed so far that the reactant flows as a coherent plug through the discharge. This concept of plug-flow is only an approximation at

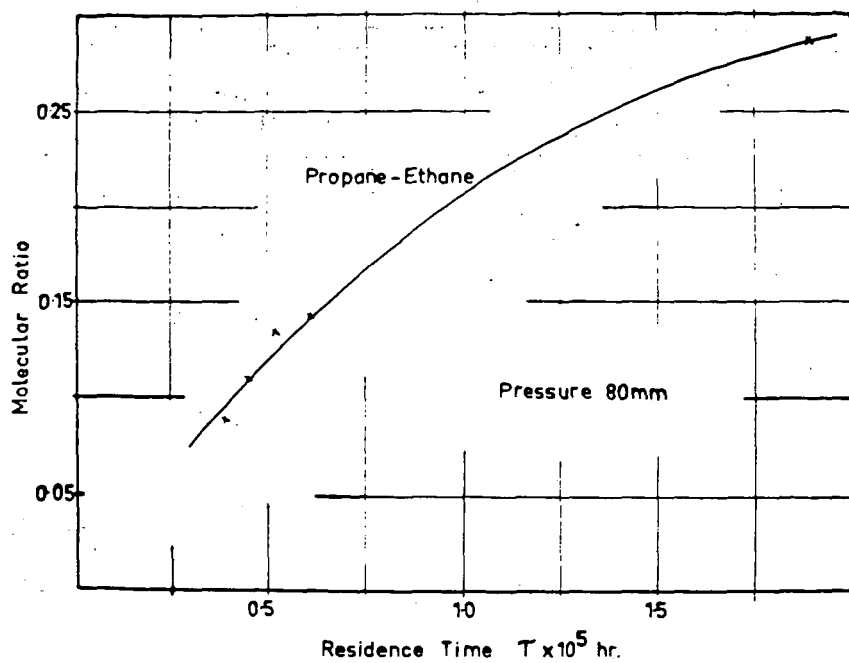


Fig. 5. The effect of residence time on propane-ethane yield from methane.

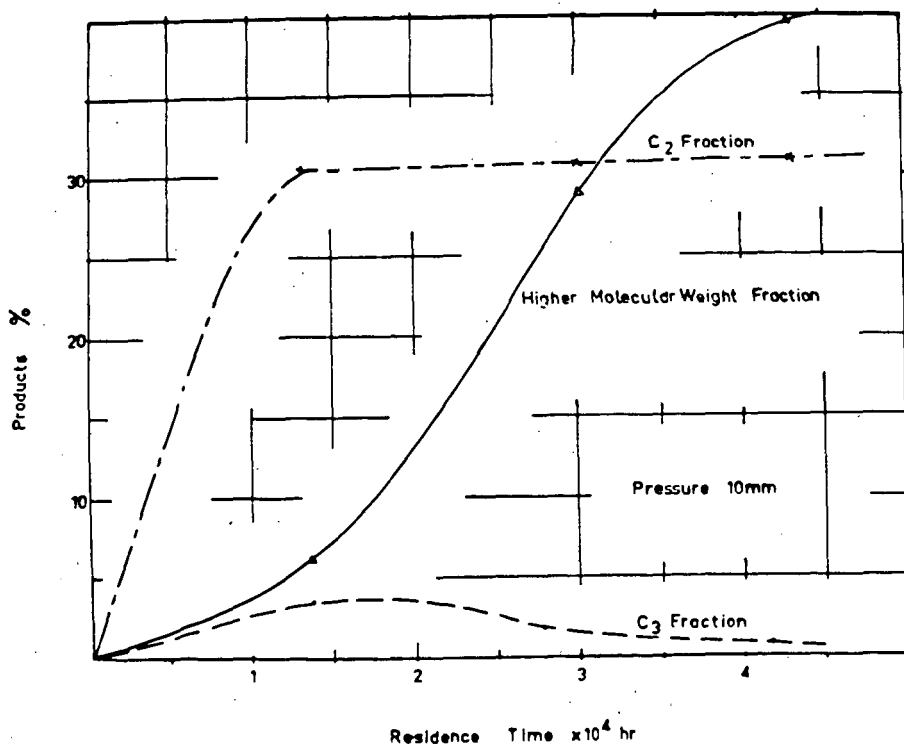


Fig. 6. The effect of residence time on the yield of higher molecular weight fraction from methane.

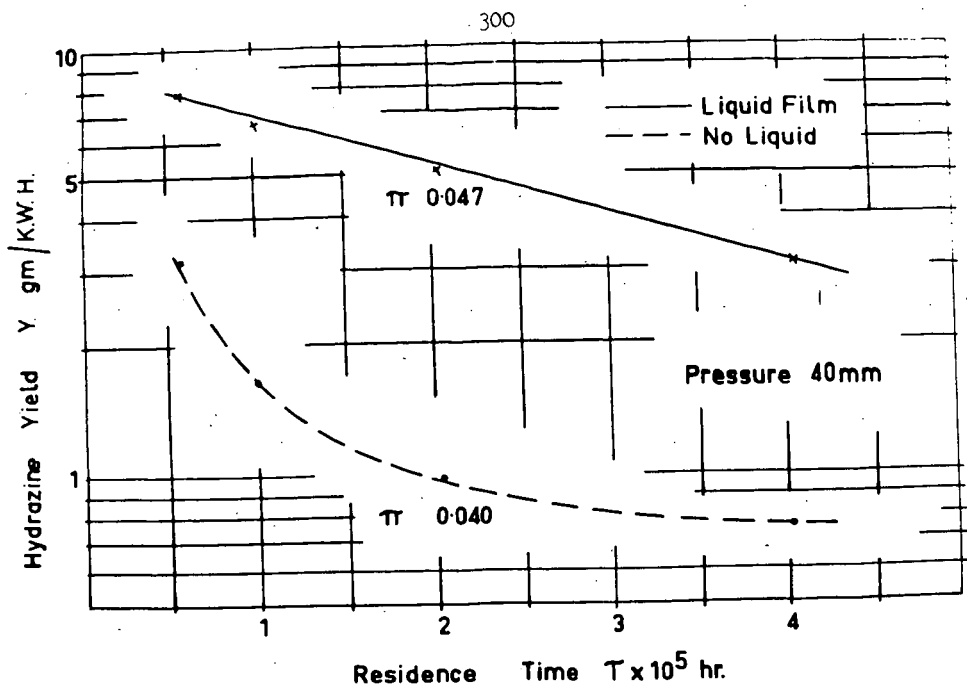


Fig.7. The effect of residence time and absorbent on hydrazine yield from ammonia.

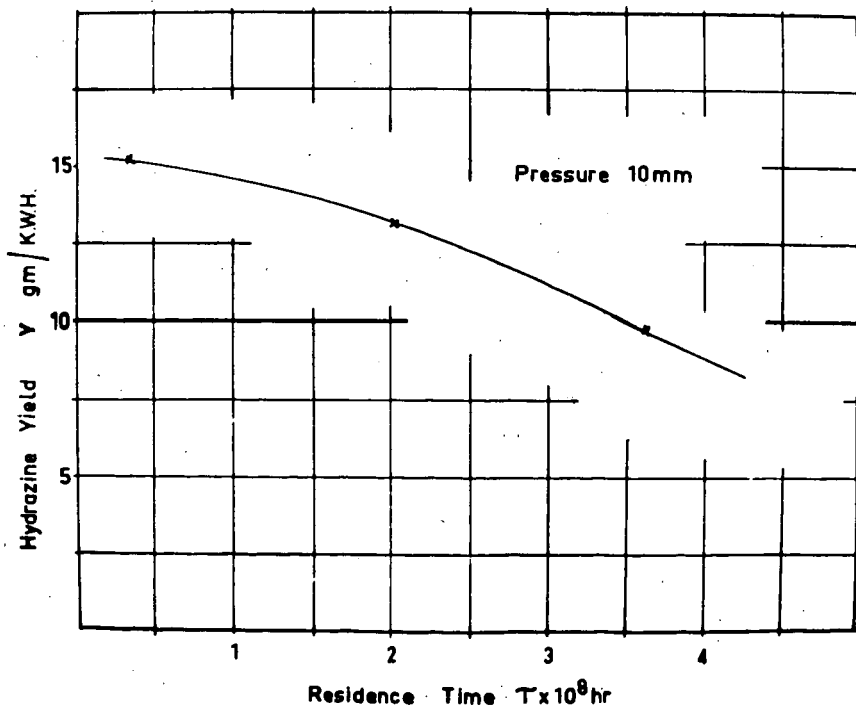


Fig.8. The effect of residence time on hydrazine yield from ammonia when residence time is dictated by the discharge waveform characteristics.

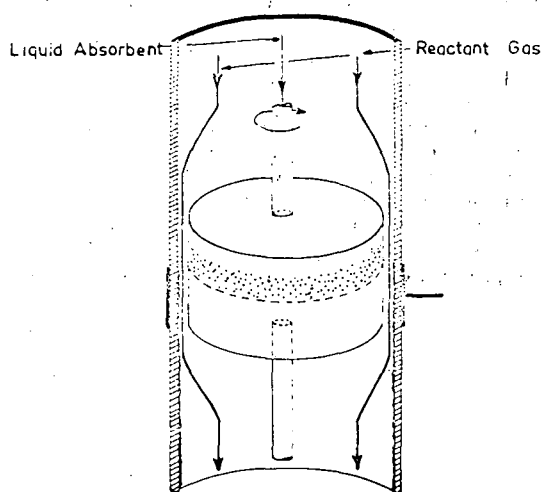


Fig.9. . Arrangement of the differential reactor for hydrazine synthesis from ammonia.

the best and in many practical situations considerable divergences are observed between the residence time ( $\tau$ ) calculated from

$$\tau = \int_0^x \frac{dx}{U_r \cdot r}$$

and the residence time observed in practice for the same conversion. Such discrepancies result from the velocity profile of the gas as it passes through the reactor; molecules adjacent to the wall will have a lower velocity than molecules travelling along an axial path and as a result there will be a distribution of residence times. The effect of such a distribution can be serious in the case of polymerisation-type reactions where a wide spread in residence-times is often accompanied by a corresponding spread in the molecular weights of the products. If therefore a product is required with a relatively narrow molecular weight distribution, steps must be taken to ensure that the distribution of residence times is correspondingly small. One way of achieving this is to promote rapid mixing in the reactor by the use of suitably designed baffles so that each element of gas spends approximately the same time in the discharge.

Acknowledgements.

The author is indebted to a number of his colleagues and to Dr. C.A.Walley of the Department of Electrical Engineering for many helpful discussions.

References.

- (1) Andersen W.H., Zwolinski B.J., Parlin R.B., *Ind.Eng.Chem.*, 1959, 51, (4), 527.
- (2) Brewer A.K., Westhaver J.W., *J.Phys.Chem.*, 1929, 33, 883 (Cf. also *J.Phys.Chem.* 1930. 34, 153)
- (3) Cotton W.J., *Trans.Electrochem.Soc.*, 1947, 91, 407, 419.
- (4) Devins J.C., Burton M., *J.Amer.Chem.Soc.*, 1954, 76, 2618.
- (5) Howatson A.M., "Introduction to Gas Discharges" (Pergamon Press, 1965).
- (6) Imperial Chemical Industries, U.K.Patents 948,772; 958,776; 958,777; 958,778; 966,406 (all 1964).
- (7) Kraaijveld Von H.J., Waterman J.I., *Brennstoff-Chemie*, 1961, 42, (12), 369.
- (8) Llewellyn-Jones F., "Ionisation and Breakdown in Gases", (Methuen & Co. Ltd. 1966).
- (9) McCarthy R.L., *J.Chem.Phys.*, 1954, 22, 1360.
- (10) Miyazaki, Takahashi, *Nippon Kagaku Zasshi*, 1958, 78, 553.
- (11) Sergio R. Unpublished Work, University of Newcastle upon Tyne. England.
- (12) Thornton J.D., *Chem.Processing*, 1966, XII (2), S6.
- (13) Thornton J.D., Charlton W.D., Spedding P.L., "Hydrazine Synthesis in a Silent Electrical Discharge" (to be published).

GENERATION AND MEASUREMENT OF AUDIO FREQUENCY POWER  
FOR CHEMICAL-ELECTRICAL DISCHARGE PROCESSES

James C. Fraser

Research and Development Center  
General Electric Company  
Schenectady, New York

In developing equipment for use in high voltage, high frequency chemical-electrical processing, we have built a number of different types of "corona" power supplies. At the start, from the standpoint of the electrical equipment, let us use "corona" in its broadest sense. We will define a "corona" discharge as an electric discharge produced by capacitively exciting a gaseous medium lying between two spaced electrodes, at least one of which is insulated from the gaseous medium by a dielectric barrier. A corona discharge may be maintained over wide ranges of pressure and frequency, although atmospheric pressure and frequencies in the audio range substantially above power transmission values are typically employed.

Since the power which can be dissipated in a corona reactor or cell is a function of the supply frequency, we have settled arbitrarily on the audio range (3,000 to 10,000 cycles per second) as a desirable compromise. It is within the limits of rotating machinery and solid state components, presents no undue corona reactor heat dissipation problems, and provides a happy compromise between operating voltages, reactor size, and economy of operation.

The ratings for the basic electrical components are dependent upon the characteristics of the corona reactor and the impedance load which it represents to the power supply. Corona reactor values which affect these ratings are:

- a. The corona power required
- b. The electrode corona power density and, thereby, the electrode cooling or heat dissipation capability
- c. The gaseous atmosphere present
- d. The gaseous gap spacing
- e. The barrier material and dielectric constant

From these values we can determine:

- a. Peak voltage required to initiate corona
- b. Barrier thickness required to withstand the total voltage across the barrier in the event of an arc across the gap
- c. Barrier, gaseous gap, and total reactor capacitance
- d. Maximum operating voltage
- e. Capacitive charging, or displacement, current drawn by the reactor
- f. Corona resistive current
- g. Resultant load current
- h. Power factor of the corona reactor load

The objectives which we attempted to meet in the design of our equipment were:

- a. Suitability for use with a wide variety of corona reactors
- b. Operation over a wide range of breakdown voltages
- c. Flexibility over a wide range of operating conditions
- d. Maximum electrical efficiency
- e. Trouble-free operation and minimum maintenance over long periods of operation

Among the types of equipment built were the inductor-alternator with step-up transformer and parallel-resonant tuned circuit, the SCR inverter with step-up transformer, and the mobile vacuum tube high power-amplifier.

#### Motor-Alternator Set

A typical power supply based on rotating equipment consists of the following major components: an inductor-alternator, by means of which 60 cycle power is converted to 10,000 cycles, at 500 volts. This output is fed to the primary of a high voltage, high frequency transformer rated for 25 or 50 KV at 10,000 cycles. The output of this transformer is fed, in turn, to a parallel resonant tuned circuit, the discharge reactor, and the high voltage instrumentation.

The KVA rating of the M-G Set (inductor-alternator) is determined by the product of the corona operating voltage and the resultant load current (or the corona power divided by the power factor). Since the corona power generated in a gaseous gap in series with a dielectric is directly proportional to frequency, and the upper limit for frequency for commercially available rotating equipment is about 10,000 cycles per second, this has generally been considered the optimum frequency. Also, the use of lower frequencies would require higher voltages or increased corona reactor capacitance for any given power level. The output voltage of the alternator can be any value consistent with usual generator practice and with the transformer primary voltage.

The KVA rating of the transformer will usually be the same as that of the inductor-alternator. Its secondary voltage will be determined by the corona reactor requirements for voltage breakdown of the gaseous gap. Secondary or load current will be the vector sum of charging, or displacement, current and resistive, or corona, current. Primary voltage must be consistent with alternator output voltage. If experimental flexibility is required, the transformer primary should be arranged for series-parallel connection.

The corona reactor represents a capacitive load on the major items of the power supply equipment, up to the time of corona initiation. Since this generally results in a poor power factor, there are two possible means of solution:

- a. The motor-alternator set must be built with sufficient KVA capacity to meet the power factor and corona power requirements.

- b. The transformer secondary and the corona reactor can be tuned with a parallel resonant circuit consisting of a choke and high voltage, vacuum capacitors. This provides power-factor correction so that the high voltage transformer secondary sees mainly the resistive load represented by the corona power.

The parallel-resonant circuit must be tuned to give maximum transformer output voltage for some arbitrarily selected value of alternator field current. With a 0.16 henry choke, for example, the capacitance required for tuning at 10,000 cycles can be found from the expression

$$f = \frac{1}{2\pi\sqrt{LC}}, \text{ or } C = \frac{1}{4\pi^2 f^2 L} \approx 1580 \text{ picofarads}$$

However, this value is reduced by the capacitance of the discharge reactor itself, by that of any instrumentation voltage dividers, and by stray capacitances, so that the actual tuning capacitance used is somewhat lower and must be determined experimentally.

The decision as to whether the motor-alternator should be built with increased KVA capacity or whether the secondary circuit should be tuned depends on the experimental versatility required, and on economic considerations. In general, the dollars per KVA for high frequency motor-alternator sets are considerably higher than for tuning circuit components.

An alternator field-control chassis supplies and regulates the current for the alternator field windings, and has a feedback system designed to meet varying conditions of high voltage output. Alternator output voltage and, thus, transformer high voltage are raised and lowered by changing alternator field current. A magnetic amplifier stabilizer circuit maintains constant high voltage output. In the event of a decrease in high voltage, it calls for an increase in alternator field current, with a corresponding output voltage increase.

Control devices and instrumentation for a corona power supply based on rotating equipment includes at least the following:

- a. Provision for varying the transformer output high voltage from zero to maximum by varying alternator field current, and a means of measuring the field current.
- b. Provision for measuring transformer primary voltage, current, and power.
- c. Provision for measuring the peak voltage applied to the corona reactor.
- d. Provision for measuring the power dissipated in the corona reactor.
- e. Some form of protective current overload relay, for removing high voltage from the corona reactor in the event of a short circuit in the reactor, or a low voltage, high current arc

between the electrodes. This will prevent exceeding the current rating of the transformer secondary.

Since the use of this equipment involves working with high voltage, the control circuit includes provision for test area safety interlocks and flasher-warning lights.

### Inverter

The solid state corona generator consists of a 3,000 cycle inverter utilizing silicon controlled rectifiers feeding a step-up transformer. A rectifier is a device or circuit for changing alternating current to direct-current. The inverter may be thought of as a rectifier operating in reverse, changing d-c to a-c. A combination of the two achieves a change from 60 cycle a-c to approximately 3,000 cycle a-c.

Rectifier circuits occur in several configurations such as half-wave, full wave, bridge, etc. Inverter circuits may be grouped in a similar manner. The key feature of an SCR (silicon controlled rectifier) as used in an inverter circuit is that a small current from its "gate" element to the cathode can fire or trigger the SCR so that it changes from being an open circuit into being a rectifier.

The inverter operates from a single phase, 220 volt, 60 cycle source, and by means of a full-wave bridge rectifier, rectifies it to 187 volts d-c which in turn is changed to 150 volts, 3,000 cycles, approximate sine wave through SCR's. Variac control of the 220 volt input provides a variable supply output.

The inverter output is fed to a step-up transformer delivering up to 12,000 volts rms. This transformer is a dry type, potted with RTV, with integral high voltage terminals. The particular transformer used was built as a compromise between low cost, size, and electrical capability. Rated at 3 KVA, the transformer was only 6" x 6" x 7" high overall.

What is noteworthy with this equipment is that the inverter, transformer, and corona reactor are not independently operating components. The concentric cylinder corona reactor was so designed that its capacitance, reflected to the primary of the transformer, formed a part of the inverter LC circuit, as did the inductance of the high voltage transformer. The reactor gaseous gap conductance forms a part of the inverter load circuit.

Since this is an untuned high voltage circuit, the inverter and the transformer were designed to carry the power factor loss current.

Advantages of the inverter supply over the motor-alternator is the absence of moving parts, ease of mounting and installation, and the "module" or building block concept whereby units can be stacked to increase voltage and current capability.

### Vaccum-Tube Amplifier

The mobile corona generating equipment was designed for operation over a wide range of frequency and voltage. Corona power is generated by a vacuum tube, high-power amplifier driven by a stable low-power, audio-frequency sine-wave oscillator. Power is taken from the secondary winding of a high-voltage step-up transformer, with one end at ground potential.

The corona output voltage may be varied from zero to 50,000 volts, depending on the impedance of the applied load, and on the settings of the frequency and amplitude controls located on the master sine-wave oscillator panel. The frequency of the output voltage is determined by the master oscillator and is independent of load impedance or output voltage level. The frequency may be varied instantaneously between the rated limits of 3 to 10 kilocycles per second.

The a-c power from the 60 cps line is converted into the high voltage variable frequency output as follows:

A master oscillator feeds a driver amplifier. This in turn drives a tetrode power amplifier stage and the output step-up transformer. A d-c plate supply source, a screen grid voltage supply, a control grid bias supply, and an a-c filament supply feed power at appropriate voltage levels to the tetrode amplifier stage. The power line control circuitry incorporates on-off switching, circuit breakers, and starting contactors for the power amplifier supplies.

Power amplification is produced by four tetrode vacuum tubes connected in pushpull-parallel as a Class AB<sub>2</sub> amplifier. Control of the master audio oscillator signal amplitude is provided by a potentiometer on the master control panel. The output voltage of the equipment may be reduced to zero even when full voltage is applied to the plates of the power tetrodes.

Power delivered by the tetrodes to the output transformer, and thence to the corona reactor load, is controlled by the oscillator and the variable autotransformer in the tetrode plate power supply. The autotransformer control keeps the total power consumed by the equipment during an experiment as low as possible, to minimize heat developed in the cabinet and to extend tube life.

The corona cell impedance, which is mainly capacitive before corona breakdown, acquires a resistive component after breakdown which depends on the rate of production of ionized and electrically conducting chemical entities. The a-c voltage at the plates of the power tetrodes will lag the plate current by a large angle before power is consumed, and the plate current will be collected at a high rather than a low value of plate voltage. Thus, the power dissipated by the tetrodes will be high under no-load conditions.

The high voltage transformer has an effective primary to secondary step-up ratio of 11 to 1. The maximum a-c current that can be drawn from the secondary winding of the transformer is 60 milliamperes rms.

## Reactor

The corona reactor or cell represents a capacitive load to the power supply equipment up to the time of initiation of the electrical discharge. The total reactor capacitance consists of the series combination of dielectric barrier and gaseous gap capacitance. The voltages appearing across the barrier and the gap divide inversely as their capacitance.

Before corona starts, the reactor current consists of the charging, or displacement, current which is proportional to the applied voltage, frequency, and cell capacitance. After the start of corona, the cell acts as an impedance load consisting of a conductance across the gaseous gap, in addition to the gap capacitance. The total current drawn by the reactor then is the vector sum of charging plus resistive currents.

If the corona reactor power supply has a tuned circuit in the transformer high voltage secondary, for power factor correction, the corona reactor capacitance functions as part of the tuning capacitance, and the reactor charging current is a part of the circulating current in the parallel resonant circuit. The total load current through the transformer secondary winding then consists chiefly of corona current plus whatever capacitive current might be present as a result of tuning unbalance.

If the power supply is untuned, the total power available for chemical processing is the product of supply volt-amperes times the power factor of the load, and in this case transformer secondary winding must carry the full reactor impedance current.

The dielectric barrier in the corona reactor serves as a built-in current-limiting device, or ballast in the event of a short circuit or arc between the cell electrodes, so that the stored energy is dissipated in the barrier at breakdown.

The maximum power density at which a corona reactor can be operated without puncturing the barrier is a function of the dielectric strength of the barrier material, the total thickness of the barrier, the ambient temperature in which it is operated, and the gap spacing between barriers. The dielectric constant of the barrier affects both the voltage gradient across the barrier, and the corona power which can be dissipated in the reactor. The dissipation factor is a measure of the electric losses which produce heating of the barrier.

The voltage at which breakdown will occur between a set of electrodes in a corona reactor depends upon the gaseous atmosphere present, the density (pressure, temperature) of the gas between the electrodes, and the gap length.

The corona power dissipated in a gaseous gap in series with one or more dielectric barriers can be calculated from the expression

$$P = 4f C_b V_{\text{gas}} \left( V_{\text{max}} - \frac{C_{\text{gas}}}{C_t} V_{\text{gas}} \right), \text{ where}$$

P = Corona power in watts

$f$  = Power supply frequency in cycles/second

$C_b$  = Dielectric barrier capacitance

$C_{gas}$  = Capacitance of corona cell gas gap

$C_t$  = Total corona cell capacitance

$V_{gas}$  = Peak voltage across the gaseous gap at the time of corona initiation

$V_{max}$  = Total operating voltage applied to the corona cell

This can be re-written as:

$P = 4f C_b V_{gas} (V_{max} - V_t)$ , where

$V_t = \frac{C_{gas}}{C_t} V_{gas}$  = voltage across the corona cell at the instant of corona initiation

An item of concern to all, in evaluating an experiment, or in scaling up for pilot plant operation, is the electrical efficiency of a process. Care must be taken not to confuse equipment power factor with what might be called "electrical efficiency of conversion", though both may contribute to the same end result. Power factor relates to ability to convert equipment input volt-amperes (not necessarily in phase) to available chemical-result-producing "watts". This is a function of electrical equipment and electrical circuit design.

"Electrical efficiency of conversion" may be considered as the effectiveness in utilizing all or most of the available wattage in the corona reactor. This is a function of reactor design, with particular emphasis on relative barrier and gap capacitance and gap spacing. As a matter of practical design, the cell geometry and gap spacing present limits to the power which can be dissipated in any given cell.

### Power Measurement

The power consumed in the discharge cell is determined by means of the parallelogram-oscilloscope technique which shows the relationship between the voltage on the cell electrodes at any instant, and the charge flow in the circuit up to that instant. Before corona initiation, the corona null value is seen on the oscilloscope as a closed figure, or slant line. With the initiation of the electrical discharge, the figure opens up into a parallelogram, and the discharge power is represented by the area of the parallelogram.

The bridge circuit for power measurement consists of two branches between the high voltage terminal of the reactor and ground, called "Voltage" and "Charge". The "Voltage" branch consists of a capacitance

voltage divider giving an approximate  $10^4$  to 1 voltage division. The "Charge" branch consists of the corona reactor in series with some value of capacitance such that a voltage division of  $10^4$  or  $10^3$  to 1 will be obtained across the divider. The outputs from the low voltage ends of these dividers are fed to the X and Y axes of the oscilloscope. A variable potentiometer across the lower end of the "Charge" divider provides phase shift control to bring the "Voltage" and "Charge" branch outputs into phase for a null reading on the scope.

It should be noted that two signals, of equal amplitude, in phase, fed to the X and Y axes of a scope, give a 45-degree line on the scope. Any variation of relative amplitude shifts the angle of the line.

The area of the parallelogram represents the total power dissipated in the cell when the parallelogram bridge circuit and the oscilloscope are calibrated in the following manner:

The X-axis deflection is calibrated with a peak reading voltmeter so that reactor voltage (peak-to-peak) is presented as volts per cm of scope deflection.

The Y-axis deflection is calibrated with the known value of capacitance in the grounded end of the "Charge" branch so that the charge flowing through the reactor is presented as coulombs per cm of scope deflection.

The X - Y product, then, is:

$$\left( \frac{\text{volts}}{\text{cm}} \right) \left( \frac{\text{coulombs}}{\text{cm}} \right) = \frac{\text{volts} \cdot \text{coulombs}}{\text{cm}^2}, \quad \text{or} \quad \frac{\text{watt-seconds}}{\text{cm}^2}$$

Since this is the energy per  $\text{cm}^2$  in one cycle, the power per  $\text{cm}^2$  of parallelogram area is obtained by multiplying the energy per cycle by the frequency in reciprocal seconds. The parallelogram area can be determined by planimeter measurement of a polaroid picture, or by direct measurement.

With a dual beam oscilloscope it is also possible to view the voltage and charge waveforms simultaneously.

## CHEMISTRY IN HIGH TEMPERATURE PLASMA JETS

CHARLES S. STOKES

RESEARCH INSTITUTE OF TEMPLE UNIVERSITY  
4150 HENRY AVE.  
PHILADELPHIA, PA.INTRODUCTION

Plasma generators, in general, have been found suitable for a variety of uses. They generally provide an electric arc which is condensed or constricted into a smaller circular cross-section than would ordinarily exist in an open arc-type device. This constriction generates a very high temperature (8,000-20,000°K) so that a superheated-plasma working fluid can be ejected through the nozzle and the composition of the plasma determine the use to which the plasma generator is put. Plasma generators have been used for cutting, welding, metal spraying and chemical processing. For chemical processing, plasma generators have provided the possibility of the production of new alloys and compounds and the processing of less commonly used materials, as well as the preparation of certain common chemicals.

PLASMA JET EQUIPMENT

Two types of plasma generators are possible: the nontransferred and the transferred arc. A nontransferred arc consists of a cathode and a hollow anode where the arc is struck between the electrodes and the flame emerges through the orifice in the anode. In the transferred arc, the cathode is placed some distance away from the anode and an arc is passed between the electrodes. The nontransferred arc is the most popular in the chemical studies made to date.

A plasma jet used in chemical synthesis can have varied designs to meet special requirements, such as the introduction of a reactant material into the flame path at a particular point.

Consumable cathodes have been used in experiments in which carbon was one of the reactants. Carbon, vaporized from a graphite cathode, was used in the synthesis of cyanogen and hydrogen cyanide. Powdered carbon introduced in a gas stream or as a constituent of a gas has also been used as the source of carbon in a plasma flame.

Electrodes of 2% thoriated tungsten are the most frequently used water-cooled nonconsumable electrodes. Water-cooled copper anodes have been widely used in experimental work. Figure 1 shows a typical plasma jet assembly. A reactor chamber may be of any configuration desired to accommodate different feeding and quenching devices.

PLASMA JET REACTIONSGAS-GAS REACTIONS TO PRODUCE A GAS AND GAS  
DECOMPOSITION REACTIONS TO PRODUCE A GAS

A considerable amount of research has been done by a number of people in the area of plasma jet gas-gas reactions. The following is the gas reaction producing gases that have been investigated.

- CATHODE ASSEMBLY  
 1. CATHODE TOP PLATE  
 2. GAS DISTRIBUTOR PLATE  
 3. CATHODE BUS BAR  
 4. CATHODE BUS BAR STUD  
 5. GAS ENTRY EXTENSION NIPPLE  
 6. GAS TUBE  
 7. ANODE ASSEMBLY  
 8. ANODE ASSEMBLY COVER  
 9. COPPER ANODE NOZZLE  
 10. NYLON INSULATOR  
 11. CATHODE  
 12.

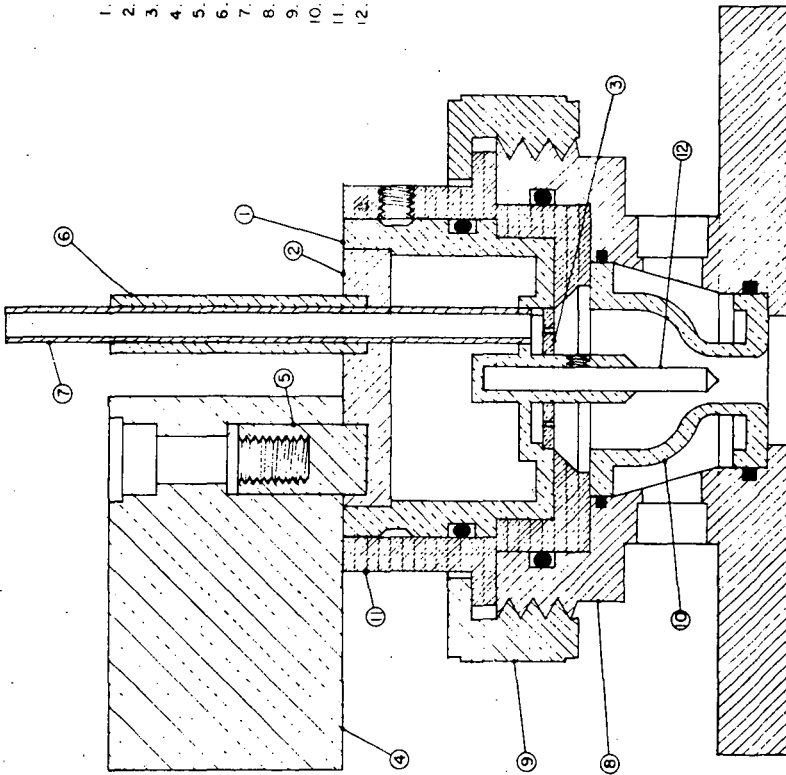
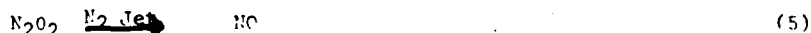
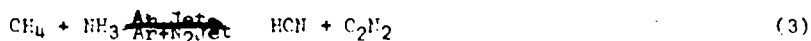
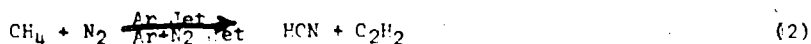
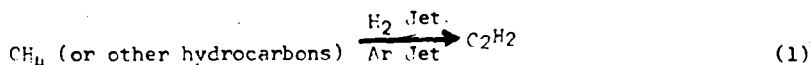


FIGURE 1



In the past several years considerable effort has been directed to the investigation of the production of acetylene from hydrocarbons (reaction 1).

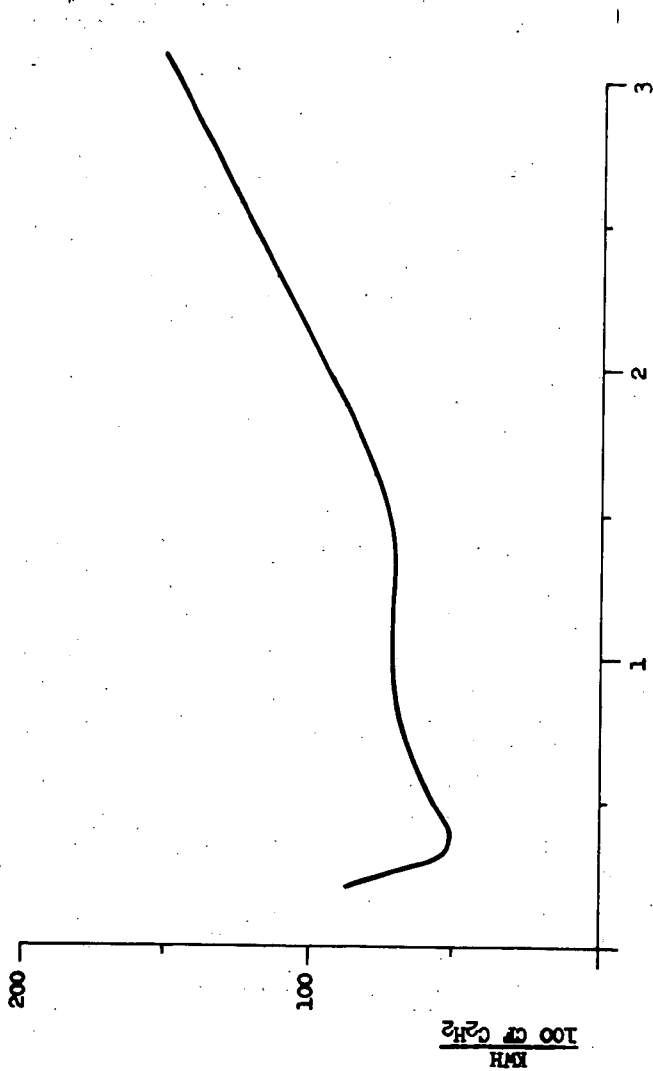
The production of acetylene by reacting methane in the flame of an argon plasma jet yielded an 80% conversion to acetylene (1). Almost all of the methane was converted to acetylene and hydrogen with little formation of soot. Figure 2 shows the power consumption vs. the feed ratio of argon to methane. This ratio is the most important parameter in the acetylene yield. The minimum power consumption 60 Kw/hr/100 cu. ft. acetylene produced, corresponded to a ratio of argon to acetylene of 0.3. Damon and White (2) selected the manufacture of acetylene as an application for plasma processing which might be of interest to the petroleum industry. Methane was one of the gases proposed with the use of recycle procedure. Anderson and Case (3) studied the methane decomposition reaction and compared it to available thermodynamic data. In these experiments a hydrogen plasma torch was used coupled to a reaction chamber and water quench system. The hot hydrogen stream emitted from the plasma jet, entered the reaction chamber and mixed with a methane feed. The gas mixture was analyzed after affluing from the reaction chamber and water quench system. The optimum cracking conditions for methane produced a 30% yield of acetylene.

In a report of the National Academy of Sciences (4) the investigation by the Linde Company of the production of acetylene using a plasma jet and natural gas was reported. This process is said to have a more efficient transfer energy to the feed stream than does the open arc process used in Germany.

Considerable research has been done on the methane-nitrogen and methane-ammonia reactions (reactions 2 & 3) to produce hydrogen cyanide and as a by product acetylene. Leutner (5 & 6) reported up to 50% conversions were obtained based on the carbon input (as methane) by using either nitrogen, argon or nitrogen-argon mixtures as the plasma gas. Figure 3 shows a schematic of the apparatus used in these studies. These experiments showed that up to 75% of the carbon input as methane was converted in HCN and acetylene for reaction 3 and 90% for reaction 2. No other hydrocarbons besides acetylene were found and cyanogen was present in only trace amounts.

Damon and White (7) proposed the production of reducer gas by reaction 4 using natural gas or propane as a hydrocarbon source. The proposed process for steam-methane reforming would operate at a temperature of 3000 to 6000°F and provide a high temperature reducing gas for metals and other high temperature processes.

The fixation of nitrogen (reaction 5) has been one of the major applications for arc induced reactions in the past. During the past several years direct fixation oxygen-nitrogen mixtures has been investigated, however, only 2% of the total nitrogen input has been converted to NO (6 & 8). The use of liquid oxygen and/or liquid nitro



Feed Ratio Ar: CH<sub>4</sub>

Figure 2

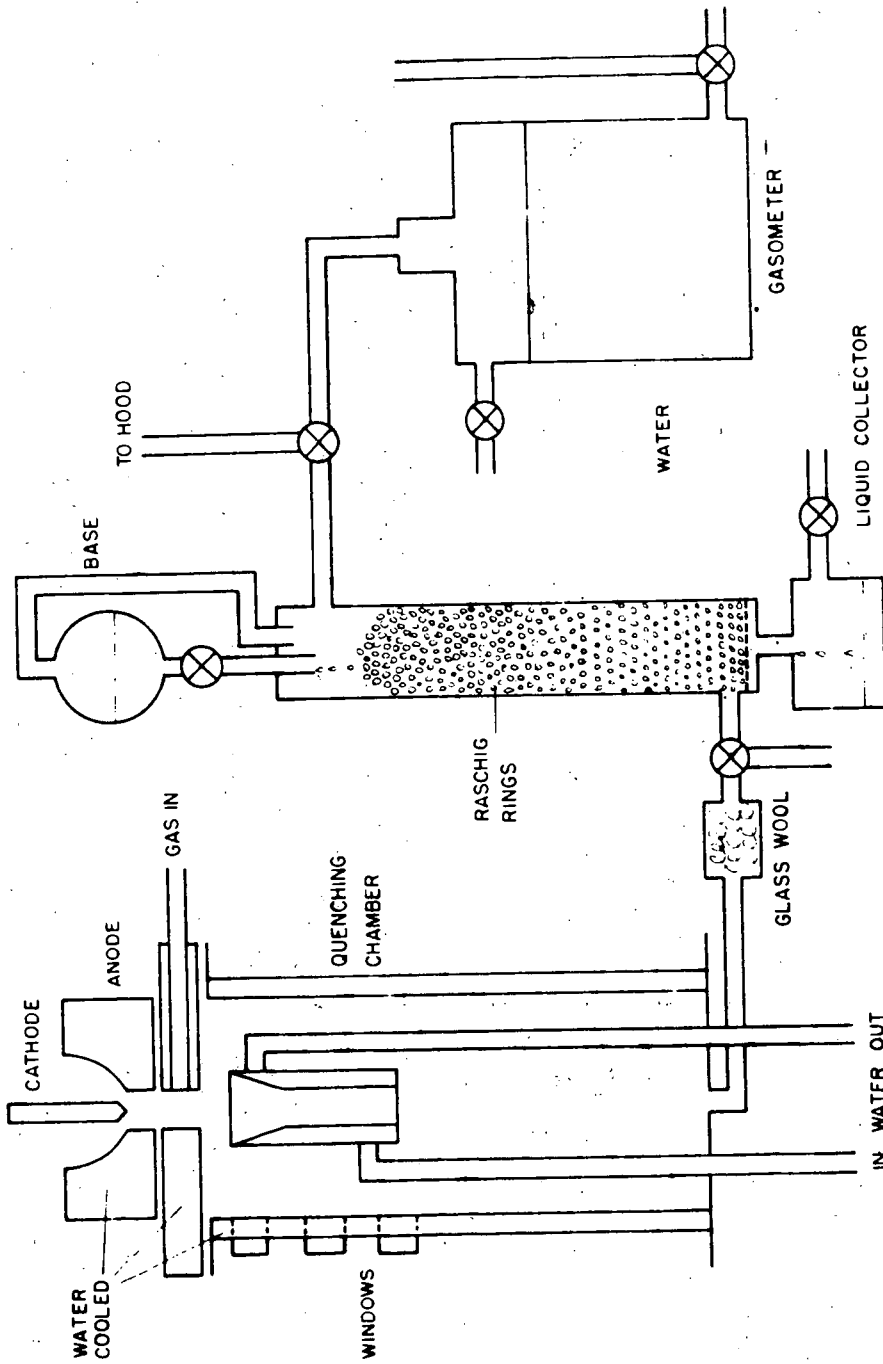


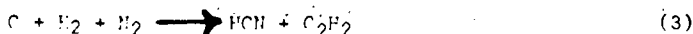
FIGURE 3

quench system with a nitrogen plasma jet have shown no improvement on the above yield(9).

Recently Fronfin and Hazlett (10) have experimented with the introduction of  $CF_4$  and  $SF_6$  into a nitrogen plasma jet. Small yields of  $NF_3$ ,  $N_2F_4$  and  $CF_3NF_3$  (reactions of 6 & 7) were produced. The yield of fixed nitrogen compounds was of the order of 1% of the nitrogen inlet. The yield of these compounds increased with both increased power input and P/N ratio.

Freeman and Skrivan (11) have studied the decomposition rate of ammonia and methane in a plasma jet (reaction 8) and have shown it to be rate limited by a diffusion process. The apparatus used has been fully characterized and shown to be a very good fit for a diffusional model.

#### GAS-SOLID REACTIONS TO PRODUCE A GAS



Recently investigations at the Research Institute of Temple University have shown that hydrogen sulfide can be synthesized from its element, hydrogen and sulfur powder fed in a helium plasma jet (12). Conversions as high as 37% based on the sulfur input have been obtained. Figure 4 shows both the % conversion and the g/Kwhr of hydrogen sulfide formed vs. Kwhr/p of sulfur input. As can be seen from the figure the maximum conversion % does not necessarily have the maximum production efficiency.

A considerable number of syntheses have been carried out using solid carbon powder or graphite elements as a carbon source for reactions with various materials including hydrogen, nitrogen, hydrogen-nitrogen and ammonia. Reactions 2 through 5 show the various productions obtained by these reactions. In the case of acetylene synthesis (reaction 2) the highest yield obtained by direct synthesis from the elements was 33% (1). Hydrogen cyanide yields up to 51% for reaction 3 and up to 39% for reaction 4 have been obtained (5). A complete study of the synthesis of cyanogen from its elements was made by Leutner (6 & 13) and this reaction gave 15% conversion based on the carbon input at the optimum reaction conditions.

Recently Graves, Kawa and Hiteshue (14) reported investigations using bituminous coal fed into an argon plasma jet. Acetylene, the principal product, was obtained in yields of 15 wt. %. This work studied the effects of coal feed rate, particle size and plasma temperature on yields and products formed.

#### GAS-GAS REACTIONS TO PRODUCE A SOLID



Harnisch, Kevner and Schallus (15) reported the preparation of titanium nitride (reaction 1) from titanium tetrachloride gas with either plasma jet heated ammonia or nitrogen/hydrogen mixtures. The reaction produced very finely divided black titanium nitride up to 95% pure. The Thermodynamics Corporation (16) has

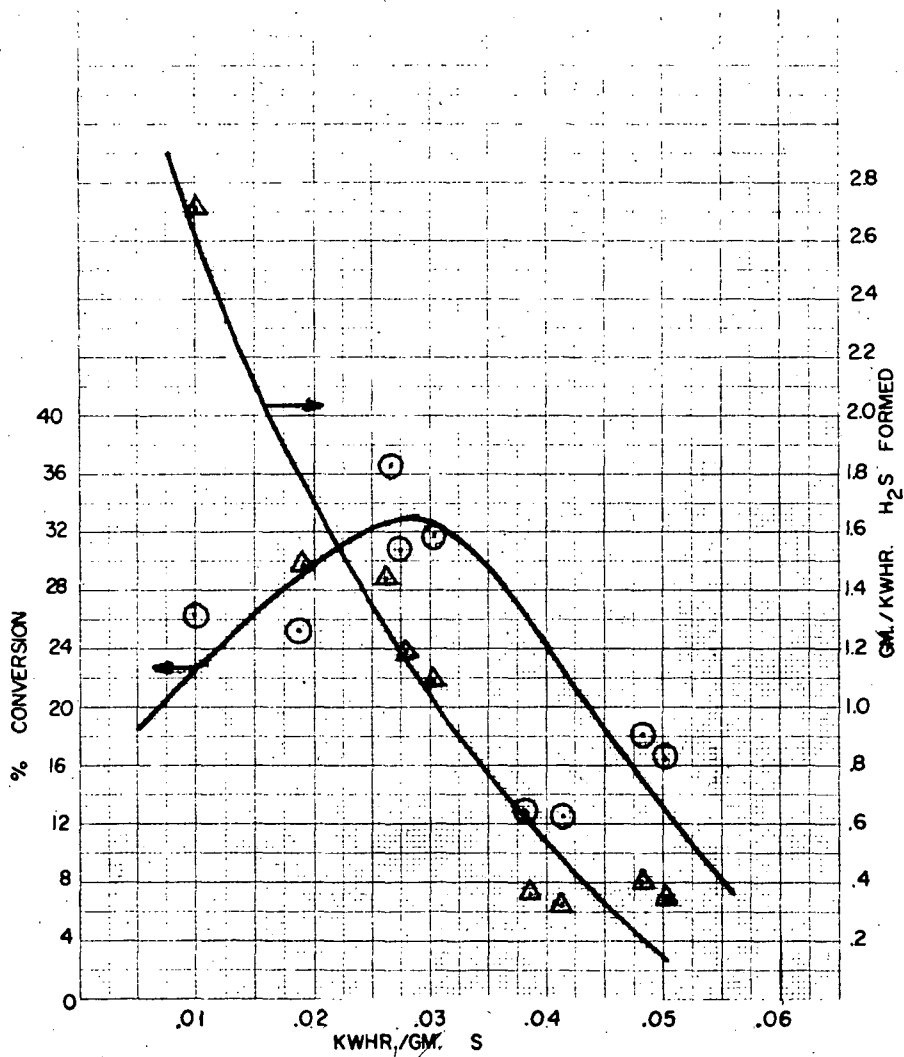
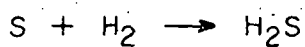


FIGURE 4

reported the possibility of producing carbon black from hydrocarbons using a plasma jet. Methane or other hydrocarbons which would be introduced into the plasma flame, would be cracked using hydrogen as the operating gas and producing carbon black. Liquid as well as gaseous hydrocarbons can be used as a source for carbon and the Vitro Laboratories (4) have experimented with carbon black production from liquid hydrocarbons.

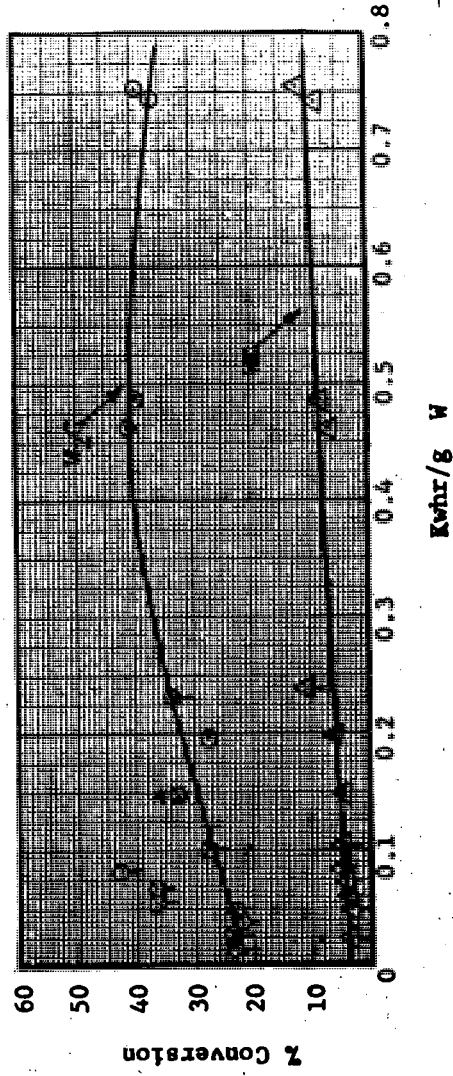
GAS-SOLID REACTIONS PRODUCING A SOLID



The production of metal nitrides (8 & 17) from the elements has been investigated for three elements, titanium, magnesium and tungsten (reactions 1 to 3). The production of titanium nitride in the 100% yield was accomplished by using 200 mesh titanium powder fed into a nitrogen plasma jet. The titanium nitride particle size was found to be 0.75 to 7.5 microns and the product was also formed in large, compact, golden yellow crystals. In a like manner tungsten nitride was formed in 25% yield. 40% conversion to magnesium nitride was obtained when magnesium was fed into a nitrogen plasma jet.

The preparation of metal carbides has also been reported (12 & 17). Figure 5 shows the % conversion vs. Kw/hr/g tungsten input for reaction 4. As can be seen, the WC conversion is directly proportional to the power input level. The highest conversions obtained were 43% for  $\text{W}_2\text{C}$  and 11% for WC. Reaction 5 above is shown in Figure 6 where % conversion is plotted vs. Kw/hr/g  $\text{WO}_3$  input. The three products of the reaction, tungsten (43 to 81% conversion), tungsten carbide (4 to 11% conversion) and ditungsten carbide (9 to 35% conversion) are formed in a total conversion of 81 to 94%. The major product is tungsten which is favored at higher Kw/hr/g  $\text{WO}_3$  inputs. The reaction of tantalum and methane in a helium plasma jet is shown in Figure 7 where a water-cooled quenching probe was placed at 1/2" and 5" below the plasma jet. The effect of the quenching distance is dramatic. The amount of  $\text{Ta}_2\text{C}$  formed is not appreciably different in either case, however, the TaC yield changed considerably by the placement of the quenching device. Conversions up to 72% TaC have been produced by this reaction. Figure 8 shows a plot of the tantalum-pentoxide plus methane reaction carried out in a helium plasma jet. The % conversion is plotted vs. Kw/hr/g tantalum pentoxide input for two different quenching probe distances from the plasma jet. In the case where the quencher was 1/2" below the jet the production of TaC

W + CH<sub>4</sub>  
 5 inch quench distance  
 ○ Δ micron size W  
 ◊ Δ -325 mesh W



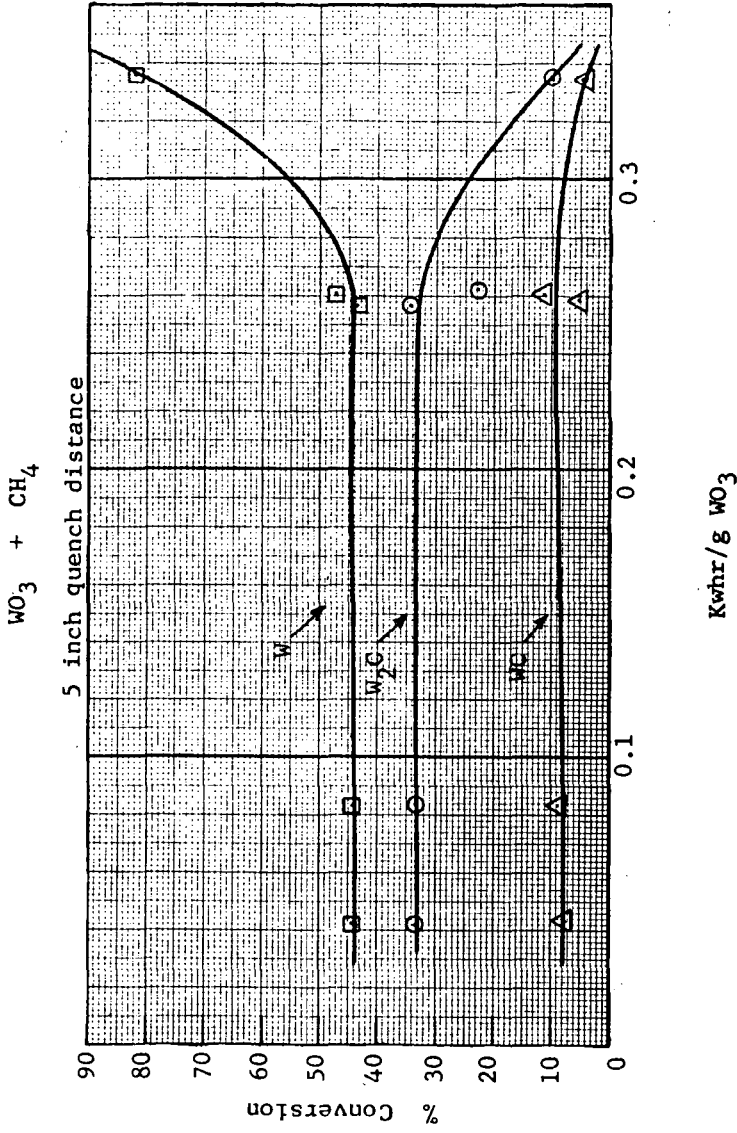


FIGURE 6

Ta + CH<sub>4</sub> IN HELIUM PLASMA JET

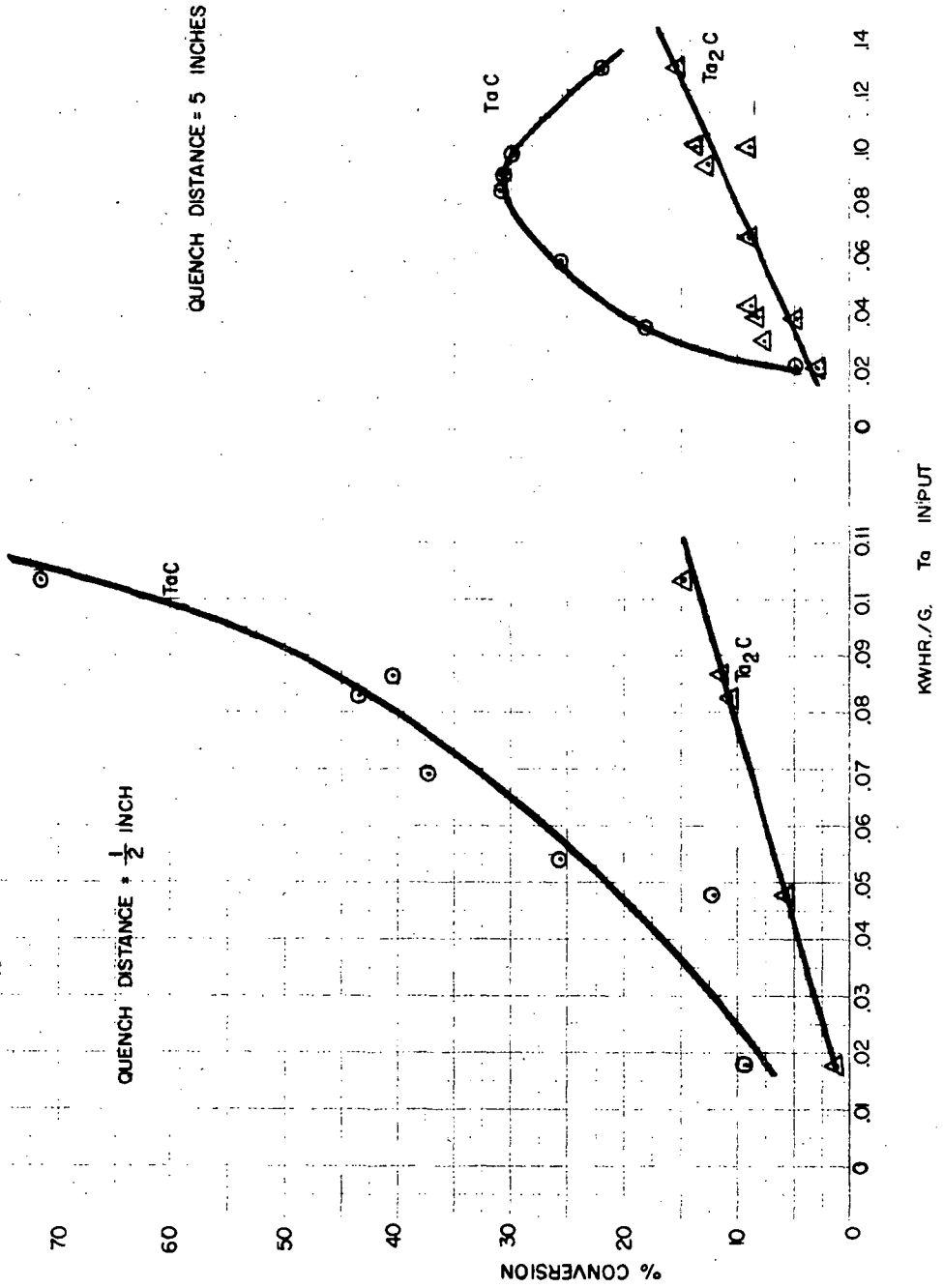


FIGURE 7

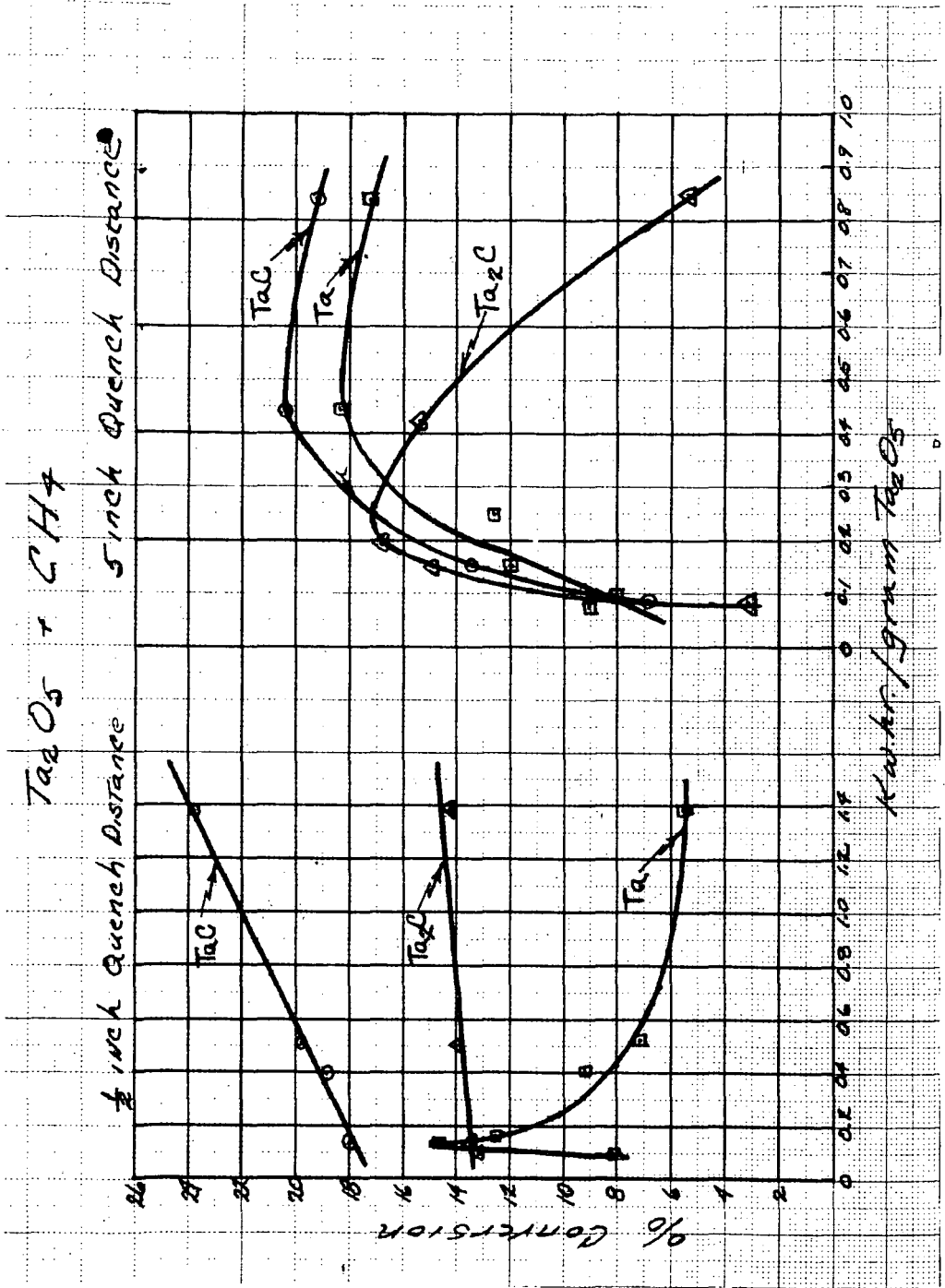


FIGURE 8

goes up linearly with the Kw/hr/g input. Where the quenching distance was 5" a peak was obtained which shows that adequate quenching does not take place beyond a value of 0.4 for Kw/hr/g. Note that in the second case the formation of Ta<sub>2</sub>C also peaks and then falls off rapidly, in contrast to the 1/2" distance. Tantalum metal is the favored product in the 5" case. Maximum conversions are 24% TaC, 17% Ta<sub>2</sub>C and 18% Ta for both cases.

The reduction of tantalum pentoxide with hydrogen (12) in a helium plasma jet to produce tantalum metal (reaction 8) is shown in Figure 9. Again the % conversion is plotted vs. Kw/hr/g Ta<sub>2</sub>O<sub>5</sub> input for two different quenching distances. As can be seen the more rapid quenching (1/2" case) gives the maximum conversion (42%), which peaks at 0.35 Kw/hr/g Ta<sub>2</sub>O<sub>5</sub>.

In a similar manner the reduction of tungsten trioxide was carried out in a helium plasma jet (17) with the quenching device 5" below the plasma jet. Conversions as high as 95% were obtained carrying the tungsten trioxide in hydrogen into the flame of the jet. The reduction of other metal oxides has also been experimentally investigated (17). Ferric oxide was reduced to iron metal in a 100% conversion using a helium plasma jet and carrying the ferric oxide in hydrogen (reaction 11). Titanium dioxide and zirconium dioxide reductions were also attempted by the same method, however, no reduction was obtained in either case. The reduction of aluminum oxide with hydrogen in a helium plasma jet produced only a 2 to 5% conversion to aluminum metal using several different quenching methods.

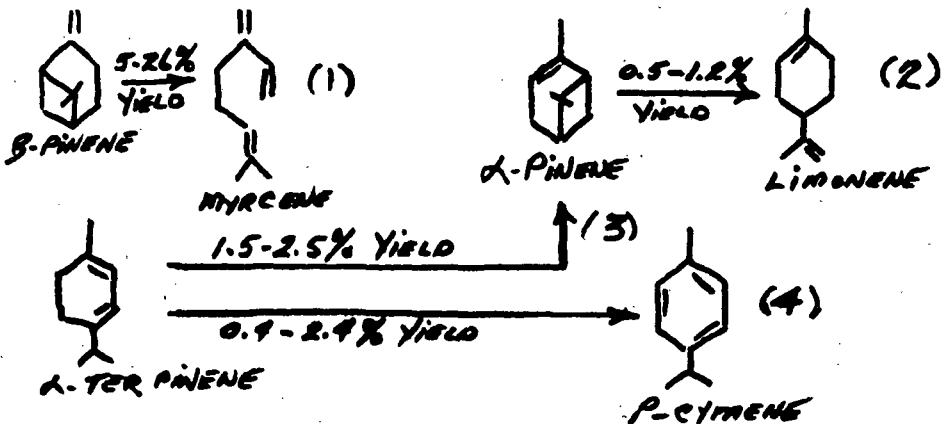
#### LIQUID-GAS REACTIONS PRODUCING A GAS



The production of ozone by means of a plasma jet was accomplished by feeding liquid oxygen into a helium jet (18). Figure 10 shows the schematic of the apparatus used and Figure 11 shows the effect of liquid oxygen flow on ozone production under constant arc conditions. The liquid oxygen acts as both a reactant and quenching medium.

Another example of this type reactant is the decomposition of hydrocarbons into acetylene by use of a plasma jet device. Thermodynamics Corporation (19) has proved the feasibility of producing acetylene from kerosene using a plasma torch. Preliminary runs gave yields of 18% acetylene.

#### LIQUID-GAS REACTIONS TO PRODUCE A LIQUID



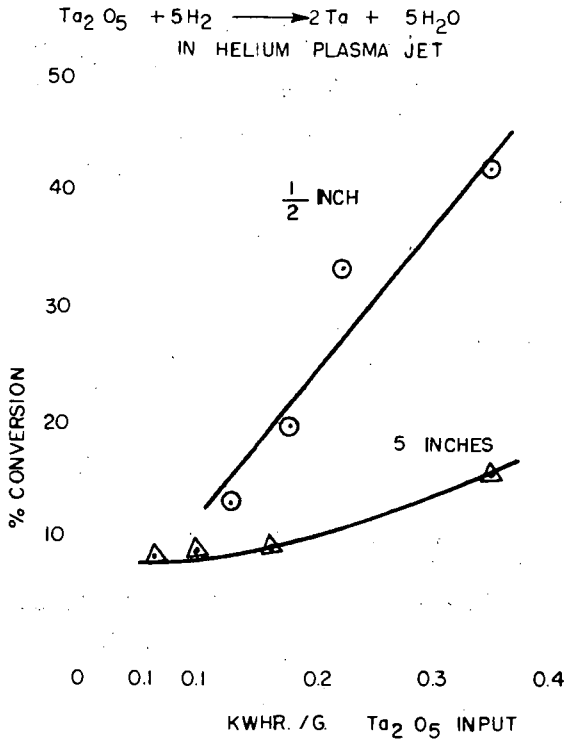


FIGURE 9

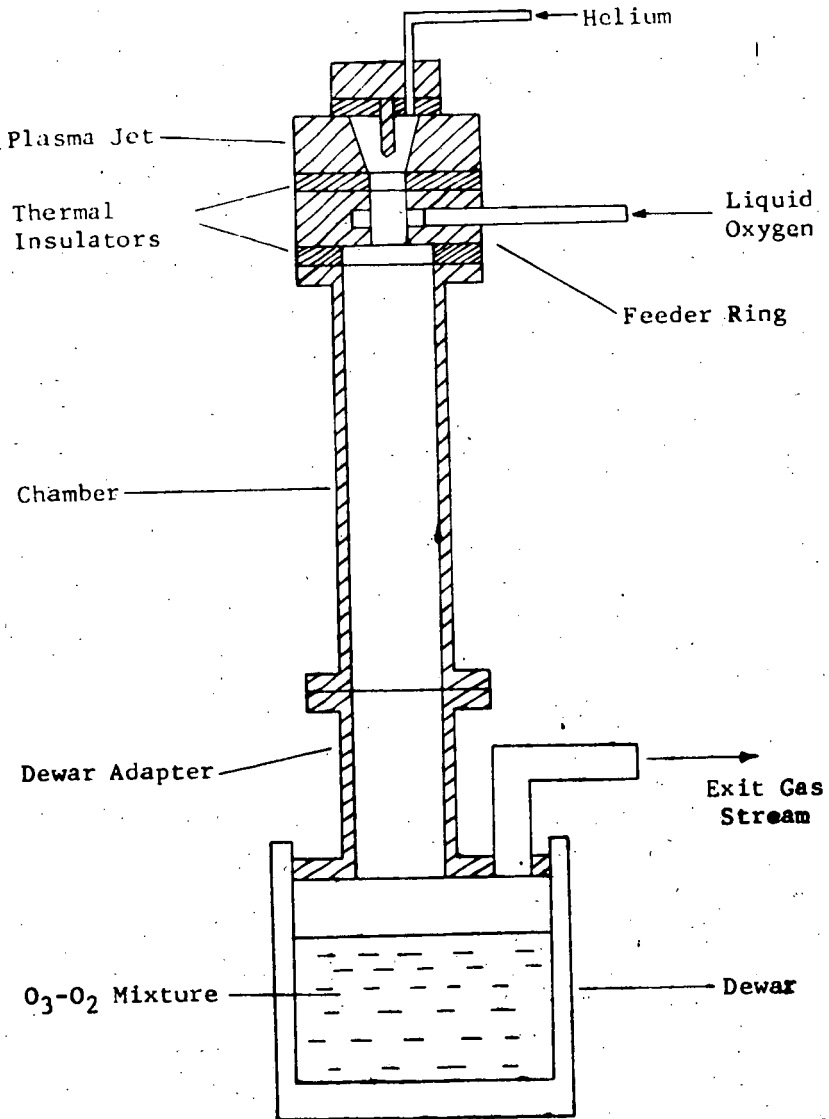


FIGURE 10

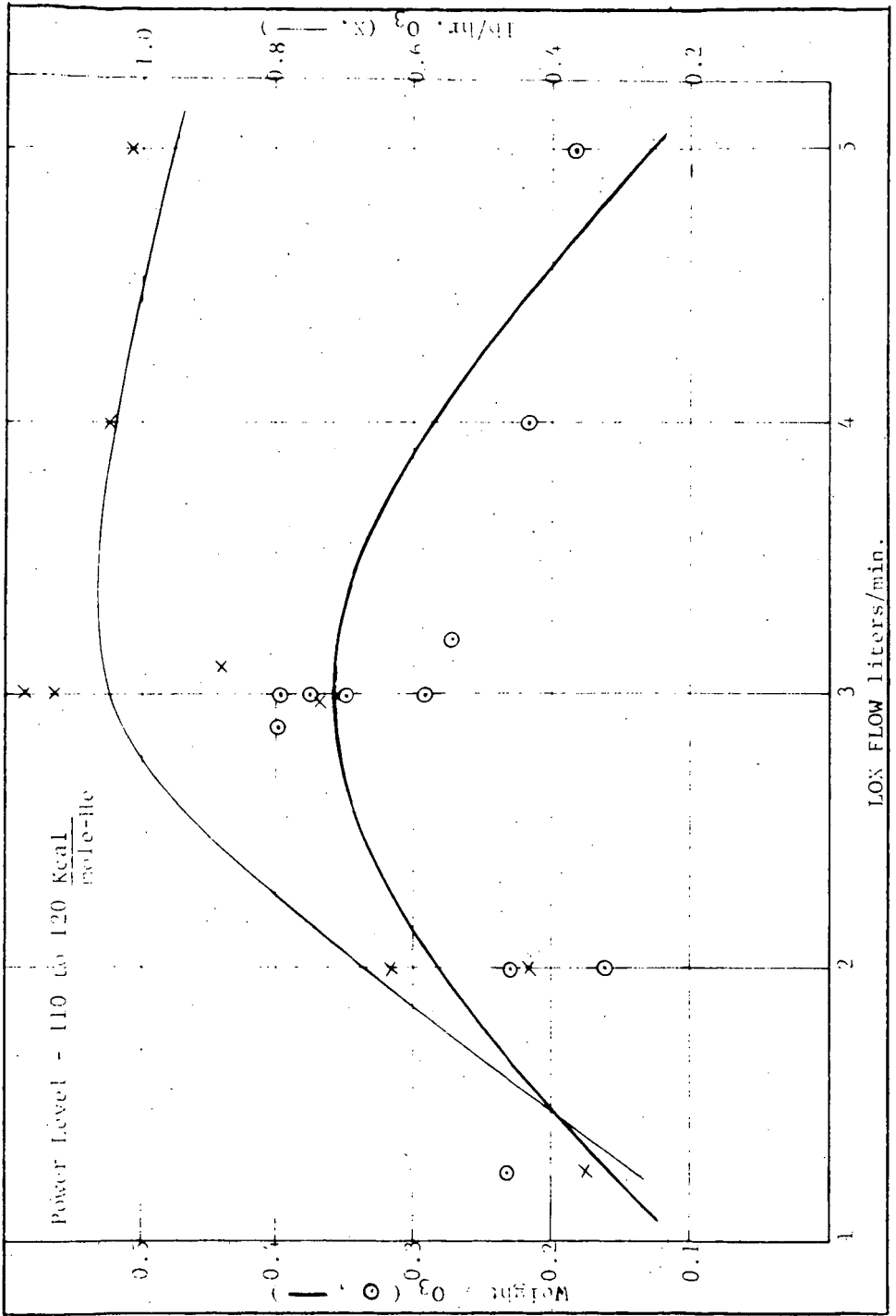


FIGURE 11

Under program carried on at the Research Institute of Temple University for the Glidden Company the reactions of terpenes in a plasma jet were studied (20). The reactions shown above were investigated by use of the apparatus showed schematically in Figure 12. All experimental data were obtained using a helium plasma jet where the terpene was added in a liquid state into the helium plasma flame. The products were analyzed by means of chromatigraphic absorption. The most productive synthesis was the conversion of B-pinene to myrcene in 26% yield (reaction 1). Although this is a normal pyrolysis product of B-pinene it is the first time that a complicated molecule has been produced by means of a plasma jet. Other reactions included the preparation of limonene from  $\alpha$ -pinene in 1% conversion and para-cymene in 2 1/2% yield and  $\alpha$ -pinene in 2 1/2% yield from  $\alpha$ -terpinene (reactions 2 to 4).

#### SUMMARY

The chemical reactions discussed above summarize the syntheses that have been accomplished thus far using a plasma jet device and are by no means all the syntheses studied using a plasma jet. The plasma jet has shown itself to be a useful tool in the area of synthesis of compounds and has moved from the preparation of simple materials to more complex ones recently. With the ever increasing number of investigations being carried out by private industry, there is no doubt that the plasma jet will become a commercial chemical process device. Its potential has been just touched and with each new use a whole field of investigation is opened.

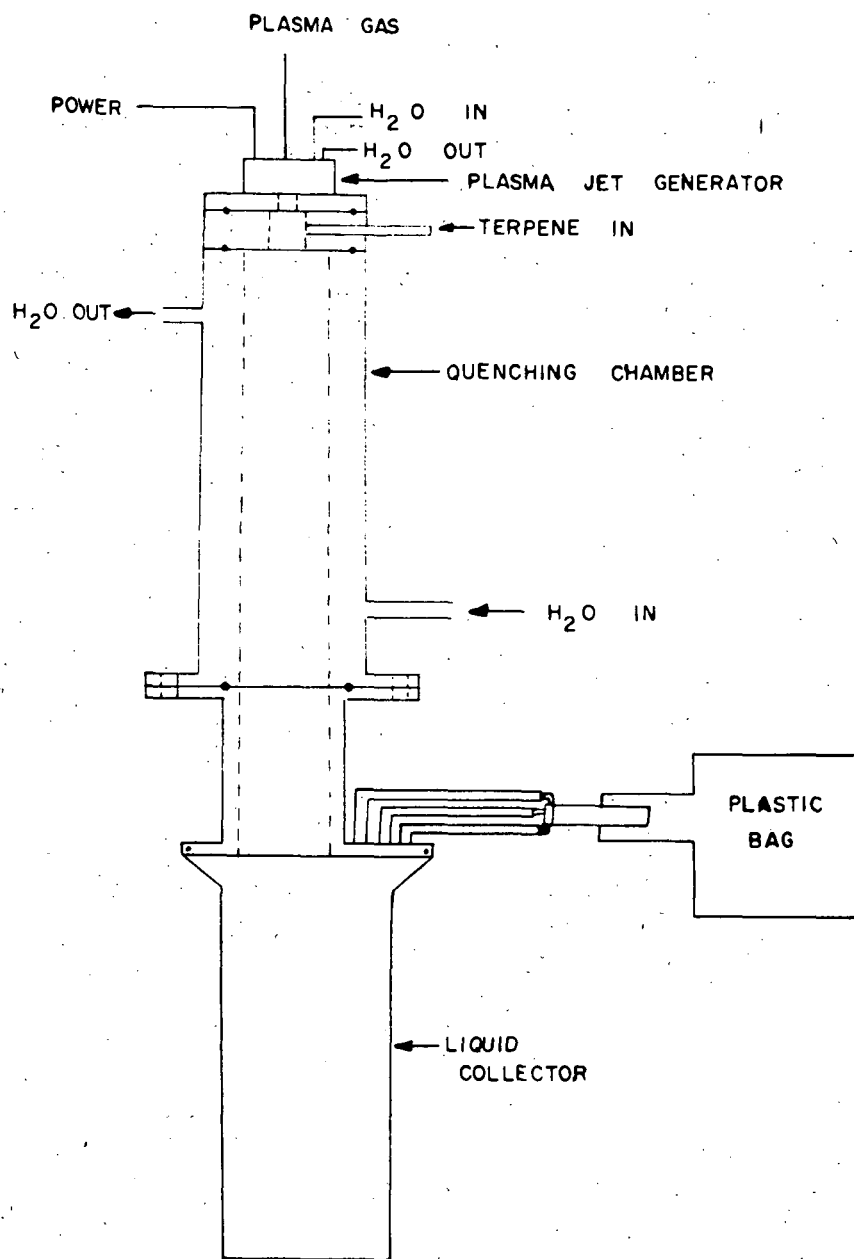


FIGURE 12

REFERENCES

1. Leutner, H. W. & Stokes, C. S., Ind. Eng. Chem. 53 341 (1961)
2. Damon, R.A. & White, D.H., Proposed Plasma Chemical Processes of Interest to the Petroleum Industry, Report No. PLR-115, Plasmadyne Corp., Santa Ana, Calif. (Feb. 8, 1962)
3. Anderson, J.E. & Case, L.K., I & F.C. Process Design and Develop. 1 (1962)
4. Development and Possible Applications of Plasma and Related High Temperature Generating Devices, Report MAP-167-M, Division of Engineering and Industrial Research, National Academy of Sciences, National Research Council, Washington, D.C. (Aug. 30, 1960)
5. Leutner, H.W. I & F.C., Process Design and Develop. 2 315 (1963)
6. Grosse, A.V., Leutner, H.W. & Stokes, C.S., Plasma Jet Chemistry, First Annual Report, The Research Institute of Temple University, Office of Naval Research Contract NONR-3085(02), (Dec. 31, 1961)
7. Damon, R.A. & White, D.H., Typical Inorganic and Inorganic High Temperature Plasma Jet Reactions, Report No. PLR-119, Plasmadyne Corp., Santa Ana, Calif. (Sept. 20, 1962)
8. Stokes, C.S. & Knipe, W.W., Ind. Eng. Chem. 52, 287 (1960)
9. Grosse, A.V., Stokes, C. S., Cahill, J.A. & Correa, J.J., Plasma Jet Chemistry, Final Report, The Research Institute of Temple University, Office of Naval Research Contract NONR-3085(02), (June 30, 1963)
10. Bronfin, D.R. & Hazlett, P.N., I & E.C., Fundamentals 5 472 (1966)
11. Freeman, M.P. & Skrivan, J.P., A.I.Ch.E. Journal 8 450 (1962)
12. Stokes, C.S. & Cahill, J.A., Plasma Jet Chemistry, Final Report, The Research Institute of Temple University, Air Force Office of Scientific Research Grant 775-65, (December, 1965)
13. Leutner, H.W., Ind. Eng. Chem. Process Design & Develop. 1 166 (1962)
14. Graves, R.D., Kawa, W. & Hiteshue, R.W., I & E.C. Process Design & Develop. 5 59 (1966)
15. Harnisch, H., Kevmer, G. & Schallus, E., Angew. Chem. Internaut. Edit. 2 238 (1963)
16. Carbon-Black Formation Using the Plasma Flame in Micro-Chemical Reactions, Plasma-Fax Bulletin PF-3, Thermal Dynamics Corp. Lebanon, N.H. (Oct. 1960)
17. Stokes, C.S., Cahill, J.A., Correa, J.J. & Grosse, A.V., Plasma Jet Chemistry, Final Report, The Research Institute of Temple University, Air Force Office of Scientific Research, Grant 62-196 (Dec. 1964)
18. Stokes, C.S. & Streng, L.A., I & E.C. Product Research & Develop. 4 36 (1965)
19. Plasma Flame Used in Formation of Acetylene from Kerosene, Plasma-Fax Bulletin PF-2, Thermal Dynamic Corp., Lebanon, N.H. (Oct. 1960)
20. Stokes, C.S. & Correa, J.J., Terpene Reaction in a Plasma Jet. Final Report. The Research Institute of Temple Univ. The Glidden Company (sponsor)(Dec. 1964)

GENERAL REFERENCES

1. Dennis, P.R., Smith, C.P., Gates, D.W. & Bond, J.B., Plasma Jet Technology NASA SP-5033, Oct. 1965
2. Stokes, C.S., Chemical Reactions with the Plasma Jet, Chem. Eng. April 12, 1965, p. 191
3. Hulburt, H.M. & Freeman, M.F., Chemical Reactions in the Plasma Jet, Trans. N.Y. Acad. of Sciences 25 770 (1963)
4. Staff Feature, Plasma - Fourth State of Matter, Ind. Eng. Chem. 55 16 (1963)
5. John, R.R. & Bade, W.L. Recent Advances in Electric Arc Plasma Generator Technology APS Journal
6. Greenlee, R.E., The Plasma Jet in Chemical Processing. Clyde Williams & Co., Columbus, Ohio (March 1, 1963), Greenlee, R.E. & Pickley, W.H., Potential Applications for Plasma Jet Processing in the Petrochemical Industry, Clyde Williams & Co., Columbus, Ohio (April 30, 1963)
7. Reed, T.E., Plasma Torches, International Science and Technology, June, 1962, p. 42
8. Marynawski, C.W., Phillips, R.C., Phillips, J.R. & Hiester, N.K., Thermodynamic of Selected Chemical Systems Potentially Applicable to Plasma Jet Synthesis, I & E.C. Fundamentals 1 52 (1962)

PRODUCTION OF HYDROGEN CYANIDE FROM METHANE IN A NITROGEN PLASMA JET

## I. Reactive Species Titration; Further Quantitative Studies

Mark P. Freeman

Central Research Division, American Cyanamid Co., Stamford, Connecticut

## INTRODUCTION

The reaction of methane with a nitrogen plasma to make hydrogen cyanide and acetylene is of considerable interest. Conversions are high enough to be of commercial interest on the one hand,<sup>(1,2)</sup> while the formation of HCN in particular proceeds in

- (1) H. M. Hulburt and M. P. Freeman, *Trans. N.Y. Acad. Sci.*, 2, No. 25, 770 (1963).  
 (2) H. W. Leutner, *Ind. Eng. Chem. Process Design Develop.*, 2, 315 (1963).

such an interesting and reproducible way that clarification of the details of the reaction should considerably advance the use of the plasma jet in synthetic chemistry, and further might be expected to contribute significantly to basic chemical knowledge.

The formally identical synthesis of HCN from "active nitrogen" and methane has been extensively studied<sup>(3-5)</sup> for more than a half century. That the systems are

- (3) K. R. Jennings and J. W. Linnett, *Quart. Rev. (London)* 12, 116 (1958).  
 (4) G. G. Manella, *Chem. Rev.* 63, 1 (1963).  
 (5) N. E. V. Evans, G. R. Freeman, and C. A. Winkler, *Can. J. Chem.* 34, 1271 (1956).

different is apparent, for the high-voltage discharge is a high excitation device, whereas the plasma jet is thought to be nearly in local thermal equilibrium and hence a low excitation device (spectroscopically speaking intermediate between arc and spark.<sup>(6)</sup>) Furthermore, the plasma jet experiments are performed at one-half at-

- (6) F. A. Kovolev and Yu. K. Kvaratskheli, *Opt. Spectr., (USSR) (English Transl.)*, 10, 200 (1961).

mosphere (as opposed to about 1 torr) and at an average temperature twenty times as high on the absolute scale as room temperature, where the bulk of active nitrogen experiments have been performed. Finally, in the plasma jet the carbonaceous species reacting is evidentially not methane. That is, the products other than HCN are acetylene and higher acetylenes with various degrees of saturation. These are the same products that would form if the jet were, say, argon. It has been shown elsewhere<sup>(7)</sup> that the precursors for these products form rapidly compared

- 
- (7) M. P. Freeman and J. F. Skrivan, A.I.Ch.E. (Am. Inst. Chem. Engrs.) J., 8, 450 (1962).
- 

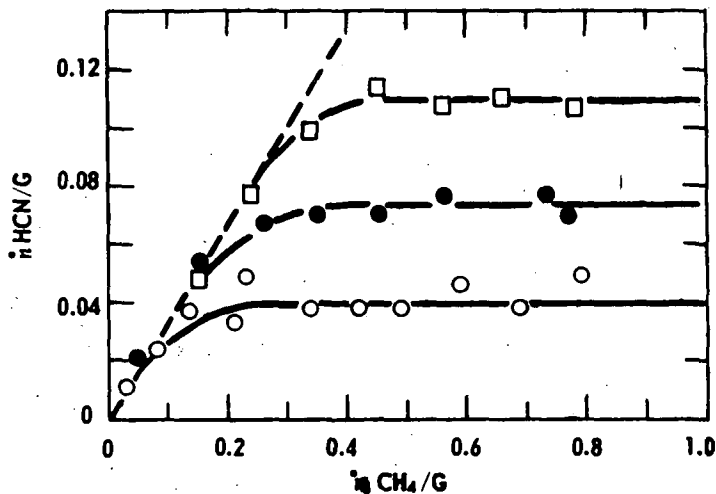
to the time for mixing of the methane with the jet.

There is no question that the plasma jet provides a difficult environment in which to do "good work" in the usual sense. The enormous temperature gradients and consequent inhomogeneities are generally thought of as being a sort of physical chemical bar sinister. On the other hand, perhaps because of their extreme magnitude, the effects due to the temperature gradients are found to be sufficiently reproducible to allow systematic investigation of the jet as a whole, which in its hotter parts represents in a steady state flow situation a chemically unique environment found only in high intensity arc devices. As compensation for tackling this difficult environment, the investigator need not work with trace quantities, but instead with partial pressures and relative conversions at least two orders of magnitude higher than those encountered in active nitrogen research.

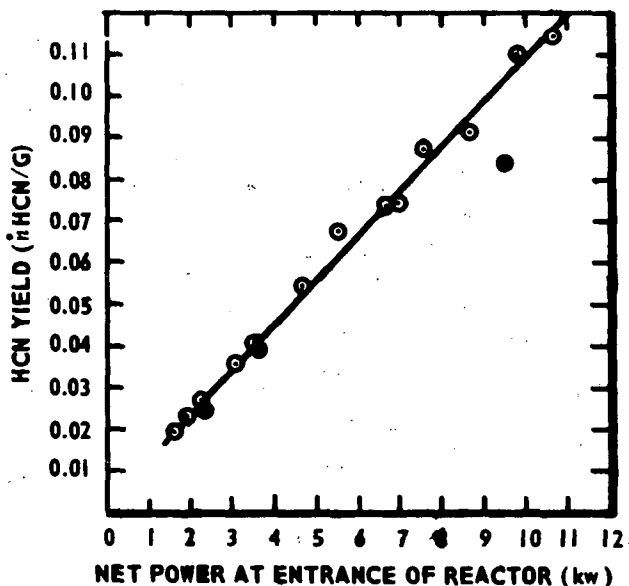
The work reported here represents a systematic continuation of a study performed some time ago.<sup>(8)</sup> The procedure followed then as now is to add methane through an an-

- 
- (8) M. P. Freeman, "The Nature and Quantitative Determination of the Reactive Species In A Nitrogen Plasma Jet," presented at the 147th Natl. Meeting, Amer. Chem. Soc., April 5-10, 1964, Philadelphia, Penn.
- 

nular slot to a confined nitrogen jet of precisely defined average enthalpy (i.e., a calibrated flow rate and a measured heat flow). It has been shown that under these conditions mixing is very rapid, as is the drop in temperature defined from average enthalpy.<sup>(7)</sup> After about one millisecond the resulting flow of high temperature species is further chilled by the entrainment of cold product gas (the fastest of several quench methods investigated on the basis of its efficacy in quenching the ammonia decomposition reaction)<sup>(7)</sup> and the flow of HCN in the product gas is chemically determined. Except as noted, the data are taken at  $350 \pm 20$  torr chamber pressure as this pressure is found to reduce the formation of solid product to an insignificant level. As the methane is added at various flow rates the corresponding rate of production of HCN is noted. Just as in e.g., Winkler's work with active nitrogen, a plateau is observed which seems to indicate that some active species is indeed being titrated (Figure 1). Of utmost interest in the older study was the provocatively simple dependence of the plateau level on jet power level (Figure 2). Because this may in turn be shown to correlate with the rate of production of ions in the arc



1. Absolute production rate of HCN vs feed rate of methane (both normalized by dividing by  $G$ , the most common flow rate of nitrogen.  $G = 0.0171$  g. moles/sec. = 0.383 liter(STP)/sec.) at three net power levels: 3522 watts--○; 6992 watts--□; and 9782 watts--●. Old data, reactor configuration of Figure 5, (0"; 2").



2. Absolute production rate of HCN (normalized) vs net power flowing in gas at entrance to reactor.  $CH_4:N_2:1:2$ . Filled data points were taken at substantially reduced nitrogen flow, 0.0125 g. moles/sec.

process,<sup>(8)</sup> it raised the question, still <sup>335</sup>unresolved, as to whether the ions might not in some way be responsible for the chemistry. As a direct consequence there is a long-term quantitative spectroscopic study of plasma jets<sup>(9)</sup> currently in progress

- 
- (9) M. P. Freeman, "A Quantitative Examination of the LTE Condition in the Effluent of an Atmospheric Pressure Argon Plasma Jet," GE-JILA-ONR Symposium on the "Interdisciplinary Aspects of Radiative Energy Transfer," Philadelphia, Penn., Feb. 24-26, 1966. In Press.

---

that is expected to ultimately yield information on the nature and quantity of ions, atoms and high temperature molecular species flowing in jets of common plasma materials.

Although thermodynamic calculations had previously been performed for the nitrogen-carbon-hydrogen system<sup>(10)</sup> they were not in a form easy to compare with plasma

- 
- (10) C. W. Marynowski, R. C. Phillips, J. C. Phillips, and N. K. Hiester, Ind. Eng. Chem. Fundamentals, 1, 52 (1962).

---

jet results obtained under normal operating constraints. The calculations were therefore reproduced<sup>(11)</sup> with the pertinent parameters varied to conform to the exigencies of

- 
- (11) B. R. Bronfin, V. N. DiStefano, M. P. Freeman, and R. N. Hazlett, "Thermochemical Equilibrium in the Carbon-Hydrogen-Nitrogen System at Very High Temperatures," Presented at the 15th CIC Chem. Engr. Conf., Quebec City, Quebec, Oct. 25-27, 1965.

---

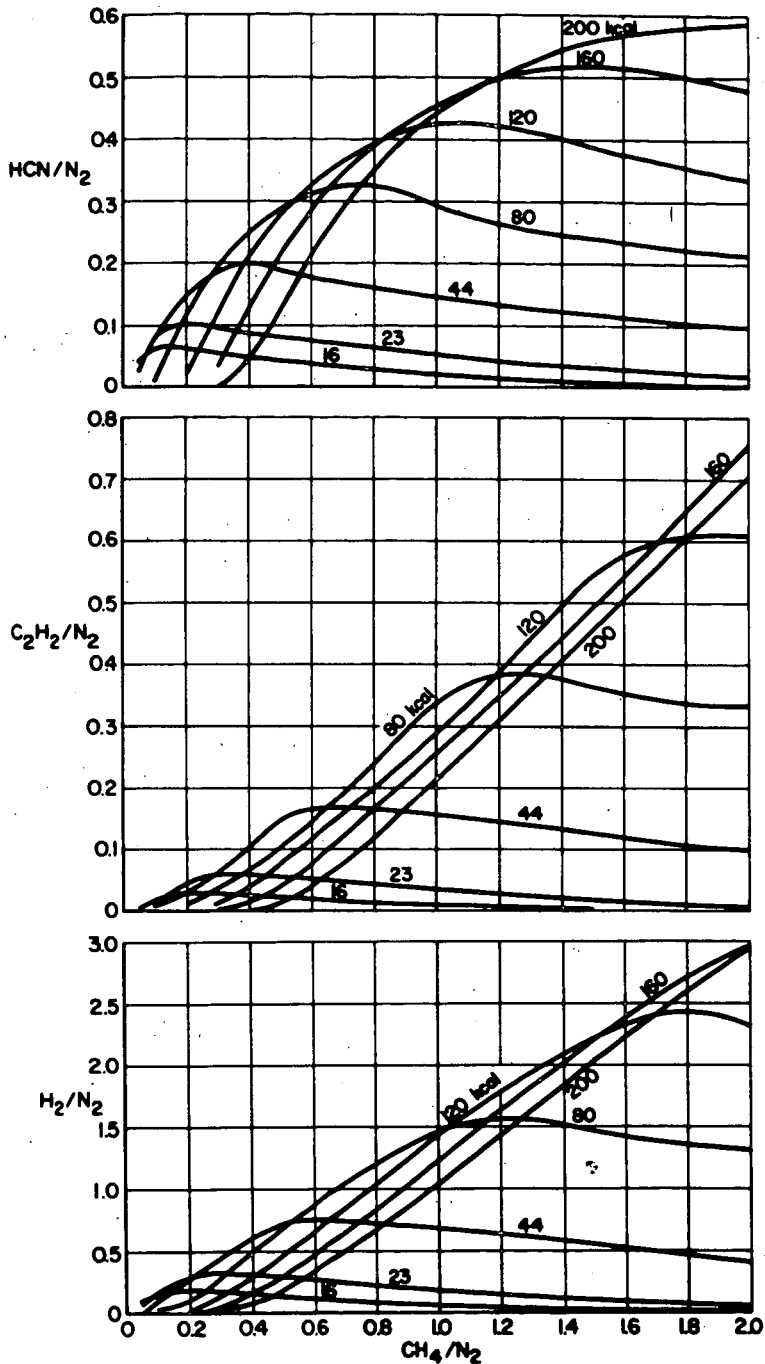
plasma jet operation. Figures 3 and 4 show the results obtained when solid carbon is suppressed in the calculations to be consistent with its absence in the observed products. An important fact immediately emerges. Neither at any experimentally attained average enthalpy, nor at any experimentally used ratio of methane to nitrogen, has the thermodynamically expected yield of HCN for a well-mixed system been exceeded. (Note that the apparent fall-off in calculated yield at high power levels and/or low methane flow rates is due to the competitive formation of cyano, CN, which may be presumed to be an HCN precursor.)

The relationship between the observed and calculated equilibrium yield for the CH<sub>4</sub>-N<sub>2</sub> System is strikingly similar to that recently reported for the F-C-N system by Bronfin<sup>(12)</sup> who thereupon advanced the plausible hypothesis that in either case the

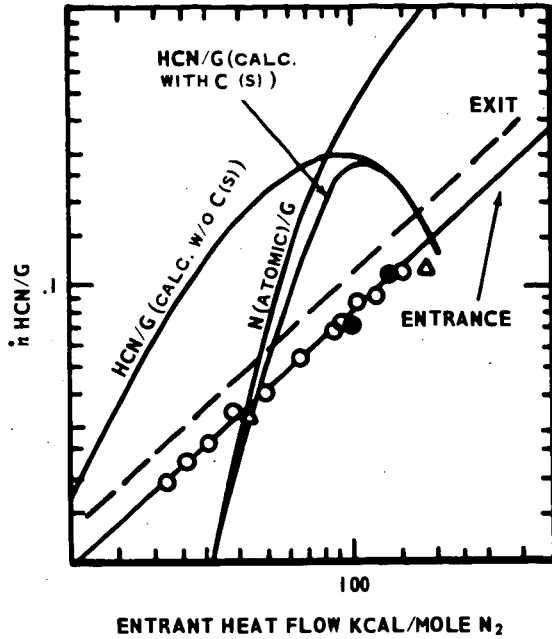
- 
- (12) B. R. Bronfin and R. N. Hazlett, Ind. Eng. Chem. Fundamentals, 5, 472 (1966).

---

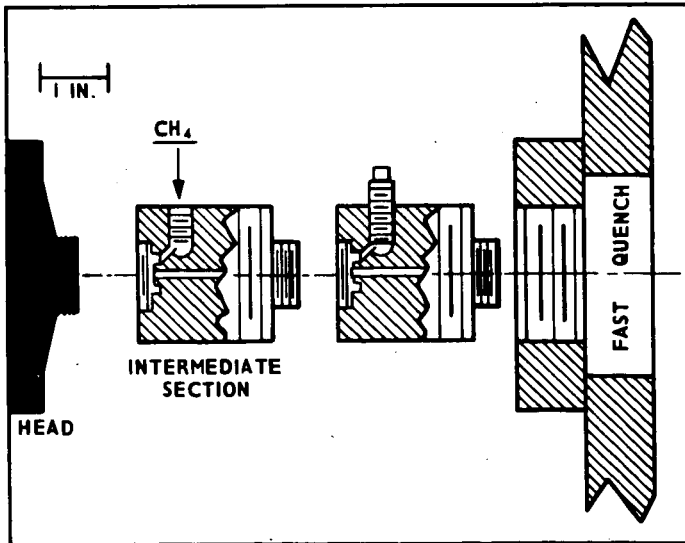
observed yield is in some way a consequence of equilibrium considerations. Now, from earlier work on the acetylene system<sup>(7)</sup> it would seem that the composition and



3. Calculated yields of HCN, acetylene and hydrogen relative to initial nitrogen resulting from the indicated nitrogen-methane mixtures. The methane is initially cold and the nitrogen initially at the indicated enthalpy. Solid carbon has been suppressed as a species in this calculation.



4. Old HCN plateau yield data plotted vs initial nitrogen enthalpy. Also shown are the appropriate theoretically calculated curves for HCN (full equilibrium), HCN (carbon suppressed) and N atoms. The dashed line indicates where the somewhat more scattered experimental data would have fallen if plotted vs 2" reactor exit enthalpy.



5. Schematic representation of modular plasma jet reactor showing but two two-inch intermediate sections.

enthalpy dependence are not what one would expect for mixing and subsequent freezing of a reaction in a confining tube and further for the shorter reactors the enthalpy at the exit is still very high. We shall therefore disregard this possibility here. (Note however, that Bronfin is currently testing this model by means of computer

---

(13) B. R. Bronfin, personal communication.

---

simulation.) The expected way in which equilibrium could control the reaction is for the product distribution to be a function of the enthalpy and composition profiles at the exit of the reactor where there is an onset of rapid quenching. The calculations indicate that composition is only of secondary importance in the "plateau" region so that presumably the enthalpy profile would be controlling. This differs from true titration in the important respect that in titration one in effect irreversibly consumes a certain potential of the nitrogen jet to form HCN that is clearly a function only of the temperature and/or composition and velocity profile in the nitrogen at the point of mixing but before mixing occurs. If we assume the velocity profile of a plasma jet is uniquely determined by the enthalpy profile,<sup>(9)</sup> then the reacting potential as a consequence would in turn be uniquely related to the heat flow in the gas.

Despite this difference, there is no way to distinguish unambiguously between these two possibilities using but one reactor. This is because fractional heat loss from a plasma in a particular reactor type has been shown to be primarily a function of reactor length and arc unit design,<sup>(14)</sup> so that the ratio of exit heat flow to inlet heat

---

(14) J. F. Skrivan and W. VonJaskowsky, Ind. Eng. Chem. Process Design Develop. 4, 371 (1965).

---

flow is nearly constant. The primary objective of the work reported here was therefore to carefully distinguish between these possibilities by performing identical titration experiments in two or more reactors that differ significantly in length in order to determine unambiguously whether inlet or exit heat flow controls the reaction.

It had been inferred from the earlier work by rather incomplete evidence that somehow the capacity to make HCN is primarily dependent on arc conditions no matter how far removed the injection point is from the arc unit itself. A further objective of this experiment was therefore to systematically check this tentative conclusion by careful control and variation of the injection point on a long reactor. From the standpoint of the titration hypothesis, if the arc unit conditions are indeed controlling, then a very long-lived reactive species is implied; such a species is hardly to be expected under these experimental conditions.

Finally, at the same time the older work was being done, Leutner<sup>(15)</sup> using a very short tubular reactor of otherwise the same design found he was able to work at

---

(15) H. W. Leutner, Ind. Eng. Chem. Process Design Develop., 2, 315 (1963).

---

atmospheric pressure and achieve a nitrogen fixation of 12.5% (erroneously reported as 21.9%)(16) in a nitrogen (62%)-argon jet (erroneously reported as pure nitrogen)

(16) C. S. Stokes, personal communication.

with a total flow of 5.0 l(STP)/min. and a power flowing in the gas of 11.5 kw X 55%(16) = 6.32 kw. It was deemed desirable to reproduce his reactor as nearly as possible to attempt to see if the two sets of results were consistent. Such comparison will be made in Part II of this paper, where the effect of argon dilution of the plasma will be discussed in some detail. The contribution such a reactor makes to the present work is of course to extend the range of reactor lengths studied.

## EXPERIMENTAL

### Apparatus

Plasma-jet reactors consist of three parts, head or arc unit, intermediate section, and quenching section. The plasma-jet heat unit used for this study is a Thermal Dynamics L-40 Plasma-jet with "turbulent nitrogen" electrodes, powered by two 12 kw welding power supplies, open circuit voltage 160 volts, connected in parallel but with opposite phase rotations on their 3  $\phi$  input so as to minimize line frequency ripple in the output. The intermediate sections (Figure 5) are made of copper and are fully water-cooled, as is the head. The three intermediate sections are themselves modular. Of length 2", 2", and 4", they are mutually compatible and can be joined in any order to make a reactor of length 2, 4, 6, or 8 inches with a feed port at any multiple of 2 inches. Note that the feed rings are not exactly reproducible in that there are residual gaps left when the surrounding gaskets are tightly compressed by the joining threaded parts. The "Leutner reactor" standard Thermal Dynamics spray nozzle with the solids injection port, which is about 1/4" from the nozzle exit, opened up to a 180° slot. The spray nozzle and the turbulent nitrogen electrode used with the intermediate reactors has a 7/32" diameter as do the intermediate reactors. Insofar as the various reactor configurations vary only in length and feed point, it will suffice to distinguish between them with a bracket specifying first the distance from the point of heat balance to the point of methane feed, and second the distance from the point of heat balance to the exit of the reactor. Thus the 8" reactor fed at the 2" point would be designated (2"; 8"), while the Leutner reactor is (-1/4"; 0").

The quenching section where the hot stream of plasma and reaction products are quenched by entrainment of cold product gas is simply a stainless steel pot 11 inches long and 11 inches in diameter sparsely wound with soldered-on copper tubing. All parts subject to heat damage are well-cooled, but between the windings the pot may get hot enough to cause flesh burns. At the outlet of the quenching section is six feet of 1 inch thick rubberized acid hose. This in turn is fastened to the bottom of a vertical mixing section consisting of a three foot long 2" diameter pipe loosely packed with glass wool. The carbon dioxide is mixed with the product stream at the inlet to the mixing section. The top of the mixing section is connected to a high capacity steam vacuum jet with an automatic control valve for maintaining desired pressures.

A Toepler pump is arranged to withdraw 522 ml of gas from the top of the mixing section at room temperature and at the reactor pressure. This aliquot is then collected for analysis in a suitable gas collection system.

Gas flows except for methane are metered by orifice gages calibrated by water displacement to within 1% for CO<sub>2</sub> and N<sub>2</sub>, respectively. Methane flow, much less critical, is determined by a rotameter calibrated by calculation. All cooling water flows are determined by experimentally calibrated rotameters. Cooling water temperature rise is determined by suitably graduated, interconsistent mercury thermometers.

#### Procedure

Heat flow in the nitrogen plasma at the point of methane introduction is determined by subtracting from the voltage-current product in the arc the heat lost to all cooling water supplies up to that point. For the most part, just the heat flowing at the exit of the head is required. For data taken at a particular heat flow an attempt is made to keep the heat flow constant. In this endeavor the relatively great intrinsic stability of plasma jets made by this manufacturer help, but especially in runs lasting for several hours it is necessary to continually introduce small corrections. This control is greatly facilitated through use of an analog computer that continuously monitors voltage, current, and cooling water temperature rise and either directly controls the rectifiers or displays the net heat flow in kilowatts continuously on a recorder chart so that manual corrections may be introduced as needed. Heat levels given are generally correct to within  $\pm 5\%$ .

Except where noted, the pressure in the quenching chamber is kept at  $350 \pm 20$  torr. The actual pressure of each sample is known to  $\pm 1$  torr but that is not a significant datum in the analysis and is used only as a consistency check. Quench section pressure measures intermediate section pressures fairly well, but probably not the arc pressures because of the pressure drop through the front orifice of the plasma jet. These arc units are not instrumented to measure the pressure inside the head.

Whenever methane flow rate, power level and/or pressure conditions are changed, the system is operated for eight minutes before taking a sample. This is found to be sufficient time to establish a constant composition.

The collected gas aliquot is slowly bubbled through 200 ml of ice cold-caustic containing 12.5 millimoles of base. The half liter space over the caustic is initially evacuated so that the entire sample, together with the air used to flush the lines, might be collected in the caustic and the space over it. This is followed by one minute of vigorous shaking. This procedure has been found satisfactory for the quantitative recovery of CO<sub>2</sub> and HCN. Total acid in the gas is then determined by back-titration with 0.500 N HCl until all the carbonate has been converted to bicarbonate (pH = 8.3). Ammoniacal KI is then added as an indicator and cyanide determined by precipitometric titration with 0.0100 N silver ion. This permits the initial ratio of HCN to CO<sub>2</sub> to be determined. Because the absolute flow rate of CO<sub>2</sub> is known, the absolute production rate of HCN follows directly. Note that for convenience in presentation the flow rate of HCN is always presented as some fraction of 0.383 l(STP)/sec. (0.0171 gram moles sec<sup>-1</sup>) so that it may conveniently be compared to the most often used flow rate of nitrogen. In the figures this "standard" flow rate is represented as G.

Accounting for the various sources of uncertainty, the actual HCN flow rate is estimated to be within about 10% of the reported value, and the heat flow to within 5%. Air leakage into the system, a potential source of error, is held below 0.05% of the total gas flow.

The upper limits of operation are fixed by the onset of plugging. For all but the Leutner reactor, solids formation is otherwise negligible though not nonexistent. At high power levels the Leutner reactor does not plug, the heat of the jet evidently serves to clear incipient plugs, but a fair quantity of a low density brown solid is produced that is about 14% polymerized HCN. Its quality is estimated to be small compared to the total methane utilized.

Although temperatures are not quoted, the temperatures corresponding to the extremes of the eight fold average enthalpy range are 3250-7000°K.

### Composition Dependence

Figure 6 shows typical "titration" curves for the different situations of interest. In every case a plot of HCN produced vs. methane added (both normalized to the "standard flow rate" of 0.0171 l(STP)/sec) divides cleanly into two regimes separated by a break to which we refer as the "equivalence point." To the left of the equivalence point, the yield is simply dependent on methane feed rate but not on the power level. Lines of slope 1/3 and 2/3 are included on the graph to facilitate intercomparison in this region. Although the data are too scattered to draw firm conclusions, it is clear that the break quite generally occurs along the line corresponding to a slope of 1/3. In this region it is as though the nitrogen were somehow present in excess. To the right of the break the HCN throughput is seen to depend only weakly on methane but, as is demonstrated below, is a strong and simple function of heat flow in the nitrogen before mixing. Excluding for the moment the (-1/4"; 0") data (Figure 6-d), the methane dependence on the right shows a real linear increase with methane flow rate in every case, but this slope is not found to be particularly reproducible since it is apt to change slightly when the apparatus is dismantled and reassembled. Hence the scale has been chosen to emphasize the plateau-like character of the curve. Note that the data excepted may be explained by the fact that in this case the exit rather than the entrant heat flow is regulated. Because of the small heat loss in this short section only a second order effect of this magnitude would be expected.

### Power Level Dependence

To take account of the residual slope of the "titration" curves, intercomparison of power-level-dependence studies is done at the same methane flow rate corresponding to one half the "standard" flow whether it is an interpolated point taken from a full titration curve as shown in Figure 6 (filled points) or an isolated measurement (open points). The best line through the old data (Figure 2) appears in Figures 7 through 9 as a reference to aid in intercomparison. Note that Figure 6-a should be exactly consistent with the older data of Figure 1 while the data of Figure 7-b should exactly reproduce Figure 2. The extent that they fail to do this is a fair measure of the nonreproducibility of this experiment when performed in different laboratories, with different equipment, with the chemical analyses performed by different persons.

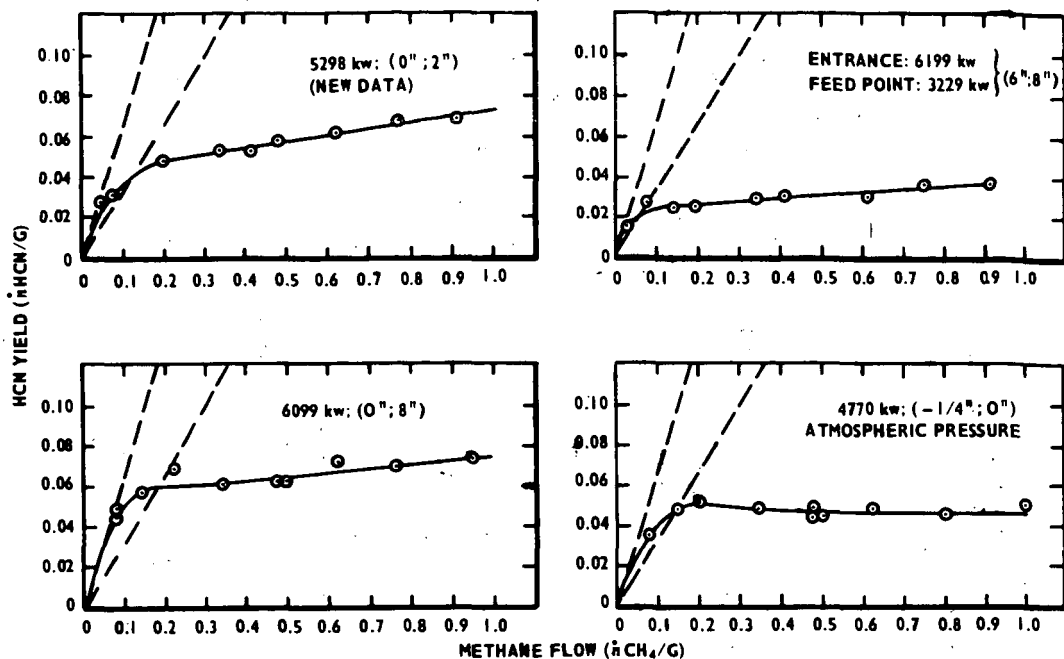
In Figure 7-b data from two different 2" reactors are intermingled as shown. This is to be compared with the (0"; 8") data of Figure 7-a. It is quite clear that within the experimental scatter it would indeed be difficult to improve the agreement. Now the heat leaving the 8" reactor for a given input is only about one half that leaving a 2" reactor for the same input, so that there can be no question but that the HCN production depends only on the heat flow at the point of mixing (or at the exit of the head) and not at all on that at the exit of the reactor.

### Mixing Point Dependence

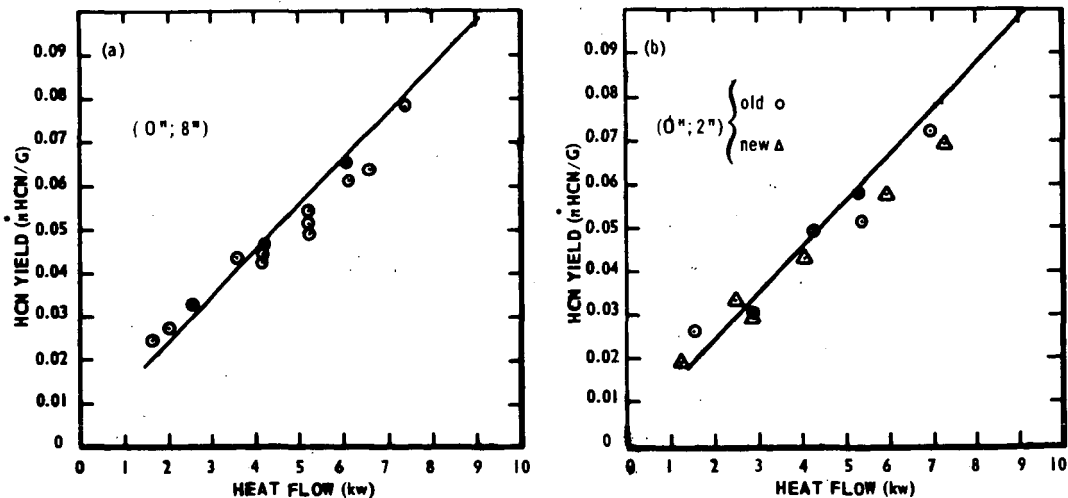
Figure 8 demonstrates clearly that the ability of the nitrogen to make HCN does not persist down the tube at its high initial level, but rather decays as the heat flowing in the gas decays. Shown are a particular set of (6"; 8") data plotted on the left vs heat flow at the exit of the head, and on the right as a function of the heat flowing at the point of mixing, the 6" point. Hence that part of the earlier work indicating the existence of a "long-lived" reactive species is wrong.

### Leutner Reactor

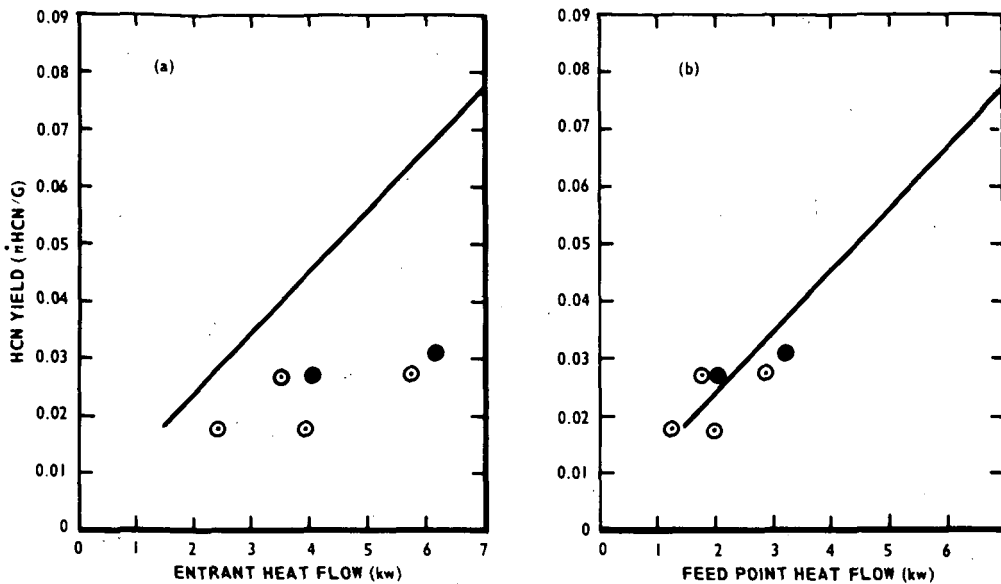
Data for the simulated Leutner reactor are shown in Figure 9. Despite the fact that these data were taken at atmospheric pressure it is clear that the results are completely consistent with those of the other reactors. This agrees with an observation made in the earlier work that there is but slight pressure dependence for this reaction.



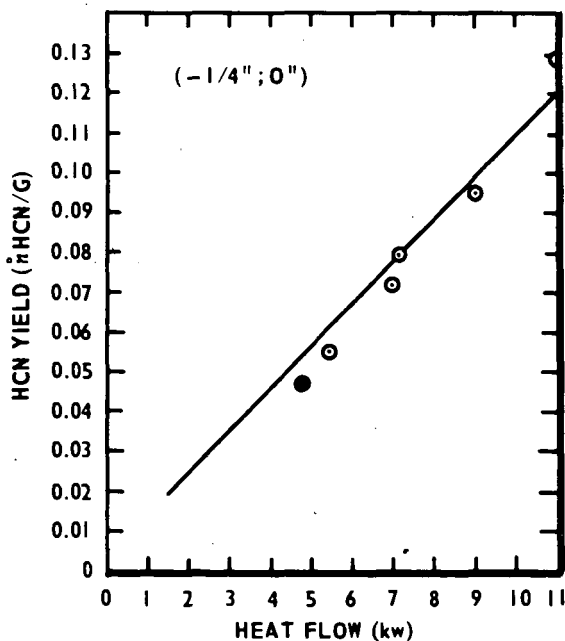
6. Typical titration curves for the case noted. Normalized production rate of HCN vs flow rate of methane. Dashed lines of slope 1/3 and 2/3 are included for reference.



7. Normalized HCN vs heat flow (head exit power) for the eight inch reactor (left) and the two inch reactor (right). Triangles and circles indicate two different 2" reactors. Filled points were interpolated from full titration curves; open points were isolated runs. The "normal" line of Figure 2 is included in either case for reference.



8. Normalized production rate of HCN for the eight inch reactor fed methane at the six inch point, (6"; 8") data, vs heat flow at (a) the exit of the head and (b) at the 6" feed point. Filled points were interpolated from full titration curves. The "normal" line of Figure 2 is included in either case for reference.



9. Normalized production rate of HCN in the Leutner reactor vs heat flow at the exit of the reactor. The "normal" curve of Figure 2 is included for reference.

Because of the use of diluent argon in his work, comparison with Leutner's results must await Part II of this paper which will explicitly treat this complication. Of significance here is the fact that reactors from 1/4" to 8" in length give the same result, dependent only on entrant heat flow. (Actually for the 1/4" reactor the exit heat flow is measured, but presumably in this case there is a nearly negligible difference.)

#### Product Distribution

Plateau Region - Mass spectrometer checks made on product formed in the "plateau" region show  $N_2$ ,  $H_2$ , HCN,  $C_2H_2$  and  $CH_4$  together with some small quantities of higher acetylenes to be the only species present to any appreciable extent. The  $N_2$  is present of course as a solvent while the  $H_2$  is simply the balance of the hydrogen. The HCN is apparently formed by some sort of irreversible process to be discussed further below while the relative amounts of methane and acetylene seem to conform to considerations investigated previously<sup>(7)</sup> for the cracking of methane in an argon jet.

Initial Region - To the left of the break region where the potential of the nitrogen jet to react is in excess, one might expect all of the methane to be converted to HCN, i.e., an initial straight line of unit slope, but such is not the case. Earlier work seemed to favor an initial slope of 1/3 for all titration curves. This would imply that one mole of acetylene is formed for each mole of HCN produced. At the time, however, admittedly crude mass spectrometer checks showed no more than two-thirds to three-quarters mole of acetylene to each mole of HCN. The work reported here indicates an initial slope corresponding to one-quarter to one half mole of acetylene for each mole of HCN. At the breakpoint, however, equimolar quantities of HCN and acetylene would still seem to be the rule. The analytical and sampling apparatuses were neither designed for accuracy nor high precision in this low yield region and it is possible that the differences in the low HCN yield region might have reflected some small change in analytical procedure. It seems more probable, though, that this region is indeed not reproducible and that product distribution here reflects some intangible of the process such as "mixing efficiency", etc. (Note that the reactors are constructed so that the widths of the slots through which the methane flows are not precisely reproducible.)

#### DISCUSSION

##### The Titration Curve

It is clear that the reactor length and hence the heat flow at the onset of sudden quenching is irrelevant; the heat flow at the mixing point evidently governs the extent of reaction. It is further seen that the ability of the nitrogen jet to react with the methane decreases as the nitrogen flows down the reactor in such a way that its potential to react with methane, at least with this reactor geometry, is a function only of heat flow in the nitrogen before mixing.

Initial Region - From a different perspective, with no methane flowing in a long tube the reactive potential of the nitrogen jet is seen to persist to some appreciable extent almost indefinitely, but decays as the heat flow decays, presumably through heat conduction processes. As the methane flow is introduced, some of this "potential to react" (PR for brevity) is now used up by the methane, while the balance decays by the heat conduction process. This gives rise to the "initial region."

Equivalence Point - As the methane flow is increased, more of the PR of the nitrogen jet is used by the methane until the equivalence point is reached. At this point none of the PR survives the mixing of the jet with the methane and the break in the curve occurs.

Plateau Region - Because mixing is not instantaneous at the point of mixing, some of the PR is still used up by heat conduction processes at the equivalence point. As the methane flow is further increased, the equivalent amount mixes closer and closer

to the slot so that less of the residual PR<sup>345</sup> is lost to heat conduction. This latter process probably gives rise to the observed residual slope in the "plateau region" of the titration curves.

#### The Potential To React

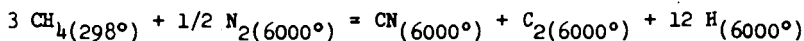
It remains to propose an explanation for the "PR." Although something is being titrated, it is by no means clear just what it is. Nor, as of the present time, has anyone experimentally characterized a nitrogen jet sufficiently well to clearly distinguish between likely alternatives. Nonetheless, it is instructive to examine some of these possibilities for their heuristic value.

Heat Balance - From Figure 2 a fairly constant heat requirement of 1280 kcal/mole may be obtained. This corresponds very nicely (and probably fortuitously) to the endothermic heat of the most probable reaction at 6000°(17):

---

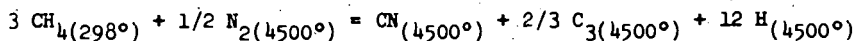
(17) "Janaf Thermochemical Tables," Dow Chemical Company, Midland, Michigan, December 31, 1960.

---



$$\Delta H = 1281 \text{ kcal}$$

or that of the equally probable reaction at 4500°:



$$\Delta H = 1225 \text{ kcal}$$

From this point of view it would appear that the heat of the jet is in some way being titrated by the methane.

Active Species - One might well ask however, if it is just the heat being titrated why does the reaction apparently stop when the core of the jet is still 4000-6000°K? And why is the amount of cyano (CN) formed so sharply limited and constrained so far below the equilibrium value? Note that below 4000° strong exothermic reactions occur that delay further cooling, so that fast quenching cannot be the answer. The most ready answer to these questions is that the HCN reaction is far too slow to equilibrate in jet residence times. Of the manifold complex of forward reaction paths leading to equilibrium, only a few of them will be fast enough to produce HCN in the time available. But these fast reaction paths might well involve nitrogenous species which at thermal equilibrium corresponding to the average enthalpy of the jet, would flow in trace amounts but which, as a consequence of the hot core, are present in the plasma jet at many orders of magnitude higher throughout. Thus we are led naturally to consider this as the titration of some sort of especially reactive species in the jet.

Consider for example a jet producing 0.00171 moles sec<sup>-1</sup> of HCN. From Figure 2, we can see that this requires about 9 kw. of heat flowing in the gas. If we assume there is a small core to the jet at 12,000° (enthalpy at one-half atmosphere = 500 kcal/mole), (18) then the heat flow can be accounted for by assuming the hot core occupies

---

(18) F. Martinek, "Thermodynamic and Transport Properties of Gases, Liquid and Solids" McGraw-Hill Book Co., Inc., New York, N.Y., 1959, p. 130.

---

about half the diameter of the jet (one fourth <sup>346</sup> the area) and that the nitrogen flowing outside this core carries negligible enthalpy. In this calculation is the unproven assumption carried over from the argon jet<sup>(9)</sup> that the mass flux of nitrogen is constant over the entire cross-section. Under the assumed core conditions the jet is 100% dissociated and the atoms 17% ionized. The fluxes are then:

$$\text{atom flow: } 1/4 \times 2 \times (1 - 0.17) \times 0.0171 = 0.0071 \text{ moles sec}^{-1}$$

$$\text{ion flow: } 1/4 \times 2 \times 0.17 \times 0.0171 = 0.00145 \text{ moles sec}^{-1}$$

The ion flow is thus seen to be in excellent agreement with the 0.00171 moles sec<sup>-1</sup> production rate of HCN. To some extent this may be due to a fortunate choice of hot core temperature but is nevertheless a promising possibility.

On the other hand there seems to be no good way to account for the reaction on the basis of nitrogen atoms, in this case present in large excess, suggesting that the nitrogen atoms are somehow deactivated before the carbonaceous species enters the hot core. Insofar as the hydrogen from the dissociation of methane must completely fill the reactor in a very short while, it seems probable that the nitrogen atoms are deactivated from this initial infusion, and that the carbonaceous species react with the nitrogen ions (which might well be molecular ions by this time) or some other species sometime later.

#### CONCLUSION

By systematic variation of reactor geometry it has been conclusively demonstrated that methane added through a peripheral slot to a nitrogen jet titrates, apparently in the true meaning of the word, some potential of the nitrogen jet to react with the thermal decomposition products of methane to form HCN. It is further demonstrated that the potential to react is simply related to heat flow even far down the reactor and is therefore probably the consequence of some steady-state temperature and/or composition profile in a flow with local thermal equilibrium.

For their heuristic value, two superficially different explanations are proposed to explain the "potential to react." On the one hand, the experimental endotherm of the reaction at the equivalence point is shown to be quite consistent with the heat flowing in the hot core of the jet, for a jet model consistent with what we might expect. On the other hand, for the same heat flow and jet model, the yield is shown to be consistent with the flow rate of e.g., ions at the point of mixing and it may equally well be postulated that the ions or some other identifiable species are in fact an active ingredient being titrated.

It is clearly pointless to attempt to conjecture further on the mechanism involved in the titration without more direct evidence on the species and velocity profiles in the jet. A spectroscopic program currently underway in these laboratories will presumably help to fill this gap.

#### Acknowledgement

Many people have contributed in some way to the success of this work, but in particular the author wishes to express his appreciation to Mr. Charles Mentzer (Chemical Engineering Department, Princeton University) who helped perform some of the experiments, and to Professor Hugh Hulburt (Chemical Engineering Department, Northwestern University) and Dr. Barry R. Bronfin (United Aircraft Laboratory) for their invaluable discussions and continuing interest.

## HYDROCARBON-NITROGEN REACTIONS IN A THERMAL INDUCTION PLASMA

Barry R. Bronfin

United Aircraft Research Laboratories  
East Hartford, Connecticut 06108

Gas temperatures above 15,000 K have been observed in plasma generated by radio-frequency induction coupling<sup>1</sup>. This high thermal energy regime becomes of interest to the chemist for the investigation of highly endothermic reactions. In particular, this paper will report reactions between methane and nitrogen fed to a thermal induction plasma and subsequently quenched to yield hydrogen cyanide, acetylene and hydrogen.

## PREVIOUS STUDIES OF THE H-C-N SYSTEM

Low Pressure Discharges. Winkler and his co-workers<sup>2-5</sup> have systematically studied the reactions of nitrogen, activated by passage through a high-voltage discharge, with various hydrocarbons. These studies were carried out at pressures near 1 torr with very low reagent flow rates. Gas temperatures were also low, typically 300 C. In this nonequilibrium system the reaction between methane and "active" nitrogen yielded hydrogen cyanide, acetylene and hydrogen<sup>2</sup>.

High Pressure Arcs. More recently high-power thermal arcs were used for the study of the H-C-N system near atmospheric pressure. Leutner<sup>6</sup> operated a nitrogen plasma jet into which methane was mixed. In his briefly reported results, up to 10 percent conversion of the nitrogen to HCN was found. At this symposium Freeman<sup>7</sup> has reported an extensive study of the synthesis of HCN from a nitrogen plasma jet intermixed with methane. Typically, a 7 percent conversion of N<sub>2</sub> to HCN was observed. In both studies H<sub>2</sub>, C<sub>2</sub>H<sub>2</sub>, and unreacted CH<sub>4</sub> were also identified as major constituents in the cooled product stream.

If the maximum mean temperature attainable in these previous studies is calculated, one finds that enthalpy input was insufficient to generate mean temperatures greater than ~ 5000 K.

Dissociating Plasmas. Upon considering the various species possible in the H-C-N system, the strongest bond found is N≡N (226 kcal/g-mole). Thermal dissociation of N<sub>2</sub> is essentially complete at temperatures in excess of 8000 K<sup>8</sup>. One can envision a high-pressure, stable plasma fed with any of a variety of carbon, hydrogen, or nitrogen compounds and supplied with sufficient enthalpy to reach this high temperature range. The constituent species of such a plasma would be primarily atomic nitrogen, atomic hydrogen, and atomic carbon near 10<sup>17</sup> cm<sup>-3</sup> concentration. The result of rapidly quenching such a highly reactive atom mixture has been generally unexplored. Ammann and Timmins<sup>9,10</sup>, however, did study the rapid quenching of the simpler atomic-nitrogen/atomic-oxygen mixtures at 10,000 K

and 1 atm, which were generated by a constricted d.c. arc. The study which is reported in this paper was undertaken to explore the chemical composition of mixtures formed by the rapid quench of atomic-nitrogen/atomic-carbon/atomic-hydrogen mixtures.

#### PLASMA REACTOR

Radio-frequency Induction Plasma. One convenient approach to achieve the required temperatures in excess of 10,000 K at atmospheric pressure is generation of a thermal plasma by radio-frequency induction heating. The techniques for generating and containing a stable high-temperature induction plasma have been described in detail by Reed<sup>1,11</sup>, Mironer<sup>12</sup>, Marynowski and Monroe<sup>13</sup>, Freeman and Chase<sup>14</sup>, and Thorpe<sup>15</sup>. Figure 1 presents a diagram of the plasma generator used. A few turns of copper tubing were wound around the outside of a water-cooled quartz reactor tube. This coil inductively coupled the supplied r.f. power into the gaseous reactants sent through the reactor. A water-cooled sampling tube with very small internal diameter which served to quench rapidly the reactive plasma species is shown. Efficient cooling allowed the entrance tip of the quench tube to be placed directly into the plasma core.

A cross-sectional diagram of the reactor is presented in Fig. 2. The isotherms indicated are those determined spectroscopically by Reed<sup>1</sup> and are representative of conditions in this study. No direct temperature measurements were attempted in the present study.

The Induction Plasma as a Chemical Reactor. Several characteristics of this system can be exploited for chemical synthesis:

1. Average temperatures in excess of 10,000 K allow essentially complete molecular dissociation. (Lower power input can reduce the specific enthalpy to preserve desired free radicals.)
2. Plasma stability is maintained while operating at very low gas velocities (<1 cm/sec). Thus long residence times and efficient mixing are achieved.
3. The power coupling involves no contact of electrodes with the plasma. Therefore electrode corrosion and contamination are eliminated, and with sufficient input power, thermal plasmas of any stoichiometry can be stabilized.
4. Quenching rates on the order of  $10^7$  K/sec can be achieved in the sampling probe. Thus the high heat of reaction released as the plasma species recombine is efficiently absorbed.

The system actually is comprised of two reactors in series: I. the plasma reactor, wherein high-temperature transient species are generated, followed by II. the quench reactor, wherein the plasma precursors are rapidly cooled within the cold-walled sampling tube to yield room-temperature stable products.

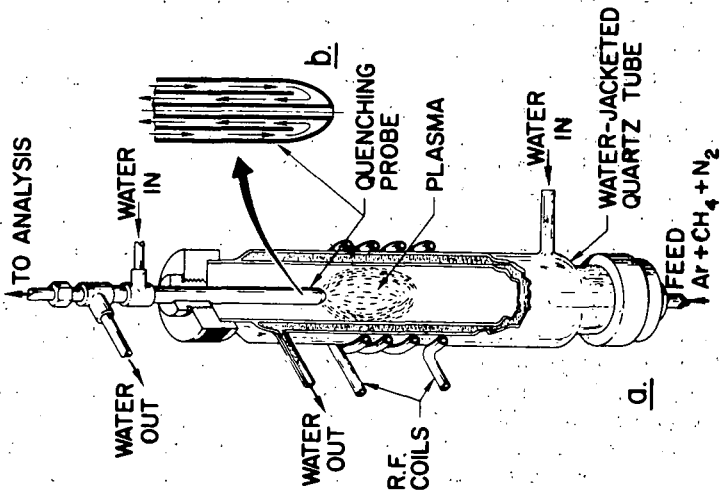


Figure 1 (a) Diagram of radio-frequency induction plasma reactor.  
 (b) Cross-section of water-cooled quenching probe.

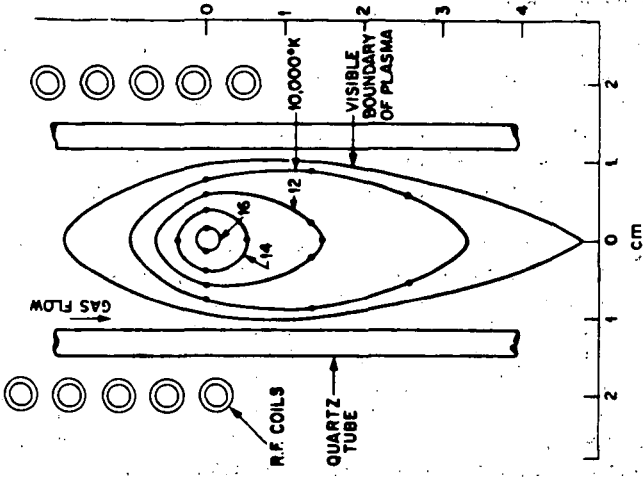


Figure 2 Isotherms in pure argon at 1 atm (1).

## PLASMA COMPOSITION

Thermochemical Equilibrium. One of the unique features of the thermal induction plasma is stable operation with low gas flow. Since flow velocities in the plasma zone are typically a few centimeters per second, residence times on the order of a second are associated with plasma species. In a plasma near atmospheric pressure the particle mean free path is very short and the collision rate very high. At plasma temperatures (c. 10,000 K) gas phase reactions can be expected to proceed quite rapidly. These facts lead to the initial assumption that local plasma composition approaches thermodynamic equilibrium.

The H-C-N System. The theoretical compositions of hydrogen-carbon-nitrogen mixtures at thermodynamic equilibrium have been computed by Kroepelin, et al.<sup>16</sup>, Marynowski, et al.<sup>17</sup>, and Bronfin, et al.<sup>18</sup>, for a variety of conditions. Computations were based on free energy minimization using tabulated thermochemical data<sup>19</sup>. Figure 3 presents calculated equilibrium composition data for a typical stoichiometry: H:C:N = 4:1:2, ( $\text{CH}_4/\text{N}_2 = 1$ ), at 1/2 atm (380 torr). Only species whose concentration is greater than 1.0 mole-percent are shown on this plot; however, twenty-one different chemical species were considered. In Fig. 3a, full equilibrium was considered for a two-phase system which included graphite. Figure 3b shows that temperature segment which is altered by the exclusion of the solid-phase, C(s).

Molecular nitrogen,  $\text{N}_2$ , is a major constituent over a broad range up to 8000 K; thereafter thermal dissociation results in the predominance of atomic nitrogen, N. As mentioned above, at temperatures over 8000 K, not shown of the graph, the system becomes completely dissociated into a simple three-component atomic state: H, C, N. At temperatures greater than 7000 K significant thermal ionization occurs, generating significant concentrations of singly-ionized atoms, e.g.,  $\text{C}^+$ ,  $\text{H}^+$ ,  $\text{N}^+$ . As noted in both plots,  $\text{CH}_4$  dissociation is well underway at 1000 K, resulting in the formation of  $\text{H}_2$  and C(s) in the two-phase system (a); but the formation of HCN and  $\text{C}_2\text{H}_2$  in the single-phase system (b). At temperatures above 3000 K,  $\text{C}_2\text{H}_2$  begins to fragment to  $\text{C}_2\text{H}$  and H, and with increasing temperature, to the atomic species. At temperatures above 3800 K, HCN begins to fragment to CN and H, and with increasing temperature, to the atomic species. Nitrogen-hydrogen species, e.g.,  $\text{NH}_2$ , occur at concentrations below 0.01 mole-percent over the entire range plotted.

In comparing the common temperature segments of the single-phase and two-phase composition diagrams, important differences are noted in that: (1) higher concentrations of species like HCN and  $\text{C}_2\text{H}_2$  are preserved at lower temperatures in the single-phase case, and (2) the maximum concentration of these species is somewhat higher in the single-phase case. Hence in the lower temperature range, the predicted yield of HCN and  $\text{C}_2\text{H}_2$  is enhanced by retarding carbon nucleation. This kinetic limitation acts to freeze the mixture composition at around 2700 K so that negligible composition change is predicted over a fairly broad temperature interval, down to 1500 K.

Composition of the Plasma. No direct determination of the plasma composition was attempted in the present study. Only a few efforts in this direction have

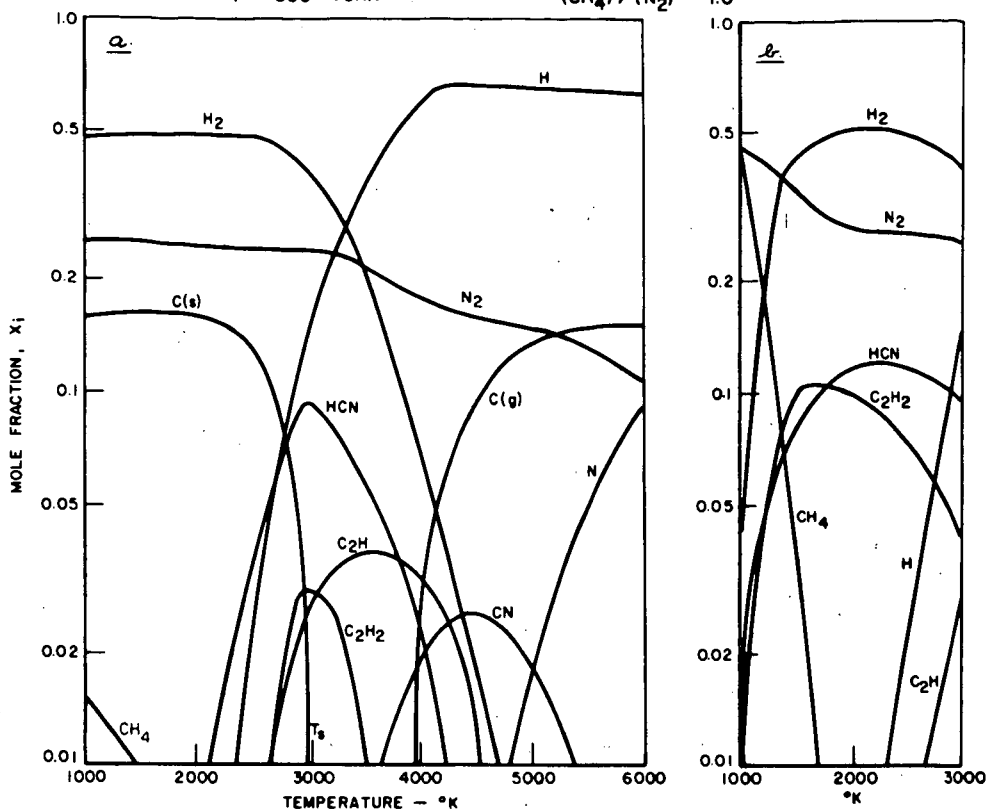


Figure 3 Equilibrium composition of equimolar CH<sub>4</sub>-N<sub>2</sub> mixture. (a) Including solid carbon; (b) Excluding solid carbon. Region above T<sub>s</sub> common.

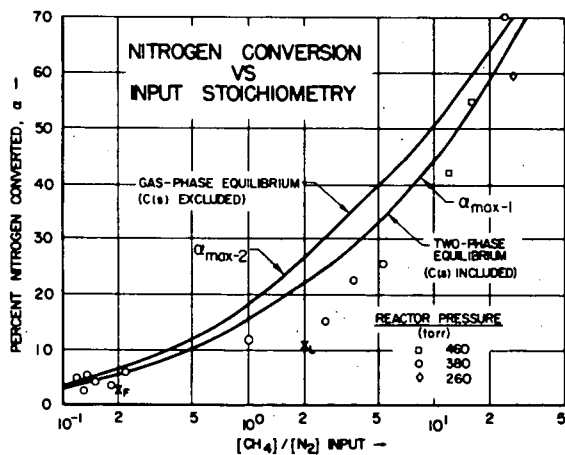


Figure 4 Yield of HCN, expressed as percent N<sub>2</sub> converted, as a function of input stoichiometry. Solid lines show maximum yield predicted by thermodynamic equilibrium. Data points show experimental results from the plasma reactor: Ar flow rate 42 std cc/sec, total reagent flow rate 2 std cc/sec, net power ~ 3.5 kw. Reactor pressure identified with key. Points labeled x from plasma jet studies<sup>6,7</sup>.

appeared in the literature. O'Halloran, et al.<sup>20</sup>, have directly sampled an argon plasma jet using a specially designed entrance cone opening to a time-of-flight mass spectrometer. Raisen, et al.<sup>21</sup>, have made spectroscopic identifications of species in an air plasma. Unlike the mass spectrometer measurements, however, emission spectroscopy is difficult to quantify due to the wide variance in the oscillator-strengths of the likely emitters.

Faced with the difficulty of determining plasma composition directly, one is prone to apply equilibrium predictions as a guide to local plasma composition. Referring both to Figs. 2 and 3, a highly dissociated composition can be expected in most of the plasma region. Temperatures in excess of 10,000 K, expected over most of the central region of the plasma, would dictate that the atomic species H, C, and N, and their ions would predominate.

### QUENCHING

At this juncture it is important to ask what changes in composition would be encountered on cooling the H-C-N atom plasma. A slow, gradual cooling of the labile intermediates resident in the plasma zone may well allow the system to revert to the original reactants along an equilibrium path. Kroepelin and Kipping<sup>22</sup> found this effect in their study of a 10 amp, 40 volt d.c. arc burning in a hydrocarbon-nitrogen atmosphere. The composition of the slowly cooled arc-heated gases was found to be mainly N<sub>2</sub>, H<sub>2</sub>, and C<sub>1</sub> and C<sub>2</sub> hydrocarbons. No HCN was observed. Under extremely rapid cooling, however, kinetic limitations can interpose along the reaction path to yield different, more interesting or valuable products.

The Cold-Wall Tube. A small-diameter, water-cooled tube was selected from the variety of available high-cooling-rate devices, to provide rapid and convenient quenching of the plasma species. Figure 1b shows a diagram of the simple design of the three-concentric tube arrangement of the quenching probe<sup>23</sup>. The overall outside diameter of the probe was 3/8 in. The internal diameter of the quenching tube which receives the hot plasma was 0.032 in. The surfaces of the inner tube were stainless steel; other parts were fabricated from copper. The effect of a variation in the composition of the cold surface was not studied.

Cooling Rate. Due to the high rate of heat transfer from plasma to adjacent cold wall, rapid cooling occurs in the quenching tube. Freeman and Skrivan<sup>24,25</sup> have measured an initial temperature decay rate of  $5 \times 10^7$  K/sec in water-cooled tubes. In their model of the heat-transfer process occurring in very small tubes, Ammann and Timmins<sup>10</sup> have calculated cooling rates greater than  $10^9$  K/sec. Probably quenching rates in this range were associated with the quenching tube used in this study.

Reaction Path During Quench. Unfortunately, there is a sparsity of high-temperature kinetic data for the H-C-N system. Hence one is unable to predict with certainty the reaction path followed as the atomic species H, C, and N, are cooled from 15,000 K to 500 K in 10 milliseconds, for example. After an examination of

the experimental results in the succeeding sections, it may be possible to infer the important steps in the reaction sequence.

### EXPERIMENTAL CONDITIONS

Radio-frequency Supply. A commercially available<sup>26</sup> 12 kw (nominal) induction heater, oscillating at 4 MHz, was the power source for the experiment. The load coil, shown in Fig. 1, consisted of five turns of 1/4-in. o.d., water-cooled, copper tubing wound tightly around the quartz reaction tube. The overall height of the coil was 1 1/2 in., with a central diameter of 3 in.

Reactor. Containment of the plasma was accomplished within a 35 cm long, 47 mm i.d. quartz tube, mounted vertically. The high-power loadings necessitated cooling which was afforded by flowing 1/3 gpm of water into a cooling jacket surrounding the central reaction tube. The plasma-forming gases were premixed and sent into the tube through a brass fitting sealed onto the tube base. Gas flow rates were monitored with calibrated rotameters. Plasma-heated gases left the reaction tube through a second brass fitting sealed onto the top of the tube. This cap, which was of approximately 1 liter volume, was water-cooled. In this configuration the top fitting functioned as a cooling chamber to reduce the average gas temperature to within a few degrees of ambient. The system pressure was controlled by a high-capacity regulated vacuum line attached to the upper cap.

A sliding O-ring seal was provided at the center of the upper cap for positioning of the 3/8-in. o.d. by 0.032-in. i.d. quench probe along the central axis of the reaction tube. Cooling water was supplied to the quench probe at a metered rate of 1/3 gpm. The entrance tip of the probe was typically located at the center of the uppermost winding of the load coil.

The flow rate through each cooling water line was metered with calibrated rotameters which were placed downstream of liquid pressure regulators. Inter-consistent mercury thermometers were mounted at each cooling water line inlet and outlet. By measurement of the temperature rise and flow rate in each cooling line, total enthalpy delivery rates could be determined.

Chemical Analysis. The gas stream withdrawn through the quench probe was sent to an on-line gas chromatograph for quantitative analysis. A triacetin column, recommended by Isbell<sup>27</sup>, followed by a molecular sieve column, recommended by Purnell<sup>28</sup>, was used for resolution of chromatogram peaks. This configuration allowed the detection of the following compounds with a thermal conductivity cell: HCN, H<sub>2</sub>, Ar, N<sub>2</sub>, CH<sub>4</sub>, and various higher hydrocarbons. A parallel flame-ionization detector was useful for detecting low concentrations of hydrocarbons, e.g., CH<sub>4</sub>, C<sub>2</sub>H<sub>2</sub>.

Experimental Variables. Total pressure in the plasma reactor was typically 380 torr; some data were also acquired in a range from 160 to 760 torr. For the data reported here the argon feed rate was 42 std cm<sup>3</sup>/sec (6.5 g-mole/hr). This

flow rate insured good plasma stability for the available r.f. power and remained with the capacity of the subatmospheric pressure regulating equipment. Added reagent gases were fed at 1/50th to 1/10th that rate, with the molal ratio varied over a broad range:  $0.1 \leq \text{CH}_4/\text{N}_2 \leq 25$ . The power coupled into the gas mixtures was  $\sim 3.5$  kw maximum, as determined from the summation of cooling water heating rates.

In the later stages of the experiment various nitrogen-substituted hydrocarbon liquids were fed to the argon plasma, namely:  $\text{CH}_3\text{CN}$ ,  $\text{CH}_3\text{CH}_2\text{CN}$ , and  $\text{CH}_2\text{CHCN}$ . Special modifications to the gas-flow system were made to insure injection of these nitriles into the plasma. A part of the argon feed stream was split off to a sealed gas-liquid bubbler containing warmed reagent. Since these compounds are all relatively volatile, a substantial amount of nitrile entrainment occurred. Rather than introduce the nitrile-laden argon stream into the relatively cool gas region at the base of the reaction tube, a special injection probe was provided to introduce the stream into the hot plasma region. This second water-cooled probe was positioned through an O-ring seal in the base cap. The probe design was identical to that previously described for quenching (cf. Fig. 1b). The tip of the injector probe was placed at the center of the lowermost winding of the load coil. Material exiting the injector thus was assured of entering the plasma zone.

#### EXPERIMENTAL RESULTS

Plasma Stability. Over the entire range of experimental variables the plasma was stable and brightly luminous. The luminous region of the plasma appeared to fill about 90 percent of the cross-sectional area of the cooled quartz tube and extended from the bottom to about 3 in. above the r.f. load coil. With high hydrocarbon flow rates a gradual build-up of soot occurred on the quartz tube walls.

#### Methane-Nitrogen Reactions

Products of Reaction. A quantitative analysis of the gas stream withdrawn through the quenching probe was made for each run. Over the entire range of stoichiometric studies, the methane fed to the plasma was completely reacted; no methane was detected in the quenched gas stream. The following major reaction products were identified:  $\text{HCN}$ ,  $\text{C}_2\text{H}_2$ ,  $\text{H}_2$ . Also present were Ar and unreacted  $\text{N}_2$ .

Nitrogen Conversion. Since essentially complete conversion of methane was observed for each run, the varying conversion of nitrogen was selected as an important datum. If the mole fraction of a species  $i$  found in the quenched product stream is defined as  $x_i$ , then the conversion of nitrogen, defined as  $\alpha$  is given by:

$$\alpha = \frac{\frac{1}{2} x_{\text{HCN}}}{x_{\text{N}_2} + \frac{1}{2} x_{\text{HCN}}}$$

Figure 4 shows the percent conversion of nitrogen as a function of feed stoichiometry,  $\text{CH}_4/\text{N}_2$ . The argon feed rate for these runs was fixed at 42 std  $\text{cm}^3/\text{sec}$ . The total flow rate of the reactant mixture was typically 2 std  $\text{cm}^3/\text{sec}$ . The key at the bottom right of the figure identifies the reactor pressure for each data point.

The measured conversion of nitrogen varied from 3 percent at the lowest stoichiometry considered,  $\text{CH}_4/\text{N}_2 = 0.1$ , to a maximum of 70 percent at a methane-rich stoichiometry,  $\text{CH}_4/\text{N}_2 = 2.5$ . This high value of nitrogen fixation is considerably in excess of previously reported nitrogen conversion levels observed in thermal plasma reactions. Pressure variations had no significant effect.

Typical Product Composition. Table I, below, presents the composition of the product stream produced under typical conditions.

Table I

Typical Product Composition

Reactor Pressure - 380 torr		Net Power Input - 3.5 kw	
<u>Input</u>	<u>Feed Rate</u> (std cc/sec)	<u>Feed Composition</u> (mole-percent)	
Ar	41.8	97.6	
$\text{N}_2$	0.5	1.2	
$\text{CH}_4$	0.5	1.2	
Total	42.8	100.0	
<u>Product</u>	<u>Composition</u> (mole-percent)	<u>Composition</u> (mole-percent, Ar-free)	
Ar	96.5	-	
$\text{H}_2$	2.0 <sup>a</sup>	57	
$\text{N}_2$	1.0	29	
HCN	0.3	9	
$\text{C}_2\text{H}_2$	0.2	5	
$\text{CH}_4$	trace	-	
Total	100.0	100	

Note a: Compositions determined from gas chromatograms;  $\pm 10$  percent.

As was seen in Fig. 4, Table I shows that about 12 percent of the nitrogen fed at this stoichiometry was converted to hydrogen cyanide. Ninety-nine percent of the methane fed was converted to the gaseous products hydrogen and acetylene and also

to an unmeasured small quantity of solid product which deposited on the wall. The minor disparity between the nitrogen and carbon material balances indicates the small fraction of material lost from the reaction zone to deposition on the reactor walls.

### Nitrile Reactions

Products of Reaction. Small quantities of nitriles could be continuously fed to the argon plasma by using the modified injection arrangement (described in the previous section). Mixed plasma which was quenched by withdrawal through the water-cooled probe was analyzed with no change in the gas chromatograph. Essentially complete conversion of the lower molecular weight compounds, acetonitrile,  $\text{CH}_3\text{CN}$ , and acrylonitrile,  $\text{CH}_2\text{CHCN}$ , was observed. A minor amount ( $\sim 10$  percent) of propionitrile,  $\text{CH}_3\text{CH}_2\text{CN}$ , was observed in the quenched gas stream, perhaps due to a bypassing of the plasma core. Each of the nitriles produced the same reaction products, a repeat of those produced in the methane-nitrogen study. High concentrations of  $\text{HCN}$ ,  $\text{C}_2\text{H}_2$ ,  $\text{H}_2$ , and  $\text{N}_2$  were observed along with the argon diluent. A complete quantitative chemical analysis of these nitrile runs has not, as yet, been performed.

## DISCUSSION OF RESULTS

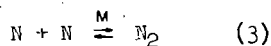
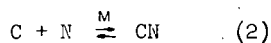
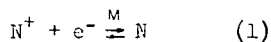
Variance in the Conversion Percentage. Considerable variance in the fraction of nitrogen converted was observed among repetitions of runs with constant stoichiometry, net power input, and pressure. The data points plotted in Fig. 4 include the maximum observed conversion levels for each stoichiometry. Sources of error in the experimental procedure which could have scattered the data down from maximum conversion were:

1. Improper adjustment of r.f. supply controls so as to mismatch the supply and plasma impedance, perhaps generating plasma irregularities
2. Minor air leaks which would add additional nitrogen to the plasma to alter the stoichiometry from preset values
3. Deposition of carbon or hydrocarbon material on the reactor walls or, the reverse, significant vaporization of carbon from the walls, to alter the preset stoichiometry.

Thermochemical Equilibrium Predictions. As described in the "Plasma Composition" section, above, a full range of composition calculations were made assuming thermochemical equilibrium. These calculations predicted that the plasma composition within the r.f. coil would be dominated by atomic species for the specific power input used in this study. Perhaps the following additional consideration of these theoretical predictions can elucidate the processes occurring during rapid quench.

Freezing. Hypothesize that equilibrium is followed during the initial stages of cooling within the quench tube. For heuristic purposes, assume that equilibrium is obeyed during temperature decay to approximately 3000 K, or more specifically, to that temperature where equilibrium predicts the maximum number of moles of HCN to be formed. Then assume that all reactions involving nitrogen species are frozen at that point, so that even as cooling continues negligible decomposition of the HCN occurs.

Chemical Reaction Kinetics. In making this series of seemingly unwarranted assumptions, some specific reaction rates have been implied to be very fast, while others, very slow. Focusing on nitrogen-containing species, the following types of reaction have been assumed to be rapid under the conditions developed in the quenching tube:



Further, the following have been assumed to be very slow:



To date a full description of the reaction kinetics of the H-C-N system, even at moderate temperatures, is unavailable. In the recent shock tube study of Marshall, Jeffers, and Bauer<sup>29</sup>, preliminary results indicate that the equilibrium in Reaction 4 may be achieved rapidly at elevated temperatures. However, the evidence points to a rather complex reaction mechanism for the thermal dissociation of HCN, wherein many more steps are involved than mentioned here. The complexity of this system was encountered in the earlier study of Robertson and Pease<sup>30</sup>, and in similar systems explored by Goy, Shaw and Pritchard<sup>31</sup>.

Rapid dissociation/recombination rates have been determined for nitrogen, Reaction 3, by Wray<sup>32</sup>. Reaction rate data is not available for Reaction 2, nor for other reactions likely to be quite important in the H-C-N system.

Atomic-ion/electron recombination reactions for each of the three atoms in the plasma are likely to be rapid<sup>33</sup> relative to the quenching time.

In summary, existing reaction rate data is far from sufficient to check the assumptions made about the reaction mechanisms appropriate to this H-C-N system. Additional kinetic studies which generate presently unknown reaction rates are needed before an accurate reaction path can be predicted theoretically for the reacting H-C-N system.

Composition at the Assumed Freezing Point. The validity of this freezing approach can be found comparing the predicted composition at the freezing temperature with the observed composition of the quenched gas stream. The following variables are defined for Table II, which facilitates the comparison.

For the equilibrium calculations let the input stoichiometry be characterized by the molar ratio  $[\text{CH}_4]/[\text{N}_2]$ , set equal to  $\phi$ ; let  $n_{\text{N}_2}$  be the number of moles of  $\text{N}_2$  introduced; and let  $n_i^*$  be the number of moles of species  $i$  present at equilibrium at a pressure,  $P$ , and a temperature,  $T$ . Then  $T_f$  is established for a given  $\phi$  and  $P$ , as the temperature at which equilibrium predicts the quantity  $n_{\text{HCN}}^*/n_{\text{N}_2}$  is a maximum.

Table II shows the mole fraction of the predominant species for a  $T_f$  value found in an equimolar input stoichiometry. As mentioned in the "Plasma Composition" section, above, solid-carbon formation may be retarded in this system. Therefore, a second set of mole fraction data have been presented in Table II which excludes the species  $\text{C(s)}$  from the calculation.

Table II

Calculated Equilibrium Composition at the Temperature  
where HCN Yield is Maximized

Pressure - 380 torr		$\phi \equiv [\text{CH}_4]/[\text{N}_2] = 1.0$		
Mole Fractions				
	Including C(s) $T_f = 3050 \text{ K}$		Excluding C(s) $T_f = 2500 \text{ K}$	
	$x_i$	$x_i^a$	$x_i$	$x_i^a$
H <sub>2</sub>	0.421	0.543	0.497	0.522
N <sub>2</sub>	0.252	0.283	0.266	0.274
HCN	0.097	0.109	0.120	0.124
C <sub>2</sub> H <sub>2</sub>	0.038	0.065	0.073	0.080
H	0.144	-	0.025	-
C <sub>2</sub> H	0.020	-	0.005	-
others	0.030	-	0.014	-
	$\frac{n_{\text{HCN}}^*}{n_{\text{N}_2}} = \alpha_{\text{max-1}} = 0.161$		$\alpha_{\text{max-2}} = 0.185$	

Note a: Adjusted to allow for the reactions:  $\text{C}_2\text{H} + \text{H} \rightarrow \text{C}_2\text{H}_2$ ,  $2\text{H} \rightarrow \text{H}_2$ .

### Frozen Composition Calculation versus Experimentally Observed Composition.

If, indeed, the original assumption that important reactions occurring in the gas withdrawn from the plasma into the cold quenching tube are frozen in the vicinity of 3000 K is valid, then agreement should be found between the compositions listed in Tables I and II. In comparing the argon-free composition listed in Table I with Column 2 in Table II, relatively good agreement is found.

This comparison has been extended to the full range of stoichiometries studied. On Fig. 4, the maximum nitrogen conversion,  $\alpha_{\max-1}$ , and  $\alpha_{\max-2}$ , has been plotted against input  $\text{CH}_4/\text{N}_2$ -mole ratio,  $\phi$ . The subscript 1 refers to calculations including C(s); subscript 2, to excluding C(s). Agreement between the freezing model and observed results is very good over more than a two-decade range in stoichiometry variation. These results strongly support the freezing model in the overall reaction path. With the existing scatter of the data, a delineation between the single-phase and two-phase equilibrium predictions of composition at  $T_f$  is not possible. Additional experimental runs may lessen this ambiguity. The retardation of carbon solid formation, however, accounts for less than a 10 percent change in predicted maximum nitrogen conversion, on the average.

Freezing Temperature. The data do not allow an exact determination of a freezing temperature appropriate to the quenching process. Referring back to Fig. 3a, a change of a few hundred degrees in the assumed  $T_f$  could account for the data points which indicate 10 to 20 percent less than the two-phase equilibrium predictions of maximum nitrogen conversion. Fig. 3b shows the HCN concentration plateaus to be quite broad. Hence the nitrogen conversion prediction would be relatively insensitive to variation in freezing temperature over the range from 1500 to 3000 K. Future experimental refinements may allow a more exact determination of  $T_f$ .

Observed Compositions in Nitrile Experiments. An analysis of the maximum nitrogen conversion predicted by thermochemical equilibrium has not been made for the different nitrile inputs described in the "Experimental Conditions" section. The similarity of product distribution and of the ratio of HCN to  $\text{N}_2$  in the product points to the same reaction mechanisms as in the  $\text{CH}_4/\text{N}_2$  studies.

### Correlation with Studies by Other Investigators

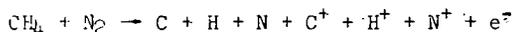
If the proposed reaction mechanism is correct, then the yields found in other studies of the synthesis of HCN by thermal reactions of hydrocarbons with nitrogen should not exceed the predicted values of  $\alpha$ . Some results of the production of HCN in plasma jets have been reported, as was mentioned in the "Previous Studies" section. While the differences in design between the plasma jet and induction plasma reactors are not detailed here, sample results from these other studies are plotted on Fig. 4. The maximum nitrogen conversion values observed in the nitrogen plasma jet experiments of Leutner<sup>11</sup> (designated  $\alpha_L$ ) and Freeman<sup>12</sup> (designated  $\alpha_F$ ) appear. These experimental data points are seen to lie below the maximum nitrogen conversion prediction.

The phenomena in the plasma jet experiments which convert less nitrogen than the maximum predicted by the freezing model may well be linked to a mixing or diffusion rate ( $\text{CH}_4$  and  $\text{N}_2$  were not premixed) or to temperatures insufficient to reach  $T_f$ . This question is the subject of a separate theoretical analysis now in progress by the author.

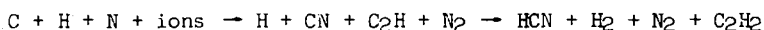
#### THE REACTION SEQUENCE

The experimental data support the following description of the overall reaction sequence:

1. Plasma Reactions. Feed reagents are dissociated to their atomic constituents in a thermal plasma. Some thermal ionization occurs at sufficiently high temperatures.



2. Initial Cooling. Plasma taken into a small-diameter cold tube rapidly cools with chemical reactions following equilibrium.



3. Frozen Reaction Kinetics. Rapid cooling continues, but at a rate much greater than the progress of the apparently complex reaction sequence necessary to destroy the species  $\text{HCN}$ ,  $\text{C}_2\text{H}_2$ , and  $\text{H}_2$ . Hence the composition of the cooling gas is frozen at the end of Step 2.

Evidence for the Freezing Model in Other Reacting Systems. The freezing model likely is applicable to a wide variety of reacting thermal plasma systems which employ a rapid quench. Ammann and Timmins<sup>15</sup> found a mechanism involving the freezing of equilibrating reactions to be applicable to their study of the quenching of nitrogen-oxygen plasma. Aided by a wealth of published rate data on chemical reactions in air, they were able to model the time-temperature-composition history of N-O plasma cooling within small-diameter tubes. A quite similar freezing temperature,  $T_f$ , was found at 3500°K for that system. The equilibrium composition of nitric oxide,  $\text{NO}$ , at  $T_f$  was preserved during continued rapid cooling.

#### CONCLUSIONS

Mixtures of methane and nitrogen can be fed continuously to a thermal argon induction plasma maintained above 10,000 K. A rapid quench of the heated plasma mixture produces  $\text{HCN}$ ,  $\text{C}_2\text{H}_2$ , and  $\text{H}_2$ . Final yields of  $\text{HCN}$ , expressed as a fraction of the nitrogen converted, range between 3 and 70 percent, a function of the input stoichiometry.

The reaction proceeds by the complete dissociation of the feed reactants in the plasma to yield a mixture of H, C, and N. As this mixture is quenched, the reaction initially proceeds along an equilibrium path, forming HCN, C<sub>2</sub>H<sub>2</sub>, H<sub>2</sub>, and N<sub>2</sub>. Below the temperature where the equilibrium yield of HCN is maximized, the slower rearrangement reactions and carbon nucleation are frozen by the rapid cooling, so that negligible alteration in the gas composition occurs upon further cooling.

## ACKNOWLEDGMENT

The author thanks William McLaughlin for his diligent assistance in performing these experiments. Thanks are also extended to Dr. M. P. Freeman, of American Cyanamid's Central Research Laboratory, and Dr. W. G. Burwell, at these laboratories, for many clarifying discussions.

## REFERENCES

1. T. B. Reed, J. Appl. Phys., **32**, 821 (1961).
2. P. A. Gartaganis and C. A. Winkler, Can. J. Chem., **34**, 1457 (1956).
3. W. Forst and C. A. Winkler, J. Phys. Chem., **60**, 1424 (1956).
4. W. Forst, H. G. V. Evans, and C. A. Winkler, J. Phys. Chem., **61**, 320 (1957).
5. C. Haggart and C. A. Winkler, Can. J. Chem., **38**, 329 (1960).
6. H. W. Leutner, Ind. Eng. Chem. Proc. Design Devel., **2**, 315 (1963).
7. M. P. Freeman, "Production of HCN from CH<sub>4</sub> in a Nitrogen Plasma Jet," 153rd National Meeting, Amer. Chem. Soc., April 13, 1967, Miami Beach, Fla.
8. G. Busz and W. Finkelburg, Z. Physik, **139**, 218 (1954).
9. R. S. Timmins and P. R. Ammann, "Chemical Reactions in a Constricted Arc;" A.I.Ch.E. Meeting, Dec. 7, 1964, Boston, Massachusetts.
10. P. R. Ammann and R. S. Timmins, A.I.Ch.E. J., **17**, 956 (1966).
11. T. B. Reed, J. Appl. Phys., **34**, 3146 (1963).
12. A. Mironer, A.I.A.A. J., **1**, 2638 (1963).
13. C. W. Marynowski and A. G. Mcroe, "R-f Generation of Thermal Plasmas," in High Temperature Technology (Butterworths, Washington, 1964), pp. 67-83.

14. M. P. Freeman and J. D. Chase, "Energy Transfer Mechanism of and Typical Operating Characteristics for the Thermal Radio-Frequency Plasma Generator," Paper No. 218, 130th Meeting, The Electrochemical Society, Oct. 12, 1966, Philadelphia, Pa.
15. M. L. Thorpe, Research/Development, 17 (1), 28 (Jan. 1966).
16. H. Kroepelin, D. E. Kipping, and H. Pietruck, "Equilibrium Partial Pressures in the Systems  $C + H_2 + N_2$  and  $C + H_2 + NH_3$  at Temperatures from 1000 to 12000 K," in J. F. Masi and D. H. Tsai, eds., Progress in International Research on Thermodynamic and Transport Properties, Proceedings of 2nd Symposium on Thermophysical Properties, Jan. 24-26, 1962, Princeton, N. J. (Amer. Soc. Mech. Eng./Academic Press, N. Y., 1962), pp. 626-48.
17. C. W. Marynowski, et al., Ind. Eng. Chem. Fund., 1, 52 (1962).
18. B. R. Bronfin, et al., "Thermochemical Equilibrium in the Carbon-Hydrogen-Nitrogen System at Very High Temperatures," 15th Chemical Institute of Canada Chemical Engineering Conference, Oct. 25-27, 1965, Université Laval, Quebec.
19. JANAF Tables of Thermochemical Data, Dow Chemical Co., Midland, Mich., Dec. 31, 1964.
20. G. J. O'Halloran, et al., "Determination of Chemical Species prevalent in a Plasma Jet," Report No. ASD-TDR-62-644, Bendix Corp. Research Laboratories, Southfield, Mich., 1964.
21. E. Raisen, et al., Appl. Spectr., 19, 41 (1965).
22. H. Kroepelin and D. E. Kipping, "Temperature Distribution in an Electric Arc Operated in a Hydrocarbon-Nitrogen Atmosphere," in J. F. Masi and D. H. Tsai, eds., Progress in International Research on Thermodynamic and Transport Properties, Proceedings of 2nd Symposium on Thermophysical Properties, Jan. 24-26, 1962, Princeton, N. J. (Amer. Soc. Mech. Eng./Academic Press, N. Y., 1962), pp. 649-55.
23. M. N. Plooster and T. B. Reed, J. Chem. Phys., 31, 66 (1959).
24. M. P. Freeman and J. F. Skrivan, A.I.Ch.E. J., 8, 450 (1962).
25. J. F. Skrivan and W. Von Jaskowsky, Ind. Eng. Chem. Proc. Design Devel., 4, 371 (1965).
26. Lepel High Frequency Labs, Inc., New York, N. Y., Model T-5-3.
27. R. E. Isbell, Anal. Chem., 35, 255 (1963).

28. H. Purnell, Gas Chromatography (John Wiley, N. Y., 1962) pp. 371-3.
29. D. Marshall, P. Jeffers, S. H. Bauer, Chemistry Dept., Cornell Univ., Ithaca, N. Y., personal communication, Nov., 1966.
30. N. C. Robertson and R. N. Pease, J. Amer. Chem. Soc., 64, 1880 (1942).
31. C. A. Goy, D. H. Shaw, and H. O. Pritchard, J. Phys. Chem., 69, 1504 (1965).
32. K. L. Wray, Res. Rept. 104, Avco Everett Res. Lab., Everett, Mass. (June, 1961).
33. D. R. Bates, A. E. Kingston, and R. W. P. McWhirter, Proc. Roy. Soc. A., 267, 297 (1962).

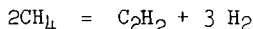
THE CONVERSION OF METHANE IN AN ARC REACTOR

P. R. Ammann\*  
R. S. Timmons  
V. Krukonis

The conversion of hydrocarbons into other products, namely acetylene, has been of considerable commercial and academic interest during the past few decades. Several types of arc devices have been reported for carrying out the pyrolysis of methane.

Thermodynamic calculations show that if the acetylene is to be recovered from an equilibrium chemical mixture, high temperatures in the range of 2000 to 3500°K are required, depending on the carbon-hydrogen ratio and the pressure of the system. Furthermore, kinetic considerations indicate that the pyrolysis of methane is fast relative to the decomposition of acetylene, and that there is an optimum reaction time to maximum both the conversion of the methane and the yield of acetylene.

The most desirable accomplishment of high temperature methane pyrolysis would be to effect the endothermic reaction.



High temperature chemical equilibria for the carbon-hydrogen system have been computed by Blanchet<sup>1</sup> and Bauer and Duff<sup>2</sup>. Assuming that chemical equilibrium is achieved in an electric arc reactor, the data indicate that the temperature at which the acetylene concentration is a maximum. The kinetics of methane pyrolysis and acetylene decomposition during heating and cooling ultimately determine the yield of acetylene.

Anderson and Case<sup>3</sup> developed a kinetic model to describe the reactions between arc heated hydrogen and methane. Calculations provided information on conditions, such as H<sub>2</sub>/CH<sub>4</sub> ratio, and reaction time, to achieve optimum conversion of methane to acetylene. The analyses indicated that conversion is not sensitive to contact time, within 0.1 and 1.3 milliseconds, and that speed of mixing is the most important parameter.

Reactions of methane and hydrogen with carbon vapor produced by an electric arc were reported by Baddour and Blanchet<sup>1</sup>. In their experiments, high acetylene concentrations of 20 to 40 percent in the product gas were found.

In an arc process, the reactions which determine the success of the process occur during the heating step and also during the cooling step. Heating of the reactant may proceed either as it passes through the discharge, or when it mixed with arc-heated gases. Cooling of the high temperature gases is usually carried out quickly, either by contact with cold surfaces, or mixing with cold fluids. This paper describes an experimental study on the conversion of methane which either (1) passed through a confined arc discharge, or (2) was mixed with an arc-heated gas. In this investigation, an attempt was made to understand the factors which affect the extent of methane pyrolysis and the yield of acetylene.

\* Avco Space Systems Division, 201 Lowell Street, Wilmington, Mass. 01887

In experiments on the direct conversion of methane, the reactant was passed through a confined arc discharge and quenched by mixing hydrogen or helium at several different quench to methane flow ratios. The net enthalpy of the gas from the arc discharge varied between 78 and 150 kcal per gram mole which correspond to equilibrium temperatures of 2500 to 3300°K. The conversion of methane, that was observed, varied from 65 percent at the low enthalpy to 85-100 percent at the high enthalpy. With a helium quench, the methane conversion varied between 90 and 98 percent, but at low He/CH<sub>4</sub> ratios, a large fraction of the methane went to carbon black, due principally to lower quenching rates and greater acetylene decomposition. Methane conversion was slightly lower with a hydrogen quench and the latter probably affected the kinetics of methane decomposition.

The conversion of methane by mixing with arc-heated hydrogen was studied in a plug-flow type reactor. Hydrogen was passed through a confined arc discharge. Methane was mixed with the hydrogen leaving the arc zone, and heated and reacted as the gases flowed co-currently through a cooled pipe. The conversion of the methane was correlated with the enthalpy of the hydrogen arc gas. Conversions were low (15-20 percent) at low enthalpies, and were nearly complete at high enthalpies (90-100 percent). These energies corresponded to 50-60 kcal per mole of methane at the low enthalpies to 220 kcal at high values, and were very large for the degree of methane reaction. Two effects were important. The arc gas lost energy to the cool reactor walls and the rate of energy transfer decreased with time due to a decrease in the energy driving force. By allowing for energy losses, the conversion was correlated and fair agreement was obtained between the data from (1) cracking methane in the arc discharge, (2) cracking methane in an arc-heated hydrogen stream, and (3) the experiments of Anderson and Casel. The yield of acetylene was also observed to be a function of the available energy, and under some conditions, acetylene yields of 90 to 100 percent of theoretical were achieved.

#### References

1. Blanchet, J. L., "Reactions of Carbon Vapor with Hydrogen and with Methane in a High Intensity Arc," Sc. D. Thesis, M.I.T., June, 1963.
2. Bauer, S. H., and Duff, R. E., The Equilibrium Composition of the C/H System At Elevated Temperatures, LA-2556, Los Alamos Scientific Laboratory, Los Alamos, N. M., September 18, 1961.
3. Anderson, J. E., and L. K. Case, An Analytical Approach to Plasma Torch Chemistry, 1, 3, 161-165 (1962).

## THERMAL CRACKING OF LOW-TEMPERATURE LIGNITE PITCH

John S. Berber, Richard L. Rice, and Delmar R. Fortney

U. S. Department of the Interior, Bureau of Mines,  
Morgantown Coal Research Center, Morgantown, West Virginia

### INTRODUCTION

The tar used in this study was produced by the Texas Power & Light Company from a Texas lignite carbonized at about 500° C in a fluidized bed. The pitch, as used in this research program, is the tar distillation residue boiling above 350° C. This pitch is about 40 to 50 percent of the crude tar. Pitch is a complex resinous mass of polymerized and polycondensed compounds (1). It is an amorphous solid material and quite brittle at room temperature. The pitch analyses average 84 percent carbon, 8 percent hydrogen, 5 percent oxygen, and 1 percent each of nitrogen and sulfur. It is chemically similar to the tar from which it is prepared, being mainly mixtures of the higher homologs of the compounds contained in the distillable fractions of the tar.

The pitch is potentially useful as a binder in the manufacture of products such as roofing cement, metallurgical electrodes, asphalt paving, and pitch fibre pipe, if its characteristics can be modified by physical and chemical techniques to approximate those of asphalt and bituminous binders (3).

Researchers of the Bureau of Mines, U. S. Department of the Interior, have investigated three methods for changing the lignite pitch characteristics.

Air-blowing, which is used successfully to treat bituminous pitch by lowering the hydrogen content and increasing the softening point and the penetrability, was not too effective with lignite pitch (1, 2).

Catalytic dehydrogenation (6) was found to be effective in reducing the hydrogen content of the pitch, but catalyst cost per pound of treated pitch is high, and the catalyst recovery cost would be prohibitive.

Thermal cracking has proven to be the most effective in changing the pitch characteristics. This report covers the preliminary work done on thermal cracking of pitch and shows the variety of products that may be obtained.

Thermal cracking is widely used in the petroleum industry, particularly for the production of olefins. Thermal cracking has also been used in the treatment of coal tar (4, 5), but seldom has been used in the treatment of pitch. The successful treatment of pitch by this process could upgrade the pitch into metallurgical coke, binders, oxidation feedstock for phthalic and maleic anhydrides, and gases such as hydrogen, methane, and ethylene.

The binding ability of the cracked pitch and oil distillation pitch can be determined by the quality of metallurgical electrodes produced using the pitches as binders. Many factors affect the binding properties of the materials being

used as binders, with different producers and consumers using entirely different standards, so the electrode quality tests were used to help evaluate the effectiveness of thermal cracking of the lignite pitch.

### EQUIPMENT

The thermal cracking system is shown in figures 1 and 2. The feed tank (figure 2, A) is made from a 13-in. length of 10-in. diameter schedule 40 pipe, to which a cone has been added for the bottom. The tank is heated by commercial electric heaters. The feed pump (B) is a small gear pump with a variable speed drive. The thermocracker (D) is a 4-1/2 ft-length of 2-1/2-in. diameter schedule 40, type 304, stainless-steel pipe, heated by external electric heaters. The heaters are controlled by outside surface thermocouples welded to the reactor. The receiver (E) is a 20-in. length of 4-in. diameter schedule 40 pipe. The receiver is flanged so that it can be bolted to the bottom of the reactor. The condenser (F) is a 30-in. length of 6-in. diameter pipe, swaged at the bottom end to 1-in. diameter and flanged at the top. The top flange supports a water-cooled tube which inserts into the condenser body in the manner of a cold finger. The knockout (G) is a 34-in. length of a 2-in. diameter pipe having a tangential gas inlet about 8-in. from the bottom. The scrubber (H) is a 30-in. length of a 4-in. diameter pipe having a water-spray nozzle near the top. The water from the scrubber drains into a standpipe water-seal tank (I). The water-seal tank is a piece of 6-in. diameter pipe. The gas meter (J) is a laboratory-type wet-test meter capable of metering 1,000 cu ft of gas at standard conditions.

### PROCEDURE

Lignite pitch at 200° C was pumped from the feed tank through electrically heated lines into the top of the thermocracker. The temperature of the thermocracker was maintained at approximately 790° C as indicated by the outside surface thermocouples. At the end of a run, the flow of pitch was stopped and the pump was flushed with a low-boiling tar fraction to keep the impeller of the pump from freezing. Reactions within the cracker produced coke, cracked pitch, oil, and gas. Both the top and bottom of the cracker were removed, and coke was removed from the sides and weighed. Cracked pitch caught in the receiver was weighed and analyzed. The oil removed by the condenser and knockout chamber was weighed and then distilled to 400° C, leaving a pitch residue. This pitch residue was analyzed and, if found to have the desired carbon-to-hydrogen atomic ratio (1.20 to 1.80), was used as a binder for electrodes. Distillate from the oil may be oxidized to phthalic and maleic anhydrides or separated into acids, bases, and neutral oils. Gas from the cracker was cooled and scrubbed, then metered, sampled, and analyzed by gas chromatography.

### RESULTS AND DISCUSSION

Results of the thermal cracking tests are given in tables 1 to 4. Of the four major products obtained from the pitch--coke, cracked pitch, oil, and gas--the coke averaged about 15 to 25 percent of the feed to the cracker, the cracked pitch amounted to about 20 to 40 percent, the oil was about 20 to 30 percent, while the balance of the feed to the cracker consisted of gas.

Distribution and yield rates of products (figures 3 to 6) are as expected considering the reaction within the cracker at different crude pitch feed rates. As the pitch is heated it begins to vaporize, and the turbulence of the vapors splashes some of the fluid onto the hot wall where it sticks and is coked. If enough heat is available, the rest of the pitch is vaporized and cracked. As the cracked materials leave the hot zone, heavy high-boiling materials condense immediately and collect in the receiver as cracked pitch; the oil and gas vapors pass on to the condenser. If there is not enough heat available to vaporize all of the pitch fed to the cracker, the unvaporized portion flows through the hot zone and into the receiver without being completely cracked. Such is the case when the crude pitch feed rate is high, the residence time in the cracker being shorter and less time being available for heat to penetrate the interior of the pitch mass. High crude pitch rates also lower the temperature inside the cracker, reducing the amount of coke formed.

Figures 3 and 4 appear to reflect these effects. The coke rate increases more slowly and the cracked pitch rate increases more rapidly than does the crude pitch feed rate. Since the gases are formed by several reactions, each related to the degree of cracking and coking, the gas production rate decreases with the increase in crude pitch feed rate (figure 5). Gases are produced by coking of pitch adhering to the cracker wall, then these gases are cracked to produce hydrogen and olefins. In addition to gas produced from coke, other gases are produced by devolatilization and thermal cracking of the pitch and are also subjected to further cracking. A significant amount of ethylene was produced in the cracker.

Oil produced in the cracker, upon distillation, yielded a pitch residue potentially useful as electrode binder, paving material, pitch fibre pipe, or roofing material, along with a distillate that can be further treated to give valuable chemical intermediates. Table 3 gives characteristics of the pitch residue and some preliminary data on electrodes made with the pitch as binder. The decrease in carbon-to-hydrogen atomic ratio of the pitch residue in relation to the crude pitch feed rate (figure 7) again reflects the inhibition of cracking by relatively high crude pitch feed rates.

The oil is produced in two ways--by cracking of the pitch, the most desirable method, and by devolatilization of pitch without cracking. This is the reason why the oil production rate can increase approximately in proportion to the crude pitch feed rate (figure 6). However, the quality of the oil decreases with decrease in degree of cracking, as is shown by the drop in the carbon-to-hydrogen atomic ratio.

## CONCLUSIONS

Thermal cracking of low-temperature lignite tar pitch converted the pitch into a material that served as a satisfactory binder in the manufacture of carbon electrodes. Compressive strength and electrical resistivity of the resulting electrodes fell within acceptable ranges. Crude pitch feed rate to the thermo-cracker significantly affected the rate of formation of products and the composition of the pitch residue from distillation of oil produced in the cracker.

## REFERENCES

1. Berber, John S., and Richard L. Rice. Oxidation of a Low-Temperature Lignite Tar Pitch. Preprints, Div. of Fuel Chemistry, Am. Chem. Soc., v. 8, No. 3, Aug. 31-Sept. 3, 1964, pp. 145-151.
2. Chelton, H. M., R. N. Traxler, and J. W. Romberg. Oxidized Asphalts in a Vertical Pilot Plant. Ind. and Eng. Chem., v. 51, No. 11, November 1959, pp. 1353-1354.
3. Greenhow, E. J., and Galina Sugowdz. The Chemical Composition of Coal-Tar Pitch. Coal Research in CSIRO, No. 15, November 1961, pp. 10-19.
4. Montgomery, R. S., D. L. Decker, and J. C. Mackey. Ethylene and Aromatics by Carbonization of Lignite. Ind. and Eng. Chem., v. 51, No. 10, October 1959, pp. 1293-1296.
5. Naugle, B. W., C. Ortuglio, L. Mafrika, and D. E. Wolfson. Steam-Fluidized Low-Temperature Carbonization of High Splint Bed Coal and Thermal Cracking of the Tar Vapors in a Fluidized Bed. BuMines Rept. of Inv. 6625, 1965, 22 pp.
6. Rice, Richard L., and John S. Berber. Catalytic Dehydrogenation of Low-Temperature Lignite Pitch. Presentation, Div. of Fuel Chemistry, Am. Chem. Soc., March 22-31, 1966.

used as binders, with different producers and consumers using entirely different standards, so the electrode quality tests were used to help evaluate the effectiveness of thermal cracking of the lignite pitch.

### EQUIPMENT

The thermal cracking system is shown in figures 1 and 2. The feed tank (figure 2, A) is made from a 13-in. length of 10-in. diameter schedule 40 pipe, to which a cone has been added for the bottom. The tank is heated by commercial electric heaters. The feed pump (B) is a small gear pump with a variable speed drive. The thermocracker (D) is a 4-1/2 ft-length of 2-1/2-in. diameter schedule 40, type 304, stainless-steel pipe, heated by external electric heaters. The heaters are controlled by outside surface thermocouples welded to the reactor. The receiver (E) is a 20-in. length of 4-in. diameter schedule 40 pipe. The receiver is flanged so that it can be bolted to the bottom of the reactor. The condenser (F) is a 30-in. length of 6-in. diameter pipe, swaged at the bottom end to 1-in. diameter and flanged at the top. The top flange supports a water-cooled tube which inserts into the condenser body in the manner of a cold finger. The knockout (G) is a 34-in. length of a 2-in. diameter pipe having a tangential gas inlet about 8-in. from the bottom. The scrubber (H) is a 30-in. length of a 4-in. diameter pipe having a water-spray nozzle near the top. The water from the scrubber drains into a standpipe water-seal tank (I). The water-seal tank is a piece of 6-in. diameter pipe. The gas meter (J) is a laboratory-type wet-test meter capable of metering 1,000 cu ft of gas at standard conditions.

### PROCEDURE

Lignite pitch at 200° C was pumped from the feed tank through electrically heated lines into the top of the thermocracker. The temperature of the thermocracker was maintained at approximately 790° C as indicated by the outside surface thermocouples. At the end of a run, the flow of pitch was stopped and the pump was flushed with a low-boiling tar fraction to keep the impeller of the pump from freezing. Reactions within the cracker produced coke, cracked pitch, oil, and gas. Both the top and bottom of the cracker were removed, and coke was removed from the sides and weighed. Cracked pitch caught in the receiver was weighed and analyzed. The oil removed by the condenser and knockout chamber was weighed and then distilled to 400° C, leaving a pitch residue. This pitch residue was analyzed and, if found to have the desired carbon-to-hydrogen atomic ratio (1.20 to 1.80), was used as a binder for electrodes. Distillate from the oil may be oxidized to phthalic and maleic anhydrides or separated into acids, bases, and neutral oils. Gas from the cracker was cooled and scrubbed, then metered, sampled, and analyzed by gas chromatography.

### RESULTS AND DISCUSSION

Results of the thermal cracking tests are given in tables 1 to 4. Of the four major products obtained from the pitch--coke, cracked pitch, oil, and gas--the coke averaged about 15 to 25 percent of the feed to the cracker, the cracked pitch amounted to about 20 to 40 percent, the oil was about 20 to 30 percent, while the balance of the feed to the cracker consisted of gas.

Distribution and yield rates of products (figures 3 to 6) are as expected considering the reaction within the cracker at different crude pitch feed rates. As the pitch is heated it begins to vaporize, and the turbulence of the vapors splashes some of the fluid onto the hot wall where it sticks and is coked. If enough heat is available, the rest of the pitch is vaporized and cracked. As the cracked materials leave the hot zone, heavy high-boiling materials condense immediately and collect in the receiver as cracked pitch; the oil and gas vapors pass on to the condenser. If there is not enough heat available to vaporize all of the pitch fed to the cracker, the unvaporized portion flows through the hot zone and into the receiver without being completely cracked. Such is the case when the crude pitch feed rate is high, the residence time in the cracker being shorter and less time being available for heat to penetrate the interior of the pitch mass. High crude pitch rates also lower the temperature inside the cracker, reducing the amount of coke formed.

Figures 3 and 4 appear to reflect these effects. The coke rate increases more slowly and the cracked pitch rate increases more rapidly than does the crude pitch feed rate. Since the gases are formed by several reactions, each related to the degree of cracking and coking, the gas production rate decreases with the increase in crude pitch feed rate (figure 5). Gases are produced by coking of pitch adhering to the cracker wall, then these gases are cracked to produce hydrogen and olefins. In addition to gas produced from coke, other gases are produced by devolatilization and thermal cracking of the pitch and are also subjected to further cracking. A significant amount of ethylene was produced in the cracker.

Oil produced in the cracker, upon distillation, yielded a pitch residue potentially useful as electrode binder, paving material, pitch fibre pipe, or roofing material, along with a distillate that can be further treated to give valuable chemical intermediates. Table 3 gives characteristics of the pitch residue and some preliminary data on electrodes made with the pitch as binder. The decrease in carbon-to-hydrogen atomic ratio of the pitch residue in relation to the crude pitch feed rate (figure 7) again reflects the inhibition of cracking by relatively high crude pitch feed rates.

The oil is produced in two ways--by cracking of the pitch, the most desirable method, and by devolatilization of pitch without cracking. This is the reason why the oil production rate can increase approximately in proportion to the crude pitch feed rate (figure 6). However, the quality of the oil decreases with decrease in degree of cracking, as is shown by the drop in the carbon-to-hydrogen atomic ratio.

## CONCLUSIONS

Thermal cracking of low-temperature lignite tar pitch converted the pitch into a material that served as a satisfactory binder in the manufacture of carbon electrodes. Compressive strength and electrical resistivity of the resulting electrodes fell within acceptable ranges. Crude pitch feed rate to the thermo-cracker significantly affected the rate of formation of products and the composition of the pitch residue from distillation of oil produced in the cracker.

## REFERENCES

1. Berber, John S., and Richard L. Rice. Oxidation of a Low-Temperature Lignite Tar Pitch. Preprints, Div. of Fuel Chemistry, Am. Chem. Soc., v. 8, No. 3, Aug. 31-Sept. 3, 1964, pp. 145-151.
2. Chelton, H. M., R. N. Traxler, and J. W. Romberg. Oxidized Asphalts in a Vertical Pilot Plant. Ind. and Eng. Chem., v. 51, No. 11, November 1959, pp. 1353-1354.
3. Greenhow, E. J., and Galina Sugowdz. The Chemical Composition of Coal-Tar Pitch. Coal Research in CSIRO, No. 15, November 1961, pp. 10-19.
4. Montgomery, R. S., D. L. Decker, and J. C. Mackey. Ethylene and Aromatics by Carbonization of Lignite. Ind. and Eng. Chem., v. 51, No. 10, October 1959, pp. 1293-1296.
5. Naugle, B. W., C. Ortuglio, L. Mafrika, and D. E. Wolfson. Steam-Fluidized Low-Temperature Carbonization of High Splint Bed Coal and Thermal Cracking of the Tar Vapors in a Fluidized Bed. BuMines Rept. of Inv. 6625, 1965, 22 pp.
6. Rice, Richard L., and John S. Berber. Catalytic Dehydrogenation of Low-Temperature Lignite Pitch. Presentation, Div. of Fuel Chemistry, Am. Chem. Soc., March 22-31, 1966.

TABLE 1. - Gas products from thermal cracking of low-temperature lignite tar pitch

Run no.	Crude pitch rate, pph	Gas rate, scfh	Constituents in gas, pct								
			N <sub>2</sub>	O <sub>2</sub>	CO <sub>2</sub>	CO	H <sub>2</sub>	CH <sub>4</sub>	C <sub>2</sub> H <sub>6</sub>	C <sub>2</sub> H <sub>4</sub>	C <sub>3</sub> +
35	2.0	16.7	49.35	0.76	0.45	4.12	21.99	19.67	0.44	2.37	0.85
37	6.0	37.0	8.77	.15	.96	8.38	15.80	42.19	4.30	14.05	5.40
38	9.0	45.2	5.06	.09	.81	7.29	22.63	37.32	4.98	12.63	9.19
43	10.0	51.3	8.35	.09	.80	7.40	20.08	37.94	4.64	12.78	8.12
40	11.0	51.4	1.13	.21	.80	7.49	37.96	35.74	2.64	11.53	2.50
30	13.1	55.1	1.17	.14	.83	7.91	30.52	41.33	3.73	12.08	2.29
42	17.0	66.6	9.84	.08	1.28	7.42	19.96	36.18	5.04	12.76	7.44
41	21.0	76.2	17.28	.13	.92	6.82	14.02	34.88	4.44	14.76	6.75

TABLE 2. - Coke, pitch, and oil products from thermal cracking of low-temperature lignite tar pitch

Run no.	Feed rate, pph	Coke rate, pph	Cracked pitch rate, pph	Oil rate, pph	Distillate from oil, wt pct	Anhydrides from distillate, wt pct		Composition of distillate, vol pct			
						FAA <sup>1</sup>	MAA <sup>2</sup>	Acids	Bases	Neutral oil	
35	2.0	0.8	0.2	0.8	40.3	16.4	14.5	30.9	10.5	6.0	83.5
37	6.0	1.4	1.4	1.4	27.2	17.0	14.4	31.4	10.0	8.0	82.0
38	9.0	2.0	2.0	2.2	29.1	11.7	15.2	26.9	10.0	7.0	83.0
43	10.0	2.0	3.6	2.6	34.4	10.1	13.9	24.0	13.5	5.0	81.5
40	11.0	2.2	3.2	3.6	32.6	11.0	12.8	23.8	15.0	5.0	80.0
30	13.1	2.4	3.3	4.1	27.8	14.3	13.8	28.1	-----	---	-----
42	17.0	3.0	6.2	5.6	25.9	10.6	14.4	25.0	12.5	4.0	83.5
41	21.0	3.8	13.4	7.2	25.9	8.0	12.9	20.9	15.0	5.0	80.0

1/ Phthalic anhydride.

2/ Maleic anhydride.

TABLE 3. - Characteristics of pitch and electrodes

Run no.	Crude pitch rate, pph	Oil, wt pct	Pitch from oil, wt pct	Properties of pitch			Properties of electrodes		
				Carbon, wt pct	Hydrogen, wt pct	C/H ratio	Softening point, °C	Coke type	Strength, kg/cm <sup>2</sup>
35	2.0	40.0	56.6	85.63	5.60	1.27	110		
37	6.0	23.3	71.0	88.86	4.69	1.58	145	Lignite <sup>1/</sup>	183
38	9.0	24.4	68.5	85.55	5.84	1.22	100	Petroleum	242
43	10.0	26.0	62.9	85.67	6.00	1.19	115	Lignite <sup>2/</sup>	355
40	11.0	32.7	66.3	85.60	5.90	1.21	104	Petroleum	323
30	13.1	31.3	68.3	85.81	6.37	1.46	116		
42	17.0	32.9	72.6	82.12	7.51	.91	65		
41	21.0	34.3	72.6	81.90	7.57	.90	65		

1/ Uncalcined lignite pitch coke.

2/. Calcined lignite pitch coke.

TABLE 4. - Material balance for thermal cracking of low-temperature lignite pitch

Run no.	Crude pitch rate, pph	Coke rate, pph	Cracked pitch rate, pph	Oil rate, pph	Gas rate, pph	Total, pph	Gain or loss, pph	Recovery, pct
35	2.0	0.8	0.2	0.8	0.9	2.7	+ 0.7	35.0
37	6.0	1.4	1.4	1.4	1.9	6.1	+ .1	1.7
38	9.0	2.0	2.0	2.2	2.2	8.4	- .6	6.7
43	10.0	2.0	3.6	2.6	2.6	10.8	+ .8	8.0
40	11.0	2.2	3.2	3.6	1.9	10.9	- .1	.9
30	13.1	2.4	3.3	4.1	2.2	12.0	- 1.1	8.4
42	17.0	3.0	6.2	5.6	3.4	18.2	+ 1.2	7.1
41	21.0	3.8	13.4	7.2	4.2	28.6	+ 7.6	36.2

- A-Feed tank
- B-Thermocracker
- C-Receiver
- D-Condenser
- E-Scrubber

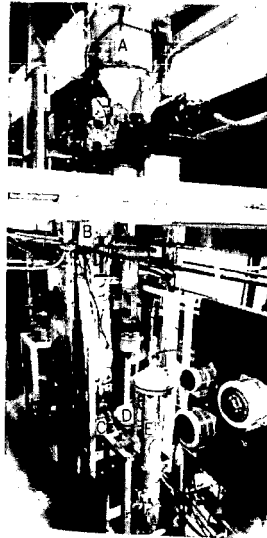


FIGURE 1. - Pitch Thermal Cracking Apparatus.

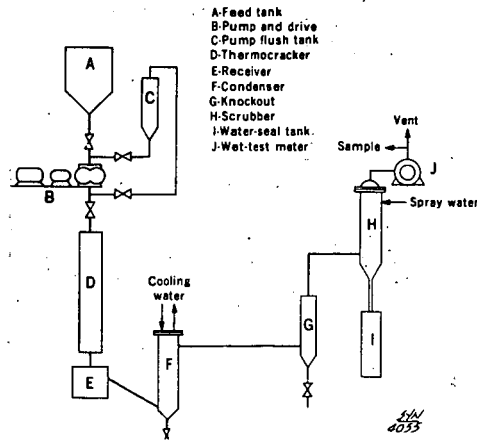


FIGURE 2. - Thermal Cracking System.

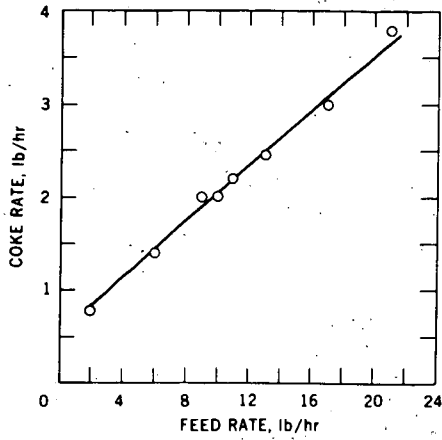


FIGURE 3. - Coke Rate Based on Crude Pitch Feed Rate - Thermal Cracking.

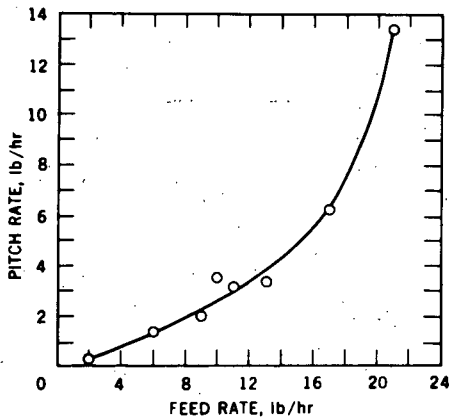


FIGURE 4. - Product Pitch Rate Based on Crude Pitch Feed Rate - Thermal Cracking.

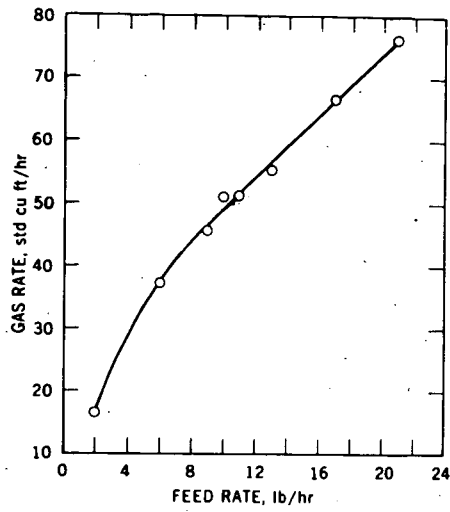


FIGURE 5. - Gas Production Rate Based on Crude Pitch Feed Rate - Thermal Cracking.

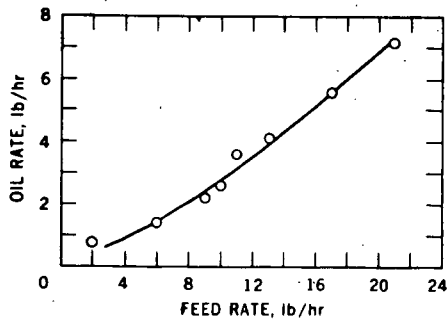


FIGURE 6. - Oil Rate Based on Crude Pitch Feed Rate - Thermal Cracking.

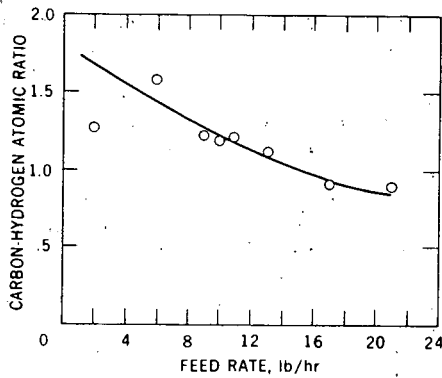


FIGURE 7. - Carbon-to-Hydrogen Atomic Ratio of Oil Distillation Residue Based on Crude Pitch Feed Rate.

378  
COAL DEASHING AND HIGH-PURITY COKE

Ward J. Bloomer , The Lummus Company, Newark, N. J. and  
F. L. Shea, Great Lakes Research Corp., Elizabethton, Tennessee

Introduction

In 1957, The Lummus Company and Great Lakes Carbon Corporation began a joint investigation into the use of coal as a source of high-purity coke. The process involved the production of a low-ash, low-sulfur deashed coal solution from high volatile bituminous coal, and the conversion of this coal solution into coke using a modification of the Lummus delayed coking operation. (1)

Experimental work on a bench scale was initiated in 1958 and completed in 1961. The experimental scope was expanded to include the production of deashed coal as well as the high-purity coke in either combined or alternate operations.

Bench programs were carried out on several scales of operation. A continuous (block operation) pilot plant was built and operated to confirm the bench work. This unit was capable of processing coal continuously at approximately 200 pounds per hour through the filtration step. At this point, the filtrate was stored for further continuous processing to either deashed coal product (performed in 150-200 pound quantities) or high-purity coke (500 pound quantities).

Summary

A process has been developed to upgrade the quality of coal to a low-ash, low-sulfur, low-chloride product. As a fuel, this material would result in reduced capital and operating costs for power stations. Investment costs would be reduced, due to the higher heating value and cleaner fuel. Operating costs would be reduced by charges associated with the transportation of ash, ash handling and disposal costs, lower maintenance costs, and fly ash removal costs. The substantial reduction in sulfur, ash, and volatile matter would greatly minimize air pollution.

Other potential applications are for use in gas turbines, as a reductant, as a raw material for synthesis gas, as an ingredient in preparing coal blends for metallurgical coke, or for high-purity coke.

The economic potential of the process in its present stage of development is covered in Table 5. The process has certain aspects requiring sustained demonstration efforts to obtain firm economic bases.

### Process Description

Figure 1 shows a schematic flowsheet for the production of either deashed coal or high-purity coke as investigated in this program.

Deashed Coal - Crushed, ground and dried raw coal is fed to agitated premix tanks where it is mixed with warm solvent. The slurry is pumped through an extraction heater and thence through either in-line reaction tubes or to agitated digestion tanks. Digestion was investigated over the temperature range of 650 to 850°F and over a pressure range of 75 to 135 psig. Residence times varied from three minutes to two hours. Solvent-to-coal ratios were varied from 1:1 to 4:1

From the digestion tanks, the coal dispersion is fed to a rotary pressure precoat filter designed for operating at 100 psig and 700°F. Washing provisions are included.

The filter cake (2) is discharged into a cake receiver. Filtrate and wash are collected and fed to the product and solvent recovery operations. Vapors from the filtrate receiver are compressed, heated and recycled to maintain pressure on the feed side of the filter drum.

Filtrate flows through the filtrate heaters into a vacuum product recovery unit. Vapors from this unit pass to a flash tower where the bottom stream is all solvent for recycle. A side stream is taken off and in part is used for solvent make-up with the remainder processed for by-product recovery.

Overhead vapors from the flash tower are condensed, and a low boiling fraction recovered as a by-product. Vapors flashing from the filtrate receiver are condensed and introduced as reflux into the bottom section of the flash tower.

Filter cake is calcined and the spent cake used as fuel for the process. Gas and distillate vapors from the kiln combined with gases from the filtrate receiver and flash tower overheads are passed into a light oil scrubber. The absorption oil -- the intermediates cut from the flash tower -- is stripped in the flash tower. Light oil fractions leave the system from a decanter on the flash tower overhead stream. Gas from the light oil scrubber is used for process heat.

High-Purity Coke - For coke product the same flow pattern prevails through the filtrate receiver. The filtrate is pumped to a coking heater and thence to coke drums. Overhead vapors from the coke drums pass to a combination tower where recycle solvent and by-product fractions are recovered. Overhead vapors from the tower pass

through a condenser, gas separator, and thence to a light oil scrubber.

The above operations were investigated on both a bench and pilot plant scale with the exception of cake calcining which was performed only on bench scale. Variables investigated are discussed in the following sections.

#### Process and Operating Variables for Deashed Coal

A review of our work on solvent deashing indicated the operating conditions necessary to optimize the process. These may be briefly summarized:

1. The development of a stable, high-extractive-efficiency solvent capable of essentially complete recovery in the vacuum recovery unit to yield deashed coal was accomplished by special treatment of a high-boiling coal tar distillate. The required solvent having excellent temperature stability and high solvent power was attained by refractorizing the high-boiling coal tar distillate, employing recycle thermal decomposition and fractionation to eliminate the less refractory and low-boiling constituents. Gratuitously, these are the less effective extraction components.

2. Recovery of from 88 to 95 weight percent of the available carbonaceous matter at extractor pressures in the range of 5 to 8 atmospheres and with solvent-to-coal ratios in the range of 2 or 3:1 was achieved using the refractorized solvent with a boiling range of 600 to 900°F. Typical extraction conditions were 750°F, 75 psig, at a solvent-to-coal ratio of 3:1.

3. Extraction at residence times of 5 to 20 minutes in a stirred solutizer vessel or, preferably, in continuous in-line solution heating coils which would permit a direct circuit from the solvent-coal mixing tank through a conventional heater with a discharge to either a rotary pressure precoat filter or a suitable hydroclone.<sup>(3)</sup> Bench extractions were successfully conducted at holding times of as low as 3 minutes. These were duplicated in a pilot furnace heater coil discharging the hot coal solution continuously through an expanded section of the transfer line to the filter charge tank.

4. Ash removal from the coal solution was accomplished at filtration rates of 200 to 300 lbs/hr/sq. ft. of filter surface. Preliminary rates of 200 to 250 were secured in the pilot rotary precoat pressure filter at low pressure differentials. Small-scale runs on cake washing and calcining were performed to obtain closed-cycle data on solvent and distillate distribution. It was anticipated that the filter cake would be washed with a light oil, calcined and the spent cake used as steam fuel for the process in a full-scale plant.

The bench and pilot plant operations in general closely approached the goals set at the start of the work for the deashed coal production phase of the program. In Table I, there are provided examples of the data relative to the composition of the raw coal, coal-to-solvent ratios, temperatures and pressures and analyses of the coal extract solutions. Yields are shown on the basis of both raw and ash-free coals. Typical coal deashing results are shown in Table 2.

#### Available Coal Charge Stocks

Extraction of coal with phenanthrene by earlier workers related the degree of extraction to the rank of the coal.<sup>(4)</sup> Thus, about 95 percent of the organic material in bituminous coal was dispersed as compared to 27 percent for subbituminous coal and 23 percent for lignite. Bench studies using a preprocessed coal tar distillate solvent matched these extraction efficiencies for the bituminous coal and lignite studied.

The coals extracted ranged in ash content from 5 to 20 weight percent and in sulfur values from 1 to over 4 percent. In each case, it was possible to secure excellent removal of the ash and a substantial portion of the sulfur, chlorides and other contaminants.

Sulfate and pyritic sulfur were fully eliminated with the ash and the organic sulfur forms were noticeably reduced. It was also possible to reduce the volatile matter contents from original values of near 40 percent to around 15 to 25 percent by distillation or by solvent precipitation<sup>(5)</sup> of the deashed coal solution.

#### Improvement of Solvent for Coal Deashing

The wide-range heavy anthracene oil fraction originally used in the coal solution studies boiled between 600°F and 1050°F. Bench delayed coking of the deashed coal solutions gave solvent losses ranging as high as 30 to 60 volume percent through polymerization of the heavy ends and decomposition of the less refractory components of the solvent.

Accordingly, studies were initiated to produce a more stable solvent. As a result, the efficiency of the coal solvent was improved to a point where 85 to better than 90% solution is achieved of the total extractable carbonaceous material of the coal (i.e., excluding the nonsoluble fusain).

This preferred solvent, freed of easily polymerizable material, is capable of essentially complete recovery from either the coal solution by vacuum stripping or from the delayed coking operation at reduced pressure.

Solvent upgrading is the result of two important factors. First, the solvent boiling range has been narrowed and, secondly, the solvent has been stabilized by removal of its less refractory (readily cracked) components. Continued use and recycle of this solvent improve its stability.

A brief discussion of the variables in coal solution and coking of its deashed solution will outline the reasons for the improvements secured by the changes in solvent boiling range and composition noted above:

It is known that the effective solvents for coal are those that have an angular configuration of the rings, and that boil above 300°C (572°F).<sup>(4)</sup> Nonangular, or linear, condensed ring systems have a greatly reduced selective solvent action on the constituents of coal that act as binding agents for the micellar portion of the coal. It is this removal of the binding material that leads to the complete disintegration of the colloidal nature of the coal, and peptization of the micelles in the solvent.

Because of the temperatures at which coal dissolution and subsequent recovery of deashed products are effected, it was found that certain high boiling fractions polymerized and were lost from the original solvent. These viscous fractions also decreased filtration rates. They were, therefore, helpfully removed in the course of refractorizing the solvent.

The narrow range solvent first prepared by distillation and employed for solution yielded 83.9 percent of the original ash-free coal. However, by successive heatings of the recovered solvent and redistillations to the original narrow boiling range, the extractive efficiency was increased to 89 to 93% in subsequent extractions.

#### Use of Other Refractory Aromatic Solvents

Numerous refinery stream fractions such as, for example, thermal-cracked, cat-cracked heavy cycle oils are rich in condensed ring aromatic compounds and their alkylated homologues. For example, a 700° to 1000°F clarified slurry oil has been reported as containing in excess of 70% condensed ring aromatics. Further, thermal cracking of this clarified oil increased the concentration of these aromatics to over 90% and these are predominantly condensed ring types. It is considered that these cracked refinery tars, after further refractorizing, could provide a low-cost coal solvent of high solution efficiency comparable to that of the coal tar solvents.

#### Removal of Ash

The efficiency of coal solution deashing has been a function of ash particle size distribution rather than of total

ash content of the initial high volatile bituminous coal. Thus, it has been repeatedly demonstrated in the bench and pilot solvent deashing studies on coal samples with ash contents varying from 5 to 20 weight percent that final ash values of 0.1 to 0.3 could be obtained in the treated coal extracts.

Likewise, inorganic chlorides have been largely eliminated with the ash. Coals containing 0.25 and 0.15 weight percent chlorine were reduced to values of 0.004 to 0.003, respectively. It is assumed that coals of considerably higher inorganic chloride contents could be reduced to similar low values. The harmful corrosive effects of ash and chlorides on furnace operation are well known and their effective reduction is obviously very desirable.

#### Sulfur Reduction

The degree of bituminous coal desulfurization by solvent deashing has proven to be a function of the original ratio of inorganic sulfate and pyritic sulfur to the organic forms. Original total sulfur contents of 1 to 4 percent are reduced to values of 0.4 to 1 weight percent in the extracts.

It is known that this ratio increases with coals of increasing total sulfur content, i.e., in the lower grade coals of correspondingly higher ash. The final sulfur of the deashed coal therefore relates to the original organic sulfur which is only partially removed in the process, whereas the inorganic sulfur is removed substantially quantitatively.

Thus, in Table 1, complete elimination of the pyritic and sulfate sulfurs has been achieved with an accompanying 26 percent reduction in organic sulfur, for an overall sulfur reduction of about 50 percent.

#### Delayed Coking

The original 1957 concept of the coal deashing process was to prepare a coal solution which, after filtration for removal of its ash, sulfur and other contaminants, would be charged to the conventional Lummus delayed petroleum coking process. The coke drum vapor would pass to the combination fractionation tower for separation of gas and light and medium distillate from a tower bottom cycle oil which would be re-used for fresh coal solution.

The bench and pilot coking of the deashed coal solution proved to be almost routine. This charge stock resembled in many of its characteristics a low temperature carbonization pitch. Lummus had previously in bench scale and pilot plant delayed coking apparatus successfully coked both low and high temperature carbonization pitches as well as Gilsonite and Athabasca tar sand pitches.

The range of temperatures and general operating characteristics proved similar to those employed for the stocks noted above. Reduced pressure is necessary for high solvent (600-900°F) recovery. Thus, it is anticipated that full scale plant operation would produce cokes with volatile matter contents approaching those normally encountered with petroleum stocks. Such cokes would be of low ash and satisfactory sulfur contents and would be secured at high yields.

The product distribution on coal solution and on coal are summarized in Table 3, based on a 2:1 solvent to coal ratio. It was found on examination of the coker total liquid products that the extraction solvent had been recovered without significant change. The properties of the coker feed and product coke are listed in Table 4.

An alternate method of producing high purity coke utilizes the pure coal extract as the raw material. This may be pulverized in a ball and ring or ring roller type mill, such as is used for powdered coal burners. The milled pure coal is then used to form a slurry with a refractory recycle stock, having a boiling range of about 500-700°F. The boiling range of this stock will vary somewhat, depending upon conditions in the heater, the coke drum, and the ratio of solids to liquid, but is selected so that sufficient liquid phase remains in the heater coils so as to convey the milled pure coal without coke build-up in the heater.

A third method of pure coke production considered, particularly where production of pure coke from coal would be conducted in conjunction with the operation of a refinery, involves utilization of petroleum coker feedstock as the liquid in which the slurry of pure coal is formed. Where a low coke yield feedstock is used, the coke produced would be predominantly from pure coal. However, the proportion might be varied, depending upon the type of coker feedstock employed and the ratio of solids to liquid in the slurry charged to the delayed coker.

#### Alternate Processes for Coal Extract Recovery

As an alternate to the recovery of coal extracts of original or decreased volatile matter contents by distillation, as noted in Tables 1 and 3, it was determined that these products could be recovered readily from solution by precipitation with hydrocarbon solvents. Thus, a paraffinic solvent yielded the complete deashed coal extract, whereas it was possible to recover a deashed coal with a volatile matter content 60 weight percent below that of the original coal with control of intermediate product values by manipulation of the aromaticity of the solvent blends.

References

1. Bloomer, W. J., and Martin, S. W., U. S. Patent 3,109,803 (November 5, 1963).
2. Dicalite 40, General Refractories Company, used for bench and pilot filtrations.
3. Patent pending.
4. Orchin, M., Golumbic, C., Anderson, J. E., and Storch, H. H., U. S. Bur. Mines Bull. 505, 1951.
5. Patent pending.

COAL SOLUTION DEASHING USING A SOLVENT AND NARROW RANGE COAL TAR DISTILLATE AND NARROW RANGE COAL TAR SOLVENT

Coal Source	I		II Illinois		III Illinois		IV Penna.		V Illinois		VI Penna.		Lignite
	Raw	Deashed	Raw	Deashed	Raw	Deashed	Raw	Deashed	Raw	Deashed	Raw	Deashed	
Coal Proximate Analysis, Percent by Weight													
Moisture	2.69		Moisture-free basis				1.4		2.75		1.4		1.9
Volatile Matter	37.7	33.6	32.6	33.5	37.2	36.6	36.6	38.90	36.6	36.6	45.2		45.2
Fixed Carbon	38.9	56.6	67.1	52.5	62.5	56.6	56.6	53.99	56.6	56.6	38.0		38.0
Ash	19.66	9.8	0.3	14.0	0.3	5.4	5.4	7.11	5.4	5.4	15.1		15.1
Sulfur	3.72	4.0	1.0	4.3	0.9	1.46	1.46	1.18(1)	1.46				
Chlorine		0.15	0.003	0.25	0.004								
Solvent													
	Wide Range	Narrow Range	Wide Range	Narrow Range	Wide Range	Narrow Range	Wide Range	Narrow Range	Wide Range	Narrow Range	Wide Range	Narrow Range	Wide Range
Refractorized	No	Yes	No	Yes	No	Yes	No	Yes	No	Yes	No	Yes	No
Deashed Coal Recovery													
On crushed coal	67.3	83.6		75.4		67.5		85.3		90.0			21.3
On ash-free coal	83.8	92.7		89.8		71.3		91.8		95.2			25.2

(continued on next page)

TABLE I (cont'd)

COAL SOLUTION DEASHING USING AS-RECEIVED WIDE-RANGE COAL TAR DISTILLATE  
AND NARROW RANGE REFRACTORIZED SOLVENT

Coal Source	I		II		III		IV		V		VI	
	Illinois		Illinois		Illinois		Penna.		Illinois		Penna.	
Filtrate	Raw	Deashed	Raw	Deashed	Raw	Deashed	Raw	Deashed	Raw	Deashed	Raw	Lignite
Sp. Gravity(100°/100°F)	1.2516	1.2250	1.2208		1.2523		1.2140		1.2355		1.2140	1.2355
Softening Point, °F(B&R)	147	131.5	111.0		212				121.5			121.5
Sulfur, Wt. %	0.63				0.44		0.51				0.51	0.57
Carbon Residue, Wt. %	32.7						23.9				23.9	28.0
Ramsbottom Conradson					35.9							
CS <sub>2</sub> Solubility, Wt. %												
Bitumen	76.81	78.56	80.71		68.35		81.01		85.13		81.01	85.13
Ash	0.06	0.08	0.03		0.07		0.05		0.02		0.05	0.02
Difference	23.13	21.36	19.26		31.58		18.93		14.85		18.93	14.85

(1)	Raw Coal		Coal Extract	
	Raw Coal	Coal Extract	Raw Coal	Coal Extract
Organic S. %	0.799	0.593	0.593	0.593
Pyritic S. %	0.370	Not Detected	Not Detected	Not Detected
Sulfate S. %	0.012	Not Detected	Not Detected	Not Detected
Total	1.181	0.593	0.593	0.593

TABLE 2

TYPICAL COAL DEASHING RESULTS

Coal Source:	Pennsylvania		Illinois		Pennsylvania	
	As Charged	Product	As Charged	Product	As Charged	Product
<b>Bench Scale</b>						
Proximate Analysis						
Moisture	1.4					
Volatile Matter	36.6	22.3-30.3	33.62	25.2	33.53	37.3
Fixed Carbon	56.6	77.4-69.4	56.56	74.5	52.54	62.5
Ash	5.4	0.02-0.5	9.79	0.3	13.93	0.3
Sulfur	1.46	0.3 - 0.6	3.95	1.0	4.32	0.9
Chlorine			0.15	0.003	0.25	0.004

Pilot Plant

Coal Source:	Illinois	
	As Charged	Product
<b>Sample</b>		
Proximate Analysis		
Moisture	2.75	
Volatile Matter (Dry Basis)	38.90	20.9+
Fixed Carbon (Dry Basis)	53.99	78.4+
Ash	7.11	0.65
Sulfur	1.18	0.593

TABLE 3

DELAYED COALING RUN - PRODUCT DISTRIBUTION

Basis: Run PF-15  
2000 lbs. Southern Illinois Coal (Moisture Free)  
4000 lbs. Coker Recycle 500-700°F

<u>Product</u>	<u>Wt. lbs.</u>	<u>Solution Basis</u>		<u>Solvent-free Basis</u>	
		<u>Wt. %</u>		<u>Wt. %</u>	
Gas	134	2.2		6.7	
Liquor & Lt. Oil	60	1.0		3.0	
Coke	1256	20.9		62.8	
Solvent	4000	66.7			
Distillate	46	0.8		2.3	
Spent Cake	<u>504</u>	<u>8.4</u>		<u>25.2</u>	
Total	6000	100.0		100.0	

TABLE 4

DELAYED COKING OF DEASHED COAL SOLUTIONRESULTS OF COKER TEST RUN DC-13

Properties of Feed (1)	Coke Drum No. 1	Coke Drum No. 2
Specific Gravity, 100/60°F	1.1928	1.1811
Softening Point, °F (R&B)	158	108.5
Benzene Insoluble, Wt. %	22.2	19.6
Properties of Coke		
Wt. Percent of Feed	25.7	22.3
Density, lbs/ft <sup>3</sup>		
By Weight of Volume Occupied in Coke Drum	50.1	38.5
By Weight of Water Displaced by Sample	66.7	51.3
Volatile Matter, Wt. %	9.17	10.06
Fixed Carbon, Wt. %	90.22	89.28
Ash, Wt. %	0.61	0.66
Sulfur, Wt. %	0.37	0.38
Heating Value, BTU/lb.	14,520	
(1) Weight percent coal extract		-26.2
Benzene insoluble, weight percent-		21.0

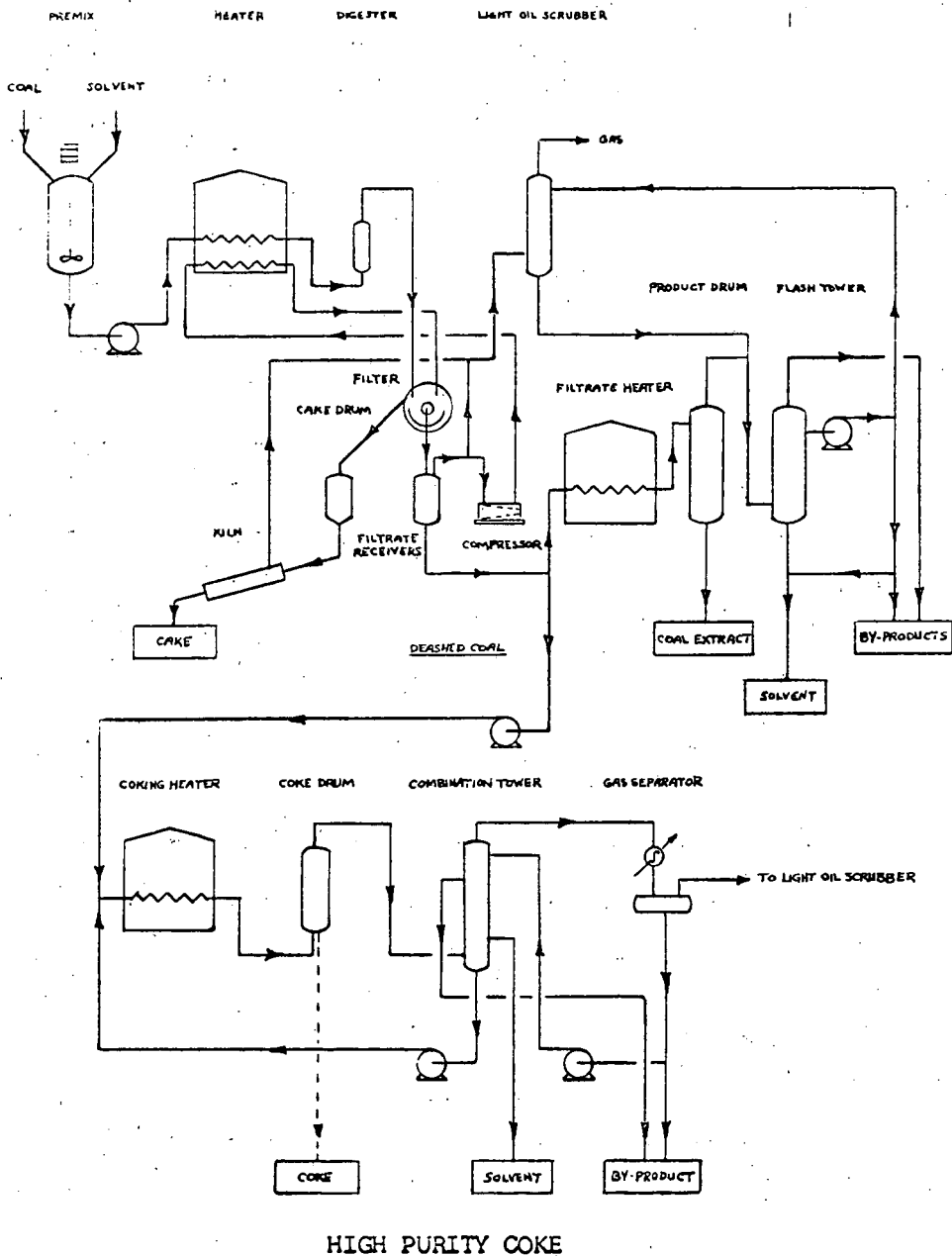
TABLE 5

ECONOMIC STUDY - DEASHED COAL PRODUCT

Plant Capacity, Tons/year	750,000		1,500,000	
Plant Cost	\$13,400,000		\$24,000,000	
	<u>Cost/Ton Product</u>	<u>¢/MM BTU</u>	<u>Cost/Ton Product</u>	<u>¢/MM BTU</u>
Raw Material (Coal)	\$6.50	21.6	\$6.50	21.6
Labor, Supervision, & Overhead	1.14	3.8	.98	3.2
Utilities	1.30	4.3	1.30	4.3
Depreciation	1.19	3.9	1.06	3.5
Maintenance	.54	1.8	.48	1.6
Insurance & Interest	.89	2.9	.80	2.7
Sales Costs	<u>.15</u>	<u>.5</u>	<u>.15</u>	<u>.5</u>
Gross Operating Costs	\$11.71	38.8	\$11.27	37.4
By-Product Credits	<u>(2.60)</u>	<u>(8.6)</u>	<u>(2.60)</u>	<u>(8.6)</u>
Net Operating Costs	\$9.11	30.2	\$8.67	28.8
Pre-tax Investment Return	<u>2.24</u>	<u>7.4</u>	<u>2.00</u>	<u>6.6</u>
Sales Price, (Coal @ \$4.00/ton)	\$11.35	37.6	\$10.66	35.3
Sales Price, (Coal @ \$3.00/ton)	\$9.72	31.9	\$9.03	29.6

- Notes: 1. Plant is a 'grass-roots' facility capable of handling run-of-mine coal from stockpile.
2. Labor - \$5.00/man hour including supervision and overhead.
3. Utilities - Electricity @ \$.006/KWH  
Steam @ \$.50/M lbs.  
Cooling Water @ \$.02/M Gallons
4. Depreciation - Straight Line over 15 year period.
5. Maintenance - 3% of investment.
6. Insurance & Interest - 5% of Plant cost.
7. By-Product Credits - \$.01/pound average for net excess distillate.
8. Pay-Out - 8 Years.

FIGURE 1  
SCHEMATIC FLOW DIAGRAM  
DEASHED COAL OR HIGH PURITY COKE



# THE HEAT OF REACTION OF <sup>393</sup>HYDROGEN AND COAL

A. L. Lee, H. L. Feldkirchner, F. C. Schora, and J. J. Henry\*

Institute of Gas Technology  
Chicago, Illinois

## INTRODUCTION

This investigation is a part of the study conducted at the Institute of Gas Technology (1,2,4,5,6,7,9,10,11) to obtain the necessary information for designing an efficient coal hydrogasification plant. A thorough literature search reveals that there is no reported data on the heat of reaction of hydrogen and coal. Therefore, two calorimeters were designed, constructed, and operated, one to measure the heat of reaction and the other to measure heat capacity by the drop method. The heat-of-reaction calorimeter can be operated at temperatures up to 1500°F and pressures up to 1500 psia; the drop calorimeter operates at atmospheric pressure and temperatures up to 1500°F. This paper reports the results of the following investigations:

1. The heat of reaction of hydrogen with coals and coal chars after various degrees of gasification.
2. The heat of reaction of coal pretreatment.
3. The heat capacity of coals and coal chars.

## APPARATUS

The heat-of-reaction calorimeter built by Dynatech Corporation is shown in Figure 1. The sample is placed in the upper portion of the neck which is cold. The calorimeter body is filled with hydrogen and heated. The temperature of the calorimeter body is measured by four thermocouples and two platinum resistance thermometers. The sample is lowered into the body after the temperature has remained steady for 2 hours. The change in temperature due to a reaction is then measured as a function of time.

The drop calorimeter, which was also built by Dynatech, is shown in Figure 2. The sample is placed in the top furnace until it reaches the desired temperature. It is then dropped into the copper receiver, and the heat capacity of the sample is determined from the temperature rise and heat capacity of the copper receiver.

## EXPERIMENTAL RESULTS

The major problem encountered in determining the heat of coal reactions at high temperature and high pressure is prereaction, since coals decompose when heated. Meaningful results can be obtained only if the coal and hydrogen react at conditions at which the desired temperature and pressure are stabilized. Therefore, the method of introducing the sample to the reaction conditions is critical. The coal must not react before the conditions are set, and the pressure must not be disturbed when the coal is introduced.

\* Dynatech Corp., Cambridge, Massachusetts.

The present method is to keep the sample at room temperature inside the calorimeter drop tube so that the reaction will not take place prematurely. Convection shields are installed to prevent a large heat loss from convection and to ensure that the sample is in a cold zone while the calorimeter is being stabilized at the reaction conditions.

Establishing a heat balance around the calorimeter was necessary in order to calculate the heat of reaction from experimental data. The heat balance is best expressed by:

$$\Delta\bar{H}_R + h_{in} = (mC_p\Delta T)_{\text{calorimeter}} + (mC_p\Delta T)_{\text{shield}} + (mC_p\Delta T)_{\text{chain}} + (mC_p\Delta T)_{\text{basket}} + (mC_p\Delta T)_{\text{coal}} \quad (1)$$

where:  $\Delta\bar{H}_R$  = heat of reaction  
 $h_{in}$  = heat input from the neck heater  
 $m$  = mass  
 $C_p$  = heat capacity  
 $\Delta T$  = temperature change

Each term in Equation 1 must be either established by calibration or accurately measured. The heat capacity of the calorimeter metal was determined in the drop calorimeter. These data are shown in Figure 3.

The effective  $mC_p$  of the reaction calorimeter was calibrated by a constant-heat-input technique in a hydrogen atmosphere at 1000 psia and temperatures from 840° to 1460°F. The results are presented in Figure 4. After the calorimeter constants were determined, the effective  $(mC_p\Delta T)$ 's of the convection shield, the chain, and the empty sample basket were calibrated in the calorimeter to determine the change of heat input with time, as shown in Equation 2:

$$K(\theta) = \int_0^{\theta} (mC_p\Delta T)_{\text{empty calorimeter}} d\theta = \int_0^{\theta} [(h_{in} - (mC_p\Delta T)_{\text{shield}} - (mC_p\Delta T)_{\text{chain}} - (mC_p\Delta T)_{\text{basket}})] d\theta \quad (2)$$

where:  $K(\theta)$  = a constant dependent only on time  
 $\theta$  = time

Combining Equations 1 and 2, we have:

$$\Delta\bar{H}_R = (mC_p\Delta T)_{\text{calorimeter}} + (mC_p\Delta T)_{\text{coal}} - K(\theta) \quad (3)$$

Equation 3 was used to calculate the heat-of-reaction data reported in this paper.

Design of a hydrogasification plant requires data on the heats of reaction of raw coal in the coal pretreatment process, the pretreated coal in the low-temperature gasifier, the residue from the low-temperature gasifier in the high-temperature gasifier, and the residue from the high-temperature gasifier (4,6). The heat-of-reaction and heat capacity measurements are given in Tables 1 and 2. Figure 5 shows the temperature and pressure profiles of a typical experimental run.

## DISCUSSION

Until now, the heat of the coal hydrogasification reaction has only been determined by calculation. These calculations have become more precise as more data became available, but no measurements were made to check the validity of the calculated data.

Initially (in the absence of accurate pilot plant yield data), the heat of reaction was estimated by assuming that coal and carbon were equivalent and that the hydrogasification reaction could be approximated by (5,8):



This approach, of course, is very crude and could not be expected to give a reliable answer, but it could be useful for comparing the thermal efficiencies of various gasification processes.

The next approach, using pilot plant data (7), was to calculate the heat of reaction from the heats of combustion of the reactants and products. The heats of combustion of various coals could be obtained by a Parr-bomb calorimeter or calculated by the modified Dulong formula. But if one attempts to calculate the heat of reaction of hydrogen and coal from heats of combustion, there are two drawbacks. First, because the calculation involves taking the differences of large numbers of the same order of magnitude, chemical analyses of all reactants and products must be very accurate and pilot material balances must be quite close to 100 percent or else the balance must be forced. If this is not the case, large errors can be made in this calculation. This makes the calculated heat of reaction dependent on the quality of the analytical data and on the method used to force the balance. The second drawback is that the calculated heat of reaction is determined for 25°C, so no information is obtained on the reaction heat at actual reaction temperatures.

Of course, if the heat of reaction could be determined at one temperature, the heat of reaction at various temperatures could be calculated from heat capacity data. Some heat capacity data are available in the literature for coals and cokes, but none are available for the particular coals used here. Moreover, the measurement methods used so far are not very accurate. In most cases the gaseous decomposition products were allowed to escape from the calorimeters during coal heatup, and, consequently, the heat capacity data are rather doubtful.

A comparison of the heats of reaction of hydrogen and coal obtained from the heat of formation data for  $C + 2H_2 \rightarrow CH_4$  and the pilot plant data with that obtained from the calorimetry studies is shown in Figure 6. Note that the pilot plant data were based on a 77°F reference

temperature, while the present experimental data were obtained at operating conditions. Moreover, the experimental data were obtained from coals at four different stages of reaction: raw coal, pretreated coal, low-temperature gasification residue, and high-temperature gasification residue. Ash balances were used to put these results on a common basis. The ash balance calculations gave the percent of carbon gasified in each coal or char. Raw coal was assumed to have 0% carbon gasified. Thus Figure 6 shows the general trend of the heat of reaction.

Accurate heat-of-reaction data are given in Table 1. Although the pilot plant data are considerably scattered, the average value is not too different from that obtained by the other methods. The calorimetry data also show some scattering, which is due to the heterogeneous nature of the coal, and the characteristics of the calorimeter and the sensing instruments. Examinations of the temperature measurement, the pressure measurement, the temperature distribution in the calorimeter, the total mass balance, and the calibration results obtained from the constant-heat-input method and experimental runs on hydrogen and n-decane reactions indicate that the data reported in Table 2 should not have a deviation greater than 10%.

#### ACKNOWLEDGMENT

This work is jointly sponsored by the American Gas Association and the U.S. Department of the Interior, Office of Coal Research. Their support is gratefully acknowledged. Valuable advice and discussions were provided by Drs. B. S. Lee, S. A. Weil, and C. W. Solbrig of the Institute of Gas Technology. J. R. DeSando assisted in the experimental work.

1. Feldkirchner, H. L. and Huebler, J., "Reaction of Coal With Steam-Hydrogen Mixtures at High Temperatures and Pressures," Ind. Eng. Chem. Process Design Develop. 4, 134-42 (1965) April.
2. Huebler, J. and Schora, F. C., "Coal Hydrogasification," Chem. Eng. Progr. 62, 87-91 (1966) February.
3. JANAF Thermochemical Tables. Distributed by: Clearinghouse for Federal Scientific and Technical Information, Springfield, Va.
4. Kavlick, V. J. and Lee, B. S., "Coal Pretreatment in Fluidized Bed," Amer. Chem. Soc. Div. Fuel Chem. Preprints 10, No. 4, 131-39 (1966) September.
5. Linden, H. R., "Pipeline Gas From Coal: Status and Future Prospects," Coal Age 71, 64-71 (1966) January.
6. Pyrcioch, E. J., Lee, B. S. and Schora, F. C., "Hydrogasification of Pretreated Coal for Pipeline Gas Production," Amer. Chem. Soc. Div. Fuel Chem. Preprints 10, No. 4, 206-23 (1966) September.
7. Pyrcioch, E. J. and Linden, H. R., "Pipeline Gas by High-Pressure Fluid-Bed Hydrogasification of Char," Ind. Eng. Chem. 52, 590-94 (1960) July.
8. Rossini, F. D. et al., Selected Values of Physical and Thermodynamic Properties of Hydrocarbons and Related Compounds. Pittsburgh: Carnegie Press, 1953.
9. Tajbl, D. G., Feldkirchner, H. L. and Lee, A. L., "Cleanup Methanation for Hydrogasification Process," Amer. Chem. Soc. Div. Fuel Chem. Preprints 10, No. 4, 235-45 (1966) September.
10. Tsaros, C. L. and Feldkirchner, H. L., "Production of High Btu Gas," Chem. Eng. Progr. 62, 49-54 (1966) August.
11. von Fredersdorff, C. G. and Vandaveer, F. E., "Substitute Natural Gas From Coal," in Segeler, C. G., Ed., Gas Engineers Handbook, Section 3, Chap. 9, 3/100-3/123. New York: The Industrial Press, 1965.

Table 1. ANALYSIS OF COAL AND COAL CHARS

	<u>Raw Coal</u>	<u>Pretreated Coal</u>	<u>Low-Temp Residue</u>	<u>High-Temp Residue</u>
Proximate Analysis, wt %				
Moisture	1.3	0.5	0.6	0.6
Volatiles	34.6	23.3	4.6	3.3
Fixed Carbon	52.0	63.5	77.6	71.6
Ash	12.1	12.7	17.2	24.5
Total	100.0	100.0	100.0	100.0
Ultimate Analysis, wt %				
Carbon	71.2	70.1	76.9	72.6
Hydrogen	5.14	3.70	2.05	1.08
Nitrogen	1.23	1.37	1.01	0.54
Oxygen	6.03	8.30	0.65	0.00
Sulfur	4.19	3.80	2.09	1.24
Ash	12.21	12.73	17.30	24.62
Total	100.00	100.00	100.00	100.00
Reaction Temperature, °F	1300	1300	1300	1300
Reaction Pressure, psia	1000	1000	1000	1000
Coal Reacted (Avg), %	49.7	47.2	27.3	28.8
Carbon Gasified (Avg), %	50.6	41.0	29.5	26.0
Avg $\Delta H_R$ , Btu/lb coal reacted	1817	1919	2432	3078

Table 2. HEAT OF REACTION OF COAL

<u>Material</u>	<u>Temperature, °F</u>	<u>Pressure, psia</u>	<u>Coal Reacted, %</u>	<u>Carbon Gasified, %</u>	<u><math>\Delta H_R</math>, Btu/lb coal reacted</u>
Raw coal	1000	1000	41.5	--	1300
Raw coal	1300	1000	52.4	50.7	1951
Raw coal	1300	1000	52.2	52.0	1723
Raw coal	1300	1000	48.1	55.6	1788
Raw coal	1300	1000	46.1	44.2	1807
Raw coal	1400	1000	51.7	52.3	1775
Pretreated coal	1300	1000	46.1	37.6	1935
Pretreated coal	1300	1000	47.3	41.2	1717
Pretreated coal	1300	1000	47.3	41.5	1844
Pretreated coal	1300	1000	47.1	40.0	2476
Pretreated coal	1300	1000	48.3	45.0	1625
Low-temp residue	1300	1000	27.3	29.5	2432
Low-temp residue	1300	1000	--	--	2566
High-temp residue	1300	1000	28.8	26.0	3078

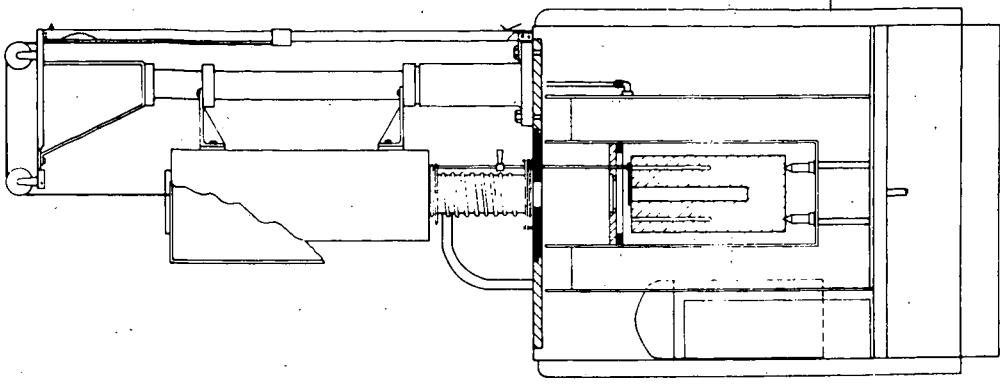


Figure 2. DROP CALORIMETER

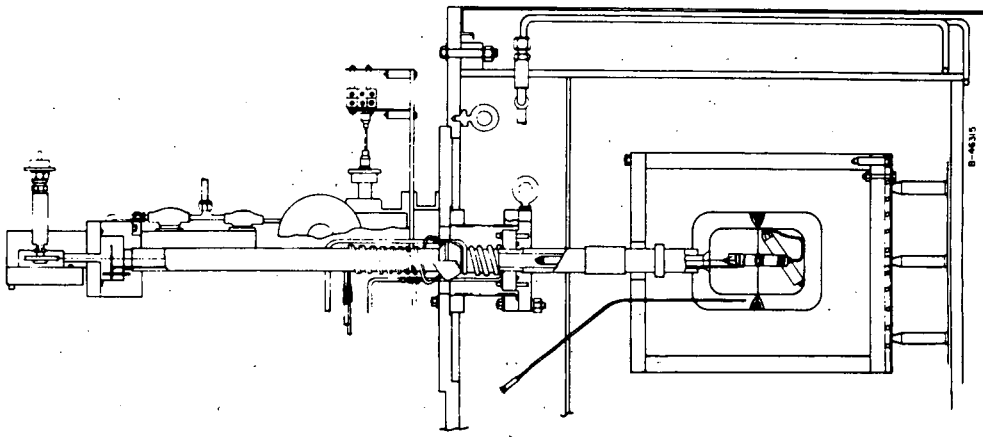


Figure 1. HEAT-OF-REACTION CALORIMETER

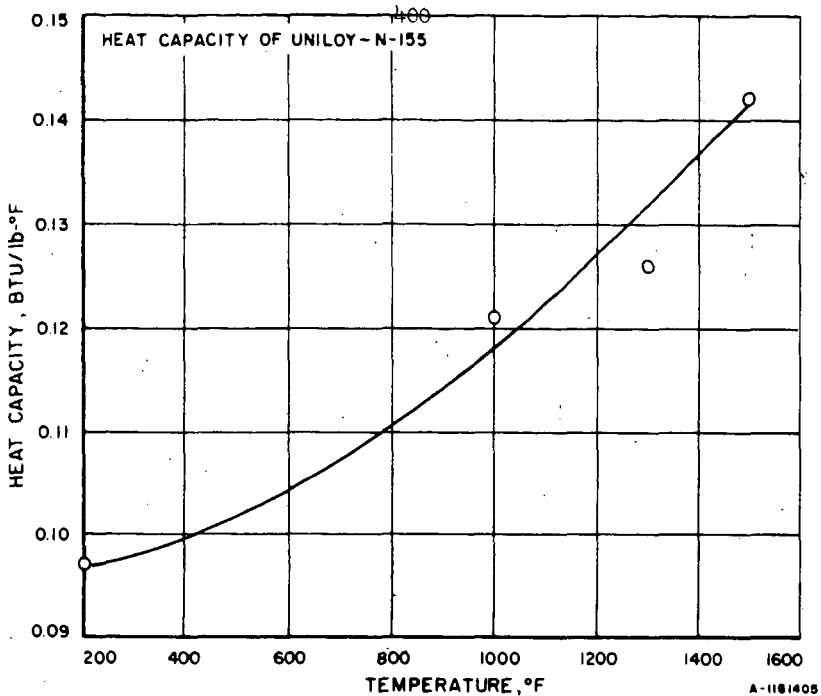


Figure 3. MEAN HEAT CAPACITY OF CALORIMETER  
(From 70°F to Temperatures Indicated)

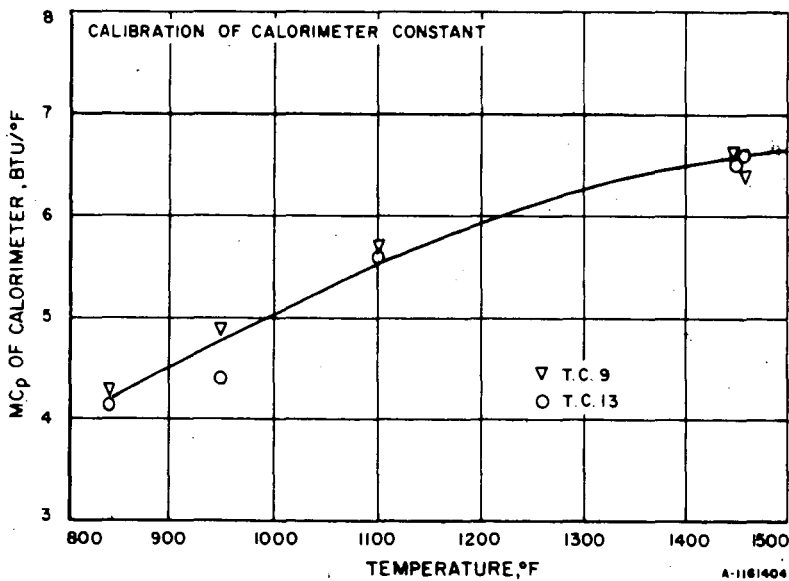


Figure 4. CALIBRATION OF HEAT-OF-REACTION CALORIMETER

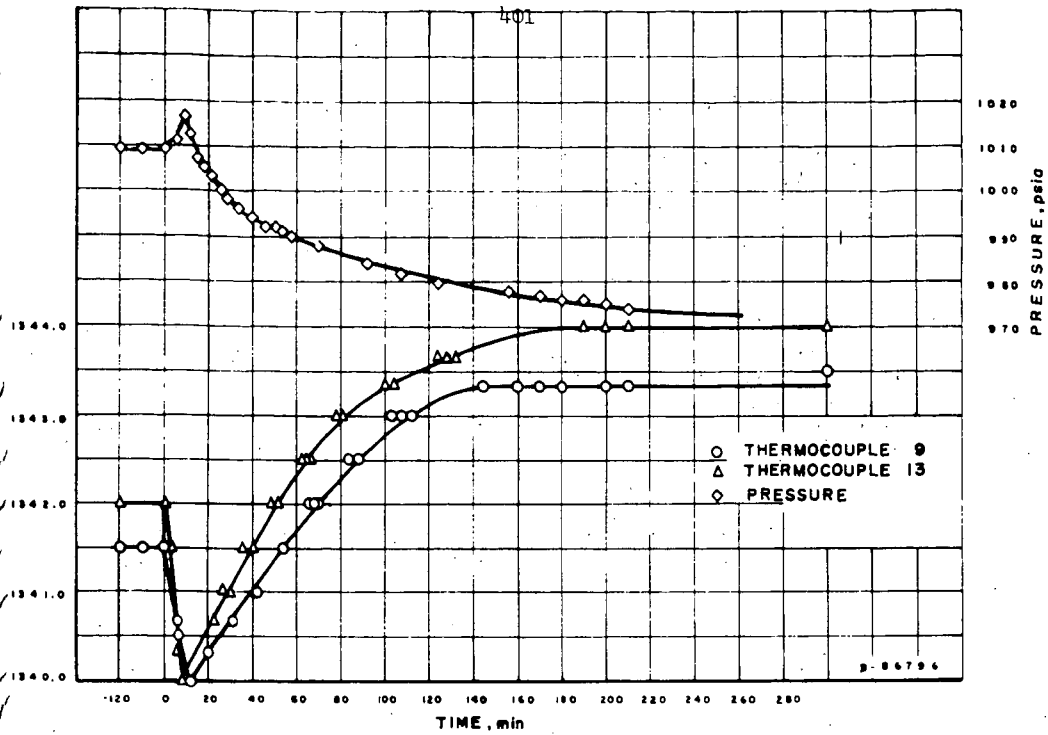


Figure 5. TIME-TEMPERATURE DATA FOR HEAT OF REACTION OF HYDROGEN AND COAL

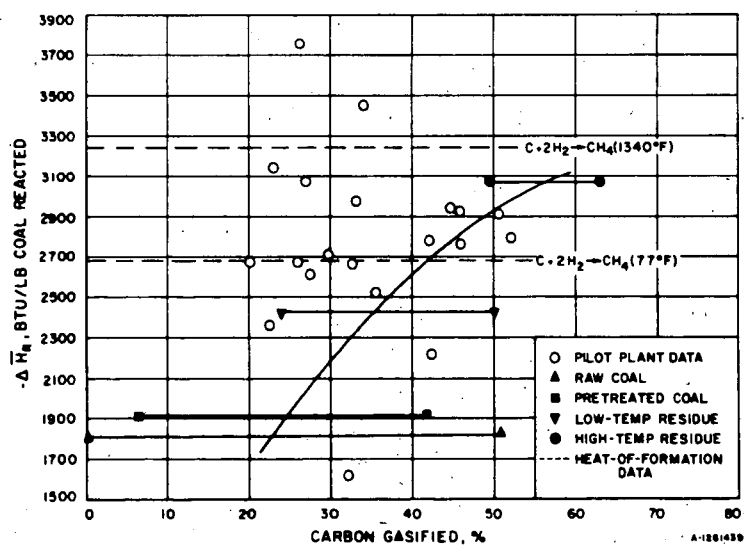


Figure 6. COMPARISON OF DATA FOR HEAT OF REACTION OF HYDROGEN AND COAL

## HYDROGEN CYANIDE PRODUCED FROM COAL AND AMMONIA

G. E. Johnson, W. A. Decker, A. J. Forney, and J. H. Field  
Pittsburgh Coal Research Center, U. S. Bureau of Mines,  
4800 Forbes Avenue, Pittsburgh, Pennsylvania 15213

## INTRODUCTION

Hydrogen cyanide (HCN) has been one of the country's strongest growth petrochemicals in recent years. U. S. production has increased from 174 million pounds in 1960 to 350 million pounds in 1964, a 100-percent increase over the 4-year period. The growth of production of hydrogen cyanide has been directly related to the expansion in production of synthetic textiles from acrylonitrile. Relative growth and production of hydrogen cyanide and acrylonitrile is as follows:

Production of Hydrogen Cyanide and Acrylonitrile

Year	Hydrogen cyanide, <sup>5/</sup> million lb	Acrylonitrile, million lb
1960	174	229 <sup>10/</sup>
1961	211	250 <sup>10/</sup>
1962	266	360 <sup>10/</sup>
1963	293	455 <sup>10/</sup>
1964	350	593 <sup>10/</sup>
1965	---	371 (6 months) <sup>4/</sup>

About 50 percent of the total output of hydrogen cyanide goes into the production of acrylonitrile; most of the remainder is used in production of adiponitrile and the manufacture of methyl methacrylate.<sup>7/</sup> However, in recent years acrylonitrile and adiponitrile are being produced by processes which generate hydrogen cyanide as a byproduct.<sup>3/</sup> The bulk of acrylonitrile is used in production of acrylic fiber (Orlon, Acrilan, Dynel, Zefran, etc.),<sup>a/</sup> a smaller amount in production of nitrile rubber, the adiponitrile in manufacture of Nylon.

The manufacture of sodium cyanide utilizes about 7 percent of hydrogen cyanide production. The remaining hydrogen cyanide goes to a large number of relatively small uses including ferrocyanides, acrylates, ethyl lactate, lactic acid, chelating agents, optical laundry bleaches, and pharmaceuticals.

The Andrussow process is the major commercial process used for producing hydrogen cyanide. It involves the reaction of methane, ammonia, and air over a platinum catalyst at 1,000° to 1,200° C.<sup>9/</sup> The platinum catalyst is usually alloyed with rhodium (10 to 20 percent).

Conversion by the Andrussow process in a single pass is limited to about 69 percent of the ammonia (about 75 percent with gas recycle) and 53 percent of the methane. A typical analysis of the reaction gases leaving a catalytic reactor is as follows in volume-percent: Nitrogen 56.3, water vapor 23.0, hydrogen 7.5, hydrogen cyanide 6.0, carbon monoxide 4.4, ammonia 2.0, methane 0.5, carbon dioxide 0.2, and oxygen 0.1.

<sup>a/</sup> Reference to trade names is made for identification only and does not imply endorsement by the Bureau of Mines.

In the catalytic Degussa process which is not in general use but is similar to the Bureau of Mines method in that heat is provided externally, the offgas from the ammonia-methane reaction contains more than 20 percent hydrogen cyanide. Utilization of methane and ammonia are reported as 91 and 85 percent, respectively.

In its search for new uses for coal the Bureau of Mines has been investigating the production of hydrogen cyanide from coal. Although hydrogen cyanide is present in coke oven gases, and at one time was recovered as a byproduct, this source of the gas has not been commonly used in the United States since the development of the newer methane-ammonia processes. Although the production of hydrogen cyanide from coal is technically feasible, production in yields that could be competitive is a problem of major concern.

#### EQUIPMENT AND PROCEDURE

Figure 1 is a flowsheet of the experimental unit. Coal ground to minus 300 mesh is dropped in free-fall through a heated reaction zone in the presence of ammonia at rates up to 1.10 lb/hr. A revolving-disk feeder especially designed by the Bureau of Mines to feed coal at low rates was constructed; it delivered to within  $\pm 5$  percent of the desired feed rate.

A special coal feed system is used to prevent agglomeration and possible plugging of the reactor by heating the coal rapidly through its plastic range (about 400° C).

The reactor itself is a 4-foot length of vitreous refractory mullite, 1-1/8 inches ID and 1-3/8 inches OD, jacketed with two electrical resistance heaters. The top heater (maximum temperature 850° C) is 12 inches long and is wound with Nichrome wire. It serves as preheater for the coal and gas. A Kanthal heater (Al-Cr-Co-Fe alloy, maximum temperature 1,250° C) encloses the center 20 inches of the tube, or the reaction zone. The bottom section of the reactor is exposed to the atmosphere for rapid cooling of the product gases.

The bottom of the reactor tube fits into a 4-liter side-arm flask or char receiver in which the heavier solids are collected. The fine solids and carbon black produced are collected in an electrostatic precipitator. After the product gases leave the precipitator they pass through a cooler, then they are either metered or sent through absorbers to remove the hydrogen cyanide for analysis.

All of the piping and vessels are stainless steel or glass in order to counteract the corrosive nature of the gases. Since the gases are toxic, the unit is completely enclosed, and the enclosure is well ventilated to prevent any accumulation of escaped gases. The whole structure (6 ft x 6 ft x 15 ft high) is covered with steel sheeting. It has an exhaust blower (400 cfm) on the roof and access doors at both ground and 8-foot levels. Figure 2 shows the exterior of the unit and figure 3 shows its interior.

Product gas can be recycled to the top of the reactor adjacent to the cooled feed tube along with part of the feed gas. This flushes away any tar vapors which might adhere to the walls and cause plugging. The remainder of the feed gas (0 to 10 scfh) enters the reactor with the coal. Ammonia, helium, methane, nitrogen, or air, or mixtures of these gases fed from cylinders have been used as feed gas.

Before startup, the system is purged with inert gas. After the reactor has been heated to 1,250° C the desired flows of coal and gas are started. Ammonia and nitrogen or helium are the gases usually used. The gas flow is generally split, part entering the top of the reactor adjacent to the cooled feed tube, and the remainder entering with the coal.

The powdered coal is fed through a steam-jacketed tube (5/16-inch OD) which extends into the preheat zone of the reactor. The coal leaves the end of the feed tube which is at the temperature of the steam to enter the preheat zone of 850° C. The temperature of the coal rises very suddenly to 850° C because of the high heat-transfer rate to the small particles. The carrier gas (usually helium, an inert gas) fed with the coal keeps the particles in motion and helps prevent agglomeration as the coal rapidly passes through its plastic range.

Proximate and ultimate analyses<sup>2, 6/</sup> are made of the char and heavier solids collected in the char receiver and of the lighter solids collected by the electrostatic precipitator. Mass spectrometric and chromatographic analyses are made on spot samples of the product gas. For cyanide determinations, metered amounts of product gas are bubbled through two scrubbers in series containing solutions of sodium hydroxide. Titration with silver nitrate solution determines the total cyanide present.<sup>1/</sup>

#### EXPERIMENTAL RESULTS AND DISCUSSION

The initial tests were made with a metallic reactor tube, but because of low yields of hydrogen cyanide and failure of the metal at the temperatures employed, the metal tube was replaced by a ceramic reactor tube.

In all the tests of this report with hvab coal, Pittsburgh seam coal from Bruceton, Pa., was used. Its ultimate analysis is as follows in percent: Carbon 75.6, ash 8.4, oxygen 8.0, hydrogen 5.1, nitrogen 1.6, and sulfur 1.3.

The effect of varying the coal-ammonia feed rates is illustrated in table 1. Hydrogen cyanide yields were computed from the wet-chemical method of analysis which is considered the more reliable method since it was determined from proportionated gas samples taken continuously throughout the test (sample volume of 0.2 to 2 cu ft). Only spot gas samples (sample volume 0.01 cu ft) were used for the chromatograph and mass spectrograph analyses.

In test C-241 the coal-feed rate was 0.37 lb/hr and the ammonia-feed rate was 1 cu ft/hr. (All process gas volumes reported are corrected to standard conditions of 0° C and 760 mm mercury pressure.) A hydrogen cyanide yield of 0.6 cu ft per cu ft of ammonia reacted was obtained, corresponding to about 12 percent hydrogen cyanide in the product gas.

In test C-243 the hvab coal-feed rate was reduced to 0.19 lb/hr, while the ammonia-feed rate was increased to 2.3 cu ft/hr. A yield of 0.4 cu ft hydrogen cyanide per cubic foot of ammonia consumed was obtained, corresponding to about 13 percent hydrogen cyanide in the product gas.

The yield of hydrogen cyanide per pound of coal was approximately doubled when the coal-feed rate was halved and the ammonia-feed rate doubled (tests C-241 to 243), while the hydrogen cyanide yield per cubic foot of ammonia consumed decreased by one-third.

Table 1.- Data from Tests with hvab Coal and Ammonia with Helium at 1,250° C

Test	Product gas, percent											
	HCN <sup>1/</sup>	H <sub>2</sub> S	NH <sub>3</sub>	H <sub>2</sub>	O <sub>2</sub>	N <sub>2</sub>	CO	CO <sub>2</sub>	CH <sub>4</sub>	C <sub>2</sub> H <sub>4</sub>	C <sub>3</sub> H <sub>8</sub>	C <sub>8</sub> H <sub>10</sub>
C-241	11.8	0.0	0.0	77.7	0.1	6.7	9.6	0.3	5.1	0.4	0.1	0.0
C-243	13.1	.0	17.5	68.6	.9	6.8	4.0	.1	1.0	.0	.0	1.1
C-239	13.2	.1	.5	75.9	.1	4.4	10.6	.5	6.9	.6	.1	.3
C-198	5.4	.3	.0	78.3	.3	3.5	11.1	.3	5.7	.5	.0	.0

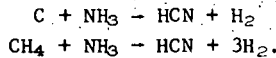
  

	Feed				Yield, cu ft			
	He, cu ft/hr	NH <sub>3</sub> , cu ft/hr	Coal feed, lb/hr	Total off gas He-free, cu ft/hr	Length of run, min	HCN/lb coal	HCN/cu ft NH <sub>3</sub> feed	HCN/cu ft NH <sub>3</sub> consumed
C-241	1.00	1.00	0.37	5.06	30	1.59	0.60	0.60
C-243	0.49	2.35	.19	4.90	30	3.31	.27	.40
C-239	.98	1.00	.73	5.59	15	1.01	.74	.76
C-198	2.12	0.20	.37-.40	3.61	15	0.51	.98	.98

<sup>1/</sup> Wet-analytical method of analysis for HCN only; other components are the average of 2 chromatograph and 2 mass spectrometer analyses, HCN-free basis.

In test C-239 (table 1) the coal-feed rate was increased to 0.73 lb/hr, while the ammonia flow was maintained at 1 cu. ft/hr. A hydrogen cyanide yield of about 0.8 cu ft per cubic foot ammonia reacted was obtained, equivalent to about 13 percent hydrogen cyanide in the product gas.

In the next listed test, C-198, the coal-feed rate was 0.37 to 0.40 lb/hr, while the ammonia flow was only 0.2 cu ft/hr. The hydrogen cyanide content in the product gas was only 5 percent, table 1, but conversions of about 100 percent of the ammonia were obtained with 1 cu ft of hydrogen cyanide formed per cubic foot of ammonia used. This yield of hydrogen cyanide approximates the stoichiometric yield according to the following reactions:



In typical commercial units using catalysts for the methane-ammonia reaction, the ammonia conversion attained is about 75 percent. Yield values include the slight amount of hydrogen cyanide that may be formed when coal is heated to high temperatures without adding ammonia.

In general, the tests of table 1 indicate that an excess coal feed is desirable in order to attain maximum utilization of the ammonia since the ammonia is by far the more expensive raw material.

Tests With Coals of Different Rank

In addition to the hvab coal, lignite, subbituminous, low-volatile bituminous, and anthracite coals, coal char, and activated carbon were tested as raw materials for producing hydrogen cyanide. It is thought that the volatile matter in coal reacts with the ammonia to form hydrogen cyanide, therefore coals with higher volatile content should produce more hydrogen cyanide. The volatile-matter contents on a moisture-free basis of the various materials tested are as follows:

Test	Identification of coal	Source of coal	Volatile matter, percent
C-123, 124, 125, 198, 239, 241, 243	Hvab, Pittsburgh seam	Bruceton, Pa.	34.0
C-207	Activated carbon, Grade SXWC	Union Carbide and Carbon Corp.	2.0
C-210	Anthracite	Anthracite Research Center, Schuylkill Haven, Pa.	7.6
C-246	Subb, Laramie seam	Erie, Colo.	38.5
C-249	Lvb, Pocahontas #3 seam	Stepheson, W. Va.	17.5
C-252	Lignite, unnamed seam	Beulah, N. Dak.	41.1
C-254	Pretreated hvab, <sup>1/</sup> Pittsburgh seam	Bruceton, Pa.	32.6

<sup>1/</sup> Treated with air at 200° C.

Table 2 shows the results of these tests. Lignite with 41 percent volatile matter produced the most hydrogen cyanide, 0.4 cu ft per cubic foot of ammonia consumed; activated carbon, containing the least volatile matter (2.0 percent), produced the least hydrogen cyanide, 0.007 cu ft per cubic foot of ammonia consumed.

The chemical nature of the volatile matter and the oxygen content of the coal may also affect the hydrogen cyanide yield. The ratio of H<sub>2</sub> to CO in the off gases varied from 2.3 to 1 for subb coal and 2.4 to 1 for lignite to 7 to 10 to 1 for hvab. The higher carbon monoxide values obtained with subb coal and lignite are due to the higher oxygen contents of these coals, being 17.1 and 20.3 percent, respectively, compared with 8.0 percent for the hvab coal.

Table 2.- Data from Tests with Various Coals and Ammonia with Helium at 1,250° C

Test	Product gas, percent										
	HCN <sup>1/</sup>	H <sub>2</sub> S	NH <sub>3</sub>	H <sub>2</sub>	O <sub>2</sub>	N <sub>2</sub>	CO	CO <sub>2</sub>	CH <sub>4</sub>	C <sub>2</sub> H <sub>4</sub>	C <sub>3</sub> H <sub>8</sub>
C-246 Subb	5.4	0.0	0.0	64.2	0.0	4.9	28.0	0.5	2.4	0.0	0.0
C-249 Lvb	4.2	.0	.0	78.9	.1	14.2	3.6	.0	3.0	.2	tr.
C-252 Lignite	6.4	tr.	.0	64.6	.1	6.1	26.3	.5	2.4	.0	.0
C-254 Pretreated, hvab	3.8	.1	.0	72.3	.8	10.6	14.3	.0	1.9	.0	.0
C-210 Anthracite	0.2	.0	.0	73.4	.3	21.4	2.9	.4	1.5	.0	.0
C-207 Activated carbon	.25	.0	.0	70.0	.0	23.0	6.6	.1	0.3	.0	.0

	Feed				
	He, cu ft/hr	NH <sub>3</sub> , cu ft/hr	Solids feed, lb/hr	Total off gas He-free, cu ft/hr	Length of run, min
C-246 Subb	0.91	1.00	0.42	6.88	30
C-249 Lvb	.97	1.00	.47	3.92	30
C-252 Lignite	1.06	1.00	.37-.40	6.38	15
C-254 Pretreated, hvab	1.04	1.00	.35	5.80	30
C-210 Anthracite	1.02	1.15	.37-.40	4.15	15
C-207 Activated carbon	1.06	1.15	.62	3.23	15

	Yield, cu ft		
	HCN/lb coal	HCN/cu ft NH <sub>3</sub> feed	HCN/cu ft NH <sub>3</sub> consumed
C-246 Subb	0.88	0.37	0.37
C-249 Lvb	.34	.16	.16
C-252 Lignite	1.05	.41	.41
C-254 Pretreated, hvab	.63	.22	.22
C-210 Anthracite	.021 <sub>2/</sub>	.007	.007
C-207 Activated carbon	.013 <sub>2/</sub>	.007	.007

- 1/ Wet-analytical method of analysis for HCN only; other components are the average of 2 chromatograph and 2 mass spectrometer analyses, HCN-free basis.  
 2/ Per pound of carbon.

#### Tests With Air in the Feed Gas

Tests were made to determine the effect that oxygen in the treating gas would have on the yield of hydrogen cyanide. It was thought that the heat for raising the temperature of the reactants to reaction temperature could be supplied by direct contact with a hot flue gas containing oxygen instead of by electric heating (table 3). In test C-125, a maximum yield of hydrogen cyanide was produced for tests with air in the treating gas--0.12 cu ft of hydrogen cyanide per cubic foot of ammonia consumed, or 9.2 percent hydrogen cyanide in the product gas. When more than 0.5 percent air was fed into the reactor, moisture condensed on the walls of the solids-collection flask; the yield of hydrogen cyanide decreased. The moisture could have been absorbing the hydrogen cyanide since hydrogen cyanide is highly soluble in water. This approach was abandoned.

Table 3.- Product Gas Analyses and Yields of Hydrogen Cyanide from Tests with hvab Coal, Ammonia, and Air at 1,250° C

Test	Product gas, percent						Length of run, min	Feed		
	HCN <sup>1/</sup>	CH <sub>4</sub>	NH <sub>3</sub>	H <sub>2</sub>	N <sub>2</sub>	CO		NH <sub>3</sub> , cu ft/hr	Air, cu ft/hr	Coal, lb/hr
C-123	10.3	1.1	10.2	62.8	16.2	9.7	20	5.90	0.52	0.17-0.20
C-124	10.9	0.6	6.9	62.1	17.2	13.2	20	2.96	.53	.17- .20
C-125	9.2	.4	9.6	48.4	31.5	10.1	20	3.08	1.08	.17- .20
Total off gas, cu ft/hr		Yield, cu ft								
		HCN/lb coal		HCN/cu ft NH <sub>3</sub> feed		HCN/cu ft consumed		NH <sub>3</sub>		
C-123	4.18	2.30		0.073		0.078				
C-124	3.05	1.77		.112		.120				
C-125	3.70	1.82		.110		.123				

1/ Wet-analytical method of analysis for HCN only; other components are the average of 2 chromatograph and 2 mass spectrometer analyses, HCN-free basis.

#### Tests With Methane and Ammonia

Tests were made without coal feed but with ammonia and methane to determine the resulting hydrogen cyanide yields for comparison. In one series of tests 2.0 cu ft/hr of methane was reacted with ammonia in flows varying from 0.3 to 2.5 cu ft/hr at 1,250° C. As illustrated in figure 4, yields of 0.18 to 0.61 cu ft of hydrogen cyanide per cubic foot of ammonia consumed were obtained, equivalent to 1.2 to 13.8 percent hydrogen cyanide in the product gas. The yield of hydrogen cyanide reached a maximum at a feed ratio of methane to ammonia of about 1 to 1.

A series of tests was made in which the methane and ammonia flow rates were maintained at 2 and 1 cu ft/hr, respectively, while the reactor temperature was increased from 1,000° to 1,275° C. Hydrogen cyanide yields are plotted with temperature in figure 5, indicating increased hydrogen cyanide yields with increased temperature. Maximum yields of about 0.6 cu ft of hydrogen cyanide per cubic foot of ammonia consumed were obtained at the higher temperatures, while at 1,000° C only 0.07 cu ft of hydrogen cyanide per cubic foot of ammonia consumed was formed.

To explore the use of coal-derived gases in the formation of hydrogen cyanide from ammonia, synthetic mixtures of a low-temperature carbonization gas, a coke oven gas, and a producer gas were prepared and reacted with ammonia at 1,250° C. Gas flows were adjusted to give a minimum methane-to-ammonia ratio of 1 to 1. In figure 6 the hydrogen cyanide yields obtained are plotted with the methane contents of the coal gases. Increasing hydrogen cyanide yields were produced with increasing methane contents of the feed gas.

## ECONOMIC EVALUATION

The Bureau of Mines Process Evaluation Group, Morgantown, W. Va., made a preliminary cost study of an integrated plant to produce hydrogen cyanide by reaction of ammonia with coal. The cost study was based on experimental results including a yield of 0.6 cu ft of hydrogen cyanide per cubic foot of ammonia. Electrical heating was assumed as in the bench-scale tests; a plant capacity of 40 million pounds per year was chosen. The total estimated capital investment was \$12,930,000 including costs for power generation.

Based on a coal cost of \$4.00 per ton and an ammonia cost of \$100.00 per ton, the operating costs before profit and taxes would be 5.82 cents per pound of hydrogen cyanide product allowing byproduct credit. Addition of 12-percent gross return on investment would give production costs of 9.7 cents per pound of product when \$4.00 per ton coal is used. The current market price is 11.5 cents per pound.<sup>8/</sup>

Credit has been allowed in the cost figures for a 7.6-percent yield of carbon black and the excess char produced in the process. Some of the char and the scrubbed product gas (containing about 75 percent hydrogen) are consumed in the steam plant for power generation. Electrical heating, which was used in the test unit and also in the cost figures, is one of the most expensive types of heating, accounting for greater than 40 percent of the capital costs in the estimate. If cheaper conventional heating could be used, production costs would be lowered considerably.

## CONCLUSIONS

Hydrogen cyanide has been produced from coal and ammonia at 1,250° C in bench-scale studies. The use of a metal reactor was unsuccessful because the metal failed at the temperatures required, and the yield of hydrogen cyanide was low. The yield was improved greatly when a refractory ceramic reactor was used.

Hydrogen cyanide yields approximating stoichiometric of 1 cu ft of hydrogen cyanide per cubic foot of ammonia reacted were obtained at low flows of ammonia. At higher ammonia flows, ammonia conversion of about 75 percent was obtained, which is the usual conversion attained in commercial units using natural gas and a platinum catalyst.

The low-volatile coals gave low yields of hydrogen cyanide; the high-volatile coals gave the best yields. The results indicated that the hydrogen cyanide is produced by reaction of ammonia with the hydrocarbons in the coal. Yields of hydrogen cyanide from reaction of ammonia with gas mixtures containing methane are directly related to the methane content of the gas.

Cost studies indicate that hydrogen cyanide can be produced from coal and ammonia at a price approximating the posted sales price.

## BIBLIOGRAPHY

1. American Public Health Association, Inc. Standard Methods for the Examination of Water and Wastewater. 11th ed., 1960, pp. 355-356.
2. A.S.T.M. Standards with Related Material. Gaseous Fuels, Coal and Coke. Part 19, 1966, 470 pp.
3. Chemical Week, Market Newsletter, v. 99, No. 23, Dec. 3, 1966, p. 65.
4. Chemicals, Quarterly Industry Report, U.S. Business and Defense Services Admin., v. 12, No. 4, Dec. 1965, p. 40.
5. Current Industrial Reports, Inorganic Chemicals and Gases 1964. U. S. Commerce Department, Series M-28A, Released Jan. 28, 1966, p. 6.
6. Fieldner, A.C., and W. A. Selvig. Methods of Analyzing Coal and Coke. BuMines Bull. 492, 1951, 51 pp.
7. Fugate, W.O. Hydrogen Cyanide, pp. 574-585 in v. 6 Encyclopedia of Chemical Technology. Interscience Publishers, New York, N.Y., 1962, 2d ed., ed. by R. E. Kirk and D.O. Othmer.
8. Oil, Paint and Drug Reporter. V. 189, No. 23, June 6, 1966, p. 20.
9. Sherwood, Peter W. Synthesis of Hydrogen Cyanide by Autothermic Reaction. Refining Engineer, v. 31, No. 2, February 1959, pp. C-22-26.
10. U. S. Tariff Commission, Synthetic Organic Chemicals, U.S. Production and Sales:
 

1960 -	Tariff Commission Publication No. 34,	p. 53,	published 1961.
1961 -	ditto	72, p. 53,	published 1962.
1962 -	do.	114, p. 56,	published 1963.
1963 -	do.	143, p. 55,	published 1964.
1964 -	do.	167, p. 55,	published 1965.

All published in Washington, D. C.

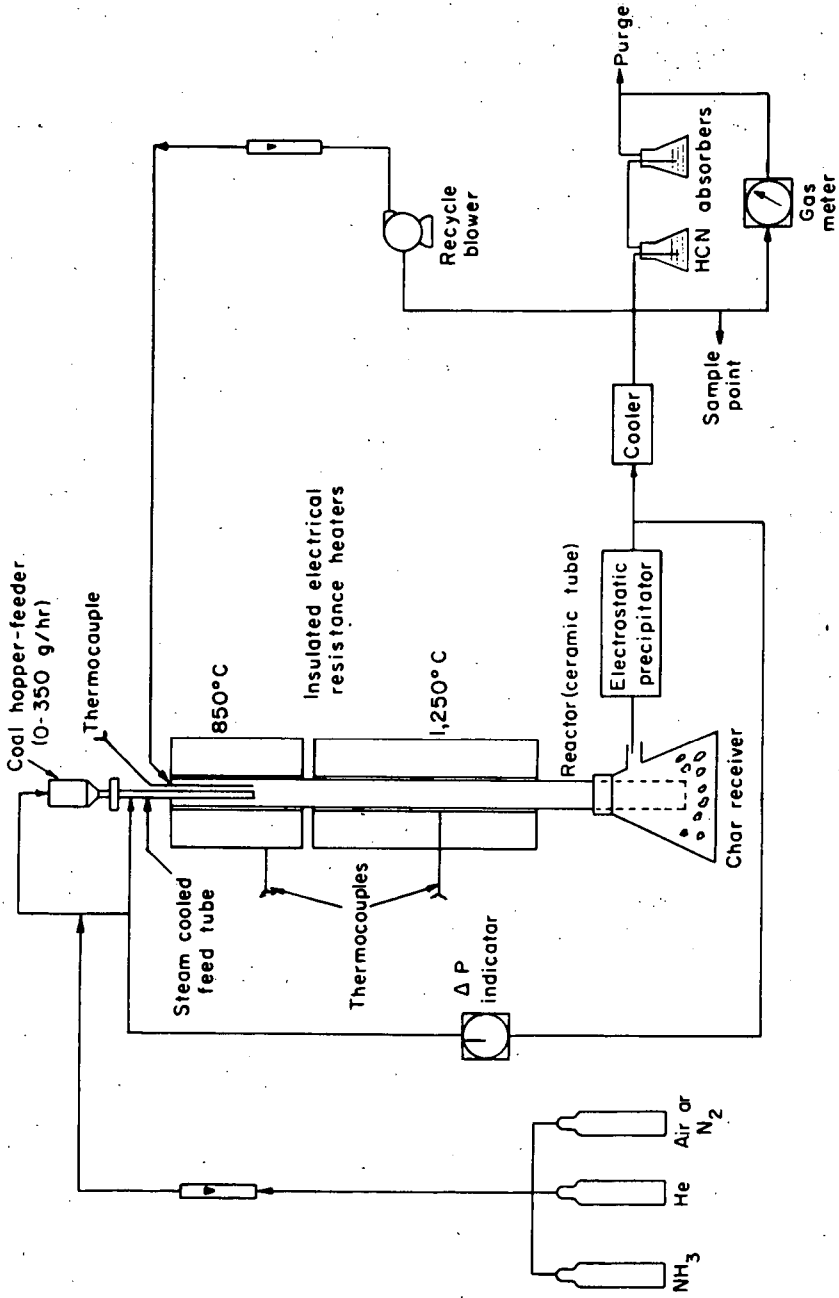


Figure 1. Flowsheet of hydrogen cyanide unit.

6-1-66

L-9365

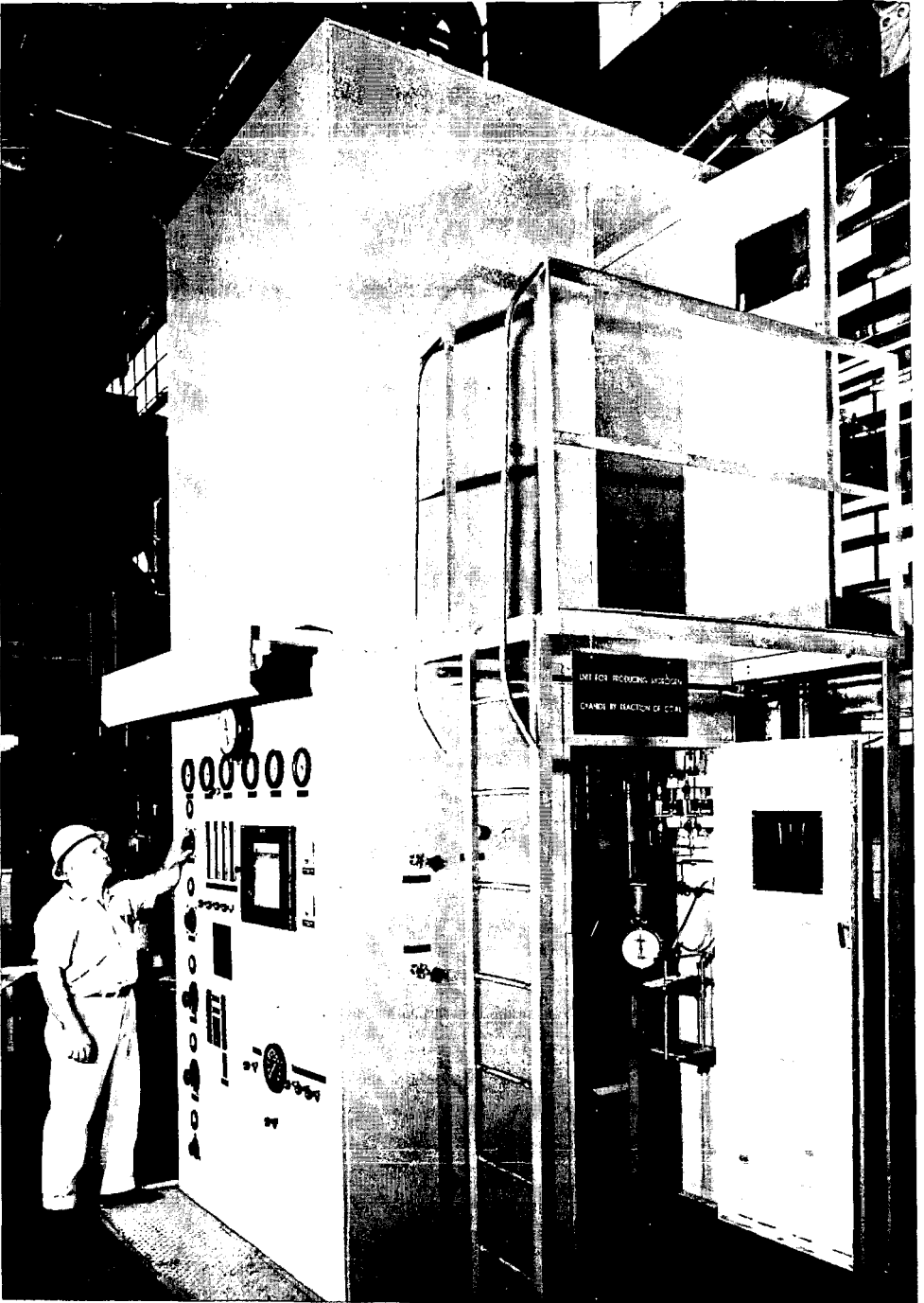


Figure 2. Enclosure surrounding hydrogen cyanide unit.

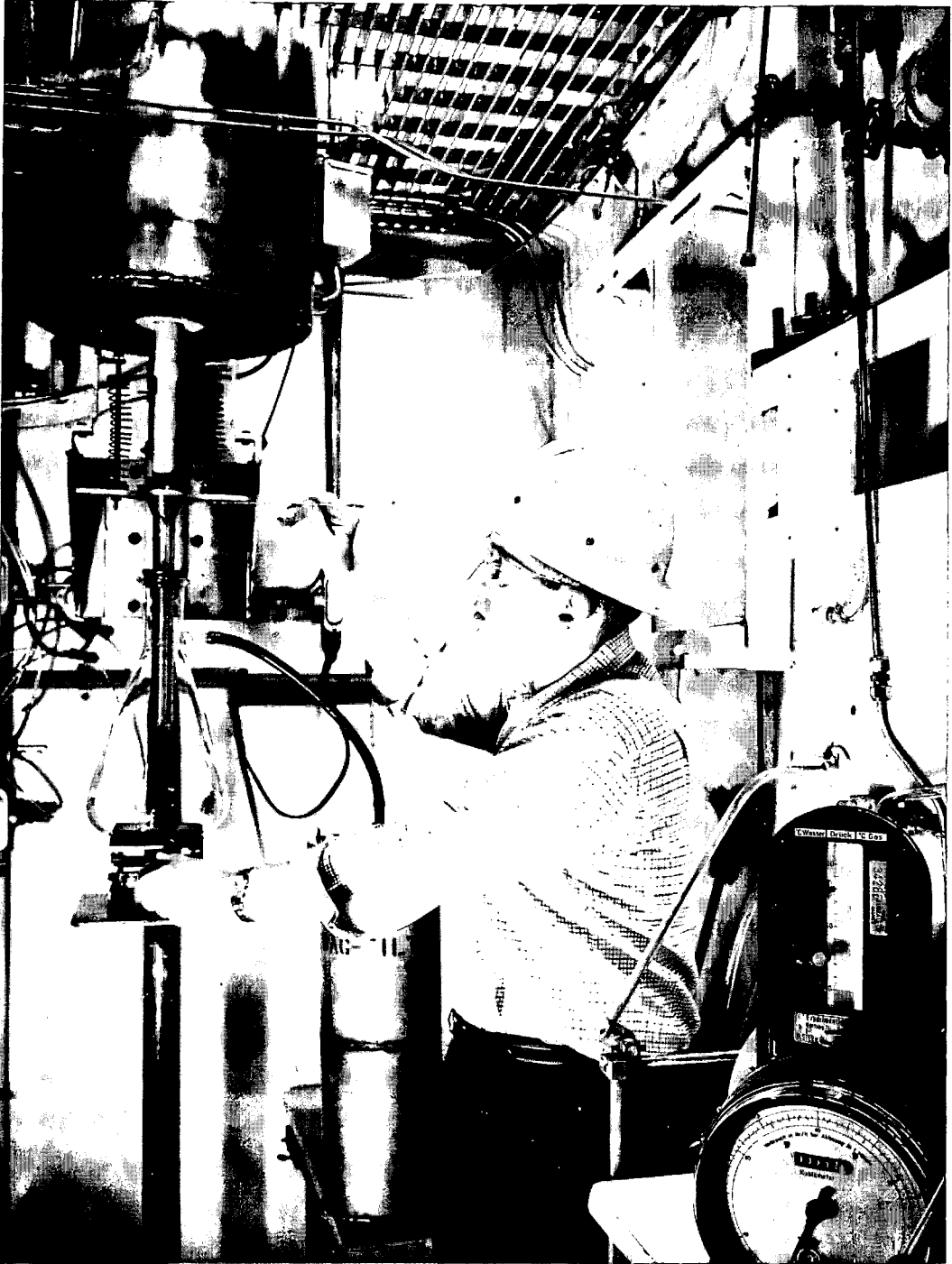


Figure 3. Hydrogen cyanide reactor.

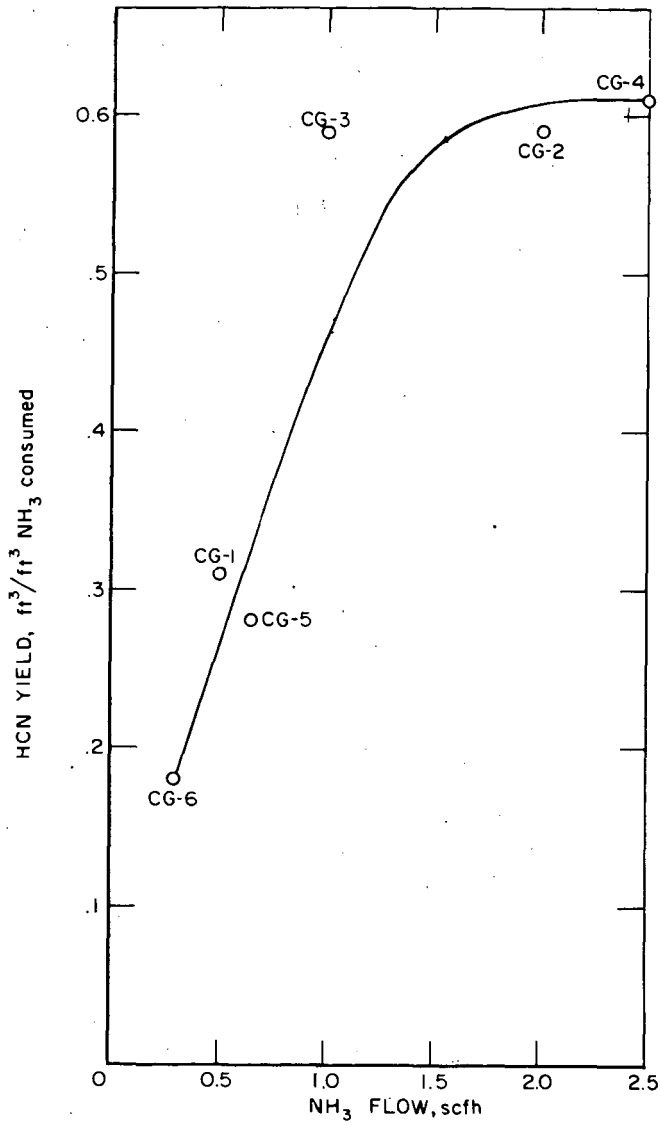


Figure 4. Effect of ammonia flow rate on yield of hydrogen cyanide from methane-ammonia reaction at 1,250° C. (Methane flow 2 scfh).

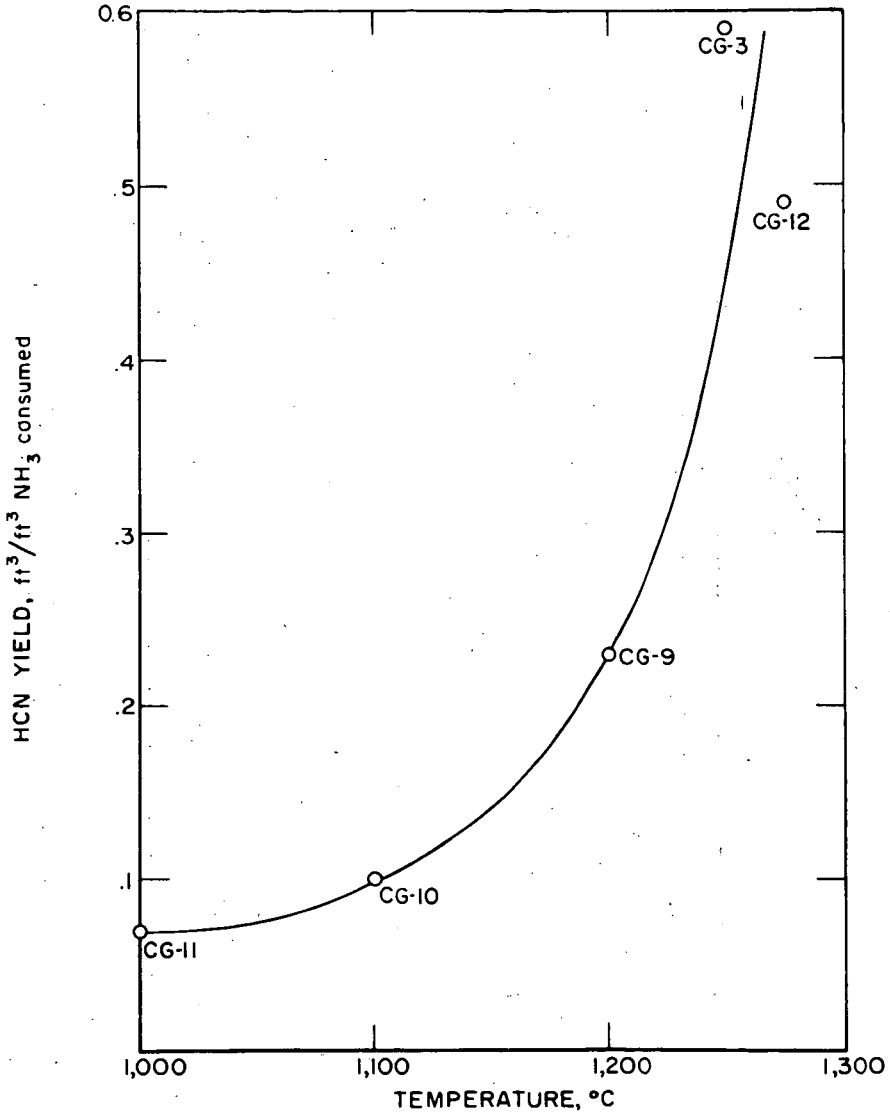


Figure 5. Effect of temperature on yield of hydrogen cyanide from reaction of methane (2 scfh) and ammonia (1 scfh).

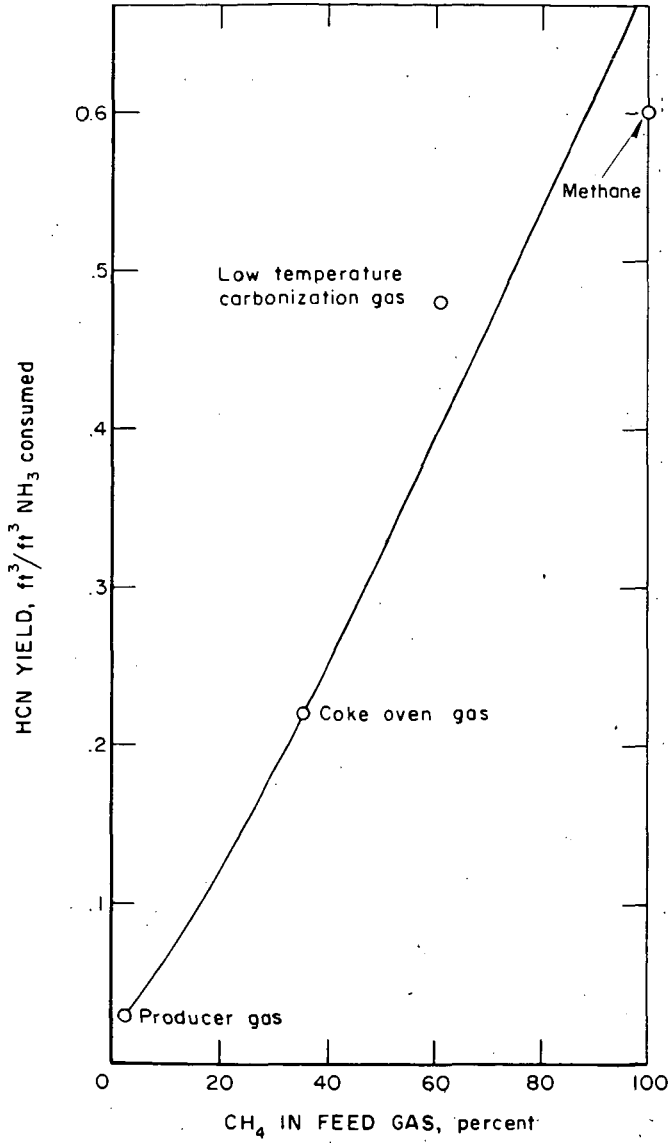


Figure 6. Variance of hydrogen cyanide yield with methane content of feed gas in reaction with ammonia at 1,250° C.

## MÖSSBAUER SPECTROSCOPY OF IRON IN COAL

John F. Lefelhocz\*, Robert A. Friedel<sup>†</sup>, and Truman P. Kohman\*

\*Department of Chemistry, Carnegie Institute of Technology  
 †Pittsburgh Coal Research Center, Bureau of Mines, U.S. Department of the Interior  
 Pittsburgh, Pennsylvania 15213

## INTRODUCTION

Metallic elements (Na, Mg, Al, Si, K, Ca, Ti, Fe) which occur abundantly in the ash obtained from the combustion of coals are present in the original coals partly as inorganic constituents or minerals. The identification of minerals present usually does not account quantitatively for several of these elements, and it is supposed that some sort of organic bonding with the coal is involved. The nature of this bonding in most coals has not been determined. Changes in the infra-red spectra of lignites and brown coals following acid and alkali treatment indicate the presence of metallic salts of carboxylic acids (1,2,3). For higher rank coals, little or nothing is known about the structures of the metallic elements "organically bound". In the case of iron, for example, it has not been determined whether the so-called "organic" iron is in the ferrous or ferric state, to what element or elements the iron is bonded, or whether there is more than one form of "organic" iron. The term "organic" must be interpreted with care; the nature of the bonding is uncertain; and presumably could be ionic, coordinate, or organo-metallic.

Mineral components containing iron can often be identified petrographically. Pyrite ( $\text{FeS}_2$ ) is common, both as distinct nodules and as veins, often intertwined with carbonaceous macerals. An electron microprobe study of several coals (4) revealed, however, many examples which lacked a correlation between Fe and S distributions. In some cases Fe was distinctly associated with Si and Al, suggesting incorporation in an aluminosilicate gel or kaolinite. A strong parallelism of Fe and Ca (but not Si, Al, K, or S) in one specimen suggested the presence of Fe as carbonate or possibly oxide. In some cases the Fe showed fairly uniform distribution with no apparent correlation with other ash-forming elements. This presumably could be "organic" iron.

Mössbauer spectroscopy has been employed to study the chemical properties of iron in a great variety of natural materials: oxides and oxyhydroxides (5,6), sulfides (7,8), numerous silicate minerals (5,6,9,10,11,12), ilmenite and related titanium minerals (5,13), siderite (6), jarosites (5,14), löllingite (15), ordinary chondrite meteorites (16), carbonaceous chondrites (17), an achondrite (16), and several tektites (11).

Recent general articles on Mössbauer spectroscopy (18,19,20,21,22) discuss the interpretation of spectra in terms of the chemical state of iron, including its oxidation state, bonding, and environmental symmetry. The isomer shift ( $\delta$ ), quadrupole splitting ( $\Delta$ ), line width ( $\Gamma$ ), line intensities, and a comparison of the spectra obtained at room temperature and at liquid- $\text{N}_2$  temperature are useful.

We have undertaken Mössbauer studies to characterize non-mineral iron in

coal. A major advantage of the Mössbauer technique is that the iron is observed without altering its chemical state or environment. The relatively low atomic number of the major elements present makes it possible for small amounts of iron to be observed in rather large amounts of coal. Samples of whole coal and vitrain as free as possible from minerals were selected in order to minimize mineral-iron interference, and a few samples whose chemical analysis indicated "organic" iron were included.

#### EXPERIMENTAL PROCEDURES

Nine specimens, vitrain or whole-coal, of seven coals with rank from lignite (72% C) to anthracite (95% C) were used. Their designations and geographic origins are given in Table 1, in order of increasing carbon content.

Table 2 is a compilation of the analytical data for C, H, N, S, Fe, ash, and O (by difference) on samples of these materials, as determined by the Coal Analysis group at the Bureau of Mines. The total iron in the coal was determined by ash analysis. HCl-soluble iron was determined by treating a separate powdered sample with 25% HCl to extract any iron present as carbonates, oxides, sulfates, etc. Pyrite iron was then removed by treating the HCl-leached coal with 25% HNO<sub>3</sub> to dissolve the iron combined with sulfur; the extract was evaporated to dryness to expel oxides of nitrogen, and the residue was dissolved in HCl. In each case the iron was reduced with SnCl<sub>2</sub>, the slight excess of which was eliminated with HgCl<sub>2</sub>. The reduced iron was titrated with potassium dichromate. "Organic" iron was then calculated by subtracting the two acid-soluble iron contents from the total iron. The resulting iron contents are listed in Table 2 as: total, HCl-soluble, pyrite, and "organic".

Mössbauer spectra were obtained on coal samples that were ground in a mortar and pestle. A cylindrical cell, open on one end with a circular aperture of 7.14 cm<sup>2</sup>, was made by gluing a sheet of lucite 1/32" thick with Duco cement to the bottom of a circular wall made from a paper card. A 3.50-g sample was then placed into this cell. The top window, also 1/32" lucite, was then cemented in place. The sample mass per unit area was thus held constant at 0.490 g cm<sup>-2</sup>. Inorganic iron compounds and mineral samples were ground and mounted either between two lucite sheets held together with Duco cement, or by mixing the solid with acetone and Duco cement and allowing this mixture to harden on a lucite sheet. This latter method was used only when the sample would not interact with acetone or the cement. The area for these samples was also 7.14 cm<sup>2</sup>. All of the materials used in this investigation contained natural iron with presumably 2.19 atom % Fe<sup>57</sup>.

The Mössbauer spectrometer incorporates a Nuclear Science and Engineering Corporation Model-B lathe-type drive modified in this laboratory for automatic operation. The operating mode employs constant velocity, advanced in increments of 0.05 mm s<sup>-1</sup>. The detector of the 14.4-keV Co<sup>57</sup> → Fe<sup>57</sup> gamma radiation is a Reuter-Stokes proportional tube containing 10% methane in krypton, feeding through a single-channel analyzer set at 11 - 17 keV. Absorbers were mounted on the moveable table perpendicular to the radiation beam. The stationary source consists of ~ 5 mCi of Co<sup>57</sup> diffused into chromium metal. A Baird-Atomic scanning count integrator and Varian chart recorder plot the number of counts in a constant time interval at each velocity in succession.

Powdered samples of sodium nitroprusside gave an isomer shift, relative to the Co<sup>57</sup>-Cr source, of -0.11 mm s<sup>-1</sup>, and a quadrupole splitting of 1.68 mm s<sup>-1</sup>. With this source a line width of 0.25 mm s<sup>-1</sup> was observed with an absorber containing 5 mg cm<sup>-2</sup> of Fe as K<sub>4</sub>Fe(CN)<sub>6</sub>·3H<sub>2</sub>O. The estimated uncertainty in the velocity setting is about 2% of the velocity and the estimated uncertainty in derived spectral parameters is ~ 0.05 mm s<sup>-1</sup>. The counting time at each velocity was ~ 5

Table 1. Designations, geographic origins, and adjusted\* carbon contents of coal samples used.

Code #	Designation†	Geographic Origin	Mass fraction C* (%)
A	Indian Head lignite	Zap Bed, Indian Head Mine, N. Dakota	72.2
B	Harmatten vitrain, hvcb	No. 7 Bed, Harmatten Mine, Illinois	76.5
C	Corbin coal, hvab	High Splint Bed, Lynch Mine, Corbin Plant, Ky.	84.3
D	Bruceston vitrain, hvab	Pittsburgh Bed, Bruceston Mine, Pa.	84.2
E	Bruceston coal, hvab	Pittsburgh Bed, Bruceston Mine, Pa.	84.7
F	Jewell Valley coal, mvb	Jewell Bed, Jewell Valley Coal Co., Va.	90.3
G	Pocahontas No. 4 vitrain, lvb	Pocahontas No. 4 Bed, McAlpine No. 2 Mine, W.Va.	90.3
H	Pocahontas No. 4 coal, lvb	Pocahontas No. 4 Bed, McAlpine No. 2 Mine, W.Va.	90.4
I	Dorrance anthracite vitrain	Dorrance Mine, Lehigh Valley Coal Co., Pa.	92.7

\* Adjusted to moisture- and ash-free basis. Calculated from C and ash contents of Table 2.

† h = high; m = medium; l = low; v = volatile; b = bituminous; a, c = sub-classifications of high-volatile coals.

Table 2. Analytical data on coal samples used.

Sample No.	Mass Fraction Fe (%) <sup>*</sup>			Mass fraction (moisture-free basis) (%) <sup>†</sup>						
	Total	HCl-sol.	Pyrite	"Organic" <sup>†</sup>	Ash	C	H	N	S	O <sup>†</sup>
A (a)	0.13	-	-	-	5.6	68.2	4.6	0.6	0.6	20.2
B (a)	0.81	0.40	0.27	0.14	1.0	75.8	5.3	1.3	1.8	14.8
C (a)	0.23	0.06 <sup>§</sup>		0.17	3.8	81.1	5.3	1.6	0.5	7.7
D (a)	0.62	-	0.33	(0.29) <sup>#</sup>	1.4	83.0	5.4	1.6	0.8	7.8
(b)	0.33	0.02	0.21	0.11						
E (a)	4.18	-	3.85	(0.33) <sup>#</sup>	1.9	83.1	5.6	1.6	0.7	7.1
(b)	0.32	0.06	0.20	0.06						
F (a)	1.39	0.24 <sup>§</sup>		1.16	1.8	88.7	4.6	1.4	0.5	3.0
(b)	0.47	0.37	0.08	0.02						
G (a)	0.46	0.03	0.00	0.44	1.2	89.2	4.6	1.5	0.8	2.7
H (a)	0.43	0.15	0.00	0.28	2.6	88.1	4.3	1.3	0.6	3.1
(b)	0.39	0.21	0.04	0.14						
I (a)	0.41	0.00	0.03	0.38	1.8	91.0	2.5	1.0	0.8	2.9
(b)	0.57	0.11	0.20	0.26						

<sup>†</sup> By difference.

<sup>\*</sup> In sample as received, before drying.

<sup>§</sup> Includes both HCl-soluble and pyrite iron.

<sup>#</sup> Includes both "organic" and HCl-soluble iron.

<sup>†</sup> Determined on samples other than those used for Mössbauer and iron determinations.

minutes, yielding ~ 600,000 counts and a relative standard deviation < 0.15%. The velocity region scanned for each sample was from  $-2.00 \text{ mm s}^{-1}$  to about  $+4.00 \text{ mm s}^{-1}$ .

Most measurements were made a room temperature. A cryostat made from styrofoam was mounted on the moveable table of the instrument for low-temperature measurements. The sample was placed in this and submerged in liquid  $\text{N}_2$ . The spectrum of each coal sample was run twice at room temperature, before and after the spectrum was taken at liquid- $\text{N}_2$  temperature.

Spectral parameters were generally read from plotted spectra. The data from sample F(a) were fitted to a double Lorentz curve by a least-squares program using an IBM 7040 computer. Isomer shifts are reported (in  $\text{mm s}^{-1}$ ) with respect to the isomer shift of sodium nitroprusside. Quadrupole splittings are reported (in  $\text{mm s}^{-1}$ ) as the velocity differences between the minima of two associated absorption lines.

#### DATA

Room-temperature spectra for the nine coal samples are illustrated in Figure 1. Each spectrum shows neither, either, or both of just two components: (1) a close doublet similar to those of pyrite and marcasite, and (2) a wide doublet similar to those of many ferrous compounds. Table 3 lists the Mössbauer parameters, including the fractional peak absorptions, for what we will call respectively the pyrite and non-pyrite resonances. Isomer shifts and quadrupole splittings obtained with our instrument on some powdered iron compounds and minerals which were regarded as possibilities for the non-pyrite spectrum appear in Table 4.

The parameters observed for the pyrite iron are: isomer shift ( $\delta$ ) =  $+0.54 \text{ mm s}^{-1}$ ; quadrupole splitting ( $\Delta$ ) =  $0.58 \text{ mm s}^{-1}$ . All of the coals having a non-pyrite absorption as shown in Figure 1 have:  $\delta = +1.38 \text{ mm s}^{-1}$ ;  $\Delta = 2.62 \text{ mm s}^{-1}$ . The computer analysis of sample F(a) indicated both lines in the spectrum had widths ( $\Gamma$ ) of  $0.39 \text{ mm s}^{-1}$ ; their intensity ratio is within 5% of unity.

Liquid- $\text{N}_2$  spectra showed the same absorption peaks as at room temperature, with  $\delta = +0.65 \text{ mm s}^{-1}$  and  $\Delta = 0.58 \text{ mm s}^{-1}$  for pyrite and  $\delta = +1.47 \text{ mm s}^{-1}$  and  $\Delta = 2.78 \text{ mm s}^{-1}$  for the non-pyrite iron.

#### INTERPRETATION

The isomer shift is a function of nuclear properties and the electron density at the absorbing nucleus relative to that of the source or a standard absorber, such as sodium nitroprusside (23,24). As the electron density at the iron nucleus, due essentially only to s electrons, increases, the isomer shift decreases algebraically. Thus, ferrous compounds have a more positive isomer shift than ferric compounds, as the additional 3d electron of the former increases the shielding effect on the 3s electrons and thereby decreases their density at the nucleus (18). For ferric iron, isomer shifts (relative to sodium nitroprusside) have been observed in the range  $-0.1$  to  $+1.1 \text{ mm s}^{-1}$ , and for ferrous iron from  $-0.1$  to  $+1.6 \text{ mm s}^{-1}$ .

Quadrupole splitting into a two-line spectrum occurs when the iron nucleus is in an asymmetric electric field. The field consists of two parts, (1) that produced by the electrons of the iron atom, including those shared with adjacent atoms, and (2) that resulting from charges of the surrounding atoms; each part can contribute to asymmetry at the nucleus. Ferric compounds show quadrupole splittings from zero to about  $2.3 \text{ mm s}^{-1}$ ; here the asymmetry is caused chiefly by charges of the surrounding atoms. Ferrous compounds show larger values, from zero to  $\sim 3.3 \text{ mm s}^{-1}$ . Ferrous iron can exist in either a high-spin or a low-spin

Table 3. Room-temperature Mössbauer spectral parameters for coal samples\*

Sample No.	Pyrite iron <sup>2+</sup>			Non-Pyrite iron		
	Isomer shift <sup>†</sup> (mm s <sup>-1</sup> )	Quadrupole splitting (mm s <sup>-1</sup> )	Fractional absorption (%)	Isomer shift <sup>†</sup> (mm s <sup>-1</sup> )	Quadrupole splitting (mm s <sup>-1</sup> ) <sup>‡</sup>	Fractional absorption (%)
A (a)	-	-	N.O.†	-	-	N.O.†
B (a)	0.59	0.55	1.6	-	-	N.O.
C (a)	-	-	N.O.	1.39	2.65	2.3
(b)	-	-	N.O.	1.30	2.65	2.1
D (a)	0.51	0.55	3.6	-	-	N.O.
(b)	0.53	0.48	3.6	-	-	N.O.
E (a)	0.50	0.58	22.7	1.41	2.70	2.6
(b)	0.50 <sub>±</sub>	0.53	2.3	-	-	N.O.
(c)	0.50	0.53	1.7	-	-	N.O.
F (a)	-	-	N.O.	1.38	2.62	11.0
(b)	-	-	N.O.	1.39	2.65	5.5
G (a)	-	-	N.O.	1.38	2.65	1.5
(b)	-	-	N.O.	1.38	2.65	1.0
H (a)	0.54	0.60	1.3	1.39	2.65	1.5
(b)	0.59	0.60	1.7	1.36	2.60	1.7
I (a)	-	-	N.O.	-	-	N.O.
(b)	0.56	0.65	1.0	-	-	N.O.

\* Weighing 3.50 g and distributed evenly over 7.14 cm<sup>2</sup>.

‡ May include marcasite.

† With respect to center of sodium nitroprusside spectrum.

‡ Zero-point uncertain by 0.10 mm s<sup>-1</sup>.

† N.O. = not observed; in general, < 0.5%.

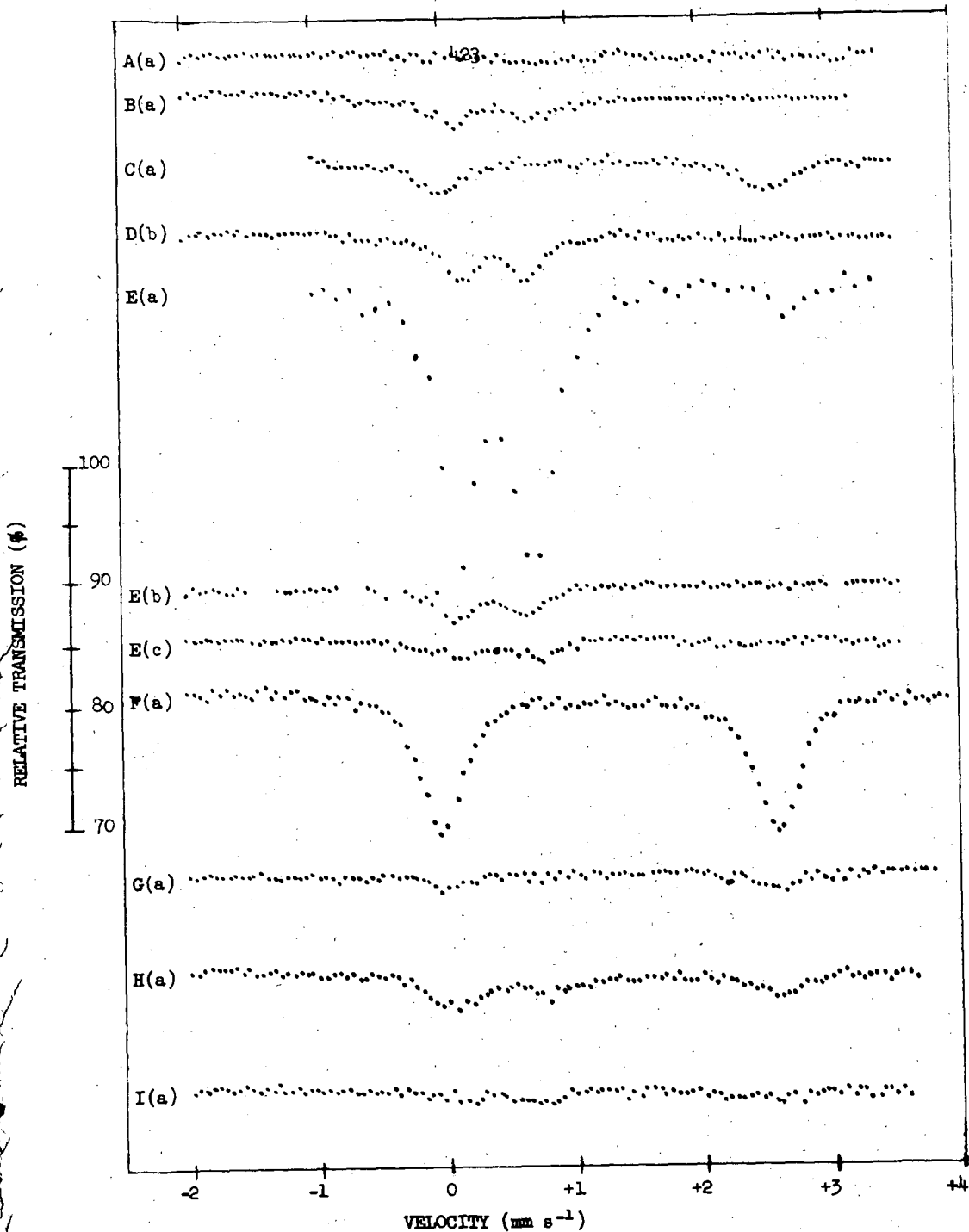


Figure 1. Mössbauer spectra of coal samples. In most cases, each point represents ~ 600,000 counts. The source was  $\text{Co}^{57}$  diffused into chromium metal. To convert the velocity scale to the sodium nitroprusside scale, add  $0.11 \text{ mm s}^{-1}$  to the indicated values.

state, depending on the strength of the ligand field around the central iron atom. In the high-spin configuration the large asymmetry of the valence shell results in considerable asymmetry at the nucleus; low-spin ferrous compounds have smaller field asymmetries, which are due chiefly to the external environments only.

Pyrite and marcasite, respectively stable and metastable forms of  $\text{FeS}_2$ , are low-spin ferrous compounds. Isomer shifts and quadrupole splittings observed in this laboratory (Table 4) are in agreement with those of Temperley and Lefevre (8). The parameters of the two minerals are so similar that the spectra cannot be resolved when both are present. A comparison of the data in Tables 3 and 4 confirms the conclusions from petrographic (25) and x-ray diffraction (26) studies that the iron sulfide in coal consists mainly of pyrite.

From the Mössbauer data on the non-pyrite iron observed in several coal samples (Figure 1 and Table 3), it can safely be concluded that this iron is in a high-spin ferrous state. Furthermore, the combination of such high values of both isomer shift and quadrupole splitting has been reported only in octahedrally-coordinated high-spin ferrous compounds, so it is highly probable that the non-pyrite iron in coals is in octahedral coordination. Neither the analytical nor the Mössbauer data yields a distinction between inorganic or organic minerals or compounds.

The natural line width ( $\Gamma_0$ ) of the  $\text{Fe}^{57}$  gamma radiation corresponds to a velocity difference of  $0.0973 \text{ mm s}^{-1}$  (27), and the minimum observable line width ( $\Gamma$ ) in a Mössbauer spectrum is twice this,  $0.195 \text{ mm s}^{-1}$ . Inhomogeneities in the source and absorber, instrumental "noise", unresolved quadrupole splitting, and atomic spin-spin relaxation effects (22,28,29) increase the apparent line widths, and further widening occurs with thick absorbers (30). The minimum width we have observed with our instrument is  $0.25 \text{ mm s}^{-1}$  for a very thin absorber. The value of  $\Gamma = 0.39 \text{ mm s}^{-1}$  observed for the strongest non-pyrite iron spectrum (sample F(a)) indicates that this doublet is caused by a fairly well-defined iron compound or mineral, though some inhomogeneity may be present.

A large number of iron compounds have strong Mössbauer absorptions (large recoil-free fractions) at room temperature. Some ferrous compounds show little or no absorption at room temperature, but at liquid- $\text{N}_2$  temperature the intensity is strongly enhanced (31,32). We have observed this effect with ferrous stearate, which must be cooled to liquid- $\text{N}_2$  temperature before resonant absorption is detected. Herzenberg and Toms (5) have observed that samples of  $\gamma\text{-Fe}_2\text{O}_3$  and  $\delta\text{-FeOOH}$  give nonresonant absorption at room temperature. These would probably exhibit an effect at liquid- $\text{N}_2$  temperature. Lack of such an effect in the coals is interpreted to mean that there are no compounds present in significant amounts that do not have appreciable resonant absorption at room temperature.

Isomer shifts and quadrupole splittings depend on the temperature. A second-order Doppler effect (22) decreases the isomer shift as the temperature is increased. Quadrupole splittings for high-spin ferrous compounds are affected by temperature much more strongly than those of other iron compounds because the population of the  $d_{\sigma}$  levels of iron in an octahedral field is determined by a Boltzmann distribution (18,22). For example,  $\text{FeSO}_4 \cdot 7\text{H}_2\text{O}$  shows a change of  $\delta$  from  $+1.53$  to  $+1.56 \text{ mm s}^{-1}$  and of  $\Delta$  from  $3.19$  to  $3.47 \text{ mm s}^{-1}$  in going from room to liquid-nitrogen temperature (18). The observed change in the non-pyrite iron spectrum in coal of  $\delta$  from  $+1.38$  to  $+1.47 \text{ mm s}^{-1}$  and of  $\Delta$  from  $2.62$  to  $2.78 \text{ mm s}^{-1}$  is in agreement with our assignment to this class of compounds.

In some iron compounds where the Mössbauer absorption ordinarily shows a 6-line hyperfine structure as a result of a magnetic field at the nucleus, very

finely comminuted samples show instead a two-line pattern at room temperature as a result of thermal disruption of the macroscopic magnetic domains. Kündig et al. (33) observed this effect in  $\alpha\text{-Fe}_2\text{O}_3$  in particles of  $\sim 50\text{-\AA}$  diameter, but at liquid- $\text{N}_2$  temperature the 6-line pattern was observed. The absence of any magnetic splitting in the coal spectra at room- or liquid- $\text{N}_2$  temperatures probably rules out the possibility that the non-pyrite doublet is caused by a magnetically ordered material (such as  $\text{Fe}_2\text{O}_3$ ,  $\text{Fe}_3\text{O}_4$ ,  $\text{FeC}_3$ ,  $\text{FeS}$ , or metal) present as very small particles.

Inequality in the intensity of the components of a doublet may result from the anisotropy of the absorption cross section relative to the crystal axes when (1) a single-crystal absorber is oriented preferentially with respect to the optical axis, or (2) there is anisotropy in the recoilless fraction of the split  $3/2$  state; the latter condition results in unequal absorption even with powdered samples (Goldanskii effect) (20,21). Most of the samples used in this work were powdered, so only the second effect could be operative, except for biotite, which was mounted as a sheet. The essential equality of intensity of the two non-pyrite coal spectrum lines would eliminate any compounds showing unequal absorption in powdered samples as possible causes of this absorption.

At the present state of Mössbauer spectroscopy, the identification of an unknown compound from its spectrum can only be made by finding a known compound having the same spectrum and temperature dependence. We have been unable to find any published combination of spectral parameters, for either natural or synthetic iron compounds, which match that of the non-pyrite iron in coal. Ankerite (Table 4), which has not been reported previously, likewise does not match.

In Figures 2 and 3 we have plotted  $\Delta$  versus  $\delta$  for all single- or two-line iron spectra for which we have been able to obtain data (5,6,8,9,10,11,14,18,31,34,35,36,37,38,39,40). Attention is called to the variations in  $\delta$  and  $\Delta$  within isomorphous silicate series (olivines, pyroxenes) in which the Fe/Mg ratio varies. Many silicate minerals show two or more coupled Mössbauer doublets, eliminating from consideration many points near the coal point on the plots. Biotite gives an apparent 2-line spectrum with  $\delta$  and  $\Delta$  similar to the coal spectrum, but with decidedly unequal intensities (our measurement), which persist in powdered samples (6), and which can be resolved into a coupled doublet (9), whereas the coal spectrum is symmetrical. Even considering the compositional variations and the uncertainties of measurement, it is apparent that the non-pyrite iron in coal is distinct from any compound whose Mössbauer spectrum is known. Minerals excluded include oxides and oxyhydroxides, sulfides and related compounds, the carbonates siderite and ankerite, titanian minerals, and the many silicates examined.

Some ferrous complexes of pyridines (35) and 1,10-phenanthrolines (37) have similar though non-matching  $\delta$  and  $\Delta$  values. These comparisons suggest that the non-pyrite iron could be bound to heterocyclic nitrogen aromatic groups in the coal macerals, or possibly in a clay-like silicate mineral or gel.

An attempt was made to correlate the Mössbauer absorption intensities in the coals with the analytical data. Mössbauer spectra were determined on mixtures of pyrite in carbon, and the fractional peak absorption was plotted against the mass fraction of pyrite iron. In a few coal samples the Mössbauer absorption and the analytically determined amount of iron as "pyrite" did agree with the above plot, but in others the agreement was poor. This may be due to the inadequacy of the chemical method for determining pyrite iron, and to differing matrix effects in the coals and the standards. Likewise, a poor correlation was found between the non-pyrite iron absorption in coals and the amount of "organic" iron deduced from the chemical analyses, although the sample with the highest "organic" iron, Jewell Valley coal F(a), showed the strongest non-pyrite Mössbauer spectrum.

Table 4. Room-temperature isomer shifts and quadrupole splittings for polycrystalline iron compounds and minerals

Compound or Mineral	This Work		Other Work		Ref.
	$\delta^*\S$	$\Delta\S$	$\delta^*\S$	$\Delta\S$	
Pyrite, $\text{FeS}_2$	0.54	0.60	0.55	0.61	8
Marcasite, $\text{FeS}_2$	0.51	0.50	0.52	0.51	8
Siderite, $(\text{Fe},\text{Mg})\text{CO}_3$	1.47	1.78	1.47	1.80	6
Ankerite, $(\text{Ca},\text{Mg},\text{Fe})\text{CO}_3$	1.46	1.50	-	-	-
Olivine, $(\text{Mg},\text{Fe})_2\text{SiO}_4$	1.39	2.95	1.39	3.04	10
Biotite, $\text{K}(\text{Mg},\text{Fe})_3(\text{AlSi}_3\text{O}_{10})(\text{OH})_2$	1.36	2.50	1.27 1.46	2.41 2.81	9
Tourmaline, $\text{Na}(\text{Mg},\text{Fe})_3\text{Al}_6(\text{BO}_3)_3(\text{Si}_6\text{O}_{18})(\text{OH})_4$	1.30	2.38	$\text{Fe}^{+2}$ 1.19 $\text{Fe}^{+2}$ 1.44 $\text{Fe}^{+3}$ 0.99	2.10 2.61 0.91	10
Ferrous sulfate, $\text{FeSO}_4 \cdot 7\text{H}_2\text{O}$	1.56	3.05	1.53	3.19	18
Ferrous acetate, $\text{Fe}(\text{C}_2\text{H}_3\text{O}_2)_2$	1.45	2.23	-	-	-
Ferrous stearate, $\text{Fe}(\text{C}_{18}\text{H}_{35}\text{O}_2)_2$	0.66†	0.70†	-	-	-
Non-pyrite iron in coal	1.38	2.62	-	-	-

\* Respect to center of sodium nitroprusside spectrum.

† At liquid nitrogen temperature; no resonant absorption observed at room temperature.

§ In  $\text{mm s}^{-1}$ .

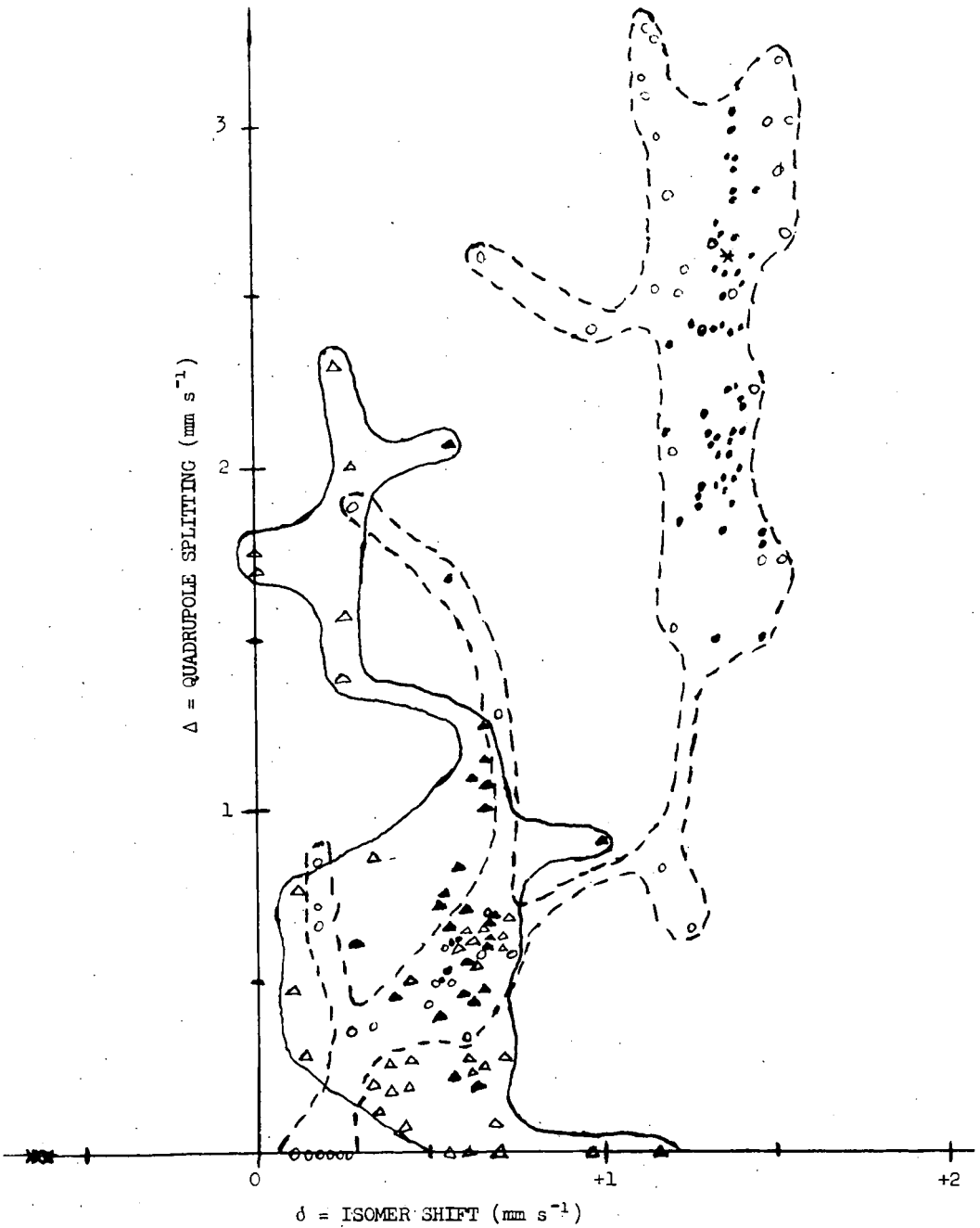


Figure 2. Representative plot of quadrupole splitting versus isomer shift (relative to sodium nitroprusside) for: — ferric compounds ( $\Delta$ ) and minerals ( $\blacktriangle$ ); ---- ferrous compounds ( $\circ$ ) and minerals ( $\bullet$ ); ferrate compounds ( $\times$ ), and the non-pyrite iron found in coal (\*).

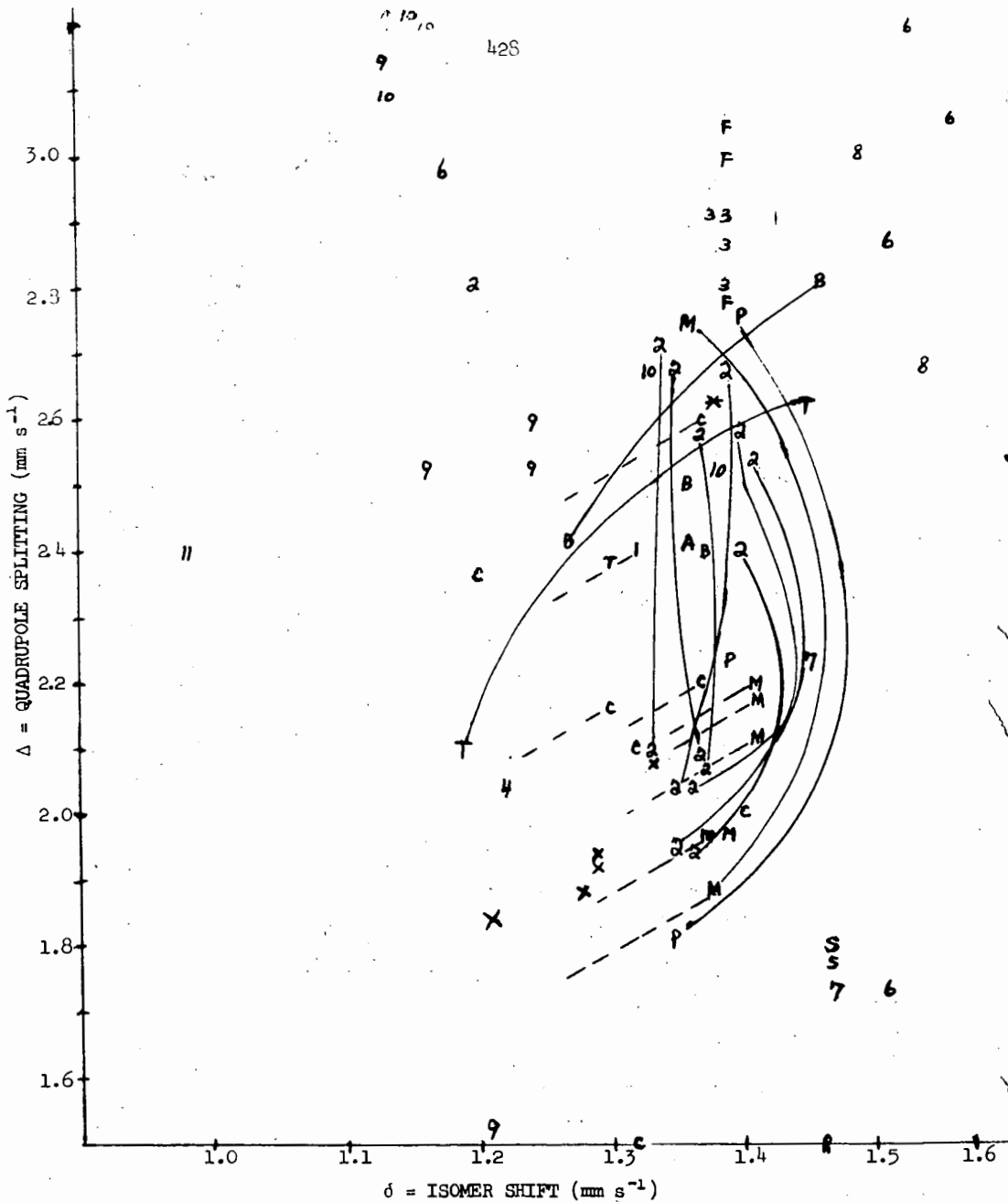


Figure 3. Enlarged section of Figure 2, showing quadrupole splitting versus isomer shift relative to sodium nitroprusside for two-line ferrous spectra. Lines connect pairs of points which are observed together in the same mineral or compound. Dashed lines indicate that a ferric spectrum is associated with the plotted ferrous point. Synthetic compounds: 1-ferrianite (synthetic mica), 2-synthetic pyroxenes, 3-synthetic olivines, 4-welding glass 5-germanium spinel, 6-oxy-salts, 7-carboxylates, 8-halides, 9-pyridine complexes, 10-phenanthroline complexes, 11-ferrous hemoglobin. Natural materials: A-actinolite, B-biotite, C-clay minerals, F-fayalite and olivine, M-clinopyroxenes, P-orthopyroxenes, R-ankerite, S-siderite, T-tourmaline, X-tektites, \*-non-pyrite iron in coal.

## CONCLUSION

In summary, several coal samples contain a form of iron which exhibits a hitherto unobserved Mössbauer spectrum, in addition to the well-known pyrite spectrum. The non-pyrite iron is ferrous, in a high-spin configuration, in octahedral symmetry, and apparently in a rather well-defined state. Comparisons with known compounds suggest that this iron may be bound in the coal macerals to heterocyclic nitrogen aromatic groups, though a clay-like silicate mineral or gel is a possibility. Mössbauer spectrometry can at the very least indicate the most suitable coal samples for further studies of this iron by chemical and other methods. It should ultimately permit unambiguous identification of the iron in coal with synthetic compounds or analogs. We intend to pursue this line of investigation.

## ACKNOWLEDGEMENTS

We wish to thank Drs. Maurice Deul and Bryan C. Parks of the Bureau of Mines for their assistance in obtaining some of the coal samples. We are especially indebted to Mr. Michael Toia for the construction and maintenance of the Mössbauer spectrometer. The work at Carnegie Institute of Technology was performed under the auspices of the U.S. Atomic Energy Commission under contract AT(30-1)-844; Report No. NYO-844-69.

## REFERENCES

- (1) Brooks J.D. and Sternhell S. (1957) Brown coals. I. Oxygen containing functional groups in Victorian brown coals. Australian J. Appl. Sci. **8**, 206-221.
- (2) Brooks J.D., Durie R.A. and Sternhell S. (1958) Chemistry of brown coals. II. Infrared spectroscopic studies. Australian J. Appl. Sci. **9**, 63-80.
- (3) Elofson R.M. (1957) Infrared spectra of humic acids and related materials. Can. J. Chem. **35**, 926-931.
- (4) Dutcher R.R., White E.W. and Spackman W. (1964) Elemental ash distribution in coal components--Use of the electron probe. Proc. 22nd Ironmaking Conf., Iron and Steel Div., Metallurgical Soc. of A.I.M.M.E., 463-483.
- (5) Herzenberg C.L. and Toms D. (1966) Mössbauer absorption measurements in iron-containing minerals. J. Geophys. Res. **71**, 2661-2677.
- (6) Pecull T.E. (1966) Thesis Georgia Institute of Technology, A study of iron in clay minerals using Mössbauer spectroscopy; Pecull T.E., Wampler J.M. and Weaver C.E. (1966) Mössbauer analysis of iron in clay minerals. Abstracts, 15th Ann. Clay Min. Conf. (Pittsburgh, Oct. 1966), 32-3.
- (7) Hafner S. and Kalvius M. (1965) Mössbauer studies of FeS minerals with the NiAs-type structures. Abstract DJ5, Bull. Am. Phys. Soc. (II) **10**, 1112.
- (8) Temperley A.A. and Lefevre H.W. (1966) The Mössbauer effect in marcasite structure iron compounds. J. Phys. Chem. Solids **27**, 85-92.
- (9) Pollak H., deCoster M. and Amelinckx S. (1962) Mössbauer effect in biotite. Phys. Stat. Sol. **2**, 1653-1659.
- (10) deCoster M., Pollak H. and Amelinckx S. (1963) A study of Mössbauer absorption in iron silicates. Phys. Stat. Sol. **3**, 283-288.
- (11) Marzolf J.G., Dehn J.T. and Salmon J.F. (1966) The study of oxidation states and ordering phenomena in tektites and iron bearing silicates using the Mössbauer effect. Symposium on the Mössbauer Effect sponsored by Nuclear Science and Engineering Corporation (New York, Sep. 1966).
- (12) Whitfield H.J. and Freeman A.G. (1966) Mössbauer studies of amphiboles. Abstracts, International Conference on Hyperfine Nuclear Spectroscopy at Victoria University (Wellington, Oct. 1966).
- (13) Avrahami M. and Golding R.M. (1966) Mössbauer spectroscopy as a tool in analytical chemistry. Abstracts, International Conference on Hyperfine Nuclear Spectroscopy at Victoria University (Wellington, Oct. 1966).
- (14) Hryniewicz A.Z., Kubisz J. and Kulgawczuk D.S. (1965) Quadrupole splitting of the 14.4-keV gamma line of  $^{57}\text{Fe}$  in iron sulphates of the jarosite group. J. Inorg. Nucl. Chem. **27**, 2513-2517.
- (15) Imbert P., Gerard A. and Wintenberger M. (1963) Étude des sulfure, arséniosulfure et arsénure de fer naturels par effet Mossbauer. Compt. Rend. Paris **256**, 4391-4393.

- 5) Sprenkel-Segel E.L. and Hanna S.S. (1964) Mössbauer analysis of iron in stone meteorites. Geochim. Cosmochim. Acta 28, 1913-1931.
- 6) Gerard A. and Delmelle M. (1964) Effet Mössbauer et caractère ionique des atomes de fer dans les météorites Orgueil et Cold Bokkweid. Compt. Rend. Paris 252, 1756-1759.
- 7) Fluck E., Kerler W. and Neuwirth W. (1963) The Mössbauer effect and its significance in chemistry. Angew. Chem. Internat. Ed. 2, 277-287.
- 8) Wertheim G.K. (1964) Mössbauer Effect, Principles and Applications. Academic Press, Inc., New York.
- 9) Goldanskii V.I. (1964) The Mössbauer Effect and its Applications in Chemistry. Consultants Bureau, New York.
- 10) Herber R.H. (1965) Introduction to Mössbauer spectroscopy. J. Chem. Educ. 42, 130-137.
- 11) DeBenedetti S., Barros F. deS. and Hoy G.R. (1966) Chemical and structural effects on nuclear radiations. Ann. Rev. Nucl. Sci. 16, 31-83.
- 12) Herber R.H. and Hayter R.G. (1964) Mössbauer effect in cis-trans isomers. J. Am. Chem. Soc. 86, 301-302.
- 13) Spijkerman J.J., Ruegg F.C. and DeVoe J.R. (1965) Standardization of the differential chemical shift for Fe<sup>57</sup>, Mössbauer Effect Methodology, pp. 115-120. Plenum Press, New York.
- 14) Thiessen G. (1945) Chemistry of Coal Utilization (Ed. H.H. Lowery), Vol. 1. John Wiley, New York.
- 15) Mitra G.B. (1954) Identification of inorganic impurities in coal by the X-ray diffraction method. Fuel 33, 316-330.
- 16) Eckhause M., Harris R.J., Shuler W.B. and Welsh R.E. (1966) Measurement of the lifetime of the 14.4-keV level of <sup>57</sup>Fe. Proc. Phys. Soc. London 89, 137-138.
- 17) Obenshain F.E., Roberts L.D., Coleman C.F., Forester D.W. and Thomson J.O. (1965) Hyperfine structure of the 14.4-keV  $\gamma$ -ray of <sup>57</sup>Fe in hydrated ferric ammonium sulfate as a function of the magnetization of the salt. Phys. Rev. Lett. 14, 365-369.
- 18) Wignall J.W.G. (1966) Mössbauer line broadening in trivalent iron compounds. J. Chem. Phys. 44, 2462-2467.
- 19) Margulies S. and Ehrman J.R. (1961) Transmission and line broadening of resonance radiation incident on a resonance absorber. Nucl. Instr. Meth. 12, 131-137.
- 20) Epstein L.M. (1962) Mössbauer spectra of some iron complexes. J. Chem. Phys. 36, 2731-2737.

- (32) Gibb T.C. and Greenwood N.N. (1966) The Mössbauer spectrum of the tetrachloroferrate(II) ion. J. Chem. Soc. London, 6989-6991.
- (33) Kündig W. and Bömmel H. (1966) Some properties of supported small  $\alpha$ -Fe<sub>2</sub>O<sub>3</sub> particles determined with the Mössbauer effect. Phys. Rev. **142**, 327-333.
- (34) Muir A.H. Jr., Ando K.J. and Coogan H.M. (1965) Mössbauer Effect Data Index, Issue 5. North American Aviation Inc., Thousand Oaks, California.
- (35) Golding R.M., Mok K.F. and Duncan J.F. (1966) Magnetic susceptibility and Mössbauer results of some high-spin iron (II) compounds. Inorg. Chem. **5**, 774-775.
- (36) Duncan J.F. and Mok K.F. (1966) A Mössbauer study of iron (II)-1,10-phenanthroline-complexes. J. Chem. Soc. London, Sec. A, 1493-1496.
- (37) König E. and Madeja K. (1967)  $^{57}\text{T}_{2-1}\text{A}_1$  Equilibria in some iron (II)-bis(1, 10-phenanthroline) complexes. Inorg. Chem. **6**, 48-55.
- (38) Lang G. and Marshall W. (1966) Mössbauer effect in some haemoglobin compounds. Proc. Phys. Soc. London **87**, 3-34.
- (39) Mathur H.B., Sinha A.P.B. and Yagnik C.M. (1965) The Mössbauer spectra of spinel oxides containing ferrous ion. Solid State Commun. **3**, 401-403.
- (40) Frank E. and Abeledo C.R. (1966) Mössbauer effect in iron (III) dithiocarbamates. Inorg. Chem. **5**, 1453-1455.

REACTIONS OF COAL AND RELATED MATERIALS IN MICROWAVE DISCHARGES IN  $H_2$ ,  $H_2O$  AND Ar

Yuan C. Fu and Bernard D. Blaustein

U. S. Bureau of Mines, Pittsburgh Coal Research Center,  
4800 Forbes Avenue, Pittsburgh, Pennsylvania 15213

## INTRODUCTION

Recent investigations on the reaction of carbon in a high frequency discharge have shown that it produces methane, acetylene and minor amounts of other hydrocarbons in the hydrogen discharge,<sup>1-3/</sup> but produces primarily an  $H_2$ -CO mixture downstream from a water discharge.<sup>3/</sup> Similar work with respect to coal, however, is almost non-existent except that carried out by Letort et al.<sup>4/</sup> and by Pinchin.<sup>5/</sup> Though some work on coal in a plasma jet<sup>6-9/</sup> has been reported, the characteristic of those reactions is generally the thermal decomposition of coal by rapid heating to high temperatures in an inert atmosphere.

In a microwave-generated discharge, hydrogen or water vapor can be excited or dissociated into atoms, ions and electrons at temperatures much lower than those attained in a plasma jet. The present study is concerned with the reactions of various coals, a polynuclear hydrocarbon, and graphite, in microwave discharges in  $H_2$ , water vapor and Ar. The results are compared in terms of the product yield and distribution in each type of discharge. Differences observed between the reactions of the various coals and the other materials suggest that the amount and type of volatile material, carbon content, and the type of the carbonaceous material, as well as the type of the gas discharge, are all factors affecting the product yield and distribution. The difference between coal and graphite in their behavior toward water vapor in the microwave discharge is of particular interest. In the water discharge, the graphite yields almost no hydrocarbons but only an  $H_2 + CO$  mixture while the coal yields appreciable amounts of  $C_2H_2$  and  $CH_4$  in addition to  $H_2 + CO$ . Experiments using  $D_2O$  and Ar discharges indicate that the  $D_2O$  and the water actually do participate in the reactions with coal to form hydrocarbons. It is also demonstrated that the  $C_2H_2$  yield from coal in the hydrogen discharge can be drastically increased by condensing at a low temperature part of the primary products formed during the discharge reaction.

## ACKNOWLEDGEMENTS

The authors wish to thank Dr. Irving Wender for his valuable discussions, Gus Pantages for his technical assistance, A. G. Sharkey, Jr. and Janet Shultz for their mass spectrometric analyses, and John Queiser for his infrared analysis.

## EXPERIMENTAL

The experiments were carried out in a static system with the discharge produced by a Raytheon microwave generator in the air-cooled Ophthos coaxial cavity at 2450 Mc/sec. Chemical analyses and origins of the vitrains of the different coals used are given in table 1. All the vitrains were -200 mesh. Ultra purity spectroscopic graphite powder (325 mesh, United Carbon) and chrysene ( $C_{18}H_{12}$ ) were used for comparison. As reactant gases, a 9.7:1  $H_2$ -Ar mixture,  $H_2O$ -Ar mixtures and Ar were used. The  $H_2$  and Ar were obtained from cylinders and passed through a liquid  $N_2$  trap prior to storage. The water vapor was obtained from distilled water degassed in high vacuum.

In the experimental procedure, a known weight of graphite or coal powder was placed in a cylindrical Vycor tube (ID = 11 mm, vol = 32 ml) and degassed in a high vacuum at an elevated temperature (150°C for graphite and 100°C for coal) for a half to one hour to remove the moisture and the air adsorbed on the carbon. A known pressure of the reactant gas or gas mixture measured by a Pace Engineering pressure

transducer was then introduced into the reactor tube. For the H<sub>2</sub>-Ar mixture, a known pressure of the water vapor was first introduced to the reactor containing the degassed carbon, and then a known pressure of the argon was introduced while the water was condensed in the end of the tube by dry ice and acetone. The portion of the tube cooled by the dry ice was so small compared to the total volume that no correction on the pressure reading seemed to be necessary. The discharge was then produced with the carbon in the discharge zone. The gaseous products were analyzed by mass spectrometer.

The solid product obtained from the high volatile bituminous coal in the H<sub>2</sub> discharge was analyzed by infrared spectrometer. The sample was obtained either by scraping the reactor wall or by solvent (benzene or acetone) extraction. In some instances, a reactor consisting of a tube divided by a fritted Vycor disc was used. The coal was placed on the disc and KBr powder was introduced on the other side of the disc. During the discharge, the lower end of the tube was immersed in liquid N<sub>2</sub>, thus permitting the condensable low volatile products to pass through the disc and be adsorbed on the surface of the KBr powder. This was later removed, pressed into a pellet, and examined by infrared analysis.

TABLE 1. - Analysis of vitrains (moisture free basis, percent)

	C	H	N	S	O (by diff.)	Volatile matter	
Anthracite <sup>1/</sup>	91.06	2.49	0.96	0.83	2.89	1.77	6.1
Low volatile aminous <sup>2/</sup>	89.57	4.67	1.25	.81	2.17	1.53	20.2
bituminous <sup>3/</sup>	81.77	5.56	1.71	.97	5.87	2.06	39.2
Lignite <sup>4/</sup>	66.45	5.40	.31	1.40	22.84	3.06	44.0

<sup>1/</sup> Dorrance Mine, Lehigh Valley Coal Co., Luzerne County, Pennsylvania.

<sup>2/</sup> Pocahontas No. 3 Bed, Buckeye No. 3 Mine, Page Coal and Coke Co., Stephenson, Wyoming County, West Virginia.

<sup>3/</sup> Bruceton, Pittsburgh Bed, Allegheny County, Pennsylvania.

<sup>4/</sup> Beulah-Zap Bed, North Unit, Beulah Mine, Knife River Coal Mining Co., Beulah, Mercer County, North Dakota.

#### RESULTS AND DISCUSSION

All results were obtained from experiments using 5 mg of the carbonaceous material in each discharge at 35 watts of power input. For consistency, an initial total pressure of about 25 mm was used for most runs, but in the runs with H<sub>2</sub>O vapor it was varied in the range of 12 to 25 mm. The time of the discharge reaction was intended to be 60 seconds in most runs, but the discharge would not sustain itself in some runs. It is suspected that the solid product (probably polynuclear hydrocarbons) formed may tend to draw away the electrons in the discharge to form negative ions and create a shortage of energetic species in the gas phase. However, under the experimental conditions employed, a large part of the reaction occurred within 30-60 seconds, and prolonged treatment resulted only in some change in the product distribution and a little increase in the extent of the gasification. A few runs were made for as long as 3 minutes.

#### Hydrogen-Argon and Argon Discharges

In preliminary runs with graphite in an H<sub>2</sub> discharge, we attempted to interpret the data on the basis of the hydrogen balance before and after reaction. It appears, however, that appreciable amounts of hydrogen were consumed in the formation of solid product or were taken up by the carbon. Therefore, to allow

interpretation of the data, Ar was introduced into the reactant gas as an internal standard. The presence of Ar in the system gives no noticeable effect on product type or distribution.

Table 2 summarizes the results obtained from the reactions of each material in microwave discharges in an H<sub>2</sub>-Ar (9.7:1) mixture and in Ar. In the Ar discharge, coal is partially gasified to give H<sub>2</sub>, CO, and C<sub>2</sub>H<sub>2</sub> as the major gaseous products, CO<sub>2</sub>, CH<sub>4</sub>, and minor amounts of other hydrocarbons (C<sub>2</sub> and C<sub>3</sub> hydrocarbons, biacetylene and benzene were detected), in addition to a solid product and residual char. In the H<sub>2</sub>-Ar discharge, the percent of carbon forming gaseous hydrocarbons is increased as compared with the Ar discharge; the total amount of carbon gasified is also increased. In this discharge, C<sub>2</sub>H<sub>2</sub>, CO, and CH<sub>4</sub> are the main constituents of the gaseous product, and minor amounts of other hydrocarbons are also formed as in the Ar discharge. Comparison of the several 60-second runs indicated that the net amount of hydrogen remaining after the reaction was decreased, except for high volatile bituminous coal and lignite. Besides that converted to hydrocarbons, part of the hydrogen was probably consumed in the formation of solid product or was taken up by the coal residue. With high volatile bituminous coal and lignite, gasification was extensive and resulted in a net increase of hydrogen.

The percent of carbon converted to gaseous hydrocarbons increases with the volatile matter of coal as shown in figure 1, suggesting that a rapid release of the volatile matter and its subsequent gas phase reaction in a discharge may be the determining factors. Figure 1 includes the data for graphite. Lignite, with the highest volatile matter, however, gave only small amounts of hydrocarbons in both discharges. The high oxygen content of the lignite results in higher yields of carbon oxides and water but apparently inhibits hydrocarbon formation. Water vapor, in a discharge, can reverse the reactions of hydrocarbon formation by reacting with the hydrocarbon species to form carbon oxides and hydrogen.<sup>10/</sup>

Chrysene did not behave particularly different from coal in both discharges; the extent of gasification was appreciably small, approximately the same as that for anthracite. Interestingly, the carbon contents of the chrysene and the anthracite are also close to each other and are much higher than the other coals.

For coal in general, the higher the carbon content the lower the volatile matter. The extent of the reaction of graphite with H<sub>2</sub> was very much smaller under comparable conditions, probably due to the absence of volatile matter. The main products from graphite were CH<sub>4</sub> and C<sub>2</sub>H<sub>2</sub>; however, the hydrogen balance indicated, for example, that with an initial pressure of the H<sub>2</sub>-Ar mixture of 25 mm Hg, the percentage of the initial hydrogen present in each component of the product is H<sub>2</sub>, 77.6; CH<sub>4</sub>, 9.2; C<sub>2</sub>H<sub>2</sub>, 3.3; C<sub>2</sub> + C<sub>3</sub> hydrocarbons, 1.6; and the remainder (8.3%) was apparently consumed in the formation of polymer or was taken up by the graphite.<sup>11/</sup>

It is interesting to note that C<sub>2</sub>H<sub>2</sub> accounted for 75-92% of the gaseous hydrocarbons produced from coal in both discharges. Hydrogasification or carbonization of coal usually gives CH<sub>4</sub> as the major hydrocarbons. It has been suggested that, in a microwave hydrogen discharge system, transport of carbon from the solid to the vapor phase takes place by bombardment of the carbon by energetic ions and electrons, and that the gaseous carbon species could react with H atoms or CH species to form hydrocarbons.<sup>2,3/</sup> A similar mechanism appears to apply to the system containing coal except that H and CH species would also be evolved from the coal in addition to gaseous carbon species, even in the absence of an initial hydrogen. The predominance of C<sub>2</sub>H<sub>2</sub>, however, is also observed in rapid heating of coal by various high temperature methods such as plasma jet,<sup>6-9/</sup> laser beam<sup>12/</sup> and flash heating,<sup>13/</sup> etc. A comparison of our experimental results with those obtained with an Ar plasma jet by Bond et al.<sup>7/</sup> indicates that the percentage of carbon converted to C<sub>2</sub>H<sub>2</sub> in our system is somewhat lower, but the effect of volatile matter on the hydrocarbon

yield is quite similar. The conversion of carbon to  $C_2H_2$  for the high volatile bituminous coal (VM = 39.2%) in table 2 is 9.2% in the  $H_2$ -Ar discharge as compared to 12.5% in the Ar plasma for a coal of similar volatile matter content.

TABLE 2. - Reactions of coal and related materials  
in microwave discharges of  $H_2$  and Ar

Material	Pressure, mm		Time, sec	Yield x $10^4$ , mole/g of solid					Percent of C present as	
	$H_2$	Ar		$H_2$	$CH_4$	$C_2H_2$	CO	$CO_2$	Gaseous products	Gaseous hydrocarbons
hvab	22.7	2.3	60	63.9	4.7	31.1	21.1	0.2	13.6	10.4
	22.7	2.3	60	53.6	10.2	28.6	20.2	.2	13.1	10.3
	23.4	2.4	60	12.5	4.5	27.0	23.6	.4	12.8	9.4
	22.8	2.4	90	$\frac{1}{1}$	3.9	29.8	22.2	.2	13.1	9.9
	21.8	2.3	105	$\frac{1}{1}$	4.8	21.0	16.9	.2	9.9	7.4
	21.9	2.3	110	$\frac{1}{1}$	3.6	20.0	16.0	.2	9.4	7.0
	-	25.7	17	3.3	.1	1.2	7.1	.1	1.5	.4
	-	24.0	60	56.4	.9	13.4	23.0	.2	7.7	4.3
	-	23.6	180	44.0	1.1	16.5	22.6	.2	8.7	5.3
lvb	23.8	2.5	34	$\frac{1}{1}$	4.1	15.6	7.3	.1	6.1	5.1
	21.6	2.2	60	$\frac{1}{1}$	3.8	17.5	8.1	.1	6.7	5.6
	-	23.5	60	19.3	.3	3.6	7.7	trace	2.1	1.1
Lignite	21.6	2.2	60	25.4	2.1	9.3	66.2	3.5	16.7	4.1
	22.6	2.3	180	22.9	2.1	7.7	80.3	1.8	18.3	3.4
	20.7	2.1	180	26.0	2.1	7.3	69.2	1.7	16.1	3.3
	-	24.7	32	50.4	.7	6.9	61.7	3.2	14.1	2.7
	-	23.0	60	18.4	.6	5.0	68.4	3.2	15.1	2.1
Anthracite	21.6	2.2	60	$\frac{1}{1}$	4.2	8.3	4.0	trace	3.6	3.1
	22.6	2.4	60	$\frac{1}{1}$	4.6	9.6	3.0	trace	3.9	3.4
	-	24.0	60	.3	trace	trace	2.0	.1	.3	-
Chrysene	22.7	2.4	10	$\frac{1}{1}$	6.5	12.8	2.0	trace	4.6	4.4
	20.0	2.0	30	$\frac{1}{1}$	10.4	5.8	trace	trace	3.4	3.4
	-	22.0	30	18.6	.8	2.6	trace	trace	.9	.9
Graphite	22.4	2.3	60	$\frac{1}{1}$	3.5	2.5	trace	trace	1.2	1.2
	22.6	2.4	60	$\frac{1}{1}$	3.4	1.8	trace	trace	1.0	1.0

$\frac{1}{1}$  Net decrease of hydrogen was indicated.

#### Solid Product

The solid product obtained from coal is brownish and is similar to that usually observed from the thermal treatment of coal. No appreciable amount of solid product was formed from anthracite or from lignite. Though the extent of the gasification for the chrysene was not appreciable, the original white powder was instantaneously converted to a brown solid upon the initiation of both discharges. The infrared spectra of the solid product and the residual char obtained from the high volatile bituminous coal in the  $H_2$ -Ar discharge showed the usual aliphatic C-H bands and some weak aromatic bands which are typical of pitch and coal.

#### Effect of Cooling by Liquid Nitrogen

Since the indications are that the water formed can retard the hydrocarbon formation and that the hydrocarbons produced may undergo further destructive reactions, it can be expected that a rapid quenching of the primary products should give a pronounced effect on the result. Experiments were carried out in a reactor consisting of the

tube divided by a fritted Vycor disc. The coal was placed on the disc, and was subjected to reaction in the  $H_2$  discharge while the lower end of the tube was cooled in liquid  $N_2$ . Though the process of condensing water and some hydrocarbons at this temperature is diffusion controlled, the effect is pronounced, as shown in table 3. For both the bituminous coal and the lignite, the yield of the hydrocarbons,  $C_2H_2$  in particular, was greatly increased. The amount of  $H_2$  remaining and the amount of CO produced after the reaction were also decreased. Therefore, the increase of hydrocarbon yield can be attributed mainly to subsequent hydrocarbon formation by reaction of  $H_2$  and CO; this hydrocarbon yield is greatly enhanced by rapid removal of  $H_2O$  formed.

#### Water-Argon Discharge

There is a marked difference between the products obtained from graphite and coal in a water discharge. In the discharge in  $H_2O$ -Ar mixtures, as shown in table 4, graphite yields hydrogen and CO but practically no hydrocarbons; while the coals yield an appreciable amount of  $C_2H_2$  and some  $CH_4$  in addition to  $H_2$  and CO. The amounts of  $H_2$  and carbon oxides produced in the reaction with graphite were stoichiometric. The extent of gasification was also much greater for the coals than for the graphite. The active hydrogen species produced in the water discharge did not react further with the graphite or the CO formed from it to produce significant amounts of hydrocarbons. This is further evidence demonstrating that the presence of water vapor retards hydrocarbon formation.

For the reaction of a given coal in a  $H_2O$ -Ar discharge, an initial  $H_2O$  pressure of less than 12 mm Hg appears to give the optimum gasification and hydrocarbon production. Higher initial  $H_2O$  pressures cause a decrease in both gasification and hydrocarbon production. So long as the  $H_2O$  pressure is not at its highest values, more hydrocarbons are formed than in the Ar discharge. (Also, with the higher initial  $H_2O$  pressures, the discharge could not be initiated readily and would not sustain itself for as long as 60 seconds, perhaps due to too large an increase in the total gas pressure in the reactor.) The data seem to indicate that 60 seconds may have been too long a period for the maximum production of hydrocarbons. The formation of the hydrocarbons should be a maximum at the time when a plateau of the extent of coal gasification is attained, and prolonged treatment probably allows the remaining  $H_2O$  vapor to diffuse into the discharge zone, giving an adverse effect. It was also noticed that, at an initial  $H_2O$  pressure of less than 12 mm, the hydrogen content of the products exceeded that which could possibly be derived from the stoichiometric amount of the  $H_2O$  initially present.

These results seem to indicate the following. The active hydrogen species formed in the  $H_2O$  discharge participate in the reactions which lead to the formation of hydrocarbons from (some of) the species derived from the coal. This occurs despite the retarding effect of  $H_2O$  on hydrocarbon formation. (If the  $H_2O$  pressure is too high, this latter effect decreases the hydrocarbon yield.) Presumably, the coals when gasified supply enough CH species to allow hydrocarbons to be formed, even though the active oxygen species present react with some of the gaseous carbon and CH species. On the other hand, graphite produces negligible amounts of CH species in a  $H_2O$ -Ar discharge, and therefore cannot produce hydrocarbons since the reaction of the CO formed with the active hydrogen species is retarded by the  $H_2O$  present.

Lignite, with its high volatile matter content, was extensively gasified but gave a relatively low hydrocarbon yield, presumably due to the inhibition by its high oxygen content. For lignite, the production of  $CO_2$  was also higher in the  $H_2O$ -Ar discharge than in the  $H_2$ -Ar or Ar discharge. Again, the extent of gasification for chrysene was rather small.

TABLE 3. - Effect of cooling at reactor end by liquid nitrogen

Material	Pressure, mm H <sub>2</sub> -Ar mixture (9.7:1)	Time, sec	Yield x 10 <sup>4</sup> mole/g of solid						Percent of C present as		
			H <sub>2</sub>	CH <sub>4</sub>	C <sub>2</sub> H <sub>2</sub>	C <sub>2</sub> H <sub>4</sub>	C <sub>2</sub> H <sub>6</sub>	CO	CO <sub>2</sub>	Gaseous products	Gaseous hydrocarbons
HVA-bituminous	23.0	60	2/	8.2	22.6	3.2	2.4	8.6	0.4	11.1	9.8
	24.6	60	2/	4.9	23.8	2.3	1.7	7.6	.2	10.0	8.9
Lignite	24.5	180	2/	4.5	51.8	5.5	3.6	13.7	.5	20.4	18.3
	25.9	60	2/	2.8	17.0	.7	.7	38.0	3.6	14.8	7.3
	23.8	180	20.8	2.0	25.2	.7	.7	39.6	5.0	18.2	10.1

1/ Peaks attributed to HCN was neglected.  
 2/ Net decrease of hydrogen was indicated.

TABLE 4. - Reactions of coal and related materials in microwave discharges of H<sub>2</sub>O-Ar mixtures

Material	Pressure, mm		Time, sec	Yield x 10 <sup>4</sup> mole/g solid						Percent of C present as	
	H <sub>2</sub> O	Ar		H <sub>2</sub>	CH <sub>4</sub>	C <sub>2</sub> H <sub>2</sub>	C <sub>2</sub> H <sub>4</sub>	CO	CO <sub>2</sub>	Gaseous products	Gaseous hydrocarbons
hvab	18.1	7.6	40	17.3	0.5	8.6	28.4	2.1	7.3	2.8	
	18.0	5.7	35	25.8	.8	10.2	30.0	1.0	8.0	3.4	
	12.3	6.9	57	40.0	.8	16.5	42.6	.7	11.7	5.3	
	12.0	8.0	40	70.0	1.7	22.7	36.0	.7	12.8	7.3	
	11.2	7.7	47	34.0	1.2	18.2	39.0	1.0	11.8	5.9	
	10.5	8.2	60	56.4	2.0	24.4	44.8	2.0	14.8	7.9	
	7.9	8.6	45	102	2.0	23.0	38.6	.7	13.2	7.1	
	7.3	6.4	60	24.2	.9	15.8	27.0	.8	10.1	5.2	
	6.6	9.3	30	42.8	1.6	23.5	28.7	.8	11.9	7.6	
	11.2	6.7	180	115	1.9	15.4	60.0	.6	14.2	5.3	
	18.4	7.3	25	13.8	.4	4.6	21.2	2.4	4.6	1.4	
	10.0	7.7	60	20.9	1.1	13.6	25.8	.5	7.6	4.0	
	Lignite	17.5	5.7	40	63.8	3.7	trace	52.6	16.6	13.4	.9
	Anthracite	11.0	8.8	60	89.0	1.5	10.0	87.2	5.0	20.9	4.1
	Chrysene	7.3	5.0	60	45.4	.6	10.4	42.4	.8	8.7	3.0
Graphite	8.2	6.6	23	30.4	2.0	6.4	7.4	.2	3.0	2.0	
	16.3	5.4	60	24.2	trace	trace	19.4	3.0	2.8	-	
	18.9	5.9	180	37.8	trace	trace	28.8	5.4	4.1	-	

## Deuterium Oxide-Argon Discharge

It is of interest to obtain further evidence as to whether water is actually involved in the reaction with coal to form hydrocarbons in addition to the production of  $H_2 + CO$ . The gaseous product obtained from the reaction of the high volatile bituminous coal in a  $D_2O$ -Ar mixture was analyzed by the high resolution mass spectrometer. At a resolution of 1 part in 20,000, precise masses for doublets and in some instances triplets that occurred at the same nominal masses could be used to identify completely deuterated, monodeuterated and nondeuterated species present in the product. For example, peaks due to  $C_2H_2$  (mass = 26.0156),  $C_2D$  (26.0141) and  $CN$  (26.0031) were observed at the nominal mass of 26 and peaks due to  $C_2D_2$  (28.0282),  $N_2$  (28.0061) and  $CO$  (27.9931) were observed at the nominal mass of 28. The whole spectrum up to the nominal mass of 44 contained peaks attributed to all species present including minor amounts of oxygenated and N-containing compounds, but the major products were  $H_2$ ,  $HD$ ,  $D_2$ ,  $C_2H_2$ ,  $C_2HD$ ,  $C_2D_2$  and partially deuterated methanes in addition to  $D_2O$ ,  $DHO$ ,  $H_2O$  and carbon oxides. Thus it is apparent that  $D_2O$  is initially dissociated into  $D$ ,  $OD$  and possibly an active oxygen species which in turn recombine to give  $D_2O$  and  $D_2$ , or react with the active species derived from coal such as  $H$ ,  $CH$ ,  $C_1$ ,  $C_2$  and  $CO$ , etc., to give  $DHO$ ,  $HD$ ,  $CO$ ,  $CO_2$  and deuterated hydrocarbons.

## CONCLUSIONS

In the microwave discharges of  $H_2$ ,  $H_2O$  and Ar, coal is gasified to give gaseous hydrocarbons and carbon oxides plus a solid product and residual char. Hydrogen is also produced either by dissociation of the water vapor or by devolatilization of the coal in the  $H_2O$  and/or Ar discharges. But, in most cases in the hydrogen discharge, hydrogen is consumed rather than produced (except for hvab coal and lignite). The yield of the hydrocarbons is highest in the hydrogen discharge and that of carbon oxides is highest in the water discharge. Both the hydrogen and the water discharges give greater extents of gasification and yield more hydrocarbon products than the Ar discharge, indicating the occurrence of gas phase reactions of  $H$ ,  $OH$ , and active oxygen species with the active species derived from the coal. The gasification of coal in the water discharge is of particular interest because it produces  $H_2 + CO$  ( $\sim 1:1$ ) plus  $C_2H_2$  and  $CH_4$ . The high oxygen content of the lignite results in a higher yield of carbon oxides but apparently inhibits the hydrocarbon formation in the discharge. The hydrocarbon yield from the lignite or other coals in the hydrogen discharge, however, can be increased dramatically by rapidly condensing part of the product species produced, especially  $H_2O$ , during the discharge reaction.

$C_2H_2$  accounts for as much as 92% of the gaseous hydrocarbons produced, and, excepting for lignite, the amount of the hydrocarbons is related to the volatile matter of coal. The extent of gasification, however, is increased with the volatile matter content of coal including lignite. Thus, if the hydrocarbons are formed by the recombination of the species derived from the volatile material and other species present in the discharge, another interesting study would be to employ a flow system in which coal is devolatilized by ordinary means and the evolved gases are subsequently reacted in a discharge.

## REFERENCES

1. Blackwood, J. D. and McTaggart, F. K. Reactions of Carbon with Atomic Gases. *Australian J. Chem.*, 12, 533 (1959).
2. Shahin, M. M. Reaction of Elementary Carbon and Hydrogen in High-Frequency Discharge. *Nature*, 195, 992 (1962).
3. Vastola, F. J., Walker, P. L. Jr., and Wightman, J. P. The Reaction Between Carbon and the Products of Hydrogen, Oxygen and Water Microwave Discharges. *Carbon*, 1, 11 (1963).

4. Letort, M., Boyer, A. F., and Payen, P. Attempting Hydrogenation of Coal with Atomic Hydrogen. *Bull. Soc. Chim. France*, 1589 (1963).
5. Pinchin, F. J. The Reaction of Coals with Atomic Hydrogen. Private Communication.
6. Bond, R. L., Galbraith, I. F., Ladner, W. R., and McConnell, G. I. T. Production of Acetylene from Coal, Using a Plasma Jet. *Nature*, 200, 1313 (1963).
7. Bond, R. L., Ladner, W. R., and McConnell, G. I. T. Reactions of Coal in a Plasma Jet. *Fuel*, 45, 381 (1956).
8. Graves, R. D., Kawa, W., and Hiteshue, R. W. Reactions of Coal in a Plasma Jet. *Ind. Eng. Chem.*, 5, 59 (1966).
9. Kawana, Y., Makino, M., and Kimura, T. Formation of Acetylene from Coal by Argon Plasma. *Kogyo Kagaku Zasshi*, 69, 1144 (1966).
10. Blaustein, B. D. and Fu, Y. C. Formation of Hydrocarbons from  $H_2 + CO$  in Microwave-Generated Electrodeless Discharges. Paper to be presented at 153rd National ACS Meeting, Miami Beach, Fla., April 1967.
11. Montet, G. L. Retention of Protons by Graphite. *Proc. Fourth Conf. on Carbon*, Pergamon, New York, pp. 159-164 (1960).
12. Sharkey, A. G., Shultz, J. L., and Friedel, R. A. Gases from Flash and Laser Irradiation of Coal. *Nature*, 202, 988 (1964); *Coal Science, Advances in Chemistry Series 55*, R. F. Gould, Editor, Am. Chem. Soc., Washington, pp. 643-649 (1966).
13. Rau, E. and Seglin, L. Heating of Coal with Light Pulses. *Fuel*, 43, 147 (1964).

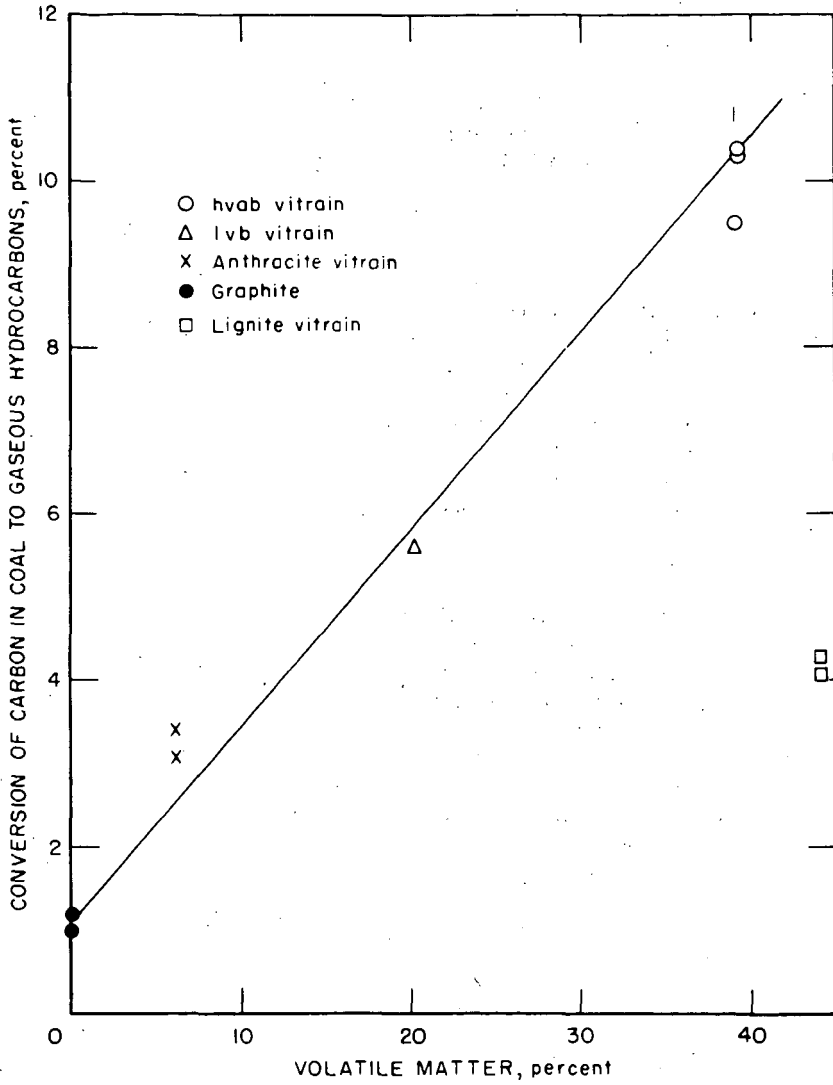


Figure 1 - Effect of volatile matter on yield of hydrocarbons in H<sub>2</sub>-Ar discharge (60 second run)

CHEMICAL REACTIONS IN A CORONA DISCHARGE I. BENZENE

M. W. Ranney<sup>1</sup>  
Wm. F. O'Connor

Department of Chemistry  
Fordham University  
New York, New York 10458

## INTRODUCTION

Corona discharges (silent) have been used to initiate chemical reactions for well over 150 years with much of the early work being confined to inorganic gases.<sup>2</sup> However, the only commercially significant development over the years has been the process for synthesizing ozone by subjecting oxygen to a corona discharge<sup>3</sup> (ozonizer). Most early investigators encountered serious difficulties in studying the interaction of high voltage electricity with organic molecules. Equipment was unreliable and dangerous, and the complexity of the reaction product mass precluded definitive performance evaluation. Since World War II, technology has advanced to the point where high frequency power can be generated and controlled at reasonable cost and many new dielectric materials such as fused quartz, alumina and mica mat are available.<sup>4</sup> Modern analytical techniques afford the opportunity to determine the composition of the product mix.

Corona electrons are accelerated by the applied voltage to an energy level of 10-20 electron volts, which is sufficient to break the covalent bond. This represents a very efficient approach when compared with high energy radiolysis (m.e.v. range) where the actual chemical work is effected by secondary electrons with an energy of 10-25 e.v., formed after a series of energy-dissipating steps. Potentially, corona energy can deliver electrons to the reaction site at the desired energy level to give products which are not readily obtainable by more conventional means. The energy available in the corona discharge is somewhat above that commonly encountered in photochemistry (up to 6 e.v.).

Bertholot reduced benzene to  $C_6H_8$  in 1876 in what appears to be the first exposure of an aromatic compound to the corona discharge.<sup>5</sup> Losanitsch obtained the following products from benzene in an electrical discharge:  $(C_6H_6)_2$ , biphenyl,  $(C_72H_96)$  and  $(C_6H_6)_{90}$ .<sup>6</sup> Benzene vapor treated at 300° in an ozonizer tube gave resinous products with a 6/4 carbon-hydrogen ratio.<sup>7</sup> Linder and Davis exposed benzene vapor to 37,000 volts and found biphenyl, gaseous products and evidence of polymerization.<sup>8</sup> The early work with benzene reactions in various types of electrical discharges is reviewed in considerable detail by Glocker and Lind.<sup>2</sup> Brown and Ripper investigated the hydrogenation of benzene flowing down the walls of an ozonizer tube and found 1,3- and 1,4-cyclohexadiene, biphenyl, and a resinous mass which gave an infrared spectrum consistent with polystyrene.<sup>9</sup>

In recent years, benzene has been subjected to direct electrode discharge<sup>10</sup> and glow discharges induced by microwave<sup>11</sup> and radiofrequency<sup>12</sup> energy. In this paper, we report some of our observations for the reaction of benzene in a corona discharge.

## APPARATUS

The corona reactor system used in this study is shown in Figure 1 and the reactor details are given in Figure 2. The system is designed to run at atmospheric or reduced pressure and, with slight modification, under recycle conditions. The use of the threaded rod center electrode affords a more uniform and higher treating potential than is obtained with a cylindrical electrode.<sup>13</sup> The electrode threads concentrate surface irregularities thereby eliminating severe discharge points. The copper electrode serves as a cooling coil and affords direct observation of the corona. In a typical run, the benzene reservoir temperature is set at 55°, the helium is adjusted to 100 ml/min. and after a two minute purge, an electrical potential of 15,000 volts is applied. A brilliant blue corona is established, the intensity being a function of helium flow, pressure, benzene content and the applied voltage. Benzene traverses the corona reactor as a vapor and is condensed by the cold water trap and collected. Yellow solids gradually deposit in the flask at the bottom of the reactor and eventually adhere to the dielectric surfaces in the reactor. Some benzene and the more volatile reaction products are condensed in the -70 and -195° traps. See experimental section for further details.

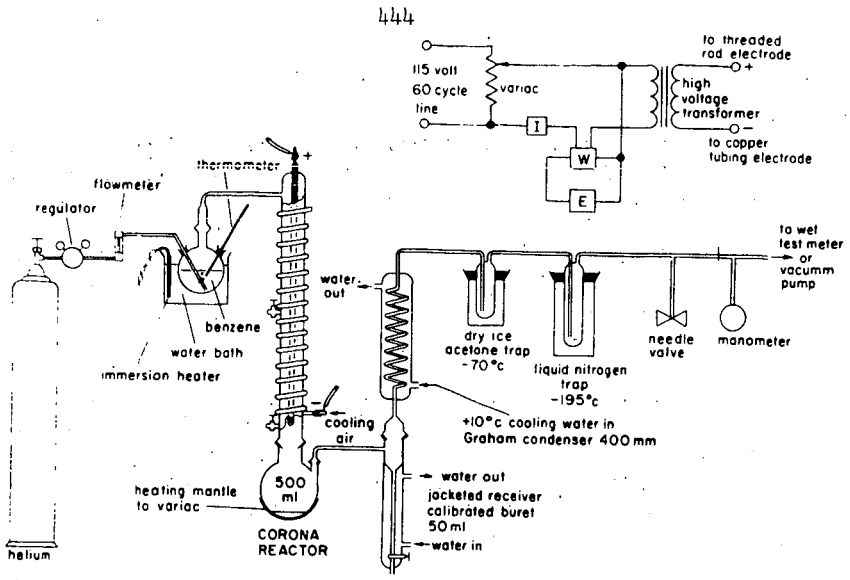
## RESULTS AND DISCUSSION

The excitation of benzene vapor in a corona discharge provides an 8.5% conversion to identifiable products. The major products are a benzene soluble polymer (6%), a benzene insoluble polymer (0.7%), biphenyl (0.3%), and acetylene (1%). The composition of the product mix obtained is given in Table 1. The overall yield obtained under our experimental conditions is similar to that produced in a radiofrequency glow discharge<sup>12</sup> (10%, with longer residence time) and somewhat higher than Streitwieser obtained using a microwave<sup>11</sup> induced glow discharge (5%). The corona discharge gives a considerably higher proportion of polymer than is obtained from these other energy sources. Benzene substitution products such as toluene, phenylacetylene and ethylbenzene were observed in the microwave discharge but were not noted in this study or in the radiofrequency investigation. The high yield of fulvene in the radiofrequency discharge is surprising in view of its tendency to polymerize or add oxygen under rather mild conditions. The sum of the carbon and hydrogen analyses for the polymeric fraction obtained by Stille in the glow discharge of benzene (86-94 per cent) suggests some fixation of oxygen and/or nitrogen during discharge or product work-up.<sup>12</sup> The pressure for these electrodeless glow discharge studies was of the order of 20 mm. or less, while the corona reactor was operated at atmospheric pressure. Schüller, using an electrode discharge in benzene, obtained products similar to those produced in the microwave glow discharge.<sup>10</sup>

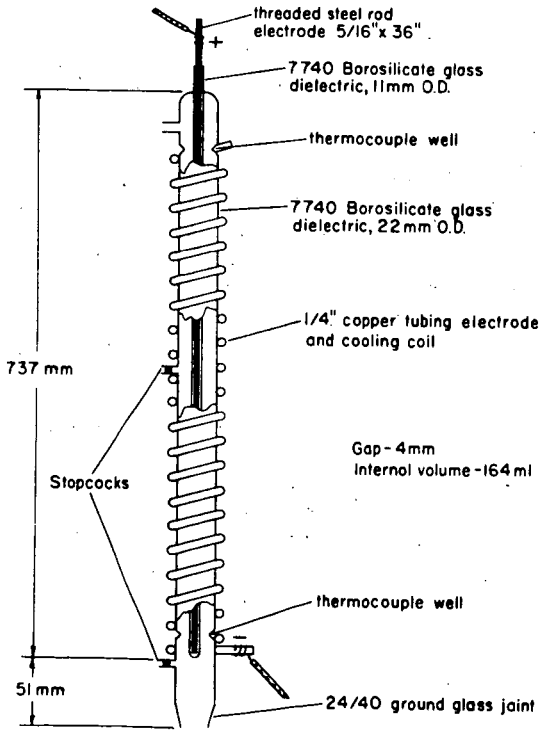
The reaction products obtained in this study are roughly categorized as the benzene fraction, biphenyl fraction and polymeric material for purposes of discussion. After initial studies indicated that the components of the -70 and -195° traps were similar to those in the benzene trap, these samples were combined. The acetylene content of the low temperature traps was determined by weight loss prior to mixing with the benzene.

Benzene Fraction

The exposed benzene, as collected in the cold traps, is bright yellow. The following reaction products have been identified in this fraction: 1,3-cyclohexadiene, 1,4-cyclohexadiene, fulvene and cyclohexene. The approximate per cent yield for each of these constituents is given in Table 2. The data were determined using a 100 foot



**CORONA REACTOR SYSTEM**  
Figure 1



**DETAIL OF CORONA REACTOR**  
Figure 2

TABLE 1

## Product Distribution in the Corona Discharge of Benzene, 15KV

Product	Yield-Per Cent Benzene Exposed	Yield-Per Cent of Product Mix	Radiofrequency <sup>(c)</sup> Yield, Per Cent
Benzene insoluble polymer	0.7	8.2	N.D. <sup>(d)</sup>
Benzene soluble polymer (a)	6.0	70.5	5.0 <sup>(e)</sup>
Biphenyl	0.3	3.5	2.0
o-, m-, and p-Terphenyl	0.1	1.2	N.D.
Phenyl, benzyl substituted cyclopentenes <sup>(b)</sup>	0.3	3.5	N.D.
1,3-and 1,4-Cyclohexadiene	0.1	1.2	N.D.
Fulvene	0.01	0.1	1.0
Acetylene	1.0	11.8	2.0 <sup>(f)</sup>
TOTAL	8.5	100.0	10.0

(a) Polymer fraction includes materials from 250 molecular weight and up.

(b) Includes several phenyl and benzyl substituted cyclopentenes similar to biphenyl and o-terphenyl in vapor pressure. See discussion.

(c) See reference No. 12.

(d) N. D. -- not determined.

(e) Benzene and toluene soluble polymer.

(f) Acetylene 1%, allene 1%.

support-coated open tubular column with a squalane liquid phase and appropriate calibration standards (Figure 3). No significant change is noted in the cyclohexane content when compared with starting benzene. The increase in the methyl cyclopentane peak is ascribed to its higher vapor pressure thus affording some accumulation of this material in the benzene distillate and a concomitant depletion in the benzene feed stock. Cyclohexene is produced in very low yield, as expected, because of the degree of hydrogenation required during its short residence time in this single pass reactor.

The reduction of benzene to the cyclohexadienes is interesting as 1,3-cyclohexadiene is thermodynamically unstable with respect to benzene, cyclohexene and cyclohexane.<sup>14</sup> The synthesis of 1,3-cyclohexadiene under these conditions is analogous to the conversion of oxygen to ozone which also represents an energetically unfavorable process. The momentary energy input and the rapid removal of the activated species from the reaction zone affords this material in low yield. As expected, the more stable 1,4-cyclohexadiene is produced in higher yield (3/1). Additionally, 1,3-cyclohexadiene would be expected to polymerize at a rapid rate under these conditions. The thermodynamic instability of 1,3-cyclohexadiene is demonstrated by its gradual disappearance from the sample after a few days standing at room temperature. The yields of both the 1,4- and 1,3-cyclohexadiene are somewhat higher than previously reported by Brown and Rippere.<sup>9</sup> The yields reported by these workers after 24 hours exposure to a 15 KV corona discharge in a counter-current hydrogen stream were 0.02 and 0.01 per cent respectively. The major variable in technique which likely accounts for this difference in yields is the use of benzene vapor in our work, versus the hydrogenation of a thin liquid benzene film running down the annular dielectric surface by Brown and Rippere.

The ultraviolet spectrum for the benzene fraction was obtained by running differentially against pure benzene in isooctane. A broad absorption band with a maximum at 258  $\mu$  is ascribed to the 1,3-cyclohexadiene. An additional absorption at 242  $\mu$  and a tailing into the visible region with a broad maximum at 360-370  $\mu$  is also observed. These spectral features are consistent with those reported for fulvene, the non-aromatic isomer of benzene.<sup>15</sup> Blair and Bryce-Smith found fulvene in the photochemical irradiation of benzene in what appears to be the first direct conversion of an aromatic hydrocarbon to a non-aromatic hydrocarbon.<sup>16</sup> Fulvene co-distilled with benzene, but could be separated from benzene using the 100 ft. squalane column (Figure 3). Fulvene prepared by the method of Meuche gave the same retention time and spectral features.<sup>17</sup> Additional evidence for assignment of the fulvene peak included its disappearance from the chromatogram after the sample was refluxed with maleic anhydride (color disappears) or exposure to a free radical catalyst. The Diels-Alder reaction product with maleic anhydride was isolated and hydrolyzed to give the adduct, 7-methylene-5-norbornene -2, 3-dicarboxylic acid. The melting point and infrared data for this adduct were identical with the sample prepared using fulvene synthesized from cyclopentadiene and formaldehyde.<sup>12</sup>

The formation of the 1,3,5-hexatrienyl diradical has been suggested as an intermediate in the photochemical decomposition<sup>18</sup> and the radiofrequency discharge<sup>12</sup> of benzene. Material isolated in the photochemical excitation gave a UV spectrum similar to 1,3,5-hexatriene, but displaced by 7.5  $\mu$  and, more disturbing, the investigators were able to separate the material from benzene by fractional distillation. No experimental evidence was given in the radiofrequency study. In our work, 1,3,5-hexatriene could not be detected (less than 100 ppm) in the benzene fraction using the squalane column. No spectral evidence was noted in the ultraviolet although the region of interest is complicated by the presence of 1,3-cyclohexadiene.<sup>19</sup>

The unidentified peak in the chromatogram (Figure 3) gives a negative test for an acetylenic hydrogen (ammoniacal cuprous chloride solution) and does not disappear after the sample is subjected to free radical catalysis for several hours. Thus, the open chain, acetylenic isomers of benzene, hexa-1, 3-diene-5-yne, 1,4-hexadiyne, 1,5-hexadiyne and 1,5-hexadien-3-yne do not appear to account for this peak. The possibility of valence isomers of benzene such as bicyclo (2.2.0) hexa-2, 5-diene, "Dewar benzene", were excluded based on the observation that the peak was stable to prolonged heating at 100°. The valence isomers would be expected to convert to benzene under such conditions.<sup>20</sup>

TABLE 2

Product Distribution in Discharged Benzene Fraction (a)

<u>Product</u>	<u>Yield % Benzene Exposed</u>
1,3-Cyclohexadiene	0.03
1,4-Cyclohexadiene	0.09
Fulvene	0.01
Cyclohexene	0.01
Unidentified	0.02

(a) Quantitative data obtained by GLC using squalane column and appropriate calibration standards.

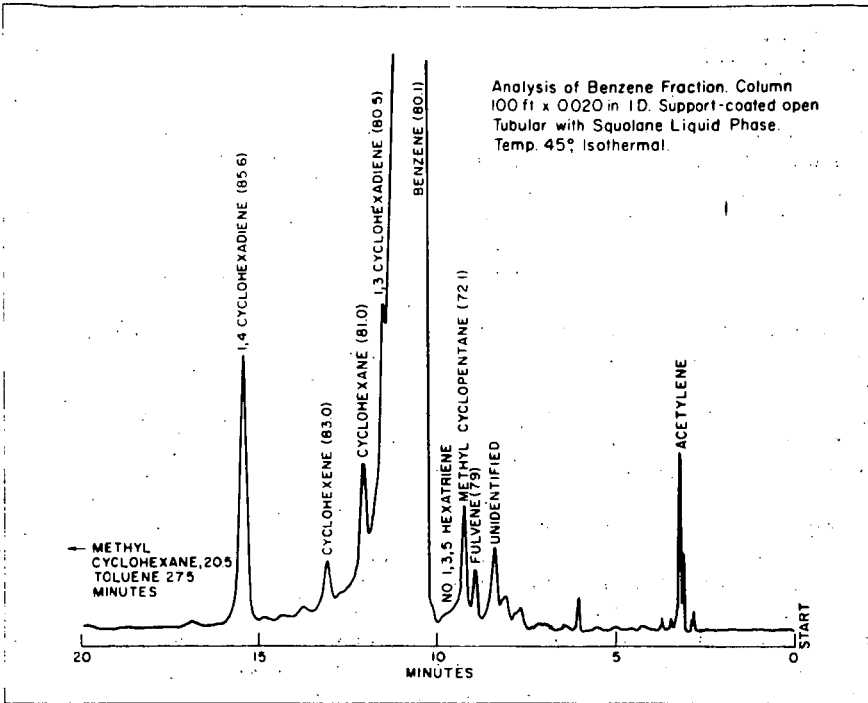


Figure 3

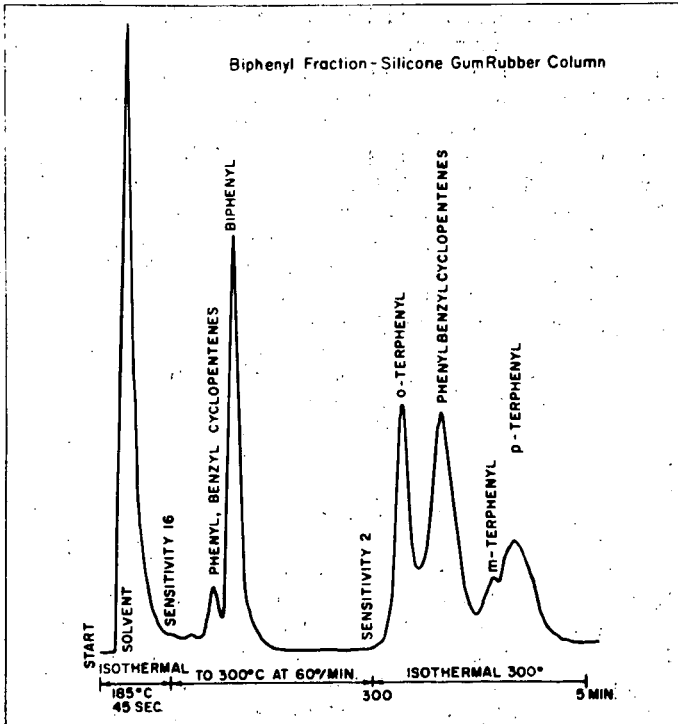


Figure 4

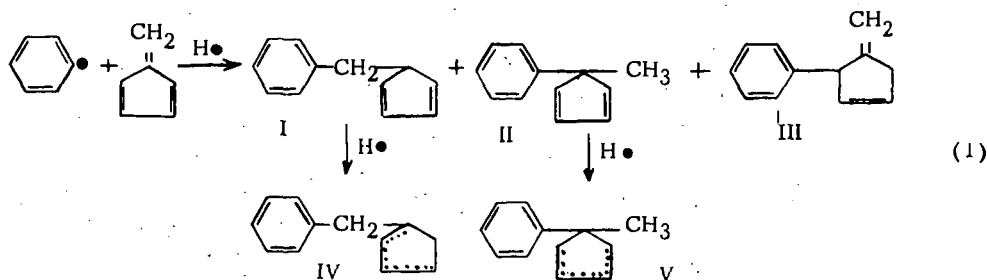
### Biphenyl Fraction

The low molecular weight compounds, soluble in isooctane and hot methanol, were primarily biphenyl and o-, m-, and p-terphenyl. These products were identified by gas-liquid chromatography using a silicone gum rubber column (Figure 4) and a Carbowax 20M column with appropriate standards. The peaks were trapped and analyzed by infrared and NMR spectroscopy for confirmation. Biphenyl was present in sufficient quantity to be readily detected in the initial infrared spectrum and was isolated by sublimation. Quantitative data, obtained using the silicone column with appropriate calibration curves are presented in Table 3. With the possible exception of biphenyl, the yields are very low considering the overall conversion noted. The o-, m- and p-terphenyl ratio (1/0.4/1) indicates a preference for the para position beyond that expected for random attack.

If hydrogenation of the polyphenyls by hydrogen radicals generated "in situ" is to be considered a primary reaction mechanism, one would expect to see components corresponding to the possible hydrogenated species of biphenyl and the terphenyls. This does not appear to be the case, however, as no significant peak can be ascribed to a hydrogenated o-terphenyl compound. The small peaks before biphenyl and after o-terphenyl in the chromatogram (Figure 4) actually include four or more components present in small proportions which have not been completely identified. The first peak, (eluted before biphenyl) amounting to less than 0.1 per cent of the total yield, was initially ascribed to a mixture of the possible hydrogenation products of biphenyl. On the Carbowax column at lower temperatures this peak is eluted between phenylcyclohexane and 1-phenylcyclohexene. Initial infrared examination of this peak after trapping indicated an intriguing similarity with the peak (s) noted after o-terphenyl and with the polymer fractions. The possibility that this component was a low molecular weight precursor to polymer formation prompted further study. Infrared indicates a phenyl substituted aliphatic compound containing some olefinic unsaturation, and the spectrum is not consistent with the anticipated phenyl cyclohexenes. Careful examination of the spectrum indicates that the following phenyl substituted compounds are not present on the basis of the indicated missing absorptions - phenyl cyclohexane (1010, 1000, 888, 865  $\text{cm}^{-1}$ ), 1-phenylcyclohexene (922, 805  $\text{cm}^{-1}$ ), and 3-phenylcyclohexene (855, 788, 675  $\text{cm}^{-1}$ ).<sup>21</sup> The spectrum is consistent with a non-conjugated benzylcyclopentene system with absorptions at 1070, 1030, and 960  $\text{cm}^{-1}$  and the expected aromatic substitution bands.<sup>21</sup> Two additional absorptions are noted, one at 850  $\text{cm}^{-1}$  which may be attributed to vinyl protons and a phenyl substitution band at 730  $\text{cm}^{-1}$ . This likely results from biphenyl contamination, but it is interesting to note that benzylidenecyclopentane has an absorption at 732  $\text{cm}^{-1}$  with the remainder of the spectrum being similar to the benzylcyclopentenes.

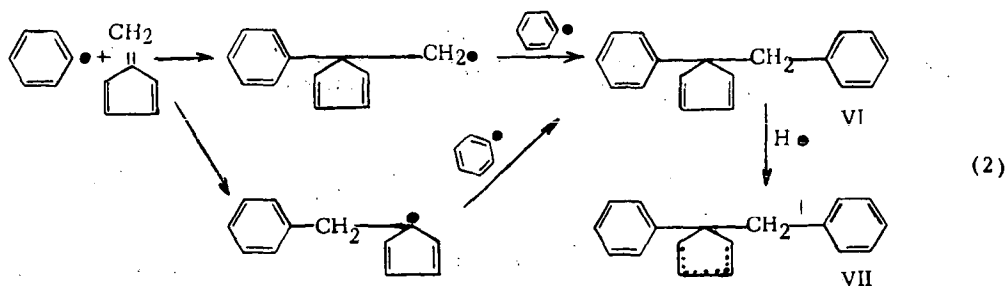
NMR data provides strong evidence for a rigid ring system (non-olefinic protons poorly resolved 1-3 ppm), non-conjugated olefinic protons at 5.7 ppm and phenyl protons at 7.1 ppm. The olefinic protons are complex, giving a closely-spaced doublet superimposed on a broad absorption, suggesting the presence of both ring and exocyclic unsaturation. Additional sharp proton resonances are noted at 1.2 ppm (methyl) and a doublet at 2.7 ppm which is attributed to benzylic protons. The lack of olefinic protons downfield from 5.7 ppm would rule out the benzylidene compounds and likely any similar structures wherein the unsaturation is conjugated with the phenyl moiety. The olefinic protons in cyclopentadiene are found at 6.42 ppm and were not obvious in this fraction. However, absorptions due to a minor component could have escaped detection because of limited sample size. The difficulty encountered in isolating the components of this peak precludes definite structural assignments, but the reaction of phenyl radicals with fulvene followed by H radical termination and hydrogenation to give

phenyl or benzyl substituted cyclopentenes is clearly indicated. The following reaction scheme is proposed to account for the experimental observations:

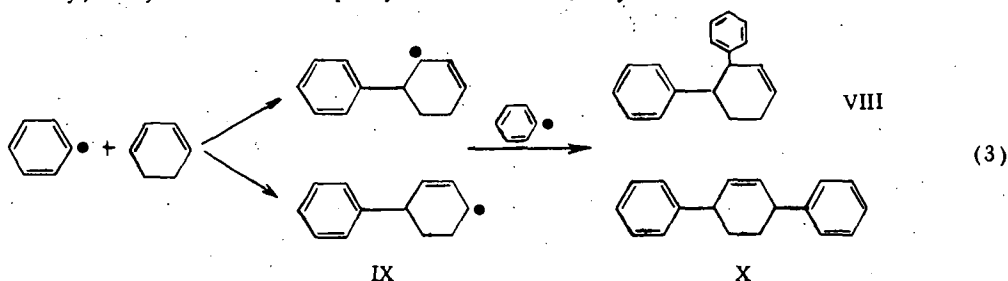


The inherent complexity of the product mix is illustrated by IV above which could be 1-, 3- and 4-benzylcyclopentene. Preliminary mass spectral data for this sample, as isolated from the chromatographic separation, indicates  $m/e$  values of 156 and 158, corresponding to the cyclopentadienes I, II and the cyclopentenes IV, V. Ring substituted compounds such as III would also have a mass of 156. Mass 91, corresponding to the benzyl radical is prominent as is mass 77, the phenyl radical, although this would be expected to arise from the biphenyl (154) contamination. Other features of the spectrum are being evaluated. The low yield is reasonable in view of the limited probability for radical termination and hydrogenation compared with the high reactivity of these olefins (or the diene precursors) under the reaction conditions. The glow discharge work of <sup>10</sup>Schüler indicates the absence of any products with vapor pressure similar to biphenyl and the other related literature generally does not give details beyond biphenyl analysis and gross polymer properties.

The peak after *o*-terphenyl (Figure 4) actually consists of 3-4 components when analyzed by varying the chromatographic conditions. This peak has the same retention time as diphenyl fulvene and is in the same general range as noted for a commercially available hydrogenated terphenyl, Monsanto HB-40. This complex peak was trapped (with trace *o*-terphenyl contamination) as a yellow liquid which gave an infrared spectrum identical to the polymer fractions and very similar to the peak before biphenyl. Again, phenylbenzylcyclopentenes are indicated and the spectrum bears little resemblance to the hydrogenated terphenyl spectrum. The NMR spectrum in carbon tetrachloride showed aromatic protons at 7.1 ppm, a broadened olefinic proton resonance at 5.7 ppm and non-olefinic protons from 0.8-3.5 ppm with poor resolution. These extremely complex olefinic and non-olefinic resonances are typical of protons in a fixed ring system such as cyclopentene. The integration for these resonances allows approximation of an average structure containing a cyclopentene ring system substituted with one phenyl and one benzyl group. The reactions appear analogous to those responsible for the components of the peak before biphenyl with termination being with a phenyl radical rather than the hydrogen radical. The mass spectrum for this material as trapped from the chromatographic analysis shows prominent peaks at mass 232 and 234 corresponding to VI and VII below. The benzyl and phenyl radical peaks are also evident at mass values of 91 and 77 respectively. Evaluation of the final structure details is continuing. The following is believed to be representative of the many reactions which are possible under the experimental conditions, to give a variety of closely related compounds:



The actual structural definition must await isolation of sufficient quantities of the components for NMR studies under various conditions. The possibility of a hydrogenated p-terphenyl was carefully considered, but the only structure even remotely consistent with the infrared and NMR data would require that the center ring of p-terphenyl be non-aromatic with mono-substituted phenyl groups attached. Such a material could be formed by preferential hydrogenation of the center ring of p-terphenyl (statistically unlikely) or by the reaction of phenyl radicals and 1,3-cyclohexadiene as follows:



This mechanism requires the formation of hydrogenated ortho terphenyl derivatives such as VIII, which were not noted by gas-liquid chromatography or infrared.

TABLE 3

Biphenyl Fraction (a)

	Yield % Exposed Benzene	Yield % Reaction Products
Biphenyl	0.30	3.5
o-Terphenyl	0.05	0.6
m-Terphenyl	0.02	0.2
p-Terphenyl	0.05	0.6
Benzyl and phenyl cyclopentenes (C <sub>12</sub> )	0.05	0.6
Phenylbenzylcyclopentenes (C <sub>18</sub> )	0.25	2.9
TOTAL	0.72	8.4

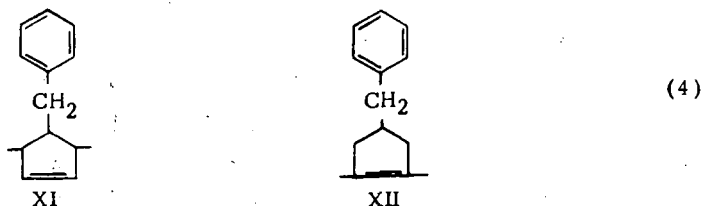
(a) Quantitative data were obtained by GLC, using a silicone gum rubber column with appropriate standard calibration curves based on peak height.

## Polymeric Products

The material which adheres to the glass dielectric surface in the reactor is a high melting solid ( $>320^\circ$ ), insoluble in benzene and all common solvents. The infrared spectrum and the carbon-hydrogen ratio are essentially the same as noted for the benzene soluble material. The benzene soluble polymer was fractionated into three molecular weight ranges based on solubility in isoctane. The polymers are all yellow with the intensity increasing as the molecular weight decreases. The ultraviolet spectrum for the low molecular weight polymer shows a gradual tailing into the visible region. The physical property data for the polymeric fractions are summarized in Table 4.

Infrared data indicate that the polymeric fractions are structurally similar to the low molecular weight products identified as benzyl and phenyl substituted cyclopentenes. The infrared evidence already presented for the low molecular weight products is applicable to the polymeric products and need not be repeated. The data are consistent with an average repeating unit containing the cyclopentene ring structure substituted with phenyl or benzyl groups. NMR data for the polymers were obtained in carbon tetrachloride at the cell holder temperature ( $40^\circ$ ). The spectrum obtained for the 300 molecular weight polymer fraction is presented in Figure 5. The extreme broadening of the proton resonances is associated with the complex, long range proton coupling in a rigid system and the motional averaging commonly noted in polymers.<sup>22</sup> Scanning the same sample at  $90^\circ$  in tetrachloroethylene did not significantly improve the resolution. The NMR spectrum of the polymer in pyridine (Figure 5) gives some improvement in the high field proton resolution, indicating a doublet at 2.6 ppm (benzylic protons) and a complex methyl proton resonance. The spectra are similar to those obtained for the low molecular weight precursors containing unresolved ring protons. The NMR spectra generally eliminate polymer formation by way of phenyl and hexatrienyl radicals as suggested for the radiolysis of benzene.<sup>23</sup> The aliphatic proton portion of the spectrum is very similar to that reported for cyclopentadiene polymers by Davies and Wassermann.<sup>24</sup> The cyclopentadiene polymers had a molecular weight range of 1200-2300, a  $\lambda$  max. at 320-360 m $\mu$  and non-olefinic proton to olefinic proton ratio of approximately 3/1.

The data are consistent with polymer formation by way of phenyl radical (or excited benzene) reaction with the fulvene produced to give phenyl or benzyl substituted cyclopentadienes which then polymerize to give a polycyclopentene chain with pendant phenyl and/or benzyl groups. The average non-olefinic to olefinic proton ratio of 2.9 indicates that the many possible structures similar to XI (5/2) predominate over the alternate type structures, XII (7/0),<sup>24</sup> assuming our analogy to cyclopentadiene type polymers is valid.



Many similar structures must be considered, including those derived from phenyl attack on the ring with polymerization through the exocyclic vinyl group of fulvene.

TABLE 4

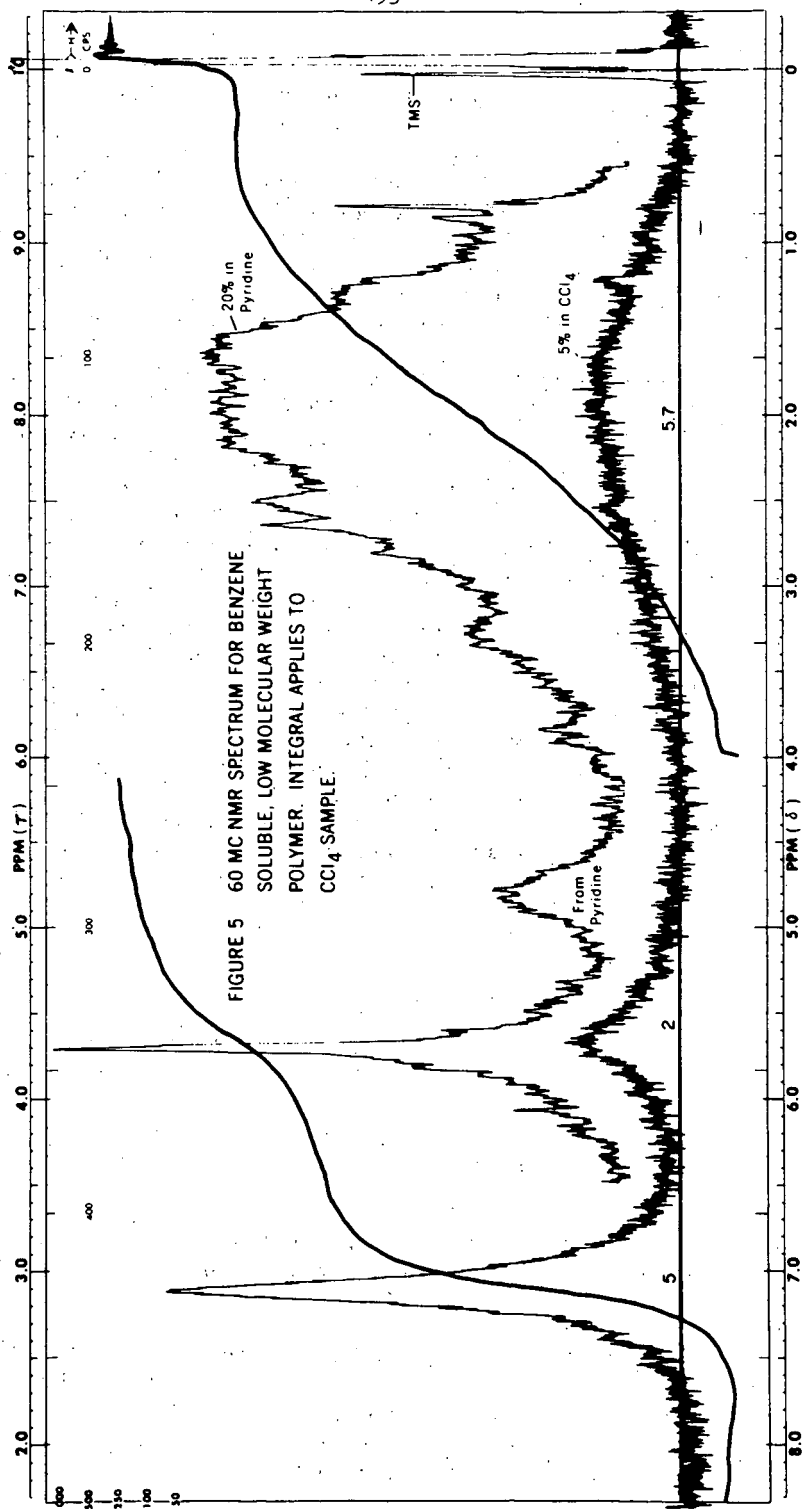
Properties of Polymers Produced  
in Corona Discharge of Benzene

	% C	% H	C/H	M. W. (a)	Infrared cm <sup>-1</sup>	(b)		
						Aromatic	Protons Olefinic	Non-olefinic
Benzene insol.	86.95	7.17	1.01	---	755, 695	---	---	---
Benzene sol. 1	88.32	7.18	1.02	4360	755, 695	5	2	5.8
2	87.26	7.09	1.03	1555	755, 695	5	2	5.7
3	87.23	7.09	1.03	305	755, 695	5	2	5.7

452

(a) Vapor pressure osmometry in benzene solution.

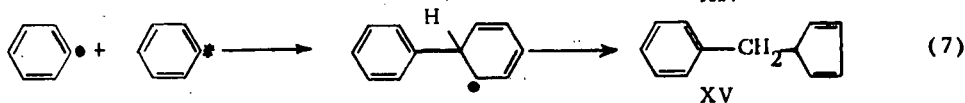
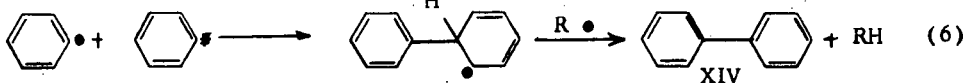
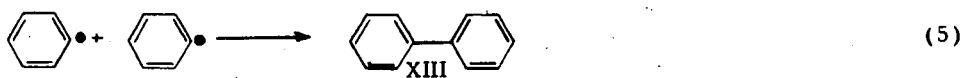
(b) Aromatic proton resonance assigned five protons.



## Mechanism

The available evidence is thus not consistent with the generally proposed mechanism of polymer formation based on the random build-up of a poly (phenylene) chain accompanied by hydrogenation,<sup>9</sup> or the interaction with the hexatrienyl diradical.<sup>23</sup> In the radiofrequency discharge of benzene, evidence was presented which clearly indicated that the polymer contained consecutive para linkages suggesting poly (p-phenylenes) as the predominant structure.<sup>12</sup> Schüller observed that the polymer (C/H 1.03, M.W. 503) was a phenyl substituted aliphatic chain based on infrared evidence.<sup>10</sup> Patrick and Burton have demonstrated that hydrogen atoms are not involved to any significant extent in polymer formation when liquid benzene is irradiated with a 1.5 m.e.v. source.<sup>24</sup>

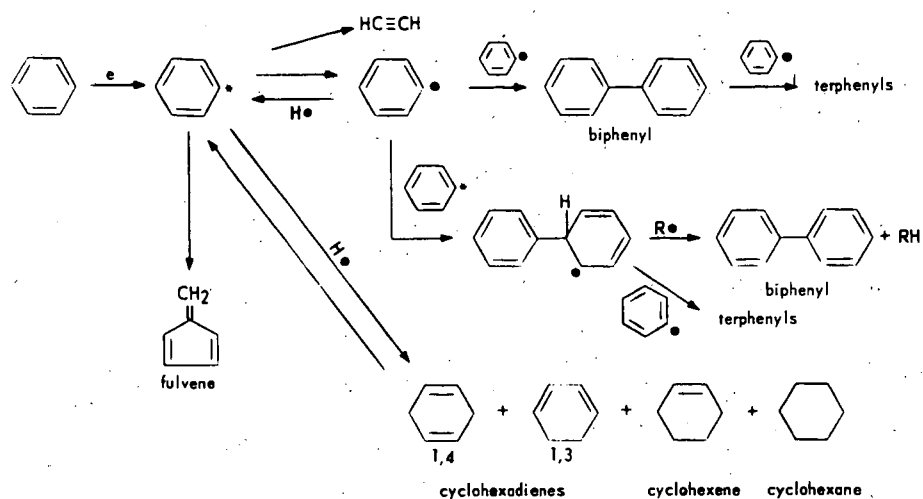
In the corona discharge many types of energy transfer are occurring, varying from photolysis (visible corona) to relatively high energy electrons responsible for fragmentation. The low yield of biphenyl in this single pass reactor suggests that phenyl radical production through loss of a hydrogen radical is not the primary reaction route leading to polymer formation. Considerable energy should be available to excite benzene to relatively high vibrational levels which would be somewhat below that energy required to actually separate the H radical. At any given time the number of these excited benzene molecules should greatly exceed the phenyl radical population. Fulvene is produced from benzene by ultraviolet energy (200 m $\mu$ , about 112 kcals, or 4.9 electron volts).<sup>25</sup> Thus, the formation of this benzene isomer with a resonance energy (11-12 kcals/mole) intermediate between benzene and 1,3 cyclohexadiene may be energetically favorable in the corona environment. Fulvene has been shown to polymerize rapidly under similar conditions with no reversion to benzene.<sup>25</sup> The uniformity of the phenyl (benzyl) - cyclopentene ratio throughout all polymer fractions makes it difficult to accept a mechanism based solely on random attack by phenyl radicals on the growing fulvene polymer. The initial synthesis of a monomeric unit comprised of the benzylcyclopentadiene system with subsequent diene type polymerization is consistent with all our observations. The phenyl radical produced in the discharge should collide with the nearest benzene molecule which will be excited to a relatively high vibrational energy level. The following reaction sequences are suggested for the phenyl radical:



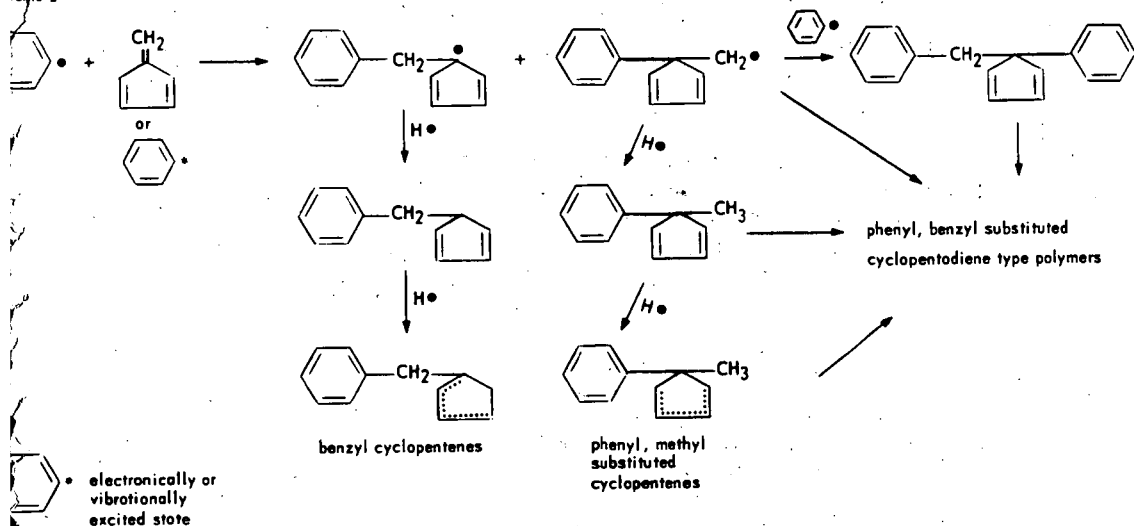
Reaction (5) is the typical termination reaction by radical coupling leading to biphenyl. The intermediate radical in (6) would be expected to lose hydrogen more readily than it would add to another benzene molecule to give polymer formation.<sup>26</sup> The possibility of ring contraction in the excited intermediate, accompanied by an intramolecular shift of a hydrogen atom is suggested in reaction (7). The benzylcyclopentadiene XV so obtained would be a very active monomer leading to the polymeric products observed. Although our data support polymer formation by the mechanism indicated, we cannot rule out participation by the cyclohexadienes and acetylene, both of these being noted in the benzene fraction and the low temperature traps.

FIGURE 6 PROPOSED REACTION MECHANISMS

Scheme 1



Scheme 2



The relatively low yield and the complexity of the reaction products does not allow an unequivocal designation of reaction mechanism or of the mode of energy transfer in the corona environment. However, where possible, we have proposed reaction mechanisms which are consistent with our results to date. These mechanisms are summarized in Figure 6. Studies are underway to obtain deuterium exchange data in the corona reactor, and mass spectral data are being evaluated. Investigation of the utility of corona chemistry will be extended to other volatile compounds.

## EXPERIMENTAL

Materials: Fisher thiophene-free benzene contained trace quantities of methyl cyclopentane, cyclohexane and toluene. Chromatogram (squalane) of original material was used as reference for irradiated benzene evaluation under the same GLC conditions.

Reference materials for chromatographic identification were generally used as obtained from commercial sources. Most of these materials were of sufficient purity to identify the major peak. However, mono-phenyl fulvene, obtained from Aldrich, gave no peak on the silicone column and infrared indicated extensive hydroxyl and carbonyl absorptions. 1,3,5-hexatriene from Aldrich gave two major and two minor peaks on the squalane column. Infrared<sup>27</sup> indicated largely the trans isomer with only a small cis absorption at  $818\text{ cm}^{-1}$ .

Fulvene was prepared by the method of Meuche.<sup>17</sup> Infrared ( $1662, 925, 890, 765\text{ cm}^{-1}$ ) and ultraviolet ( $\lambda_1 = 242\text{ mu}, \lambda_2 = 360\text{ mu}$ ) were in good agreement with literature values.<sup>15</sup>

### Reaction Conditions

The equipment used in these experiments was presented in Figures 1 and 2. Helium was bubbled through the benzene reservoir ( $55^\circ$ ) at  $100\text{ ml/min.}$  to carry  $4.2\text{ gm.}$  ( $0.054\text{ moles}$ ) benzene through the corona reactor per hour. The reactor temperature was  $45^\circ \pm 2^\circ$ . A total of  $101\text{ gm.}$  ( $1.3\text{ moles}$ ) benzene was passed through the  $15\text{ KV, } 60\text{ cycle,}$  corona discharge in  $23.7\text{ hours.}$  A small helium purge was maintained throughout all sampling operations and necessary downtime to preclude oxidation.

### Product Isolation and Analysis

At the conclusion of the run, the reactor was partially filled with benzene and refluxed on a steam bath for 2 hours. The benzene soluble material from the column was combined with the yellow brown solid which collected in the lower receiver. The insoluble material was swelled by benzene and generally loosened from the glass dielectric surface. This insoluble material was filtered off, washed several times with chloroform and dried overnight at  $70^\circ$  in a vacuum oven. The reactor was cleaned with a 5 per cent hydrofluoric acid solution to remove final traces of polymer after each run. Benzene insoluble polymer -  $0.7\text{ gm.}$  yellow brown color, % C 86.95, % H 7.17, C/H 1.01.

The benzene containing all solid products from the reactor and pot residue was reduced to  $30\text{ ml.}$  volume by vacuum distillation at  $50^\circ$ . Considerable foaming was encountered, requiring careful control of the distillation. The  $30\text{ ml.}$  of

brown benzene solution was added to 300 ml. isooctane at room temperature. A yellow solid precipitated immediately and was collected by filtration. After several washings with hot methanol, the material was dried for 8 hours at 70° in a vacuum oven. Benzene soluble polymer - Fraction 1, 2.3 gm., M. W. 4360, %C 88.32, %H 7.18, C/H 1.02.

The isooctane-methanol solution was reduced to 100 ml. volume (all methanol removed) by vacuum distillation at 60°. The solution was a brilliant yellow color at this point. On cooling to room temperature, a small proportion of a deep yellow polymeric solid precipitated and was collected by filtration. After washing with hot methanol, this yellow material was dried at 70° for 8 hours in a vacuum oven. Benzene soluble fraction 2, 0.2 gm., M.W. 1555, %C 87.26, %H 7.09, C/H 1.03.

The isooctane-methanol soluble portion was reduced to 20 gm. by vacuum distillation and sufficient benzene added to insure solubility of all components. The per cent solids was determined for this sample, being careful to limit sublimation of biphenyl (about 2 hours at 70° in a vacuum oven). This sample contains the low molecular weight products and a yellow resinous polymer. Qualitative analysis for the low molecular weight components was accomplished by gas-liquid chromatography using the following liquid phases: silicone gum rubber, Carbowax 20 M, and Reoplex 400. Quantitative data were obtained on the silicone column (Figure 4) using calibration curves (peak height) prepared from appropriate standards. The concentration of the small peak eluted before biphenyl was estimated using the biphenyl calibration curve and the peak after o-terphenyl was estimated using a commercial hydrogenated terphenyl mixture (Monsanto HB-40) as a reference. The F & M 500 gas-liquid chromatograph equipped with a standard thermoconductivity detector was used for these analyses. These low molecular weight products (biphenyl, o-, m-, p-terphenyl and phenylcycloalkenes, M. W. up to ~250) amount to 0.72 gms. (See Table 3). Peak confirmation was provided by infrared and NMR analysis after fraction collection from the chromatographic separation.

The concentration of the low molecular weight resinous polymer was determined by subtracting the total biphenyl fraction weight from the total isooctane-methanol soluble material. A sample of this material was placed in the vacuum oven at 100° until the GLC trace indicated negligible biphenyl content and the molecular weight was determined. Benzene soluble fraction 3, 3.5 gm., M. W. 305, %C 87.23, %H 7.09, C/H 1.03. Prolonged heating at 150° in air gives a hard, brittle yellow film. Infrared analysis indicates oxidation is involved in the drying process.

The benzene fraction was initially examined by GLC using 100 ft. support coated open tubular columns containing Carbowax 1540 poly (ethylene glycol) and squalane (Figure 3) as the liquid phase. Quantitative data were obtained at 45° on the squalane column with a helium flow of 3.0 ml/min. The Perkin Elmer Model 380 gas-liquid chromatograph, equipped with a stream splitting device and hydrogen flame detector was used for these analyses. Peak identification was by comparison with commercial standards and the synthesized fulvene. Additionally, the benzene fraction was refluxed in pressure bottles with maleic anhydride, azobisisobutyronitrile, and ammoniacal cuprous chloride solution prior to chromatographic analysis to note peak changes due to adduct formation, polymerization or presence of acetylenic hydrogen. Acetylene content was estimated from weight loss of the -70° and -195° traps. The vapor space above those cold traps and the gas stream directly below the corona were analyzed by infrared using an 8 cm. gas cell. Although the study was not exhaustive, several samplings were made and only acetylene was detected.

Methylacetylene, allene and butadiene were not present in sufficient quantity to be detected.

The yellow benzene from several runs (1000 ml.) was fractionated and 900 ml. distillate obtained from 79-80°. The distillate was refluxed with maleic anhydride until colorless and the benzene removed at reduced pressure. Dilute sodium hydroxide solution was added and the resulting solution was extracted several times with chloroform. After acidification with dilute hydrochloric acid, the solution was extracted with ether. The ether was removed after drying to give a white solid which, on recrystallization from chloroform and pet ether, gave the adduct 7-methylene-5-norbornene-2, 3-dicarboxylic acid which melted at 146°-150°. The infrared showed maxima at 1553, 875 and 710  $\text{cm}^{-1}$ , (lit <sup>(12)</sup> 1555, 874, 712  $\text{cm}^{-1}$ ). Fulvene was prepared in low yield (less than one per cent) from cyclopentadiene and formaldehyde with sodium ethoxide catalyst. <sup>17</sup> The adduct was prepared by adding maleic anhydride to the crude fulvene reaction product in Freon 113 (b.p. 47.6°) and refluxing until colorless. After removal of the solvent, hydrolysis and recrystallization yielded the adduct, m.p. 147-150°, which gave properties identical with the fulvene adduct obtained from the corona discharge. Bryce-Smith obtained a melting range of 105-110° for this adduct which was likely a mixture of the exo and endo isomers. <sup>25</sup> Stille prepared the fulvene-maleic anhydride adduct with a melting point of 149-150° which may be a single isomer. <sup>12</sup>

Through the courtesy of the Perkin Elmer Company at Norwalk, Connecticut, the discharged benzene was analyzed by combination of gas-liquid chromatography and mass spectroscopy. The peak attributed to fulvene gave a parent mass of 78 and fragments at m/e 77, 52, 51, 50 and 39 in good agreement with the literature. <sup>17</sup> Confirmation of other assignments was obtained by this technique and the one unidentified component on the squalane column gave a parent mass of 78.

Molecular weight and carbon-hydrogen determinations were made by Schwarzkopf Microanalytical Laboratories, New York, New York. Molecular weight was determined in benzene by vapor pressure osmometry.

#### LITERATURE CITED

- 1 Present address: Tarrytown Technical Center, Union Carbide, Tarrytown, New York.
- 2 G. Glockler and S. C. Lind, "The Electrochemistry of Gases and Other Dielectrics," John Wiley and Sons, New York (1939).
- 3 Ozone Chemistry and Technology, Advances in Chemistry Series No. 21, American Chemical Society (1959).
- 4 J. A. Coffman and W. A. Browne, Scientific American, 89, June (1965).
- 5 M. Bertholot, Compt. rend., 82, 1357 (1876).
- 6 S. M. Losanitsch, Bull. soc. stin. Bucharest, 233 (1914).
- 7 A. P. Davis, J. Phys. Chem., 35, 3330 (1931).
- 8 V. Karapetoff, W. H. Trebler, E. G. Linder, and A. P. Davis, Research Reports, Detroit Edison Company, Cornell Univ. (1928-32).
- 9 G. P. Brown, R. E. Rippere, Am. Chem. Soc., Div. Petrol. Chem., Preprints 2, No. 3, 149-54 (1957).
- 10 H. Schüller, K. Prchal, and E. Kloppenburg, Z. Naturforsch., 15a, 308 (1960).
- 11 A. Streitwieser, Jr., and H. R. Ward, J. Am. Chem. Soc., 84, 1065 (1962), 85, 539 (1963).
- 12 J. K. Stille, R. L. Sung, and J. Vander Kooi, J. Org. Chem., 30, 3116 (1965).
- 13 U. S. I. Chemicals, Polyolefin News, Feb. (1964).

- 14 G. J. Janz, *J. Chem. Phys.*, **22**, 751 (1954).
- 15 J. Thiec and J. Wiemann, *Bull. Soc. chim., France*, 177 (1956).
- 16 J. M. Blair and D. Bryce-Smith, *Proc. Chem. Soc.*, 1287 (1957).
- 17 D. Meuche, N. Neuenschwander, H. Schaltegger, and H. V. Schlunegger, *Helv. Chim. Acta*, **47**, 1211 (1964).
- 18 G. E. Gibson, N. Blake, and M. Kalm, *J. Chem. Phys.*, **21**, 1000 (1953).
- 19 G. F. Woods and L. H. Schwartzman, *J. Am. Chem. Soc.*, **70**, 3394 (1948).
- 20 E. E. Van Tamelen and S. P. Pappas, *J. Am. Chem. Soc.*, **85**, 3297 (1963).
- 21 E. L. Eliel, J. W. McCoy, and C. C. Price, *J. Org. Chem.*, **22**, 1533 (1958).
- 22 J. G. Powles, *Polymer*, **1**, 219 (1960).
- 23 W. N. Patrick and M. Burton, *J. Am. Chem. Soc.*, **76**, 2626 (1954).
- 24 A. G. Davies and A. Wassermann, *J. Polymer Sci.*, **4**, 1887 (1966).
- 25 H. J. F. Angus, J. M. Blair, and D. Bryce-Smith, *J. Chem. Soc.*, 2003 (1960).
- 26 G. A. Mortimer and L. C. Arnold, *J. Am. Chem. Soc.*, **84**, 4986 (1962).
- 27 J. C. H. Hwa, P. L. de Bonneville and H. J. Sims, *J. Am. Chem. Soc.*, **82**, 2538 (1960).

VAPOR PHASE DECOMPOSITION OF  
AROMATIC HYDROCARBONS BY ELECTRIC DISCHARGE

Masayuki Kawahata

Research and Development Center  
General Electric Company  
Schenectady, New YorkIntroduction

Decomposition of organic compounds in presence of electric discharge generally involves fragmentation and polymerization induced by inelastic collision with high energy electrons. When hydrogen is added, active hydrogen atoms produced by electric discharge also participate in the decomposition reactions. The reaction mechanisms are complex involving excited molecules, free radicals, and ions.

In this laboratory hydrocracking of coal, coal volatiles and related materials by electric discharge in hydrogen was studied. It is postulated by Given<sup>1</sup> that coal (vitrinite) molecules contain aromatic and hydroaromatic structures and probably fused aromatic ring nuclei linked together by methylene or ethylene groups forming hydroaromatic rings. Many of the replaceable hydrogens in the structure are substituted by hydroxyl or carbonyl groups. Short alkyl groups and alicyclic rings may also be attached as side chains. In pyrolysis at 500 - 600°C., dissociation of hydroxyl groups and dehydrogenation of naphthenic rings take place. These acts lead to formation of OH and H radicals which in turn help to break the linkages between aromatic nuclei, forming smaller, partly aromatic volatile fragments, and at the same time leaving a more aromatic residual structure behind.

On the other hand, high pressure hydrogenation of coal gives partial or complete hydrogenation of the aromatic structure. When this is subsequently cracked, the light products tend to be aliphatic rather than aromatic hydrocarbons. It was thought that hydrocracking of coal by electric discharge might be somewhere between pyrolysis and high pressure hydrocracking. In the course of study it was thought important to test this hypothesis by subjecting several aromatic or hydroaromatic compounds to electric discharge in a hydrogen stream for better understanding of the process. Organic compounds selected were m-cresol,  $\alpha$ -methylnaphthalene, tetrahydronaphthalene, decahydronaphthalene, and 9, 10-dihydrophenanthrene.

Experimental Apparatus and Procedures

The apparatus consisted of a vaporizer, a preheater, a discharge reactor, and a product collecting system. The organic compound was fed into the vaporizer at a certain rate and vaporized. Hydrogen was also

---

<sup>1</sup> P. H. Given, presented Am. Chem. Soc., January, 1963 in Cincinnati, Ohio

fed into the vaporizer at a certain flow rate and mixed with the organic vapor. The resultant mixture was then fed into the reactor through the preheater. The liquid products condensed in a water cooler were collected in a receiver and the gaseous products were collected in a liquid nitrogen trap. These products were analyzed by mass spectroscopy and vapor phase chromatograph employing a 6 ft. column of 10% silicone rubber, SE-30 and 60-80 Chromosorb P.

The discharge reactor was fabricated with quartz and was of a concentric tube design similar to an ozonizer. The inside of the inner barrier (40 mm OD and 38 mm ID) and the outside of the outer barrier (48 mm OD and 46 mm ID) were coated with conductive, transparent, tin oxide. The former was connected to the high voltage terminal and the latter to ground. In this arrangement the electric discharge was sustained in an annular space, 46 mm OD, 40 mm ID, and 200 mm long. The inside barrier tube was filled with stainless steel wool and a thermometer was placed in the center. This thermometer and three thermistors attached to the outside electrode were used to determine the reactor temperature. The reactor was insulated with glass wool, and the reactor temperature was maintained at approximately 300°C. for all the runs.

The electric discharge power was supplied by feeding the output of a 10,000 Hertz, 30 kilowatt inductor-alternator to the primary of a 50 kilovolt transformer and, in turn, to a tuned circuit, to the reactor and to the high voltage instrumentation. The electric discharge power was determined by measuring the area of parallelogram on the oscilloscope<sup>2</sup>.

When making the run, hydrogen was fed into the reactor at a definite flow rate and the electric discharge was applied to heat the reactor. When the reactor temperature was stabilized at about 300°C., the feed of the organic compound was started. The discharge power sustained for the reaction was in a range from 140 to 170 watts.

### Experimental Results and Discussions

For cresol-hydrogen mixtures, two runs were made using the empty reactor and three runs were made by filling the reactor space with porous or activated aluminum oxide grains. For all the runs, the reactor pressure maintained at 300 mm Hg. Experimental results, including product distribution, are listed in Table 1. The principal products were phenol, toluene, benzene, aliphatic hydrocarbons, carbon dioxide and water. Among the aliphatic hydrocarbons, acetylene was present in the largest amount and about 80% was unsaturates except for Run 5. In this run the concentration of unsaturates was 55%. This is probably due to a higher hydrogen concentration in the feed causing somewhat

---

<sup>2</sup> T. C. Manley, Trans. Am. Electro Chem. Soc. 84 83, 1943

more efficient hydrogenation. The bond energies of  $C_6H_5-CH_3$  and  $C_6H_5-OH$  are 90 and 73 Kcal/mol. respectively. Despite this, it was observed that, in the products, phenol was in higher concentration than toluene.

Use of aluminum oxide packing in the discharge space was intended to investigate the possibility of increasing the energy yield. Narrowing the gaseous discharge gap with dielectric packings may cause the following two effects on the discharge: (1) increase of discharge current for the same discharge power dissipated, and (2) increase of gaseous space breakdown field strength, if the gap decreases beyond a certain limit. The exact nature of the electric discharge employed in this study is still debatable.<sup>3,4</sup> However, it can be reasonably assumed that the primary reaction rate of the organic vapor with either high energy electrons or active hydrogen atoms may be dependent on discharge current density and field strength, if the system pressure and partial pressure of the reactant are constant. In electric discharge product of ozone, an increase in ozone concentration after filling the discharge gap with various dielectric packings is also reported by Morinaga and Suzuki.<sup>5</sup> In this study for approximately the same concentration of cresol vapor, the use of aluminum oxide grains in the discharge space appeared to increase the energy yield somewhat, but not conclusively.

In all the runs, the formation of brown solid films was observed on the reactor wall or on the surface of the grains. These solid films were not analyzed but they were insoluble in methylethyleketone or toluene. It is presumed that they are indicating possibly highly cross-linked polymerized products derived from the cresol. The energy yield for film formation was estimated to be in a range from 30 to 50 g/KWH; considerably higher than that for the fragmentation products.

Experimental results for the polycyclic compounds are summarized in Table 2. Methyl-naphthalene vapor in hydrogen was tested under pressures of 760 and 74 mm Hg. The principal lighter products were aliphatic hydrocarbons, benzene and toluene. At the higher pressure the concentration of the lighter aliphatic hydrocarbons was in the order  $C_2 > C_3 > C_4 > C_5$ . At the lower pressure, however, this order was reversed. In both cases about 32 - 35% were unsaturates. The energy yield was approximately doubled by lowering the pressure.

For tetrahydronaphthalene, three experiments were made under different pressures. Among the lighter aliphatic hydrocarbons produced, the  $C_2$  fraction was present in the largest amount, in which ethylene was in highest concentration followed by acetylene and ethane. The total percentage of unsaturates increased as the pressure decreased. This increase was essentially due to the increase in  $C_2$  and  $C_3$  unsaturates. As observed for methyl-naphthalene, the energy yield at 70 mm Hg was twice as high as that at 760 mm Hg. A considerably higher

---

<sup>3</sup> R. W. Lunt, Advanced Chem. Series, "Ozone Chemistry and Technology", Am. Chem. Soc., p. 286 (1959)

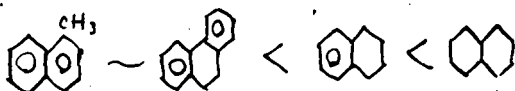
<sup>4</sup> M. Suzuki and Y. Naito, Proc. Japan Academy, 28 469 (1959)

<sup>5</sup> K. Morinaga and M. Suzuki, Bull. Chem. Soc., Japan 35 429 (1962)

energy yield than for the other two runs was observed at the intermediate pressure, 300 mm Hg.

When decahydronaphthalene was tested, one experiment was made under 760 mm Hg using 6.7% concentration in hydrogen. Another run was made under 300 mm Hg using 67% concentration. In the latter run, a higher energy yield was obtained. The product distribution was richer in the C<sub>2</sub> and C<sub>3</sub> fraction and also unsaturate concentration was higher.

One experiment was made to test dihydrophenanthrene in hydrogen. The gaseous products were essentially in the C<sub>2</sub> fraction; about 50% being unsaturated. Vapor phase chromatography of the liquid product showed two peaks. They were not identified but by the combined results of the VPC and mass spectroscopy one of the peaks was tentatively identified as butylbenzene. Biphenyl, which is a likely decomposition product, was not found. For the polycyclic aromatic and hydroaromatic compounds tested in this study, the energy yield from electric discharge hydrocracking for production of the lighter hydrocarbons was in the following order:



As observed in cresol runs, solid films were formed on the reactor wall, but they were not analyzed.

The number of experiments are not sufficient to permit drawing a concrete relationship between energy yield and molecular structure. The resonance energies of benzene, naphthalene, and phenanthrene are 39, 75, and 110 Kcal, respectively. It is reasonable to assume that the condensed aromatic ring structure absorbs large amounts of energy and requires high energy for cracking. The radiation effect on various polycyclic aromatic compounds were studied by Weiss et al.<sup>6</sup> They discussed correlations between the radiation stability and various structural factors. These include resonance energy, electron affinity, and ionization constant. Since there is a close similarity between radiation and electric discharge in principle, further information along this line would be helpful for a better understanding of the electric discharge hydrocracking process.

Elucidation of the reaction scheme in detail is beyond the scope of this study. However, it was indicated that in electric discharge hydrocracking of aromatic or hydroaromatic hydrocarbons, dissociation of the side chains and rupture of the rings are followed by secondary reactions involving the decomposed species; this leads to the formation of aromatic or aliphatic lighter compounds. Energy requirement to form these lighter compounds appear to be too high for practical applications. The formation of the solid polymerized products, which takes

<sup>6</sup> J. Weiss, C. H. Collins, J. Sucker, and N. Carciello, *Ind. Eng. Chem, Prod. Res. and Development*, 3, 73 (1964)

place in parallel with fragmentation, as seen for cresol runs, requires considerably less energy. Study on the formation of polymer films starting with various monomers and using the present discharge system presents an extremely interesting problem which is currently under investigation.

This is a part of the work supported by the Office of Coal Research, U. S. Department of Interior. The author is thankful for their generous support.

Table 1

Exp. No.	m-cresol Conc. %	Reactor packings	Organic Products Distributions, g/KWH			Energy Yield g/KWH	Unsaturates in Aliphatic %	
			Aromatic H/C	Aliphatic H/C	Phenol			
			C <sub>6</sub>	C <sub>7</sub>				
1	88.8	no	0.8	2.7	1.4	4.3	9.2	78
2	65.5	no	0.5	2.3	1.0	3.2	7.0	85
3	93.0	porous alumina	1.0	4.1	2.2	4.4	11.7	82
4	35.5	porous alumina	0.8	2.1	1.5	3.1	7.5	55
5	67.5	activated alumina	0.2	0.9	1.4	6.8	9.3	80

Electric Discharge Hydrocracking of m-cresol

Table 2

Exp. No.	Organic Vapor	Vapor Conc. %	Pressure mmHg	Energy Yield g/KWH	Product Distribution, Wt. %								
					C <sub>1</sub>	C <sub>2</sub>	C <sub>3</sub>	C <sub>4</sub>	C <sub>5</sub>	C <sub>6-C<sub>9</sub></sub>	Unsaturated		
6		4.5	760	0.66	2	33	24	21	13	7	32		
7		5.8	74	1.2	8	5	24	29	40	2	35		
8		5.8	760	1.5	5	77	12	3	1	2	74		
9		7.3	300	8.8	1	78	16	3	1	2	85		
10		7.4	70	3.0	--	74	23	2	.5	.5	90		
11		6.7	760	3.9	4	38	20	10	7	21	49		
12		66.7	300	5.4	4	56	27	7	2	7	76		
13*		4.5	760	0.69	3	23	7	3	2	1	71**		

466

\* The balance of the product distribution for this run (60%) was the heavier fractions which were not identified by VPC.

\*\* Percentage of unsaturates in C<sub>1</sub>-C<sub>9</sub> fractions

Hydrocracking of Polycyclic Aromatic and  
Hydroaromatic Compounds

## HYDROCARBONS AND CARBON FROM A ROTATING ARC HEATER

C. Hirayama and D. A. Maniero

Westinghouse Electric Corporation, Pittsburgh, Pa.

INTRODUCTION

A brief description of the rotating arc heater utilized in this work, and some preliminary hydrocarbon processing data, were described a year ago.<sup>1</sup> A more detailed description of the heater, and some of the operating characteristics have also been presented within the past year.<sup>2</sup> The arc heater consists essentially of water-cooled, toroidal electrodes, in which the arc is rapidly rotated as a result of interaction of the arc current with a magnetic field. The heater is a high current, low voltage device with a rating of 3 megawatts into the arc. Both alternating and direct current power operation are possible with this device. In contrast, most arc devices previously reported<sup>3</sup> are of the long arc, high voltage type which are operated on d.c. only.

We wish to report, herewith, some of the results obtained more recently in the pyrolysis of methane at atmospheric and at slightly elevated pressures.

EXPERIMENTAL

The feed gas was commercial grade methane of 96 per cent purity which was injected into the heater at ambient temperature. The flow rate was controlled by regulating the pressure drop across a sonic orifice.

The arc heater was operated only on a.c. power at electrode separations of 0.38, 0.75 and 1.0 inch. The arc power with methane ranged from 550 to 2200 kilowatts, with thermal efficiencies between 25 and 76 per cent, depending on operating conditions. For operation at elevated chamber pressure, the nozzle was choked with a graphite plate which had an orifice of 0.5 or 0.75 inch diameter in the center of the plate. The chamber pressure was as high as 100 psig.

The heater was operated at two different field coil currents to determine arc rotation velocity on the degree of reaction.

The products of the reaction were quenched and collected through a water-cooled copper probe, 1/8 or 1/4 inch I.D., inserted about an inch inside of the nozzle. The product from the probe was first passed through a fiber filter (Purolator Co.) to separate the carbon, then collected at appropriate intervals in gas sampling tubes on a manifold, as previously described.<sup>1</sup>

The gas analyses were made mass spectrometrically. A typical composition of a sample is shown in Table I; Table II shows the approximate material balance based on the  $H_2/C$  ratios of the feed and product gases. The only variation with operating conditions is in the relative concentration of the different species.

TABLE I. COMPOSITION OF GASEOUS PRODUCT, MOLE PERCENT

$H_2$	CO	CO <sub>2</sub>	CH <sub>4</sub>	C <sub>2</sub> H <sub>2</sub>	C <sub>2</sub> H <sub>4</sub>	C <sub>3</sub> H <sub>4</sub>	C <sub>4</sub> H <sub>2</sub>	C <sub>6</sub> H <sub>6</sub>
77.68	1.27	0.09	5.81	13.58	1.01	0.12	0.32	0.14

TABLE II. MATERIAL BALANCE OF PRODUCTS IN MOLE PERCENT

$H_2$	CO	CO <sub>2</sub>	CH <sub>4</sub>	C <sub>2</sub> H <sub>2</sub>	C <sub>2</sub> H <sub>4</sub>	C <sub>3</sub> H <sub>4</sub>	C <sub>4</sub> H <sub>2</sub>	C <sub>6</sub> H <sub>6</sub>	C
73.06	1.19	0.08	5.46	12.77	0.95	0.11	0.30	0.13	15.00

Electron micrographs were obtained on a number of the carbon samples by replicating an amyl acetate suspension on a carbon film. X-ray spectra were obtained by packing the soot into a disc-sample holder and irradiating with Cu K- $\alpha$  radiation. The sample packing and irradiation were kept as nearly identical as possible for all of the samples. The d-spacing and line intensity were compared against AUC graphite measured under identical conditions.

### RESULTS AND DISCUSSION

As shown in Table II, the product consists of species which are expected from the high temperature pyrolysis of methane. The primary products are  $H_2$ ,  $C_2H_2$ , and carbon, with varying concentration of  $CH_4$ , depending on the degree of reaction. The diacetylene and benzene are formed from the polymerization of the acetylene; the methyl acetylene, although not an intermediate in the conversion of  $CH_4$  to  $C_2H_2$ , is known to be a minor product found in the pyrolysis of diacetylene.<sup>4</sup> The  $C_2H_4$  is an intermediate in the  $CH_4 \rightarrow C_2H_2$  reaction. There is a slight error in the material balance since the hydrogen content of the soot was not taken into account because of sampling difficulty. The soot usually contains about one percent of hydrogen, and the presence of aromatic constituents is evident from the odor.

Considering the difficulty of obtaining exact experimental parameters during an experiment, quite good correlation was obtained between the degree of reaction and arc enthalpy, whereas the correlation was poor with respect to the net enthalpy increase of the gas. Figure 1 shows the relative degree of methane pyrolysis as a function of the arc enthalpy. The curves show the comparison between runs made at 2500 and 1500 amperes field coil current. The former effects an arc rotation velocity approximately 66 percent greater than that at the 1500 amps field coil current. There is a significantly steeper slope at higher arc rotation velocity, this result probably arising from the greater degree of mixing. Note that the curves saturate at high enthalpies, where the system is at equilibrium, or near equilibrium condition. A minimum just above the critical enthalpy (or initiation temperature).

The electron micrographs of the soot, quenched at the heater nozzle, at 25,500X magnification, Figure 2, shows spherical particles of less than 100 Å to approximately 5000 Å diameter. The nature of the background is not known at present, but blow-ups of the photomicrographs to approximately 153,000X suggests that the cloud consists of extremely fine, smokey carbon dust.

The d-spacings obtained from the x-ray diffraction of the soot varies between 3.45 and 3.49 Å, compared to 3.35 Å for pure, crystalline graphite. The lower value of 3.45 Å was obtained on the carbon collected from the high pressure runs, where the residence times were up to seven times longer than the runs at atmospheric pressure. The degree of crystallinity of the soot, based on the x-ray intensity, varied from two to ten percent of AUC graphite. The x-ray crystallinity, as suspected, is a function of the residence time.

It was of interest to plot the major product compositions on a semi-log plot, as a function of reciprocal arc enthalpy since the latter is proportional to the temperature in the gas. Figure 3 shows that the slopes for acetylene and hydrogen are approximately the same, whereas the slope for carbon is much steeper. The difference in slopes for carbon, as compared to  $C_2H_2$  and  $H_2$ , clearly shows the different mechanisms for the formation of these species.

REFERENCES

1. C. Hirayama and D. A. Maniero, "A New Rotating Arc Heater for Chemical Processing," Preprints, Div. of Fuel Chem., Am. Chem. Soc. Meeting, Pittsburgh, March 22-31, 1966, Vol. 10, No. 1, pp. 123-132.
2. D. A. Maniero, P. F. Kienest, and C. Hirayama, Westinghouse Engineer 26, 66 (1966). Also, same authors, paper presented at Electrochem. Soc. Nat. Meeting, Phila., Oct. 12, 1966.
3. See, for example, S. A. Miller, "Acetylene, Its Properties, Manufacture and Uses." Vol. I, Academic Press, New York, 1965, pp. 391-405.
4. K. C. Hou and H. B. Palmer, J. Phys. Chem. 69, 858 (1965).

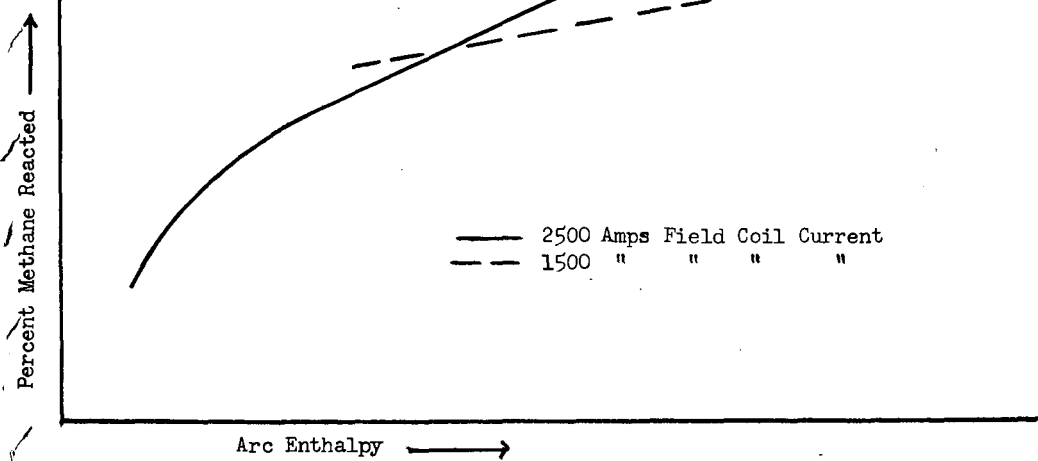


Fig. 1. Methane conversion as functions of arc enthalpy and arc rotation



Fig. 2. Electron micrographs of carbon at 25,500X

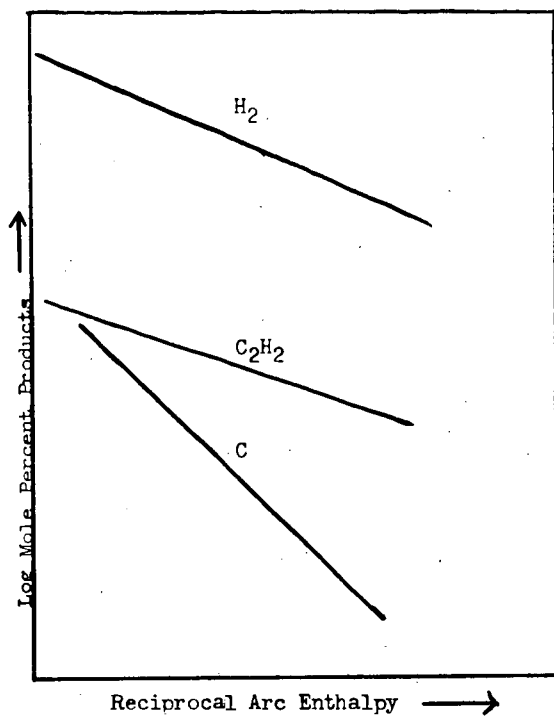


Fig. 3. Product composition as a function of reciprocal arc enthalpy

## THE REARRANGEMENT OF METHANE AND METHYL CHLORIDE IN A MICROWAVE DISCHARGE

J. P. Wightman

Virginia Polytechnic Institute, Blacksburg, Virginia

N. J. Johnston

NASA - Langley Research Center, Hampton, Virginia

## I. INTRODUCTION

In a previous paper(1) the rearrangement of a series of hydrocarbons including methane in a microwave discharge was reported. The work reported here is an investigation of the effect of the introduction of a functional group in methane on the nature of both the gaseous and solid products of rearrangement. Such measurements should ultimately support a model of the rearrangement mechanism in a microwave discharge. Methane and methyl chloride were passed separately in the absence of a diluent through a microwave discharge.

## II. EXPERIMENTAL

## A. Materials

Methane (ultrahigh purity grade) was obtained from the Matheson Co. and used without further purification. The following analysis was supplied with the methane:  $\text{CO}_2$  - <5 ppm;  $\text{O}_2$  - 5 ppm;  $\text{N}_2$  - 19 ppm;  $\text{C}_2\text{H}_6$  - 14 ppm;  $\text{C}_3\text{H}_8$  - <5 ppm. Methyl chloride (high purity grade) was obtained from the Matheson Co. and used without further purification.

## B. Apparatus and Procedure

The rearrangements were carried out in a high vacuum flow system. The power source for the microwave discharge was a Raytheon generator (Model KV-104) and was operated at a power level corresponding to about 40 r.f. watts at 2450 Mc. The generator was connected to an air-cooled cavity (Raytheon - KV series) by a coaxial cable. Two procedures were used depending upon whether an analysis of the gaseous products was being made or whether solid film was being deposited for subsequent analysis. In the former case, the parent gas was passed through a variable leak valve (Veeco - VL). The pressure in a typical experimental run was 0.15 torr at a mass flow rate of  $1 \times 10^{-5}$  moles/min. and a linear flow rate of 20 cm./sec. In the latter case, the parent gas was passed through a Teflon needle valve (Fischer-Porter). The pressure in a typical experimental run was 0.50 torr. Normal deposition time was 20 min.

The gaseous rearrangement products of methane and methyl chloride were determined using a mass spectrometer (Associated Electronics Industries - MS-10). The sampling volume was located about 140 cm. downstream from the discharge. After establishment of a constant flow rate, the parent gas stream was sampled. An off-on valve upstream from the discharge allowed the system to

be pumped down without altering the setting of the variable leak. Between analyses pumpdown resulted in faster attainment of steady state concentrations of rearrangement products. Flow was again started and the discharge initiated with a Tesla coil. After establishment of a constant flow rate the discharged gas stream was sampled.

The solid polymeric films were removed mechanically from the walls of the Pyrex tubing. The infrared spectra of the films of both gases were obtained using either a Perkin-Elmer 421 or 621 spectrophotometer. The electron spin resonance spectra of the neat films from both gases were obtained on a Varian ESR 6 spectrometer. Elemental analyses of both films were made by Gailbraith Labs.

### III. RESULTS

#### A. Gaseous Products

##### 1. Mass spectra

Selected peaks from the mass spectra of methane and methyl chloride obtained with the discharge on and off are shown in Figures 1a and 1b. The most significant features in the methane spectra (Figure 1a) were the increase in the  $m/e = 2$  ( $H_2^+$ ) peak and the decrease in the  $m/e = 15$  ( $CH_3^+$ ) peak when methane was passed through the discharge. Trace quantities of higher molecular weight hydrocarbons were also noted. The most significant features of the methyl chloride spectra (Figure 1b) were the increase in the  $m/e = 2$  ( $H_2^+$ ) peak, the appearance of the  $m/e = 30$  ( $C_2H_6^+$ ) peak and the decrease in the  $m/e = 50$  ( $CH_3Cl^+$ ) peak when methyl chloride was passed through the discharge. Further, HCl was noted when the liquid nitrogen cooled trap downstream from the discharge was opened.

#### B. Solid Films

A solid film was observed to form in the discharge region when either methane or methyl chloride was passed through the discharge. Both films were characterized in several ways.

##### 1. Elemental analysis

Empirical formulas for the solid films were established by elemental analysis. The formulas for the solid films formed from methane and methyl chloride were  $(CH_{1.5})_x$  and  $(CH_{0.65}Cl_{0.045})_x$ , respectively.

##### 2. Infrared spectra

The infrared spectrum of the film obtained from methane is shown in Figure 2 where a neat sample was used. Peaks ascribed to the film were noted in the region of the following frequencies: 2900, 1700, 1450, 1380 and  $880\text{ cm}^{-1}$ . The assignments of these frequencies follow those given by Jesch et al (2). The band at  $880\text{ cm}^{-1}$  may be due to rocking vibration of  $-CH_3$  in a multiple carbon atom chain. The band at  $1380\text{ cm}^{-1}$  is characteristic of  $-CH_3$  deformation. The band at  $1450\text{ cm}^{-1}$  is characteristic of  $-CH_2$  symmetric scissors vibration. The band at  $1700\text{ cm}^{-1}$  was probably due to carbonyl formed on exposure of the film to air. The  $2900\text{ cm}^{-1}$  band

is due to C-H stretching vibration.

The infrared spectrum of the film obtained from methyl chloride is shown in Figure 3 where a neat sample was used. The low intensity peaks were a characteristic of the methyl chloride films whether run as a neat sample or as a KBr pellet. Peaks ascribed to the film were noted in the region of the following frequencies: 2900, 1700, 1580, 1440 and 875  $\text{cm}^{-1}$ . The peak at 1380  $\text{cm}^{-1}$  observed in the methane film is absent in the methyl chloride film and a new peak at 1580  $\text{cm}^{-1}$  is observed in the methyl chloride film.

### 3. Electron spin resonance

The electron spin resonance spectra of the films produced from methane and methyl chloride are shown in Figures 4a and 4b. A significantly larger free spin concentration on the order of one thousand times greater was noted in the case of the methyl chloride film. No fine structure was observed in the case of the methyl chloride film. g-values for both films were essentially identical to the value for pitch ( $g = 2.000$ ).

### 4. Solubility studies

An extensive series of liquids were tested as possible solvents for the films prior to NMR measurements. Solubility of the methane film was observed only in the case of hexamethylphosphamide and concd.  $\text{H}_2\text{SO}_4$ .

## IV. DISCUSSION

Investigations of chlorinated hydrocarbons in a microwave discharge have not been reported in the literature previously. Swift et al (3) however have investigated the effect of an rf discharge on  $\text{CCl}_4$  in the absence of a diluent. A number of chlorinated gaseous products were reported in addition to a chlorinated polymer. The present work indicated a limited number of gaseous products. The results are consistent with the argument that molecules in a microwave discharge are subjected to a greater degree of fragmentation than in an rf discharge thereby limiting both the number and the complexity of gaseous products.

From the previous work of Vastola and Wightman (1) the following postulate could be advanced: if a parent hydrocarbon has a hydrogen to carbon (H/C) ratio greater than about 1.6, a hydrogen saturated solid film will be produced on passage of the hydrocarbon through a microwave discharge in addition to hydrogen. Conversely, if a parent hydrocarbon has a (H/C) ratio less than about 1.6 a hydrogen deficient film will be produced and no hydrogen will be observed.

The present work is an attempt to test the validity of this postulate if a functional group is introduced into the hydrocarbon molecule. Methyl chloride was chosen since it represents a straightforward extension of the methane case. Methyl chloride has a (H/C) ratio of 3 and if the Cl is neglected, the formation of a hydrogen saturated film would be predicted. However, HCl was observed as a rearrangement product. Hence the Cl can not be neglected and yet assuming the limiting case of a 1:1 correspondence between  $\text{CH}_3\text{Cl}$  and HCl, the (H/C) ratio of the remaining fragment would be 2. Thus the formation of a hydrogen saturated film would still be predicted but which in fact was not observed.

Instead a hydrogen deficient film was produced. The formation of a hydrogen deficient film from a parent molecule which has a high enough (H/C) ratio to form a hydrogen saturated film can be attributed to two factors. In the first instance, Cl preferentially appears in the gas phase as is indicated by the low percentage of Cl in the film, the absence of a significant C-Cl absorption peak in the infrared spectrum (Figure 3) and the presence of HCl downstream from the discharge. The extension of this work to other functional groups is anticipated to determine if this is a general scheme. In the second instance, the tendency to form hydrogen in a microwave discharge is again noted in the case of methyl chloride as in the case of methane (Figures 1a and 1b). Apparently for hydrocarbons containing functional groups, the formation of hydrogen is favored even at the expense of the formation of a hydrogen deficient film. The formation of ethane observed as a product of the methyl chloride discharge could be due to the recombination of methyl radicals produced in the discharge.

Films formed in various types of electrical discharges have not been extensively characterized. The recent work of Jesch et al (2) described the infrared analysis of a series of films produced from hydrocarbons in a glow discharge. Direct comparison between the present results and those of Jesch et al is not possible since two different types of electrical discharges were used. The type of discharge used dramatically alters the nature of both the gaseous and solid rearrangement products as indicated above.

The properties of the film produced from methyl chloride are similar to those reported previously (1) for the hydrogen deficient films formed from acetylene, benzene and naphthalene. The color of the methyl chloride film was dark (brownish-black) characteristic of hydrogen deficient films in contrast to the light yellow methane film characteristic of hydrogen saturated films. The high electron spin concentration of the methyl chloride film had also been observed for the hydrogen deficient film from acetylene.

The films produced from both methane and methyl chloride appear to be highly cross-linked as evidenced by the negligible solubility in liquids used as solvents for other polymeric systems. The methyl chloride film contains a greater number of free electrons than the methane film indicative of a significant number of unsaturated valences in the methyl chloride film. The methyl chloride film appears to be characterized by a greater degree of unsaturation than the methane film. Highly unsaturated polymeric systems have been found difficult to analyze by infrared spectroscopy\* which has also been noted in the present results. Definitive NMR work would be helpful in elucidating the nature of these polymeric films.

\* private communication with Dr. Vernon Bell (NASA - Langley Research Center)

Acknowledgements - The authors would like to acknowledge the help of Dr. R. E. Dessy in obtaining the ESR spectra and the experimental assistance of Mr. R. O. McGuffin.

#### REFERENCES

- (1). F. J. Vastola and J. P. Wightman, *J. Appl. Chem.*, 14, 69 (1964).
- (2). K. Jesch, J. E. Bloor and P. L. Kronick, *J. Poly. Sci. A-1*, 4, 1487 (1966).
- (3). E. Swift, jr., R. L. Sung, J. Doyle and J. K. Stille, *J. Org. Chem.*, 30, 3114 (1965).

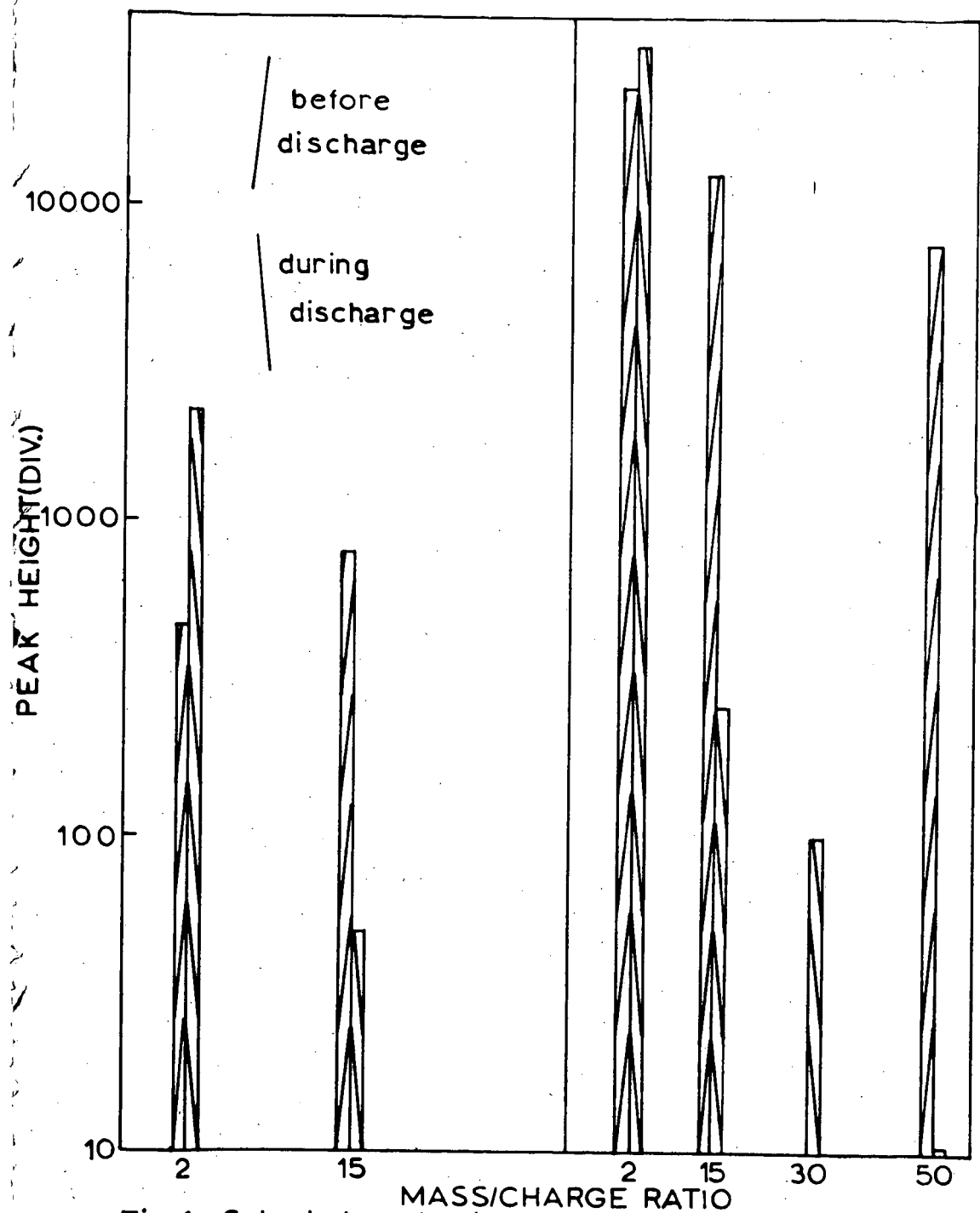
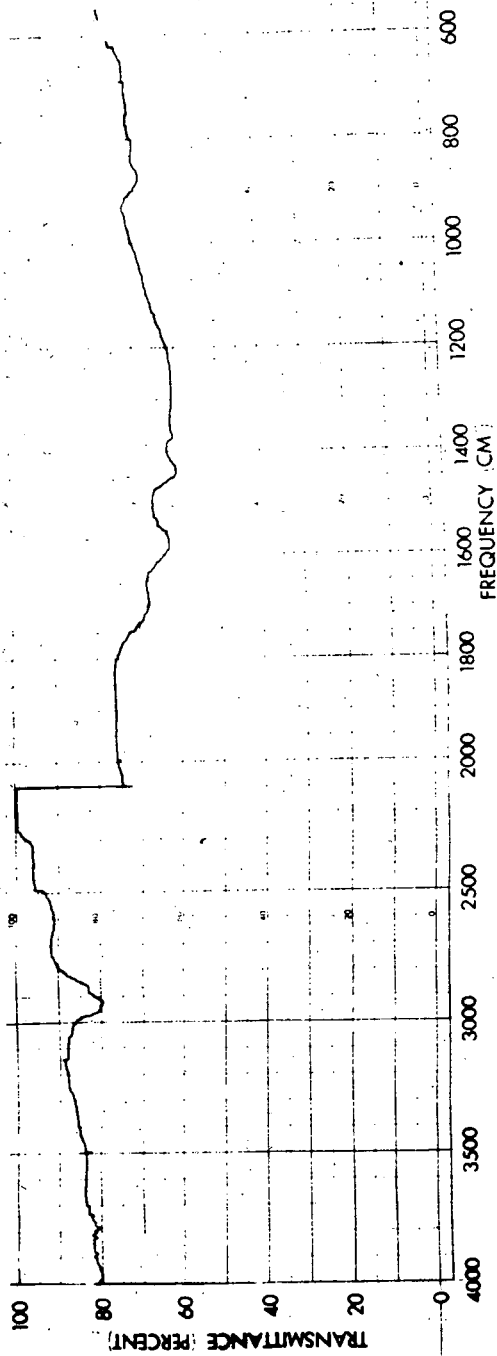


Fig. 1a. Selected peaks from Fig. 1b. Selected peaks from mass spectra of methane in a microwave discharge. mass spectra of methyl chloride in a discharge.



478

Fig.3. Infrared spectrum of polymer produced from methyl chloride.

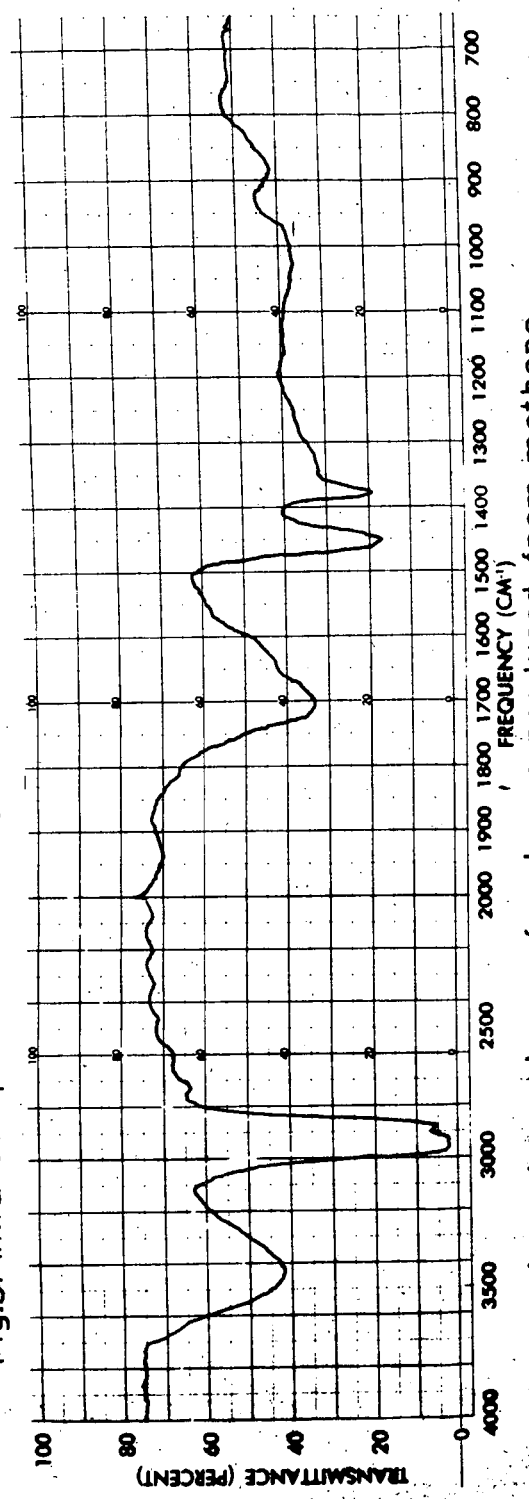


Fig.2. Infrared spectrum of polymer produced from methane.

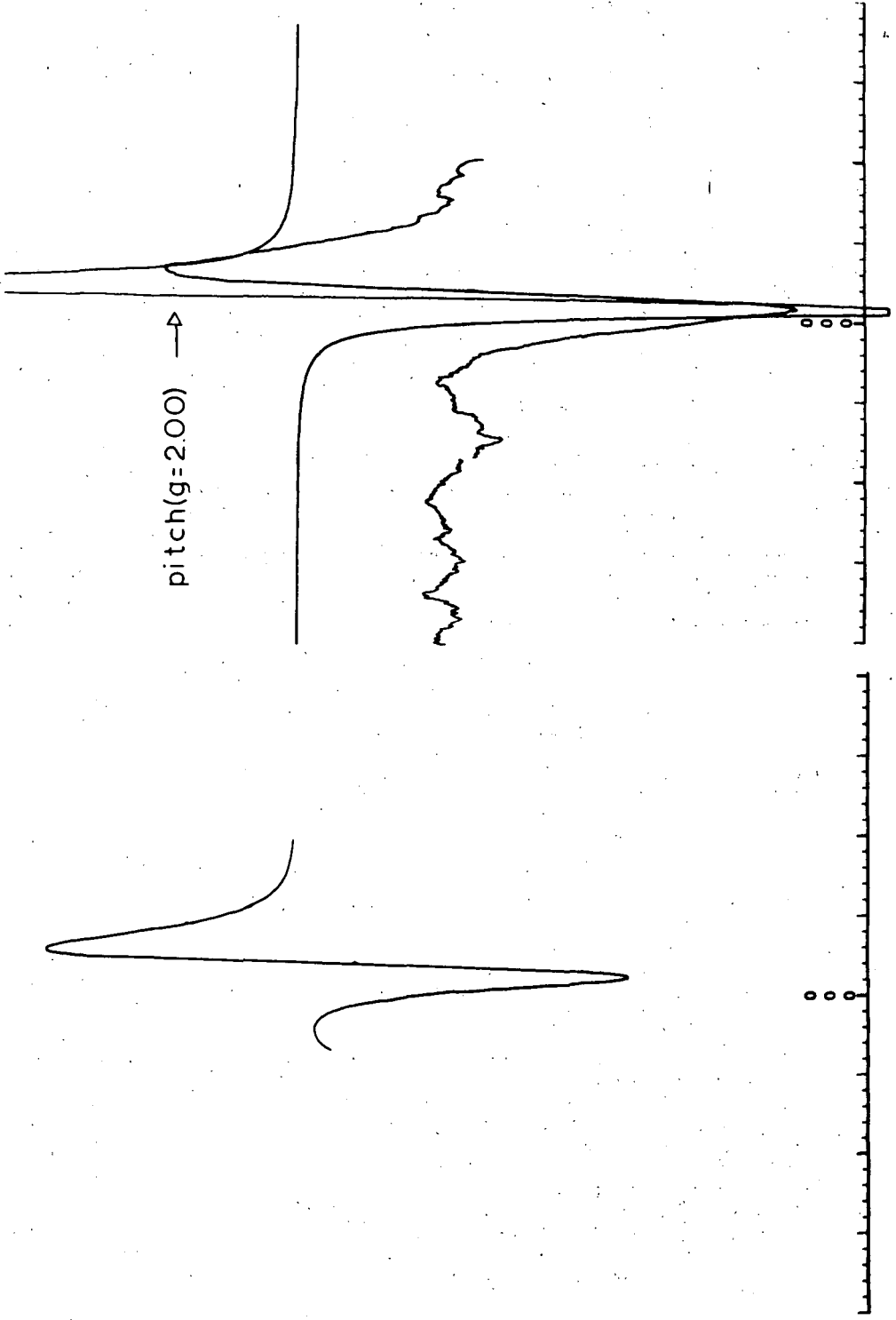


Fig.4b. ESR spectrum of polymer produced from methyl chloride.

Fig.4a. ESR spectrum of polymer produced from methane.

FATTY ACIDS AND n-ALKANES IN GREEN  
RIVER OIL SHALE: CHANGES WITH DEPTH

Dale L. Lawlor and W. E. Robinson

Laramie Petroleum Research Center, Laramie, Wyoming

## INTRODUCTION

Many papers have been published relating fatty acids to n-alkanes in ancient sediments. Breger (1) postulated that n-alkanes may be formed in sediments by beta-keto acid decarboxylation. Jurg and Eisma (5) demonstrated in the laboratory that a homologous series of n-alkanes can be produced by heating the C<sub>22</sub> fatty acid in the presence of bentonite. Cooper and Bray (2) suggested that odd-carbon-numbered n-alkanes and odd-carbon-numbered fatty acids may be produced from naturally occurring even-carbon-numbered fatty acids by a free-radical decarboxylation mechanism. Mair (7) and Martin and coworkers (8) have discussed the relationship between fatty acids and n-alkanes in petroleum genesis.

If fatty acids are converted to n-alkanes in sediments, a distributional relationship would likely be apparent between the two compound classes. Such a relationship would be most relevant if both the acids and the alkanes were indigenous to each sample taken from one geological formation. In this respect the Green River Formation is ideal for study of the relationship between fatty acids and n-alkanes. This formation represents 6 million years of accumulation of organic debris from a highly productive Eocene lake which existed approximately 50 million years ago. A 900-foot core representing 3 million years of the Green River Formation was sampled and the fatty acids were extracted and analyzed.

An earlier paper (6) presented a correlation between the carbon number distribution of the fatty acids and the carbon number distribution of the n-alkanes in the Mahogany zone portion of the Formation. The present paper tests the postulate that n-alkanes are formed from fatty acids by maturation processes resulting from the time differential existing between the bottom and the top of the core. The results showed that both maturation and changes in organic source material explain the differences in samples taken from several stratigraphic positions in the formation.

## EXPERIMENTAL

Ten oil-shale samples were taken from the Green River Formation, nine from a 900-foot core (Equity Oil Co., Sulfur Creek No. 10), and one from the Mahogany zone. The stratigraphic positions and the oil yields of the 10 samples are presented in table 1. The samples were the same as those used by Robinson and coworkers (9) in a study of the distribution of n-alkanes at different stratigraphic positions within the formation.

The samples, ground to pass a 100 mesh screen, were treated with 10 percent hydrochloric acid to remove mineral carbonates and to convert salts of acids to free acids. Two-hundred grams of each of the acid-treated samples were refluxed with 400 ml of 7 percent borontrifluoride in methyl alcohol for 6 hours. This reaction converted free and esterified acids to methyl esters. The reaction mixture was cooled, filtered, and washed with methyl alcohol until the washing was clear. The filtrate was transferred to a separatory funnel, water was added, and the solution was extracted with successive portions of carbon tetrachloride until the solvent was colorless. The carbon tetrachloride solution of the methyl esters was dried overnight using anhydrous sodium sulfate. The fatty acid methyl esters were isolated from the carbon tetrachloride solution by urea adduction.

TABLE 1. - Stratigraphic position and pyrolytic oil yields of the oil-shale samples

Sample Number	Stratigraphic position, feet from surface	Approximate pyrolytic oil yield, gallons per ton of shale
0	830	60
1	1036-1056	35
2	1056-1081	34
3	1152-1178	42
4	1236-1241	48
5	1450-1462	39
6	1597-1628	35
7	1668-1696	37
8	1786-1825	28
9	1884-1924	20

Fatty acid methyl esters were further purified by thin layer chromatography using silica gel. The thin layer plate was developed with a mixture of n-hexane, ethyl ether, and acetic acid (90/10/1). The adsorbant zone where esters occur was scraped from the plate and extracted with a solution of 10 percent methyl alcohol in carbon tetrachloride. The solvent was removed from the methyl esters by evaporation at room temperature under a stream of nitrogen. The carbon number distribution of these isolated fatty acid methyl esters was determined by mass spectrometry using the intensity parent peak as a measure of the quantity.

Carboxyl and ester contents were determined for the 10 shale samples by analytical procedures developed by Fester and Robinson (4).

#### RESULTS AND DISCUSSION

The fatty acid distribution with depth (table 2), shows that the predominant acid at various stratigraphic depths within the formation is not constant. The sample number, percentage, and chain length of the predominant acid of the samples are: No. 0, 16.2, C<sub>30</sub>; No. 1, 14.1, C<sub>24</sub>; No. 2, 21.7, C<sub>28</sub>; No. 3, 9.8, C<sub>28</sub>; No. 4, 16.6, C<sub>24</sub>; No. 5, 9.2, C<sub>28</sub>; No. 6, 12.8, C<sub>14</sub>; No. 7, 12.6, C<sub>14</sub>; No. 8, 12.1, C<sub>28</sub>; and No. 9, 23.9, C<sub>28</sub>. The C<sub>28</sub> acid is the predominant acid in five of the samples, and is among the three most abundant acids in all the other samples except samples 1 and 4 where it is present in small amounts. The C<sub>20</sub> acid content in samples 5 through 9, despite being more abundant in nature than the C<sub>19</sub> and C<sub>21</sub> acids, is less than the C<sub>19</sub> and C<sub>21</sub> acids in these samples. The C<sub>18</sub> acid is quite low in samples 1 and 2 relative to the other eight samples. The C<sub>32</sub> acid is present in large amounts only in sample No. 0. There appears to be no consistent relationship between the acids of one sample to that of another sample. This lack of relationship may be due to differences in source material or environmental changes rather than maturation changes.

Significant differences are apparent in the relative distribution of the fatty acids and the n-alkanes from published data (3,9), shown in figures 1 and 2, where the data from four samples are plotted for comparative purposes. These particular samples were chosen because they represent three stratigraphic levels below the Mahogany zone sample approximately equi-distant from each other. If maturation of sediments causes decarboxylation of fatty acids to form n-alkanes, a relationship between the distribution of the two components would be expected. Except for sample No. 0, little similarity is evident. Since the distributions correlate poorly, either the original postulate is untrue and n-alkanes are not produced from fatty acids having one more

TABLE 2. - Carbon number distributions of fatty acids

Carbon Number	Fatty acids, wt percent of total									
	Sample number									
	0	1	2	3	4	5	6	7	8	9
14	5.1	7.1	2.8	6.3	2.3	8.0	12.8	12.6	11.4	6.5
15	3.0	3.4	2.8	6.3	2.8	7.2	2.1	6.3	8.1	3.7
16	2.7	7.1	2.4	5.6	4.0	5.8	6.4	7.8	9.4	5.4
17	2.0	4.0	1.9	4.9	2.9	5.1	5.9	4.3	2.4	2.0
18	3.4	2.6	2.1	4.2	4.2	5.4	8.0	7.4	7.4	6.1
19	2.4	3.4	1.8	3.5	3.8	4.0	4.3	3.6	2.0	2.0
20	2.7	8.2	1.9	2.8	4.5	2.9	4.2	2.9	2.0	1.3
21	2.4	7.1	2.2	2.8	5.6	3.6	4.8	3.6	2.0	1.7
22	7.4	8.8	3.6	4.9	9.7	5.8	11.6	8.3	10.7	13.0
23	4.7	4.7	4.4	5.6	12.5	5.8	3.8	4.7	3.4	3.3
24	7.1	14.1	6.2	4.2	16.6	3.3	8.0	6.3	8.7	12.0
25	3.7	7.6	5.0	3.5	8.3	2.5	3.8	3.4	2.7	2.6
26	12.1	11.8	13.3	8.4	11.8	6.5	4.9	5.9	4.7	5.2
27	2.7	2.6	8.2	6.3	3.7	8.0	2.7	4.9	3.4	3.7
28	11.1	4.2	21.7	9.8	4.0	9.2	9.8	8.5	12.1	23.9
29	2.7	1.3	5.7	4.2	1.2	4.3	1.5	2.9	2.7	2.4
30	16.2	1.3	8.6	7.7	1.1	5.8	2.5	3.2	2.7	2.8
31	1.7	0.4	2.5	4.2	0.3	4.0	0.8	1.6	2.0	1.3
32	7.1	0.4	2.9	4.9	0.5	3.3	0.9	1.6	2.0	1.1

carbon atom or other factors are more significant. One factor to consider is that the fatty acids recovered from the lower portions of the core may not be representative of the acids originally present since they may be residual acids from selective maturation.

Groups of even numbered acids vary in abundance as shown graphically in figures 1 and 2. Sample No. 0 has predominant acid peaks between C<sub>26</sub> and C<sub>30</sub>, sample No. 4, between C<sub>22</sub> and C<sub>26</sub>, sample No. 6, between C<sub>22</sub> and C<sub>28</sub>, and sample No. 9, between C<sub>22</sub> and C<sub>28</sub>. The latter two samples show the greatest overall similarity.

The carboxyl content of the shale generally decreases with depth, table 3, beginning with sample No. 0 having 23.6 mg of carboxyl per gm of organic carbon and ending with sample No. 9 having 4.8 mg of carboxyl per gm of organic carbon. This general decrease in carboxyl content with depth, and a corresponding increase in the n-alkane content, as shown by Robinson and coworkers (9), implies that the fatty acids may have been converted to n-alkanes by decarboxylation.

The ester content of the samples, table 3, did not show a trend; this is in contrast to the trend shown by the acids. Random distributions found for the ester samples reflect more accurately changes in organic source material than do the acid distributions.

Maturation changes are evident in the decreasing amount of carboxyl content with depth, the increasing amount of n-alkane content with depth, and the decreasing ratio of odd to even-carbon-numbered n-alkanes. Source material or environmental changes are evident in the variations in the amount and carbon number of the dominant fatty acids, and n-alkanes and the random distribution of ester content with depth.

TABLE 3. - Carboxyl and ester contents of the 10 shale samples

Sample Number	Carboxyl, mg/gm carbon	Ester, mg/gm carbon <sup>1/</sup>
0	23.6	36.6
1	18.3	22.2
2	10.1	33.9
3 <sup>2/</sup>	--	--
4	3.8	26.7
5	6.7	17.9
6	4.0	37.1
7	4.7	26.0
8	4.9	42.9
9	4.8	29.0

<sup>1/</sup> Calculated as COOH

<sup>2/</sup> Insufficient sample.

#### CONCLUSIONS

The postulate that fatty acids from the organic debris in the Green River Formation may form n-alkanes of one less carbon atom was found to be subject to question. Relatable fatty acid and n-alkane distributions were shown to be present in the younger portions of the Formation but the older portions showed little relation.

Maturation and organic source material differences may account for the observed distributions of fatty acids in sections of Green River Formation oil shale. Evidence of maturation is found in the decreasing amount of odd-carbon-numbered n-alkanes and in the decreasing amount of carboxyl content with depth. Evidence of organic source material differences is found in the inconsistent distribution of the predominant fatty acids from sample to sample.

The ester content is not related to the free-acid content, indicating different formative histories.

#### REFERENCES

1. Breger, I. A. Diagenesis of Metabolites and a Discussion of the Origin of Petroleum Hydrocarbons. *Geochim. et Cosmochim. Acta*, v. 19, 1961, pp. 297-308.
2. Cooper, J. E., and E. E. Bray. A Postulated Role of Fatty Acids in Petroleum Formation. *Geochim. et Cosmochim. Acta*, v. 27, 1963, pp. 1113-1127.
3. Cummins, J. J., and W. E. Robinson. Normal and Isoprenoid Hydrocarbons Isolated from Oil-Shale Bitumen. *J. Chem. Eng. Data*, v. 9, 1964, pp. 304-307.
4. Fester, J. I., and W. E. Robinson. Oxygen Functional Groups in Green River Oil Shale and Trona Acids. Ch. in "Advances in Chemistry Series." American Chemical Society, Washington, D.C. (1966), pp. 22-31.
5. Sarg, J. W., and E. Eisma. Petroleum Hydrocarbons: Generation from Fatty Acids. *Science*, v. 144, 1964, pp. 1451-1452.

6. Lawlor, D. L., and W. E. Robinson. Division of Petroleum Chemistry, Am. Chem. Soc., Detroit, Mich., April 1965, Petroleum Division General Papers No. 1, 1965, pp. 5-9.
7. Mair, B. J. Terpenoids, Fatty Acids and Alcohols as Source Materials for Petroleum Hydrocarbons. *Geochim. et Cosmochim. Acta*, v. 28, 1964, pp. 1303-1321.
8. Martin, R. L., J. C. Winters, and J. A. Williams. Distributions of n-Paraffins in Crude Oils and Their Implication to Origin of Petroleum. *Nature*, v. 199, 1963, pp. 110-114.
9. Robinson, W. E., J. J. Cummins, and G. U. Dinneen. Changes in Green River Oil Shale Paraffins with Depth. *Geochim. et Cosmochim. Acta*, v. 29, 1965, pp. 249-258.

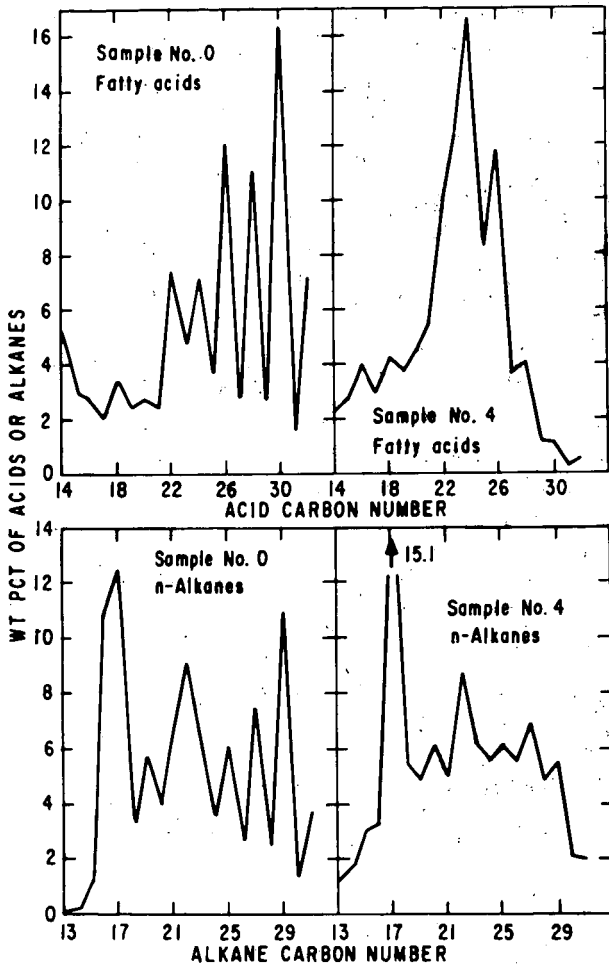


Figure 1. Comparison between fatty acid and n-alkane distributions, Sample Nos. 0 and 4

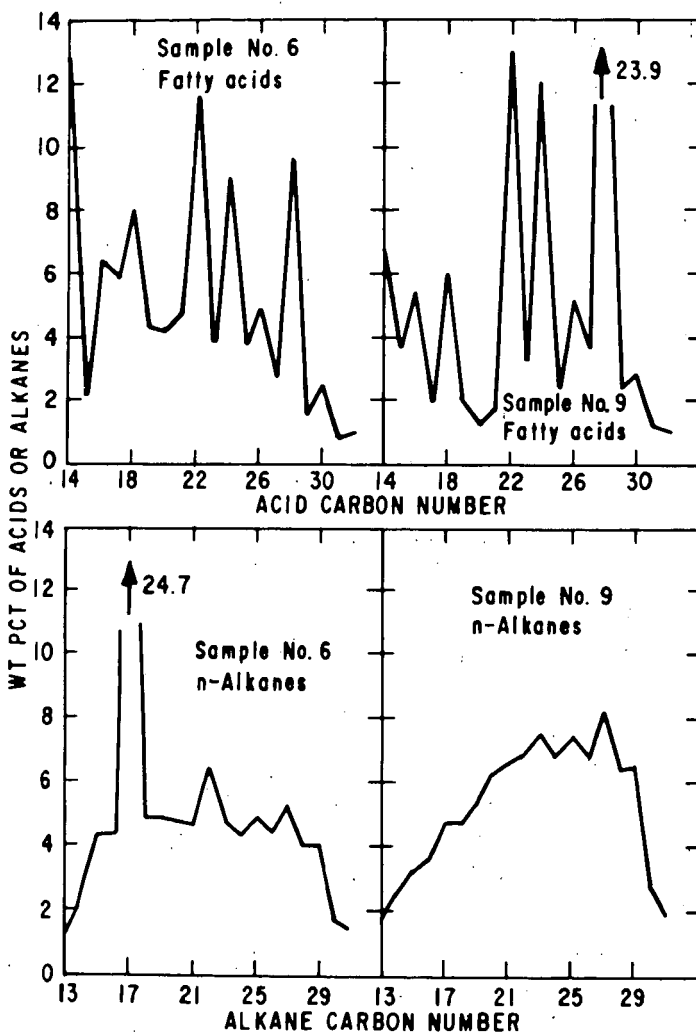


Figure 2. Comparison between fatty acid and n-alkane distributions, Sample Nos. 6 and 9

## ELECTRICAL PROPERTIES OF IODINE COMPLEXES OF ASPHALTENES

Gustave A. Sill and Teh Fu Yen

Mellon Institute  
Pittsburgh, Pennsylvania 15213

## INTRODUCTION

Polynuclear aromatic hydrocarbons generally form charge-transfer complexes with halogens. Some of the fused aromatic hydrocarbons, e.g., perylene, violanthrene, yield solid complexes exhibiting extremely good semiconduction (1,2,3) while others, e.g., coronene, show only fair to poor semiconduction (4). A number of charge-transfer complexes of aromatic containing polymers have been investigated for possible differences in electrical properties (5,6,30).

A polymeric dielectric may be converted to a polymeric semiconductor by increasing the aromaticity of the insulator, followed by complex formation with a halogen (7,8). The increase in aromaticity can be effected by radiation--e.g., cyclization of polyethylene and followed by dehydrogenation (7); or by heat--e.g., pyrolysis or graphitization to a pyropolymer (8). The resulting products when treated with iodine exhibit a wide range of interesting electrical properties.

From a structural standpoint asphaltene (9) are considered to consist of two-dimensioned fabrics of condensed aromatic rings, intermingled with short aliphatic chains and fused naphthenic ring systems (10). X-ray diffraction (11,12) and ESR investigations (13) have indicated that these aromatic systems tend to form stacks of graphite-like layers surrounded by a disorganized zig-zag chain structure of saturated carbons. Morphologically they may be considered as a highly associated "multipolymer" (14), the

molecular weight of which can vary from a few thousand (unit or particle weight) to a few million (micelle weight) (15). The aromatic centers, roughly 15Å in diameter, are considered to be pericondensed (23,18). It has been demonstrated that asphaltics can form charge-transfer complexes, due to the presence of such aromatic systems (20).

Most polynuclear aromatic compounds form well defined crystals, the iodine complexes of which are stable and stoichiometric in composition. Asphaltics are mesomorphic (17) owing to the random distribution and isotropic orientation of the structural units, and it is to be anticipated, therefore, that the conduction mechanism will be different from that of the crystalline environment (due to diffusion and phonon processes) (16). Since there is a difference in the conduction mechanism between crystalline and amorphous aromatics, one would like to know whether the mesomorphic nature of asphaltics would retard or inhibit the conductivity, and if so to what extent.

The aims of this research were two-fold. The first was simply to observe where asphaltenes fall in the conductivity range and to determine the extent to which conductivity can be enhanced by iodine complex formation. The second was a more general study of the electrical properties of asphaltics as another approach to a better understanding of their structure. To the authors' best knowledge, there is no published work on the electrical characteristics of these materials. Iodine may be visualized as a tracer or indicator for condensed aromatic systems, even when buried in a matrix of paraffinic or cycloparaffinic material. It was thought, therefore, that iodine complex formation and its effect

on the overall electrical properties of the asphaltene might yield independent information of the size and distribution of the aromatic centers in these multipolymers.

## EXPERIMENTAL

### Resistance Measurements

A General Radio type 1230A electrometer was used for specimens with resistance less than  $10^{12}$  ohms (ambient temperature), and a Cary model 31 electrometer was used for specimens of higher resistance. In each case a glass vessel equipped with a ball joint and appropriate electrostatic shielding was coupled to the head of the electrometer (Fig. 1). Each specimen (approximately  $1 \times 0.5 \times 0.1$  cm) was pelleted with a Beckman KBr press at  $7.09 \times 10^3$  kg/cm<sup>2</sup> between two pieces of 52 mesh platinum screen. The pellet was degassed for eight hours and the electrical measurements made in a vacuum of  $5 \times 10^{-4}$  Torr. Using the high resistance leak method, a standard resistor served as calibrating reference (21); data were taken under conditions of both falling and rising temperature, a minimum of 30 minutes being allowed for equilibration at  $10^\circ$  levels. Upon completion of the temperature dependence measurements, the physical dimensions of the specimen block were obtained with a travelling microscope (10X) with an x,y micrometer attachment (0.0001 cm precision).

### Preparation of Sample

The asphaltene sample was prepared by our standard procedure (9). Two native asphaltenes were investigated, one from the Boscan crude oil from Venezuela (Sample VY), the other from the Baxterville crude from

Mississippi (Sample GS). Stock solutions in benzene of iodine and of the individual asphaltenes were made up in fixed concentration and samples of varied composition prepared by mixing appropriate quantities of these stock solutions at room temperature and lyophilizing at reduced pressure to yield powdered solids with a homogeneous iodine distribution. These samples were analyzed before and after the electrical measurements for %I by ignition in oxygen, reduction with hydrazine sulfate, and potentiometric titration of the resulting iodide with  $\text{AgNO}_3$  using a Beckman model K automatic titrator. Usually there was no observable loss of free iodine during electrical measurements; 10-15% loss of iodine was found after degassing. The iodine values used in the present work are those values obtained after completion of the electrical measurements for the entire specimen.

#### Treatment of Data

The resistance values along with the corresponding temperature data and dimensions of the specimen were key punched on IBM cards and evaluated on an IBM 7090-1401 digital computer system. Given A, the area of the cross section, and L, the length of the specimen, the resistivity,  $\rho$ , can be evaluated from the resistance, R, as follows:  $\rho = AR/L$ . The temperature dependence of the resistivity is then evaluated by the relationship:

$$\rho_T = \rho_0 \exp (\epsilon/2kT),$$

where k is Boltzman's constant,  $\epsilon$  is the energy gap in eV and  $\rho_0$  is the resistivity extrapolated to  $\frac{1}{T} = 0$ . By use of a California Computer Products 30-in. plotter (300 steps; 1/500-in. per step) the temperature dependence data were fitted to straight lines (Fig. 2) as given by the equation

$$\log \rho = \log \rho_0 + \epsilon / (2kT \ln 10)$$

From the digital output,  $\rho_{25^\circ\text{C}}$  and  $\epsilon$  can be obtained. The applied voltage was limited to values under 10 V; in this region Ohm's law was followed.

The temperature range examined was from ambient to  $90^\circ\text{C}$ .

There is error involved in any single measurement of resistance, owing to systematic errors in the electrometer; errors also enter in the measurement of the dimensions of the specimen. That the results were not influenced by such systematic errors is evident from the two sets of data for two different preparations of an asphaltene (VY)-iodine complex, as given in Table I. The uncertainties in the per cent iodine and sample size may be judged from the variations in the independent measurements. Despite these variations, the resistivity at  $25^\circ\text{C}$  and the energy gap are within ca. 5% of the mean values.

#### Infrared Analysis

Differential IR spectra were obtained from a scan of an iodine-containing asphaltene versus a reference asphaltene at equal asphaltene concentration in  $\text{CS}_2$  (the iodine-containing sample is normalized to 100% asphaltene for purposes of comparison) using a Beckman IR-12 instrument. A control scan of asphaltene in  $\text{CS}_2$  solution against itself also was made for each sample.

#### X-ray Diffraction

A Norelco x-ray diffractometer equipped with a  $\text{CuK}\alpha$  radiation source and a geiger tube detector was used to study the asphaltene-iodine system. In order to record the shift of the d-spacing due only to change in mass absorption coefficients, adamantane was added to an asphaltene-iodine complex (24% I) and to the original asphaltene. Strong (111) and (200) reflections due to the adamantane mixed with the VY asphaltene were

found at 5.7 and 4.9Å; for the VY asphaltene-iodine complex shifts were observed to 5.5 and 4.7Å, respectively. The spacing is reproducible to  $\pm 0.2\text{\AA}$ .

#### Electron Spin Resonance

ESR spectra were taken with a Varian V-4502 x-brand EPR spectrometer system in conjunction with a 12-inch magnet and a "Fieldial." The relative intensity observed was used as a guide for the spin concentration of the asphaltene (VY)-iodine complexes and native asphaltene (VY) (13).

#### RESULTS

All asphaltene-iodine samples studied gave repeatable linear relations in the temperature range investigated as shown in Fig. 2. There is no significant deviation from Ohm's law through the range 2.5 to 97 V as indicated by Fig. 3 in the temperature interval 313° to 372°K.

The native asphaltenes (Points 1, Fig. 4) fall generally in the insulator range. Upon the addition of iodine the resistivity falls, a to b, then increases sharply, b to c, and finally drops, c to d, as iodine content rises. Both complexes appear to yield curves of similar shape. The gap energy values for the asphaltene-iodine complexes are plotted versus their iodine contents (Fig. 5). The smallest energy gap measured in each case was  $\sim 0.5\text{eV}$ , but the absolute minimum is uncertain. These minima (points b) correspond to the sharp transitions of resistivity shown in Fig. 4.

Scanning in the far IR region revealed no C-I stretching frequencies for those iodine complexes for which  $\rho$  was determined. However, the differential IR measured in the 700-1200  $\text{cm}^{-1}$  did show an additional band at

1080  $\text{cm}^{-1}$  (Fig. 6), and freshly prepared asphaltene-iodine complexes in  $\text{CS}_2$  also exhibited an enhancement in absorption in the region of 1000 to 1150  $\text{cm}^{-1}$ , which is generally ascribed to complex formation.

The x-ray spectrograms in the region  $2\theta = 2 - 42^\circ$  of the asphaltene (VI)-iodine system yielded an amorphous pattern with broad halos as shown in Fig. 7. For samples with an iodine content of less than 5 per cent, the 3.5Å band still appeared as a shoulder. In the meantime a new band was formed at around 8.7Å. At higher iodine contents (>10%), the 3.5Å band has apparently disappeared and the 8.7Å band became clearly visible. There is a general overall decrease of total intensity as %I increases since the iodine itself absorbs an increasingly large fraction of the diffracted x-rays. In the present case, the noise level coupled with the intensity reduction has made the disappearance of the 3.5Å shoulder difficult to detect.

In general, the ESR spectra obtained from the asphaltene-iodine samples indicated an increase in free radical concentration with increase in iodine content. The increase in relative intensity for an asphaltene (VI)-iodine complex containing 20% I over the corresponding native asphaltene is about 3.8 fold.

#### DISCUSSION

In all the samples studied, including both native asphaltenes and their iodine adducts, a negative temperature coefficient of resistivity was obtained. The linearity of  $\log \rho$  vs. reciprocal T is substantiated by the plots shown in Fig. 2. The resistivity is inversely related to the concentration of the charge carriers (holes and electrons), but the fact that the number of charge-carriers increases exponentially with temperature does not enable a choice to be made between electronic or ionic conduction

mechanisms. However, the voltage dependence for the current at a relatively low electric field is linear, indicating that Ohm's law is valid (Fig. 3). This adherence to Ohm's law supports the belief that the conduction is electronic (19).

The fact that the asphaltene-iodine sample exhibits (Fig. 6) strong enhancement of absorption near  $1080\text{ cm}^{-1}$  suggests that an iodine molecule forms a donor-acceptor complex with the aromatic portion of the asphaltenes. It is known that the iodine molecule forms such a charge-transfer complex with benzene and other alkylated benzenes, and that these complexes, in general, exhibit bands from  $992\text{ cm}^{-1}$  to  $1200\text{ cm}^{-1}$  (24,25). Arguing from analogy, it is plausible that the complex assumes the axial model (model A of Mulliken) while the acceptor molecule is sitting perpendicular to the plane of the aromatics (26). Further, our failure to locate any C-I stretching frequencies in the  $400\text{-}600\text{ cm}^{-1}$  region supports the view that iodination of the asphaltene samples did not occur.

Most charge-transfer complexes of iodine with aromatics are crystalline. An exception to this is the violanthrene-iodine system, which x-ray diffraction indicates to be amorphous (2). X-ray results also indicate a low degree of order for the asphaltene-iodine complexes. If the acceptors ( $\text{I}_2$ ) are homogeneously distributed in the host matrix (asphaltene), these systems may be considered analogous to the impurity or valence-controlled semiconductor systems. Disappearance of the  $3.5\text{\AA}$  spacing of the (002) band means that the layered structure of asphaltene must have been altered (Fig. 7). The  $4.6\text{\AA}$   $\gamma$ -band, due to the saturated carbon in the structure, did not change in the complexing process.

The new band at  $8.7\text{\AA}$  then may be due to the expansion of the aromatic interplanar distance to allow for complexing by the iodine molecule. In the case of the perylene-iodine systems, the spacing found at  $10.7\text{\AA}$  was interpreted (5) as the distance between perylene molecules when iodine molecules were sandwiched between the aromatic layers. The present observed value of  $8.7\text{\AA}$  can be viewed as the sum of the interplanar distance ( $5.5\text{\AA}$ ) and the iodine length ( $4 \times 1.53\text{\AA}$ ). The picture of these interlinked layers resembles that of an intercalation compound of graphite (Fig. 6).

Referring again to Fig. 4, the room temperature resistivities for the two native asphaltenes are seen to be in the insulator range ( $>10^{14}$  Ohm). Upon addition of the iodine, the resistivity decreases about six decades or a million fold. This is essentially the same behavior as that observed for polymeric charge-transfer complexes such as poly(vinylpyridium TCNQ) and its derivatives. These polymeric salts are dependent upon the TCNQ concentration which at best increases the conductivity six decades. Here we have to point out that it is not easy to prepare a polymeric charge-transfer complex with good semiconduction. Slough (5) made a number of polymeric complexes from aromatic-containing polymers, with acceptors such as tetracyanoethylene, chloranil, etc., and found the conductivities of these complexes were not measurably higher than those of the original polymeric donors. These mesomorphic materials may lack the order of the  $\pi$ -systems needed to open a path for charge carriers. More likely, the aromatic systems are too small to form stable charge-transfer complexes.

For pure polynuclear aromatic hydrocarbons, donor-acceptor complexes, especially the iodine complexes (2,3), exhibit increases in conductivity of 12 to 16 decades when compared to the parent hydrocarbon.

The enhancement in conduction by the addition of iodine can be illustrated by comparison of the complexes with a valence controlled semiconductor, a typical example being nickel (II) oxide doped with lithium oxide (22). In Fig. 9 a comparison is made between this system and the aromatic-iodine complexes. The trends in resistivity with the concentration of impurity are quite similar.

Asphaltenes contain fused ring aromatics, the peripheral hydrogens of which are substituted heavily by short chain alkyl groups (23). Owing to the relatively large porportion of methyl groups (20%) and the large average layer diameters ( $L_a \sim 15\text{\AA}$ ), the asphaltic molecule can be viewed as a typical aromatic donor (D); halogens such as iodine can behave as an acceptor (A). Through charge-transfer by overlapping of the molecular orbitals of the two moieties, the dative structure ( $D^+A^-$ ) should result in which asphaltene is the positive ion.

Fig. 4 clearly indicates that the increase of conductivity follows two different paths, the first a to b, is the path followed for small increments of iodine, terminating at b with fixed composition (VY, 15.5%; GS, 10.0%); the other, c to d, is for higher percentages of iodine. Line bc represents the transition state. The curve cd may be extrapolated to a resistivity value of  $5.8 \times 10^6$  ohm-cm, corresponding to that for pure  $I_2$  (27). The same results were found (23) for violanthrene-iodine system with a minimum corresponding to a 2:1 iodine-violanthrene molar ratio for the complex. Apparently b in Fig. 4 corresponds to a stoichiometric ratio of

a stable complex where conductivity is at a maximum. It is assumed that for iodine contents less than that corresponding to the minimum the amount is insufficient to form the complex. At bc the resistivity is highly sensitive to the number of iodine molecules. When c is passed, excess iodine acts as an impurity in the stoichiometric complex. The transition at b is also reflected by the energy gap plot in Fig. 5. The same fixed composition (VY, 15.5%; GS, 10.0%) is obtained in either plot. At these minima, the energy gap value is ca. 0.5eV suggesting favorable conditions for conduction.

A number of aromatic-iodine complexes have been reported (2,3) and from their phase diagrams (either temperature or density vs. mole per cent of iodine) the complexes are found to be stoichiometric (29). For example perylene-iodine can have 2:3, or 1:3; pyranthrene-iodine is 1:2; violanthrene-iodine is 1:2; pyrene-iodine is 1:2. In all cases for peri-type aromatics the ratio of  $I_2$  to aromatic is higher than unity. Since the diameter of the aromatic system in asphaltics falls in the range 8-15Å (12), the system would be comparable in size to violanthrene or perylene.

Assuming the composition at the transition (VY, 15.5%; GS, 10.0%) is stoichiometric, then for any given ratio of aromatic and iodine, the molecular weight of the asphaltene can be calculated. We have taken the liberty of calculating this weight for VY and GS asphaltenes based on sample ratios of  $I_2$ :asphaltene of 2:1, 3:2 and 1:1. Since all layers contain the aromatic moieties and the sample is free of wax contamination, the molecular weight obtained is that of the unit sheet weight (weight of an average sheet containing both aromatic and saturated carbon atoms). These

values are listed in Table II. Next, provided aromaticity is also known ( $f_a$  for VY, 0.35; for GS, 0.51), the disk weight (weight of aromatic carbon atoms in a single sheet) and the layer diameter also can be approximated. These values are also listed in Table II. Experimental values for the VY and GS asphaltenes from a previous paper (15) are included. It is of interest that the unit weight values obtained from GPC, mass spectrometry, x-ray diffraction and the electron microscopic measurements agree in general magnitude with the weights obtained by the present method. Deviations of the disk weight of GS calculated from resistivity from that obtained by mass spectrometry may be due to the polydispersity of the GS asphaltene (e.g.,  $M_w/M_n$  for VY is 1.27; for GS, 1.74 (15)).

From Table II, the asphaltene-iodine complexes formed appear to correspond to an  $I_2$ :asphaltene ratio of about 1.5:1. This composition is shown in model A of Fig. 8. Actually aromatic disks of the size present in asphaltenes should be able to accommodate more than one molecule of iodine.

Finally the increase in the free spins, as demonstrated by the EPR spectra, may be indicative of an increase in carrier concentration (2). The nature of these charge carriers will have a strong bearing on the conduction mechanism and will be the subject of a separate investigation.

#### ACKNOWLEDGMENT

The authors thank Mr. Timothy R. Drury, Mellon Institute, Research Services, for his technical assistance; and Mrs. Marianne P. Hoy and Dr. Sidney S. Pollack, Mellon Institute, Research Services for the x-ray diffraction work.

This work was sponsored by Gulf Research & Development Company as part of the research program of the Multiple Fellowship on Petroleum.

## REFERENCES

- (1) Inokuchi, H., and Akamatu, H., *Solid State Physics*, 12, D3 (1961).
- (2) Uchida, T., and Akamatu, H., *Bull. Chem. Soc. (Japan)*, 35, 981 (1962).
- (3) Uchida, T., and Akamatu, H., *Bull. Chem. Soc. (Japan)*, 34, 1015 (1961).
- (4) Labes, M. M., Sehr, R. A., and Bose, M., "Proceedings of the Princeton University Conference on Semiconductors in Molecular Solids," Princeton, N. J., 1960.
- (5) Slough, W., *Trans. Faraday Soc.*, 58, 2360 (1962).
- (6) Bakh, N. A., Vannikov, A. V., Grishina, A. D., and Nizhnil, S. V., *Russian Chemical Rev.*, 34, 736 (1965).
- (7) Vannikov, A. V., and Bakh, N. A., *Doklady Akad. Nauk., S. S. S. R.*, 159, 230 (1963).
- (8) McNeill, R., Suidak, R., Wardlaw, J. H., and Weiss, D. E., *Aust. J. Chem.*, 16, 1056 (1963).
- (9) The asphaltene fraction of a crude oil or refinery residue is a brown-to-black, amorphous, powdery, solid material, insoluble in n-pentane but soluble in benzene; see Ref. 11 for sample preparation.
- (10) Yen, T. F., and Erdman, J. G., *A. C. S., Div. Petroleum Chem., Preprints*, 7, No. 1, 5 (1962).
- (11) Yen, T. F., Erdman, J. G., and Pollack, S. S., *Anal. Chem.*, 33, 1587 (1961).
- (12) Yen, T. F., and Erdman, J. G., in "Encyclopedia of X-rays and Gamma-rays" (G. L. Clark, Ed.), Reinhold Publishing Co., New York, N. Y., 1963, p. 65.
- (13) Yen, T. F., Erdman, J. G., and Saraceno, A. J., *Anal. Chem.*, 34, 694 (1962).
- (14) The word "multipolymer" refers to a polymer with a very large number of different building blocks, say ca. 100. Simpler structures can be referred to by more specific terms, as for example, "copolymer" (2 blocks) or "terpolymer" (3 blocks).

- (15) Dickie, J. P., and Yen, T. F., to be presented at A. C. S., Div. Petroleum Chemistry, Symposium on "Modern Instrumental Methods for the Analysis of Petroleum Fractions," Miami Beach, 1967.
- (16) LeBlanc, Jr., O. H., J. Chem. Phys., 37, 916 (1962).
- (17) Yen, T. F., Erdman, J. G., and Hanson, W. E., J. Chem. Eng. Data, 6, 443 (1961).
- (18) Yen, T. F., and Dickie, J. P., A. C. S., Div. Petroleum Chem., Preprints, 11, No. 3, 49 (1966).
- (19) Seamon, D. A., Adv. Polymer Sci., 4, 317 (1965).
- (20) Yen, T. F., and Erdman, J. G., A. C. S., Div. Ana. Chem., Abstracts, Detroit, Michigan, 1965, p. 29B.
- (21) This is essentially a method using voltage drop across a standard resistor (potential drop method); see Ref. 26 for example.
- (22) Morin, F. J., in "Semiconductors" (N. B. Hannay, Ed.), Reinhold Publishing Co., New York, N. Y., 1959, p. 600.
- (23) Yen, T. F., and Erdman, J. G., A. C. S., Div. Petroleum Chem., 7, No. 3, 99 (1962).
- (24) Haller, W., Jura, G., and Pimentel, G. C., J. Chem. Phys., 22, 720 (1954).
- (25) Ferguson, E. E., Spectrochim. Acta, 10, 123 (1957).
- (26) Ferguson, E. E., J. Chem. Phys., 25, 577 (1956).
- (27) Rabinowitsch, M., Z. Physik. Chem., 119, 82 (1926).
- (28) Akamatu, H., Inokuchi, H., and Matsunaga, Y., Bull. Chem. Soc. (Japan) 29, 213 (1956).
- (29) Kommandeur, J., and Singer, L. S., in "Symposium on Electrical Conductivity in Organic Solids," (H. Kallmann and M. Silver, Ed.) Interscience, New York, N. Y., 1961, p. 325.
- (30) Hatano, M., Nomori, H., and Kambara, S., A. C. S., Div. Polymer Chem., Preprints, 2, No. 2, 848 (1964).

TABLE I

Resistivity and Gap Energy Measurements  
 from Asphaltene (VI)-Iodine Complexes

Sample No. <sup>a</sup>	Iodine	A. (cm)	L. (cm)	$\rho_{25^\circ\text{C}} \times 10^{-12}$ (ohm-cm)	$\epsilon$ (eV)
23	17.1	1.262 <sub>8</sub>	0.099 <sub>4</sub>	1.75 <sub>6</sub>	1.74 <sub>2</sub>
25	16.8	1.266 <sub>4</sub>	0.103 <sub>3</sub>	1.61 <sub>4</sub>	1.82 <sub>5</sub>
27	17.2	1.259 <sub>2</sub>	0.119 <sub>2</sub>	1.77 <sub>3</sub>	2.00 <sub>7</sub>
24	15.8	1.267 <sub>5</sub>	0.102 <sub>7</sub>	2.15 <sub>5</sub>	1.95 <sub>0</sub>
28	15.7	1.276 <sub>6</sub>	0.051 <sub>9</sub>	2.06 <sub>3</sub>	1.75 <sub>3</sub>
29	15.8	1.147 <sub>9</sub>	0.048 <sub>0</sub>	2.25 <sub>4</sub>	1.81 <sub>4</sub>

(a) Same numbers used in curves of Fig. 4; Sample Nos. 23, 25, and 27 are from one preparation; Sample Nos. 24, 28, and 29 are from another preparation.

TABLE II

Determination of the Molecular Weight and Aromatic Sheet Size  
of Native Asphaltenes by Various Physical Methods

Physical Methods	Unit Weight <sup>a</sup>		Disk Weight <sup>b</sup>		Layer Diameter (Å) <sup>c</sup>	
	VY	GS	VY	GS	VY	GS
<u>Resistivity Calculation</u>						
I <sub>2</sub> :Asphaltene						
2:1	2770 <sup>d</sup>	4570	969 <sup>e</sup>	2330	14.6 <sup>f</sup>	22.6
3:2	2080	3430	727	1750	12.6	19.5
1:1	1380	2290	484	1170	10.3	16.0
GPC (M <sub>n</sub> ) <sup>g,h</sup>	3160	3780	-	-	-	-
<u>Mass Spectrometry<sup>h</sup></u>						
(Mean)	-	-	634	543	-	-
<u>X-ray Diffraction<sup>h</sup></u>						
(L <sub>a</sub> )	-	-	-	-	11.9	17.0
<u>Electron Microscope<sup>h,i</sup></u>						
(Particle weight)	3440	4030	-	-	-	-

(a) Weight of a single sheet containing both aromatic and saturated carbon atoms (see J. P. Dickie and T. F. Yen, A. C. S., Div. Petroleum Chem., Preprints, Miami meeting, April, 1967).

(b) Weight of aromatic carbon atoms in a single sheet.

(c) Diameter of aromatic cluster; see T. F. Yen, J. G. Erdman, and S. S. Pollack, Anal. Chem., 33, 1587 (1961).

(d) Calculated based on  $254t^{-1}R$  (100- $t$ ) where R is the ratio of I<sub>2</sub> to asphaltene and t is the %I corresponding to the transition in resistivity and gap energy.

(e) Calculated from  $f_a \times$  (unit weight).

(f)  $L_a = (2.62 C_A)^{1/2}$ , C<sub>A</sub> from disk weight without contribution of hydrogens.

(g) From gel permeation chromatography data on the native asphaltene, number average molecular weight.

(h) Experimental data from J. P. Dickie and T. F. Yen, A. C. S., Div. Petroleum Chem., Preprints, Miami meeting, April, 1967.

(i) J. P. Dickie and T. F. Yen, A. C. S., Div. Petroleum Chem., Preprints, 11, 39 (1966).

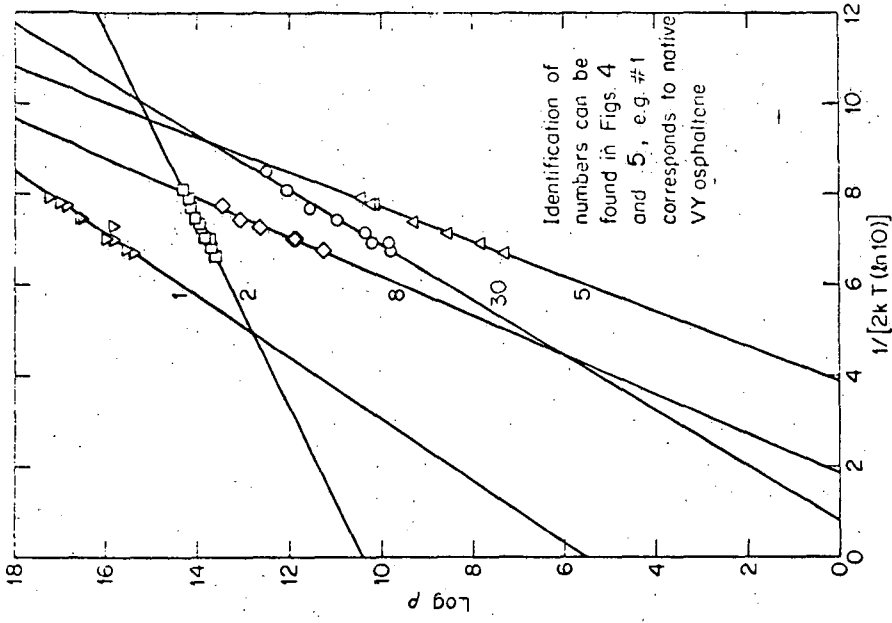


Fig. 2-Temperature Dependence of Resistivity for the Asphaltene-Iodine System.

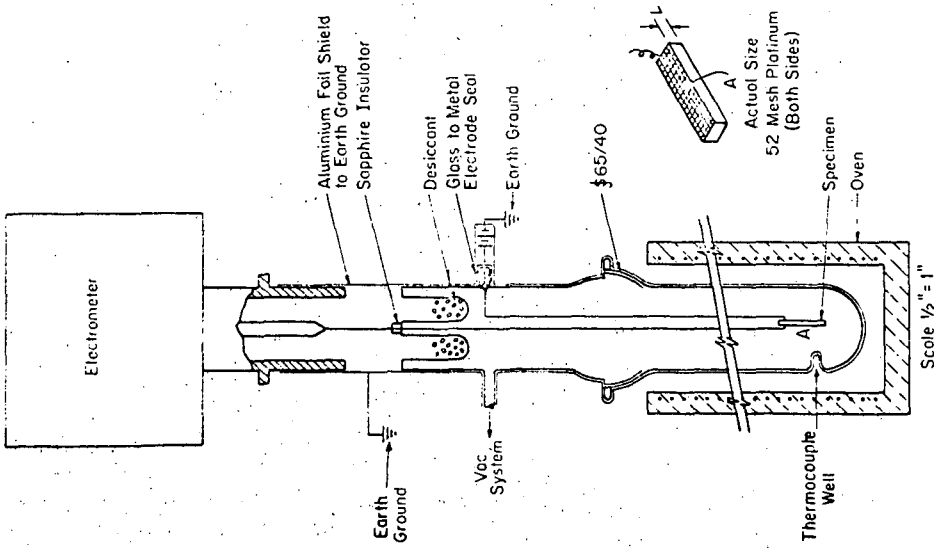


Fig. 1-Apparatus for Resistance Measurement

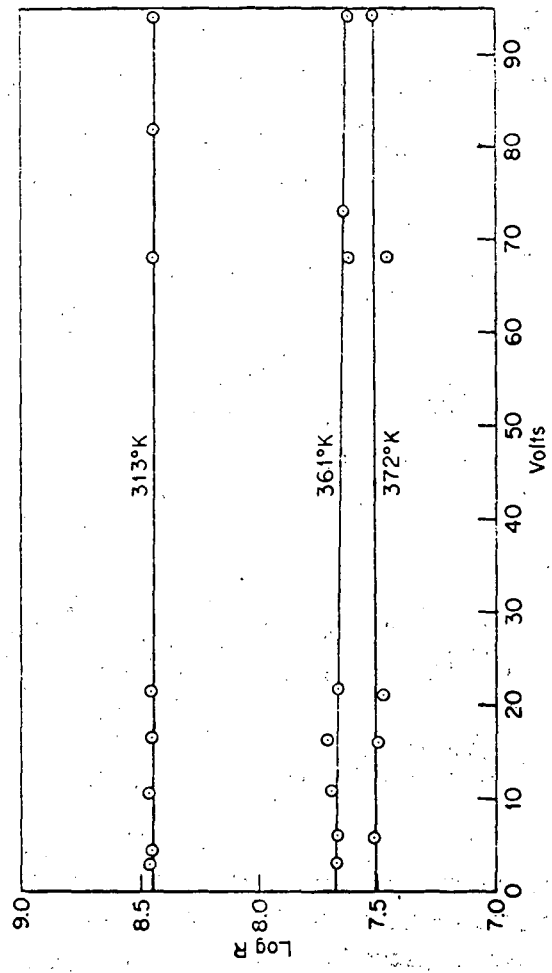


Fig. 3-Voltage Dependence of Resistance for an Asphaltene-Iodine Complex (1% = 11).

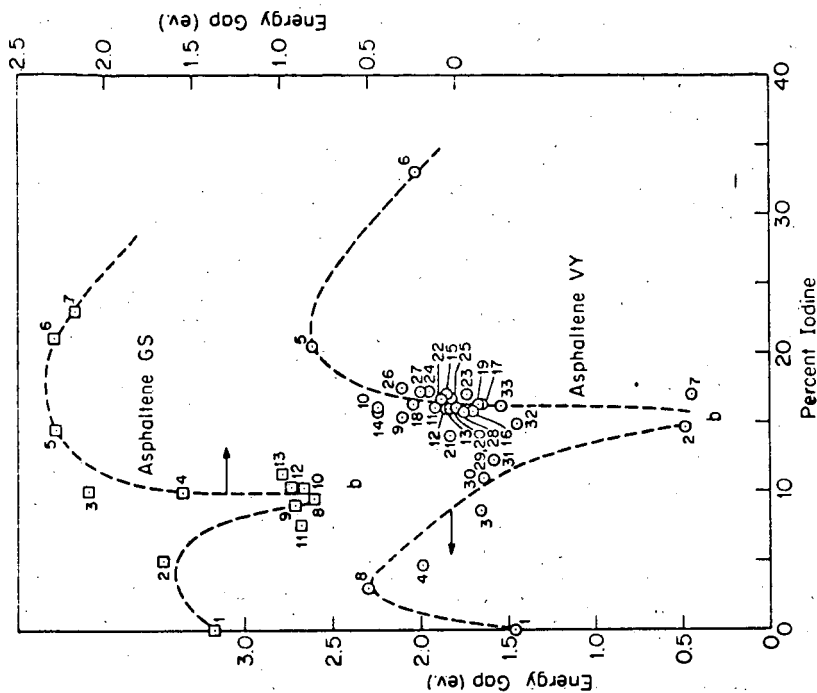


Fig. 5-Gap Energy of the Asphaltene-Iodine Complex as a Function of Iodine Content.

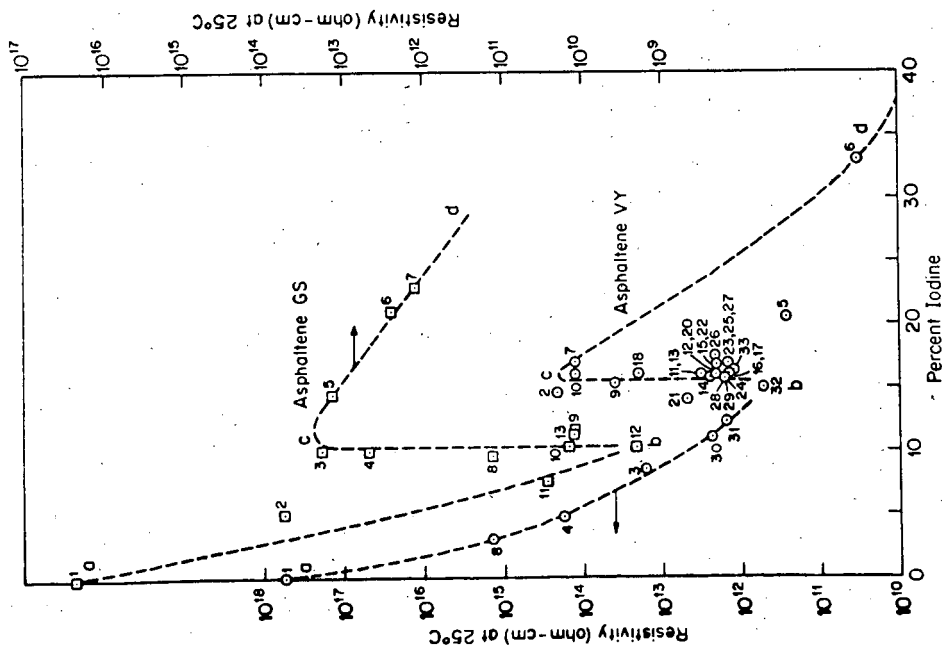


Fig. 4-Resistivity of the Asphaltene-Iodine Complex as a Function of Iodine Content.

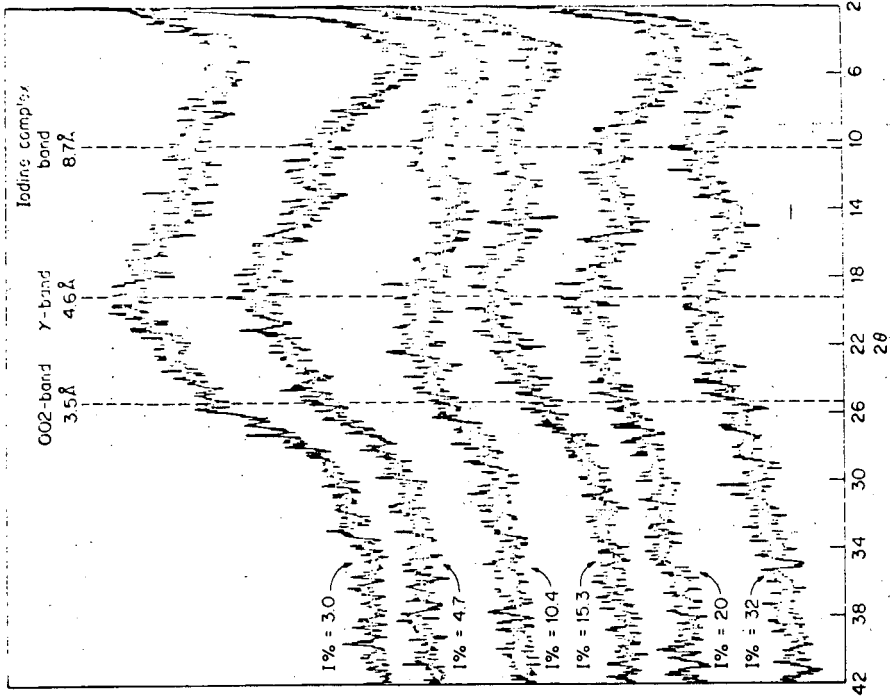


Fig. 7 - X-Ray Patterns of the Asphaltene (VY)-Iodine System

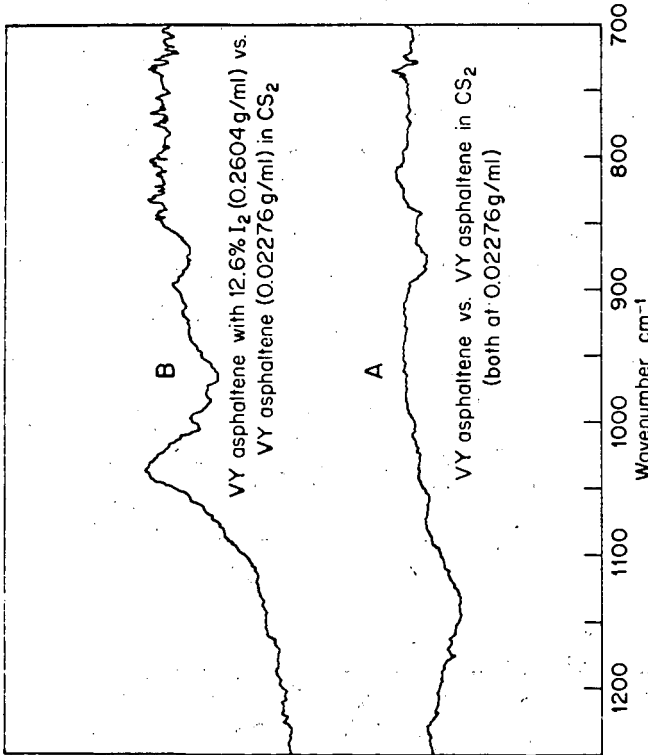


Fig. 6 - Differential Infrared Spectra of Asphaltene-Iodine Complex.

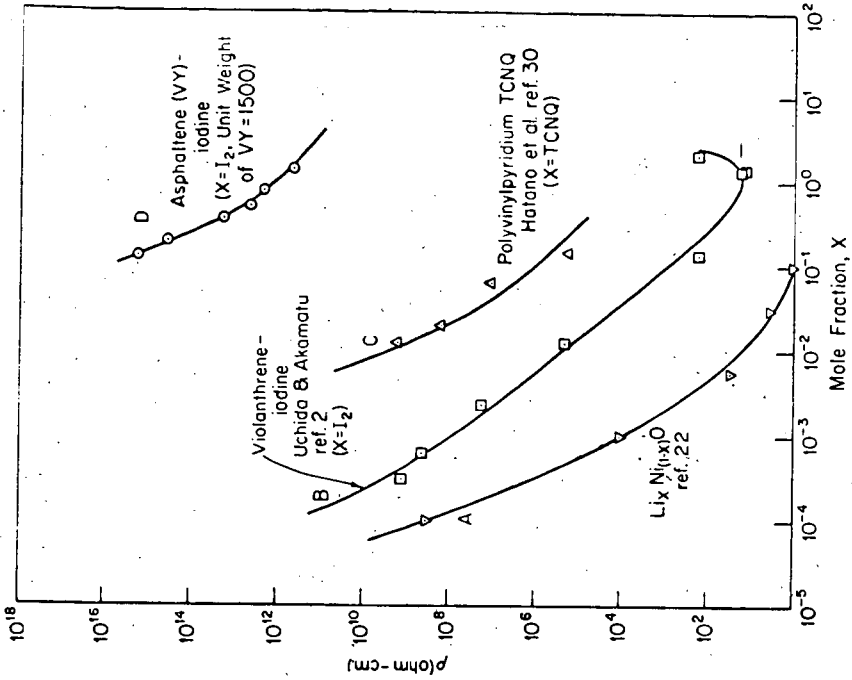


Fig. 9-Aromatic-Iodine Complexes Vs. a Valence Controlled Semiconductor with Resistivity as a Function of Impurity Content.

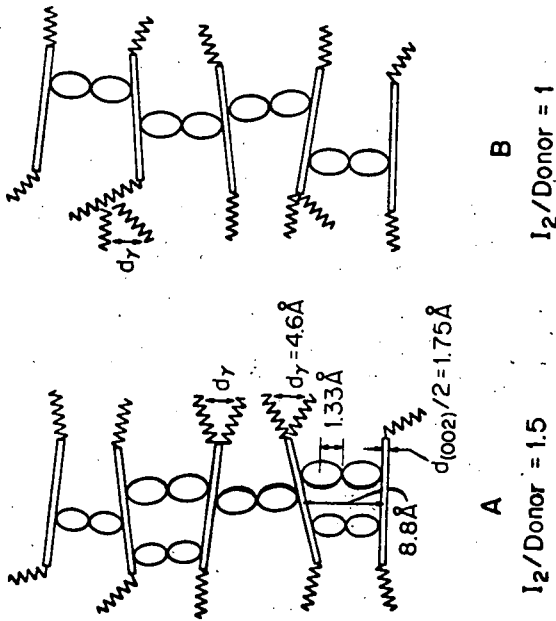


Fig. 8-Proposed Model of Asphaltene-Iodine Complexes  
A, 2 Asphaltene  $\cdot 3 \text{I}_2$ ; B, Asphaltene  $\cdot \text{I}_2$ .

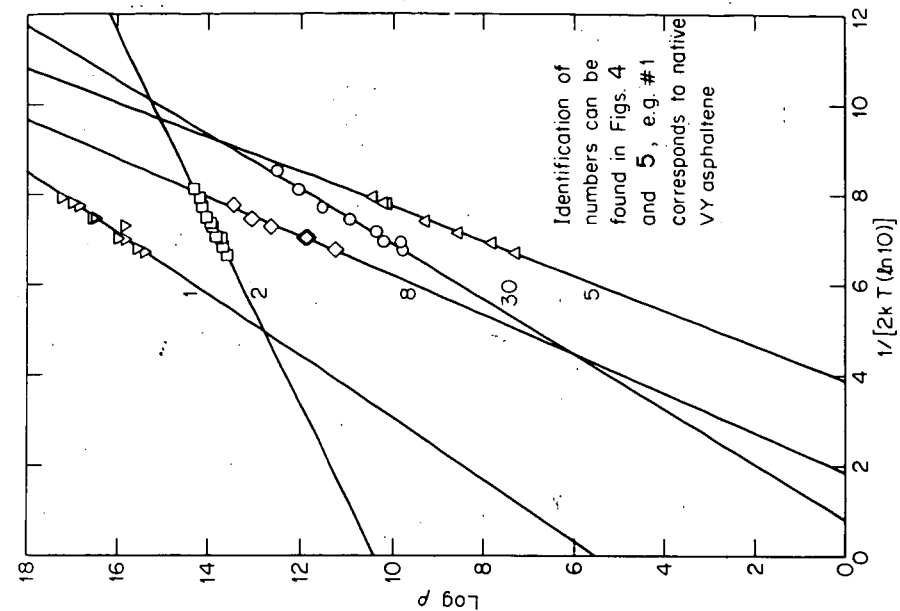


Fig. 2-Temperature Dependence of Resistivity for the Asphaltene-Iodine System.

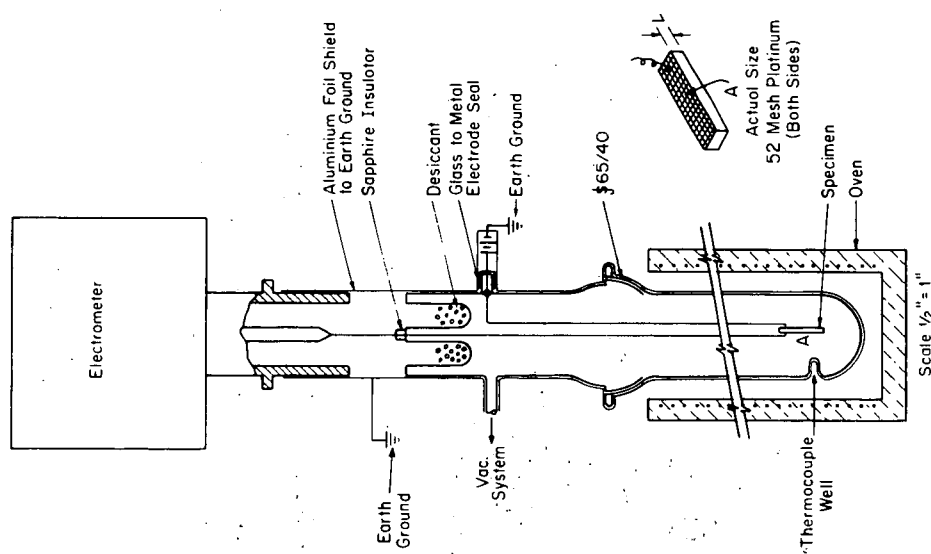


Fig. 1-Apparatus for Resistance Measurement

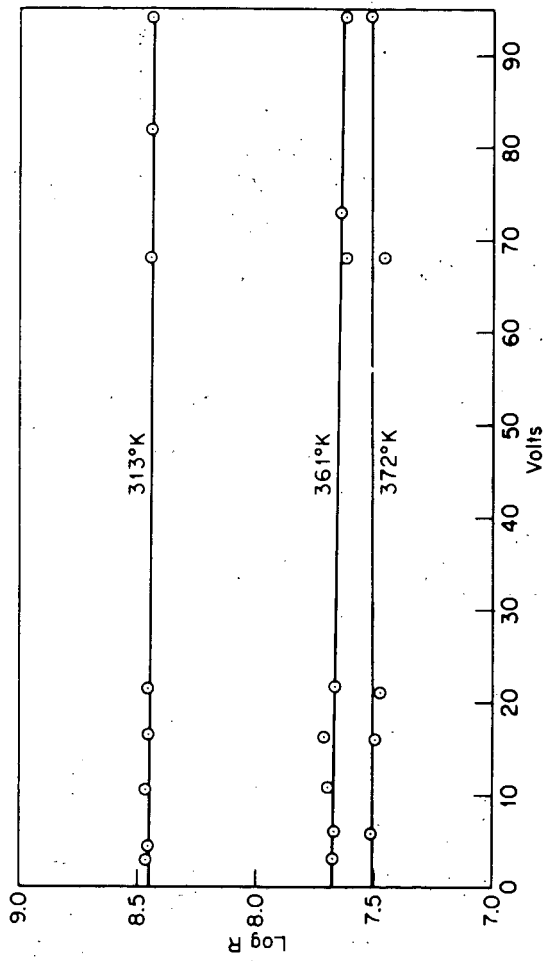


Fig. 3-Voltage Dependence of Resistance for an Asphaltene-Iodine Complex (1% = 11).

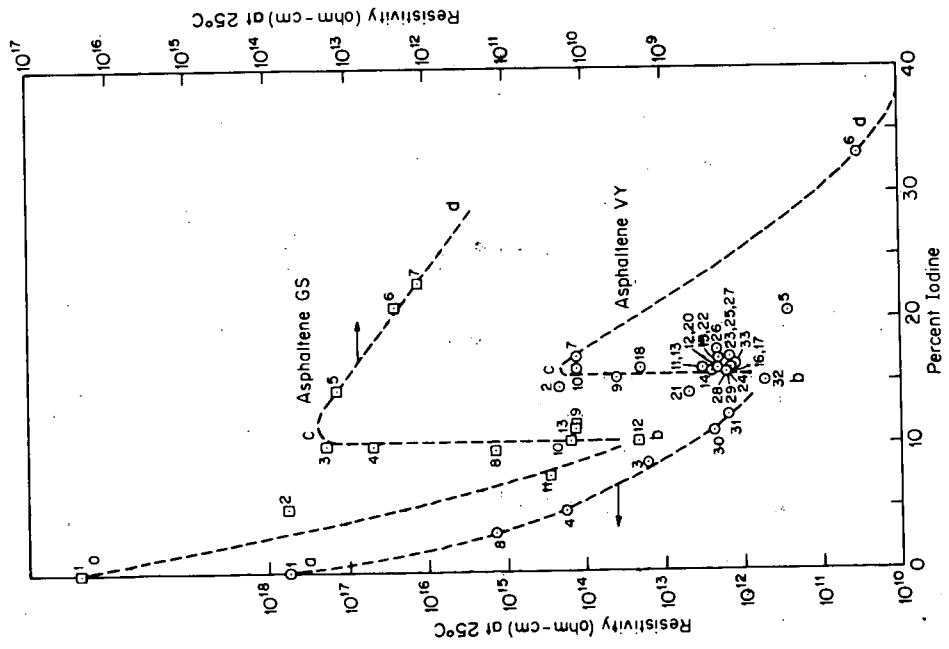


Fig. 4-Resistivity of the Asphaltene-Iodine Complex as a Function of Iodine Content.

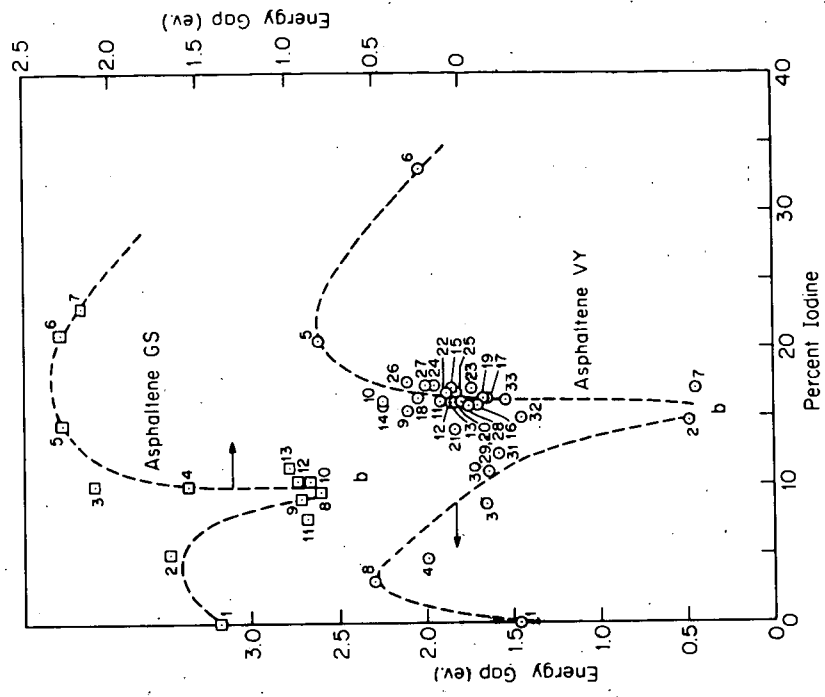


Fig. 5-Gap Energy of the Asphaltene-Iodine Complex as a Function of Iodine Content.

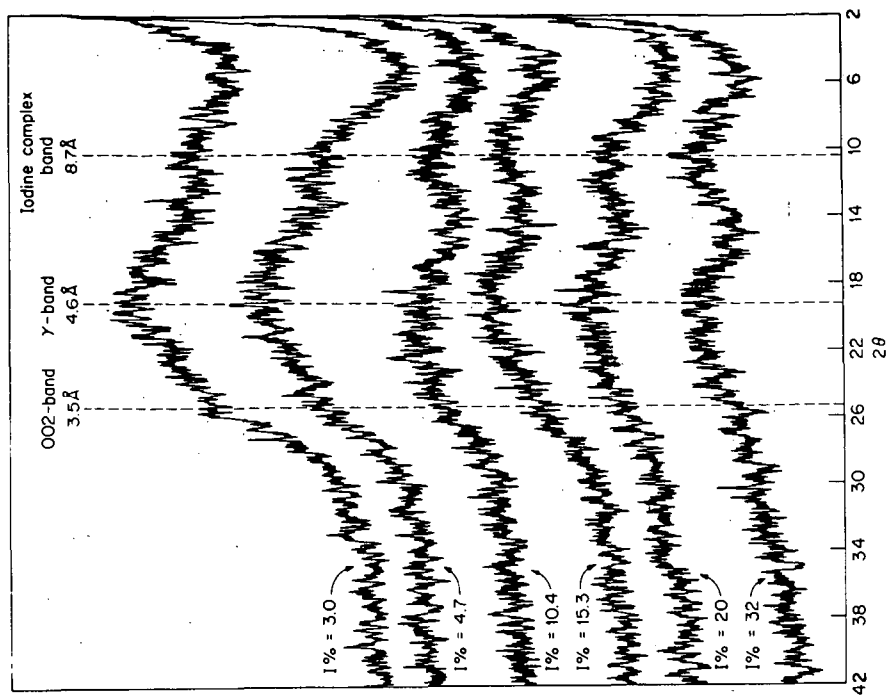


Fig. 7 - X-Ray Patterns of the Asphaltene (VY)-Iodine System

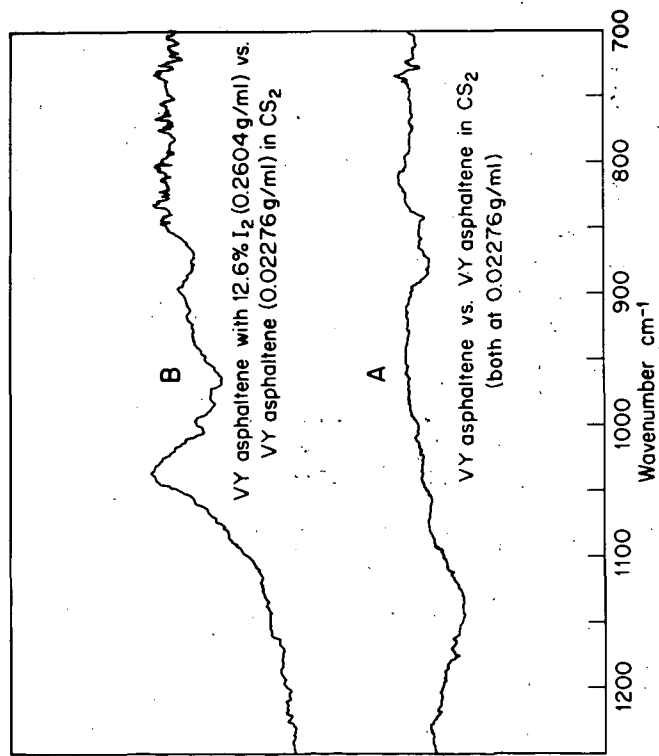


Fig. 6 - Differential Infrared Spectra of Asphaltene-Iodine Complex.

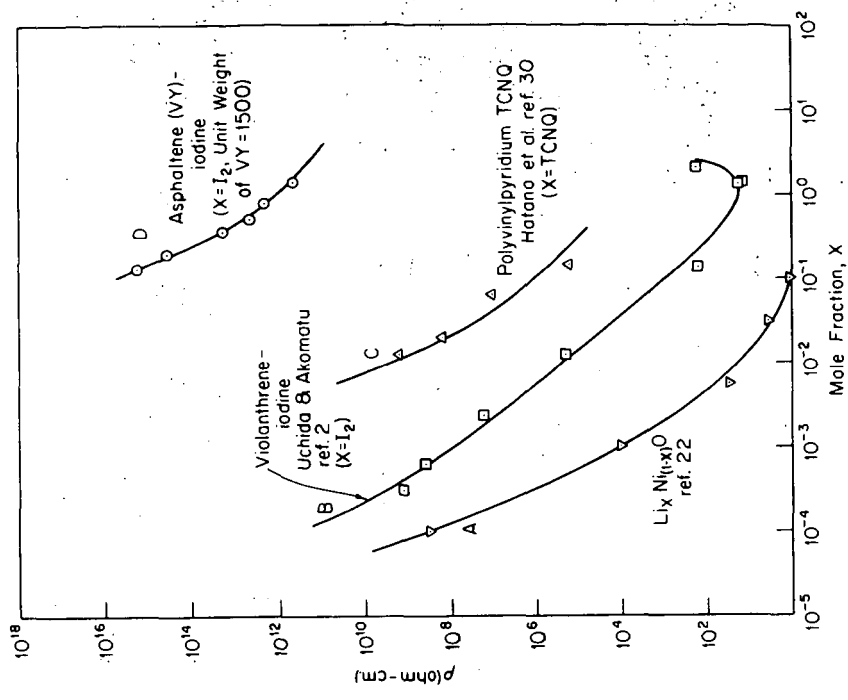


Fig. 9--Aromatic-Iodine Complexes Vs. a Valence Controlled Semi-conductor with Resistivity as a Function of Impurity Content.

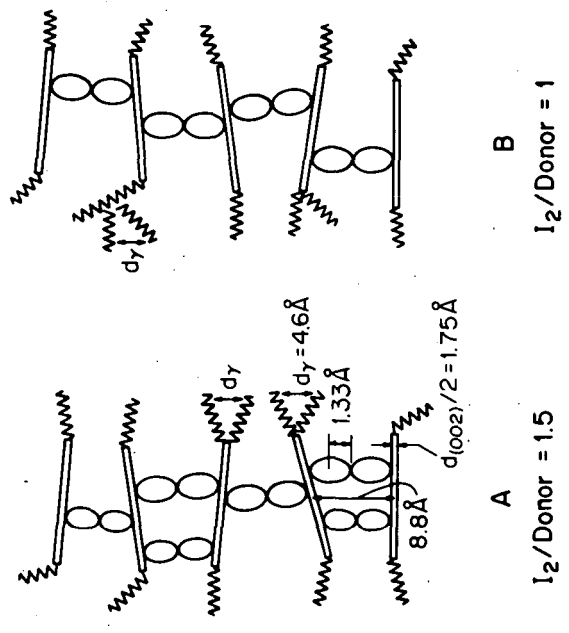


Fig. 8--Proposed Model of Asphaltene-Iodine Complexes  
 A, 2 Asphaltene  $\cdot 3 I_2$  ; B, Asphaltene  $\cdot I_2$ .

## THE ELECTRON SPIN RESONANCE SPECTRA OF CELLULOSE CHARS TREATED WITH HALOGENS\*

### Evidence for Donor-Acceptor Complexes in Coals and Chars

R. M. Elofson and K. F. Schulz

Research Council of Alberta  
Edmonton, Alberta

### INTRODUCTION

Coals and low- and medium-temperature chars have been shown to be paramagnetic by bulk magnetic susceptibility measurements<sup>1,2,3</sup> and by electron spin resonance studies<sup>4,5,6</sup>. If due care is taken to eliminate errors, reasonable agreement in the estimate of the number of unpaired electrons present can be obtained<sup>7</sup>. While there is agreement on the existence of paramagnetic centres in these materials, the origin and nature of these free radicals is not understood<sup>8,9,10,11,12</sup>. It is the purpose of this article to present new evidence to suggest that these unpaired electrons arise from donor-acceptor forces present in these materials.

One way of studying the nature of free radicals is by observing the behavior of the electron spin resonance signals when the substrate is treated with adsorbed gases and other reagents. Early workers in the field found that paramagnetic gases such as oxygen affected only the spin-lattice relaxation times of chars prepared at from 300° to 500°C. For chars prepared in the 550° to 800° temperature range, however, reversible line broadening occurred with an apparent decrease in free radical concentration at higher oxygen pressures. Removal of oxygen restored the original signal, which indicated that the phenomenon was due to physical and not chemical processes. Halogens were at first found to have no effect on coals and chars and the oxygen effect was attributed to spin broadening due to the paramagnetism of the oxygen molecules. Similar results to oxygen were obtained with nitric oxide.

In 1963 Wynne-Jones<sup>13</sup> and co-workers found that e.s.r. signals in chars obtained by heating polyvinylidene chloride (saran) were affected by adsorption of halogens. These workers noted that IBr, ICl, I<sub>2</sub>, Br<sub>2</sub>, and Cl<sub>2</sub> caused partial or complete reduction in spin concentration at constant line width. The original signal was not restored by outgassing in vacuo at room temperature but could be partially restored by reheating the specimen at 100°C in vacuo. Since, as mentioned above, no halogen effect had been obtained on coals or more common chars, these authors attributed the susceptibility to halogens of these saran chars to a high degree of porosity. Reinvestigation of the interaction of a series of cellulose chars with iodine, bromine and hydrogen iodide in this laboratory has shown pronounced effects on the electron spin resonance of some of these materials.

### EXPERIMENTAL

Cellulose chars were prepared by first charring cellulose powder (Whatman Cellulose Powder, Standard Grade) in an autoclave at 195°-200°C under nitrogen. Subsequently this char

---

\* Contribution No. 360 from the Research Council of Alberta, Edmonton, Alberta.

was heated under nitrogen in a Vycor tube to the desired temperature and held at temperature for one hour. Aliquots of the chars were then treated with a large excess of 0.1 M solutions of iodine or bromine in carbon tetrachloride. After standing in the solutions for twenty-four hours, the samples were washed once with carbon tetrachloride and dried. Samples for e.s.r. measurements were placed in 3 mm. o.d. glass tubes and evacuated.

Samples to be treated with hydrogen iodide were placed in open 3 mm. o.d. tubes placed in the cavity of the spectrometer and purged with purified nitrogen. Gaseous hydrogen iodide (Matheson) was passed directly over the sample in the cavity. Excess hydrogen iodide was removed after treatment by subsequent purging with nitrogen.

Electron spin resonance measurements were performed with a Varian Model 4500 electron spin resonance spectrometer fitted with a TE102 cavity and a 100 Kc modulation attachment. Saturation phenomena were avoided by working at 10 db attenuation and checks for saturation were made. Line widths and spin concentrations were measured from first derivative curves, generally by direct inspection but in the case of very wide and very narrow signals resort was made to graphical integration. A standard 500° cellulose char, used for calibration, was standardized against DPPH,  $\text{CuSO}_4$  and a Varian Standard char. The amount of sample was always less than 10 mg. and asymmetric line shapes were not observed, indicating the absence of serious skin effects.

## RESULTS

In Figures 1 and 2 are summarized the results of iodine and bromine treatment on line width and spin concentration as measured at room temperature. The untreated chars prepared at 625° and 650° show a marked decrease in line width as compared with those prepared at higher or lower temperature — an effect attributed to exchange<sup>4</sup>. It is seen that both iodine and bromine remove this intense narrowing in the 625° and 650° chars. Neither has a significant effect on the 300° to 500° chars but both broaden further the signal from the 700° char. The broadening due to bromine is not as great as that due to iodine and for the 600° char, in particular, the broadening effect of the bromine is minimal. The effect on spin concentration shows that line broadening is accompanied by a considerable drop in concentration in both the bromine and iodine treated chars.

Measurements made at 78°K showed that whereas the signals for the 300° to 500° chars were broadened somewhat, those from the iodine- and bromine-treated chars in the 600° to 700° range were narrowed. Washing the iodine-treated chars with cold 0.1 M sodium thiosulfate solution restored the original narrow signals. This showed that no chemical reaction had occurred to alter the signals.

Treatment of a series of chars with hydrogen iodide gas for sixty hours resulted in reduction of the signal strength and broadening of the signals as shown in Table I. The broadening for the 300°, 400° and 500° chars was moderate but that of the exchange narrowed chars (600° to 700°) was extensive. Cold 0.1 M sodium thiosulfate produced no further change in the signals but refluxing for twenty-four hours with thiosulfate restored the original signals<sup>1,4</sup>. The restored signals of the 600°, 625°, 650° and 700° chars were sensitive to air whereas the restored signals of the 300°, 400° and 500° chars were not. The e.s.r. signals of the untreated chars refluxed with 0.1 N  $\text{Na}_2\text{S}_2\text{O}_3$  were unchanged.

TABLE I

Effect of Hydrogen Iodide on Free Radical Content of Chars

Electron Spin Resonance Signals

spins/g in vacuo and width in gauss\*

Char Temperature	Untreated	HI Treatment 60 hours	Na <sub>2</sub> S <sub>2</sub> O <sub>3</sub> 0.1 M Refluxed 24 hours
300	2.1 × 10 <sup>18</sup> 4.9	2.0 × 10 <sup>17</sup> 7.9	8.3 × 10 <sup>17</sup> 5.76
400	2.3 × 10 <sup>19</sup> 6.1	5.3 × 10 <sup>18</sup> 8.3	2.6 × 10 <sup>19</sup> 6.3
500	5.1 × 10 <sup>19</sup> 4.8	3.3 × 10 <sup>19</sup> 5.9	5.4 × 10 <sup>19</sup> 4.1
600	1.4 × 10 <sup>20</sup> 0.45	1.3 × 10 <sup>19</sup> 19.1	1.4 × 10 <sup>20</sup> 0.49
625	1.3 × 10 <sup>20</sup> 0.40	1.7 × 10 <sup>19</sup> 22.4	9.8 × 10 <sup>19</sup> 0.49
650	1.0 × 10 <sup>20</sup> 1.4	4.8 × 10 <sup>19</sup> 41.0	1.0 × 10 <sup>20</sup> 1.2
700	7.4 × 10 <sup>19</sup> 1.4	1.2 × 10 <sup>19</sup> 43	7.2 × 10 <sup>19</sup> 2.0

\* Width measured between points of maximum slope.

## DISCUSSION

Two aspects of these results must be considered – the interaction with the halogens which are typical electron acceptors and the interactions with hydrogen iodide. In agreement with Wynne -Jones and co-workers, we are of the opinion that iodine, and to a lesser extent bromine, can form donor-acceptor complexes with the chars and in so doing affect the e.s.r. signals. Presumably the iodine and bromine act as acceptors and aromatic ring systems of the char act as donors in these complexes. The low-temperature chars, 300° to 500°, having few aromatic ring systems as large or larger than four or five rings<sup>15</sup>, are not affected by iodine or bromine. The 600° char apparently has a high enough donor ability – low enough ionization potential – to interact with iodine but not sufficient to react definitely with bromine, which is a much weaker acceptor. Both bromine and iodine readily form complexes with the 625°, 650° and 700° chars. The fact that the signals of the halogen affected chars are narrowed on cooling to 79°K is also indicative of donor-acceptor interaction between halogens and aromatic moieties<sup>16</sup>. It is possible that lack of porosity is sufficient explanation of the failure of the 300° to 500° chars to be affected by iodine<sup>13</sup>. However, the difference between iodine and bromine on the 600° char suggests that the electrophilicity and not the size of the adsorbed molecule is important.

The line broadening at 79°K of the 300°, 400° and 500° chars treated with halogens is not only indicative of no complex formation between halogen and the aromatic system but also suggests that the initial signals of these chars are due to complexes between quinonoid acceptors and carbocyclic donors<sup>16</sup>. This is further borne out by the effects of hydrogen iodide on these chars. Treatment of all the chars with hydrogen iodide causes a reversible reduction in the number of spins/g. Aromatic hydrocarbons would not be expected to show such reversible behavior<sup>17,18</sup>, but electron acceptors such as quinones, which have been shown by Given and Peover<sup>19</sup> to be present in coals and related materials, would interact with hydrogen iodide. A reasonable explanation is that the e.s.r. signals of these chars are associated with acceptor moieties. These acceptor or quinonoid moieties apparently exist in the 300° to 500° chars as well as the 600° to 700° chars, since the signals are all reduced reversibly by hydrogen iodide. Since the halogen treatments suggest that the free radicals of the 600° to 700° chars, and probably of the 300° to 500° chars as well, are associated with aromatic centres, the presence of both donor and acceptor moieties associated with free radicals in the untreated chars is indicated. Hence, we suggest that the free radicals in the 600° to 700° chars are due to donor-acceptor complexes between aromatic donors and quinonoid acceptors. It is likely that the signals in the 300° to 500° chars are similar in nature but the aromatic centres are too small to form complexes with iodine or bromine.

Russian workers<sup>21</sup> reached similar conclusions, but only by a process of elimination, in order to account for the free radicals in a series of polyarylene polyacetylenes that had been heated to various temperatures. They concluded that complexes with charge-transfer were the only possible explanation after eliminating in turn the presence of paramagnetic ion impurities, radicals arising in the process of polymerization, and the existence of a triplet ground state. The first reference to charge-transfer complexes in coals or chars was made by Schuyer<sup>22</sup> to explain why the molar increment of refractive index per gram of aromatic carbon ( $I_M/C_{ar}$ ) decreases in the range between ninety per cent carbon and graphite. Some of the semiconductor properties of anthracites and chars were also explained on the basis of such a model.

In order to illustrate the relative importance of charge-transfer complexes in these chars a plot has been made in Figure 3 of the number of free radicals vs. carbon content. There has also been plotted the reciprocal of crystallite size in no./g. vs. carbon content calculated from the work of Hirsch<sup>15</sup> and van Krevelen<sup>23</sup> assuming that there is an average crystallite height of three graphitic layers and that there is no unordered material. It should be noted that the average height of the crystallites would be somewhat less than three in the low temperature chars and possibly somewhat greater than three in the higher temperature chars. In any event, it is seen that in the 600° to 650° range the number of crystallites closely approximates the number of free radicals, accounting for the results of Schuyer<sup>22</sup>. In fact these latter chars are apparently composed of little but charge transfer complexes in close proximity to one another which explains the intensive exchange narrowing of the e.s.r. signals of these materials. The decrease in free radicals at higher temperatures is at least in part due to the decrease in number of crystallites at higher charring temperatures.

Extending the conclusions on cellulose chars to coal and related materials, suggests that e.s.r. signals in all these materials result from donor-acceptor complexes which, while reaching a maximum of importance in anthracites and 600° to 700° chars, may still be of significance in lower rank coals and humic acids. Such a conclusion finds support from a number of other aspects of the behavior of coal and humic acids. Charge-transfer forces between coal and solvent can be used to explain the order of effectiveness of coal solvents. Thus catechol and anthracene oils, which are donor molecules, are very effective in extracting or dispersing coal or humic materials. Charge-transfer equilibria can also rationalize the failure of coal extracts once dried to redissolve completely in the original solvent used for extraction. Free

radicals in coals and chars are physically affected by oxygen, as indicated by line broadening of the e.s.r. signal, but are stable to chemical attack. Such behavior could be explained as due either to spin-spin coupling of the oxygen molecule with the free electron of the charge-transfer complex or to formation of new donor-acceptor complexes between aromatic centres and oxygen<sup>24</sup>.

The so-called molecular weight of humic acids and coal extracts should be re-examined in the light of the concept of donor-acceptor complexes. Thus molecular weight determinations of humic acids in catechol<sup>25</sup>, a substance conceivably capable of breaking up donor-acceptor complexes of humic acids, resulted in a low molecular weight estimate. Determinations on apparently similar material in sulfolane, a poor complexing agent, produced very much higher estimates of molecular weight<sup>26</sup>.

Finally, coals and related materials have a well-known broad absorption band at  $1600\text{ cm}^{-1}$  in the infrared region which has defied interpretation. Donor-acceptor phenomena have been shown to produce strong and broad absorption in this region<sup>27,28</sup> in aromatic systems, as shown in Figure 4, and hence may be the cause of this band in coal and chars.

#### REFERENCES

1. Honda, H., and Ouchi, K., Rep. Resources Inst. Japan No. 1, 1952.
2. Adamson, A.F., and Blayden, H.E., Proc. of the 3rd Conference on Carbon (1957), Pergamon Press, London, 1959, p. 147.
3. Berkowitz, N., Cavell, P.A., and Eloffson, R.M., Fuel 40, 279 (1961).
4. Ingram, D.J.E., and Bennett, J.E.P., Oil Mez. 45, 545 (1954).
5. Uebersfeld, J., Etienne, A., and Combrisson, J., Nature 174, 614 (1954).
6. Winslow, F.H., Baker, W.O., and Yager, W.A., J. Am. Chem. Soc. 77, 4751 (1955).
7. Akamatu, H., Mrozowski, S., and Wobschall, D., Proc. of the 3rd Conference on Carbon (1957), Pergamon Press, London, 1959, p. 135.
8. Singer, L.S., Spry, W.J., and Smith, W.H., Proc. of the 3rd Conference on Carbon (1957), Pergamon Press, London, 1959, p. 121.
9. Ingram, D.J.E., Free Radicals as Studied by Electron Spin Resonance, Butterworths, London, 1958, p. 213.
10. Uebersfeld, J. and Erb, E., Proc. of the 3rd Conference on Carbon (1957), Pergamon Press, London, 1959, p. 103.
11. Antonowicz, K., Proc. of the 5th Conference on Carbon (1961), Pergamon Press, London, 1963, p. 61.
12. Mrozowski, S., Proc. of the 4th Conference on Carbon (1959), Pergamon Press, London, 1960, p. 271.

13. Campbell, D., Jackson, C., and Wynne-Jones, W.F.K., *Nature* 199, 1090 (1963).
14. Toland, W.G., U.S. Patent 2,856,424 (1958).
15. Hirsch, P.B., *Proc. Roy. Soc. (London)*, A226, 143 (1954).
16. Bose, M., and Labes, M.M., *J. Am. Chem. Soc.* 83, 4505 (1961).
17. Mitchell, H.K. and William, R.J., *J. Am. Chem. Soc.* 60, 2723 (1938).
18. Deno, N.C., Freedman, N., Hodge, J.D., MacKay, F.P. and Saines, G., *J. Am. Chem. Soc.* 84, 4713 (1962).
19. Given, P.H., and Peover, M.E., *J. Chem. Soc.* 394 (1960).
20. Voet, A.C. and Teter, A.C., *Amer. Ink Maker* 38, No. 9, 94 (1960).
21. Dulov, A.A., Slinkin, A.A., Rubinshtein, A.M., and Kotlyarevski, I.L., *Izvestia Akad. Nauk S.S.S.R. Seriya Khim.* No. 11, p. 1910 (1963).
22. Schuyer, J., *Brenn. Chemie.* 37, 74 (1956).
23. van Krevelen, D.W. and Schuyer, J., *Coal Science*, Elsevier Publishing Co., London (1957), p. 176.
24. Tsubomura, H., and Mulliken, R.S., *J. Am. Chem. Soc.* 82, 5966 (1960).
25. Polansky, T.S., and Kinney, C.R., *Fuel* 31, 409 (1952).
26. Wood, J.C., Moschopedis, S.E., and Elofson, R.M., *Fuel* 40, 193 (1961).
27. Elofson, R.M., Anderson, D.H., Gutowsky, H.S., Sandin, R.B., and Schulz, K.F., *J. Am. Chem. Soc.* 85, 2622 (1963).
28. Sandin, R.B., Elofson, R.M., and Schulz, K.F., *J. Org. Chem.* 30, 1819 (1965).

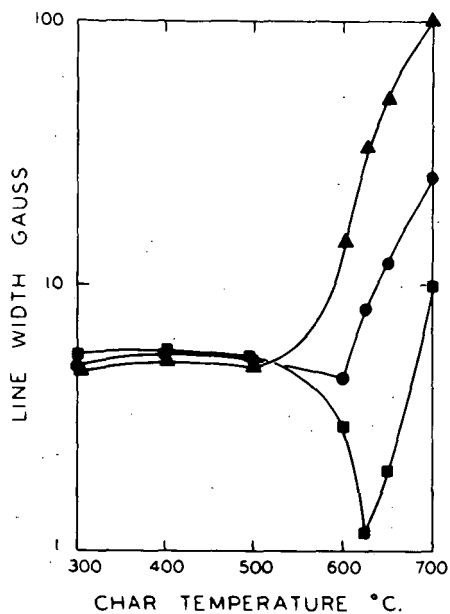


Figure 1.

Effect of  $I_2$  and  $Br_2$  on line widths of cellulose chars measured in vacuo at room temperature.

- no treatment
- ▲ treated with 0.1 M  $I_2$  in  $CCl_4$
- treated with 0.1 M  $Br_2$  in  $CCl_4$

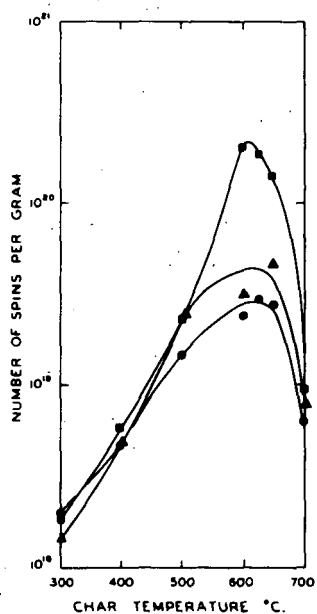


Figure 2.

Effect of  $I_2$  and  $Br_2$  on spin concentrations in cellulose chars measured in vacuo at room temperature

- no treatment
- ▲ treated with 0.1 M  $I_2$  in  $CCl_4$
- treated with 0.1 M  $Br_2$  in  $CCl_4$

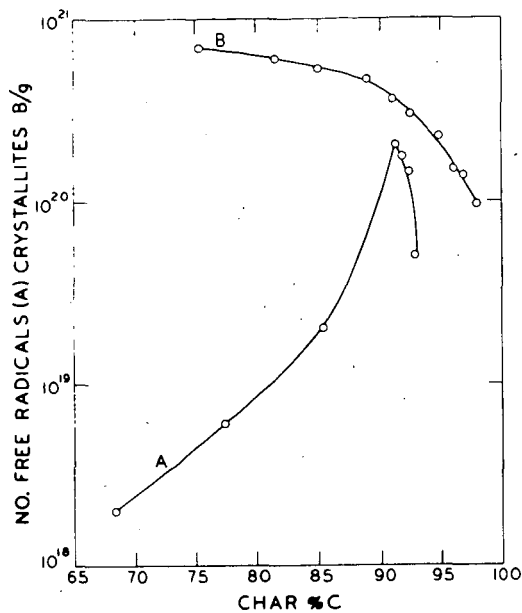


Figure 3.

Comparison of the number of free radicals with the size of crystallites in cellulose chars.

- A. number of free radicals per gram vs. Carbon content
- B. number of crystallites possible per gram vs. Carbon content

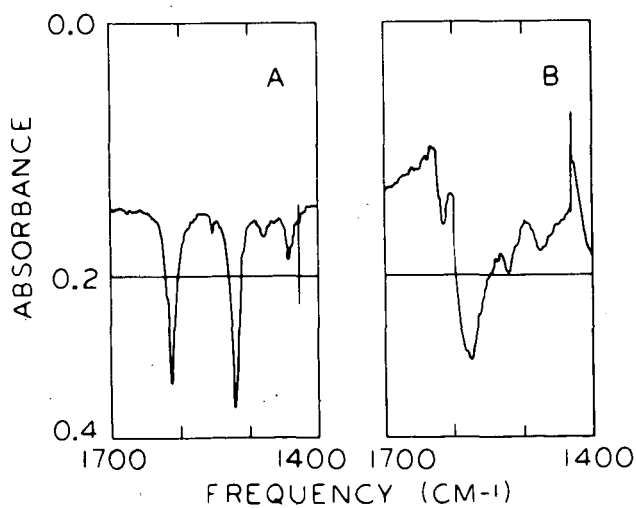


Figure 4.

The influence of charge transfer forces on infrared spectra.

- A. Tetrakis [p-dimethylaminophenyl] ethylene in fluorolube mull
- B. Iodine complex of tetrakis [p-dimethylaminophenyl] ethylene in fluorolube mull

## INFRARED SPECTRA OF OXYGEN-18 LABELED CHARs

R. A. Friedel

Pittsburgh Coal Research Center, Bureau of Mines,  
U.S. Department of the Interior, Pittsburgh, Pa.

R. A. Durie and Y. Shewchuk

Commonwealth Scientific and Industrial Research Organization,  
Chatswood, New South Wales, Australia

## SUMMARY

Chars of four O-18 labeled compounds were prepared. Infrared spectra were examined for isotopic shifts. On the basis of a few published results on pure compounds the shifts for C=O<sup>18</sup> at 1600 cm<sup>-1</sup> were expected to be -20 cm<sup>-1</sup> or more. The observed shifts are less than 5 cm<sup>-1</sup>; this result may indicate that chelated carbonyls are not involved. However, very strong hydrogen bonding as in chelated, conjugated carbonyl structures may be responsible for the small shifts. An O<sup>18</sup>-labeled chelate is being prepared at the CSIRO laboratories in order to investigate this point.

IntroductionChars

Since the early work at the Bureau of Mines on carbohydrate chars<sup>1,2/</sup> the infrared spectra of chars ( $\leq 500^\circ$  C) of various chemicals have been studied.<sup>3,4,5/</sup> Spectral investigations of structure of chars have included studies of the effect of elemental constitution; the effect of introducing oxygen into chars of hydrocarbons indicated that spectral absorption bands, particularly the intense 1600 cm<sup>-1</sup> band, were attributable to oxygenated structures.<sup>4,6,7/</sup> Isotope-labeling of chars has been utilized; a successful study of deuterium labeling was carried out by comparing infrared spectra of chars of an aliphatic hydrocarbon and a corresponding deuterocarbon. From this study definite evidence was obtained for assignment of the 730-910 cm<sup>-1</sup> absorption bands to CH out-of-plane aromatic vibrations.<sup>6,7/</sup> Also, further indications were found that the most intense band in char spectra, 1600 cm<sup>-1</sup>, was attributable to oxygenated structures.

A more direct investigation of the specific structures responsible for the 1600 cm<sup>-1</sup> band seemed desirable. Charring of compounds labeled with oxygen-18 was judged to be a direct method with good chances for success. Three structures were considered on the basis of their intense absorption, near 1600 cm<sup>-1</sup>, to be possible sources of the 1600 cm<sup>-1</sup> band in chars:

(1) Carbonyl groups in ketones, quinones, or conjugated chelate structures should show a shift to low frequency in going from C=O<sup>16</sup> to C=O<sup>18</sup>; (2) aromatic nuclei should produce no change in spectral frequency; (3) aromatic nuclei with enhanced intensities due to oxygenated substituents on the ring should not undergo any appreciable frequency shift in the 1600 cm<sup>-1</sup> region; a shift should occur in the C-O stretch region at 1100 cm<sup>-1</sup>.

## Coals

Studies of the 1600  $\text{cm}^{-1}$  band in char spectra may produce information on the origin of the same band in the spectra of coals. Spectral data from chars of carbohydrates would be particularly applicable for comparison with coal spectra as carbohydrate chars produce spectra nearly identical to spectra of coals.<sup>1,2/</sup> Unfortunately  $\text{O}^{18}$ -labeled carbohydrates are not available.

Information on the intense 1600  $\text{cm}^{-1}$  band in coals has been obtained in studies of absorption intensities for many pure compounds in an effort to determine what structures could produce the 1600  $\text{cm}^{-1}$  absorption.<sup>8/</sup> The principal type of structure found to have sufficient intensity is the conjugated chelated carbonyl group. These groups can only produce the 1600 band if all or nearly all of the oxygen in the coal is in the form of hydroxyl chelated carbonyl groups.

## $\text{O}^{18}$ -Labeled Compounds

The minimum spectral shift in the infrared spectra for a labeled carbonyl group ( $\text{C}=\text{O}^{18}$ ) relative to an unlabeled group ( $\text{C}=\text{O}^{16}$ ) is  $-40 \text{ cm}^{-1}$ , on the basis of the simple ratio of the reduced masses. Hooke's law for the stretching vibration of  $\text{C}=\text{O}^{16}$  is:  $\nu_{16} = \frac{1}{2\pi c} \sqrt{\frac{k}{\mu_{16}}}$ , where

$$\mu_{16} = \frac{m_{\text{C}} + m_{\text{O}^{16}}}{m_{\text{C}}m_{\text{O}^{16}}}; \quad \nu = \text{frequency, cm}^{-1}; \quad k = \text{constant};$$

For  $\text{C}=\text{O}^{18}$  the same equation applies; dividing,

$$\frac{\nu_{16}}{\nu_{18}} = \sqrt{\frac{\mu_{16}}{\mu_{18}}} = \sqrt{1.05}$$

$$\text{or } \nu_{18} = \frac{\nu_{16}}{\sqrt{1.05}}$$

For  $\nu_{16} = 1600 \text{ cm}^{-1}$ ,  $\nu_{18} = 1560 \text{ cm}^{-1}$ ;  $\Delta\nu = -40 \text{ cm}^{-1}$ . If this 1600  $\text{cm}^{-1}$  band in a char or coal spectrum is due to a simple carbonyl structure, the corresponding labeled carbonyl group should produce an absorption band shifted to 1560  $\text{cm}^{-1}$ . If the stretching vibration of the carbonyl structure is complex the simple value obtained from the reduced mass calculation will differ somewhat from 40  $\text{cm}^{-1}$ . A ketone investigated by Karabatsos<sup>9/</sup> showed an appreciable deviation; 2,3-dimethyl-3-pentanone- $\text{O}^{18}$  shows a shift of 31  $\text{cm}^{-1}$  instead of the expected 40. This shift is in the neighborhood predicted by Francis<sup>10/</sup> for a mixed vibration composed of about 80 percent  $\text{C}=\text{O}$  stretch and 20 percent  $\text{C}-\text{C}$  stretch. With conjugation the shift does not change for the benzenoid carbonyl compounds: Benzoic acid, two benzoates, benzophenone, and benzoquinone.

	$\Delta\nu, \text{ cm}^{-1}$
Benzoic acid (monomer)	-32 <sup>11/</sup>
Methylbenzoate	-31 <sup>11/</sup>
Cinnamyl nitrobenzoate	-30 <sup>12/</sup>
Benzophenone	-30 <sup>13/</sup>
p-Benzoquinone	-30 <sup>14/</sup>
Benzoylchloride	-25 <sup>11/</sup>
Benzamide	-24 <sup>15/</sup>

The decreased shift for benzamide is attributable to greater participation of other groups of the molecule in the carbonyl vibration.<sup>15/</sup> Apparently the same explanation may be given for the decreased shift observed for benzoylchloride. It is surprising that the shifts observed indicate no particular increase due to conjugation with an aromatic ring. (A large effect due to ring conjugation is observed by comparison of the spectra of nitromethane- $\text{O}^{18}$  and nitrobenzene- $\text{O}^{18}$ .<sup>16,17/</sup>) Future investigations of more aliphatic ketones may produce different results.

The only published indication of the effect of conjugated chelation is on benzoic acid dimer:

	$\Delta\nu, \text{ cm}^{-1}$
Benzoic acid dimer	-20
Benzoic acid monomer	-32

Thus hydrogen bonding is seen to produce a significant decrease in the  $\text{O}^{18}$  shift of a conjugated carbonyl system. It was anticipated that the spectra of chars having carbonyl groups enriched in  $\text{O}^{18}$  may show shifts for the  $1600 \text{ cm}^{-1}$  band of -20 to  $-30 \text{ cm}^{-1}$ . Such shifts in char spectra would be measurable, even though absorption bands are broad.

#### Experimental

On the initiation of this work only three usable  $\text{O}^{18}$ -labeled organic compounds were commercially available. They were investigated in the following order: Linoleic acid, phenol, and benzoic acid; sodium phenate and sodium benzoate- $\text{O}^{18}$  were also prepared and charred. First the unlabeled compounds were charred under various conditions in order to determine the most favorable condition for producing intense  $1600 \text{ cm}^{-1}$  bands. Temperatures required to eliminate the absorption of monosubstituted benzenes in order to produce coal-like absorption bands in the  $730\text{-}900 \text{ cm}^{-1}$  aromatic band region were usually so high that other spectral details, including the  $1600 \text{ cm}^{-1}$  band, were weakened.

Samples of  $\text{O}^{16}$  compounds were placed in a glass tube or a steel bomb, sealed or unsealed, in vacuo or under nitrogen. Amounts of sample used were 50-100 mg because of the scarcity of  $\text{O}^{18}$  samples. Pyrolysis temperatures were varied from  $350^\circ \text{ C}$  to  $620^\circ \text{ C}$ ; times were varied from 1 to 58 hours.

Linoleic acid- $O^{18}$ 

Two samples were investigated: (a) A sample of 22 percent  $O^{18}$ -enriched acid (kindly given by Dr. A. Miko, of the Yeda Research and Development Co., Rehovoth, Israel), and (b) a commercial sample of 38 percent enriched acid. The best conditions found for obtaining  $1600\text{ cm}^{-1}$  bands were  $400^\circ\text{ C}$ , 2 hours, under 1 atmosphere of nitrogen in a sealed pyrex tube. The 22 percent enriched sample was donated, with the warning that polymerization probably had occurred; it is also possible that polymerization occurred in the 38 percent enriched sample. Yeda has taken linoleic acid- $O^{18}$  off the market.

Phenol- $O^{18}$ , 86 percent

Pyrolysis of phenol of 86 percent  $O^{18}$  enrichment was carried out at temperatures near  $550^\circ\text{ C}$  for about 18 hours in a sealed tube under nitrogen.

Sodium phenate

The  $O^{18}$ -labeled phenate was not prepared because of insufficient phenol- $O^{18}$ . Sodium phenate- $O^{16}$  was prepared from ordinary phenol and charred. Conditions were similar to those used for phenol.

Benzoic acid- $O^{18}$ , 95.6 percent

Conditions were similar to those used for phenol.

Sodium benzoate- $O^{18}$ 

A nitrogen atmosphere and a temperature of  $500^\circ\text{ C}$  were used. Pyrolysis times were about 24 hours.

In all samples except the sodium phenate and sodium benzoate, char was obtained in the form of a thin film on the walls of the sealed tube. These films were sufficiently thin to give spectra of good quality directly; data obtained from such films was qualitative or semi-quantitative as thicknesses of the film varied considerably. In all cases spectra were also obtained by means of KCl pellets which were better for quantitative absorption measurements.

Spectra were determined first on gases produced. Then the samples were washed with hexane and/or benzene and the spectra of the soluble products were obtained. The benzene-insoluble char was then investigated.

Ultimate analyses of all of the chars are given in table 1.

Results and Discussion of Results

Results obtained on the four substances investigated show that the spectral shifts are very small or negligible (table 2); no shift was definitely detectable for any of the chars. In figure 1 the spectra of chars from benzoic acid- $O^{16}$  and - $O^{18}$  are given; they are practically identical, including the positions of the two  $1600\text{ cm}^{-1}$  bands.

$1600\text{ cm}^{-1}$  bands were obtained in all chars but in no case were they intense bands. This is a possible indication that carbonyl groups may not have been involved. For linoleic acid and benzoic acid it is nearly certain that no oxygen-containing group could be an important contributor to the  $1600\text{ cm}^{-1}$  band, as the oxygen contents of the chars were found to be negligible. Hydrocarbon structures could have produced the weak bands found.

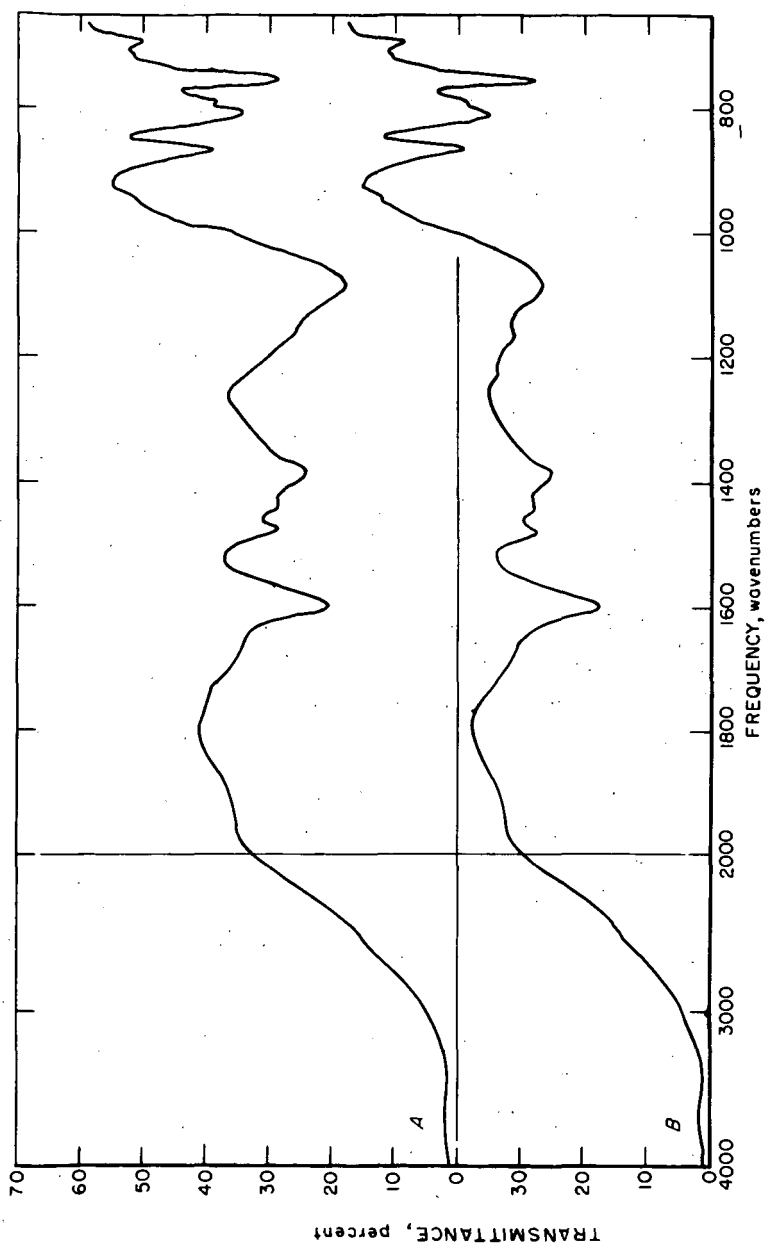


Figure 1. Infrared spectra of chars prepared from 50 mg heated at 550 C for 72 hours. KCl pellets, 2 percent in 100 mg KCl. Curve A, benzoic acid; curve B, benzoic acid-O<sub>18</sub>.

Table 1.- Ultimate analyses of chars

	C	H	O	State
Benzoic acid	96.2	3.8	< 0.5	Film
Benzoic acid	70.08	2.86	(6.35) <sup>2/</sup>	Powder
Benzoic acid- <sup>18</sup> O	95.17	3.89	1.35	Film
-----				
Sodium benzoate	93.00	3.71	3.88	Powder
Sodium benzoate- <sup>18</sup> O	91.47	3.22	2.60	Powder <sup>3/</sup>
-----				
Phenol	71.80	3.35	20.0	Powder
Phenol	93.26	3.46	3.42	Film
Phenol- <sup>18</sup> O	91.20	3.81	3.73	Film.
-----				
Sodium phenate	76.76	2.98	19.4	Powder
-----				
Linoleic acid <sup>1/</sup>	95.9	3.7	0.4	Powder

1/ <sup>18</sup>O-labeled chars were not analyzed.

2/ Very small sample; oxygen analysis dubious.

3/ Ash, 3.5 percent, apparently due to a trace of glass from vial opening.

Table 2.- Negative spectral shifts of oxygen-18 labeled chars

	Spectral shift, cm <sup>-1</sup> <sup>1/</sup>
Linoleic acid- <sup>18</sup> O (22 and 36 percent)	< 5
Phenol- <sup>18</sup> O (86 percent)	< 5
Benzoic acid- <sup>18</sup> O (95.6 percent)	< 5
Sodium benzoate- <sup>18</sup> O	< 5

1/ Bands were broad. Small shifts were difficult to measure accurately.

The phenol chars also showed no shift from  $1600\text{ cm}^{-1}$ , even though one char contains 20 percent oxygen. It is not surprising if the pyrolysis of phenol at  $550^\circ\text{C}$  does not produce carbonyl groups. The  $1600\text{ cm}^{-1}$  band observed in the spectrum of the phenol char must be due to aromatic absorption enhanced by oxygen-containing substituents on the aromatic rings (ethers and phenols).

The char of sodium benzoate also shows a negligible shift. It was the most likely possibility for producing an isotope shift, as the elimination of oxygen encountered in the chars of linoleic and benzoic acid does not occur for the char of sodium benzoate. The sizeable percentage of oxygen present in the char, 4 percent, is likely to exist in the char as carbonyl groups of some sort; even so, no appreciable shift is observed.

The lack of appreciable shift in the spectra of  $\text{O}^{18}$ -labeled chars may be attributable to extremely strong association (chelation, or other). With the sizeable oxygen content of some of these chars there are presumably some carbonyl groups present. Unfortunately no  $\text{O}^{18}$ -labeled pure compounds having very strong hydrogen-bonding have been investigated. As mentioned above, the spectrum of benzoic acid- $\text{O}^{18}$  shows a smaller shift for the associated dimer acid ( $-20\text{ cm}^{-1}$ ) than for the free monomer ( $-32\text{ cm}^{-1}$ ).<sup>10</sup> These results are for a rather weakly associated acid dimer; the vibration of the C=O group in the dimer obviously involves participation of other groups in the molecule. For a more strongly hydrogen-bonded chelate, as acetylacetone, the participation of other groups in the molecule would be greater and the shift probably would be less. On this basis the small shifts in chars are explainable. Certainly the negligible shift observed for chars does not exclude the presence of C=O groups in structures producing the  $1600\text{ cm}^{-1}$  band. In order to investigate the effect of strong chelation on the C=O $^{18}$  shift preparation of dibenzoylmethane,  $\text{H}_5\text{C}_6\text{-CO}^{18}\text{-CH}_2\text{-CO}^{18}\text{-C}_6\text{H}_5$ , is being carried out at the CSIRO laboratories. Little or no C=O $^{18}$  shift is expected. If an appreciable shift is observed for this compound it will be necessary to conclude that chars do not contain strongly chelated carbonyls.

Further studies will be carried out on labeled chars as other  $\text{O}^{18}$ -containing compounds become available. It is expected that prices of these compounds will decrease greatly, for cheaper methods of preparation are being developed.<sup>18/</sup>

#### References cited

1. Friedel, R. A., and M. G. Pelipetz. Infrared Spectra of Coal and Carbohydrate Chars. *J. Opt. Soc. of Am.*, v. 43, No. 11, November 1953, pp. 1051-1052.
2. Friedel, R. A., and J. A. Queiser. Infrared Analysis of Bituminous Coals and Other Carbonaceous Materials. *Anal. Chem.*, v. 28, 1956, pp. 22-30.
3. Friedman, S., R. Raymond, L. Reggel, I. Wender, and R. A. Friedel. Chemistry and Structure of Coal. Formation of Coallike Chars From Pure Organic Compounds. Abstracts, Am. Chem. Soc. meeting, Dallas, Texas, April 1956.
4. Friedel, R. A. Spectra and the Constitution of Coal and Derivatives. Proc. 4th Carbon Conf., Univ. of Buffalo, Pergamon Press, London, 1960, pp. 320-336.
5. Brown, T. H., and Turkevich, J. A Study of the Low-Temperature Carbonization of d-Glucose Using Electron Magnetic Resonance and Infrared Absorption. Proc. 3rd Conf. on Carbon, Pergamon Press, London, 1959, pp. 113-120.

6. Friedel, R. A., and H. Retcofsky. Spectral Studies of Coal. Proc. 5th Biennial Conf. on Carbon, The Pennsylvania State Univ., Pergamon Press, London, 1963, v. 2, pp. 149-165.
7. Friedel, R. A. The Use of Infrared Spectra of Chars in Coal Structure Research. Applied Optics, v. 2, No. 11, Nov. 1963, pp. 1109-1111.
8. Friedel, R. A., R. A. Durie, and Y. Shewchuk. The Origin of the 1600 Wavenumber Absorption Band in the Infrared Spectra of Various Coal Vitrains. To be published.
9. Karabatsos, G. J. Infrared Spectra of Isotopically Labelled Compounds. I. Diisopropyl Ketones. J. Org. Chem., v. 25, 1960, pp. 315-318.
10. Francis, S. A. Intensities of Some Characteristic Infrared Bands of Ketones and Esters. J. Chem. Phys., v. 19, 1951, pp. 942-948.
11. Pinchas, S., D. Samuel, and M. Weiss-Brodsky. Infrared Absorption of  $O^{18}$  Labelled Benzoic Acid, Benzoylchloride, and Methylbenzoate. J. Chem. Soc., 1961, p. 2382.
12. Braude, E. A., and M. Turner.  $O^{18}$  Isotope Effect on Infrared Spectra of Benzophenone. Chem. and Ind. 1955, p. 1223.
13. Halman, M., and S. Pinchas. The Isotope Effect of  $O^{18}$  on the Infrared Spectrum of Benzophenone. J. Chem. Soc., 1958, p. 1703.
14. Becker, E. D., E. Charney, and T. Anno. Molecular Vibrations of Quinones. VI. A Vibrational Assignment for p-Benzoquinone and Six Isotopic Derivatives. Thermodynamic Functions of p-Benzoquinone. J. Chem. Phys., v. 42, 1964, pp. 942-944.
15. Pinchas, S., D. Samuel, and M. Weiss-Brodsky. Infrared Absorption of  $O^{18}$ -Labelled Benzamide. J. Chem. Soc., 1961, p. 1688.
16. Pinchas, S. and M. Halman. The Infrared Absorption of  $O^{18}$ -Labelled Nitromethane. J. Chem. Soc., 1960, p. 1242.
17. Pinchas, S., D. Samuel, and B. L. Silver. The Infrared Absorption Spectrum of  $O^{18}$ -Labelled Nitrobenzene. Spectrochim. Acta, v. 20, 1964, p. 179.
18. Richter, W. J., M. Senn, and A. L. Burlingame. Convenient Labelling Technique for Mass Spectroscopy: Acid Catalyzed Deuterium and Oxygen-18 Exchange Via Gas-Liquid Chromatography. Tetrahedron Letters, No. 17, 1965, pp. 1235-1239.

Recovery of Nitrogen Bases with  
Weak Acids

by

T. F. Johnson, P. X. Masciantonio  
and J. H. Schelling

Applied Research Laboratory  
United States Steel Corporation  
Monroeville, Pennsylvania

Introduction

The recovery of nitrogen bases is of particular interest in chemical plants that operate in conjunction with coal-carbonization facilities. Traditionally, nitrogen bases such as ammonia, pyridine, and quinoline have been recovered by processes that involve acid extraction followed by neutralization with caustic soda or lime.<sup>1,2)</sup> Such processes have inherent disadvantages with regard to excessive consumption of acids and bases as well as concomitant waste-disposal problems.

Recently, several processes have been developed for nitrogen-base recovery by regenerative cyclic techniques. For example, recovery of ammonia from coke-oven gas and pyridine from coke-oven light oil have been reported.<sup>3,4,5)</sup> These processes for recovery of nitrogen bases are characterized by the use of an aqueous acid solution for the extraction step followed by a high-temperature stripping, or springing, operation that liberates the nitrogen bases and simultaneously regenerates the acid extractant. The selection of an appropriate acid extractant for a particular nitrogen-base system is an important factor in designing or developing a regenerative process. Previously reported studies<sup>3,4,5)</sup> have demonstrated that monoammonium acid phosphate is a suitable extractant for ammonia recovery, whereas either phosphoric acid or monopyridinium sulfate is adequate for pyridine recovery. However, the theory for selection of appropriate reagents for regenerative nitrogen-base recovery has not been developed and, consequently, the general applicability of this recovery technique has not received significant attention. It is the object of this paper to demonstrate that readily available thermodynamic data can be used to determine the feasibility of a regenerative technique for recovery of particular nitrogen bases. The discussion is based on the behavior of particular acids during the extraction and springing operations. Data are also presented on the extraction and springing steps for recovery of pyridine and quinoline from coal-tar fractions.

Discussion of the Regenerative Technique

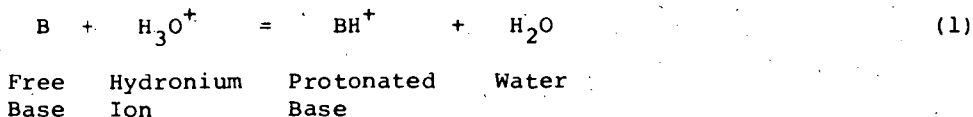
The general scheme for a regenerative recovery process for

\* See References.

nitrogen bases involves three steps: a) extraction, b) separation, and c) regeneration. The system can be seen in Figure 1 as a generalized flow diagram. Usually, nitrogen bases are recovered from streams in which they are present in low concentrations (about 0.1 to 5%), such as coke-oven light-oil streams.

### Selection of Reagents for Regenerative Systems

The selection of an appropriate acidic extractant for a particular nitrogen base is the initial problem encountered in developing a regenerative process. Although such factors as solubility, volatility, decomposition, and side reactions must be considered, the acid component essentially must be strong enough to effect efficient removal of the nitrogen base from the hydrocarbon stream during the extraction step and yet be sufficiently weak to allow decomposition of the resultant acid salt during the regeneration step. Therefore the values of the equilibrium constants at the springing and extraction temperatures ( $K_{T_2}$  and  $K_{T_1}$ ) for the following reaction are of significance in determining whether the regenerative technique is feasible.



The temperature dependence of the equilibrium constant follows the expression

$$\ln \frac{K_{T_2}}{K_{T_1}} = \frac{-\Delta H}{R} \left( \frac{1}{T_2} - \frac{1}{T_1} \right) \quad (2)$$

where

$\Delta H$  = the heat of reaction, and  
 $R$  = the gas constant.

It is desirable that the ratio ( $K_{T_2}/K_{T_1}$ ) be less than unity for a regenerative system ( $\Delta H$ , the heat of reaction, must be negative).

In an effort to develop suitable parameters for the selection of reagents for regenerative systems, the ionization equilibria of acids and bases have been examined.

In a discussion of acid-base systems, the following equations are applicable. Acid extraction of a nitrogen base (B) from a hydrocarbon stream involves the equilibrium reaction



which can be represented by an equilibrium constant

$$K_e = \frac{[\text{BH}^+]}{[\text{B}][\text{H}_3\text{O}^+]} \quad (4)$$

The ionization constant of the base involves the equilibrium



expressed by an ionization constant

$$K_b = \frac{[BH^+][OH^-]}{[B]} \quad (6)$$

By using the ionization constant for  $H_2O$

$$K_w = [OH^-][H_3O^+] \quad (7)$$

and combining Equations 4, 6, and 7, the following expression is obtained to show the concentration of protonated base in an aqueous extract.

$$[BH^+] = \frac{K_b}{K_w} [B][H_3O^+] \quad (8)$$

The dependence of  $[BH^+]$  on  $[H_3O^+]$  can be represented in terms of the strength of any acid (HA) by using the equilibrium dissociation constant of the acid.



$$K_a = \frac{[H_3O^+][A^-]}{[HA]} \quad (10)$$

$$[H_3O^+] = \left( [HA] K_a \right)^{1/2} \quad (11)$$

Combining (11) with (8) gives

$$[BH^+] = \frac{K_b}{K_w} K_a^{1/2} [HA]^{1/2} [B] \quad (12)$$

Equation 12 indicates that, for a given concentration  $[B]$  and strength ( $K_b$ ) of base, the concentration  $[BH^+]$  can be increased by increasing the strength of acid ( $K_a$ ).

$$[BH^+] \propto K_a^{1/2} \quad (13)$$

A similar discussion of the regeneration step is pertinent. The reaction involved is



The equilibrium constant for the reaction can be represented as

$$K_r = \frac{[B][H_3O^+]}{[BH^+]} \quad (15)$$

and can be expressed in terms of Equation 8 to give

$$K_r = \frac{K_w}{K_b} = \frac{[B][H_3O^+]}{[BH^+]} \quad (16)$$

Therefore

$$[B] = \left(\frac{K_w}{K_b}\right)^{1/2} [BH^+]^{1/2} \quad (17)$$

$$[B] \propto K_b^{-1/2} \quad (18)$$

Thus, for a given concentration  $[BH^+]$  in the aqueous extract, the concentration  $[B]$  of base is high for bases of low base strength ( $K_b$ ).

From Equations 12 and 17, the following generalizations can be made concerning the selection of an acid and a base for recovery of nitrogen bases by a regenerative process. To get good extraction, maximize  $[BH^+]$  by using an acid with as large a value for  $K_a$  as is possible, consistent with other requirements of the process. To get good regeneration, maximize  $[B]$  (a base with a small  $K_b$  value should be involved).

Accordingly, suitable systems appear to involve an acid extractant with a large  $K_a$  value and a nitrogen base with a small  $K_b$  value. Consistent with the above, the  $\Delta pK$  was examined as a useful guide in selecting components for regenerative systems,

where

$$pK = -\log K \quad (19)$$

$$\Delta pK = (pK_b - pK_a), \text{ and} \quad (20)$$

$\Delta pK$  is expressed as the absolute value of  $(pK_b - pK_a)$ . It is anticipated that the larger the  $\Delta pK$  of a system, the better it will function in a regenerative recovery process. Therefore it appears that recovery of nitrogen bases is facilitated by combinations of relatively weak bases and relatively strong acids or relatively strong bases and weak acids.

#### Systems for Recovery of Ammonia and Pyridine Bases

As mentioned above, several processes have previously been reported for recovery of ammonia and pyridine bases from coke-oven product streams. The data on ammonia and pyridine are consistent with the discussion presented above, Tables I and II. Experimentally it has been demonstrated that, although ammonia can be recovered in a regenerative manner using monoammonium phosphate, neither phosphoric acid nor sulfuric acid can be used ( $H_2PO_4^-$  is suitable for  $NH_3$  recovery, whereas  $H_3PO_4$ ,  $HSO_4^-$ , and  $H_2SO_4$  are not applicable).

It has also been shown that pyridine can be recovered successfully with either  $H_3PO_4$  or  $HSO_4^-$ ; however, neither  $H_2PO_4^-$  nor  $H_2SO_4$  can be employed.

The use of the parameter  $\Delta pK$  does not appear to fit the observed behavior of all the systems examined. However, the elementary ionization equilibrium theory explains certain inconsistencies with  $\Delta pK$  values. For example, in general, (1) systems in which both components have  $pK$  values greater than about 6 are not useful since interaction is too weak to effect extraction, (2) systems in which both components have  $pK$  values less than about 6 are not useful since interaction is too strong for dissociation of the acid-base salt during regeneration, and (3) when either component is a strong acid or a strong base, the system is not applicable because interaction is too strong for regeneration of the reagent.

### Recovery of Pyridine and Quinoline from Coal-Tar Fractions

A regenerative system for recovery of pyridine from coal-tar fractions has been examined on the basis of the above consideration of  $\Delta pK$ . Values of  $\Delta pK$  for the pyridine -  $\text{HSO}_4^-$  and pyridine -  $\text{H}_3\text{PO}_4$  systems are 6.85 and 6.64, respectively, Table II. Each system was examined to determine the behavior of these acids in the extraction and regenerative steps. Data on the quinoline regenerative recovery system are presented for comparison. Ionization data on quinoline ( $K_b = 6.3 \times 10^{-10}$ ,  $pK = 9.87$ ) suggest that either  $\text{HSO}_4^-$  or  $\text{H}_3\text{PO}_4$  could be used as the extractant. The respective values of  $\Delta pK$  are 7.95 and 3.22. Since  $\text{HSO}_4^-$  gives a larger value of  $\Delta pK$ , the recovery of quinoline with quinolinium acid sulfate solution as the extractant was examined for comparison.

### Experimental

Data on the extraction of pyridine and quinoline bases were obtained by using conventional laboratory equipment consisting of a stirred 1-liter 3-neck flask equipped with a bottom outlet stopcock. Single-stage extraction tests were conducted over the temperature range 0 to 55 C. The data on the pyridine - sulfuric acid system are presented in Table III, and data on the pyridine - phosphoric acid and the quinoline - sulfuric acid systems appear in Tables IV and V, respectively. The extraction data indicate that the nitrogen bases can be concentrated in the aqueous phase by the extraction technique.

To examine the vapor-liquid equilibrium data for the pyridine - phosphoric acid system, the pyridine - sulfuric acid system, and the quinoline - sulfuric acid system, solutions were prepared of various strengths of acid and concentration of the respective nitrogen bases. Acid strengths covered the range 20 to 40 percent and base-to-acid mole ratios varied from 0.6 to 1.9.

An Othmer equilibrium still was used to determine concentrations of pyridine and quinoline in the vapor and liquid phases for the various sample solutions.

### Discussion

The Othmer equilibrium data indicate that pyridine concentration

in the vapor increases with increasing concentration of acid (consistent with Equation 17) and, at a given level of acid strength, with increasing pyridine-to-acid mole ratio, see Figures 2 and 3, Tables VI and VII.

Although it was expected that quinoline should behave similar to pyridine, such was not the case. Quinoline was realized in the distillate of the Othmer still; however, the quinoline concentration is significantly lower than pyridine for a given mole ratio of base to acid. Two factors, low vapor pressure and low solubility, cause problems in the quinoline system. Because of the relatively poor solubility of quinoline in water (0.08 g/100 ml at 25 C), recovery of quinoline as a distillate product depends on the limitations of a steam distillation system. Accordingly, the distillate composition is a function of the vapor pressure of quinoline at the boiling point of the mixed liquid phase. Because of the low volatility of quinoline, only about 2 weight percent quinoline is realized in the distillate during the regeneration step. Thus, typical Othmer equilibrium data are not realized for quinoline.

Therefore, although quinoline can be recovered by a cyclic regenerative process, the system is not analogous to the pyridine system. The quinoline system appears suitable on the basis of  $\Delta pK$  data, but other factors such as solubility and volatility must be considered for practical application.

#### Summary

A method for selecting reagents for recovery of weak bases from hydrocarbon streams has been developed, based on thermodynamic ionization equilibrium constants. An acid can be selected for recovery of a given base according to the value of  $\Delta pK$  calculated for the system. Experimental data have been presented on the pyridine - sulfuric acid system, the pyridine - phosphoric acid system, and the quinoline - sulfuric acid system and demonstrate the utility and limitations of the method.

The technique should also be applicable to development of systems for recovery of acids from effluent streams by extraction with selected nitrogen base reagents. When it is required to effectively remove nitrogen impurities in conjunction with a subsequent refining operation on a hydrocarbon stream, a regenerative process may also be applicable; however, provision must be made for adequate removal of nitrogen bases by using a sufficient number of extraction stages.

#### References

1. H. H. Lowry, "Chemistry of Coal Utilization," Vol II John Wiley & Sons, Inc., New York, 1945.
2. P. J. Wilson and J. H. Wells, "Coal, Coke and Coal Chemicals," McGraw Hill, N. Y., 1950.

3. H. L. Stewart, U. S. Patent 2,410,906, November 12, 1946.
4. R. D. Rice, U. S. Patent 3,024,090, March 6, 1962.
5. G. D. Kharlampovich and R. I. Kudryashova, Coke and Chemistry (USSR),  
2, 29, (1964).

Table I

Data on Regenerative Recovery Systems  
for Nitrogen Bases<sup>1)</sup>

<u>Nitrogen Bases</u>	<u>Extractant</u>	<u>K<sub>a</sub></u>	<u>K<sub>b</sub></u>
NH <sub>3</sub>	(NH <sub>4</sub> )H <sub>2</sub> PO <sub>4</sub>	6.23 x 10 <sup>-8</sup> <sup>2)</sup>	1.79 x 10 <sup>-5</sup>
NH <sub>3</sub>	H <sub>3</sub> PO <sub>4</sub>	7.52 x 10 <sup>-33</sup> )	1.79 x 10 <sup>-5</sup>
NH <sub>3</sub>	(NH <sub>4</sub> )HSO <sub>4</sub>	1.20 x 10 <sup>-22</sup> )	1.79 x 10 <sup>-5</sup>
NH <sub>3</sub>	H <sub>2</sub> SO <sub>4</sub>	-4)	1.79 x 10 <sup>-5</sup>
Pyridine	(PyH)H <sub>2</sub> PO <sub>4</sub>	6.23 x 10 <sup>-8</sup> <sup>2)</sup>	1.71 x 10 <sup>-9</sup>
Pyridine	H <sub>3</sub> PO <sub>4</sub>	7.52 x 10 <sup>-33</sup> )	1.71 x 10 <sup>-9</sup>
Pyridine	(PyH)HSO <sub>4</sub>	1.20 x 10 <sup>-22</sup> )	1.71 x 10 <sup>-9</sup>
Pyridine	H <sub>2</sub> SO <sub>4</sub>	-4)	1.71 x 10 <sup>-9</sup>

- 1) Handbook of Chemistry and Physics, 44th Ed., Chemical Rubber Publishing Co., Cleveland, Ohio, 1963.
- 2) K<sub>a</sub> for second hydronium-ion dissociation.
- 3) K<sub>a</sub> for first hydronium-ion dissociation.
- 4) Completely dissociated.

Table II

ΔpK Values for Acid-Base Systems

<u>Systems</u>	<u>ΔpK</u>	<u>Suitability of System</u>
NH <sub>3</sub> -(NH <sub>4</sub> )H <sub>2</sub> PO <sub>4</sub>	2.46	Yes
NH <sub>3</sub> -H <sub>3</sub> PO <sub>4</sub>	2.63	No
NH <sub>3</sub> -NH <sub>4</sub> HSO <sub>4</sub>	2.83	No
NH <sub>3</sub> -H <sub>2</sub> SO <sub>4</sub>	*	No
Pyridine-(PyH)H <sub>2</sub> PO <sub>4</sub>	1.55	No
Pyridine-H <sub>3</sub> PO <sub>4</sub>	6.64	Yes
Pyridine-(PyH)HSO <sub>4</sub>	6.85	Yes
Pyridine-H <sub>2</sub> SO <sub>4</sub>	*	No

\* ΔpK Not applicable.

Table III

Extraction of Pyridine Bases from Light Oil  
With Pyridinium Sulfate Solution\*

<u>Test No.</u>	<u>Mole Ratio of Pyridine to H<sub>2</sub>SO<sub>4</sub></u>	<u>Pyridine in Washed Light Oil, %</u>	<u>Pyridine in Extract, %</u>
1	1.68	0.15	29
2	1.67	0.12	29
3	1.63	0.08	28
4	1.54	0.05	27

\* In each test, light oil containing 0.44 percent of P-bases was washed with a lean pyridinium sulfate solution (mole ratio 1.05) prepared by adding crude P-bases to a 30 weight percent sulfuric acid solution.

Table IV

Extraction of Pyridine Bases from Light Oil  
(30 Percent Phosphoric Acid at 55 C)

<u>Test No.</u>	<u>Mole Ratio of Pyridine to H<sub>3</sub>PO<sub>4</sub></u>	<u>Pyridine in Light Oil, %</u>	<u>Pyridine in Washed Light Oil, %</u>	<u>Pyridine in Extract, %</u>
1a)	1.0	5.67	0.44	19.5
2a)	1.0	2.10	0.40	19.2
3a)	0.70	4.60	0.24	14.5
4a)	0.92	4.60	0.59	18.1
5b)	0.95	4.60	0.58	18.6

a) One-stage wash.

b) Two-stage wash.

Table V

Extraction of Quinoline from a Tar Fraction  
With Sulfuric Acid<sup>1,2)</sup>

<u>Test No.</u>	<u>Mole Ratio of Quinoline to H<sub>2</sub>SO<sub>4</sub></u>	<u>Quinoline in Washed Oil, %</u>	<u>Quinoline in Acid Extract, %</u>
1	1.46	1.59	36.7
2	1.41	2.06	35.7

- 1) Tar fraction contained 12.1 weight percent quinoline bases.  
2) Extractant contained 30 weight percent H<sub>2</sub>SO<sub>4</sub>.

Table VI

Pyridine Concentrations in Vapor at Equilibrium With  
Refluxing H<sub>2</sub>SO<sub>4</sub> Solutions - Othmer Still Data

<u>Initial H<sub>2</sub>SO<sub>4</sub> Concentration, wt %</u>	<u>Mole Ratio of Pyridine to H<sub>2</sub>SO<sub>4</sub></u>	<u>Pyridine Content of Vapor, wt %</u>
20.4	1.63	4.7
19.9	1.95	21.1
30.9	1.60	10.4
30.4	1.81	23.8
30.6	1.98	41.6
40.3	1.60	21.3

Table VIII

Pyridine Concentrations in Vapor at Equilibrium With  
Refluxing H<sub>3</sub>PO<sub>4</sub> Solutions - Othmer Still Data

Initial H <sub>3</sub> PO <sub>4</sub> Concentration, wt %	Equivalent Ratio of Pyridine to Acid	Pyridine Content of Vapor, wt %
10.45	0.60	0.54
10.44	0.80	2.08
10.41	0.98	6.86
19.88	0.40	0.0
20.42	0.60	0.87
20.40	0.81	4.72
20.34	0.97	13.84
31.20	0.60	1.11
30.38	0.80	6.52
31.08	0.98	21.46
30.98	0.99 <sup>a)</sup>	19.92
31.06	0.99 <sup>b)</sup>	21.65 <sup>c)</sup>

- a) Pyridine contained 23.4 percent picoline.  
 b) Pyridine replaced with picoline.  
 c) Analyzed as picoline.

D. M. Mason

Institute of Gas Technology  
Chicago, IllinoisINTRODUCTION

Luminescence is the emission of nonequilibrium or nonthermal radiation as opposed to incandescence. A number of materials have been observed to luminesce when placed in a flame. This phenomenon, called candoluminescence, must be distinguished from thermoluminescence - in which a material is excited by radioactivity or other means but luminesces only when raised to a higher temperature - and from incandescence and luminescence of the flame itself. The blue luminescence of an aerated methane flame is an example of the latter. Candoluminescence is of interest from two standpoints - that of obtaining a better understanding of flames and flame-solid interactions, and secondly the possibility, though remote, of developing a new method of gaslighting. The work reported here was supported in part by the American Gas Association.

Candoluminescence has been known and studied for many years. It was probably first reported by Balmain in 1842 (3) in his description of the material boron nitride, which he was the first to prepare. Apparently the phenomenon was not recognized with other materials until it was reported by Donau in 1913 (5). The subject was reviewed by L. T. Minchin in 1938 (8) and by E.C.W. Smith in 1941 (11).

The materials that luminesce in flames share the characteristics of phosphors generally; that is, they are comprised of a colorless crystalline host or matrix material into which a small concentration of foreign atoms or ions, called the activator, is incorporated. The radiation is typically continuous and extends over only a small wavelength range, thus having a definite color. The color is usually characteristic of the activating ion and can also be obtained with other means of excitation, such as ultraviolet light or cathode rays.

Excitation by a hydrogen flame has been used in most studies of candoluminescence, although Tiede and Buescher reported that, in addition to hydrogen, flames of ethyl alcohol, hydrogen sulfide, and carbon disulfide excited the luminescence of boron nitride (14). Excitation by the flame of city gas has also been reported (9).

The existence of the phenomenon at relatively low temperatures has not been seriously questioned. The temperature range here is from the temperature attained when a flame impinges on a thin film of phosphor spread on a cool metal support up to a bright red heat. This upper limit is based on the observation of Tiede and Buescher (14) that blue luminescence occurred when a flame touched boron nitride in a carbon boat heated electrically to redness.

E. L. Nichols (10) claimed that at much higher temperatures he had observed light outputs from materials heated in an oxyhydrogen flame that were several times greater than the light output from a blackbody at the same temperature. Apparently this work was inspired by the

limelight which was produced by heating a cylinder of lime with an oxyhydrogen flame. The fact that a fresh portion of the lime had to be brought to the flame from time to time was interpreted to mean that something other than thermal radiation was involved (8). Neunhoeffer (9) reports that the natural chalks from which the lime was prepared contain rare earths. If this were known to Nichols, it would no doubt have suggested to him that the rare earths were activators in a luminescence process. However, the work of later investigators indicated that the limelight was similar to the light of the Welsbach mantle in that both are only excited thermally.

Nichols applied his "phosphors" on ceramic adjacent to a uranium-oxide-coated area and heated both areas evenly with an oxyhydrogen flame. Observations were made of both areas with an optical pyrometer; the uranium oxide was taken to behave essentially as a blackbody and to have the same temperature as the companion material. Many mixtures of colorless oxides with small amounts of rare earths, or with some other elements that were also regarded as activators, had a greater emittance than uranium oxide. E.C.W. Smith (11) repeated some of Nichols's experiments and obtained similar emittance readings. He then proceeded to determine or approximate the actual temperature of the two coatings - a matter of some difficulty. By means of thermocouples made of extremely fine wires, he was able to show large differences in the temperatures of the two coatings - differences sufficient to conclude that at incandescence temperatures there was no emission other than thermal. This conclusion has been confirmed by Sokolov and his co-workers (12), (13).

In hydrogen flames, at least, recombination of hydrogen atoms is generally accepted as the major source of energy for the low-temperature excitation (1), (7); earlier Donau (5) and Nichols (10) considered an oxidation-reduction mechanism, and Neunhoeffer (9) thought that electrons in the flame were responsible. Smith, and Arthur and Townend (1), (2) investigated this question with phosphors composed of calcium oxide activated with manganese, antimony, or bismuth. They found that:

1. Activated oxides that luminesce in hydrogen flames also luminesce when subjected to the action of hydrogen atoms produced in an electrical discharge. When subjected to the latter action and heated electrically, the color of the luminescence approached the color produced in the flame. Presumably, the temperature of the heated oxides approached the temperature of oxides in the flame.
2. The intensity of hydrogen flame luminescence increases when the hydrogen is burned under reduced pressure. This effect was presumed to be caused by a decrease in the number of three-body collisions. These collisions remove hydrogen atoms by recombination.
3. The luminescence is strongest in hydrogen, erratic and very faint in town gas, and absent in carbon monoxide flames. It is also absent in methane and ethylene flames tested at pressures from atmospheric to 10 cm Hg.
4. The luminescence is extinguished when small amounts of hydrocarbon gases or vapors are added to the hydrogen.

According to recent studies of flame mechanisms, hydrogen atoms are present in the methane-air flame as well as in the hydrogen flame (15). Thus it appeared reasonable to search for phosphors that candoluminesce in the methane-air flame. This search and the study of the characteristics of this phenomenon were the objectives of our investigation.

## PROCEDURES

### Preparation of Phosphors

#### Materials

Rare earths were obtained as 99.9% pure oxides from Lindsay Chemical Division of American Potash and Chemical Corporation. Other chemicals were research grade.

#### Calcium Oxide Phosphors

Calcium and rare earth nitrate solutions were prepared and mixed in the required amounts. The mixed nitrate solution was slowly poured into hot ammonium carbonate solution with stirring. The precipitate was filtered, washed with hot ammonium carbonate solution, dried at 100°C, and ignited at 900°C for 30 minutes. The pure rare earth oxides were prepared by precipitation from the nitrate in the same manner.

#### Yttrium Europium Tungstate - $(Y_{0.9}Eu_{0.1})_2O_3WO_3$ - and Gadolinium Europium Molybdate - $(Gd_{0.8}Eu_{0.2})_2O_3.MoO_3$

The required amounts of the oxides (tungstic acid in the case of tungsten) were mixed, heated in a platinum crucible at 1000°C for 2 hours, ground with mortar and pestle, and reheated at 1000°C for 2 hours. The X-ray patterns of the two products showed that in both a new phase had been formed.

#### Screening Tests

Mounting strips about 2 cm wide and 10 cm long were made of insulating fire brick and of copper sheet. Phosphor powder, thick enough to hide the surface of the strip, was pressed on to it with a spatula. The nearly vertical face of the strip was observed as it was passed through a methane-air flame (bunsen burner) and a hydrogen diffusion flame in a dark room.

#### Spectra

Three different methods of mounting the phosphors were used in obtaining the spectra. When we wished to observe the effect of temperature, the phosphor was applied as a paste to a silicon carbide rod. Pastes made with monomethyl ester of ethylene glycol seemed to adhere after drying somewhat better than those made with other liquids. The silicon carbide rod, about 6 mm in diameter, was held between two water-cooled electrical terminals to allow the electrical current passing between the terminals to heat the silicon carbide rod and the phosphor.

When hydrogen was used as a fuel, the phosphor could be coated dry on the fritted disk of a gas-dispersion tube. The fritted disk was operated as a porous-plate burner (Figure 1) without primary air. Known amounts of other gases could be added to the hydrogen.

The phosphor was coated on a water-cooled copper plate when a methane-air flame was to be used. The plate was 1 in. square x 1/4 in. thick with two 1/4-in. copper tubes soldered to the back for cooling water. Plating the face with silver was found to be necessary to prevent slow poisoning of the phosphor by the copper. The phosphor was settled onto the plate from a water suspension. The plate was mounted facing upwards at about 45° to the horizontal and the flame of a National Welding Equipment Co. Type-3A blowpipe was directed downward onto it.

A Beckman DK-2 spectrophotometer with an IP 28 photomultiplier was used to record spectra. The backplate of the lamp housing was removed to allow direct entrance of the radiation from the excited phosphor into the spectrophotometer. A slit opening of 0.4 mm without an auxiliary light-gathering system gave sufficient energy. Varying light intensity from the flickering of the flame was troublesome and made it necessary to use the highest time constant and the slowest recording rate of the instrument. The porous-plate burner gave the steadiest radiation.

## RESULTS

Screening tests to discover phosphors that candoluminesce in methane-air flames or in hydrogen flames were run on a number of commercial phosphors and on others prepared in our laboratories. The latter were principally rare earths - pure and in calcium oxide. The phosphors were spread on fire-brick slabs and on copper strips - the latter to hold down the temperature of the phosphor at least momentarily - and tested by impingement in both hydrogen and methane-air flames. Several phosphors that candoluminesce in both flames were found. Detailed results are shown in Tables 1 and 2. These results should be regarded as tentative rather than conclusive.

A few additional phosphors not listed in the tables were tested. Three General Electric silver-activated zinc sulfides (Nos. 118-2-3, 118-2-11, and 118-3-1) showed emission in the blue. Their spectra, obtained with a hydrogen diffusion flame on a fritted glass disk, showed that the emission was the band spectrum of S<sub>2</sub> and that no candoluminescence was present (6). The S<sub>2</sub> was undoubtedly formed by decomposition of the phosphor. Zinc sulfide activated by silver and copper showed both candoluminescence and the band spectrum of S<sub>2</sub> (Figure 2). A boron nitride sample from Carborundum Co., Electronics Division showed weak, green luminescence in hydrogen and methane flames. Two recently developed rare earth phosphors, (Y<sub>0.9</sub>Eu<sub>0.1</sub>)<sub>2</sub>O<sub>3</sub>·WO<sub>3</sub> and (Gd<sub>0.8</sub>Eu<sub>0.2</sub>)<sub>2</sub>O<sub>3</sub>·MoO<sub>3</sub> were prepared and tested (4). Both luminesced red in hydrogen and methane flames on the fire-brick strip.

Light emission in some of the screening tests may have had a source other than candoluminescence. The emission from magnesium germanate was probably thermal. This is indicated by the color of the emission (white to yellowish white), by the absence of a maximum of emission intensity with increasing temperature of the phosphor, and by equal emission when the phosphor is heated to the same temperature with or without the flame. For this test, the phosphor was mounted on the electrically heated silicon carbide rod, and temperature equivalence was indicated by the emission of the phosphor at 2.25 microns. Light

Table 1. LIGHT EMISSION OF YTTRIUM OXIDE AND RARE EARTHS (Pure and in CaO) IN HYDROGEN AND METHANE-AIR FLAMES

Element	Atomic No.	Symbol	Metal Conc in CaO, wt %	Light Emission				Color
				With H <sub>2</sub>		With CH <sub>4</sub> -Air		
				On Cu Strip	On Fire Brick	On Cu Strip	On Fire Brick	
Yttrium	39	Y	0.2 1.0 PO*	Trace Trace Weak	Weak Trace Trace	Nil Nil Trace	Nil Nil Nil	Violet Violet Green and Orange
Lanthanum	57	La	0.2 1.0 PO	Trace Trace Weak	Weak Trace Trace	Nil Nil Nil	Nil Nil Nil	Lavender Lavender Green and Orange
Praseodymium	59	Pr	0.2 1.0 PO	Trace Trace Nil	Strong Strong Trace	Nil Trace Nil	Strong Strong Nil	Red Red Red
Neodymium	60	Nd	0.2 1.0 PO	Trace Trace Nil	Trace Weak Trace	Nil Nil Nil	Nil Nil Nil	Violet Lavender Red
Samarium	62	Sm	0.2 1.0 PO	Trace Trace Nil	Trace Trace Nil	Trace Nil Nil	Trace Trace Nil	Orange Orange --
Gadolinium	64	Gd	0.2 1.0 PO	Trace Trace Strong	Trace Weak Strong	Nil Nil Trace	Nil Nil Weak	Violet Violet Red
Dysprosium	66	Dy	0.2 1.0 PO	Trace Trace Nil	Trace Weak Nil	Nil Nil Nil	Nil Nil Nil	Lavender Blue --
Holmium	67	Ho	0.2 1.0 PO	Trace Trace Nil	Trace Weak Trace	Nil Nil Nil	Nil Nil Trace	Aqua to Blue Aqua Red
Erbium	68	Er	0.2 1.0 PO	Trace Trace Nil	Trace Weak Trace	Nil Nil Nil	Nil Nil Nil	Blue White Red
Ytterbium	70	Yb	0.2 1.0 PO	Trace Trace Nil	Trace Trace Nil	Nil Nil Nil	Nil Trace Nil	Lavender Red --

\* Pure oxide.

Table 2. LIGHT EMISSION OF COMMERCIAL PHOSPHORS IN HYDROGEN AND METHANE-AIR FLAMES

Mfr. No.	Name	Host Crystal	Formula	Crystal Structure	Activation Name	Wt. %	Color In		Light Emission		Color
							Comer. Applic.	On Cu Strip	With Mg	With CH <sub>4</sub> -Air	
<b>Sylvania Fluorescent Lamp and Sign Tubing Phosphors</b>											
242	6-Barium pyrophosphate	Ca <sub>2</sub> CaP <sub>2</sub> O <sub>7</sub>	---	---	Titanium	7.6	Blue	---	Nil	Nil	---
2313	Cadmium borate	CaB <sub>2</sub> O <sub>7</sub>	---	---	Manganese	0.2	Deep pink	Weak	Weak	Nil	Red orange
5553	Calcium halophosphate	Ca <sub>10</sub> (PO <sub>4</sub> ) <sub>6</sub> (F,OH) <sub>2</sub>	Apatite	---	Antimony	0.3	White	Trace	Trace	Nil	Pale orange
290	Calcium silicate	CaSiO <sub>3</sub>	Wollastonite	---	Lead	1.0	Red	Trace	Weak	Trace	---
2402	Calcium tungstate	CaWO <sub>4</sub>	Scheelite	---	Manganese	2.8	Deep blue	Nil	Nil	Nil	---
281	Calcium zinc orthophosphate	Ca <sub>2</sub> Zn <sub>2</sub> (PO <sub>4</sub> ) <sub>2</sub>	Whitlockite	---	TiN	0.8	Red	Nil	Nil	Nil	---
2301	Magnesium tungstate	MgWO <sub>4</sub>	Scheelite	---	In	1	Blue	Trace	Trace	Trace	Blue
283	Strontium pyrophosphate	Ca <sub>2</sub> StrP <sub>2</sub> O <sub>7</sub>	---	---	Mn	1	Blue	Trace	Trace	Trace	Green
2822	Zinc orthosilicate	ZnSiO <sub>3</sub>	Willemite	---	Manganese	2.5	Green	Trace	Weak	Trace	Green
<b>General Electric Lamp Phosphors</b>											
151	Zinc phosphate	Zn <sub>3</sub> (PO <sub>4</sub> ) <sub>2</sub>	---	---	Manganese	1.2	Red	Strong	Strong	Strong	Yellow-orange
161	Zinc orthosilicate	ZnSiO <sub>3</sub>	Willemite	---	Manganese	0.4	Green	Trace	Trace	Trace	Yellow-orange
<b>General Electric Lamp Phosphors</b>											
	Barium silicate	BaSiO <sub>3</sub>	---	---	Lead	---	Ultraviolet	Trace	Trace	Nil	Green
	Barium titanium phosphate	(BaTi) <sub>2</sub> (PO <sub>4</sub> ) <sub>2</sub>	---	---	None	---	White	Trace	Trace	Nil	---
	Cadmium borate	Ca <sub>2</sub> CaB <sub>2</sub> O <sub>7</sub>	---	---	Manganese	---	Orange	Trace	Trace	Nil	Pale orange
	Calcium halophosphate	Ca <sub>10</sub> (PO <sub>4</sub> ) <sub>6</sub> (F,OH) <sub>2</sub>	Apatite	---	Manganese, Ant. 1	---	Cool white	Trace	Trace	Nil	Pink
	Calcium halophosphate	Ca <sub>10</sub> (PO <sub>4</sub> ) <sub>6</sub> (F,OH) <sub>2</sub>	Apatite	---	Antimony	---	Blue	Trace	Trace	Nil	Orange
	Calcium phosphate	Ca <sub>3</sub> (PO <sub>4</sub> ) <sub>2</sub>	---	---	Mercury	---	Red	Trace	Trace	Nil	Pink
	Calcium metasilicate	CaSiO <sub>3</sub>	---	---	Manganese	---	Plum	Trace	Trace	Trace	Green
	Calcium tungstate	CaWO <sub>4</sub>	---	---	Manganese	---	Plum	Trace	Trace	Trace	Green
	Magnesium germanate	3MgO·GeO <sub>2</sub>	---	---	Lead	---	Deep blue	Trace	Trace	Nil	Light blue
	Magnesium tungstate	3MgO·2WO <sub>3</sub>	---	---	Manganese	0.01	Red	Trace	Trace	Trace	Light yellow
	Strontium halophosphate	Str <sub>10</sub> (PO <sub>4</sub> ) <sub>6</sub> (F,OH) <sub>2</sub>	Apatite	---	None	---	Light blue	Trace	Trace	Trace	Pink
	Strontium halophosphate	Str <sub>10</sub> (PO <sub>4</sub> ) <sub>6</sub> (F,OH) <sub>2</sub>	Apatite	---	Antimony	---	Green	Trace	Trace	Trace	Pink
	Strontium magnesium orthophosphate	(SrMg) <sub>2</sub> (PO <sub>4</sub> ) <sub>2</sub>	---	---	Manganese	---	Green	Trace	Trace	Trace	Pink
	Zinc orthosilicate	ZnSiO <sub>3</sub>	---	---	Stannous tin	2	Pink-white	Trace	Trace	Trace	Blue
	Zinc orthosilicate	ZnSiO <sub>3</sub>	---	---	Manganese	---	Green	Weak	Weak	Trace	Green
<b>General Electric Lamp Phosphors</b>											
	Zinc orthosilicate	ZnSiO <sub>3</sub>	---	---	Copper	---	Yellow	Trace	Trace	Trace	Yellow
	Zinc orthosilicate	ZnSiO <sub>3</sub>	---	---	Manganese	---	Yellow	Trace	Trace	Trace	Yellow
	Zinc orthosilicate	ZnSiO <sub>3</sub>	---	---	Silver	---	Black-blue	Trace	Trace	Trace	Green
	Zinc orthosilicate	ZnSiO <sub>3</sub>	---	---	Copper	---	Black-blue	Trace	Trace	Trace	Green
<b>General Electric Lamp Phosphors</b>											
	Strontium and Ba silicate	(BaSr) <sub>2</sub> SiO <sub>4</sub>	---	---	None	---	Black-blue	Trace	Trace	Trace	Green

3. Based on the following: 1. J. H. Van Vleet, J. Appl. Phys., 22, No. 22, p. 22-23, and the remainder calcium halophosphate.  
 2. J. H. Van Vleet, J. Appl. Phys., 22, No. 22, p. 22-23, and the remainder calcium halophosphate.  
 3. J. H. Van Vleet, J. Appl. Phys., 22, No. 22, p. 22-23, and the remainder calcium halophosphate.  
 4. J. H. Van Vleet, J. Appl. Phys., 22, No. 22, p. 22-23, and the remainder calcium halophosphate.

emission in a few cases may be caused by decomposition of the phosphor, as was shown in the case of the silver-activated zinc sulfides.

The manganese-activated zinc phosphate (Sylvania No. 151) phosphor appeared to give the most intense luminescence emission in methane-air flames of any tested, and, accordingly, its light emission was investigated further. When the phosphor was coated on a fritted disk and the disk used as a porous-plate burner, a steady emission was obtained with a hydrogen diffusion flame. However, no emission could be obtained in this manner when the fritted-disk burner was fed with pure methane or with a methane-air mixture. Only when the phosphor was brought into a Bunsen flame was the light emission observed. We do not know the cause of this effect. A greater concentration of hydrogen atoms in the hydrogen flame may play a role. The high diffusivity and other properties of hydrogen that cause its flame to burn closer to the solid surface may be of equal or greater importance.

Spectra recorded with the Beckman DK-2 spectrophotometer were used to compare the light emission of this phosphor in the hydrogen flame with its emission in the methane-air flame. The phosphor was coated on a silicon carbide rod for this experiment. No significant difference other than that of the emission from the flame itself was observed (Figure 3).

The effect of temperature on the light emission of the phosphor was investigated by electrically heating the silicon carbide rod. With a methane-air flame impinging on the phosphor-coated rod, and with the spectrophotometer focused on the rod near one of its water-cooled ends, the light emission increased to a maximum with an increase in electrical heating, then decreased to near extinction with further heating. This agrees with the observation of Neunhoeffler (9) that the hydrogen flame candoluminescence of calcium oxide impregnated with various activators exhibits temperature maxima.

When the phosphor was heated to a still higher temperature, thermal emission appeared. When the emission of the phosphor was corrected for the emission of the flame, no essential difference in emission at high temperatures with and without the flame was evident. These experiments indicated that the low-temperature light emission experienced with this phosphor is candoluminescence, but that candoluminescence is not involved in the high-temperature emission.

This phosphor was the only one of several tested that luminesced in a carbon monoxide flame. The question of excitation in this flame by high-energy species other than hydrogen atoms was not pursued.

Spectra of the luminescences from several phosphors excited by hydrogen burning on the surface of a sintered glass disk were obtained, and the effect of the addition of small amounts of carbon monoxide and methane to the fuel was observed. The phosphors were calcium silicate activated with lead and manganese (Sylvania No. 290), calcium oxide activated with ytterbium, calcium oxide activated with praseodymium, and calcium oxide activated with samarium. The spectra obtained from the first three of these phosphors when they are excited with pure hydrogen burning on a fritted disk are shown in Figure 4. The Sylvania No. 290 phosphor emits with a broad peak in the green. Praseodymium-activated calcium oxide shows two peaks - one at 595 millimicrons (yellow) and a weaker one at 490 millimicrons (blue-green). Ytterbium-

547  
activated calcium oxide also shows two peaks - one at 375 millimicrons, which is in the ultraviolet. Samarium-activated calcium oxide also emits with a similar peak in the ultraviolet and another at 570 millimicrons (yellow), as shown in Figure 5.

The effect of the addition of small amounts (1 to 10 volume percent) of carbon monoxide or methane to the hydrogen burning on the fritted disk was different for each of these phosphors. Luminescence of the Sylvania No. 290 phosphor was substantially unchanged with addition of as much as 10% of the carbon monoxide or methane. Luminescence of the praseodymium-activated calcium oxide was not greatly affected by addition of 1% of the carbon monoxide or methane, but decreased rapidly with greater amounts. Only about 10% of the original intensity was obtained with 6% carbon monoxide or 8% methane. The luminescence of the ytterbium-activated calcium oxide was even more strongly quenched by the addition of carbon monoxide or methane. With these phosphors, only the intensity of the luminescence was affected.

With samarium-activated calcium oxide, the spectral distribution of the luminescence was also affected, as shown in Figure 5. Upon the addition of carbon monoxide, emission by this phosphor in both wavelength regions decreased in intensity, and, at about 3% carbon monoxide, emission in the 375-millimicron region had virtually disappeared. The 570-millimicron peak, however, was replaced by two narrower emission bands with peaks at about 560 and 595 millimicrons. With further addition of carbon monoxide the intensity of this emission increased to a maximum several times more intense than the original peak emission, then decreased. These effects were not observed upon the addition of methane to the flame. The variation of the intensity of the luminescence in the two cases is shown in Figure 6.

At a late stage of the work, phosphors were deposited by settling from a water suspension onto a water-cooled copper plate. A few spectra were obtained in this way with methane-air excitation.

Enhancement of the luminescence from the manganese-activated zinc silicate (Sylvania No. 161) by the cooling of the copper plate was very pronounced. (Figure 7).

#### ACKNOWLEDGMENT

The author wishes to thank the American Gas Association for their support and for permission to publish these results. John Hasenberg did most of the experimental work. Peter Mrdjin identified the S<sub>2</sub> bands in the spectra of the zinc sulfide phosphors.

1. Arthur, J. R. and Townend, D.T.A., "Fundamental Aspects of Combustion - Some Reactions of Atomic Hydrogen in Flames," J. Inst. Fuel 26, 44-51, 61 (1953) July.
2. Arthur, J. R. and Townend, D.T.A., "Some Reactions of Atomic Hydrogen in Flames," in U.S. Natl. Bur. Standards, Circ. 523, "Energy Transfer in Hot Gases," 99-110. Washington, D.C.: Govt. Print. Office, 1954.
3. Balmain, W. H., "Observations on the Formation of Compounds of Boron and Silicon With Nitrogen and Certain Metals," Phil. Mag. 21, 270-77 (1842).
4. Borchardt, H. J., "Rare Earth Phosphors," J. Chem. Phys. 38, 1251 (1953) March 1.
5. Donau, J., "New Kind of Luminescence of Alkaline Earth Preparation, Especially Calcium Preparations Which Contain Bismuth or Manganese Brought Out by the Hydrogen Flame; as Well as the Detection of Traces of the Latter," Monatsh. 34, 949-55 (1913).
5. Gaydon, A. G., The Spectroscopy of Flames, 244. New York: John Wiley, 1957.
7. Gorban, A. N. and Sokolov, V. A., "On the Question of the Physico-Chemical Nature of Candoluminescence," Opt. Spectr. (U.S.S.R.) English Transl. 7, 164-65 (1959) August.
8. Minchin, L. T., "Luminescence of Oxides Under Flame Excitation," Trans. Faraday Soc. 35, 163-70 (1939); "Luminescence of Substances Under Flame Excitation," Trans. Faraday Soc. 36, 505-06 (1940).
9. Neunhoeffler, O., "The Hydrogen Flame as a Source of Electrons," Z. Physik. Chem. 197, 179-85 (1951).
10. Nichols, E. L., Howes, H. L. and Wilber, D. T., "Cathodo-luminescence and the Luminescence of Incandescent Solids," Carnegie Inst. Publ. No. 348 (1928).
11. Smith, E.C.W., "The Radiation From Solid Substances Under Flame Impact: Part 1," Institution of Gas Engineers Comm. 237. London, 1941; Gas J. 233, 202-05, 247, 250-51, 256, 293, 298 (1941).
12. Sokolov, V. A., "Candoluminescence From the Viewpoint of the Vavilov-Wiedemann Criterion and of Contemporary Physicochemical Ideas," Izv. Akad. Nauk. U.S.S.R., Ser. Fiz. 26, 514-17 (1962).
13. Sokolov, V. A., Grozina, I. S. and Gorban, A. N., "The Nature of Candoluminescence of Calcium Oxide," Izv. Tomskogo Politekhn. Inst. 95, 253-56 (1958).
14. Tiede, E. and Buescher, F., "Inorganic Luminescent Phenomena. II. Luminous Boron Nitride (Balmain's Aethogen and the Flame Excitation of Luminescence)," Ber. 53B, 2206-14 (1920).

15. Wise, H. and Rosser, W. A., "Homogeneous and Heterogeneous Reactions of Flame Intermediates," in Ninth Symposium (International) on Combustion, 733-42. New York: Academic Press, 1963.

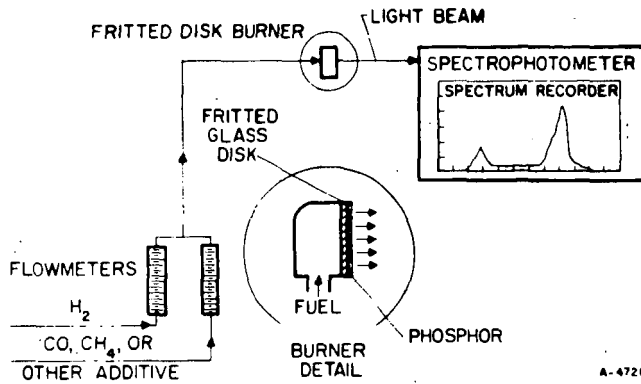


Figure 1. SCHEMATIC REPRESENTATION OF THE POROUS BURNER APPARATUS FOR LIGHT EMISSION STUDIES

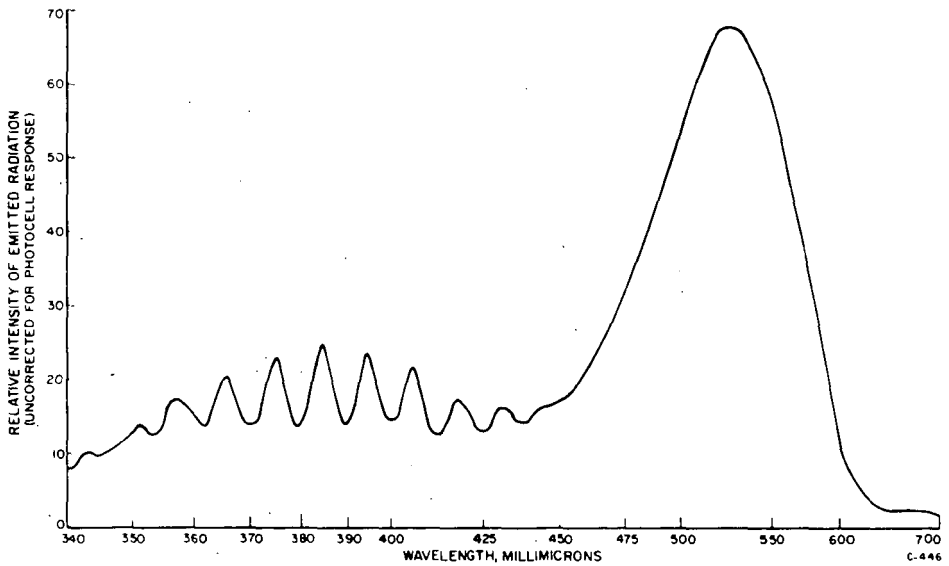


Figure 2. EMISSION SPECTRUM OF ZnS:Cu:Ag EXCITED BY A HYDROGEN DIFFUSION FLAME

15. Wise, H. and Rosser, W. A., "Homogeneous and Heterogeneous Reactions of Flame Intermediates," in Ninth Symposium (International) on Combustion, 733-42. New York: Academic Press, 1963.

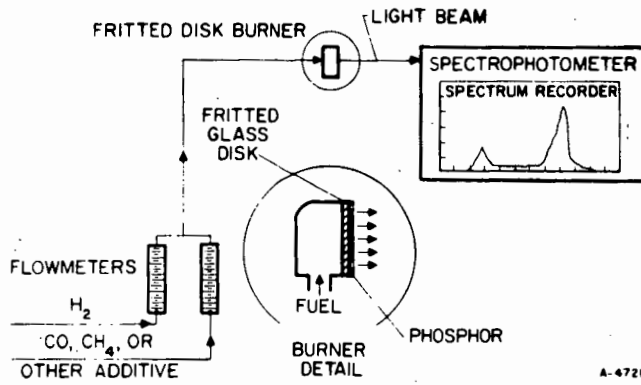


Figure 1. SCHEMATIC REPRESENTATION OF THE POROUS BURNER APPARATUS FOR LIGHT EMISSION STUDIES

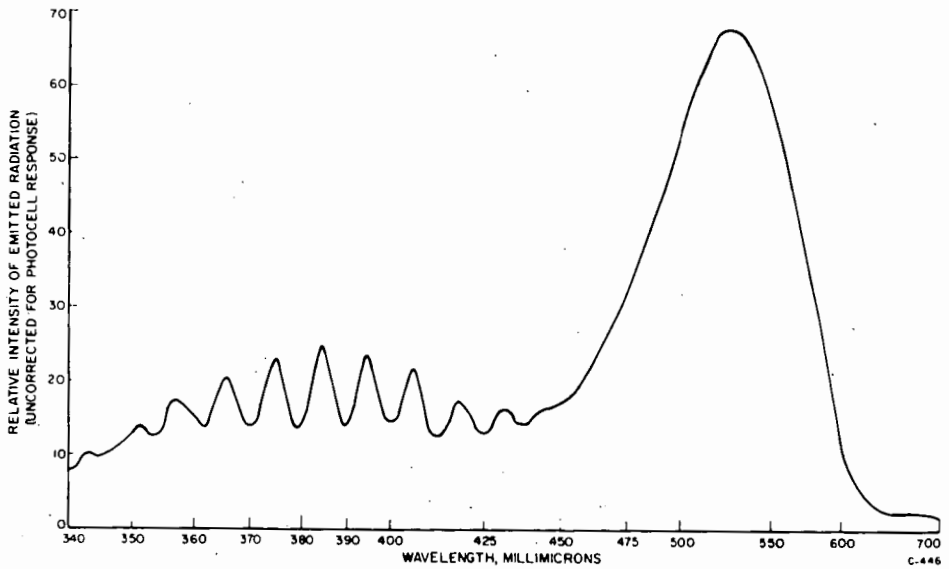


Figure 2. EMISSION SPECTRUM OF ZnS:Cu:Ag EXCITED BY A HYDROGEN DIFFUSION FLAME

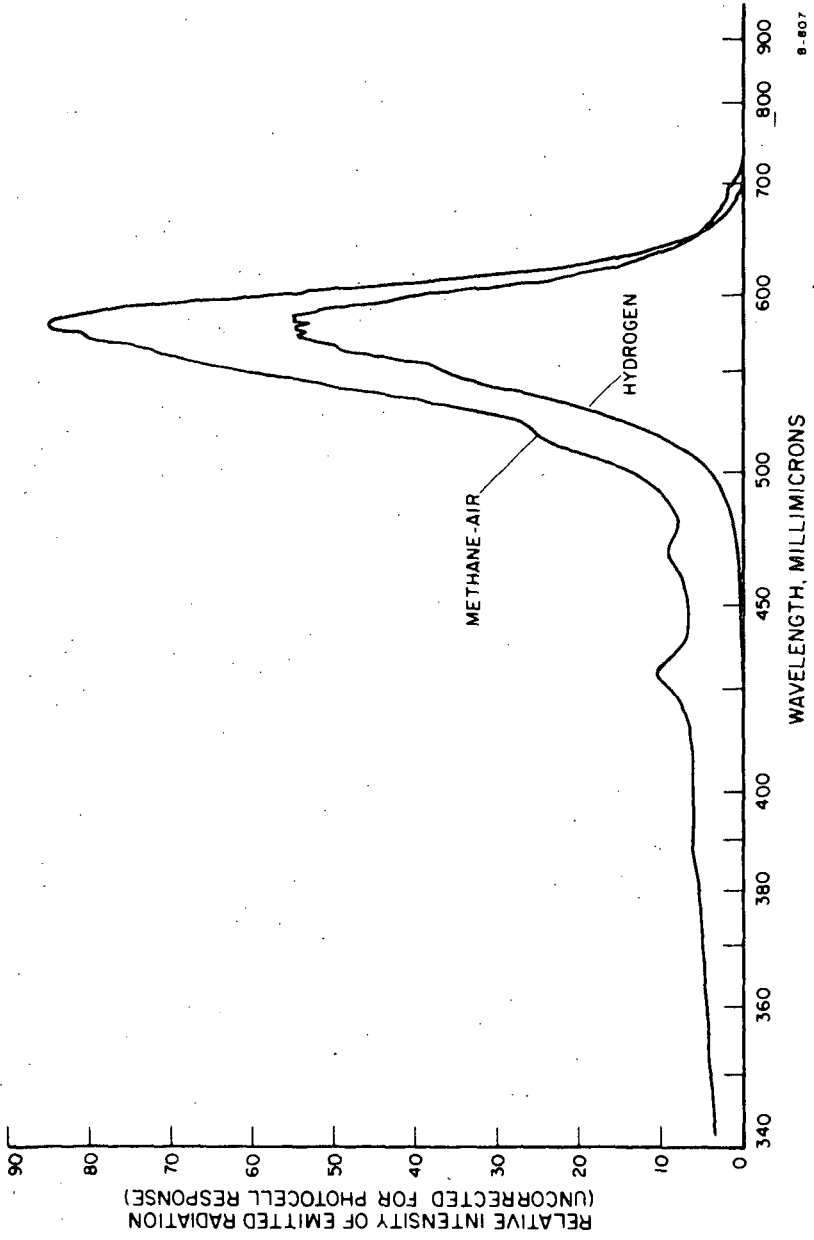


Figure 3. EMISSION SPECTRA OF SYLVANIA NO. 151 PHOSPHOR EXCITED BY HYDROGEN AND METHANE-AIR FLAMES

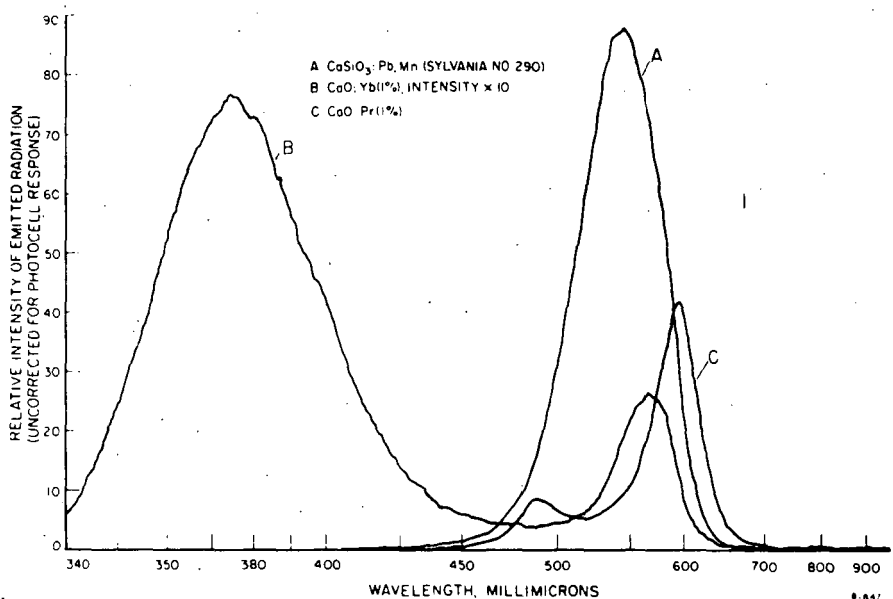


Figure 4. EMISSION SPECTRA OF PHOSPHORS EXCITED BY A HYDROGEN DIFFUSION FLAME

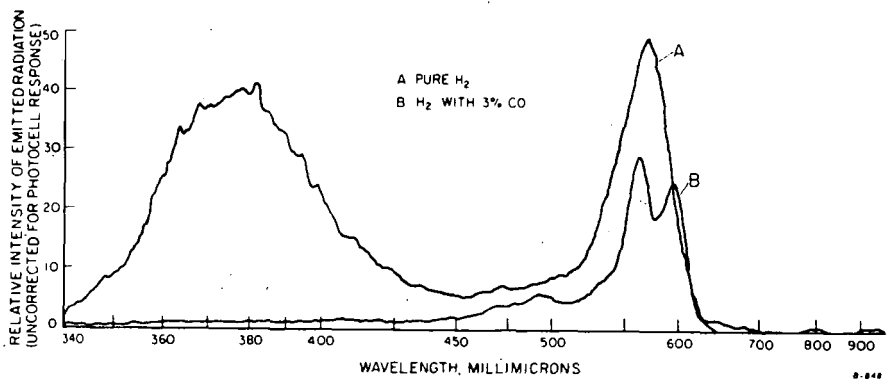


Figure 5. EFFECT OF CARBON MONOXIDE ON THE EMISSION SPECTRUM OF SAMARIUM-ACTIVATED CALCIUM OXIDE

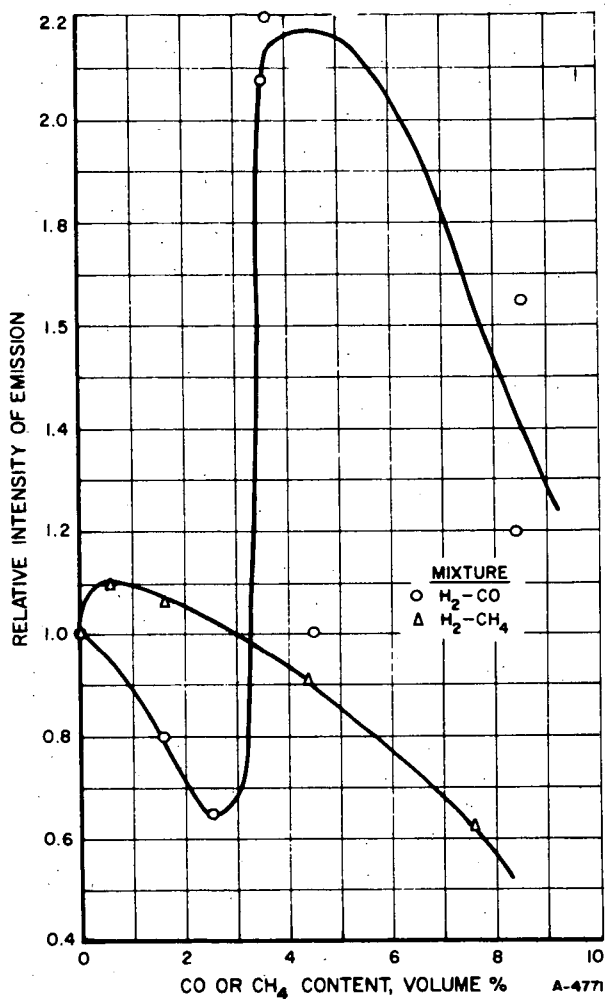


Figure 6. EFFECT OF FUEL COMPOSITION ON THE CANDOLUMINESCENCE OF SAMARIUM-ACTIVATED CALCIUM OXIDE

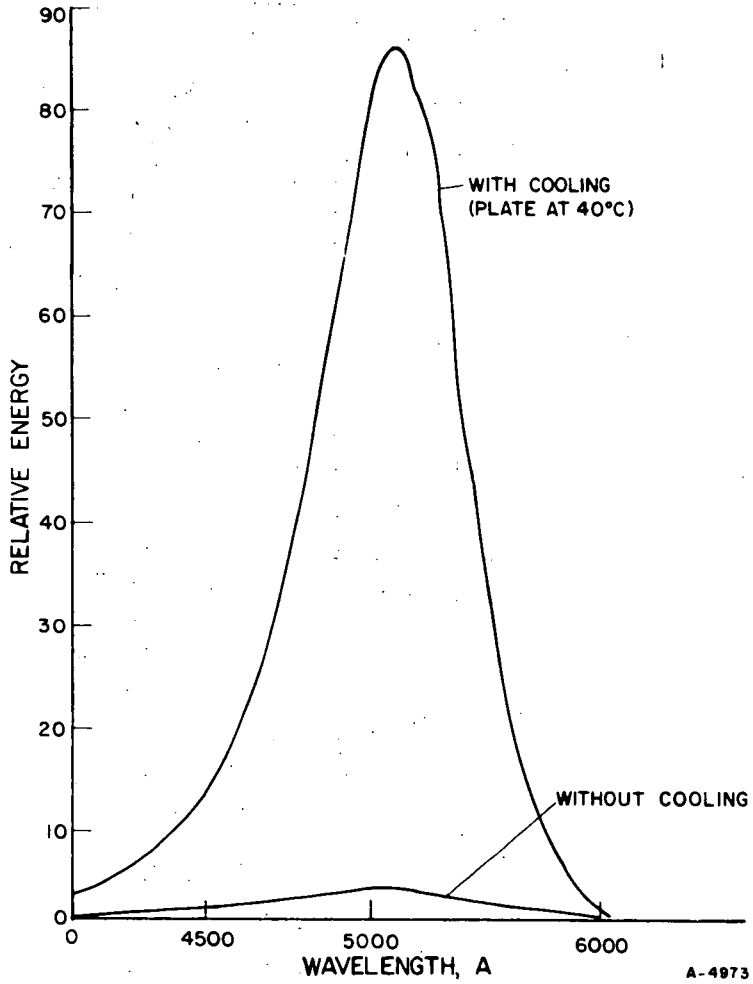


Figure 7. THE EFFECT OF TEMPERATURE ON THE EMISSION SPECTRUM OF SYLVANIA NO. 161 PHOSPHOR EXCITED BY A METHANE-AIR FLAME

A-4973

A RAPID, SIMPLE METHOD FOR THE DETERMINATION  
OF THE THERMAL CONDUCTIVITY OF SOLIDS

Neal D. Smith  
Fay Fun  
Robert M. Visokey

UNITED STATES STEEL CORPORATION  
Research Center  
Monroeville, Pennsylvania

The rational design of equipment such as shaft coolers, heaters, and rotary kilns for the heating and cooling of solids requires that the thermal properties of the solids be known. Thermal conductivity is one of these properties that to measure necessitates elaborate equipment and time-consuming techniques.

A rapid, simple method has been developed for determining the thermal conductivity of solids. The solids can be either porous or non-porous and of either high or low conductivity. If high-conductivity materials are tested, then both the thermal conductivity and heat capacity can be simultaneously measured by the method.

The procedure involves preparing a cylindrical briquette of the test solid that has a thermocouple located in the center. This briquette is heated to a constant temperature after which it is suspended in an open-end glass tube and cooled by a known flow of nitrogen or any other nonreactive gas. The thermal conductivity is then computed from a digital computer comparison of the cooling curves for the test solid versus a reference solid of known thermal properties and similar size that has undergone the same heating and cooling cycle. The method was validated by using the known thermal properties of lead, aluminum, and silver and computing the theoretical cooling curves. The theoretical curves were in close agreement with the experimentally measured cooling curves for these materials.

### Theory

The mathematical basis for determining thermal conductivity by the described method is discussed in a paper by Newman<sup>1)</sup> and is summarized as follows. Consider a cylindrical briquette as shown in Figure 1. The differential equation for unsteady state heat transfer by conduction in the x-direction is (see nomenclature for definition of the variables):

$$\frac{\partial t}{\partial \theta} = \alpha \left( \frac{\partial^2 t}{\partial x^2} \right) \quad (1)$$

For a briquette of thickness  $2a$ , the central plane being at  $x = 0$  and assuming:

- 1) uniform temperature at the start of cooling of the initially hot briquette

then  $t = t_0$  when  $\theta = 0$  (2)

2) the final temperature of the briquette will be the temperature of the surroundings:

therefore  $t = t_s$  when  $\theta = \infty$  (3)

3) there is no heat flow across the central plane because of symmetry:

consequently  $-k \left( \frac{\partial t}{\partial x} \right) = 0$  at  $x = 0$  (4)

The heat balance on the briquette surface is made by equating heat transferred to the surface by conduction with heat transferred from the surface by convection. In differential form, the heat balance is:

$$-k \left( \frac{\partial t}{\partial x} \right) = h (t - t_s) \text{ at } x = \pm a \quad (5)$$

Newman<sup>1)</sup> showed that the solution to Equations (1) through (5) expressed in terms of a dimensionless temperature ratio  $Y_x$  is:

$$Y_x = \frac{t - t_s}{t_0 - t_s} = 2 \sum_{n=1}^{\infty} A_n e^{-(\beta_n^2 X_a)} \cos(\beta_n \frac{x}{a}) \quad (6)$$

where  $A_n = \frac{m_a}{(1 + \beta_n^2 m_a^2 + m_a) \cos \beta_n}$  and

$\beta_n$  are defined as the first, second, third, etc., roots of the transcendental equation:

$$\beta_n \tan \beta_n - 1/m_a = 0 \quad (7)$$

The surface to solid thermal resistance ratio,  $m_a$ , is defined as:

$$m_a = k/ha \quad (8)$$

and  $X_a$  is defined as:  $X_a = \alpha \theta / a^2$  (9)

where the thermal diffusivity is:  $\alpha = k/\rho C_p$  (10)

Similarly, considering radial heat transfer, the radial briquette heat balance is

$$\frac{\partial t}{\partial \theta} = \alpha \left[ \frac{\partial^2 t}{\partial r^2} + \frac{1}{r} \frac{\partial t}{\partial r} \right] \quad (11)$$

The initial condition equation is:

$$t = t_0 \text{ WHEN } \theta = 0 \quad (12)$$

The final temperature equation is:

$$t = t_s \text{ WHEN } \theta = \infty \quad (13)$$

The boundary condition equations are:

$$-k \left( \frac{\partial t}{\partial r} \right) = 0 \text{ AT } r = 0 \quad (14)$$

and 
$$-k \left( \frac{\partial t}{\partial r} \right) = h(t - t_s) \quad \text{AT } r = R \quad (15)$$

Solving Equations (11) through (15) gives:

$$\frac{t - t_s}{t_0 - t_s} = 2 \sum_{n=1}^{\infty} A_n e^{-(\beta_n^2 X_r)} J_0(\beta_n \frac{r}{a}) = Y_r \quad (16)$$

where

$$A_n = \frac{m_r}{(1 + \beta_n^2 m_r^2) [J_0(\beta_n)]} \quad (17)$$

and  $\beta_n$  are the first, second, third, etc., roots of the equation:

$$\beta_n J_1(\beta_n) - 1/m_r J_0(\beta_n) = 0 \quad (18)$$

The surface to solid thermal resistance ratio,  $m_r$  is

$$m_r = k/hR \quad (19)$$

and

$$X_r = \alpha \theta / R^2 \quad (20)$$

The complete differential equation for the case shown in Fig. 1 is:

$$\frac{\partial t}{\partial \theta} = \alpha \left( \frac{\partial^2 t}{\partial r^2} + \frac{1}{r} \frac{\partial t}{\partial r} + \frac{\partial^2 t}{\partial x^2} \right) \quad (21)$$

and the solution to Equation (21) is:

$$Y = \frac{t - t_s}{t_0 - t_s} = Y_r \cdot Y_x \quad (22)$$

If the center temperature defined at  $r = 0$ ,  $x = 0$  is  $t_c$ , then eqn. 22 becomes:

$$Y_c = \frac{t_c - t_s}{t_0 - t_s} = Y_r \cdot Y_x \quad (23)$$

where  $Y_r$  and  $Y_x$  are evaluated at  $r = 0$  and  $x = 0$ .

The preceding mathematical analysis shows that the rate of cooling, or change in center temperature for a cylindrical briquette is a function of time ( $\theta$ ), density ( $\rho$ ), thermal conductivity ( $k$ ), the surface heat transfer coefficient ( $h$ ), specific heat ( $C_p$ ) and the briquette dimensions as expressed by Equation (23).

The experimental technique can now be described in terms of the previous discussion. If the change in center temperature with time is measured experimentally for a material of known thermal and physical properties (standard briquette), the surface heat transfer coefficient can be calculated from Equation (23), since it is the only unknown.

The surface heat transfer coefficient ( $h$ ) is a function of the flow rate of the cooling gas and the geometry and size of the briquette. It is independent of all other physical, thermal, or chemical properties of the briquette. Therefore, any other briquette having similar dimensions and cooled at the same flow rate will have the same value for ( $h$ ).

Once ( $h$ ) has been determined using the standard briquette, the thermal conductivity of any test material can be determined from Equation (23) since all other variables are known.

A computer program has been written which through an iterative process determines the best value of ( $h$ ) which makes the calculated values for the dimensionless temperature ratio equal to the experimental values obtained when the standard briquette is cooled.

With ( $h$ ) determined, another computer program is run for the test specimen. Thermal conductivity is now the unknown variable and through another iterative scheme, the best value for ( $k$ ) that makes the calculated and experimental values for the temperature ratios equal is found.

The input data for both programs consist of density, specific heat, time, briquette dimensions, and several experimental values for the temperature ratio. The output from the first program (standard) is the best value for ( $h$ ). Using this value for ( $h$ ), the second program used to determine the  $k$  value for any test material. If a highly conductive material is tested, then it is possible to determine its heat capacity since the solid thermal resistance will be small compared to the surface thermal resistance. A transient heat balance can be written for the test solid cooling in a stream of coolant gas.

$$V\rho C_p \frac{dt}{d\theta} = hA(t - t_s) \quad (24)$$

In the above equation,  $t = t_c$  since the thermal gradient in the solid is neglected. Integrating Equation (24) and using the dimensionless temperature ratio,  $Y_c$  gives:

$$Y_c = \exp(hA/\rho C_p V)\theta \quad (25)$$

Thus, if the internal solid thermal resistance is negligible, a plot of the experimental  $Y_c$  versus  $\theta$  data on semilog paper should be linear as shown by Equation (25). The heat capacity,  $C_p$ , can be calculated from the slope of the line for  $Y_c$  versus  $\theta$  since ( $h$ ) is the same as for the standard briquette and the density,  $\rho$ , and total surface area,  $A$ , for the test material are also known.

#### Materials and Experimental Work

A primary advantage of the transient technique for determining thermal conductivities is the ease and swiftness with which the experiment can be conducted.

In so far as sample preparation is concerned, any solid that can be briquetted, cast, or fabricated around a centrally located rigid

thermocouple ( $x = 0$ ;  $r = 0$ ) may be tested. Finished test sample cylinders should be approximately one inch in diameter, and one-half inch in height; however, other dimensions can be used.

### Experimental Apparatus

The experimental apparatus (see Figure 2) consists simply of a 3-inch diameter glass tube approximately 3 feet in length. One end of the tube is completely stoppered except for a one-half inch circular opening through which the coolant gas flows. The other end of the tube is open to the atmosphere. A small electric furnace is used to heat the briquette, and an automatic single point temperature recorder connected to the embedded thermocouple is used to measure the center temperature of the briquette.

### Experimental Procedure

The experimental procedure is the same for both the standard and test briquettes. Either the standard (aluminum was chosen since its thermal properties are well established), or the test briquette is connected to the temperature recorder by way of the thermocouple leads. The briquette is heated until the center temperature has reached a constant, predetermined value. The briquette is then quickly removed from the furnace and suspended in the cooling tube with the cooling gas flowing at a constant rate. The briquette is usually cooled to the temperature of the cooling gas within 20 minutes.

### Data Processing

For the standard briquette, the experimental dimensionless temperature ratio versus time data points for the standard briquette along with the known thermal properties are used to calculate the surface coefficient,  $h$ , in the following manner. A digital computer program is written to compute  $Y_c$  from Equations (6) through (23). By iteration and assuming various values of ( $h$ ), the computed values of  $Y_c$  can be made to converge on each of selected experimental  $Y_c$  versus  $\theta$  data points. Thus, for a selected data point, the best experimental ( $h$ ) is that which when used in Equations (8) and (19) results in equal values for the computed and experimental  $Y_c$  values.

For low conductivity test materials, the same method is used to determine the best experimental value of  $k$  by using the  $h$  determined for the standard and the other properties of the test material. If the test material is a good conductor as discussed in the theory section, then experience has shown that  $h$  should be computed from the experimental cooling curve and then this value is used to compute  $k$  by the same method as for low conductivity test materials.

## Discussion and Results

Three briquettes of aluminum, lead and silver were made to test the validity of the experimental technique since their thermal properties were available from the literature as shown in Table I. Sintered, dense hematite ( $\text{Fe}_2\text{O}_3$ ) and a briquette of porous carbon made from a partially devolatilized coal were used as test materials. For these materials, all properties except the thermal conductivities shown in Table I were previously measured. Cooling curves for each briquette were measured for a nitrogen flow rate of 0.9 scfm. Surface heat transfer coefficients for lead, silver and aluminum were calculated by the method discussed in the data processing section. For these materials, the literature conductivity values were used to calculate the surface coefficient. Table I shows that the calculated or experimental  $h$  values for each metal are nearly identical. This result is consistent with the theoretical basis of the experiment and may be considered as establishing the validity of the method. Also as additional evidence, aluminum was chosen as the standard and  $k$  values for lead and silver were calculated using the  $h$  value for aluminum. Table I shows that the calculated or experimental  $k$  values were within 0.5 percent of the literature values. The conductivities for hematite and porous carbon were calculated using aluminum as the standard. Figure 3 shows the experimental data points with the solid lines calculated from the theory. Note that the line for the carbon is curved whereas those for the metals and hematite are linear. As discussed previously, a linear cooling curve is obtained if the surface to solid thermal resistance ratios are relatively large. Note that for the metals, lead which has the lowest conductivity and thermal diffusivity cooled the fastest. This result is explained by examination of eqn. (25) which shows that for similar gas flows and briquette dimensions, the rate of cooling for different materials is determined by the heat content,  $\rho C_p$ . It can be seen in Table I that the heat content for lead is the lowest of all metals tested.

## Summary

A rapid, simple method for determining thermal conductivity for a solid has been developed. The solid can be either porous or non-porous and of either high or low conductivity. If high conductivity materials are tested, then both conductivity and heat capacity can be simultaneously measured from one cooling experiment. The method was validated by using the known thermal properties of lead, aluminum, and silver and the experimental cooling curves in a comparison with the computed results.

## References

1. Newman, A. B., Industrial and Engineering Chemistry, Vol. 28, 1936, pp. 545-548

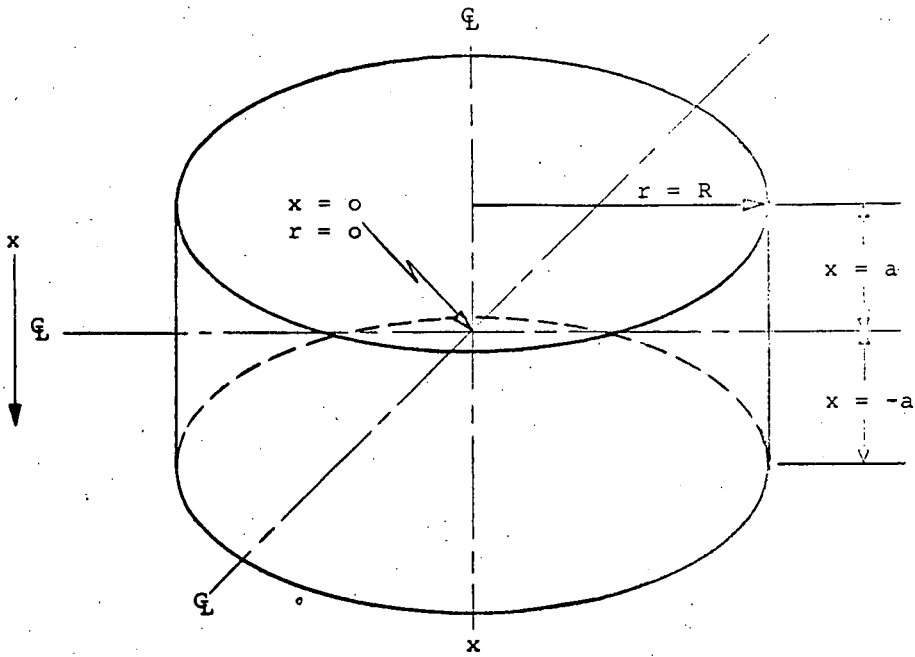
Nomenclature

- $a$  = Half height of briquette; ft  
 $A$  = Area; ft<sup>2</sup>  
 $A_n$  = Coefficient in infinite series solution for temperature distribution in Briquette  
 $C_p$  = Specific heat; BTU/lb °F  
 $H$  = Overall heat transfer coefficient; BTU/hr ft<sup>2</sup> °F  
 $h$  = Surface heat transfer coefficient; BTU/hr ft<sup>2</sup> °F  
 $k$  = Thermal conductivity; BTU/hr ft<sup>2</sup> °F/ft  
 $m_a$  = Axial surface resistance; dimensionless  
 $m_r$  = Radial surface resistance; dimensionless  
 $Q$  = Heat flux; BTU/hr  
 $R$  = Maximum radius of briquette; ft  
 $r$  = Radius of briquette; ft  
 $s$  = Half width of infinite plate; ft  
 $t$  = Temperature; °F  
 $t_c$  = Temperature at center of briquette; °F  
 $t_o$  = Initial temperature of briquette; °F  
 $t_s$  = Temperature of cooling gas; °F  
 $x$  = Distance of direction; ft  
 $X_o$  =  $\frac{a\theta}{\alpha^2}$  Dimensionless time parameter for axial component  
 $X_r$  =  $\frac{a\theta}{r^2}$  Dimensionless time parameter for radial component  
 $Y_x$  = Symbol for temperature ratio, axial component; dimensionless  
 $Y_r$  = Symbol for temperature ratio, radial component; dimensionless  
 $\alpha$  =  $(k/\rho C_p)$  Thermal diffusivity; ft<sup>2</sup>/hr  
 $\theta$  = Time; minutes or hours  
 $\rho$  = Density; lb/ft<sup>3</sup>

Table I  
THERMAL AND PHYSICAL PROPERTIES FOR THE BRIQUETTES

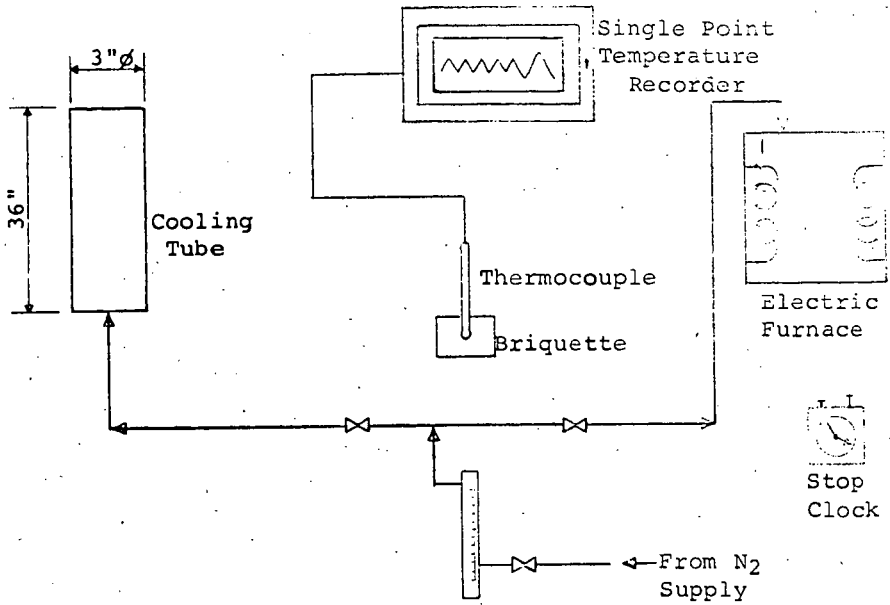
	Aluminum	Silver	Lead	Hematite	Porous Carbon
a	.01842	.02059	.01842	.01842	.01958
R	.04208	.04210	.04117	.04208	.04121
$\rho$	168.50	655.20	707.43	306.00	75.0
$C_p$	.2273	.0578	.0306	.2090	.2360
$\rho C_p$	38.30	39.31	21.65	63.95	17.70
h (experimental)	5.58	5.70	5.60	5.58	5.58
k (experimental)		240.3	18.99	12.10	.0307
k (literature)	121.7	240.0	19.00	none	none
$\alpha$ (experimental)	3.178*	6.113	.8770	.1892	.00173

\* Average of literature sources



STANDARD CYLINDRICAL BRIQUETTE

Figure 1



EXPERIMENTAL APPARATUS

Figure 2

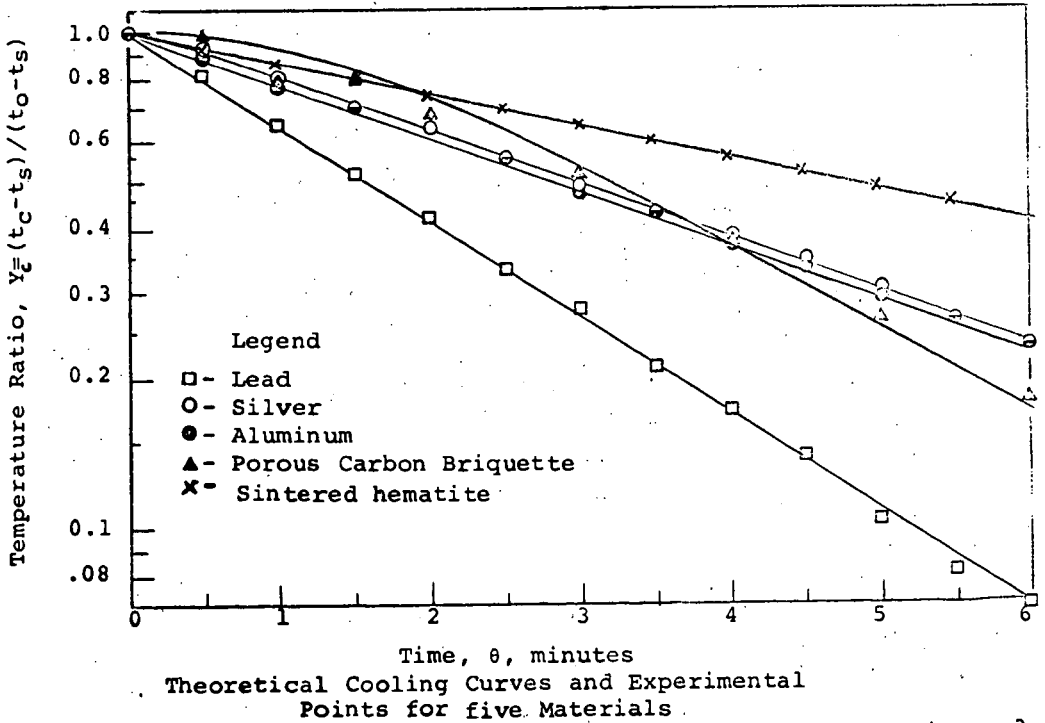


Figure 3